NASA
TT
F-557
c.1

AKADEMIYA NAUK SSSR

M.V. Pridantsev, Editor

STRUCTURE AND PROPERTIES OF HEAT-RESISTANT METALS AND ALLOYS

LOAN COPY: RE
AFWL (WLO
KIRTLAND AFB,
0068999
TECH LIBRARY KAFB, NM

Translated from Russian

Published for the National Aeronautics and Space Administration
and the National Science Foundation, Washington, D.C.
by the Israel Program for Scientific Translations

TECH LIBRARY KAFB, NM
0068999

AKADEMIYA NAUK SSSR. INSTITUT METALLURGII im.
Academy of Sciences of the USSR. A. A. Baikov Institute of Metallurgy

M.V. Pridantsev, Editor

STRUCTURE AND PROPERTIES OF HEAT-RESISTANT METALS AND ALLOYS

(Struktura i svoistva zharoprochnykh metallicheskikh materialov)

Izdatel'stvo "Nauka"
Moskva 1967

Translated from Russian

Israel Program for Scientific Translations
Jerusalem 1970

NASA TT F-557
TT 69-55020

Published Pursuant to an Agreement with
THE NATIONAL AERONAUTICS AND SPACE ADMINISTRATION
and
THE NATIONAL SCIENCE FOUNDATION, WASHINGTON, D.C.

Copyright © 1970
Israel Program for Scientific Translations Ltd.
IPST Cat. No. 5439

Translated by Ch. Nisenbaum, Chem. Eng.
Edited by D. Slutzkin

Printed in Jerusalem by Keter Press
Binding: Wiener Bindery Ltd., Jerusalem

Available from the
U.S. DEPARTMENT OF COMMERCE
Clearinghouse for Federal Scientific and Technical Information
Springfield, Va. 22151

XII/15/4

Table of Contents

I Heat-Resistant Metals and Alloys 1

E. M. SAVITSKII and G. S. BURKHANOV. The problem of cold shortness in heat-resistant metals and alloys 1
V. S. IVANOVA, I. M. KOP'EV, and Yu. P. LIBEROV. The susceptibility of refractory metals to brittleness and creep 14
M. P. MATVEEVA and V. A. MOROZOV. Study of creep of cast and wrought chromium in vacuo 20
P. L. GRUZIN and S. V. ZEMSKII. Influence of local inhomogeneities in the distribution of impurities on the brittleness of chromium 26
A. K. BUTYLENKO, V. N. GRIDNEV, and V. N. MINAKOV. The absence of polymorphism in chromium 33
I. I. KORNILOV. Metallides—A new basis for refractory materials 40
D. A. PROKOSHKIN and M. I. ZAKHAROVA. Isothermal sections of the phase diagram of the molybdenum—titanium—zirconium system at 1200°C, 900°C, and 800°C 50
A. M. YAKIMOVA. Study of the properties of molybdenum modified by refractory compounds at elevated temperatures 57
V. K. GRIGOROVICH. Electron structure and crystal structure of transition metals 61
V. G. OSIPOV, V. D. MUTOVIN, and V. V. VINOGRADOV. Rolling, heat treatment, and deep drawing of thin sheets of molybdenum 71
I. S. GAEV and E. V. SHEYANOVA. Study of the weldability of molybdenum associated with variation in its structure 74
I. A. TREGUBOV and L. N. KUZINA. High-temperature (1400°C) hardness of tungsten-base alloys containing tantalum and rhenium 79
K. B. POVAROVA, M. A. TYLKINA, and E. M. SAVITSKII. Refractory ternary alloys of the tungsten—molybdenum—rhenium system 82
V. G. OSIPOV, V. M. AMOSOV, E. V. USHAKOV, E. K. DROBYSHEVA, N. M. ZELENTSOVA, and A. G. BORISOV. The ductility of tungsten . . 88
V. G. OSIPOV, E. V. USHAKOV, E. K. DROBYSHEVA, V. I. KASHIN, and G. Kh. VASYUKOV. Forging tungsten produced by arc melting 94
L. I. IVANOV, E. A. ABRAMYAN, and V. A. YANUSHKEVICH. Nature of high-temperature creep of refractory metals and alloys 97
A. F. ORLOV. Creep of niobium under high stresses 101

V. G. CHERNYI and I. M. NEDYUKHA. Physical factors leading to the strengthening of alloyed niobium 104
A. P. SEMENOV and V. V. POZDNYAKOV. Methods and results of a study on the friction and the adhesion between metals at elevated temperatures in vacuo and in gases 110
A. P. SEMENOV and V. V. POZDNYAKOV. Preliminary results of a study on adhesion and friction at elevated temperatures between oxides and refractory metals and oxides in vacuo and in gases 118
S. O. TSOBKALLO, M. D. NIKITIN, V. A. CHELNOKOV, V. I. TIMOFEEVA, I. G. VALTER, and L. A. PRIVALOV. Study on the vibration energy (internal friction) as a reserve of strength of refractory alloys at elevated temperatures 123

II. Iron- and Nickel-Base Steels and Alloys 130

I. L. MIRKIN, A. A. YUDIN, Yu. A. RYBAKOVA, M. B. GUTERMAN, and A. S. TREKALO. Substructure and grain boundary porosity under conditions of creep 130
K. I. TEREKHOV. Alloying, structure and phase composition of heat-resistant nickel-chromium alloys containing niobium 137
Yu. P. ROMASHKIN. Influence of temperature and deformation on the nature of activation and the behavior of stressed metals at elevated temperatures 142
L. A. RYABTSEV, I. I. KORNILOV, and L. I. PRYAKHINA. Heat resistance and physicochemical properties of complex nickel-base alloys 155
M. V. RASTEGAEV, M. V. PRIDANTSEV, M. Ya. DZUGUTOV, and Yu. V. VINOGRADOV. The nonuniform crystal structure of the KhN77TYuR (EI437B) alloy 160
M. Ya. DZUGUTOV and V. P. STEPANOV. Prevention of the formation of a nonuniform grain structure in a critically deformed KhN77TYuR alloy 167
B. I. MEDOVAR, L. G. PUZRIN, G. A. BOIKO and Yu. N. KROKHMAL'. Isothermal crystallization during pressure brazing of heat-resistant nickel-base alloys 173
V. G. VOLKOV, S. A. YUGANOVA, I. A. STEPANOVA and N. S. KRESHCHANOVSKII. Influence of metallurgical factors on the structure of heat-resistant nickel alloy EI765 179
V. I. PROSVIRIN, V. D. MORTIKOV, and S. A. GORYUNOV. The specific behavior of heat-resistant alloys during thermal cycling 185
V. K. TSVETKOVA, V. N. ZHUCHIN, V. V. TOPILIN, A. P. BOYARINOVA, V. P. STEPANOV, L. N. ZIMINA, and G. F. KOSHELEVA. Properties of super alloys of the EP487 type 189
L. N. ZIMINA, G. F. KOSHELEVA, E. A. KARDONOV, and V. K. TSVETKOVA. Structure and properties of the KhN60MVTYu (EP487) alloy 194
N. F. LASHKO, O. A. KHROMOVA, A. A. BURMISTROVA, and N. I. ZHURAVLEVA. Influence of cobalt on the phase composition of some heat-resistant alloys 200

M. A. FILATOVA, G. T. KUZ'MINA, and L. I. OSTROVSKII. Changes in the properties and structure of vanes of gas turbines made of nickel-base industrial alloys during service in an experimental installation .. 204
E. E. LEVIN, E. M. PIVNIK, M. G. TAUBINA, D. B. LIVSHITS, and E. F. TRUSOVA. Some problems of alloying nickel-base alloys 211
O. A. BANNYKH, I. F. ZUDIN, R. M. VOLKOVA, Yu. K. KOVNERISTYI, M. V. PRIDANTSEV, E. D. SUROVTSEVA, and G. A. SGIBNEVA. Study of the structure and properties of EP357 steel..... 217
I. L. MIRKIN, Z. N. PETROPAVLOVSKAYA, and I. A. SHCHENKOVA. Influence of alloying elements on the strength of interatomic bonds of ferrite, the composition and type of strengthening phases and the resistance of steel to stress relaxation 225
K. V. GOREV, L. I. SHVEDOV, Z. D. PAVLENKO, and S. L. LIFSHITS. Study of structural changes in chromium-nickel steel alloyed with aluminum 231
O. A. BANNYKH, M. Ya. DZUGUTOV, V. M. DORONIN, I. F. ZUDIN, M. V. PRIDANTSEV, V. V. TOPILIN, A. M. UGLOVA, E. G. FEDORINOVA, and E. V. SHAL'NEV. Study of the heat resistance of chromium—manganese—aluminum austenitic steels 239
Yu. P. BELOLIPETSKII, M. A. ENDZELIN, M. A. FILATOVA, S. P. BARABANOV, L. P. ALISHOEV, and D. I. BEREZHKOVSKII. Study of the influence of the grain size and of grain size nonuniformity on the heat resistance and strength of vane materials 245
L. Ya. LIBERMAN. Relaxation and creep strength of hardening stainless chromium steels 250
A. S. TERESHKOVICH, S. P. NESTERTSEV, and A. E. RUNOV. Austenitic heat-resistant steel for castings 257

III. Strengthening of Steels and Alloys 264

V. D. SADOVSKII, B. D. TITOROV, E. N. SOKOLKOV, V. K. FARAFONOV, V. D. NEGODYAEV, M. M. NICHKOVA. High-temperature ausforming of large steel forgings 264
V. S. IVANOVA and N. A. VOROB'EV. Kinetics of failure of heat-resistant alloys during high-temperature deformation 267
L. K. GORDIENKO, Z. G. FRIDMAN, and V. M. STEPANOV. Influence of temperature on the stability of heat-resistant alloys strengthened by thermomechanical treatment (TMT) and multistage thermomechanical treatment (MSTMT) 274
M. I. ZAKHAROVA, Yu. S. EGOROV, and A. B. IVANOVA. The structure of aluminum and aluminum alloys containing 3% of copper after thermomechanical treatment..... 283
I. A. EPSHTEIN. Influence of low-temperature thermomechanical treatment (LTTMT) on the properties of manganese austenitic steels 288
M. G. LOZINSKII, A. S. NIKISHOV, N. Z. PERTSOVSKII, and Yu. I. KAPLIN. Influence of high temperature thermomechanical treatment on the heat resistance of KhN70VMTYu alloy 291

E. N. SOKOLKOV, M. A. SMIRNOV, M. G. GAIDUKOV, and M. M. SHTEINBERG. Influence of the temperature of preliminary plastic deformation on the long-time strength of austenitic steels 297
N. S. ALFEROVA and T. M. BOGDANOVA. Increase in workability during pressing of heat-resistant steels of the martensitic and martensitic-austenitic types 305
A. A. CHIZHIK. A new method for investigating creep and relaxation in metals and alloys 308
N. V. AGEEV, S. G. GLAZUNOV, L. A. PETROVA, G. N. TARASENKO, and L. P. GRANKOVA. Short-time and long-time strength of the β-alloy of the Ti—Mo—Cr—Fe—Al system at elevated temperatures 316
A. M. KOROL'KOV, L. M. GUROVA, and E. V. BEZUS. Heat-resistant copper alloys 322

IV. Kinetics and Mechanism of Oxidation, and Protective Coatings 329

N. N. KOZLOVA and A. R. KRYLOVA. Principles of long-time oxidation of heat-resistant steels and alloys 329
P. T. KOLOMYTSEV, R. I. ANDREEVA, L. A. KOSTINA, and S. A. STREKOPYTOV. Behavior of diffusion coatings on nickel alloys at elevated temperatures 336
O. S. IVANOV, I. I. RAEVSKII, and M. S. SKRYABINA. Comparative study on the oxidizability and heat resistance of niobium-base alloys 340
G. V. ZEMSKOV, R. L. KOGAN, and A. V. KOSTENKO. Study of binary heat-resistant silicon-base diffusion coatings for nickel alloys 347
D. V. IGNATOV, R. S. IVANOVA, and N. B. ABRAMOVA. Electron diffraction and kinetic studies on the reaction between heat-resistant metals and oxides and residual gases and vapors in vacuo (10^{-3}—10^{-6} torr) at elevated temperatures 354
N. F. SHUR. Investigation of the serviceability of heat-resistant steels in carbon-containing atmospheres 361
V. S. POSTNIKOV, I. M. SHARSHAKOV, V. V. USANOV, A. M. BELIKOV, and I. V. ZOLOTUKHIN. The mechanism of the hardening of some Fe—Cr—Ni alloys 364
M. Ya. DZUGUTOV, Yu. V. VINOGRADOV, S. A. GOLOVANENKO, and A. N. CHERNOV. Study of the macrostructure and properties of extruded rods of high-strength alloys 368

EXPLANATORY LIST OF ABBREVIATED NAMES OF USSR INSTITUTIONS AND PERIODICALS APPEARING IN THE TEXT

Abbreviation	Full name (transliterated)	Translation
AN	Akademiya Nauk	Academy of Sciences
FMM	Fizika Metallov i Metallovedenie	Physics of Metals and Metallurgy
IL	Izdatel'stvo Inostrannoi Literatury	Foreign Literature Publishing House
IMET	Institut Metallurgii im. A. A. Baikova	A. A. Baikov Institute of Metallurgy
LGU	Leningradskii Gosudarstvennyi Universitet	Leningrad State University
ONTI	Otdel Nauchno-Tekhnicheskoi Informatsii	Department of Scientific and Technical Information
OTN	Otdelenie Tekhnicheskikh Nauk (Akademii Nauk SSSR)	Department of Engineering Sciences (of the Academy of Sciences of the USSR)
TsNIIChM	Tsentral'nyi Nauchno-Issledovatel'skii Institut Chernoi Metallurgii imeni I. P. Bardina	Central Scientific Research Institute of Ferrous Metallurgy im. I. P. Bardin
TsNIITMASh	Tsentral'nyi Nauchno-Issledovatel'skii Institut Tekhnologii i Mashinostroeniya	Central Scientific Research Institute of Technology and Machine-Building
ZhNKh	Zhurnal Neorganicheskoi Khimii	Journal of Inorganic Chemistry

This book contains new theoretical and experimental data on the heat resistance of metals and metal alloys. The role of dissolved atoms in the strengthening and diffusion processes in metals and alloys, and their influence on the cold shortness of heat-resistant metals are reviewed.

Experimental data are given on the thermal stability of the defects of crystal lattices, on creep, and on the nucleation and development of cracks during failure.

The physicochemical properties and structure of alloys, as well as basic methods of controlling the dislocation structure of metals and alloys by thermal and mechanical processes, are discussed. Problems of corrosion in gases and of protective coatings are also clarified. The book contains data on methods of surface alloying to reduce the oxidizability of heat-resistant alloys.

The book has been written for wide circles of research workers, scientists, industrial engineers, and workers in metallurgical laboratories of the aircraft, machine-building, and other industries.

I. HEAT-RESISTANT METALS AND ALLOYS

E. M. Savitskii and G. S. Burkhanov

THE PROBLEM OF COLD SHORTNESS IN HEAT-RESISTANT METALS AND ALLOYS

The recent intense development of industry has greatly increased the importance of heat-resistant metals in the production of the most heat-resistant alloys, and alloys with special physical properties /1/. Some examples of the application of heat-resistant metals to modern industry are given in Figure 1 /2—4/. The main drawbacks of heat-resistant metals which hinder their introduction into modern industry are not only their oxidizability and poor weldability, but also their cold shortness. If heat-resistant metals are cooled, they become embrittled over a rather narrow range of temperatures. The metals with a body-centered cubic crystal lattice belonging to groups VA and especially VIA of the periodic system become embrittled during cooling. The ductile-brittle transition temperatures of these metals (commercial grade) are approximately as follows: tantalum – 196°C, niobium 20°C, molybdenum 20—300°C, chromium 250—400°C, and tungsten 400—600°C. Thus, metals belonging to group VIA, and especially tungsten, have the highest ductile-brittle transition temperature. Iron with a body-centered cubic lattice is a classical example of a metal susceptible to cold shortness. Some metals with hexagonal crystal lattices, e.g., zinc, cadmium, magnesium, ruthenium, and osmium (the last two metals have a high melting point) also suffer from cold shortness. Cold shortness is found in some metal compounds (intermetallic compounds) and in certain semiconductor elements (germanium, silicon).

Cold shortness is an important problem in heat-resistant metals, but is also one of the main problems of physical chemistry, metallurgy, metal physics, and mechanics. Cold shortness is very important industrially and economically in the fields of cosmonautics, aircraft building, electronics, railways, the automobile industry, water transport, and the building industry, particularly in Siberia, the Arctic and the Antarctic. Many institutes have been busy investigating the problem of cold shortness in the Soviet Union and outside. A review of the present state of the studies carried out in this field would require a large, specialized book. The purpose of this short article is to give a review of modern theories on the problem of cold shortness.

Today the study of the nature of cold shortness is based on four points of view which can be approximately classified as follows: 1) the mechanical, 2) the energetic; 3) the metallophysical, and 4) the physicochemical.

The mechanical or phenomenological point of view is based on the relationship between σ_T and σ_B which varies with temperature (σ_T grows considerably more rapidly than σ_B with decrease in temperature). This

point of view was developed by the school of Davidenkov. A review of modern theories on cold shortness is given in /5, 6/.

The energy of failure /7/ is calculated in the energetic method.

The metallophysical standpoint is based on the decisive role of crystal defects /7—9/. This has been developed in Soviet and non-Soviet metallophysical institutes. According to modern metallophysical theories, the cracks which determine brittle failure are caused by the resistance to the motion of dislocations. The development of these theories from qualitative descriptions, which are frequent in the literature, to a determination of quantitative relationships is very important, since this will help to answer the question of the dislocation structure (type and number of dislocations and other defects, their location in the metal or alloy) that will ensure the required minimum ductility at ordinary and low temperatures.

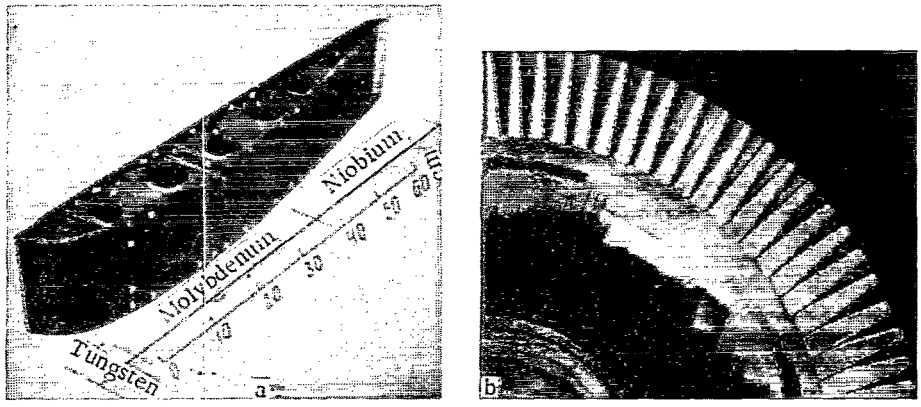

FIGURE 1. A complex part made of three heat-resistant metals: tungsten, molybdenum, and niobium (a); turbine blades made of a Mo—0.5% Ti alloy (b).

The physicochemical theory on ductility is based on the assumption that the metallic bonds and the freedom of metals and alloys from interstitial impurities exert a decisive influence on the ductility of metals. This theory has been developed in the Laboratory of Heat-Resistant Alloys and Rare Metals of IMET AN SSSR, and in a number of other Soviet and non-Soviet scientific institutions /10—14/.

The above four points of view are not contradictory, but complement one another and emphasize the importance of the detailed study of the complex problem of cold shortness. Ductility, like strength, of solid-crystalline materials, including metals and alloys, is dependent on a number of factors. The most important are: the nature of the interatomic bonds, the macro- and microstructures, various defects, external factors (temperature, pressure, composition), testing conditions (stresses, rate of deformation, presence or absence of notches, surface finish, dimensional factors, etc.). Thus, ductility is not only a property but also a state of the substance.

Let us see what are the most important assumptions on which the physicochemical theory of ductility is based. The nature of the interatomic bonds is one of the most important factors which determines the behavior of a material under the influence of external forces. The idea of high

ductility can be derived from the very definition of a metal. The metallic state, and the metallic nature of interatomic bonds, are most favorable to the ductile state of substances, since only metallic bonds, i.e., the presence of free electrons, allow atoms to shift relatively to one another without upsetting the continuity of the material. This has been confirmed by the experience of mankind over many centuries. The malleability of metals besides their hardness and strength was the most important factor which led to the bronze age, the iron age, and the technical progress in our days. Lomonosov wrote: "Metals are those bright bodies which can be forged" /15/. It is important to point out that the whole development of science and industry has confirmed this brillant generalization of Lomonosov.

Materials with covalent bonds in which the valence electrons are shared by a given atom and its closest neighbors are the most brittle. This type of bond is found in diamonds, silicon, germanium, and semiconductor compounds at room and low temperatures. Once the covalent bond is disturbed it can be restored with great difficulty only. The behavior of crystals with ionic bonds, for example, metal oxides and natural salts, is similar. However, if covalent or ionic crystals are heated to relatively high temperatures, close to the melting point, and if nonuniform compressive forces are applied at all sides, these crystals become ductile /10/.

Pure metals may become ductile at any temperature. A metal or alloy becomes brittle or ductile according to the amount and structural location of interstitial impurities, and the influence of external factors. Metals with a face-centered cubic lattice show no brittle failure even if they are cooled to a temperature close to absolute zero. The same is true of alkali metals with a body-centered cubic structure /5, 10/. The monomorphic heat-resistant metals of groups VA and VIA with a body-centered lattice retain this type of structure and the metallic nature of the bond even if they are cooled to absolute zero. Consequently, from the physical point of view, there is no reason why such metals should have temperature zones of brittleness. Brittleness is a characteristic property of metals of the commercial grade of purity, and is associated with difficulties encountered in the production of pure metals and in the preservation of this purity during later processes /12/. Some authors believe that cold shortness is an inherent characteristic of metals with body-centered lattices but this idea has not been proved, and it does not conform to the nature of the metallic state of substances. Apparently, metals with body-centered lattices are brittle only if they contain impurities which form interstitial solid solutions or nonmetallic inclusions, mainly along the boundaries of grains and blocks. It has been experimentally shown that metals such as tantalum, niobium, molybdenum of a high degree of purity, and also potassium and sodium, show no signs of cold shortness down to temperatures of liquid helium /10—14/. Tungsten with a low content of carbon is highly ductile in liquid nitrogen /13/, and if the metal is completely free of carbon or other interstitial impurities it can be deformed even in liquid helium. We do not share the opinion that heat-resistant metals are brittle because they contain a certain amount of covalent bonds. There is nothing new in this statement on the covalent bonds, since it is known that natural substances often have mixed interatomic bonds, and the presence of covalent bonds is derived from the very definition of transition metals. It should be pointed out that metallic bonds are always predominant in metals, and that these determine

the mechanical and electrical properties of metals. Covalent bonds apparently determine the susceptibility of metals to impurities. One of the main tasks of the physical chemistry of metals is to translate qualitative theories into a quantitative determination of the distribution of electrons in metals and alloys. This is possible by the following modern physical methods: study of the distribution of electrons using Fourier series /16/, study of X-ray emission spectra /17/, determination of the spin superstructure using neutron scattering, resonance methods, experimental determination of the Fermi surface in metals /18—20/, measurement of different physical properties, etc. These problems must be solved in close cooperation with institutes of physics.

The ductile—brittle transition in metals, characterized by a critical temperature of brittleness, is associated with a change in the mechanism of failure. At temperatures above the critical point the failure takes place after considerable plastic deformation as the result of plane slipping, while below the critical temperature the failure is due to the development of cracks along cleavage planes, or sometimes along the grain boundaries, with little or no plastic deformations /21/.

Let us consider for a moment the method of determining the temperature, or more accurately, the temperature range, of the ductile—brittle transition. The transition temperature cannot be determined by the relationship between hardness and temperature, as attempted by some authors, since experiments on the determination of this relationship do not bring the metal to failure. The zones of brittleness can be found by determining measures of ductility by means of mechanical tests with the application of tensile stresses. These measures are elongation or reduction of area during monoaxial tensile tests, impact strength, angle of deflection during bending tests, etc. The energy required to bring about the failure of the specimen during impact tests and the notch sensitivity can be considered as the most objective and rigid criteria of the cold shortness of materials. The most rigid conditions are created during testing for impact strength of notched specimens. For steel the ductile—brittle transition temperature is fixed as the point at which the impact strength of at least one specimen falls below 2 kgm/cm^2. This method gives the highest ductile—brittle transition temperature. According to Semchyshen and Barr, the ductile—brittle transition temperature of recrystallized molybdenum rods, determined by impact tests, is by about 350—450°C higher than that found from tensile tests /3/. The influence of the type of loading on the transition temperature conforms with the variation in the relationship between tangential stresses and normal stresses. For tensile tests this relationship is 1:1, for torsion tests 1:2, and for compression tests 1:4. Therefore, according to /3/, the ductile—brittle transition temperature of commercial chromium as determined by tensile tests, torsion tests, and compression tests, is 355, 250, and 0°C, respectively. During bending the maximum tensile stresses act on the external surface of the specimen. Therefore, to avoid accidental results because of impurities, the surface of the specimen must be polished before testing. Tensile tests on notched specimens clearly reveal the principal parameters of the ductile—brittle transition of materials. Notching specimens leads to two effects during tensile tests: it increases the strain in the localized region of the specimen, and it induces triaxial stresses which increase the ratio of normal stresses to tangential stresses.

An interpretation of the experimental data and an exact determination of the range of the ductile—brittle transition temperature by methods of mathematical statistics are given in /22/. The graphical method of determination of the ductile—brittle transition temperature is described in /23/.

The ductile—brittle transition temperature is not a constant physical characteristic of the metal but is determined by a number of factors: the purity of the metal, the rate and type of deformation, the gaseous environment, etc.

According to modern physicochemical theories of ductility, an actual metal or alloy is a physicochemical system consisting of crystals of the basis metal, and impurities, alloying elements, and crystal defects distributed inside the metal and along the grain boundaries. The mechanical and other physical properties of such a system are determined by the nature of the basis metal, and especially by the properties and relative distribution of the structural components of metalloid and metal impurities and crystal defects. This distribution may be either favorable or unfavorable to the plastic deformation of the crystals of metals or alloys /11/. Today nobody doubts that the purity of a metal is one of the chief factors influencing the ductile—brittle transition temperature /10/. The greatest influence is exerted by interstitial impurities; the purer the metal the lower is the transition temperature /10—14/.

Not all interstitial impurities influence the ductility of heat-resistant metals to the same extent. From recent studies on the reactions between interstitial impurities and metals of the VIA group, it is possible to place the impurities into a series according to their descending influence on metals of the VIA group: carbon (most embrittling), oxygen, nitrogen, hydrogen (exerts the smallest influence) /10, 13/. According to Jaffee et al. these elements can be placed according to their influence on metals of the VA group in the following series: hydrogen (most embrittling), nitrogen, oxygen, carbon (exerts the smallest influence) /24/. According to the data obtained in our laboratory, oxygen exerts the most detrimental influence on rhenium /25/.

The highly brittle and hard nonmetallic compounds are particularly harmful if they form films or coatings along the grain boundaries. This leads to a weakening of the bonds between the crystallites and to a brittle failure of the material along the grain boundaries. For example, in molybdenum a content of 0.006% of oxygen is sufficient for the formation of molybdenum oxides along all grain boundaries. If the content of interstitial impurities does not exceed their solubility in the solid material, metals of groups VA and VIA remain ductile at low temperatures. Highly pure metals have a considerably lower ductile—brittle transition temperature. A decrease in the content of carbon in tungsten from 0.01 to 0.001% decreases the transition temperature from room temperature to -196°C /13/. The influence of the content of carbon on the transition temperature for molybdenum is shown in Figure 2 /24/. The purification and analysis of interstitial impurities in metals of group VIA is most difficult, since at room temperature the solubility of these impurities is only 0.0001%. Since metals are embrittled mainly by interstitial impurities along the grain boundaries, the extent of the boundaries is of great importance. The surface area of grain boundaries per unit of volume is an important factor which determines the ductility of heat-resistant metals /26/.

Therefore, it is desirable to have the surface area of grain boundaries as large as possible, i.e., to have a fine-grained structure, irrespective of the content of impurities. This will reduce the relative concentration of interstitial impurities and the ductile—brittle transition temperature /1/. The influence of the grain size on the ductile—brittle transition temperature of some heat-resistant metals of groups VA and VIA is shown in Figure 3. The dimensions of the subgrains and the field of coherent dispersion apparently also exert a certain influence on the ductility of the metals, although not as great as that of the grain size. Cold working, and the existence of texture, have a favorable influence on the ductility of heat-resistant metals. Drawn wire of heat-resistant metal with a critical amount of cold working readily endures subsequent cold drawing to small sizes.

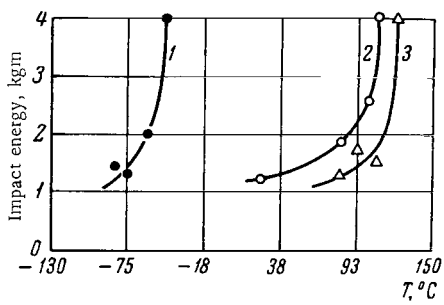

FIGURE 2. Influence of the content of carbon on the ductile—brittle transition temperature of molybdenum (Charpy tests on unnotched specimens made of rolled rods):

1—0.004% C; 2—0.008; 3—0.017.

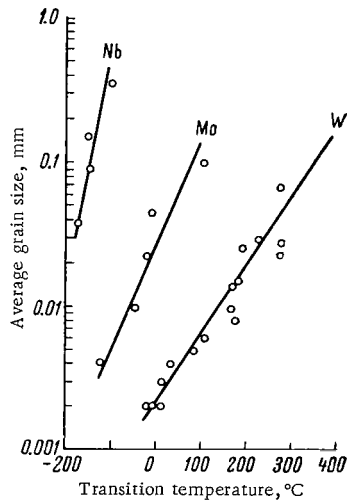

FIGURE 3. Influence of grain size on the ductile—brittle transition temperature of metals of groups VA and VIA.

We have discussed how cold shortness of heat-resistant metals is influenced by interstitial impurities at concentrations exceeding their solubility. Impurities which have not dissolved form nonmetallic inclusions along the grain boundaries.

Interstitial impurities in the solid solution also have a highly unfavorable effect on the ductility of heat-resistant metals, mainly because they hinder the movement of dislocations and reduce the resistance to propagation of cracks /27, 28/.

There is also a purely geometric theory which explains the influence of interstitial impurities which form solid solutions on the cold shortness of metals with a body-centered cubic lattice. According to this theory, the atoms of the interstitial impurities which occupy the octahedral or

tetrahedral interstices of the body-centered cubic lattice distort its cubic symmetry, and impart a tetragonal orientation in a certain crystallographic direction. This leads to a considerable increase in shear stresses during deformation, which creates favorable conditions for the nucleation and propagation of cracks.

Let us now discuss the influence of substitutional elements. Alloying of heat-resistant metals with substitutional elements usually leads to an increase in the ductile—brittle transition temperature, which is apparently due to the additional distortions of the crystal lattice which arise during alloying. The considerable decrease in the ductile—brittle transition temperature of heat-resistant metals deoxidized by small amounts of thermodynamically active elements, such as zirconium, titanium, lanthanum, cerium, yttrium, is apparently due to a refining and not to an alloying influence of these elements /12, 29, 30/. The appreciable increase in the ductile—brittle transition temperature caused by alloying heat-resistant metals (commercial grade) is a serious obstacle to the production of new alloys on the basis of the most heat-resistant metals. Modern molybdenum-base and tungsten-base alloys produced in vacuo are not true alloys, but deoxidized and modified metals (tungsten and molybdenum) of commercial purity.

This will continue until the heat-resistant basis metals of alloys (chromium, molybdenum, tungsten) can be prepared in a sufficiently pure state so that their strength can be increased by alloying that will lead to the formation of substitutional solid solutions of considerable concentration. This method has already been carried out during a study of titanium alloys. After methods for freeing of titanium from oxygen and hydrogen had been developed, the pure metal showed a ductility characteristic of all pure metals. It was thus possible to produce titanium-base constructional and heat-resistant alloys that according to their compositions could be classified as highly alloyed materials. Similar investigations have been carried out recently with niobium and its alloys. Niobium obtained by electron-beam vacuum melting can be alloyed with considerable amounts of other elements, and a minimum ductility necessary for shaping the material can be maintained. The ultimate strength of niobium can be increased by 500% by alloying /1/. The problem of producing highly alloyed materials with VIA group basis metals (chromium, molybdenum, tungsten) has not yet been solved. The only exception is alloying these metals with rhenium, and apparently with ruthenium and osmium also /11, 26/. The limit of cold shortness of chromium, molybdenum, and tungsten can be considerably lowered by alloying with rhenium. The decrease in the ductile—brittle transition temperature and increase in the ductility of molybdenum and tungsten alloyed with rhenium may be due to the redistribution of oxygen and the formation of complex oxides, which because of their high surface tension are distributed as globular particles along the grain boundaries and within the grains /31/, or to the process of twinning /11, 26, 32—35/. At the same time, some authors point out that twin crystals may form the sources of the nucleation of cracks, particularly in iron and in steel /5/. It would be interesting to clarify the influence of twin crystals on the cold shortness of metals with a body-centered cubic lattice. It should be pointed out that the mechanism of the influence of rhenium on the ductility of metals of the VIA group is not yet clear, although there are indications that the hexagonal metals of the VIIth

and VIIIth groups increase the ductility of metals of the VIA group /11, 24/. But at present rhenium is the only element which effectively reduces the ductile—brittle transition temperature of metals with a body-centered cubic lattice of commercial purity.

The rate of deformation greatly influences the ductility and resistance to deformation of heat-resistant metals /10/. An increase in the rate of deformation leads to an increase in the temperature of the cold shortness limit, and to a certain widening of the temperature range of the transitional zone. The behavior of the material during high deformation rates, comparable to the velocity of sound, is of great interest. We believe that there is no directly proportional relationship between the ductile—brittle transition temperature and the rate of deformation of the material, at very high deformation rates. The rapid deformation of metals or alloys is accompanied by a considerable thermal effect, and consequently by softening processes. It has been pointed out in /36, 37/ that the temperature—velocity factor during the deformation of metals and alloys must be taken into account. The heating caused by explosion deformations is associated not only with dynamical plastic deformation, but also with instantaneous elastic deformation of an all-sided compression /38/. In the field of very high deformation rates each metal or alloy has apparently a certain critical deformation rate and a corresponding maximum transition temperature. The decrease in the transition temperature is due to the thermal effect of deformation, the distinctive features of the stressed state, and the nature of the deformation process.

The environment usually exerts a considerable chemical influence on the behavior of metals and alloys during plastic deformation. This is particularly true in the case of heat-resistant metals of high chemical activity. The environment may dissolve the surface and boundary layers of the metal being deformed, may lead to corrosion of these layers, a change in the chemical composition of the substance due to adsorption, and facilitate or inhibit the process of deformation. The process of plastic deformation considerably increases the influence of the environment on the metal. Stresses usually accelerate corrosion, and the softening of the metal during deformation accelerates the penetration of gases. Corrosion, deterioration of the grain boundaries, and a change in the chemical composition under the influence of the corrosive environment, lead to such deep structural changes that plastic deformation is impossible because of the considerable embrittlement of the metal. These factors lead to the formation of the so-called zones of hot shortness /10/. It is thus necessary to reduce the temperature of deformation of heat-resistant metals and alloys, or to carry out the deformation in an inert environment or a protective atmosphere.

It should be pointed out that storage in the air even at ordinary temperatures leads to a selective absorption of gases from the atmosphere by the heat-resistant metal; for example, titanium absorbs hydrogen, chromium absorbs nitrogen, etc. These processes have not yet been sufficiently investigated.

As we have already mentioned, stresses are also one of the most important factors which determine the behavior of metals during deformation. The ductility of the metal increases with increase in the role of compressive stresses. The most detrimental for plastic deformation are tensile stresses acting on all sides, while the most favorable influence is exerted by nonuniform compressive stresses on all sides. A deformation induced by tensile stresses on all sides may lead to brittle failure of even highly ductile materials. On the other hand, nonuniform compressive stresses applied on all sides facilitate deformation, and it is possible to

shape heat-resistant metals, even commercially pure, and intermetallic compounds extruded through a die, which would show brittle failure under deformation /10/. The influence of stresses on the ductility of metals has been convincingly demonstrated by Kurnakov and Zhemchuzhny, and Karman in their well-known experiments with marble, red sandstone, and natural salts /39/. These brittle substances could be deformed if a side pressure was exerted. The ability to become deformed increased with increase in the side pressure /40/.

The beneficial influence of compressive stresses applied at all sides on the ductility of brittle materials, including heat-resistant metals, can be explained by the following physicochemical factors: 1) space compression prevents intercrystalline deformation, which rapidly leads to failure of the polycrystal and an increase in intracrystalline slip; 2) space compression makes the metal more dense and restores the intracrystalline and intercrystalline bonds which were impaired during plastic deformation; 3) these stresses completely or partially annul the negative influence of nonmetallic inclusions and of liquid phases. Nonmetallic inclusions are dangerous if the metal is subjected to tensile stresses. The compressive stresses crush the nonmetallic inclusions, which then cannot influence the ductility of the material; 4) compressive forces applied at all sides reduce the embrittling influence of tensile stresses, which are induced as a result of the nonuniform plastic deformation.

The dependence of the ductile—brittle transition temperature on the dimensional factor has not yet been sufficiently studied. The influence of this factor is closely connected to the influence of the structural factor and the surface finish.

The existing methods of combating cold shortness of heat-resistant metals can be classified into chemical and physical. Chemical methods include removal of interstitial impurities during the different stages of the preparation of pure metals, the deoxidation and modification of metals during vacuum melting, and the production of an optimum structure by alloying with substitutional elements. Some examples of a considerable increase in the ductility of heat-resistant metals achieved by completely removing interstitial impurities or by annulling their unfavorable influence by adding alloying elements which are more thermodynamically active than the basis metal are given below. It has been found /12/ that yttrium and other rare-earth metals which bind the nitrogen present in chromium into nitrides can appreciably increase the ductility of chromium as a result of their refining action. The heat of formation of yttrium nitride (72 kcal/mole) is almost three times greater than that of chromium nitride (25 kcal/mole).

The experimental studies carried out in the Laboratory of Heat-Resistant Alloys and Rare Metals of IMET AN SSSR /41/ and in other research institutes confirmed the effectiveness of this method. Trefilov et al. of the Institute of Metallophysics AN SSSR recently obtained highly ductile chromium by treating it with rare-earth metals /42/. The metal in the form of plates could be bent to an angle of 180° at room temperature. It has also been found that rare-earth metals have a favorable influence on the ductility of molybdenum. The deoxidation oi molybdenum by rare-earth metals reduces the temperatures of the ductile—brittle transition by about 300°C /43/. Molybdenum deoxidized by lanthanum boride could be further rolled at room temperature into 0.15 mm thick foil after preliminary forging and rolling at 700°C. The total deformation was 98% /30/. The increase in the ductiliy of molybdenum is due to the deoxidizing influence of lanthanum (heat of

formation of La_2O_3 is equal to 457 kcal/mole, and the heat of formation of MoO_2 to 120 kcal/mole).

Single crystals of molybdenum very carefully freed from interstitial impurities by electron-beam zone melting in vacuo are highly ductile (Figure 4) /11/. Metals of groups IVA and VA (titanium, zirconium, halfnium, vanadium, niobium, and tantalum) have a high degree of ductility at low temperatures, even as a result of electron-beam vacuum remelting, since they dissolve interstitial impurities over a wider range than metals of group VIA. It has recently been determined that most of the oxygen is removed from the metal in the form of lower oxides. The so-called Duplex process consists of electron-beam melting in the presence of an active deoxidizing agent that removes interstitial impurities, and of arc melting in the presence of a modifying agent to obtain a fine-grained structure. The method is very promising for the production of ductile metals of group VIA. A very promising method for combating the contamination of metals by carbon during the melting process is removal of the gases by chemically active substances (getters) such as zirconium, titanium, boron, different ion-exchange resins (for example zeolites, etc.), rather than degassing by a vacuum oil pump.

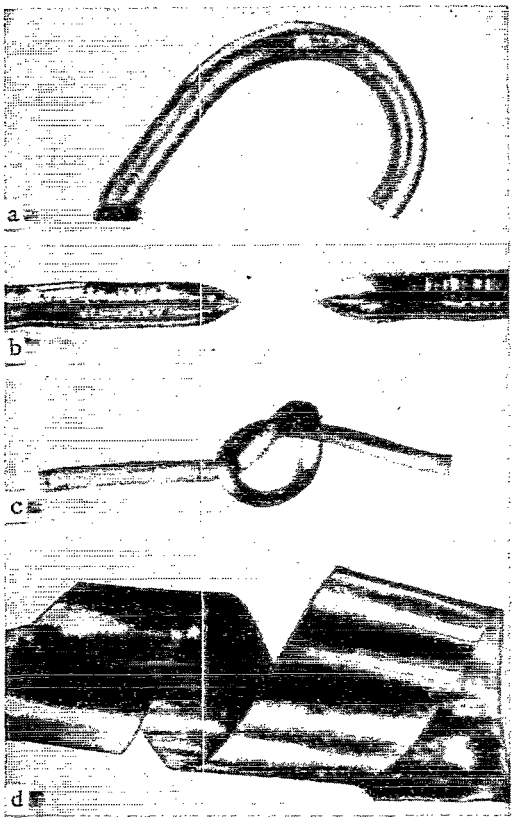

FIGURE 4. Highly ductile molybdenum produced by electron-beam zone melting:

a—single crystal, bent at room temperature; b—100% reduction in area by stretching; c—loop made of a 3 mm diameter wire obtained by rolling a single crystal; d—100 μ thick foil produced by cold rolling a single crystal of molybdenum.

The most interesting example of the efficiency of chemical methods in combating cold shortness of refractory metals is the considerable increase in the ductility of tungsten from which carbon has been removed (down to 0.001% C) by cyclic heat treatment in a medium containing a few hundredths of one percent of oxygen /44/.

Single crystals of tungsten obtained by electron-beam zone melting in vacuo from carbonless materials prepared by the above method were bent

to an angle of 180° in liquid nitrogen. Carbon forms heat-resistant carbides with tungsten, and is apparently the most harmful and tenacious impurity, since oxygen, nitrogen, and hydrogen, which with tungsten form easily dissociable low melting compounds, can be almost completely removed by evaporation during melting or when tungsten is heated in vacuo. The numerous inclusions of carbides hinder the movement of the dislocations, and also form the nuclei for the formation of microcracks. Therefore, the ductile—brittle transition temperature of tungsten is increased by hundreds of degrees /13/. The task of producing carbon-free tungsten and of maintaining its purity during service must be undertaken by the mutual efforts of chemists, metallurgists, technologists, and consumers. Our article has also shown that to obtain ductile refractory metals, special efforts must be made, starting from the preparation of ores and during all the chemical, metallurgical, and technological processes.

We have already mentioned that the ductility of tungsten and molybdenum can be improved if these metals are alloyed with rhenium. This is also true if chromium is alloyed with hexagonal ruthenium.

The physical methods of combating cold shortness of refractory metals include the application of nonuniform compressive stress at all sides of the article during its plastic deformation (extrusion), and the preparation of the best texture, and the optimum dislocation structure, and structure of subgrains, by thermomechanical processes and by cold working. This can also be achieved by treatment in an ultrasonic field, by freeing the metal from dissolved gases, by plastic deformation in vacuo, etc. It should be pointed out that until recently, the most widely used of these methods has been cold working below the recrystallization point. Today, refractory metals are extruded using all-sided nonuniform pressures and also a counter pressure. Thermomechanical methods of increasing ductility of refractory metals are now being developed. We can only give suggestions on the purity of metals, grain size, grain boundaries, necessary for the structure of deformation, but we are not able to recommend the best fine structure or the methods by which it can be achieved.

The above examples of increasing ductility of refractory metals are an example of the efficiency of the physicochemical approach to the problem of cold shortness.

Certain successes have been achieved in solving the problem of cold shortness of refractory metals. But the final solution requires a great deal of work by scientists and industrial engineers. Because of the considerable susceptibility of refractory metals and alloys to interstitial impurities, the production and treatment of these materials require highly developed technical and industrial skill. We should like to point out again that the brittleness of refractory metals must be avoided during the whole production cycle, and therefore all the available techniques of chemical technology for the production of pure substances, of vacuum metallurgy, and of heat-treatment must be used to attain and keep the required purity of the metal.

It is important not only to produce a pure refractory metal or alloy with a low ductile—brittle transition temperature, but also to maintain the necessary purity during later treatment and service of the article /45/.

Today, we should revise the theoretical and experimental data, the studies carried out by different institutes should be coordinated, and a permanent commission set up to deal with this problem.

Bibliography

1. Savitskii, E.M., G.S.Burkhanov, and Ch.V.Kopetskii. — Izvestiya AN SSSR, Metallurgiya i Gornoe Delo, No. 6. 1963.
2. Kieffer, R. and H.Braun. Vanadin—Niob—Tantal. Die Metallurgie der reinen Metalle und Ihrer Legierungen.—Berlin (Göttingen), Springer Verlag. 1963.
3. Levinstein, M.A.—Refractory Metals and Alloys, 11:269, Chicago, Illinois, New York—London, April 12—13. 1962.
4. Metal Progress, p. 83, May. 1964.
5. Davidenkov, N.N. and G.N.Chuchman. Sbornik—Issledovaniya po zharoprochnym Splavam (Collection—Investigation of Refractory Alloys).—Izdatel'stvo AN SSSR. 1959.
6. Davidenkov, N.N. Sbornik—Issledovaniya po zharoprochnym splavam (Collection—Investigation of Refractory Alloys).—Izdatel'stvo AN SSSR. 1959.
7. Ivanova, V.S. and R.I.Ragozin.—Neorganicheskie Materialy, No.11. 1965.
8. Oding, I.A. Teoriya dislokatsii v metallakh i ee primenenie (Theory of Dislocations in Metals and its Application).—Izdatel'stvo AN SSSR. 1959.
9. Sbornik —Fizicheskaya priroda khrupkogo razrusheniya metallov (Collection—Physical Nature of the Brittle Failure of Metals). Kiev. 1965.
10. Savitskii, E.M. Vliyanie temperatury na mekhanicheskie svoistva metallov i splavov (Influence of Temperature on the Mechanical Properties of Metals and Alloys).—Izdatel'stvo AN SSSR. 1957.
11. Savitskii, E.M.—Izvestiya AN SSSR, Metally, No. 5. 1965.
12. Savitskii, E.M.—Izvestiya AN SSSR, Metallurgiya i Toplivo, No. 5. 1960.
13. Savitskii, E.M. and G.L.Tsarev.—Izvestiya AN Belorusskoi SSR, No. 2. 1965.
14. Hahn, G.T., R.I.Gilbert, and R.I.Jaffee. Effects of Solutes on the Ductile—Brittle Transition in Refractory Metals.—Proceedings of the Symposium on Refractory Metals, Chicago, April 15. 1962.
15. Lomonosov, M.V. Polnoe sobranie sochinenii (Complete Works), 1.—Izdatel'stvo AN SSSR. 1950.
16. Ageev, N.V. Priroda khimicheskoi svyazi v metallicheskikh splavakh (Nature of Chemical Bonds in Metal Alloys).—Izdatel'stvo AN SSSR. 1947.
17. Korsunskii, M.I. and Ya.E.Genkin.—Izvestiya AN SSSR, Seriya Fizicheskaya, 28, No. 5. 1964.
18. Sbornik— Sverkhchistye metally Metallurgiya (Collection—Super-Pure Metallurgy). 1966.
19. Zimon, J.M. Principles of the Theory of Solids. [Russian translation. 1966.]
20. Sbornik—Elektronnaya struktura perekhodnykh metallov i khimiya ikh splavov. Metallurgiya (Collection—Electronic Structure of Transitional Metals and the Chemistry of Their Alloys. Metallurgy). 1966.

21. Hahn, G.T. and R.I.Jaffee. Ekspress-informatsiya (Rapid Information).—Metallovedenie i Termoobrabotka, No. 4. 1965.
22. Shvetsova, E.M.—Zavodskaya Laboratoriya, **4**, No. 6. 1935.
23. Pogodin—Alekseev, G.I. Svoistva metallov pri udarnom nagruzhenii (Properties of Metals under Impact Loading).—Metallurgizdat. 1953.
24. Jaffee, R.I.—J. Metals, May. 1964.
25. Savitskii E.M. and G.E.Chuprikov. Sbornik—Renii (Collection—Rhenium).—Izdatel'stvo Nauka. 1964.
26. Savitskii, E.M. Redkie metally i splavy (Rare Metals and Alloys).—Moskva, Izd. Doma tekhniki. 1959.
27. Cottrell, A.H. Dislocations and Plastic Flow in Crystals. [Russian translation. 1958.]
28. Cottrell, A.H. and B.A.Bilby.—Proc. Roy. Soc., **62A**:49. 1949.
29. Savitskii, E.M.—Metallovedenie i termoobrabotka metallov, No. 9. 1961.
30. Savitskii, E.M., V.V.Baron, Yu.V.Efimov, and V.A.Frolov. Voprosy teorii i primeneniya redkozemel'nykh metallov (Problems of the Theory and Application of Rare-Earth Metals).—Izdatel'stvo Nauka. 1964.
31. Jaffee, R.I., D.J.Meikat, and R.U.Douglas. Rhenium and Refractory Metals of the Platinum Group. [Russian translation.]
32. Savitskii, E.M. and T'ao Tsu-ts'ung.—Fizika Metallov i Metallovedeniya, **14**, No. 1. 1962.
33. Savitskii, E.M., M.A.Tylkina, and K.B.Povarova. Splavy reniya (Rhenium Alloys).—Izdatel'stvo AN SSSR. 1965.
34. Savitskii, E.M., M.A.Tylkina, and K.B.Povarova.—Doklady AN SSSR, **119**, No. 2. 1958.
35. Savitskii, E.M., K.B.Povarova, and M.A.Tylkina.—ZhNKh, **5**. 1960.
36. Gubkin, S.I. Teoriya obrabotki metallov davleniem (Theory of Treating Metals by Pressure).—Metallurgizdat. 1947.
37. Gubkin, S.I. and E.M.Savitskii.—Izvestiya Sektora Fiziko-Khimicheskogo Analiza, **14**. 1946.
38. Atroshchenko, E.S., P.O.Pashkov, and I.M.Rodinskaya.—Fizika Metallov i Metallovedeniya, **19**, No. 4. 1965.
39. Kurnakov, N.S.—Izbrannye Trudy, I and II, Izdatel'stvo AN SSSR. 1960 and 1961.
40. Gubkin, S.I. Plasticheskaya deformatsiya metallov (Plastic Deformation of Metals). **2**.—Moskva, Metallurgizdat. 1960.
41. Savitskii, E.M., V.F.Terekhova, I.V.Burov, I.A.Markova, O.P.Naumkin. Splavy redkozemel'nykh metallov (Alloys of Rare-Earth Metals).—Izdatel'stvo AN SSSR. 1962.
42. Sbornik nauchnykh trudov (Collection of Scientific Works). No. 20.—Institut Metallofiziki AN USSR, Kiev. 1964.
43. Savitskii, E.M., V.V.Baron, Tao Tsu-ts'ung.—Izvestiya AN SSSR, OTN, Metallurgiya i Toplivo, No. 1. 1962.
44. Savitskii, E.M. and G.L.Tsarev. Sbornik—Rost Kristallov (Collection—Growth of Crystals).—Kiev, Izdatel'stvo Naukova Dumka. 1966.
45. Savitskii, E.M. and G.S.Burkhanov. Metallovedenie tugoplavkikh metallov i splavov (Metallurgy of Refractory Metals and Alloys).—Izdatel'stvo Nauka. 1967.

V. S. Ivanova, I. M. Kop'ev, and Yu. P. Liberov

THE SUSCEPTIBILITY OF REFRACTORY METALS TO BRITTLENESS AND CREEP

The interest in refractory metals as promising constructional materials has greatly increased recently. Studies on the behavior of these materials under load, especially the brittleness, have increased.

As we shall show later, the brittleness of metals of the VIA group is closely connected with their high creep at low and medium temperatures. Since these phenomena are interconnected, they should be discussed together. The problem of creep of refractory metals at low temperatures has arisen only recently, and therefore time is needed to discover the principle of the processes which give rise to creep of refractory metals at low and medium temperatures.

It has been found that in transition metals, especially in metals of the VIA group (tungsten molybdenum, chromium), the interatomic bonds can be considered as a superimposition of an ordinary metallic bond on a covalent bond /1, 2, and others/. Hence, it follows that we should expect strong anisotropy of ductility, since the covalent bonds can exert a great resistance to the motion of dislocations in certain directions. This means that effective natural dislocation barriers such as the Peierls-Nabarro forces exist in metals of the VIA group, and that these barriers can only be overcome by a sufficient amount of thermal energy and time. In addition to the frictional forces, the behavior of dislocations under stress is also greatly influenced by their own properties. The considerable stacking faults of the metals of the VIA group make the splitting of dislocations energetically difficult. According to Pavlov /3/, the stacking fault energy of molybdenum, tungsten, and chromium is close to 300 erg/cm^2, which should lead to a considerable interaction of the dislocations and interstitial impurities. The velocity of dislocations is a very important dynamic property. In general, the velocity of a single dislocation in a lattice at a given rate of deformation depends on the time t_1 during which the dislocation is present in the potential well, and on the time t_2 during which it travels a distance equal to the Burgers vector ($t_1 \gg t_2$). Other conditions being equal, the time increases with increase in the energy of a single dislocation and in the potential barrier which has to be overcome.

Since the Peierls forces in metals of the VIA group are rather strong, the acceleration of the formation of dislocations per unit time will be low, that is the retardation will be high /4/. These phenomena should also be facilitated by the high energies of dislocation. The table gives the approximate values of the elastic energy of dislocations of different metals (calculated from Gb^2 or Gb^3), and indicates that tungsten and molybdenum have the highest energy of dislocations. Thus, the elastic energy of dislocations of tungsten is more than 4 times higher than that of aluminum and magnesium. At the same time the energy of dislocations of chromium is close to that of iron.

All factors which reduce the acceleration of formation of dislocations per unit time and increase the retardation of creep facilitate the development of brittleness. On the other hand, the same factors should also increase the ability of metals to store excess elastic energy at high deformation rates. The value of this excess energy can be found from the acceleration

of the increase in the elastic limit with increase in the rate of deformation. It is clear that the more a given metal is able to store excess elastic energy, the greater will be the tendency of this metal to creep at low and medium temperatures, since if a constant stress is applied the excess stored elastic energy can be used to develop plastic deformation. Therefore, since because of their structure the metals of the VIA group should have a high ability to store excess elastic energy, the following effects should accompany the deformation of these metals:

1) an anomalously high creep rate over the temperature range of brittleness, and an intense development of the processes of relaxation at these temperatures;

2) a high tendency to creep at temperatures considerably below 0.5 T_{mp};

3) a high ductility at low rates of deformation, comparable to the rates of creep.

The tendency of refractory metals (tungsten, molybdenum and chromium) to creep over the temperature range of brittleness was predicted in /5/.

Fracture energy and energy of dislocations of pure metals at room temperature

Type of lattice	A_f, kgm/cm^3	$Gb^3 \cdot 10^9$, kg	$Cb^2 \cdot 10^{16}$, kg mm	$Cb^2 \cdot 10^{16}$, ev	$\rho_{crit} = \frac{A_f}{Gb^2}$, 1/cm$^2 \cdot 10^{13}$	Type of lattice	A_f, kgm/cm^3	$Gb^3 \cdot 10^9$, kg	$Gb^2 \cdot 10^{16}$, kg mm	$Gb^2 \cdot 10^{16}$, ev	$\rho_{crit} = \frac{A_f}{Gb^2}$, 1/cm$^2 \cdot 10^{13}$
BCC	320	1.13	3.1	19.0	3	FCC	198	0.47	1.16	7.1	4
	253	0.90	2.46	15	3		115	0.30	0.77	4.70	4
	170.0	0.57	1.62	9.9	3		62.3	0.22	0.64	3.9	3
	136	0.45	1.13	6.7	3	HCP	102	0.33	0.95	5.8	3
	156	0.52	1.28	7.8	3		28.9	0.18	0.57	3.5	2

The above characteristic behavior of metals of the VIA group has been investigated by special experiments which we shall discuss below.

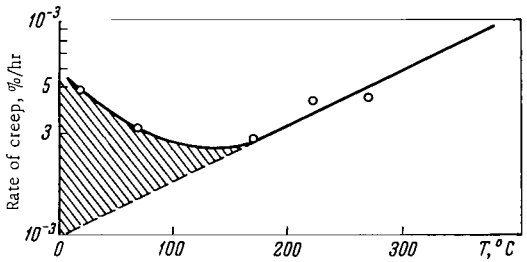

FIGURE 1. Dependence of the creep rate on temperature for TsM-2 molybdenum produced by vacuum melting (according to data of long-time hardness tests).

The behavior mentioned in 1) is confirmed by the data of Figure 1. These data were obtained from a study on the time-dependence of the hardness of TsM-2 molybdenum obtained by vacuum melting.

The creep rate was calculated by the Osipov—Tieh-ch'êng /6/. The hatched area represents a temperature range of 20—170°C over which

there is an anomalous relationship between the creep rate and the temperature. At 20°C the creep rate is about twice that at 170°C. The decrease in the creep rate with increase in temperature can be explained by a decrease in the ability of the metal to store the excess elastic energy at higher temperatures.

The above assumption is again confirmed by the data in Figure 2 on the relaxation of stresses during tensile tests. The tests were carried out on a ZM-4 machine using molybdenum wire (M4) with $\sigma_в = 220\,kg/mm^2$. It is obvious that the intense relaxation of stresses takes place at $\sigma_0 = 0.5\sigma_в$, and the decrease in stresses during 90 min is about $17\,kg/mm^2$, i.e., about 20%. This is a very high rate of relaxation of stresses (considerably higher than for nickel or iron) which indicates that the processes of creep at room temperature are very effective. We think that these results are also of practical interest, since they indicate a low relaxation stability of commercial molybdenum even at room temperature. It is possible that at low temperatures the tendency of molybdenum to creep and to relaxation will be even higher.

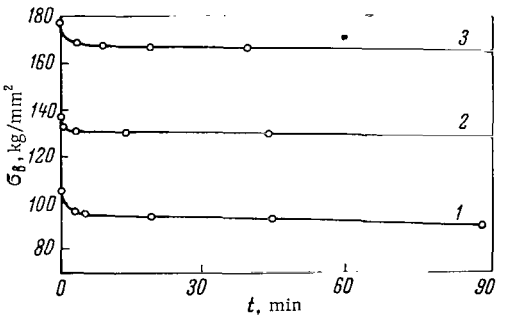

FIGURE 2. Relaxation curves of molybdenum wire recorded during tensile tests on molybdenum wire (M4) with a diameter of 100μ:

1— $\sigma_0 = 105\,kg/mm^2$; 2—138; 3—178.

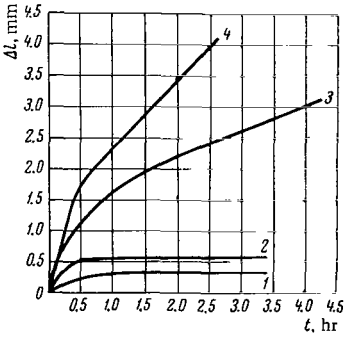

FIGURE 3. Creep curves of 0.1 mm tungsten wire:

1—temperature 20°C; 2—350°C; 3—415°C; 4—450°C, $\sigma = 150\,kg/mm^2$.

The experiments which we carried out with tungsten (group VIA) also indicate a high creep at low temperatures. This has been confirmed by the data on Figure 3. After 3 hr of testing at 450°C the elongation of a 250 mm long wire specimen was about 0.8%, which indicates a very high creep rate.

The high tendency of tungsten to creep at low temperatures is directly confirmed by the data of Bechtold /7/ on the influence of the rate of deformation on the ductility of tungsten. An increase in the rate of deformation at 250°C from $9.8 \cdot 10^{-3}$ to $9.8 \cdot 10^{-8}\,sec^{-1}$ increases the ductility to 50% with almost no macroscopic deformation at ordinary deformation rates ($9.8 \cdot 10^{-3}\,sec^{-1}$). The above data indicate that despite their tendency to brittle failure tungsten and molybdenum, and apparently also chromium, have a high tendency to creep and to a relaxation of stresses over the temperature range of brittleness or at low temperatures.

This analysis indicates that the metals of the VIA group should be inherently more sensitive to the rate of deformation than other metals with a body-centered cubic lattice. For these metals it is therefore necessary to develop principles of alloying and methods of thermoplastic treatment different than those for metals with a body-centered cubic and a face-centered cubic lattice.

To obtain a complete picture of the influence of different factors on the deformation and failure of metals of the VIA group, we should like to discuss an analysis of the dislocation energy, and to consider together the behavior of dislocations and the specific energy needed for plastic deformation and for failure of metals.

Plastic deformation is accompanied by a strengthening and a softening of the metal. From the point of view of the theory of dislocations, strengthening is the hindering of dislocations in the metals, since this leads to an increase in the flow stresses, while softening is a shift of dislocations to the surface, since in this case a "stepped" failure takes place.

Since the deformation of actual metals leads to a shifting of dislocations to the surface and hindering of dislocations at the obstacles, plastic deformation is clearly accompanied by a strengthening of some and a softening of other volumes of the metal.

Failure takes place at the moment when the volume of a metal which leads to failure absorbs a maximum energy A_f, determined by the binding forces of a given metal /7, 8/. According to the above, the specific energy determined by A_f consists of the strengthening energy A_{st}, fixed by the dislocations and other defects retained in the metal, and the fracture energy fixed by the dislocations and other defects formed during deformation which have shifted to the surface, i.e.,

$$A_f = A_{st} + A_{surf}, \tag{1}$$

where the specific energy A_{st} is used for the formation and a development of brittle cracks as a result of the concentration of a critical number of dislocations, while A_{surf} is the energy used for the formation and development of ductile cracks as a result of the shifting of a critical number of dislocations to the surface at a given slip plane.

Thus,

$$A_f = A_{bc} + A_{dc}. \tag{2}$$

It has been shown earlier that the magnitude A_f can be determined experimentally or calculated as before /5/ from the data on the thermodynamic constants.

The data on the fracture energy (A_f) determined as

$$A_f = L_{den} - \int_0^{T_x} C_p dT. \tag{3}$$

are given in the table.

Here $\int_0^{T_x} C_p dT$ determines the heat content of a metal at a given temperature or the energy of the thermal vibrations of the atoms (C_p is the heat capacity, T_x is the given temperature).

An analysis of this equation is given in /5/.

The data in the table indicate that with increase in the fracture energy the energy of dislocations increases. The specific energy stored in metals consists mainly of the energy of single dislocations, vacancies, and interstitial atoms, the energy of reaction between the dislocations and between dislocations and intersititial atoms, and also the stacking fault energy.

However, the share of dislocations in the stored energy is highest. Therefore, to a certain approximation, if we assume that the total energy A_f is associated with the dislocations either in the interior of the metal or shifted to the surface, it is also possible to calculate the maximum density of dislocations formed in a metal during deformation from the formula

$$\rho_{crit} \cong A_f/Gb^2.$$

The table also indicates that different metals have different values of A_f and of dislocation energies. However, in all metals A_f is equivalent to the energy necessary for the formation of the same density of individual dislocations ($10^{13} \cdot cm^{-2}$). The energy of the interaction of dislocations can be different, depending on whether the dislocations remain in the metal or are shifted to the free surface during deformation. For this reason, and also due to the presence and interaction of other defects, the real magnitude of ρ_{crit} decreases.

The strength of a given metal, its ductility, and also the type of failure depend on the relationship between the fractions of specific energy used for the formation and development of brittle and of ductile cracks (the relationship between the dislocations which remain in the metal and those shifted to the surface). This is determined by the conditions of deformation and the structure of the metal.

We propose the following energy diagram for ductile and brittle failure as a function of the rate of deformation (Figure 4). The continuous line in Figure 4 represents the dependence of the energy of strengthening, which is a function of the number of dislocations remaining in the metal and of their interaction with one another and with impurity atoms, on the rate of deformation. The ordinates above this curve represent the fraction of specific energy consumed for the formation and development of ductile cracks (A_{dc}) and those below the fraction of the specific energy used up for the development of brittle cracks at a given rate of deformation (A_{bc}). The total fracture energy is $A_f = A_{dc} + A_{bc} = \text{const}$.

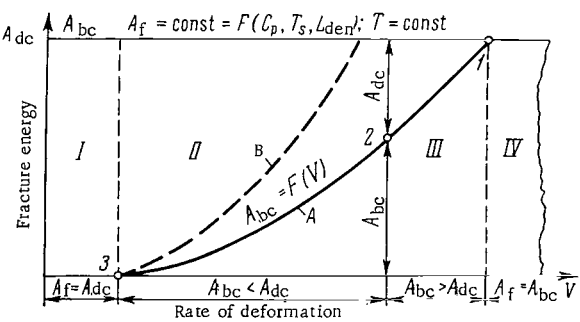

FIGURE 4. Energetic diagram of brittle and ductile failure.

The increase in $A_{bc} = F(V)$ is limited by the maximum energy A_f, which depends on the binding forces. This curve shows three critical points.

Point 1 is the intersection of the curve $A_{bc} = F(V)$ with the straight line A_f = const. At $V = V_1$ the failure is purely brittle, since $A_f = A_{bc}$, and $A_{dc} = 0$. A further increase in the rate of deformation is not expected to have any influence on the mechanical properties of the materials, and the failure will take place when the breaking stress is reached.

Point 2 is a point corresponding to the rate of deformation at which A_{bc} is equal to A_{dc}, i.e., this failure is both brittle and ductile. The area between the ordinates of points 1 and 2 is an area of a brittle—ductile failure in which brittle failure predominates.

Point 3 corresponds to a rate at which $A_f = A_{dc}$; $A_{bc} = 0$, i.e., at these rates and below no brittle cracks are formed, which means no dislocations of critical density are formed, and the failure is due to the formation of ductile cracks as a result of the shifting of a critical number of dislocations to the surface.

The area between the ordinates of points 2 and 3 is an area of ductile—brittle failure in which ductile failure predominates.

This diagram shows that with increase in the ability of a metal to hinder dislocations, the relationship $A_{bc} = F(V)$ becomes more marked, and the tendency of the metal to brittle failure under dynamic loads and to creep over the temperature range of brittleness increases.

As we have already mentioned, as a result of their inherent dislocation barriers and also because of the high energy content of individual dislocations, metals of the VIA group should have a higher tendency to hinder dislocations than other metals with a body-centered cubic or face-centered cubic lattice, and consequently the $A_{bc} = F(V)$ relationship should be more marked for these metals.

The above diagram also explains the high sensitivity of tungsten, molybdenum, and chromium to impurities. If the metal has strongly blocked dislocations the hindering of new dislocations formed during deformation is even more effective, i.e., other conditions being equal the relationship $A_{bc} = F(V)$ for metals containing interstitial impurities should be more marked than for pure metals, and the curve representing this relationship is located higher (dashed curve). This means that the susceptibility of metals with interstitial impurities to brittle failure increases, i.e., brittle failure takes place at lower rates of deformation, or the ductile—brittle transition during impact tests is shifted toward higher temperatures.

CONCLUSIONS

The following conditions are necessary to reduce the tendency of metals of the VIA group to creep in the range of brittleness.

1. Special principles of alloying these metals should be developed to reduce the Peierls forces, the stacking fault energy, and the energy of individual dislocations, i.e., alloying should not lead to a strengthening of the metal, as in other cases, but to a certain softening. Such alloying should also decrease the tendency of the metal to brittle failure.

2. The content of interstitial impurities should be reduced by high purification or by alloying.

3. Special methods of thermoplastic treatment should be developed to produce a structure which will not hinder dislocations (as in the strengthening of other metals), but will facilitate their shift to the surface, i.e., lead to a decrease in the internal and external barriers and to an increase in the number of centers through which dislocations can be shifted.

Bibliography

1. Goodenough, J.B.—Phys. Rev., 126, No. 6. 1962.
2. Trefilov, V.I. Sbornik—Fizicheskaya priroda khrupkogo razrusheniya metallov (Collection—Physical Nature of Brittle Failure of Metals). p. 22, Kiev, Izdatel'stvo Naukova Dumka. 1965.
3. Pavlov, V.A.—Fizika Metallov i Metallovedeniya. 21, No. 2. 1966.
4. Ivanova, V.S., L.K.Kondienko, V.N.Geminov, et al. Sbornik—Rol' dislokatsii v uprochnenii i razrushenii metallov (Collection—Role of Dislocations in the Strengthening and Failure of Metals).—Izdatel'stvo Nauka. 1965.
5. Ivanova, V.S. and Yu.I.Ragozin.—Neorganicheskie materialy (Inorganic Materials), 1, No.10. 1965.
6. Osipov, K.A. and T'ien-Tieh-ch'êng.—Izvestiya AN SSSR, OTN, Metallurgiya i Toplivo, 4. 1959.
7. Bechtold, J.N.—Trans AIME, 206. 1956.

M.P. Matveeva and V.A. Morozov

STUDY OF CREEP OF CAST AND WROUGHT CHROMIUM IN VACUO

Chromium-base alloys have recently been developed for service at temperatures above 1000°C. The plastic deformation of chromium above 1000°C and the mechanism of the deformation of chromium at temperatures above 0.5 T_{mp} have been little investigated, especially under conditions of variable factors such as stresses, temperatures, and environment. The development of plastic deformation and failure at temperatures of 0.5—0.75 T_{mp} are influenced chiefly by heat-activated processes. Therefore, it is of great interest to study the development of the deformations under conditions of creep at these temperatures. When the heat-activated processes predominate, we can expect: 1) a relatively close relationship between the temperature and the creep rate; and 2) the absence of any dislocation—slip deformation. However, at temperatures above 1000°C chromium has a high tendency to volatilize, which facilitates the shift of dislocations to the surface. At temperatures above 0.5 T_{mp} conditions can be created for a dislocation—slip process, and as a result the resistance to plastic deformation can be greatly reduced. From this point of view it is probable that materials which are more susceptible to vaporization under conditions of constant stress will have a higher resistance to creep.

The purpose of this study is to investigate the process of creep in cast and wrought chromium. We studied the variation in density of the specimens, their electric resistivity, and their microstructure. The activation energy for creep was studied by creep test methods based on monoaxial tensile tests, and on twisting by different forces in vacuo at temperatures of $0.525-0.74\,T_{mp}$. The cast specimens were prepared from twice-refined electrolytic chromium of 99.9% purity, and the wrought specimens of pressed chromium rods. The billet for cast specimens was obtained by melting chromium suspended in an atmosphere of dry, purified helium. The molten metal was poured in the same atmosphere into copper molds 6 mm in diameter and 50 mm long /1/.

Both the cast and wrought specimens were prepared by machining. The working surface was ground by emery paper. The specimens were not electropolished to avoid contaminating their surfaces. The tensile test specimens were 15 mm long and 2.5 mm in diameter, and the torsion test specimens 15 mm long and 3 mm in diameter.

The creep tests were carried out on a VPR-1 machine designed and built in the laboratory. The specimens were heated in a vacuum chamber by a molybdenum heater consisting of two thin molybdenum cylinders connected by a molybdenum ring (vacuum up to $1\cdot10^{-5}$ mm Hg). The stress applied to the specimen was maintained constant by a cam gear. The elongation of the specimen under a constant load was measured by an indicator. The temperature was recorded and maintained constant by an automatic electronic potentiometer of the EPD type with a platinum—platinum—rhodium thermocouple, with its hot end attached to the surface of the specimen.

Over the temperature range mentioned above the creep curves were recorded at constant temperatures and at constant stresses of 2.56 kg/mm^2. Creep was measured not only by tensile tests but also by torsion on the IMET-4K machine /2/ under different stresses and at different temperatures, and at a pressure of $1\cdot10^{-5}$ mm Hg. The tests were carried out by recording creep curves at constant temperatures and also by the temperature—cyclic stress method, i.e., under conditions when the creep rate was recorded continuously under the action of a constant torsion moment but at a gradually changing temperature.

Before the specimens were tested they were annealed at 1200°C for 1 hr. Because of the large number of defects in chromium the specimens were selected according to their density and their electric resistivity. The density of the specimens was measured by the method of hydrostatic weighing of specimens in the air and in distilled water, and the electric resistivity at room temperature by the compensation method using a double resistor bridge.

All stages of the creep process were studied under the microscope. After the load was removed the specimens were cooled, and taken from the machine. Then microsections were prepared from longitudinal strips and electrolytically etched in a 10% solution of oxalic acid at a current density of 0.7 amp/cm^2. The test and the volatilization were carried out in a nonoxidizing atmosphere so that the microstructure directly on the surface of the specially prepared specimens could be investigated. A small dent about 1 mm wide was made along the generatrix of the cylinder, and its surface was prepared in the same way as for the microsections.

Experimental data on the creep rate of chromium plotted in the ordinates of logarithm of creep rate versus reciprocal of temperature are shown in Figure 1. The data are the average values of the creep rate of cast specimens, since despite the selection the scattering of the experimental data is quite high (about 1 order of magnitude). No such scattering was encountered in wrought specimens. Almost all points lie on a straight line which represents a $\log V = f(1/T)$ function. Over the temperature range investigated the creep rate is greatly influenced by temperature. An increase in temperature of 100°C leads to an increase in the creep rate of one order of magnitude. The creep rate during torsion at T = const can be found from the formula $V = A\tau^{\alpha}$, where V is the creep rate, A is a constant, τ is the torsional stress, α is an exponent which depends on the mechanism of creep of a given material. The activation energies given in the table were calculated from experimental data. The activation energy of creep decreases with increase in stress.

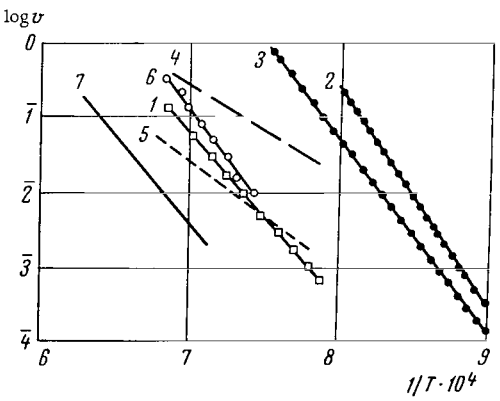

FIGURE 1. Dependence of the creep rate of chromium on temperature:

a—investigation by the temperature-cyclic method of torsion at $\tau = 2.05$ kg/mm^2; 1—wrought; 2—cast; 3—cast; b—at a constant temperature; 4—cast, torsion, $\tau = 2.05$ kg/mm^2; 5—the same, $\tau = 4.39$ kg/mm^2; 6—wrought by stretching, $\sigma = 2.56$ kg/mm^2; 7—cast, stretched, $\sigma = 2.56$ kg/mm^2.

The activation energies of tensile and torsional tests were very similar, although the activation energy of torsion found from the creep curves at T = const is only about half that calculated from the data of the temperature-cyclic stress method. This phenomenon has not yet been clarified, but it is quite possible that it is due to the specific influence of the structure and of the defects in the surface layers during torsion tests.

The loss of metal due to its volatilization from the working surface of stressed chromium was determined by weighing the specimens before and after the test. Cast chromium specimens had a polished surface and the experiments were carried out over a temperature range of 1150—1311°C. Specimens covered by an oxide film were tested at 1112—1290°C. The

oxide film was formed by first heating the specimens to 1200°C in the atmosphere. Wrought specimens with a polished surface were also tested at 1050—1205°C. It was found that the surface finish and the structure of the chromium specimens directly influenced the rate of volatilization. Thus, cast chromium specimens covered by an oxide film had a lower rate of volatilization than uncoated specimens. Wrought chromium specimens showed higher weight losses due to volatilization than cast specimens (Figure 2). The oxide films covering chromium specimens affect the evaporation process only. No conclusions on the influence of the oxide film on the creep rate of cast could be drawn because of the great scattering of the experimental data. Microstructural studies on the surface of the specimens confirmed the conclusion that volatilization effectively facilitates the shift of dislocations to the surface. The structures of chromium specimens during different stages of creep tests are shown in Figure 3.

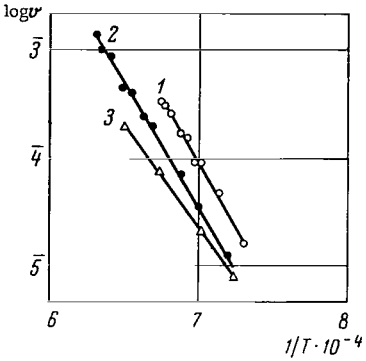

FIGURE 2. Dependence of the volatilization of chromium on temperature found by the weight loss method:

1—wrought; 2—cast; 3—cast with oxide film.

The photographs shown in Figure 3 indicate that beside symptoms characteristic of heat-activated processes (migration of boundaries, recrystallization at the grain boundaries, etc.) symptoms of the dislocation-slip mechanism of plastic deformations can also be found.

During the first stage of creep the stresses lead to grain rotation, fragmentation of the structure, and development of polygonization /4/. The dislocations become ordered into walls which form a substructure. Characteristic lines are also formed (Figure 3,c). However, the damage and the defects cannot be noticed under a microscope.

Activation energies calculated from experimental data

Method of testing	Starting material	Temperature range, °C	Stresses, kg/mm²	Activation energy, kcal/g-atom
		Torsional tests		
Temperature-cyclic stress	Cast chromium	1080—1300	2.05	117
The same	Wrought	1000—1208	2.05	107.8
" "	Cast	840—1000	4.39	91.8
" "	"	840—1070	4.39	94.8
Standard	"	1000—1200	2.05	65
"	"	950—1100	4.39	56.8
		Tensile tests		
"	Wrought	1050—1205	2.56	128
"	Cast	1150—1311	2.56	113

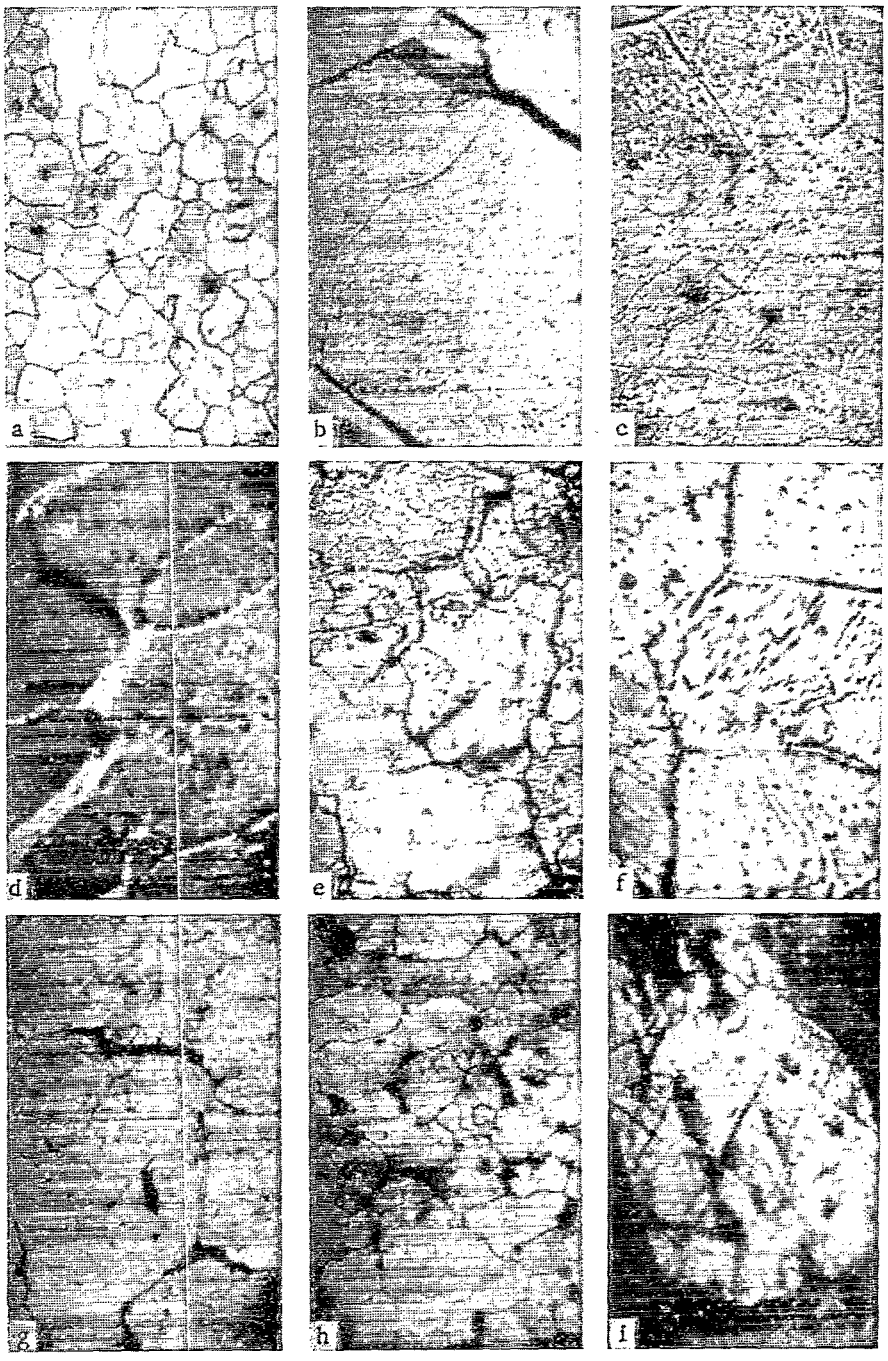

FIGURE 3. Microstructure of chromium during creep:

a—wrought (initial material), ×115; b—end of first stage of creep, ×500; c—second stage of creep, ×1000; d—the same, ×450; e—the same, ×450; f—the same, ×1000; g—third stage of creep, ×450; h—the same, ×115; i—the same, ×500.

During the second stage of creep characterized by processes of strengthening and recovery, we can distinctly see mosaic blocks (Figure 3, d). During this stage polygonization and the formation of a substructure take place. On the microsection where the microstructure has been revealed by vacuum etching (Figure 3, e, f) we can see how sinuous the grain boundaries have become. On certain areas the migration of boundaries, slip bands and the formation of blocks can also be noticed. The shift of dislocations to the surface is also visible on certain grains (Figure 3, f). The deformation of the boundary zones indicates slipping of grains in relation to one another. It is also possible to distinguish individual pores, which however become annealed during the second stage. A moment is reached when annealing lags behind deformation, which means that a combination of dislocations and excess vacancies occurs in the weakened zones. Stable pores (Figure 3, g) which are lengthened and widened by the acting stresses begin to appear along the grain boundaries. This leads to considerable weakening of the material and the beginning of failure. The surface of a specimen near failure is shown in Figure 3, h. Slip lines in two (Figure 3, i) intersecting systems and the formation of planes along the boundaries are visible.

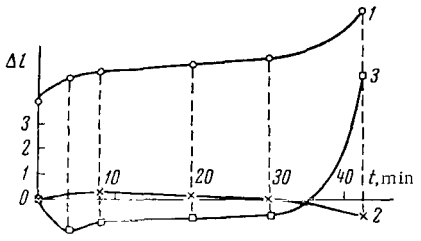

FIGURE 4. Variation in density and electric resistivity of wrought chromium during creep at 1200°C and at $\sigma = 2.56\ kg/mm^2$:

1—elongation of specimen; 2—density $\Delta d/d \cdot 100\%$; 3—electric resistivity, $\Delta\rho/\rho \cdot 100\%$.

The data of the microstructural analysis agree well with those on the density and electric resistivity of the materials.

It should be pointed out that the electric resistivity (which reflects the structure of the metal) changes in the same way as in other metals tested at lower temperatures, i.e., at temperatures at which the dislocation—slip mechanism of deformation is predominant /3/.

The variation in the density and electric resistivity of wrought chromium specimens during creep tests is shown in Figure 4. During the first stage of creep the electric resistivity decreases, reaches a certain minimum, and then smoothly increases to a certain value corresponding to the beginning of the second stage of creep. The density of the material increases slightly during this stage. Since several processes are taking place simultaneously, it is difficult to determine which exerts the highest influence on the electric resistivity and density of the material. The formation of a deformation texture accompanied by a drop in the electric resistivity during the first stage apparently has a considerable influence.

During the second stage of creep, characterized by an equilibrium between the processes of strengthening and recovery, the electric resistivity somewhat increases which indicates that the annealing of the dislocations lags somewhat behind their formation, and therefore their number gradually increases. If the number of dislocations begins to grow rapidly and the density of the specimen decreases, the electric resistivity increases sharply.

CONCLUSIONS

The creep of chromium in vacuo at temperatures of $(0.5-0.75)\,T_{mp}$ can be characterized by the following factors.

1. The creep rate is very influenced by temperature. Creep is greatly influenced by heat-activated and dislocation—slip processes.
2. Wrought chromium specimens have a higher rate of volatilization during creep than cast chromium specimens or specimens covered by an oxide film. Therefore, the absolute creep rates of cast chromium are lower than of wrought.
3. The nature of the variation in the electric resistivity of chromium reflects the structural changes taking place in the metal during different stages of creep, and is the same as the variation in the electric resistivity of other metals during creep at temperatures below $0.5\,T_{mp}$.

All these factors indicate that the creep of chromium below $(0.5-0.75)T_{mp}$ is greatly influenced by the dislocation—slip mechanism, which may be due to the volatilization of chromium which facilitates the free shift of dislocations to the surface.

Bibliography

1. Fogel', A.A.—Izvestiya AN SSSR, OTN, No. 2. 1959.
2. Bystrov, L.N. and L.I.Ivanov. —In: Sbornik "Issledovanie po zharoprochnym splavam." Izdatel'stvo AN SSSR, p. 286. 1961.
3. Oding, I.A., V.S.Ivanova, V.V.Burdukskii, and V.N. Geminov. Teoriya polzuchesti i dlitel'noi prochnosti (Theory of Creep and Long-Time Strength).—Metallurgizdat. 1959.
4. Prokoshkin, D.A., M.P.Matveeva, and V.A.Morozov.—In: Sbornik "Issledovaniya po zharoprochnym splavam." Izdatel'stvo AN SSSR, p.22. 1963.

P. L. Gruzin and S. V. Zemskii

INFLUENCE OF LOCAL INHOMOGENEITIES IN THE DISTRIBUTION OF IMPURITIES ON THE BRITTLENESS OF CHROMIUM

Even small amounts of several metallic and nonmetallic impurities reduce the ductility of chromium /1, 2/. The mechanism of this influence of impurities on the ductility of chromium has been discussed in a number of works /3, 4, 5, 6/. However, some problems have not yet been fully clarified. It is believed /6/ that the embrittlement of refractory metals of group VI, chromium subgroup, is caused by the accumulation of interstitial impurities along the grain boundaries in the form of solid solution precipitates, by the increase in the resistance to the movement of dislocations, and by the decrease in the resistance to the propagation of cracks. This hypothesis apparently assumes that the existence of a close antiferromagnetic order of chromium /3/, and the mechanism of the deformation of chromium /7/, be taken into account.

In their studies on the influence of impurities on the ductility of chromium many authors assumed that this metal consists of a chemically homogeneous solid solution. The possibility of precipitation of stable and metastable particles along the grain boundaries and other interfaces has not been considered or sufficiently investigated. The uneven distribution of the carbide phase in metals with a high carbon content (0.5 wt%) has been determined metallographically. The distribution of the carbide phase in chromium, and the kinetics of its precipitation in chromium containing less than 0.01% of carbon, have not yet been sufficiently studied.

We carried out direct investigations of the distribution of a number of impurities and alloying elements present in chromium in small amounts. If chromium contains small or medium concentrations of impurities, a study of their distribution by metallographic and other classic methods involves certain difficulties, and therefore we employed methods with artificial radioactive isotopes. The distribution of carbon, sulfur, phosphorus, iron, copper, tungsten, molybdenum, tantalum, calcium, and zirconium, in chromium, and also the solubility and diffusion of carbon in electrolytically refined chromium during its remelting, were investigated by adding isotopes of these elements to chromium. The distribution of the above elements in cast and annealed cast chromium, and the distribution of carbon and sulfur in hot-formed and heat-treated chromium, were studied by the autoradiographic method.

The distribution of carbon in chromium after crystallization in metal ingots is shown in Figure 1,a. The dark network along the grain boundaries indicates an accumulation of carbon. The intensity of the dark color of the grain boundaries, and the variation in this intensity as we pass from dark areas to bright, indicate that the concentration of carbon at the grain boundaries is more than ten times that in the grain, and that the changes from the carbon-rich zones to zones with a low content of carbon are stepwise. This is another proof that under existing conditions carbon forms carbides along the grain boundaries of chromium.

Phosphorus is present in chromium in concentrations of 0.001 — 0.005%. A study of the distribution of phosphorus under the above conditions showed that phosphorus also accumulates along the grain boundaries of this metal (Figure 1, b). The distribution of phosphorus seems to differ from that of carbon, but this is apparently due to the specific features of the application of autoradiography to the determination of phosphorus. However, as in the previous case, it can be seen that phosphides are precipitated along the grain boundaries of chromium. The autoradiogram showing the distribution of sulfur in chromium (Figure 1, c) indicates that at the given concentrations sulfur is present in chromium as sulfide inclusions distributed at random along the grain boundaries and within the grains. The content of impurities in the alloys is given below.

Alloy	Content of impurity, wt %	Alloy	Content of impurity, wt %
Chromium — iron	0.3	Chromium — tungsten	0.03
Chromium — tantalum	0.3	Chromium — calcium	0.5
Chromium — silicon	0.5	Chromium — carbon	0.02
Chromium — copper	0.006	Chromium — sulfur	0.01
Chromium — zirconium	0.1	Chromium — phosphorus	0.005
Chromium — molybdenum	0.14		

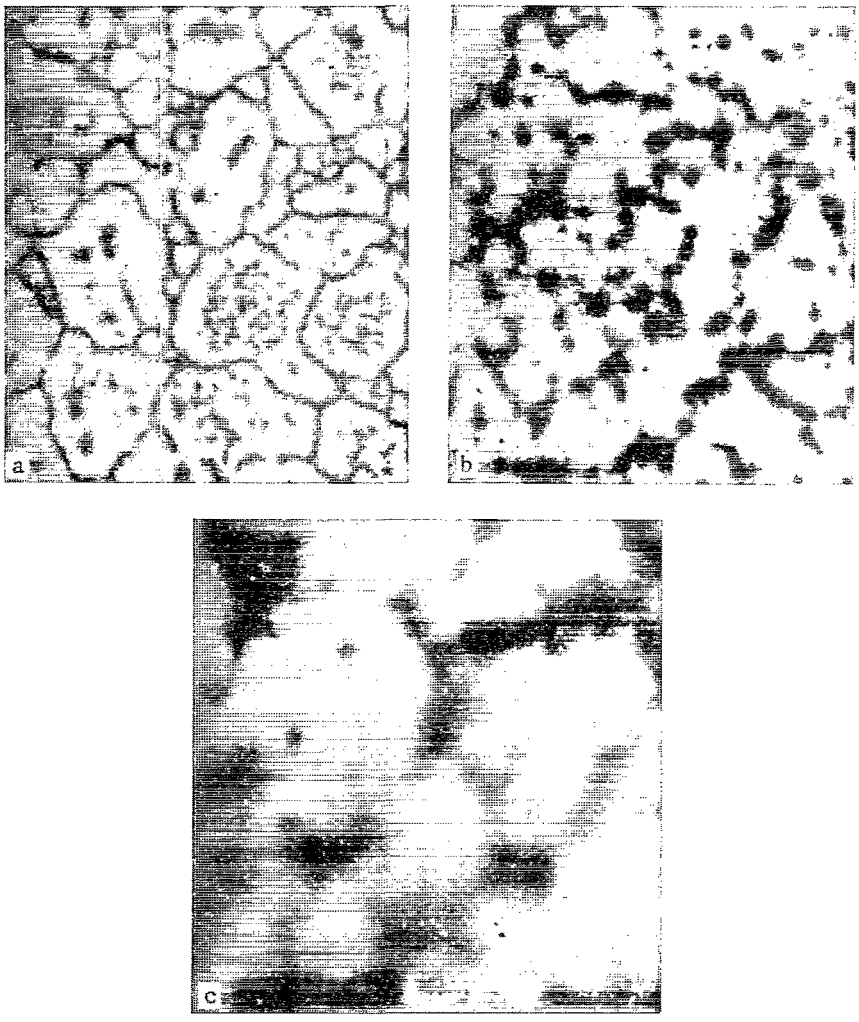

FIGURE 1. Autoradiodiagrams showing the distribution in chromium of: a—carbon; b—phosphorus; c—sulfur, ×150.

On all the autoradiograms the blackened areas are much wider than the zones containing impurities.

The distribution of carbon, sulfur, and phosphorus, described above, is also retained in annealed cast chromium and in hot-worked chromium. In the latter case only carbon is distributed in this way provided that no hardening is caused by cooling.

The distribution of iron, tantalum, copper, molybdenum, tungsten, calcium, and zirconium in cast and annealed chromium has been investigated by the method of autoradiography. The conditions were the same as above. At the concentrations given (see page 27), all the above elements, except tungsten, are present at the grain boundaries of chromium. But the concentration of tungsten in the grains is higher than in the grain boundaries.

No enrichment of the grain boundaries of chromium specimens containing 10 and 20% of molybdenum could be found by the autoradiographic method. The autoradiograms showing the distribution of tantalum, calcium, and zirconium in chromium indicate that, in addition to the fields with a high concentration of these impurities along the grain boundaries, very dark areas also exist, which apparently contain compounds formed by these elements with nonmetallic impurities, and also precipitated mainly along the grain boundaries.

These data indicate that the concentration of many impurities and alloying elements in cast and annealed chromium is considerably higher along the grain boundaries than in the grains themselves. The precipitates of carbides and phosphides of chromium, and apparently also of impurity metals, and also oxide precipitates are present mainly along the grain

Cast chromium and chromium-base alloys are more brittle than the hot- or cold-worked metal /8/. This may be related to the data given above. Apparently the distribution of precipitates is influenced by the higher concentration of alloying elements along the grain boundaries.

Great attention should be paid to the behavior of carbon in chromium, since according to literature data carbon and nitrogen have the greatest influence on the ductility of the metal /2, 6/. The distribution of nitrogen cannot be determined by the autoradiographic method because no convenient radioactive isotopes of this element are available.

The distribution of carbon in chromium of the type shown in Figure 1, a, can be found in metal specimens which were forged and isothermally heated at 1100°C or above, and quenched from these temperatures in oil or cooled more slowly. In both cases the carbides were precipitated during the cooling process. The presence of large amounts of a carbide phase along the grain boundaries of chromium indicates that one of the conditions of brittle failure suggested in /6/ has been established.

To clarify the influence of impurities present in solid solutions, it is necessary to have data on the solubility of these impurities and on the parameters which influence the kinetics of precipitation. We investigated the solubility of carbon in chromium and the influence of alloying on the maximum content of carbon in saturated solid solutions, and on the diffusion of carbon in chromium. The data on the solubility of carbon in chromium were obtained by Smith (metallographic investigations) /9/, and are apparently only qualitative.

We studied the equilibrium in the carbon—chromium system at concentrations of carbon of 0.004—0.05%, over a temperature range of 1100—1500°C. The forged chromium specimens were heated at a given temperature for a specific time, quenched, and examined by the autoradiographic method. Specimens in which chromium had been distributed uniformly after such a heat treatment were further treated at a lower temperature, and vice versa. The results are given in Figure 2. Points 1 indicate conditions corresponding to a uniform distribution of carbon at which no precipitates were found, and only a solid solution of carbon in chromium existed; points 2 represent a condition at which the specimens contain both a solid solution and a $Cr_{23}C_6$ carbide, whose structure was determined by an X-ray structural analysis. The data are plotted in the log C—1/T coordinates. The straight line which separates the points of different phases of chromium—carbon alloys represents a maximum concentration of carbon in the solid solution of chromium. The heat of dissolution calculated

according to the data of Figure 2 is equal to 32 ± 2 kcal/g-atom. The results of the extrapolation of the data of the field of lower temperatures indicate that to obtain chromium with no carbide precipitates at 900°C the total content of carbon must be less than 10^{-3} wt %. To avoid carbide precipitates at 700°C and 600°C, the content of carbon must be less than 10^{-4} and 10^{-5} wt %, respectively. Even if this dependence of the maximum concentration of carbon in chromium on temperature is retained down to lower temperatures, it is nevertheless difficult to produce chromium with no carbide precipitates in a state of equilibrium with the metal at room temperature.

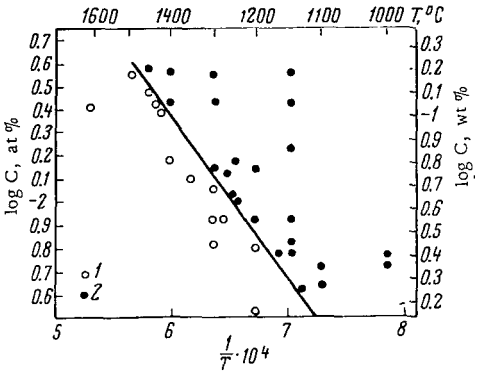

FIGURE 2. Results of a study of the chromium—carbon phase diagram (C = 0.004—0.05%).

To find the influence of alloying on the solubility and distribution of carbon in chromium we studied the phase diagram of chromium with small amounts of molybdenum and nickel by the method of autoradiography. The addition of molybdenum to chromium reduces the concentration of carbon in saturated solid solutions at 1200°C (Figure 3). This is also true of the addition of nickel, tantalum, and titanium to chromium. If the concentration of these elements at the grain boundaries is higher than in the grains, carbon can migrate into the former and thus facilitate an increase in the amount of the carbide phase or supersaturation of the solid solution.

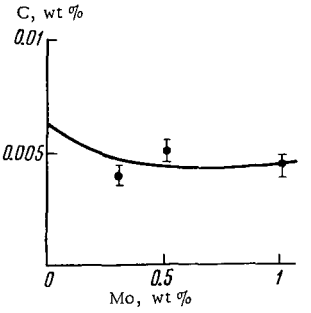

FIGURE 3. Influence of molybdenum on the solubility of carbon in chromium at 1200°C.

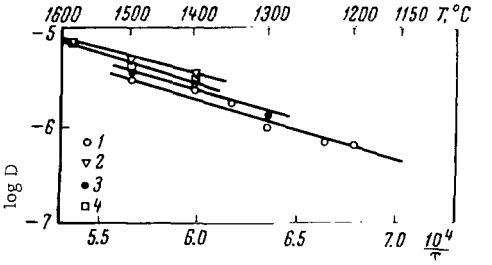

FIGURE 4. Dependence of the coefficient of diffusion of carbon on temperature:

1—in unalloyed chromium; 2—in chromium—0.5% iron alloys; 3—in chromium—1% iron alloys; 4—in chromium—1% tantalum alloys.

The growth of the particles precipitated from the solid solution depends on the intensity of the diffusion currents which supply carbon from the solid solution. It is believed /6/ that coagulation may take place at a diffusion rate in the solid solution of not less than 10^{-11}—10^{-12} cm^2/sec. To determine the diffusion rate of carbon in chromium and its alloys containing 0.5 and 1% of iron and 0.5% of tantalum, the dependence of the diffusion coefficients of carbon on temperature were investigated. Because of the low solubility of carbon in chromium, the diffusion coefficients of carbon at elevated temperatures were determined by the concentration method, by freeing the specimens of carbon, and then making a radiometrical analysis of parallel layers /10/, and at lower temperatures (140—162°C) by the method of a low-frequency internal friction at free torsional vibrations /11/. The dependence of the diffusion coefficients on temperature is shown in Figure 4. The diffusion coefficients of alloys are somewhat higher than of unalloyed chromium. The diffusion coefficient at about 400°C is about 10^{-11} cm^2/sec, and at 350°C it is 10^{-12} cm^2/sec. The data obtained on the aging of chromium /12, 13/ indicate that the precipitation of nitrides from solid solutions may take place at lower temperatures. However, these precipitates are very small and the problem of whether the precipitation from the solid solution is complete has not yet been solved.

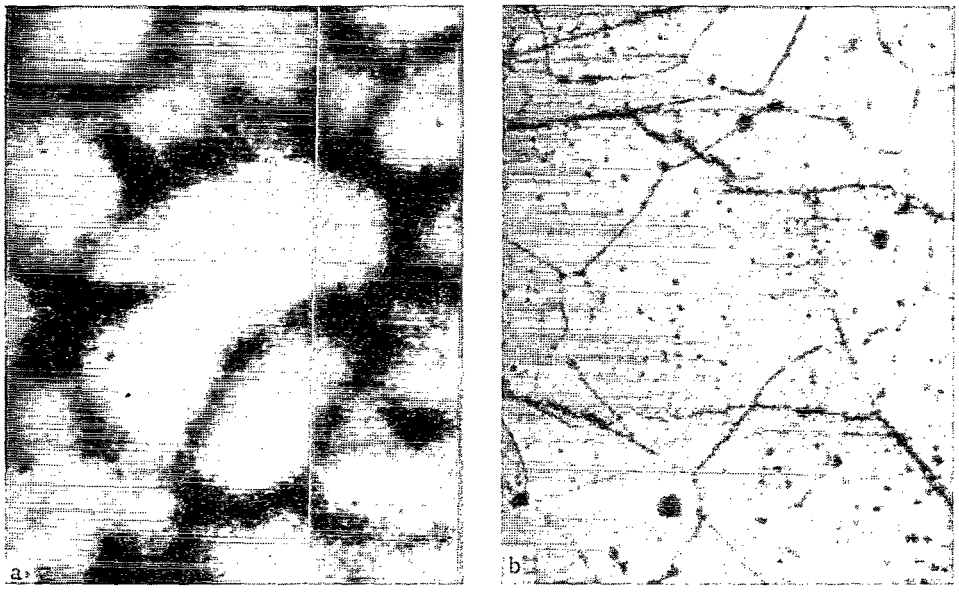

FIGURE 5. Distribution of cracks in chromium:

a—autoradiogram; b—microstructure of the same region, ×150.

A comparison of the data on the diffusion and solubility of carbon in chromium indicates that at low temperatures (below 100°C) the solid solution of carbon in chromium is supersaturated.

The impurities present in solid solutions increase the yield point of the metal and lead to uneven deformation. The differences between the chemical compositions of the grain boundaries and of the grains increase the

unevenness of deformation, raise local stresses, and thus facilitate the formation of cracks. Supersaturated solid solutions may decrease the resistance to crack propagation. An example of the nucleation of cracks in grain boundary zones of chromium with a high content of impurities is shown in Figure 5. The cracks nucleated during the bending of the specimens at a point close to the grain boundary.

A study on the influence of alloying elements on the solubility of carbon in chromium indicates that alloying elements affect the coefficient of thermodynamic activity. The distribution of carbon and phosphorus in chromium should be studied as in steels in which the mutual influence of carbon and phosphorus on their distribution has been determined.

CONCLUSIONS

The results confirm that brittle failure in chromium is caused by two processes, and that these are greatly accelerated if the distribution of impurities within the grains is uneven. To obtain more homogeneous and ductile metals, the distribution of impurities must be made more uniform by heat treatment, so that homogenizing of some impurities will not lead to nonuniform distribution of others.

Bibliography

1. Sully, A.H. Ductile Chromium, p. 14.—A.S.M. Cleveland, Ohio. 1957.
2. Asai, G. and E.T. Hayes. Ductile Chromium, p. 138.—A.S.M. Cleveland, Ohio. 1957.
3. Ageev, N.V., V.N. Bykov, and V.A. Trapeznikov. Sbornik—Sovremennye problemy metallurgii (Collection—Modern Problems in Metallurgy), p. 556.—Izdatel'stvo AN SSSR. 1958.
4. Wain, H.L. Ductile Chromium, p. 27.—A.S.M. Cleveland, Ohio. 1957.
5. Gridnev, V.N., V.I. Trefilov, and A.K. Butylenko. Sbornik—Issledovaniya po zharoprochnym splavam (Collection—Investigation of Refractory Alloys), No. 4:266.—Izdatel'stvo AN SSSR. 1959.
6. Hahn, G.T., A. Gilbert, and R.I. Jaffee. Refractory Metals and Alloys.—Interscience, 2:23, New York. 1963.
7. Hull, D. Fracture of Solids.—Interscience, p. 417, New York. 1963.
8. Gendersen, Kvaas and Vein.—Problemy Sovremennoi Metallurgii, No. 3:62. 1955.
9. Smith, W.H.—Trans. AIME, 209:47. 1957.
10. Borisov, E.V., P.L. Gruzin, and S.V. Zemskii. Sbornik—Problemy metallovedeniya i fiziki metallov (Collection—Problems of Metallurgy and of Physics of Metals), No. 8:321.—Izdatel'stvo AN SSSR. 1964.
11. Zemskii, S.V. and M.N. Spasskii.—Fizika Metallov i Metallovedeniye, 21, No. 1. 1966.

12. Weaver, C.W.—Acta Met., 10:1151. 1962.
13. Spasskii, M.N. and L.M.Utevskii. Sbornik—Problemy metallovedeniya i fiziki metallov (Collection—Problems of Metallurgy and Physics of Metals), No. 9.—Moskva, Izdatel'stvo Metallurgiya. 1967.
14. Law, J.R. Fracture of Solids.—Interscience, p. 197, New York. 1963.

A. K. Butylenko, V. N. Gridnev and V. N. Minakov

THE ABSENCE OF POLYMORPHISM IN CHROMIUM

The problem of polymorphism in chromium arose in connection with X-ray structural studies of electrolytic deposits of chromium, and with an investigation of binary chromium-base alloys containing Ni, Ta, and Fe. Close-packed hexagonal /1—4/, hexagonal /5, 6/, isomorphic α-Mn cubic /6/, and face-centered /7, 8/ modifications have been found. These modifications of electrodeposited chromium proved to be unstable, and the metal regained its usual compact body-centered structure soon after deposition or as the result of heating.

It has been found /7—9/, that a change in the structure of chromium during electrodeposition is due to hydrogen pickup, and to the formation of hydrides or other structures characteristic of this process.

The existence of a high-temperature face-centered modification of chromium above 1840°C was proved during a study of Cr—Ni systems /10—15/, an X-ray microstructural analysis of the phase composition of quenched alloys, and a thermal analysis at temperatures up to the melting point. The existence of this modification of chromium has been proved indirectly by data on the decomposition of solid solutions of the Cr—Ni system. Other authors who carried out similar studies /16—20/ are doubtful of these results. Nevertheless, polymorphism of pure chromium has also been confirmed by other authors who used the method of extrapolation of the data from phase diagrams of alloys. Great attention has been paid to the study of the Cr—Ni system. In /21, 22/ the formation of a β-phase in chromium—nickel alloys was associated with the existence of a high-temperature modification of chromium. In these works, however, as in the preceding ones, no attention was paid to the heterogeneous mechanism of the decomposition of solid solutions which leads to the formation of eutectoid structures. An analysis of these may lead to erroneous conclusions on the polymorphism of metals /23, 24, 25/. We believe that the same erroneous conclusions were drawn in /26—35/ also. In these works the results of the differential thermal analysis of chromium and of X-ray microstructural studies of binary and ternary chromium-base systems (Cr—Co, Cr—Fe, Cr—Ni, Cr—Mo, Cr—W, Cr—Nb, Cr—Ta, Cr—Fe—Ni, Cr—Fe—Mo, Cr—Co—Ni, Cr—Mo—Ni) led to the conclusion that chromium can exist in five modifications, and can undergo the following transformations: $\alpha \rightleftarrows \beta$ at 930°C; $\beta \rightleftarrows \gamma$ at 1300; $\gamma \rightleftarrows \delta$ at 1650°C; and $\delta \rightleftarrows \varepsilon$ at 1830°C. An X-ray analysis of quenched alloys confirmed the existence of crystallographic structures of the following modifications: α, γ, ε -body-centered cubic, β-face-centered cubic, and δ-hexagonal.

These conclusions do not agree with the results of a study on the Cr—Ni system /36—39/, Cr—Fe system /39/, and pure chromium /40, 41/, in which the existence of a single body-centered cubic modification of chromium was proved. This has also been confirmed by the authors of /42—44/, and /45/. It should be pointed out that a thermodynamic analysis of the equilibrium between α- and γ-phases (body-centered cubic and face-centered cubic modifications) in the Cr—Fe system carried out in /46, 47/ indicates that no face-centered cubic modification of chromium can exist at elevated temperatures (the difference between the free energies of the γ- and α-phases increases with increase in temperature).

These theoretical calculations were confirmed by a study of the behavior of chromium /48, 49/ and of Cr—Ni alloys /48/ at elevated temperatures and high pressures, when a transformation of the body-centered cubic modification of chromium into more close-packed structures is probable. However, the authors could not transform the body-centered cubic modification into any other structure at temperatures up to 2400°C and at a pressure of 50 kbar.

The existence of polymorphism in chromium is disproved by numerous studies of many physical properties of chromium. These properties should undergo sudden changes during a phase transformation of the first type.* First, we should like to point out that Krauss /51/ found that the thermal capacity of chromium increases smoothly from 20 to 1400°C, although he also pointed to previous unpublished works which indicate that a transformation takes place in chromium at about 1375°C. However, no change in the thermal capacity at this temperature was observed in later investigations /52/.

It has been found /53/ that the magnetic susceptibility of highly purified chromium undergoes no sudden changes over the range of temperatures from 100 to 2000°K. Therefore, the results of studies on the magnetic susceptibility of chromium, which show hysteresis at temperatures between 1250 and 1480°C /54/, cannot be considered valid, since this hysteresis is apparently caused by impurities (up to 1.2% of chromium oxide). A linear dependence of the logarithm of the coefficient of self-diffusion of chromium on temperature was found over this range of temperatures in /55, 56/, and a similar dependence of the logarithm of vapor pressure on temperature for the same range in /57, 58/. No sudden changes are indicated by the curve representing the temperature dependence of the electric resistivity of chromium up to 1700°C /59/, or on the curve of the dependence of thermal expansion on temperature up to 1600°C /45/.

Direct X-ray studies on the changes in crystal lattices of chromium at elevated temperatures are very important in clarifying the problem of polymorphism in chromium.

A study of the variation in the parameters of body-centered cubic lattices of chromium above 200°C, when a deviation in the lattice parameters is expected because of the complete disappearance of antiferromagnetic regions, was very accurately carried out in /60/. The parameters of body-centered cubic lattices of chromium up to 800°C were measured in /61/. The structure of chromium at temperatures of 700 to 1700°C was examined in /62/, from 20 to 1500°C in /63/, and from 20 to 1850°C in /64/. The data

* Changes in the physical properties and in the symmetry of the body-centered cubic lattice of chromium at 35—40°C are due to a transformation of the second type caused by the antiferromagnetism of chromium, which has been described in /50/.

of experiments with prolonged heating at given temperatures agree, and this confirms the existence of only one body-centered cubic modification of chromium.

However, the above review indicates that the structure and the properties of chromium were investigated at temperatures up to 1600—1700°C, which is clearly insufficient for final confirmation of the absence of polymorphism in chromium, as this metal sublimes readily and becomes oxidized at elevated temperatures. Despite the number of experimental and theoretical data which seem to confirm that chromium exists in a single modification only, the problem of its polymorphism is still the subject of great discussions.

To solve the problem of polymorphism in chromium, we carried out continuous X-ray structural studies on chromium in rays of Cr_{k_α} (method of scanning /65/), expecting the line (211) of chromium, and also by special complex studies of the variation in temperature, elongation, and electric resistivity /66/ during rapid heating of specimens up to their melting point. To prevent the oxidation of specimens, they were heated by electricity at the rate of 1000—1600 degree/sec in a stream of argon. During the above rapid X-ray studies and the recording of the above characteristics of chromium the temperature was measured by a VR-5-20 thermocouple 0.1 mm in diameter.

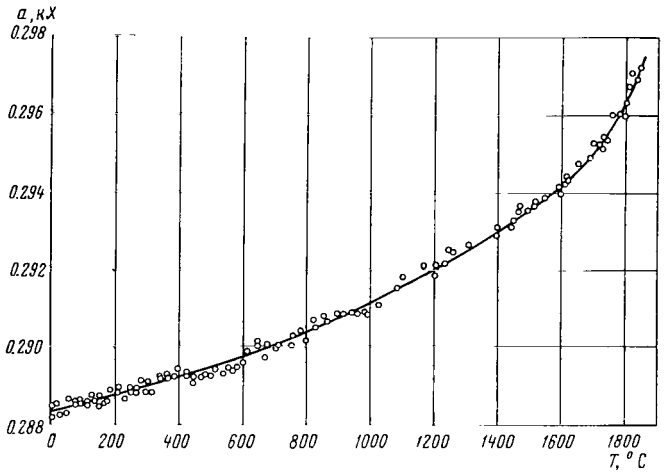

FIGURE 1. Variation in the lattice parameters of body-centered cubic chromium with temperature.

The specimens for X-ray analysis were made of plates (0.5 × 12 × × 70 mm) of wrought and annealed chromium of small grain size. For complex studies of the physical properties, electropolished wires 1.4 and 1.8 mm in diameter, and plates (2 × 3 × 100 mm) cut from an ingot were used. The specimens were made of highly purified chromium containing not more than 0.002% nitrogen, 0.002% oxygen, 0.004% carbon. In addition, we used specimens of chromium deoxidized by adding 0.4% Y and 0.4% La.

Figure 1 shows the results of X-ray studies on chromium up to its melting point, with an accuracy of ± 0.005 mμ. The data given indicate

that the parameters of the body-centered cubic lattice of chromium increase with increase in temperature, and show no jumps of temperatures at which a face-centered modification or a hexagonal modification could exist /26—35/. Figure 2 shows the X-ray oscillograms of lines (211) of chromium in the range of temperatures where the above transformations of the body-centered modification are expected to take place. Figure 2 also shows that line (211) exists over all ranges of the assumed transformations: from 885 to 985°C, from 1260 to 1350°C, from 1565 to 1600°C, and above 1800°C. The intensity of line (211) decreases smoothly with increase in temperature. In all cases, however, line (211) stands out against the background, and even at the moment of melting of the specimen it can be instrumentally resolved (see Figure 2,c).

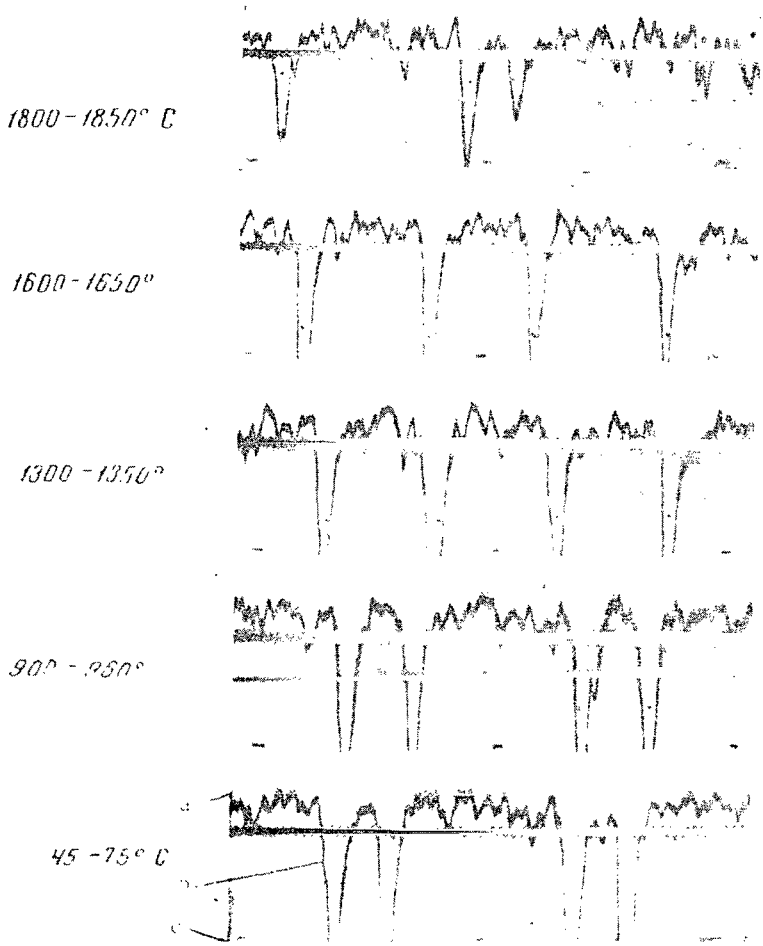

FIGURE 2. Sections of oscillograms of chromium heated in the range of the expected formation of α, β, γ, δ and ε modifications according to /26—35/:

a—variation in temperature; b—variation in the intensity and position of the (211) line of chromium; c—position of scanning aperture.

The data of X-ray studies on chromium agree well with those obtained by continuous oscillography, by measuring thermal expansion, and the potential drop and decrease in current along the specimen. Not one of the oscillograms of electrically heated chromium (an example is shown in Figure 3) indicates any deviations from the monotonous temperature dependence of thermal expansion and of the potential drop along the specimen. The specimens usually start to melt simultaneously at several places, with considerable oxidation. This oxidation is apparently the reason for the decrease in the melting point of chromium to 1795°C (Figure 3,a).

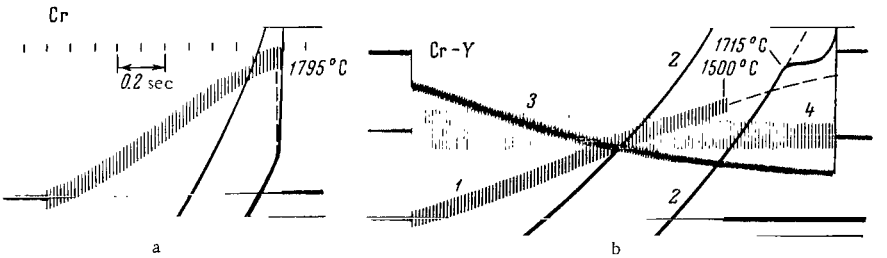

FIGURE 3. Oscillogram of heating:

a—pure chromium; b—chromium deoxidized by the addition of 0.4% Y.
1—variation in temperature; 2—variation in thermal expansion; 3—variation in the potential drop; 4—variation in current along specimen.

The oscillograms of electrically heated chromium containing rare-earth elements indicate that these specimens heated to 1700—1720°C are denser than pure chromium (Figure 3,b). However, we believe that this density increase does not prove the existence of a new modification of chromium, since the metal contains considerable amounts of an uninvestigated phase located preferentially along the grain boundaries /67/. In addition, the Cr—Y and Cr—La phase diagrams indicate that the addition of 0.4% Y or 0.4% La reduces the solidus temperature to about 1700°C. These chromium specimens showed no signs of age hardening, and their ductility was higher than that of chromium with no deoxidizing agents /68/. Apparently, the formation of a second phase by deoxidation or by some other process in insufficiently pure chromium might lead to erroneous conclusions during the analysis on the properties of chromium, especially during a study of polymorphism by indirect metallographic methods.

CONCLUSIONS

From an analysis of different investigations on various physical characteristics of highly purified chromium over a wide range of temperatures, and direct X-ray studies of chromium at elevated temperatures, as well as our own investigations, we conclude that chromium is a monomorphic metal with a body-centered cubic lattice.

Bibliography

1. Bradley, A.J. and E.A.Ollard.—Nature, 117:122. 1926.
2. McNaughton, D.J.—Metal Industry, 28:173. 1926.
3. Wood, W.A.—Phil. Mag., 12:583. 1931.
4. Wright, L., H.Hurst, and J.Riley.—Trans. Faraday Soc., 31:1253. 1935.
5. Dean, R.S. and F.X.McCawley.—Nature, 182:746. 1958.
6. Sasaki, K. and S.Sekito.—Trans. Electrochem. Soc., 59:437. 1931.
7. Salli, A. Khrom (Chromium).—Moskva, Metallurgizdat. 1958.
8. Snavely, C.A.—Trans. Electrochem. Soc., 92:537. 1947.
9. Albrecht, G., F.D.Doenitz, K.Kleinstück, and M.Betzl.—Phys. Status Solidi, 3:7. 249K. 1963.
10. Bloom, D.S. and N.J.Grant.—Trans. AIMME, 191:1009. 1951.
11. Bloom, D.S., J.W.Putman, and N.J.Grant.—Trans. AIMME, 194:626. 1952.
12. Bloom, D.S. and N.J.Grant.—Trans. AIMME, 200:261. 1954.
13. Stein, C. and N.J.Grant.—Trans. AIMME, 203:127. 1955.
14. Abrahamson, E.P. and N.J.Grant.—Trans. AIMME, 206:975. 1956.
15. Abrahamson, E.P. and N.J.Grant.—Ductile Chromium and its Alloys.—ASM, p. 277, Ohio. 1957.
16. Taylor, A. and R.W.Floyd.—J.Inst. Metals, 80:577. 1951—1952.
17. Duwez, P. and H.Martens.—Trans. AIMME, 194:523. 1954.
18. Köster, W. and S.Kabermann.—Arch. Eisenhüttenw., 26:627. 1955.
19. Williams, R.O.—Trans. AIMME, 209:1257. 1955.
20. Wyman, L.L. and J.T.Sterling. Ductile Chromium and its Alloys.—ASM, p. 180, Ohio. 1957.
21. Abrahamson, E.P. and N.J.Grant.—J.Metals, 8:975. 1956.
22. Vasyutinskii, B.M., V.S.Kogan, and G.N.Kartmazov.—FMM, 9:558. 1960.
23. Haynes, F.G. and R.F.Smart.—J.Inst. Metals, 90(5):189. 1960—1961.
24. Haynes, F.G. and R.F.Smart.—J.Inst. Metals, 91(4):153. 1962—1963.
25. Ageev, N.B. and M.S.Model.—Doklady AN SSSR, 148(1):84..1963.
26. Grigor'ev, A.T., L.N.Guseva, E.M.Sokolovskaya, and M.V.Maksimova.—ZhNKh, 4:2168. 1959.
27. Grigor'ev, A.T., E.M.Sokolovskaya, M.V.Maksimova, I.G.Sokolova, and I.A.Nedumova.—ZhNKh, 5:2640. 1960.
28. Grigor'ev, A.T., E.M.Sokolovskaya, and Yü-p'u.—ZhNKh, 5:2642. 1960.
29. Grigor'ev, A.T., E.M.Sokolovskaya, et al.—ZhNKh, 6:2136. 1960.
30. Grigor'ev, A.T., E.M.Sokolovskaya, et al.—Vestnik MGU, Khimiya, 4:23. 1960.
31. Grigor'ev, A.T., E.M.Sokolovskaya, et al.—Vestnik MGU, Khimiya, 2:19. 1961.
32. Grigor'ev, A.T. and E.M.Sokolovskaya.—Vestnik MGU, Khimiya, 6:3. 1961.
33. Grigor'ev, A.T., E.M.Sokolovskaya, et al.—ZhNKh, 6:1248. 1961.

34. Grigor'ev, A.T., E.M.Sokolovskaya, I.G.Sokolova, and M.V.Maksimova. Sbornik—Issledovaniya po zharoprochnym splavam (Collection—Investigation of Refractory Alloys), 8.—Moskva, Izdatel'stvo AN SSSR. 1962.
35. Grigor'ev, A.T., E.M.Sokolovskaya, L.I.Pyatigorskaya, and M.V.Maksimova. —ZhNKh, 8:1105. 1960.
36. Svechnikov, V.N. and V.M.Pan. —Doklady AN USSR, 7:917. 1960.
37. Svechnikov, V.N. and V.M.Pan. Sbornik—Issledovaniya po zharoprochnym splavam (Collection—Investigation of Refractory Alloys), 6.—Izdatel'stvo AN SSSR. 1960.
38. Svechnikov, V.N. and V.M.Pan. Sbornik—Voprosy fiziki metallov i metallovedeniya (Collection—Problems of Physics of Metals and Metallurgy), No. 15.—Kiev, Izdatel'stvo AN USSR. 1962.
39. Wyder, W.C. and M.Hoch. —Trans. Met. Soc. AIME, 227(3):588. 1963.
40. Svechnikov, V.N., G.F.Kobzenko, and Yu.A.Kocherzhinskii. Sbornik—Voprosy fiziki metallov i metallovedeniya (Collection—Problems of Physics of Metals and Metallurgy), No.11.—Kiev, Izdatel'stvo AN USSR. 1960.
41. Svechnikov, V.N. and G.F.Kobzenko. Sbornik—Issledovaniya po zharoprochnym splavam (Collection—Investigation of Refractory Alloys), 6.—Izdatel'stvo AN SSSR. 1960.
42. Edwards, A.R., J.I.Nish, and H.L.Wain. — Metallurg. Rev., 4(16):403. 1959.
43. Wain, H.L. and A.Ya.Edwards. —Metall., 14(5):387. 1960.
44. Edwards, A.R.—J.Austral.Inst. Metals, 5(2):182. 1960.
45. Svechnikov, V. N.—FMM, 15(4):616. 1963.
46. Svechnikov, V.N. and A.G.Lesnik. —FMM, 3:87. 1956.
47. Lesnik, A.G. Modeli mezhatomnogo vzaimodeistviya v statisticheskoi teorii splavov (Models of Interatomic Reactions in the Statistical Theory of Alloys).—Moskva, Fizmatgiz. 1962.
48. Coliber, E.W. and K.H.McKee. Progress in Very High Pressure Research.—Proc. Conf. at Lake George, N.Y., June. 1960, p. 126, J.Wiley and Sons, N.Y. 1963.
49. Kinzokee, C.—J.Metals, 33(3):30. 1963.
50. Butylenko, A.K. Sbornik—Elektronnye svoistva metallov i splavov (Collection—Electronic Properties of Metals and Alloys).—Kiev, Izdatel'stvo Naukova Dumka. 1966.
51. Krauss, F.—Z.Metallkunde, 49(7):386. 1958.
52. Kohlhaas, R., M.Braun, and O.Vollmer. —Z.Naturforschung, 20a(8):1077. 1965.
53. Weiss, W.D. and R.Kohlhaas.—Z.Naturforschung, 19a(13):1631. 1964.
54. McGuire, T.R. and C.J.Kriesman. —Phys. Rev., 85:452. 1952.
55. Ivanov, L.I., M.P.Matveeva, V.A.Morozov, and D.A. Prokoshkin. —Izvestiya AN SSSR, Metallurgiya i Toplivo, 2. 1962.
56. Hagel, W.C.—Trans. Met. Soc. AIME, 224(3):430. 1962.
57. Speiser, R., H.S.Johnstone, and P.Blackburn. —J. Amer. Chem. Soc., 72:3142. 1950.
58. Gulbrausen, E.A. and K.F.Andrew. —J.Electrochem. Soc., 99:402. 1952.

59. Grube, G. and R. Knabe. — Z. Elektrochemie, 42:793. 1936.
60. Smirnov, Yu. N. and V. A. Finkel. — FMM, 16(4):437. 1963.
61. Hidnert, P. — J. Res. Nat. Bur. Stand., 27:113. 1941.
62. Vasyutinskii, B. M., G. N. Gartmazov, and V. A. Finkel'. — FMM, 12(5):771. 1961.
63. Müller, S. and P. Dünner. — Z. Naturforschung, 20a(9):1225. 1965.
64. Ross, R. G. and W. Hume-Rothery. — J. Less-Common Metals, 5(3):258. 1963.
65. Gridnev, V. N., V. N. Minakov, and V. I. Trefilov. Sbornik — Issledovanie stalei i splavov (Collection — Investigation of Steels and Alloys), p. 384. — Izdatel'stvo Nauka. 1964.
66. Meshkov, Yu. Ya., S. P. Oshkaderov, and N. F. Chernenko. Sbornik — Voprosy fiziki metallov i metallovedeniya (Collection — Problems of Physics of Metals and Metallurgy), No. 20:199. — Kiev, Izdatel'stvo AN USSR. 1964.
67. Savitskii, E. M., V. F. Terekhova, et al. Splavy redkozemel'nykh metallov (Alloys of Rare-Earth Metals). — Izdatel'stvo AN SSSR. 1962.
68. Gridnev, V. N., R. K. Ivashchenko, Yu. V. Mil'man, and V. I. Trefilov. Sbornik — Voprosy fiziki metallov i metallovedeniya (Collection — Problems of Physics of Metals and Metallurgy), 25, No. 20. — Kiev, Izdatel'stvo Naukova Dumka. 1964.

I. I. Kornilov

METALLIDES — A NEW BASIS FOR REFRACTORY MATERIALS

INTRODUCTION

Ideas on high-temperature strengthening of metals described in /2/ were further developed in a lecture given at the 19th scientific session on refractory alloys /1/. Besides the two mechanisms of strengthening metals by the formation of solid solutions and by precipitation of dispersed particles from supersaturated solutions, this report mentions another way of increasing the heat resistance of metals by the formation of refractory compounds.

The history of the development of refractory alloys shows that the mechanism of strengthening metals by dissolution and precipitation of dispersed phases was very often the starting point for producing new refractory alloys, irrespective of which was the basis metal.

Yet another method of strengthening metals is based on the formation of metallides, i.e., of compounds of metals with other elements /3/. In the general system of inorganic compounds metallides occupy a particular position. They have a specific electron structure and may have different chemical bonds such as metallic, ionic, metallic — covalent, and covalent — ionic, etc. Because of the great variety of chemical bonds and crystal structures, metallides have also different physicochemical, mechanical,

and other properties. The characteristic properties of metallides can be summarized as follows /3/:

1) they are usually more heat resistant than their components;

2) they are very hard and strong at low and elevated temperatures, but brittle at low temperatures;

3) they are considerably less weakened by heating than pure metals, solid solutions, or alloys with a heterogeneous structure;

4) they exhibit low-temperature brittleness, but the ductility of metallides tends to increase at temperatures above $0.5-0.7T^{\circ}_{mp}$;

5) it has recently been found that some metallides are sufficiently ductile to be cold worked as well as hot worked;

6) they are chemically less active than their components, and are highly resistant to corrosion and oxidation at elevated temperatures;

7) metallides, like all chemical compounds, can react with one another and with other elements to form continuous and limited solid solutions, as well as ternary or more complex compounds.

Many of these properties of metallides and their reactions are discussed in a special monograph /3/. The mechanical and other properties of intermetallic compounds at both low and elevated temperatures are reported in /3, 4/ and they were discussed at the International Symposium in the USA (in 1959), and compiled in the form of a book edited by Westbrook, which has been translated into Russian /5/.

Refractory metallides formed by transition metals with elements of groups IIA and IIB—VIB of the second and third short periods are of the greatest interest from the point of view of the thermal resistance of materials.

These elements include beryllium, boron, carbon, nitrogen, oxygen, aluminum, and silicon. The reaction between transition metals with incomplete d shells and the above elements with sp electrons leads to the production of strong chemical bonds due to hybridization of the external ds and sp electrons and to the donor—acceptor properties of the reacting elements. It has been found experimentally that metallides containing the above elements, called beryllides, borides, carbides, nitrides, aluminides, and silicides, have the highest melting points and are very heat resistant.

Many of these compounds and materials formed from them are used not only for strengthening metals, and solid solutions of alloys, but also for the production of heat-resistant alloys. They are also employed as heat-resistant protective coatings against oxidation and corrosion in corrosive media, and as materials with special physical properties /3/.

The most important heat-resistant materials are aluminides, beryllides, borides, carbides, and silicides /6, 7/.

Some metallides are also found in metallic systems, and as already mentioned these are ductile to a certain extent. The problem of the ductility of such compounds needs special study.

These compounds are found in the Ni—Al, Ni—Ti, Ti—Al, Ti—Ag, and other systems /8/.

HEAT-RESISTANT COMPOUNDS Ni_3Al AND NiAl

Some compounds (Ni_3Al, NiAl, Ni_2Al_3 and $NiAl_3$) are formed in the nickel—aluminum system. Two of these alumindes, Ni_3Al and NiAl, are

very heat resistant. The Ni_3Al compound is formed by a peritectic reaction at 1410°C and NiAl crystallizes at an extended maximum at 1640°C. The first of these compounds has a face-centered cubic lattice and the second a body-centered cubic. The differences in the structure of the lattices is reflected by the differences in the heat resistance and other properties. The Ni_3Al compound exhibits a certain ductility at elevated temperatures and a low ductiliy at room temperature, but NiAl is not ductile.

At temperatures above 600—700°C both compounds show appreciable elongation during slow deformation (during tensile strength tests and long-time strength tests), which increases with increase in the testing temperature.

Some literature data /51/ on the strength of these compounds at room temperature and during long-time tests at elevated temperatures are given in Table 1.

TABLE 1. Mechanical properties of Ni_3Al and NiAl compounds in the cast and homogenized states

Compound	σ_b, kg/mm^2 (20°C)	δ, % (20°C)	σ_b, kg/mm^2 (815°)	δ, % (815°C)	σ_b, kg/mm^2 (980°C)	δ, % (980°C)	Long-time strength, kg/mm^2 (815°C)	Time to failure, hr	Long-time strength, kg/mm^2 (980°C)	Time to failure, hr
Cast Ni_3Al	21	1.1	—	—	—	—	—	—	—	—
Homogenized Ni_3Al	15	0.2	8	—	6.0	—	7.0	61	5.2	4.6
Cast NiAl	10.1	0	—	—	—	—	—	—	—	—
Homogenized NiAl	30.7	0	10.0	20	7.0	5.2	—	—	8.8	23.0
NiAl + 0.5% Mo	13	0	18	27	—	—	—	—	—	—
NiAl + 2% Mo	24	0.5	18	44	—	—	—	—	—	—

These data show that both compounds fail in a brittle manner during tensile tests at room temperature, but at 815°C and 980°C the specimens show a certain elongation. Long-time tests on NiAl specimens at 815°C also resulted in a 40% elongation. Thus, the pure compounds do not have good mechanical properties at room or at elevated temperatures. It has been found /5/ that the long-time strength of these compounds at 815°C is considerably higher than that of pure nickel, and only a little less than that of nickel-base Inconel alloy. The NiAl compound with its body-centered cubic lattice has a lower long-time strength than the Ni_3Al compound with its face-centered lattice, although the former has a higher melting point.

It has been found /2, 9, 10/ that the strength and heat resistance of alloys made of intermetallic compounds can be considerably increased by producing solid solutions and precipitating dispersed phases. Many alloying elements (Cr, Mo, W, Nb, etc.) have a limited solubility in Ni_3Al and NiAl compounds, and at saturation point can form dispersed phases which will additionally strengthen these alloys. The favorable influence of up to 2% of molybdenum on the properties of NiAl is shown in Table 1 /5/. A new heat-resistant nickel-aluminum alloy based on the Ni_3Al compound has been developed by correctly choosing the alloying elements and their maximum concentrations. The heat resistance of this alloy at 800—1000°C exceeds that of some nickel Nimonic alloys /2, 9/. Heat-resistant alloys based on intermetallic

compounds, including Ni_3Al, can be developed by studying the phase diagrams of metallides and the dependence of the properties of these systems on their compositions. One of these original works /10/ describes the study of the Ni_3Al-Ni_3Nb system, in which the solubility of Ni_3Nb in Ni_3Al is limited and which includes heat-resistant alloys with compositions close to the maximum solubility of Ni_3Nb in Ni_3Al. A detailed study of alloys of this section /11/ confirmed the high heat resistance of alloy compositions close to the solubility limits of Ni_3Nb in Ni_3Al (40—50 wt % Ni_3Nb). Aluminides of other transition metals may also be of interest as heat-resistant materials. Aluminides of vanadium, niobium, molybdenum (V_3Al, Nb_3Al, Mo_3Al, etc.) may be very promising from the theoretical and practical point of view. Some properties of such compounds are given in /6/.

DUCTILE TiNi METALLIDE OF THE Ni—Ti SYSTEM

The equilibrium Ni—Ti system contains three compounds: $TiNi_3$, TiNi, and Ti_2Ni. The first and second compounds crystallize over an extended maximum, while the third compound is formed during a peritectic reaction. The $TiNi_3$ compound is very important for strengthening nickel-base heat-resistant alloys, and Ti_2Ni is apparently important for strengthening titanium alloys. These two compounds are rather brittle. The equiatomic titanium nickelide, TiNi, unlike the two other compounds, has a narrow field of homogeneity and sufficient ductility not only at elevated but also at low temperatures. Therefore, the TiNi compound has been thoroughly studied /8, 12—16/. The chief properties and the structure of this compound are given below:

Melting point, °C	1240°
Crystal structure	CsCl type $a = 3.015$ Å
Density, g/cm^3	6.45
Electric resistivity, mohm·cm:	
at 25°C	80
at 900°C	132
Coefficient of linear expansion (25—900°C)	$10.4 \cdot 10^{-6}$
Recrystallization temperature, °C	550—650
Ultimate strength, kg/mm^2	77—87
Yield point, kg/mm^2	28—38
Elongation, %	15—16
Necking down, %	16
Toughness at 25°C, kgm/cm^2	3.9

The TiNi compound has a relatively low melting point, a lower specific gravity than nickel alloys, and may be of interest as a basis for ductile heat-resistant alloys. The properties of this compound should be further investigated. A study of the reactions of this compound with other compounds or metals is also important in order to increase its strength at low and elevated temperatures.

Together with Dubkina we have begun a systematic study of the interaction of the TiNi metallide and the TiFe and TiAl intermetallic compounds. We

should like to give some results of the study of the phase diagram of the TiNi—TiFe system. Both these compounds have an isomorphic structure of the CsCl type. The alloys of this system were prepared from pure charges suspended in a furnace without a crucible in an atmosphere of helium.

The specimens were annealed at 1100°C for 40 hr and cooled together with the furnace. At both 800 and 500°C the alloys were held for 25 hr.

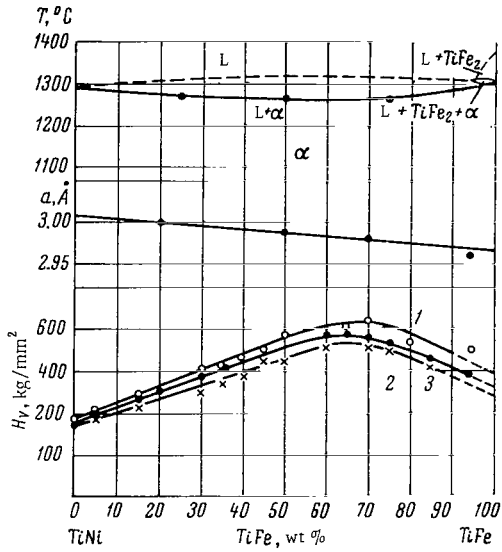

FIGURE 1. Diagram of fusion, lattice parameters, and hardness of alloys of the TiNi—TiFe system:

1—annealed alloy; 2—alloys quenched from 500°C; 3—quenched from 800°C.

The phase diagram of this system, shown in Figure 1, was constructed from the results of a thermal analysis of the structure and properties of homogenized alloys. These data show that the TiNi—TiFe system forms continuous solid solutions according to the rules of mutual solubility of metallides /3/, except in a small field where a $TiFe_2$ compound is formed by a peritectic reaction. The formation of solid solutions in this system is confirmed by the monotonous dependence of the lattice parameters and of the hardness on the composition. The curve passes through a sloping maximum (see Figure 1). We found that the fields of TiNi and TiFe metallides are separated by continuous solid solutions. The properties of heat-resistant alloys on the basis of TiNi compounds are now being investigated further.

REFRACTORY TITANIUM ALUMINIDE, Ti_3Al

The phase diagram of the Ti—Al system /8/ is very useful for a study of many titanium alloys which are important in industry, and in particular

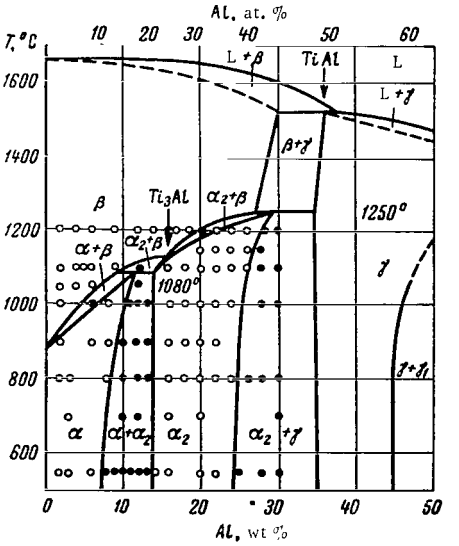

FIGURE 2. Phase diagram of the Ti—Al system showing the formation of the aluminide Ti_3Al from β-solid solutions.

for clarifying the nature of many refractory titanium alloys. The titanium—aluminum system has also been widely investigated. A review of the works on this problem published before 1963 is given in /17/. In these works the existence of two aluminides TiAl (γ-phase) and $TiAl_3$ is confirmed, but until recently the problem of the phase transformations over a wide field of β- and α-solid solutions of titanium and aluminum, and the formation of the Ti_3Al compound, were under discussion, and the results of many authors were contradictory. A certain light was shed on these problems in our last work /18/, in which we proved the existence of a Ti_3Al compound in the Ti—Al system.

As can be seen from Figure 2, this compound is formed at 1130°C as a result of the transformation of the β-solid solution. This compound has a homogeneous field of an α_2-phase, and is separated from the α- and γ-phases by fields of $(\alpha+\alpha_2)$- and $(\alpha_2+\gamma)$-binary phases (see Figure 2). The Ti_3Al compound has an ordered hexagonal lattice and is represented by single points on the composition—elasticity modulus and composition—heat of formation diagrams /19/. We proved that the Ti_3Al compound can be produced by arc melting in an atmosphere of argon (or helium), and that the ingots obtained can be deformed if the forging is started in the field of β-solid solutions (about 1300°C) and is finished at 1000°C. The cast alloy has a polyhedral structure with coarse grains (Figure 3,a), but forged specimens have a fine-grained structure (Figure 3, b). The homogenized Ti_3Al compound retains its polyhedral fine-grained structure (Figure 3, c) up to 1100°C, but specimens quenched from 1200°C (from the field of the β-solid solution) have an acicular structure (Figure 3, d).

From a study of experimental heats we can give the following properties of this compound:

Temperature of formation of Ti_3Al from a β-solid solution, °C	1130
Type of crystal structure	Hexagonal (ordered) structure of the Mg_3Cd type
Density, g/cm³	4.21
Electric resistivity, μ ohm·cm	120—125
Elasticity modulus, kg/mm²	~16,000
Hardness after quenching from 1150—1200°C, kg/mm²	450—465
Ultimate strength after homogenizing at 25°C, kg/mm²	60—65
Elongation at failure, %	0.5—1.5
Ultimate strength at 800°C, kg/mm²	40—50
Time to failure (hr) during long-time strength tests at 800°C:	
σ = 10 kg/mm²	> 500
σ = 15 kg/mm²	> 200

These data show that the Ti_3Al aluminide differs from many metallides in its low specific gravity and high heat resistance. It has a low ductility but a high heat resistance at 700—800°C, and can be used as a basis for the production of new refractory alloys.

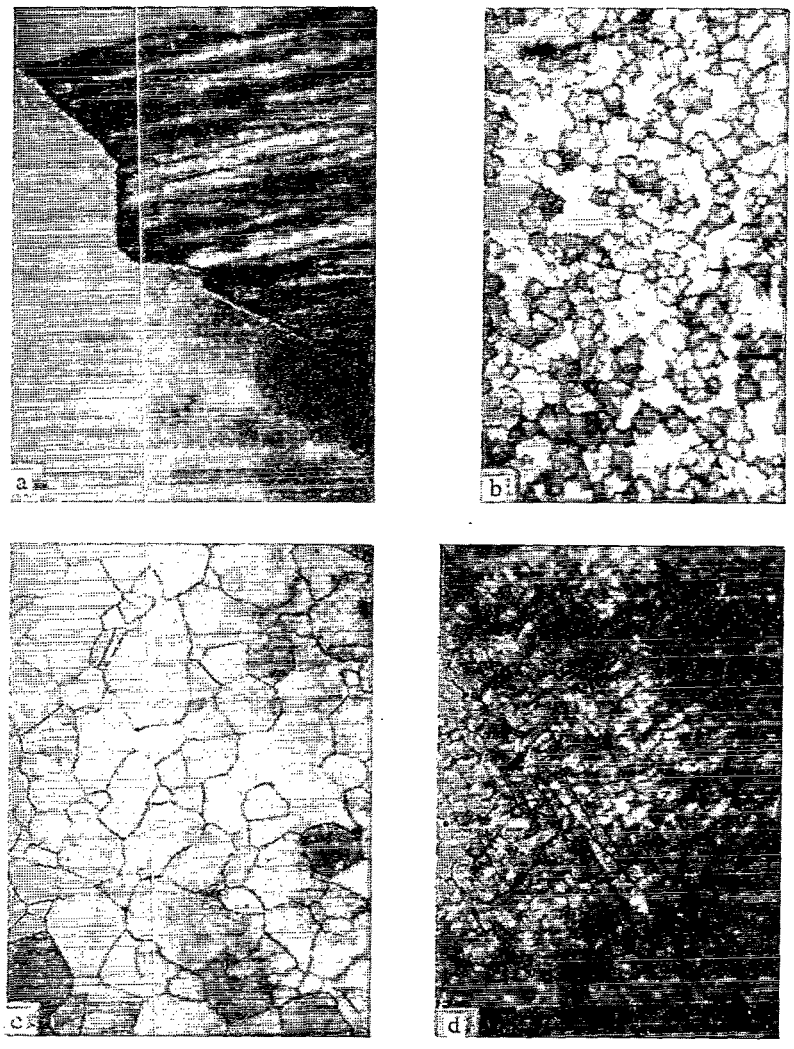

FIGURE 3. Microstructure of Ti_3Al in different states:

a—structure of cast specimen; b—structure of forged specimen; c—after homogenizing at 1100°C; d—after quenching from 1200°C (from the β-field).

To investigate similar alloys on the basis of Ti_3Al it is very important to know the reaction of this compound with other compounds or metals. We studied this question to determine the nature of these reactions and the formation of solid solutions on the basis of Ti_3Al. For example, the

formation of continuous solid solutions between the isomorphic compounds of Ti_3Al and Ti_3Sn was confirmed /20/. The alloys represented on this section of the Ti—Al—Sn ternary system are more heat-resistant than the Ti_3Al compound. It has also been shown that alloying Ti_3Al with elements of low solubility increases the heat resistance of this compound, which can be hot worked in spite of its low ductility.

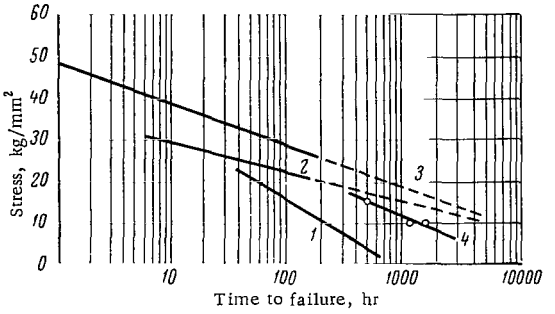

FIGURE 4. Long-time strength of an alloy based on Ti_3Al and of heat-resistant nickel alloys at 800°C:

1—EI437A; 2—EI437B; 3—EI617; 4—Ti_3Al.

We produced some experimental titanium alloys based on Ti_3Al which had a high heat resistance at 800°C /21/. On Figure 4, the ultimate long-time strength at 800°C of one of the experimental Ti_3Al-base alloys is compared with that of some refractory nickel-base alloys, in semilogarithmic coordinates. The investigations in this direction are being continued.

There are indications in the literature that other heat-resistant and ductile metallides exist. For example, the TiAg compound of the Ti—Ag system is soft (130—150 kg/mm²), and can be cold pressed to a 75% reduction in area. This compound is formed during a peritectic reaction at 1030°C, and has a lattice of the AuCu type /22/. Some compounds of niobium and tantalum with metals of the platinum group (Rh and Ir) are also ductile /23/.

REFRACTORY BERYLLIDES OF TRANSITION METALS

Besides metallides which are ductile at low temperatures, other compounds exist which become ductile after being heated to above $0.6—0.8\,T_{mp}$. We are thus able to test metallides for long-time strength and for creep at elevated temperatures to determine their heat resistance, and also to choose the best compositions of refractory compounds. One of the most recent studies in this field was carried out by Stonehouse, Pein and Beever /24/. Many beryllium-rich beryllides (from $MeBe_{12}$ to $MeBe_{17}$) have a high melting point (above 1700—1900°C), and are resistant to oxidation in the air above 1200°C. Of particular interest are the beryllides of titanium, zirconium, niobium, tantalum and molybdenum,

which because of their high heat resistance can be used at 1200—1600°C. Some data on the composition, specific gravity, testing temperature, and ultimate strength (or bending) and on the elasticity modulus are given in Table 2 /24/. It is interesting to point out that the ultimate strength of beryllides is sometimes higher at 1370—1520°C than at 1260°C, probably as a result of brittleness, and that the ultimate strength of some beryllides at such high temperatures is greater than 35—40 kg/mm^2. Therefore, the authors of /24/ believe that the beryllides of these metals can be used up to 1260—1600°C. The high temperature strength of beryllides can be increased by additional alloying.

TABLE 2. Results of bending tests on beryllides

Compound	Specific gravity of specimen, g/cm^3	Testing temperature, °C	Ultimate strength, kg/mm^2	Young's modulus, kg/mm^2	Compound	Specific gravity of specimen, g/cm^3	Testing temperature, °C	Ultimate strength, kg/mm^2	Young's modulus, kg/mm^2
$NbBe_{12}$	2.88	1260	7.4		$ZrBe_{13}$	2.78	1520	8.84	
$NbBe_{12}$	2.86	1260	6.6		$MoBe_{12}$	2.96	1260	29.4	10550
$NbBe_{12}$	2.83	1370	27.6		$MoBe_{12}$	3.02	1370	21.2	8450
$NbBe_{12}$	2.91	1485	>28.6		$MoBe_{12}$	3.02	1370	20.8	7740
$TaBe_{12}$	4.07	1260	34.4	16900	$MoBe_{12}$	3.02	1520	8.85	700
$TaBe_{12}$	4.07	1260	40.5	16900	$MoBe_{12}$	3.02	1520	7.74	
$TaBe_{12}$	4.07	1370	30.2	9850	$TiBe_{12}$	2.29	1260	6.4	
$TaBe_{12}$	4.07	1370	20.4	9150	$TiBe_{12}$	2.29	1260	9.14	4920
$TaBe_{12}$	4.07	1520	18.65	6330	$TiBe_{12}$	2.29	1370	2.46	
$ZrBe_{13}$	2.78	1260	13.0		$TiBe_{12}$	2.29	1370	2.46	
$ZrBe_{13}$	2.79	1370	10.6		$TiBe_{12}$	2.29	1520	1.62	

The high ductility and high strength at elevated temperature is characteristic not only of aluminides and beryllides but also of other inorganic compounds, including refractory oxides.

It is claimed that single crystals of titanium carbide /25/ are ductile at temperatures of from 800 to 2200°C. At 1100°C such crystals can withstand stresses of up to 10 kg/mm^2 without failure, and without the production of slip lines.

It is also claimed that fused aluminum oxide is ductile during creep tests by the bending method at 1000—1100°C.

Refractory metallides such as aluminides, beryllides, borides, carbides, silicides, etc., are very promising for service at elevated temperatures. However, the properties of these compounds for this purpose have so far been very little studied.

CONCLUSIONS

1. Metallides are a special class of inorganic compounds, and have been widely studied for possible use as refractory materials. They have many of the properties of metals: mechanical, physical, chemical, and others.

2. Metallides, in contrast to their components, are more heat resistant and stronger, and retain their properties better at elevated temperatures, than metals or solid solutions.

3. Many metallides have a high resistance to heat and corrosive media. They can be used as protective coatings for metals and alloys which are readily oxidized on heating.

4. Metallides, like other chemical products, can interact with one another. The regularities of the formation of metallide solid solutions and complex compounds have been found.

5. The properties of these compounds and their dependence on the composition are governed by Kurnakov's laws, but in metallide systems the variation in properties is many tens of times greater than in solid solutions of metals.

6. Certain metallides have been found with a ductility sufficient for hot working or sometimes even cold working. These metallides are Ni_3Al, NiTi, Ti_3Al, TiAg, etc.

7. The strength and heat resistance of intermetallic materials can be increased by producing metallide solid solutions and different alloys with dispersed precipitates on the basis of these solid solutions.

8. Metallides and alloys on their basis are important for the production of refractory materials. These compounds include aluminides, beryllides, borides, carbides, silicides, etc. New alloys of great practical interest have been produced on the basis of nickel and titanium aluminides (Ni_3Al, Ti_3Al).

9. It is most important that a number of problems on the heat resistance of these refractory metallides and their use in various fields of the industry should be solved as soon as possible.

Bibliography

1. Kornilov, I.I. Fiziko-khimicheskaya teoriya zharoprochnosti primenitel'no k tugoplavkim metallam (Physicochemical Theory of the Heat Resistance of Refractory Metals).—Sbornik trudov nauchnoi sessii po zharoprochnosti, Izdatel'stvo Nauka. 1966.
2. Kornilov, I.I. Fiziko-khimicheskie osnovy zharoprochnosti splavov (Physicochemical Principles of the Heat Resistance of Alloys).—Izdatel'stvo AN SSSR. 1961.
3. Kornilov, I.I. Metallidy i vzaimodeistvie mezhdu nimi (Metallides and their Interaction with One Another).—Izdatel'stvo Nauka. 1964.
4. Savitskii, E.M. Vliyanie temperatury na mekhanicheskie svoistva metallov i splavov (Influence of Temperature on the Mechanical Properties of Metals and Alloys).—Izdatel'stvo AN SSSR. 1957.
5. Westbrook, J. Mechanical Properties of Metal Compounds. [Russian translation. 1962.]
6. Sinel'nikova, V.S., V.A. Podorgin, and V.N. Rechkin. Alyuminidy (Aluminides).—Kiev, Izdatel'stvo Naukova Dumka. 1965.
7. Samsonov, G.V. Tygoplavkie soedineniya (Refractory Compounds).—Metallurgizdat. 1963.

8. Hansen, M. and K. Anderko. Structure of Binary Alloys. [Russian translation. 1962.]
9. Mints, R.S. Sbornik—Issledovaniya po zharoprochnym splavam (Collection—Investigation of the Heat Resistance of Alloys), 5.—Izdatel'stvo AN SSSR. 1959.
10. Mints, R.S., G.F. Belyaeva, and Yu.S. Malkov. —Izvestiya AN SSSR, Metallurgiya i Gornoe Delo, No. 4. 1963.
11. Chuprina, V.G. Izuchenie struktury i nekotorykh svoistv splavov sistemy $Ni_3Al - Ni_3Nb$ (Investigation of the Structure and Properties of Alloys of the $Ni_3Al - Ni_3Nb$ System). Author's Summary of Candidate Thesis, Kiev. 1966.
12. Poole, D.M. and W. Hume-Rothery. — J. Inst. Metals, p. 173, July 1955.
13. Purdy, G.R. and I.G. Parr. —Trans. Met. Soc. AIME, 221:636. 1961.
14. Buchlera, C.I. and R.C. Wiley. —Trans. Am. Soc. Metals, 55, No. 1. 1962.
15. Buehler, W.I., I.V. Gilfrich, and R.C. Wiley. —J. Appl. Phys., 34:1475. 1963.
16. Dautovich, D.P. and G.R. Purdy. —Canad. Metallurgical Quarterly, 4, No. 2. April-June. 1965.
17. Molchanov, E.K. Atlas diagramm sostoyaniya titanovykh splavov (Atlas of Phase Diagrams of Titanium Alloys). —Oborongiz. 1964.
18. Kornilov, I.I. et al. —Doklady AN SSSR, 161, No. 4. 1965.
19. Matveeva, N.M. Novye issledovaniya titanovykh splavov (New Investigations of Titanium Alloys). — Izdatel'stvo Nauka. 1966.
20. Kornilov, I.I. and T.T. Nartova. Nepreryvnye tverdye rastvory metallidov $Ti_3Al - Ti_3Sn$ v sisteme Ti—Al—Sn (Continuous Solid Solutions of $Ti_3Al - Ti_3Sn$ Metallides in the Ti—Al—Sn System). — Doklady AN SSSR, 140, No. 4. 1961.
21. Kornilov, I.I. and T.T. Nartova. Dlitel'naya prochnost' titanovogo splava na osnove soedineniya Ti_3Al pri 800°C (Long-time Strength of Titanium Alloys on the Basis of Ti_3Al Compounds at 800°C). —Doklady AN SSSR, 148, No. 3. 1963.
22. Thyne, R. van, W. Rostocker, and H. Kessler. —J. Metals, p. 670, May. 1953.
23. Ritter, D.L., B.C. Giessen, and N.J. Grant. —Trans. Met. Soc. AIME, 230:1251, October. 1964.
24. Stonehouse, J., P.M. Pein, and V.V. Beever. Mechanical Properties of Beryllium and Some Other Transition Metals. [Russian translation.]
25. Williams, W.S. and R.D. Schall. —J. Appl. Phys., 33(3):935. 1962.

D.A. Prokoshkin and M.I. Zakharova

ISOTHERMAL SECTIONS OF THE PHASE DIAGRAM OF THE MOLYBDENUM—TITANIUM—ZIRCONIUM SYSTEM AT 1200°C, 900°C, AND 800°C

Molybdenum, titanium, and zirconium have many valuable properties. Alloys prepared from these metals have the necessary physical, chemical,

and mechanical properties for service under normal, low and elevated temperatures. A thorough knowledge of the molybdenum—titanium—zirconium system is necessary for any wide study of these alloys.

The ternary molybdenum—titanium—zirconium system has not yet been investigated, no phase diagram has been constructed, and we have data on only part of the diagram near the titanium apex up to 1.3 at. % of zirconium /1/.

In this work we have summarized the results of a study on the isothermal sections at 1200°C, 900°C, and 800°C, of the molybdenum—titanium—zirconium system.

To construct the diagram, we used 120 alloys represented by 11 sections with a constant content of titanium: 10, 20, 30, 40, 45, 50, 55, 60, 70, 80, and 90 at. % Ti. The composition of the alloys is shown in the concentration triangles. In this article the alloys are designated according to their titanium content (first number) and zirconium content (second number) in atomic percent.

Most alloys were prepared by induction melting in the suspended state in an atmosphere of purified helium (preliminary vacuum of $1 \cdot 10^{-4}$) using a Vogel device /2/. The most heat-resistant alloys containing more than 50% of molybdenum were melted in an arc furnace with a nonconsumable tungsten electrode and a water-cooled copper hearth. The atmosphere was chemically pure argon at a pressure of 150 mm Hg (preliminary vacuum of $1 \cdot 10^{-3}$). Iodide zirconium was used as a getter. The 20—30 g ingots were remelted 6 times.

To prepare the alloys we used the following materials: molybdenum (99.9% pure); iodide zirconium (99.87% pure); and iodide titanium (99.85% pure). The phase composition of the alloys was investigated with preliminarily homogenized and solution heat-treated alloys. The homogenizing annealing was carried out in a vacuum of $2 \cdot 10^{-5}$ mm Hg at 1750, 1600, and 450°C for 50, 100, and 200 hr, respectively, depending on the melting point of the alloy.

For solution heat-treatment the alloys were heated at 800°C and 900°C for 600 and 450 hr, respectively, in double evacuated quartz ampules. To quench from 1200°C, the alloys were held at this temperature for 175 hr in a vacuum furnace, and then placed into a container made of tantalum sheet. The container was held for 25 hr in a double quartz ampule from which the air had been evacuated. The specimens were quenched (from all temperatures) in water by breaking the double quartz ampules.

After the alloys had been quenched they were studied by metallographic and X-ray methods, and the hardness of alloys and microhardness of individual phases were measured.

The X-ray analysis of powdered alloy specimens was carried out in a 57.3 mm diameter Debye chamber, by asymmetric recording of K_α radiation passed through a nickel filter, and in some cases of vanadium irradiation without a filter.

The powder specimens were freed from iron filings by a magnet. The cold-working effect was relieved by annealing. The powder in the double quartz ampule was put into containers made of tantalum sheet. The annealing was carried out at the same temperatures as the solution heat-treatment, and was followed by rapid quenching in water by breaking the external ampule.

The hardness of the alloys was measured by a Vickers tester with a load of 10 kg, and the microhardness by a PMT-3 device with a load of 50 g.

It was found in /3/ and confirmed in /4, 5, 6/ that the phase diagram of the titanium—zirconium system has two regions of unlimited solubility of two modifications of titanium and of zirconium: at elevated temperatures the modification with a body-centered cubic lattice (β-phase) and at low temperatures the modification with a close-packed hexagonal lattice (α-phase).

However, the above works /3, 5 and 6/ are very contradictory on the location of the boundaries of the binary region (α+β). According to the data of /5/, the (α+β)-region is much narrower than that given by the data of Fast /3/.

From an investigation of four alloys at the titanium apex of the diagram, quenched from 700, 600, 575, 525, and 500°C, Ence and Margolin /6/ found that the boundary of the $\beta \rightarrow \alpha$ transformation lies at much lower temperatures, and that the α+β-region is wider than suggested in /5/. The location of the boundaries of the (α+β)-region according to /6/ differs from that given in /3/.

The initial metals used in /3, 5, 6/ were of different degrees of purity. In /3/ the alloys were prepared of iodide titanium and of zirconium. In /5/ titanium and zirconium of commercial purity were used, which had been contaminated by carbon (from 0.38 to 1.85%) when melted in graphite crucibles. The investigations in /6/ were carried out with titanium and zirconium which initially had a Brinell hardness of 63 and 150 kg/mm^2, respectively.

According to our data the boundaries of the (α+β)-region at 800, 750, and 600°C at the titanium apex of the system almost coincide with the boundaries of this region determined by Fast. At the zirconium apex the (α+β)-region is somewhat wider than found in /3/.

Molybdenum greatly stabilizes the β-modification of titanium and therefore the α-phase exists in the molybdenum—titanium system at the titanium apex only, and at 600°C the (α+β)- region stretches to 17 at. % of molybdenum /7, 8/.

The interaction between molybdenum and zirconium differs appreciably from that between the components in the above binary systems. The $ZrMo_2$(δ-phase) compound is formed at 1880°C by a peritectic reaction; at 1520°C a eutectic reaction $L \rightarrow \beta+\delta$ takes place in the system, and at 780°C a eutectoid reaction associated with the polymorphic transformation of zirconium $\beta \rightarrow \alpha+\delta$ /9, 10/.

The isothermal section at 900°C is shown in Figure 1. The X-ray diagrams of alloys 10—0 and 10—2 of the section with 10 at. % of titanium show lines of the β_1-phase (solid solution) only. The X-ray diagrams of the 10—5 alloy show not only strong β_1-lines but also weak lines of the δ-phase. The intensity of the lines of the δ-phase increases with increase in the zirconium content, up to the composition of the 10—35 alloy.

At the same time the intensity of the lines of the β_1-phase decreases, and although the X-ray diagram of the 10—28 alloy still shows faint lines of the β_1-phase, the X-ray diagram of the 10—35 alloy has lines of the δ-phase only. Further increase in the content of zirconium leads to the formation of a β_2-phase (10—40 alloy), and the intensity of the lines of the δ-phase decreases. The 10—85 alloy gives lines of the β_2-solid solution only.

The sharp increase in the hardness as we pass from the 10—0 to 10—28 alloys and the equally rapid decrease on passing to the 10—80 alloy (see table) also confirm the regularity of the variation in the amount of the hardest phase determined by X-ray analysis. The position of the $\beta_1/(\beta_1+\delta)$, $(\beta_1+\delta)/\delta$; $\delta/(\beta_2+\delta)$, and $(\beta_2+\delta)/\beta_2$ phase boundaries was found from the inflections on the curves representing the variation in the [lattice] parameters and hardness of some phases. The position of the phase boundaries was confirmed by a microstructural analysis of the alloys.

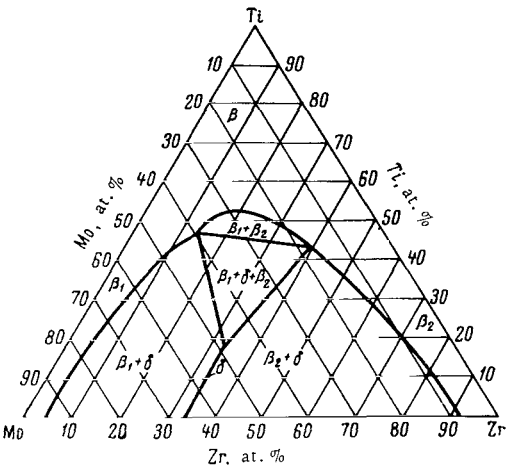

FIGURE 1. Isothermal section at 900°C of the phase diagram of the molybdenum—titanium—zirconium system.

Hardness of alloys investigated

No. of alloy	Hardness, kg/mm²	No. of alloy	Hardness, kg/mm²	No. of alloy	Hardness, kg/mm²	No. of alloy	Hardness, kg/mm²
10—0	240	20—25	670	30—55	352	50—35	350
10—2	315	20—30	690	30—60	330	50—45	330
10—5	400	20—35	680	30—65	315	50—50	305
10—10	514	20—40	600	30—70	305	60—0	375
10—22	705	20—45	525	40—0	425	60—5	375
10—28	745	20—55	422	40—5	408	60—10	385
10—35	720	20—60	378	40—10	390	60—20	380
10—40	615	20—65	355	40—15	485	60—25	370
10—45	535	20—70	320	40—20	515	60—35	302
10—50	485	20—75	265	40—30	415	60—40	324
10—55	435	20—80	320	40—40	385	70—0	360
10—60	390	30—0	450	40—45	330	70—5	340
10—65	360	30—2	435	40—50	327	70—15	330
10—70	340	30—8	435	40—60	305	70—25	285
10—80	310	30—15	535	50—0	410	70—30	335
10—85	325	30—20	580	50—5	425	80—0	280
10—90	290	30—25	590	50—10	440	80—5	305
20—0	350	30—30	535	50—15	465	80—10	295
20—2	430	30—35	515	50—18	450	80—15	280
20—5	515	30—40	460	50—20	430	80—20	345
20—12	570	30—45	425	50—25	375		
20—18	618	30—50	385	50—28	358		

We should point out that the β-phase lying along the zirconium—titanium side of the diagram is not formed in the alloy on quenching.

This confirms that the alloys are essentially free of gaseous impurities, since it has been found /11/ that the amount of residual β-phase in this system decreases with decrease in the content of nitrogen and oxygen impurities.

An X-ray analysis of alloys belonging to the section with 20 at. % of titanium showed that the 20—12, 20—18, and 20—25 alloys contain β_1- and δ-phases.

X-ray photographs of the 20—30 alloy show lines of the δ-phase only. The 20—35, 20—40, 20—45, 20—50, 20—55, 20—60, and 20—65 alloys contain β_2- and δ-phases.

Lines of a β_2-solid solution only were found on the X-ray photographs of 20—70 and 20—75 alloys. These data were confirmed by microstructural studies and by hardness measurements (see table). The boundaries of the $(\beta_1+\delta+\beta_2)$ three-phase regions in the given section were fixed by extrapolating the experimental results for sections with 30, 40, and 45 at. % of titanium. The three-phase region in the ternary system is shown on the isothermal section as a triangle. The sides of the triangle $(\beta_1+\delta+\beta_2)$, which were accurately determined on the above three sections, were prolonged to intersect at a point on the line of formation of the δ-phase. This point determines the composition of the δ-phase which is part of the three-phase region. The two other apexes of the three-phase triangle give the compositions of the β_1- and β_2-phases.

In this section the [lattice] parameter of the β_2-phase changes, within the limits of the binary $(\beta_2+\delta)$-region more sharply (from 3.366 kX in the 20—35 alloy to 3.468 kX in the 20—70 alloy) than in the same phase region of the section with 10 at. % of titanium (from 3.498 kX in the 10—40 alloy to 3.516 kX in the 10—80 alloy). This indicates an increase in the slope of the conoid $\delta-\beta_2$ from the molybdenum—zirconium side to the zirconium—tianium side.

The 20—30 alloy has the highest hardness, equal to 690 kg/mm², which is however 60 units lower than the maximum hardness of alloys of the section with 10 at. % of titanium, although the amount of the second phase (β_1-solid solution) in the 20—30 alloy (only the δ-phase could be found by X-ray analysis) is lower than in the 10—28 alloy. X-ray analysis showed the existence of δ- and β_1-phases. The hardness of the 10—28 alloy is equal to 750 kg/mm². This is apparently because the δ-phase somewhat changes its composition in the 20—30 alloy due to substitution of molybdenum atoms by titanium ones. This was confirmed by the position of region of the δ-phase on the isothermal section.

The 20—80 alloy is harder than the ternary solid solution of the 20—75 alloy (see Table 1). This can be explained by the metastable state of the 20—80 alloy (α-phase). The hardness of the 20—80 alloy is equal to 320 kg/mm², and that of the 20—75 alloy to 265 kg/mm².

The $(\beta_1+\delta+\beta_2)$ three-phase region in the section with 30 at. % and in the section with 40 at. % (see Figure 1) was determined from the presence of lines of lattices of 3 phases on the X-ray photographs of 30—30 and 40—30 alloys, and from the constant parameters of the δ-, β_1'-and β_2-phases of the 30—25, 30—35, and 40—20 alloys. The parameters of the δ, β_1-and β_2-phases in this region are equal to 7.596, 3.248, and 3.364 kX, respectively.

The homogeneous region of the ternary β-solid solution stretches into the ternary system from the molybdenum—titanium and titanium—zirconium binary systems, and covers a considerable area of the concentration triangle. At 52 at. % of titanium and 20 at. % of zirconium the β-solid solution decomposes into two solid solutions, β_1 and β_2. X-ray photographs of alloys containing ($\beta_1 + \beta_2$)-phases show two systems of lines of a body-centered lattice, but with different lattice parameters.

The boundaries of this binary phase field were determined from the inflections on the curves of lattice parameters and of hardness of the section with 45 and 50 at. % of titanium.

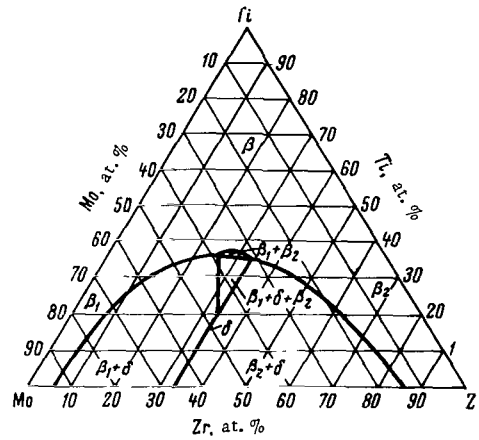

FIGURE 2. Isothermal section at 1200°C of the phase diagram of the molybdenum—titanium—zirconium system.

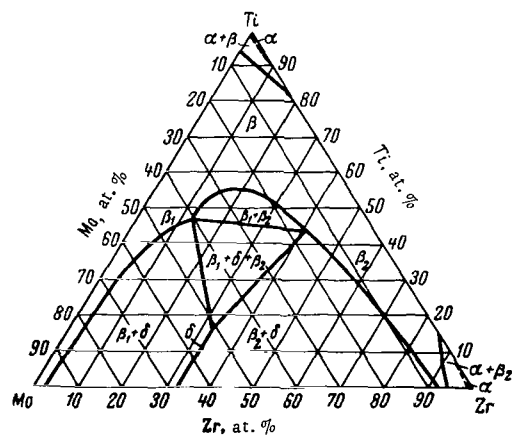

FIGURE 3. Isothermal section at 800°C of the phase diagram of the molybdenum—titanium—zirconium system.

Thus, from the side of the titanium apex of the system the ternary phase ($\beta_1+\delta+\beta_2$) triangle is limited by a binary phase region which is the result of the decomposition of the ternary solid solution into β_1- and β_2-phases.

The region of the ternary solid solution becomes wider as the temperature increases. Thus, at 1200°C (Figure 2) the homogeneous field of the β-phase occupies a large part of the concentration triangle. The solid solution decomposes at a content of 37 at. % cf titanium and of 20 at. % of zirconium.

The nature and the number of phase regions at 1200°C are the same as at 900°C.

The titanium and zirconium apexes of the isothermal section at 800°C (Figure 3), which is located in the temperature range below the polymorphic transformation of titanium and zirconium, has not only the phase regions which exist at 1200 and at 900°C, but also a region of an α-solid solution based on close-packed hexagonal modifications of titanium and zirconium, and also binary-phase ($\alpha+\beta$)- and ($\alpha+\beta_2$)-regions.

CONCLUSIONS

We constructed isothermal sections at 1200, 900, and 800°C for molybdenum—titanium—zirconium systems from data of X-ray structural and microstructural analyses, and also from hardness and microhardness measurements of specimens quenched from an equilibrium state at the above temperatures.

1. We found that a large homogeneous region of a ternary β-solid solution exists at 800, 900, and 1200°C. As the temperature is increased, this region increases, and at 1200°C it occupies a large part of the concentration triangle. This indicates a considerable variation in the mutual solubility of molybdenum, titanium, and zirconium with temperature.
2. The phase based on the $ZrMo_2$ intermetallic compound can dissolve up to 21 at. % of titanium. But this phase has no large region of homogeneity at either the molybdenum on zirconium side.
3. We found that this system contains 5 two-phase regions which are adjacent to the regions of the ternary β-solid solution, and to the regions of the α-solutions. We also proved the existence of one three-phase region, which consists of a phase based on $ZrMo_2$ and β_1- and β_2-solid solutions.

Bibliography

1. Kornilov, I.I., V.S.Mikheev, and O.K.Belousov. Sbornik—Titan i ego splavy (Collection—Titanium and its Alloys), p. 120.—Izdatel'stvo AN SSSR. 1962.
2. Fogel', A.A.—Izvestiya AN SSSR, OTN, Metallurgiya i Toplivo, 2:24. 1959.
3. Fast, Y.D.—Rev. trav. Chim., 58:973. 1939.
4. Duwez, P.—J. Inst. Metals, 80:525. 1952.
5. Hayes, E.T., A.H.Roberson, and O.G.Paasche.—U.S.Bur. Mines. Rep. Invest., No. 4826. 1951.
6. Ence, E. and H.Margolin.—Trans. Met. Soc. AIME, 221(1):205. 1961.

7. Hansen, M., E. L. Kamen, H. D. Kessler, and D. Y. McPherson.—J. Metals, 3(10):881. 1951.
8. Duwez, P.—Trans. Met. Soc. AIME, 191:765. 1951.
9. Domagala, R. F., D. Y. McPherson, and M. Hansen.—Trans. Met. Soc. AIME, 197:73. 1953.
10. Duwez, P. and C. B. Jordon.—J. Amer. Chem. Soc., 73:5509. 1951.
11. Natt, B. A. and G. I. Williams.—Acta Met., 7, No. 10. 1959.

A. M. Yakimova

STUDY OF THE PROPERTIES OF MOLYBDENUM MODIFIED BY REFRACTORY COMPOUNDS AT ELEVATED TEMPERATURES

Molybdenum and molybdenum-base alloys are very promising constructional materials for service at temperatures above 1200°C. This metal has a number of very valuable properties: high melting point, high thermal conductivity, low coefficient of thermal expansion, and considerable high-temperature strength. However, molybdenum and its alloys with titanium, zirconium, tantalum, etc., have poor technological properties (poor weldability, high threshold of cold shortness), and therefore new multiphase alloys obtained by alloying pure molybdenum with refractory compounds should be developed and studied.

By correct choice of the phase and its amount, it is possible to regulate the technological and service properties of alloys based on refractory metals over wide limits.

In this work we studied the influence of refractory compounds (ZrC, ZrN, and ZrB_2) on the properties of molybdenum at room and elevated temperatures. The molybdenum—refractory compound alloys were prepared in a vacuum arc furnace of the TsEP-374 type. The refractory compounds were added to molybdenum during the melting process. At the same time we also prepared a 10 kg master ingot of molybdenum with no additions. The ingots were then pressed and rolled on a vacuum rolling mill into 1 mm thick strips. The chemical compositions of the alloys and their mechanical properties at room temperature are given in the table. Cold-worked and recrystallized alloys were studied. The annealing process was as follows: heating to 1800°C at the rate of 140°C/min with no soaking time.

Mechanical properties of molybdenum—refractory compound alloys

Alloy	Initial state	σ_B, kg/mm^2	δ, %	Alloy	Initial state	σ_B, kg/mm^2	δ, %
Mo	Cold worked	42	7.1	Mo—0.5%	Cold worked	81.5	9.0
Mo—0.1%	Cold worked	49.0	3.5	ZrN	Recrystallized	44.5	4.2
ZrC	Recrystallized	41.5	5.5	Mo—0.1%	Cold worked	78.5	12
Mo—0.5%	Cold worked	60.0	7.8	ZrB_2	Recrystallized	52.0	14.2
ZrC	Recrystallized	41.0	4.5	Mo—0.5%	Cold worked	21.0	6.8
Mo—0.1%	Cold worked	73.0	10.7	ZrB_2	Recrystallized	19.0	1.5
ZrN	Recrystallized	46.0	6.0				

The data in the table show that alloys containing refractory compounds (ZrC, ZrN and ZrB_2) have a higher strength at room temperature than pure molybdenum but about the same ductility. It is interesting to point out that the strength and ductility of the Mo—0.1% ZrB_2 alloy are about twice as high as those of pure molybdenum. However, a further increase in the content of $ZrBr_2$ to 0.5% leads to premature brittle failure of the alloy.

The recrystallization of experimental alloys was studied at 1000—1800°C by hardness measurements and metallographic analysis. The holding times during annealing were 1 hr and 5 hr. The results are given in Figure 1. The data in Figures 1, a and 1, b indicate that a longer holding time during the annealing of molybdenum—carbide and molybdenum—nitride alloys leads to a greater softening of the alloy.

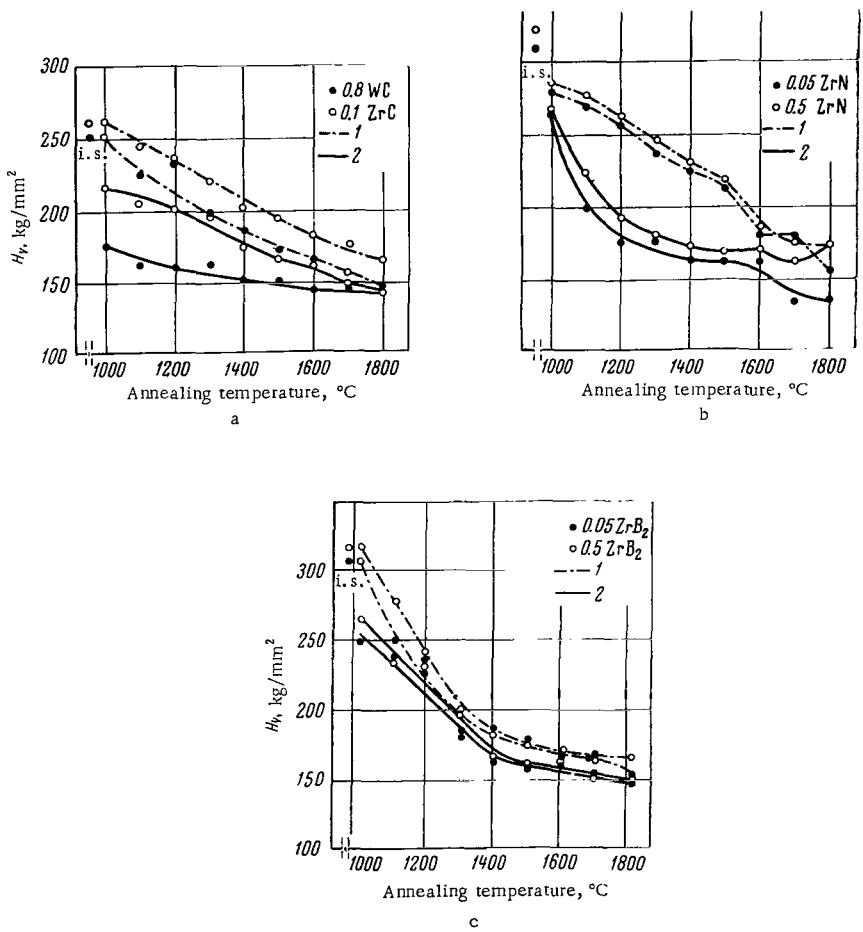

FIGURE 1. Dependence of hardness on the annealing temperature and annealing time of alloys (P = 10 kg): a—Mo—ZrC; b—Mo—ZrN; c—Mo—ZrB_2; i.s.—hardness of alloy before annealing. 1—holding time during annealing 1 hr; 2—5 hrs.

The Mo—ZrB_2 alloys do not lose strength when heated for these periods (1 and 5 hr). A comparison of the data on the dependence of hardness on temperature shows that the alloys of the molybdenum—boride system are the most stable.

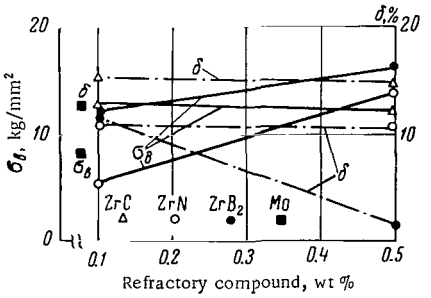

FIGURE 2. Mechanical properties of molybdenum—refractory compound alloys at 1500°C.

A study of the mechanical properties of molybdenum—refractory compound alloys at 1500°C (Figure 2) shows that the strength of the experimental alloys is about 1.5 times greater than that of the initial molybdenum, but the ductility remains the same. An exception is the Mo—0.5% ZrB_2 alloy which becomes very embrittled.

The above metallographic investigation showed that the temperature of recrystallization is increased by the addition of refractory compounds to molybdenum. The maximum temperature of recrystallization is exhibited by Mo—ZrB_2 alloys (Figure 3).

CONCLUSIONS

1. The addition of ZrC and ZrN in amounts of 0.1—0.5 wt % increases the strength of molybdenum without reducing its ductility at room temperature.

2. The addition of 0.1% ZrB_2 to molybdenum causes its strength and ductility to be doubled at room temperature. A higher content of ZrB_2 (0.5%) leads to a premature brittle failure of the alloy.

3. A study of the recrystallization of molybdenum—carbide, molybdenum—nitride, molybdenum—boride alloys at 1000—1800°C by hardness measurements and by a metallographic analysis showed that molybdenum is strengthened more by ZrC than by WC.

Molybdenum—carbide and molybdenum—nitride alloys lose much of their strength if the annealing time is increased. Mo—ZrB_2 alloys lose less of their strength with increase in the holding time of annealing than alloys of the molybdenum—carbide and molybdenum—nitride systems.

4. It has been found that the addition of 0.1—0.5% ZrC, 0.1—0.5% ZrN, and 0.1% ZrB_2 increases the short-time strength of molybdenum at 1500°C by one and a half times. Such alloying has no influence on the ductility of molybdenum.

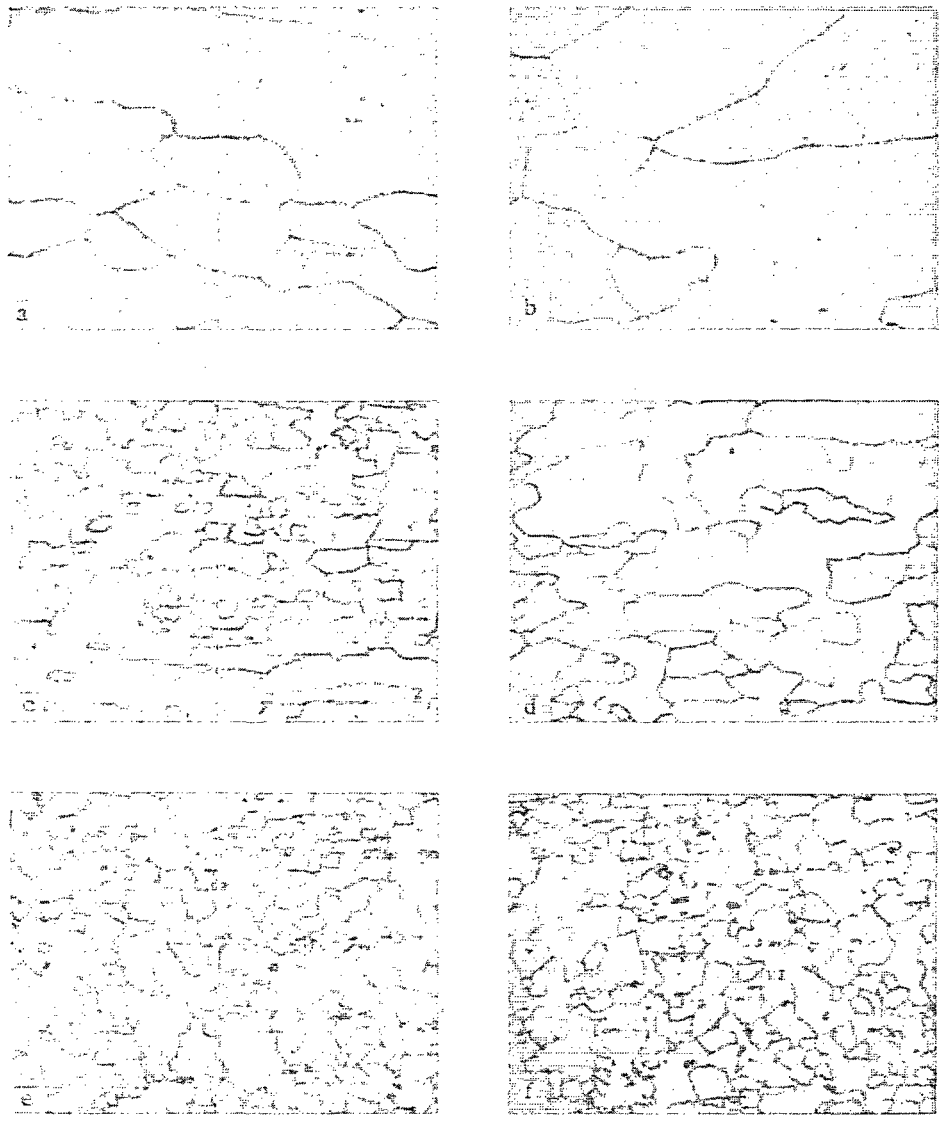

FIGURE 3. Microstructure of molybdenum (a, b), of Mo—0.5% ZrN (c, d) and of Mo—ZrB_2 (e, f) alloys at 1500°C:

a, b, c—holding time 1 hr; d, e, f—holding time 5 hr, ×200.

If the content of ZrB_2 in molybdenum is increased to 0.5%, the alloy is greatly embrittled.

5. It has been found that the strength and ductility of molybdenum at room and elevated temperatures is favorably influenced by the following compounds:

a) ZrN—0.1%; b) ZrB_2—not more than 0.1%; and c) ZrC—up to 0.5%, over the concentration range studied.

V. K. Grigorovich

ELECTRON STRUCTURE AND CRYSTAL STRUCTURE OF TRANSITION METALS

In his book "The Structure of Iron Alloys" /1/ Hume-Rothery pointed out that the theory of alloys has not yet been completely clarified, and that we have no clear understanding of the factors which lead to the stabilization of body-centered cubic α-solid solutions by many elements which have no such structure (Al, Si, P, etc.). "The absence of any well-developed theory on alloys will not appear so unexpected if we consider that today we have no single reliable quantitative theory on the structures of even pure transition metals." During the period from 1958 to 1962, we developed a theory /2, 3—5/ which states that the body-centered cubic structure of metals is the result of the overlap of the p-orbitals of their atomic shells, and of the formation of six exchange bonds directed along the edges of the body-centered cubic cell. The polymorphism of iron has been explained by this theory in /6/. The influence of the electron structure of alloying elements on the widening of the regions of α- and γ-solid solutions in iron alloys is discussed in detail in /7/.

Since the valency electrons in metals are collective, they cannot explain the directional bonds in the body-centered cubic lattices. We must therefore apply the modern theory of valency, underlying the quantum theory of the chemistry of molecules, to the physics of metals based on the conception of conductivity electrons interacting with the periodic field of the crystal lattice.

The Schrödinger wave equation for a single electron approximation for the central field of an atom can be written as

$$\frac{h^2}{8\pi^2 m}\left(\frac{\partial^2\Psi}{\partial x^2}+\frac{\partial^2\Psi}{\partial y^2}+\frac{\partial^2\Psi}{\partial z^2}\right)+(E-V)\Psi=0$$

or

$$\frac{h^2}{8\pi^2 m}\nabla^2\Psi+(E-V)\Psi=0,$$

where E is the total energy of the particle with a mass m; V is its potential energy, and ψ is a wave function. The solution of this formula for an electron on the s-level will give a spherically symmetric wave function $\psi_{ns}=R_{ns}(r)$, while the solution of this equation for electrons on the p-level

will give dumbbell wave functions of ψ_{p_x}, ψ_{p_y} and ψ_{p_z} which are aligned along three axes of rectangular coordinates

$$\psi_{np_x} = \sqrt{\frac{3}{4\pi}} R_{np}(r) \sin\theta \cos\varphi,$$

$$\psi_{np_y} = \sqrt{\frac{3}{4\pi}} R_{np}(r) \sin\theta \sin\varphi,$$

$$\psi_{np_z} = \sqrt{\frac{3}{4\pi}} R_{np}(r) \cos\theta.$$

The probability density of finding electrons $|\psi|^2$ in the s-state has the shape of a spherical layer, and for the p_x, p_y and p_z states this density has the shape of three dumbbells meeting at a common center and extending along three axes of the coordinates. The electrons of shell p^6 also form extended electron clouds consisting of combined dumbbells produced by two coupled electrons with antiparallel spins.

The main type of valence bonds in molecules and crystals of the diamond-type is the two-electron exchange bond of the σ-type. An accurate quantitative theory of this has been developed for the H_2 molecule by Gaitler and London, and then extended to other molecules and covalent crystals by Pauling, Millikan, Slater, et al. The solution of Schrödinger's equation for a hydrogen molecule consisting of 1, 2 protons and 1, 2 electrons

$$\frac{h^2}{8\pi^2 m}\left(\frac{\partial^2\psi}{\partial x_1^2} + \frac{\partial^2\psi}{\partial y_1^2} + \frac{\partial^2\psi}{\partial z_1^2} + \frac{\partial^2\psi}{\partial x_2^2} + \frac{\partial^2\psi}{\partial y_2^2} + \frac{\partial^2\psi}{\partial z_2^2}\right) -$$
$$- e^2\left(\frac{1}{r_{1a}} + \frac{1}{r_{2b}} + \frac{1}{r_{1b}} + \frac{1}{r_{2a}} - \frac{1}{r_{12}} - \frac{1}{R}\right)\psi = E\psi$$

leads to an exchange integral

$$K = e^2 \iint \psi_a(1)\,\psi_b(1)\left\{\frac{1}{R} + \frac{1}{r_{1,2}} - \frac{1}{r_{1b}} - \frac{1}{r_{2a}}\right\}\psi_a(2)\,\psi_b(2)\,d\tau_1 d\tau_2,$$

which indicates a strong exchange directional bond of two atoms of hydrogen with electrons with antiparallel spins. The formation of covalent bonds in crystals of elements of groups VII—IV is determined by the number of unpaired coupling electrons which is equal to the number of the nearest neighbors of each atom. In halogens and in elements of the oxygen, nitrogen, and carbon subgroups, the numbers of unpaired p- and s-electrons and the coordination numbers are equal to 1, 2, 3, and 4, respectively.

The existence of close-packed cubic and hexagonal structures of metals can be explained by the random interaction of spherically symmetric ions with almost free or collective valence electrons. The exchange directional bonds existing in body-centered cubic metals prevent the atoms from becoming close-packed, despite their interaction with the electron gas. Since the valence electrons in the metals are collective, the natural explanation for the origin of body-centered cubic structures lies in the exchange interaction of subvalent electrons of the external shells of ions which have an inert gas configuration (s^2p^6). The activity of the filled shells and the ability of their p-orbitals to form exchange bonds are now widely

known, and are being confirmed by the developing chemistry of the inert gases Kr, Xe, Rn, etc. Numerous compounds of these elements with fluorine, and oxygen, and also salts, bases, acids, complex compounds, clathrate hexahydrates, etc., are well known. The fluorides have the following formula: KrF_2, KrF_4, XeF_2, XeF_4, XeF_6, and RnF_6. Oxides XeO_3 and XeO_4 are also known. All paired electrons of the p^6-shell of xenon take part in the formation of six octahedrally oriented bonds with six atoms of fluorine during the formation of hexafluorides. The transition of six electrons from xenon to fluorine atoms is impossible, since the sum of the ionization potentials of p-electrons is equal to 25 ev or 5750 kcal/mole, which is two orders of magnitude higher than the heat of formation of XeF_6 (79 kcal/mole). The $p-d$-hybridization is also forbidden, since the transition of three p-electrons into the vacant d-orbits of xenon is energetically impossible. Consequently, the spin fission of all six p-orbitals and the formation of six asymmetric p-electrons able to form σ-bonds is the only real possibility of forming bonds. The exchange reaction of these electrons with one of the unpaired p-electrons of six atoms of fluorine leads to the formation of an octahedral molecule XeF_6 (Figure 1). The strong shift of p-orbitals from xenon atoms to fluorine yields Xe^+ and F^- charges and an additional ionic component in this essentially covalent compound. The formation of two-electron bonds by p-electrons of the external filled p^6-shells takes place in all compounds of inert gases. The energy of these covalent bonds is extraordinarily high ($\Delta H^0_{298} = 79$ kcal/mole for XeF_6) and is commensurable with the heat of sublimation of the most heat-resistant body-centered cubic metals ($\Delta H_{subl} = 201.9$ kcal/g-atom for W). This

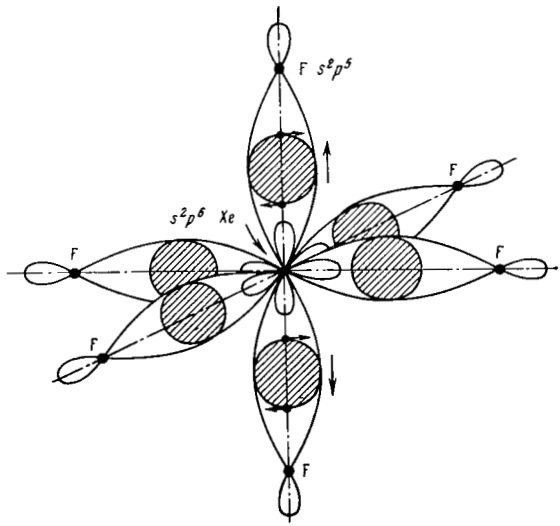

FIGURE 1. Formation of hexafluorides of inert gases as a result of the fission of p-orbitals in the filled external p^6-shell, and of the formation of six interchangeable valence two-electron bonds directed along the axes of rectangular coordinates:

Energy of formation of valence bonds ($-\Delta H°_{298}$): 37 kcal/mole for XeF_2; 60 for XeF; 79 for XeF_6.

indicates that the participation of covalent energy in the total energy of the lattices of body-centered cubic metals is quite considerable.

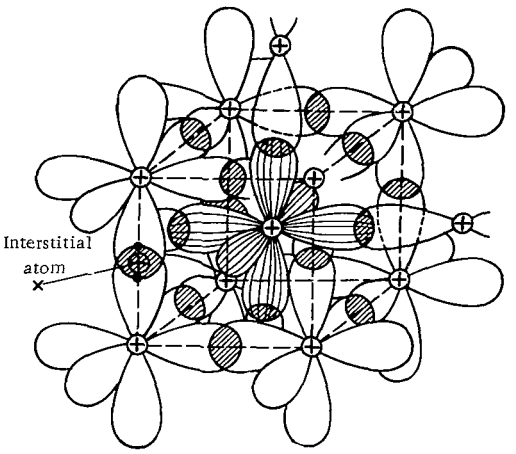

FIGURE 2. Formation of body-centered cubic structures of alkali, alkaline-earth, refractory *d*-transition metals of groups III—VI, lanthanides and actinides. This is the result of the overlap of external p^6-shells of ions during the reaction of ions with collective electrons, which leads to the formation of additional exchange covalent and orthogonally directed σ-bonds of the *p*-orbitals.

Let us now consider the problem of the origin of the body-centered cubic structures of metals of the longer periods, including refractory metals of groups IV—VI. The Hall coefficient of solid potassium, rubidium, and cesium, at 20°C indicates that their only valence *s*-electron is a conduction electron, i.e., the concentration of collective almost free electrons is equal to 1 electron/atom. This means that the free atoms of alkali metals with an external $s^2p^6s^1$ shell are transformed into Me^+ ions with an external p^6-shell during association into a crystal. This external shell of inert gases has an orthogonal symmetry and consists of six *p*-orbitals. These undergo spin fission as they approach neighboring atoms, with increase in the asymmetry and length of the *p*-orbitals, and with the formation of six exchange two-electron orthogonal bonds as a result of overlap. The shortening of the distances between ions with p^6-shells as a result of interaction with an electron gas leads to overlap of the external parts of the *p*-orbitals and the formation of six exchange valence σ-bonds directed along the axes of rectangular coordinates. This leads to the formation of a primitive cubic cell with another ion in the vacant center. The *p*-orbitals of this form bonds with similar ions in six neighboring cells (Figure 2). This mechanism leads to the formation of the body-centered cubic structures of potassium, rubidium, and cesium, in which the energy of the lattice is derived mainly from the metallic interaction between the conductivity electrons and ions, but also from the covalent exchange σ-bonds of the subvalent electrons of the external p^6-shells of ions which determine the crystal structure. The Hall coefficient indicates that solid

alkaline-earth metals, calcium, strontium, and barium, which have an external configuration of $s^2p^2s^2$, and their compounds form Me^{2+} ions with an external p^6-shell. The same mechanism leads to the formation of a body-centered cubic structure in the high-temperature modifications of β-calcium, and β-strontium, and body-centered cubic structure of barium. The assumption that all valence electrons in metals of groups III—VI, including all lanthanides and actinides, are collective indicates that the ions of these metals in the lattice have external p^6-shells. The approach and overlap of these as a result of the metallic interaction between ions with collective electrons will lead to the formation of additional exchange bonds directed along the edges of the cube <100>, and to the formation of body-centered cubic structures characteristic of these metals or of their high-temperature modifications. The valence electrons in this case are considered to be collective, i.e., they belong to the lattice as a whole. However, they are in no case free electrons, even in alkali metals, and they react with the lattice more strongly with increase in their concentration and decrease in the dimensions of the ions. As we pass from alkali metals to Ca, Sr, Ba, and then to Cr, Mo, and W, the concentration of electrons responsible for the interaction between the metals increases from 1 to 6 electrons/atom, and their effective mass m^* increases so much as the result of their reaction with ions that the effective number of conduction electrons is considerably less than the number of collective valence electrons. The collective heavy electrons in the transition metals occupy quite a wide d-band and a very wide s-band, forming an energy spectrum which determines the electron and many other physical characteristics of metals. The electrons in the d-band are more strongly bound to the lattice than the freer electrons of the s-band. However, none of these is localized in the atoms but they are collective. From the body-centered cubic, face-centered cubic and close-packed hexagonal lattices, which we know from X-ray studies, it is possible to construct Brillouin zones for individual metals, and to calculate the distribution of electrons along the zones to determine the energy model of a given metal. The zone model alone does not explain the formation of a lattice, and the theory of the origin of crystal structures should start from a theory on the shape and interaction between atomic orbitals, as in quantum chemistry, to explain the structure of molecules. For body-centered cubic metals, and also for diamond, silicon, and germanium, it is possible to explain the origin of the crystal lattice by the hypothesis of interchangeable σ-bonds, and then proceed further to the construction of a zone model and of an energy spectrum of the electrons. Consequently, we should consider the formation of body-centered cubic structures in all metals to be the result of exchange reactions between subvalent p-electrons of the external p^6-shells of ions.

All energy characteristics of the lattice and the strength of interatomic bonds increase from 1 to 6, according to the increase in the number of collective electrons responsible for the metal bonds and to decrease in the atomic radius, as we pass from alkali metals to metals of group VI. The thermodynamic and physical properties of body-centered cubic metals of groups I—VI are given below:

Group	I	II	III	IV	V	VI
	K^1	Ca^2	Sc^1	Ti^4	V^5	Cr^6
Metal radius						
r_{met}, Å	2.35	1.97	1.62	1.47	1.34	1.27
t_{mp}, °C	63.7	838	1539	1668	1900	1920
t_{bp}, °C	760	1440	2730	3260	3450	2668
ΔH_{mp}, kcal/g-atom	0.143	0.218	0.015	0.024	0.04	0.078
ΔH_{bp}, kcal/g-atom	18.9	36.74	81	106.5	106	72.97
x, electronegative	0.8	1.0	1.3	1.5	1.6	1.6
d, g/cm³	0.86	1.55	3.0	4.51	6.1	7.19
E, kg/mm²				9000	13,500	25,000
H_v, kg/mm²				60	80	100
	Rb^1	Sr^2	Y^3	Zr^4	Nb^5	Mo^6
Metal radius						
r_{met}, Å	2.48	2.15	1.80	1.60	1.46	1.39
t_{mp}, °C	38.9	708	1509	1852	2415	2610
t_{bp}, °C	688	1380	2927	3580	3300	5560
ΔH_{mp}, kcal/g-atom	0.55	2.1	2.7	4.0	6.4	6.6
ΔH_{bp}, kcal/g-atom	18.1	33.8	93	120	—	128
x, electronegative	0.8	1.0	1.3	1.4	1.6	1.8
d, g/cm³	1.53	2.6	4.47	6.49	8.4	10.2
E, kg/mm²				8960	9080	33,000
H_v, kg/mm²				67	80	150
	Cs^1	Ba^2	La^3	Hf^4	Ta^5	W^6
Metal radius						
r_{met}, Å	2.67	2.22	1.87	1.58	1.46	1.39
t_{mp}, °C	28.7	714	920	2222	2996	3410
t_{bp}, °C	690	1640	3470	5400	5425	5930
ΔH_{mp}, kcal/g-atom	0.5	1.83	1.5	5.2	6.8	8.05
ΔH_{bp}, kcal/g-atom	16.3	35.7	96	155	180	185
x, electronegative	0.7	0.9	1.1	1.3	1.5	1.7
d, g/cm³	1.90	3.5	6.17	13.1	16.6	19.3
E, kg/mm²				9800	188.30	41,500
H_v, kg/mm²				160	125	290
Electron configuration	$p^6—s^1$	$p^6—s^2$	$p^6—d^1s^2$	$p^6—d^2s^2$	$p^6—d^3s^2$ $p^6—d^4s^1$ (Nb)	$p^6—d^5s^1$ $p^6—d^4s^2$ (W)
Crystal structure	BCC	β-BCC α-FCC	(γ La-BCC) (β La-FCC) β-BCC α-CPH	β-BCC α-CPH	BCC	BCC

In fact, the melting point, boiling point, heats of fusion and sublimation, moduli of elasticity, hardness, strength, and other properties of body-centered cubic metals increase as we pass from group I to VI. As we pass further to metals of the copper subgroup, these characteristics decrease down to group I as a result of the decrease in the number of collective electrons and ionic charges:

I	II	III	IV	V	VI	VII	VIII	I
K^1	Ca^2	Sc^3	Ti^4	V^5	Cr^6	Mn^1	$Fe^2Co^2Ni^2$	Cu^1
Rb^1	Sr^2	Y^3	Zr^4	Nb^5	Mo^6	Tc^5	$Ru^4Rh^3Pd^2$	Ag^1
Cs^1	Ba^2	La^3	Hf^4	Ta^5	W^6	Re^5	$Os^4Ir^3Pt^2$	Au^1

The variation in the properties of transition metals over long periods confirms our hypothesis.

Direct experimental proof that all valency electrons in the body-centered cubic lattices of metals of group I—VI are collective is their paramagnetism, i.e., the absence of any magnetic moments in atoms due to the collectivization of all *d*- and *s*-electrons. Magnetic neutronographic studies of all metals of groups I—VI, including vanadium, showed no traces of *d*-electrons in the atoms, and only chromium has antiferromagnetic properties below 39°C as a result of partial localization of *d*-electrons. However, above 39°C all *d*- and *s*-electrons of chromium are delocalized, and this metal has paramagnetic properties and a body-centered cubic structure up to the melting point. The collectivization of all valence *d*-, *s*-electrons in metals of groups I—VI is confirmed by Matthiessen's rule, since all these electrons are taken into account during the calculation of the electron concentration of superconductive alloys.

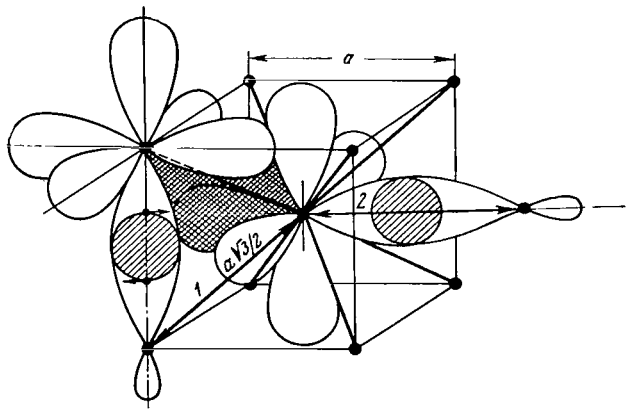

FIGURE 3. Nature of interatomic bonds in body-centered cubic metals:

1—metal bond between central atom and the eight nearest neighbors, located in the directions [111], at a distance of 0.86 a ($K = 8$) as a result of the concentration of electron gas in the interionic space along the eight octants; 2—covalent, exchange, and orthogonally directed bonds along [110] of the central atom with six neighboring atoms at a distance a ($K = 6$).

We shall see whether the bonds of the central atom with its neighbors of the first and second coordination spheres are equivalent. The central atom in a body-centered cubic cell neighbors on eight other atoms ($K_1 = 8$) located at the vertices of a cube at a distance of $a\sqrt{3/2} = 0.86\,a$, and with six other atoms of the second spheres ($K_2 = 6$), located along the axes of the coordinates at distances a. The interaction between the central atom and its neighbors of the first and second spheres is of a different nature, although the differences in the distance are only 14%. The collective electrons which lie in the interionic space in the middle part of the eight octants which are not occupied by the orbitals (Figure 3) are responsible for the metallic interaction of the central atom with its eight nearest neighbors in the direction of the space diagonals. The central atom is

connected to the six electrons of the second coordination sphere by six exchange 2-electron directed bonds of a covalent type. Thus, the interaction between mobile ions and collective electrons in metals, which leads to the ductility and elasticity of metals with a body-centered cubic lattice, is superimposed by more rigid covalent bonds <100> directed along the edges of the cube. If the overlap of orbitals is sufficiently great, this can lead to a reduction in ductility, and under unfavorable conditions of deformation to embrittlement of these metals.

What experimental data prove the existence of directed bonds in body-centered cubic metals? Firstly there are data on the anisotropy of the elasticity moduli in single crystals. In fact, in the cubic structures of diamond, silicon, and germanium, and in the diamond-like compounds of the $A^{III}B^{V}$ -type, the coefficient of anistropy $A = \frac{2C_{44}}{C_{11} - C_{12}} > 1$ (table), and therefore, $E_{<111>} > E_{<100>}$, which means that the diamond-type lattice is most rigid in the direction of the exchange valence bond aligned along the space diagonal of the cube <111>. According to the data in /8/, the ratio of Young's moduli $E_{<111>}/E_{<100>}$ for silicon and germanium is equal to 1.465 and 1.485, respectively, which means that Young's modulus in the direction of the valence bond is 1.5 as great as in the <100> direction. For alkali metals with a body-centered cubic lattice, Young's modulus in the direction of the space diagonal is 6.3—9.4 greater than in the direction of the <100> edge (see Table 2), which indicates that in metals with a body-centered cubic lattice the energy of the elastic metallic bond plays a considerably greater role than that of the exchange bonds. The coefficient of anisotropy decreases appreciably as we pass to metals of the Vth and VIth groups. For vanadium, niobium, chromium, and molybdenum this coefficient is less than unity, and for tungsten it is equal to unity. This indicates an increasing overlap of the orbitals in polyvalent metals, and the predominant role of the covalent bonds in these overlaps, which lead to an increased susceptibility to cold shortness.

Coefficient of anistropy of elastic moduli (A) of body-centered cubic metals and the critical ductile—brittle transition temperature, (t_{cr}) /8—11/

C diamond	Li[1]					
1.214	9.4					
Brittle	Plastic					
Si	Na[1]					
1.666	8.1					
Brittle	Plastic					
Ge	K[1]	Ca	Sc	Ti	V	Cr
1.665	6.3	—	—	—	0.79	0.86
Brittle	Plastic	Plastic	Plastic	Plastic	Brittle from —110 to —65°C	Brittle from —20°C to + 200°C
Element	Rb[1]	Sr	Y	Zr	Nb	Mo
A	8.9	—	—	—	0.51	0.76
t transition temperature, °C	Plastic	Plastic	Plastic	Plastic	Plastic	Brittle from —200°C to + 300°C
Element	Cs[1]	Ba	La	Hf	Ta	W
A	8.6	—	—	—	1.6	1.0
t transition temperature, °C	Plastic	Plastic	Plastic	Plastic	Plastic	Brittle from + 200°C to + 450°C

Yound's modulus is highest along the less close-packed edges of the body-centered cubic cell <100> and not along the most close-packed rows <111>. This conflicts with the model of rigid spherical atoms, and the elastic anisotropy of such cells must be explained by the theory of valence bonds. In ionic crystals of the NaCl type the modulus E is highest along the edges <100>, i.e., along the direction of exchangeable bonds /2/.

The presence of rigid orbital bonds along the edges of the body-centered cubic lattice is the cause of the susceptibility of refractory metals of groups V—VI to brittle failure and their low ductility, especially marked if the metals are contaminated by interstitial impurities. The susceptibility to brittle failure depends on many factors: contamination by interstitial impurities (H, O, N, C, B) size of grains and mosaic blocks, dislocation characteristics, and applied stresses (notches, bending, stretching, etc.). The ductile—brittle transition temperatures of polyvalent body-centered cubic metals of groups V—VI are given in the table. The purification of body-centered cubic metals from interstitial impurities which appreciably increase the brittleness is very important. From the point of view of electron structure, the role of intersititial impurities is as follows. The atoms of interstitial impurities (H, C, N, O) in body-centered cubic metals occupy mainly the smaller and compressed octahedral pores and not the more available tetrahedral pores. It has been found /12/ that the atoms of carbon in α-Fe and in other metals occupy the middle of the edges of the unit cell /12/.

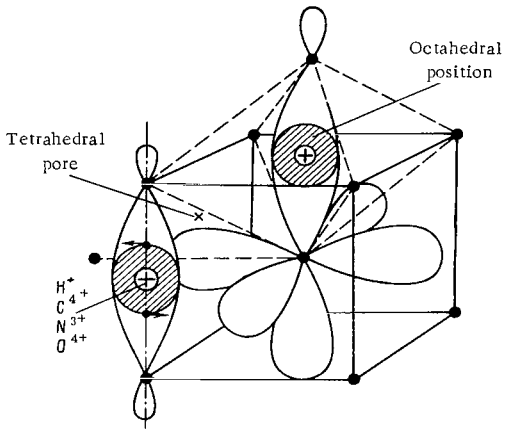

FIGURE 4. The strengthening of the exchange directed bonds in body-centered cubic metals as a result of the capture of interstitial impurity cations (H^+, O^{4+}, N^{3+}, C^{4+}, B^{3+}, etc.) by the field of overlapping orbitals and the formation of a three-centered bielectron molecular orbit Me—E—Me.

According to the hypothesis of orbital models, the H^+ (proton) and N^{3+}, C^{4+}, and B^{3+} ions which have small spherical shells $2s^2(N^{3+})$, $1s^2(C^{4+}, B^{3+})$, with radii close to 0.30 Å (N^{3+} and C^{4+}) and 0.60 Å (B^{3+}) can be captured into the field of overlap of two p-orbitals (Figure 4), where they are

strongly held as a result of the formation of a stable bond with a pair of electrons with antiparallel spins. This leads to the formation of a three-centered bielectron bond, which increases the rigidity of the exchange bond along the edge of the body-centered cubic cell. The same bond can be formed by an O^{1+} oxygen ion with a small radius (0.38 Å) and a great affinity for electrons. As C^{1+}, N^{3+}, and O^{4+}, ions are located in the overlap zone, their charge is reduced by two units. The freeing of body-centered cubic metals from interstitial impurities by vacuum arc melting and electron-beam melting greatly increases their ductility, and reduces the ductile—brittle transition temperature.

Bibliography

1. Hume-Rothery, W. The Structure of Iron Alloys.— [Russian translation. 1966.]
2. Grigorovich, V.K. Periodicheskii zakon Mendeleeva i elektronnoe stroenie metallov (Periodic Law of Mendeleev and the Electron Structure of Metals).—Izdatel'stvo Nauka. 1966.
3. Grigorovich, V.K. Periodicheskoe izmenenie struktury i svoistv elementov (Periodic Variations in the Structure and Properties of Elements).—Tezisy VIII Mendeleevskogo s"ezda po obshchei i prikladnoi khimii, No. 14:94, Izdatel'stvo AN SSSR. 1958.
4. Grigorovich, V.K. Struktura zhidkikh metallov v svyazi s ikh elektronnym stroeniem (Structure of Liquid Metals and their Electron Structure).—Izvestiya AN SSSR, OTN, Metallurgiya i Toplivo, No. 6:93. 1960.
5. Grigorovich, V.K. Kristallicheskie struktury i svoistva metallov bol'shikh periodov v svyazi s ikh elektronnym stroeniem (Crystal Structures and Properties of Metals of the Long Periods and their Electron Structure).—Trudy Instituta Metallurgii, No. 12:241, Izdatel'stvo AN SSSR.
6. Grigorovich, V.K. K prirode khimicheskoi svyazi v fazakh sistemy zhelezo—uglerod (The Nature of Chemical Bonds in Iron—Carbon Systems).—Izvestiya AN SSSR, Neorganicheskie Materialy, 1(10):1764. 1965.
7. Grigorovich, V.K. Vliyanie elektronnogo stroeniya legiruyushchikh elementov na polymorfnye prevrashcheniya zheleza (Influence of the Electron Structure of Alloying Elements on the Polymorphic Transformations of Iron).— Ibid., p. 1710.
8. Wortman, J.J. and R.A. Evans.—J. Appl. Phys. 36(1):153. 1965.
9. Aleksandrov, K.S. and T.V. Ryzhova.—Kristallografia, 6(2):287. 1961.
10. Huntington, G.—UFN, 74(3):461. 1961.
11. Bolef, D.I.—J. Appl. Phys., 32, No. 1. 1961.
12. Hume-Rothery, W. and G.V. Raynor. Structure of Metals and Alloys. [Russian translation. 1959.]

V. G. Osipov, V. D. Mutovin, and V. V. Vinogradov

ROLLING, HEAT TREATMENT, AND DEEP DRAWING OF THIN SHEETS OF MOLYBDENUM

Molybdenum sheet is today widely used in industry, and a study of its mechanical and technological properties is of great interest.

Molybdenum sheet is usually rolled at temperatures below the recrystallization point, and therefore this process should be classified as cold rolling (or more accurately, warm rolling). If the temperature of rolling is close to the recrystallization point, the required increase in strength and ductility cannot be attained /1/. Belk /2/ showed that to obtain ductile molybdenum sheet with a thickness of 6.3 mm the rolling should be started at 1350°C and terminated at 850°C.

Sheets 1—0.5 mm thick are rolled at 200—400°C, and sheets thinner than 0.5 mm at room temperature. It is recommended that cold-rolled molybdenum sheet be annealed between passes to relieve stresses and the effect of cold working.

The deformation of molybdenum below the recrystallization temperature leads to the formation of a crystalline texture. Thus, single direction rolling gives a texture with the face of the cube parallel to the surface of the sheet, and the diagonal of the face of the cube is parallel to the direction of rolling /3/.

Crystalline textures lead to anisotropy of the mechanical properties in the plane of the sheet, which harms the material during further extrusion.

A study of the anistropy of the mechanical properties of sheets rolled longitudinally and transversely was carried out with a cermet molybdenum of the M4-type. The specimens were 0.8, 0.5, 0.3, and 0.1 mm thick. The blanks were made of annealed 1.5 mm thick sheet from which the scale had been removed. This sheet was prepared by rolling a forged plate with a 5 × 40 mm cross-sectional area.

The dependence of the mechanical properties (δ_{10} and σ_b) of the specimen on the direction of longitudinal and cross rolling is shown on Figure 1. For tensile tests ten specimens 5 mm wide and 0.5 mm thick were used.

The tests of deep-drawn materials showed that the coefficient of drawing can be calculated from the formula

$$K = \frac{D_{max}}{d_{av}}$$

where D_{max} is the maximum diameter of the blank which did not fail during the tests; d_{av} is the average diameter of the extruded cup. Cross-rolled sheets have a coefficient of drawing 20—25% higher than that of sheet rolled in a single direction.

Sheet with less directional mechanical properties is obtained by cross rolling, starting from a certain thickness.

The relationship between the final thickness of the sheet and the initial thickness of the blank at which cross rolling can be started was found

experimentally (Figure 2). Molybdenum undergoes no phase transformations, and retains its body-centered cubic structure up to a temperature of 2125°C. A heat treatment of wrought molybdenum consists of recrystallization annealing, or of annealing below the recrystallization temperature.

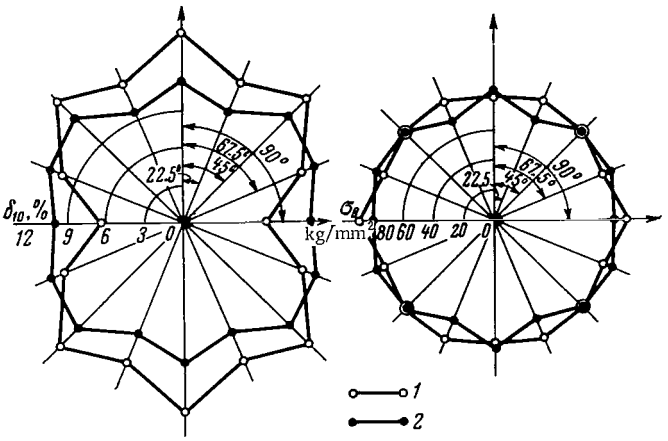

FIGURE 1. Dependence of the elongation δ_{10} and the ultimate strength σ_B on the direction of rolling:

1—longitudinal rolling; 2—cross rolling.

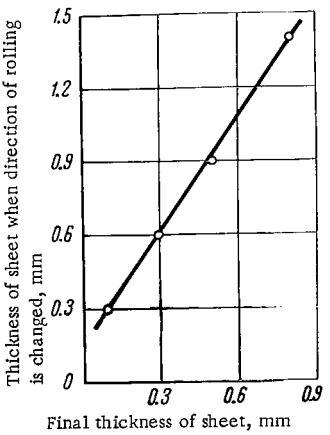

FIGURE 2. Thickness of molybdenum blanks at which cross rolling can be started.

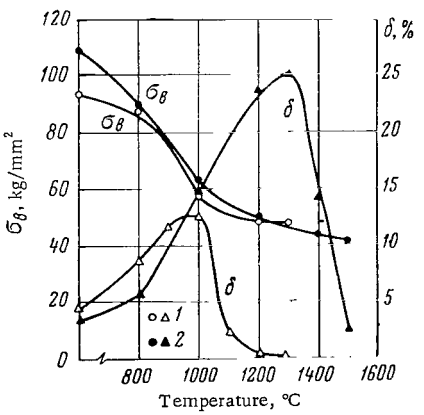

FIGURE 3. Dependence of elongation (δ, %) and ultimate strength (σ_B) on the annealing temperature:

1—commercial molybdenum; 2—molybdenum purer than commercial.

The dependence of the mechanical properties ($\sigma_в$, δ_{10}) on the annealing temperature in vacuo was investigated with cermet molybdenum of commercial or higher grade.

The specimens were cut out of a 0.5 mm thick sheet, and heated at each temperature for 1 hr. The tensile tests were carried out at the rate of 4% per minute, and the results are given in Figure 3.

A study of the microstructure of specimens annealed at different temperatures showed that recrystallization always takes place above 900°C. This leads to embrittlement of commercial molybdenum, but the ductility of pure molybdenum increases up to an annealing temperature of 1300°C, and it then drops sharply. The decrease in ductility caused by annealing at 1400°C or above coincides with the start and development of secondary recrystallization.

A study of the mechanical properties of molybdenum at different rates of deformation showed that an increase in the rate of stretching sharply reduces the ductility of the recrystallized metal, but has much less influence on molybdenum with a fibrous structure. Thus, molybdenum recrystallized at 1300°C, with an elongation of 25—28% during static tests ($V_t = 0.04\ mm^{-1}$), appears to be brittle if it is drawn at the rate of 0.5—0.8 m/sec. If molybdenum annealed below the recrystallization temperature is drawn, no such embrittlement appears.

The embrittlement of recrystallized molybdenum at high rates of deformation is associated with the critical ductile—brittle transition temperature. This critical temperature is not constant /3/, and can vary over a wide range even for molybdenum of the same chemical composition, depending on the degree of its preliminary deformation, microstructure, rate of deformation during testing, and the method of applying the load. Therefore, the ductility of molybdenum from the point of view of extrusion can be determined by a test which simulates the stresses and the drawing rate. This test should also be carried out at the same temperature as the extrusion.

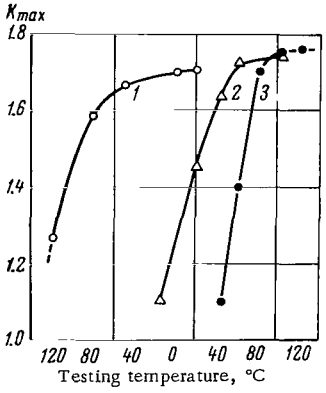

FIGURE 4. Dependence of the coefficient of drawing of molybdenum on the deformation temperature:

1—annealing at 900°C; 2—annealing at 1100°C; 3—annealing at 1300°C.

The temperature range for the deformation of molybdenum sheet of a high degree of purity in which complex stresses had been induced during drawing was found in a die, with a variation in the temperature of the blank of from − 150 to +300°C.

A rate of deformation of 0.8 m/sec corresponded to the rate of a crank press working at 50—60 rpm. The results of the investigation are shown in Figure 4. The testing temperature is plotted on the abscissa and the coefficient of drawing on the ordinate. These data indicate that molybdenum with a fibrous structure annealed at 900°C can be drawn to temperatures of − 60°C, but molybdenum recrystallized to about 50% (annealing at 1100°C) can be subjected to deformation under the given conditions at a temperature of not less than 35—50°C. The critical

ductile—brittle transition temperature of molybdenum recrystallized at 1300°C lies at 60—100°C. The drawing coefficient of recrystallized molybdenum at temperatures above this critical temperature is higher than that of nonrecrystallized molybdenum. This corresponds to an increased ductility of recrystallized molybdenum during static tensile tests. Recrystallization does not reduce the ductility of molybdenum during drawing, but shifts its ductile—brittle transition temperature toward higher temperatures.

CONCLUSIONS

1. The anisotropy of the mechanical properties of molybdenum sheet was studied after longitudinal and cross rolling.
2. We determined the relationship between the annealing temperature in vacuo and the structure and mechanical properties ($\sigma_в$, δ_{10}) of cermet molybdenum of commercial or higher grade.
3. We found the ductile—brittle transition temperature of wrought and recrystallized molybdenum of high purity, under conditions of stresses induced by deep drawing at a rate of deformation of 0.8 m/sec.
4. The results for static uniaxial drawing of recrystallized molybdenum do not characterize its ductility during drawing at the rate of 0.5 m/sec at the same temperature.

Bibliography

1. Morgunova, N.N. Zharoprochnye splavy na osnove molibdena (Refractory Molybdenum-Base Alloys).—VINITI, Moskva. 1959.
2. Belk, O.A.—J. Less-Common Metals, No. 2. 1960.
3. Tietz, T.E. and S.W.Wilson. Behavior and Properties of Refractory Metals, p. 156, New York—London. 1965.

I.S. Gaev and E.V. Sheyanova

STUDY OF THE WELDABILITY OF MOLYBDENUM ASSOCIATED WITH VARIATION IN ITS STRUCTURE

The structure of welded joints is usually studied by preparing microsections and etching them with chemical reagents or oxidizing them. At present, the processes occurring at elevated temperatures are studied by high-temperature metallography.

A better metallographic control of the structure of welded joints in refractory metals can be obtained by examining the topography of the surface revealed directly during heating and cooling which is caused by welding without any special preparation of microsections or etching (autometallography).

Since electron-beam welding is carried out in vacuo, the structure is revealed by cooling the molten zone. Plates welded by electron beams can be metallographically studied during all stages of heat treatment and mechanical tests on the welded joint.

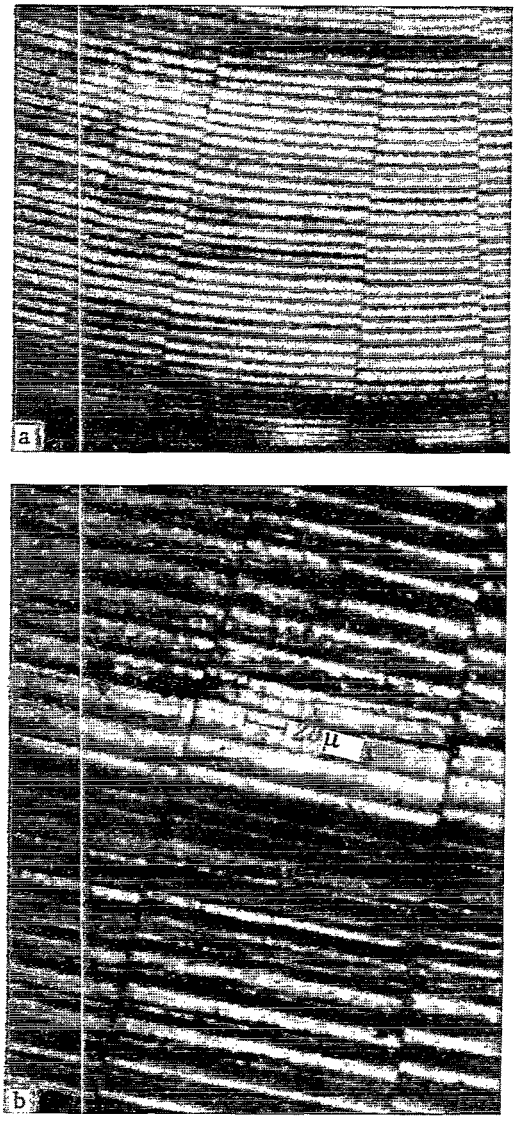

FIGURE 1. Microstructure of a welded joint in molybdenum: a—×100; b—×300.

The metal in a molybdenum joint welded by an electron beam does not solidify smoothly but periodically, and as a result the surface of the joint is uneven. The crystallization isotherms are shown in Figure 1, a.

The grains grow normally to the direction of cooling, and the grain boundaries are revealed due to a selective vaporization.

The stresses which lead to structural displacements arise as the result of the different thermal expansion and contraction, and of anisotropy of the metal. The displacements can be observed by autometallographic control methods. At the beginning of solidification of the molten metal of the joint, periodic crystallization takes place, which leaves geometrically regular lines on the surface called crystallization isotherms. A polyhedral network of grains is then formed. From the displacement of the crystallization isotherms along the grain boundaries it is possible to determine the stresses from the magnitude of the shear deformation.

The shear deformation can be observed at a 300-fold magnification. If the grains are coarser (Figure 1, b), the shear deformation is more marked. The absolute size of the linear displacement varies from 3 to 5 μ.

On Figure 2, a we can see not only the crystallization isotherms and the grain boundaries but also wavy lines which include the edges of the slip bands, and develop within individual grains. These lines often propagate beyond the grain boundaries. The presence of slip bands indicates that intragranular deformation has taken place in the welded joint. Sometimes the slip bands give rise to cracks (Figure 2, b). In addition to the above structural changes, the boundaries migrate in the welded joint (Figure 2, c). During the short period when the metal is cooled after welding, the grain boundaries do not remain stable but continue to shift, which indicates incomplete recrystallization of the solidifying metal of the joint. As a result, the decrease in the dislocation density leads to equilibrium of the metal deformed by welding.

We used an IMASh-5 machine, and showed that the intragranular deformation takes place in molybdenum mainly below the recrystallization temperature, but the displacements along the grain boundaries occur above this temperature. The thermal conditions for migration of the grain boundaries and shear deformation within the grains were determined by Lozinskii, who used an IMASh-18 machine. He found that the grain boundaries migrate at temperatures of from 2200 to 2400°C, and deformation within the grains occurs at 500—1000°C.

Welded joints in which these phenomena take place are susceptible to embrittlement (the bending angle is equal to or close to zero).

If an intragranular shear deformation develops, the welded joint is not always broken along the grain boundaries. Not only the intergranular fractures (Figure 3, a) but also fractures along several grains (Figure 3, b) or parallel to the edges of the slip bands can be observed (Figure 3, c).

Thermal stresses in the zone of the welded joint are determined by the coefficient of thermal expansion of the metal, the width of the molten zone, and the temperature differences during welding. The last factor can be regulated by heating the plates being welded during the process, which according to literature data is very favorable.*

The width of the molten zone of metal during welding can be regulated by controlling the energy parameters of welding. In such cases it is very useful to alloy the welded joint additionally, which changes the coefficient of thermal expansion and the configuration of grains in the desired direction.

* "Referativnyi zhurnal metallurg.," No. 12, 121, 480. 1964.

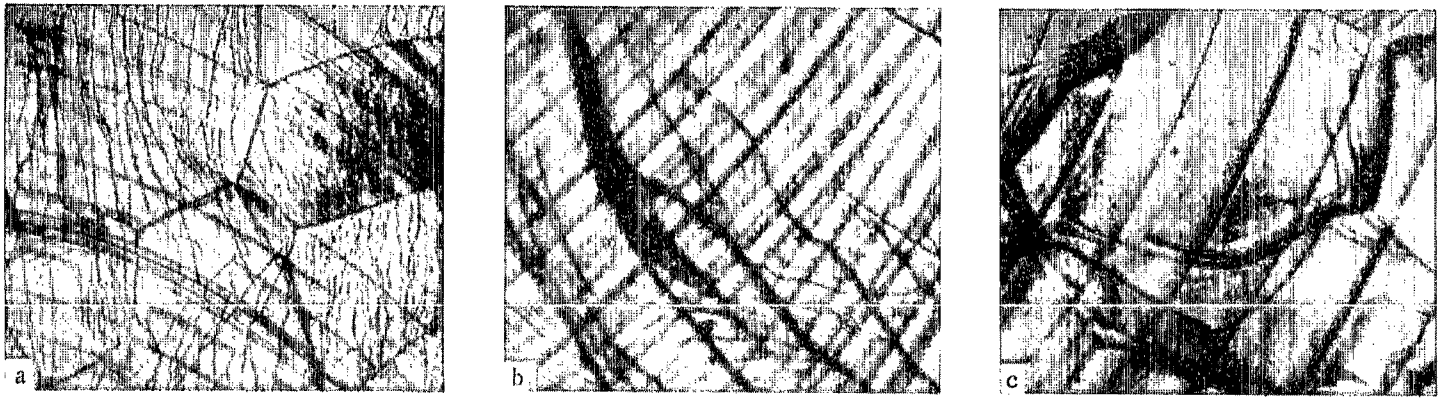

FIGURE 2. Microstructure of a welded joint in molybdenum:
a—× 100; b, c—× 200.

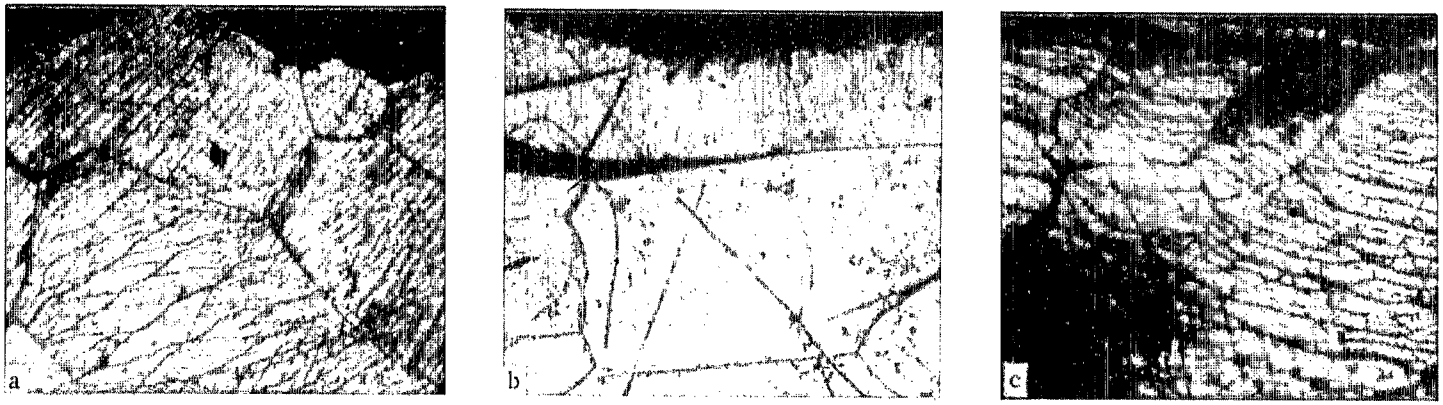

FIGURE 3. Failure of a welded joint in molybdenum, × 100.

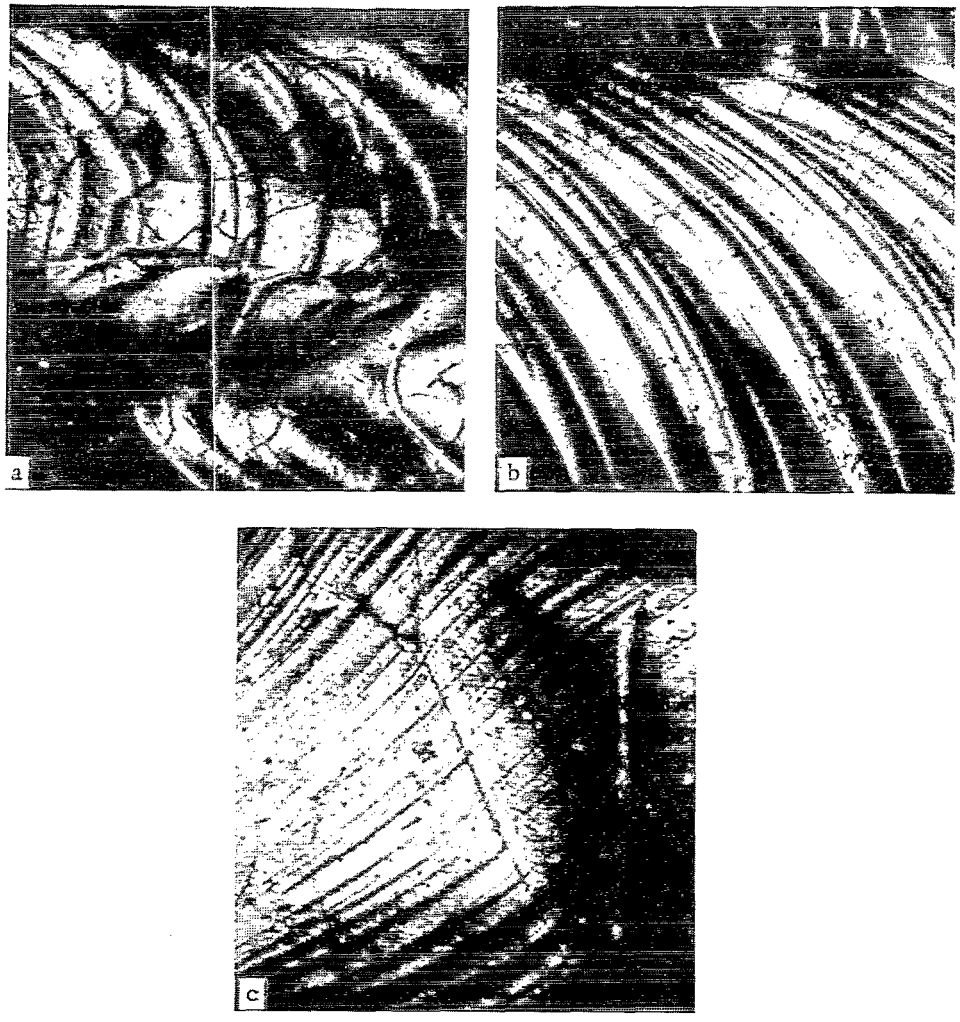

FIGURE 4. Microstructure of a welded joint in molybdenum after welding at the rate of ~60 m/hr, × 100.

Since the grain size determines the mechanical properties of the metal, a fine-grained structure can be produced by varying the rate of welding. Photographs of welded joints after welding at the rate of ~60 m/hr are shown in Figures 4, a and b. The average bending angle was about 30°. The structure is revealed less clearly.

Correct alloying elements added to the welded joint during welding can increase the bending angle of the joint to 180°. It is characteristic that the isotherms of crystallization pass smoothly from one grain to the other without any displacement at the grain boundaries (Figure 4, c).

To relieve stresses in the joint, the welded articles should be annealed, avoiding any absorption of gases by the metal. The following annealing process is recommended: heating at 900°C and 1000°C for 1 hr, or heating

in special containers (vessels) with getters at the same temperatures. Annealing is not always helpful if the metal is overstressed before welding.

CONCLUSIONS

1. The difficulties of producing a ductile welded joint are due not only to rapid recrystallization and absorption of gases, but also to the thermal stresses which lead to displacements along the grain boundaries and within the grains.
2. To produce a ductile welded joint, conditions for the minimum development of stresses must be created, and absorption of gases by the metal prevented, by choosing the correct technology of welding, alloying the weld zones, heating the metal during the process of welding, and annealing after welding in vacuo or in special vessels with getters.

I. A. Tregubov and L. N. Kuzina

HIGH-TEMPERATURE (1400°C) HARDNESS OF TUNGSTEN-BASE ALLOYS CONTAINING TANTALUM AND RHENIUM

The ternary tungsten—tantalum—rhenium alloys are prepared from the three most heat-resistant elements, with melting points of 3410°C, 2996°C, and 3180°C, respectively.

The W—Ta—Re system has been studied /1/ by metallographic and X-ray methods, and by determining the temperatures at which the alloys start to melt. The specimens were annealed at 2680°C, 2530°C, 2020°C, and 1200°C. A schematic phase diagram of the W—Ta—Re system was constructed from the data obtained /1/.

The wide field of solid solutions adjacent to the W—Ta side with up to 45 wt % of rhenium in the Ta—Re system, and with up to 30 wt % of rhenium in the W—Re system, includes heat-resistant and quite ductile alloys. The phase diagrams of the limiting W—Re, Ta—Re and W—Ta binary systems have been widely investigated /2—6/.

Our aim was to determine the hardness of tungsten-base alloys containing tantalum and rhenium at 1400°C.

Data on the variation in hardness at elevated temperatures are very important for practical purposes, for example for planning the process of mechanical shaping. On the other hand, there is a certain relationship between the data on hardness at elevated temperatures and the strength of these alloys.

Of the tungsten-base alloys, binary materials with 1—5 wt % of tantalum and 25—45 wt % of rhenium have been thoroughly investigated, and are today used in industry. However, there are very few data on ternary tungsten-base alloys containing tantalum and rhenium.

STARTING MATERIALS AND METHODS

We used tungsten rods (99.9%), tantalum strips (99.93%), and rhenium rods (99.8%).

The alloys were prepared in an arc furnace in an atmosphere of argon. The metal was melted on a water-cooled copper hearth with a nonconsumable tungsten electrode. To obtain homogeneous ingots the alloys were turned over and remelted 8—10 times. The weight of the ingots was 20 g.

The ingots were remelted twice in an electron-beam furnace in a vacuum of $2 \cdot 10^{-5}$ mm Hg. The specimens were flat plates 15 mm in diameter and 5 mm in height.

The homogenizing annealing was carried out in a special vacuum furnace at 2500°C for 2 hr.

The hardness at elevated temperatures was measured by a special device, in which the specimens could be heated in vacuo ($1 \cdot 10^{-3}$ mm Hg) up to 1600°C. We used a reinforced saphire indentor.

The hardness of the tungsten-base ternary alloys was measured at 1400°C with a 2.5 kg load.

Results

On the figure, curve 1 shows the dependence of the hardness of alloys on their composition for the 95 wt % tungsten section, and indicates that at 1400°C tungsten alloys with 5 wt % of tantalum or 5 wt % of rhenium have almost the same hardness, equal to about 55 kg/mm^2. The hardness of ternary alloys is represented by a twisting curve, and its value increases with increase in the content of rhenium. For example, an alloy with 95 wt % W + 3 wt % Re + 2 wt % Ta has a hardness of $\sim$75 kg/mm^2. If the content of tantalum is increased to 4 wt % and the content of rhenium decreased to 1 wt %, the hardness decreases to 60 kg/mm^2. The irregular course of the curve representing the dependence of hardness on composition is apparently explained by the existence of liquidation microheterogeneity in the alloys.

An analysis of curve 2 of the figure which represents the dependence of the hardness of alloys containing 90 wt % of tungsten shows that the binary tungsten-base alloys with 10 wt % of rhenium is considerably softer (H_V = = 65 kg/mm^2) than the tungsten-base alloy with 10 wt % of tantalum (H_V = = 85 kg/mm^2). In ternary alloys the hardness is represented by a curve with a smooth minimum. Alloys with 3 wt % of tantalum and 7 wt % of rhenium have the lowest hardness (H_V = 60 kg/mm^2). If the content of tantalum is increased to 6 wt %, and the content of rhenium is correspondingly reduced to 4 wt %, the hardness increases to 85 kg/mm^2 and remains almost constant if more tantalum is added. Consequently, ternary alloys with 90 wt % of tungsten and from 6 to 10 wt % of tantalum, and from 4 wt % to 0 wt % of rhenium, have the most stable hardness.

Alloys with a constant content of tungsten of 80 wt % (curve 3 in figure) are of the greatest interest. An analysis of the curve representing the variation in hardness with composition shows that the hardness remains almost constant over the range of compositions investigated. Apparently, this series of alloys has a stable hardness, and possibly even a stable resistance to heat. At 1400°C the average hardness of this series of alloys

is ~85 kg/mm^2. This has been confirmed by the US patent /7/, which recommends ternary tungsten-base alloys containing tantalum (1—10 wt %), and rhenium (1—10 wt %). Alloys with 8 wt % of tantalum or rhenium are preferable. These alloys can be hot-worked and in some cases even cold-worked.

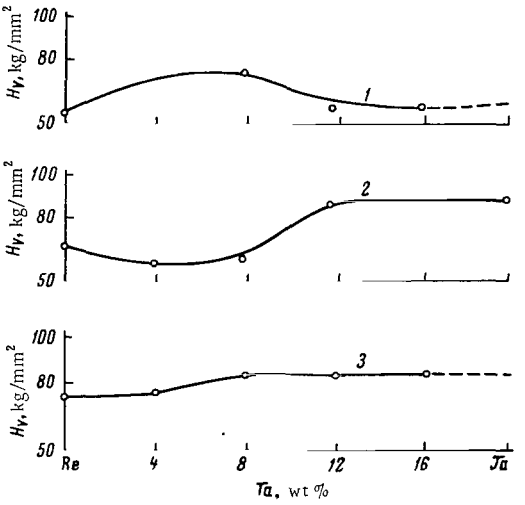

Dependence of the hardness of alloys at 1400°C on their composition:

1—section with 95 wt % of tungsten; 2—the same, 90 wt % of tungsten; 3—the same, 80 wt % of tungsten.

CONCLUSIONS

Ternary tungsten-base alloys with up to 20 wt % of tantalum and rhenium have the highest hardness stability at 1400°C. The hardness of these alloys at 1400°C is about 1/4 of that at room temperature.

Bibliography

1. Brophy, J.H., M.H.Kamdar, and J. Wulff.—Trans. Met. Soc. AIME, 221:1137. 1961.
2. Dickinson, J.M. and L.S.Richardson. The Constitution of Rhenium— Tungsten Alloys.—Trans. A.S.M., 51:758. 1959.
3. Brophy, J.H., P.Schwarzkopf, and J.Wulff. The Tantalum—Rhenium System.—Trans. Met. Soc. AIME, 218:910. 1960.
4. Schramm, C.H., P.Gordon, and A.R.Kaufmann.—Trans. Met. Soc. AIME, 188:195. 1950.

5. Tylkima, M.A., I.A.Tsyganova, and E.M.Savitskii. Diagramma sostoyaniya sistemy tantal-renii (Phase Diagram of the Tungsten—Rhenium System).—ZhNKh, 5, No. 8. 1960.
6. Savitskii, E.M., M.A.Tylkina, and I.A.Tsyganova. Fazovaya diagramma vol'fram-renii (Phase Diagram of the Tungsten—Rhenium System).—Metallovedenie i Termicheskaya Obrabotka Metallov, No. 9. 1960.
7. W—Ta—Re Alloys. US Patent No. 3160501, Class 75—17c, 8.12. 1964.

K.B.Povarova, M.A.Tylkina, and E.M.Savitskii

REFRACTORY TERNARY ALLOYS OF THE TUNGSTEN-MOLYBDENUM-RHENIUM SYSTEM

Alloys for service at 1500°C or above can be prepared from refractory metals only, especially from tungsten and molybdenum. However, these metals like all their alloys of commercial purity have a common drawback: they are brittle under certain conditions such as after recrystallization, working at elevated temperatures, or welding, and at low temperatures. They are thus difficult or sometimes even impossible to use, for example, for service under conditions of regular variation in temperature and strong vibrations. Alloying of tungsten and molybdenum with rhenium eliminates this disadvantage.

This work is a continuation of the studies carried out for many years on new alloys containing rhenium. Due to the large number of investigations on phase diagrams /1/, new alloys with the required properties can be developed.

Binary tungsten-base alloys with 27% rhenium and molybdenum-base alloys with 47% rhenium have a high strength at elevated temperatures, high ductility at low temperatures, and can be welded in the recrystallized state to give a ductile joint. They have been developed by vacuum melting ($\delta = 15-25\%$).

We also believe that some alloys of the tungsten—molybdenum—rhenium system should have high strength and high ductility. Therefore, further studies were directed toward developing alloys of this system.

We studied the part of the ternary W—Mo—Re system with 50 wt % of rhenium (Figure 1a, b) /2/. The concentration triangle (Figure 1, b) shows the solubility limits of the ternary solid solution of rhenium in tungsten and molybdenum at different temperatures, and the limit of twinning, which includes the region of ternary alloys. These alloys, like the binary W—Re, Mo—Re, and other alloys, can be deformed not only by slip but also by twinning. Deformation by twinning is the result of the unique favorable influence of rhenium on the ductility of tungsten and molybdenum. The reasons for this beneficial influence may also be changes in the structure of the oxides, redistribution of oxygen, solubility of interstitial impurities, and also mechanism of deformation and of the production of deformation twins /1—6/.

Studies /7—10/ have been carried out to develop alloys with an optimum composition, that is alloys with the highest mechanical and technological

properties and the lowest amount of rhenium (hatched field in Figure 1, b) /11/.

The purpose of this work was to develop a technique for the production of wires of these alloys, and to investigate the properties of some of these wires. We took alloys of the MVR-27VP series with 27% rhenium and different molybdenum to tungsten ratios (Table 1).

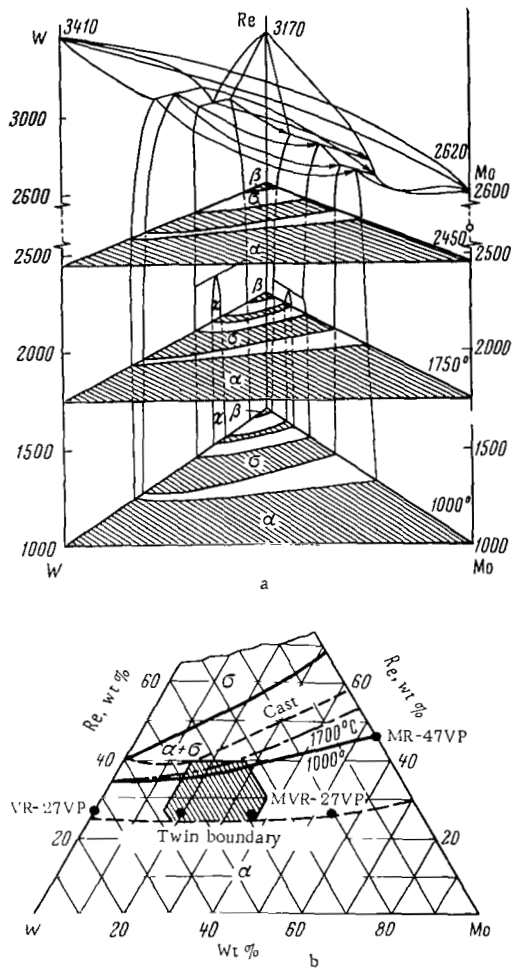

FIGURE 1. Rhenium—tungsten—molybdenum system:

a—diagram of reactions in the system; b—concentration triangle with solubility limits of rhenium in tungsten and molybdenum at different temperatures.

The alloys were prepared by vacuum melting, and a technique has been developed for the production of wires with a diameter of up to 50 μ.

Chemical analysis of the alloys showed that the content of the chief components varies within the permissible limits of ± 3%. The contents of the chief impurities are (in wt %): 0.003—0.006 N_2; 0.028—0.043 O_2; 0.013—0.026 C; and 0.09—0.019 Cu.

TABLE 1. Composition of alloys of the MVR-27VP series

Alloy	Composition of charge, wt %		
	W	Mo	Re
MVR-27VP1	55	18	27
MVR-27VP2	39	34	27
MVR-27VP3	20	53	27

We have studied the mechanical properties of alloys at room and elevated temperatures, as well as their physical properties (ductility, electric properties, and thermal expansion).

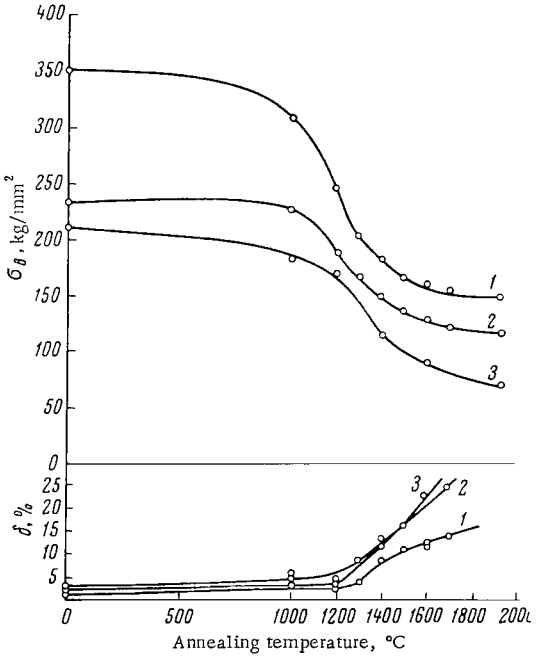

FIGURE 2. Influence of the annealing temperature on the mechanical properties of alloys containing rhenium, tungsten, and molybdenum:

1—VR-27VP; 2—MVR-27VP3; 3—MR-47VP.

We investigated the dependence of the mechanical properties of 0.6—0.05 mm diameter wire at room temperature on the degree of deformation (hot and cold) and on the annealing temperature. The ternary tungsten—molybdenum—rhenium alloys of the MVR-27VP series are greatly hardened

by both cold and hot (400—500°C) working. The strength of an annealed alloy is 120—140 kg/mm^2 and its elongation $\delta = 20\%$. After a deformation of 50—70% the strength of the same alloy increases to 200 kg/mm^2, and after a deformation of 98—99% (diameter of the wire 50—60 μ) the strength increases to 380—400 kg/mm^2, i.e., it increases to three times that of the annealed wire. However, even after this amount of working the ternary tungsten—molybdenum—rhenium alloys containing 27% Re are sufficiently ductile and machinable to be rolled into a strip with a ratio of sides of 1:10 and a thickness of less than 10 μ, which means that the technological properties of this alloy are not inferior to those of binary molybdenum-base alloys with 47% rhenium.

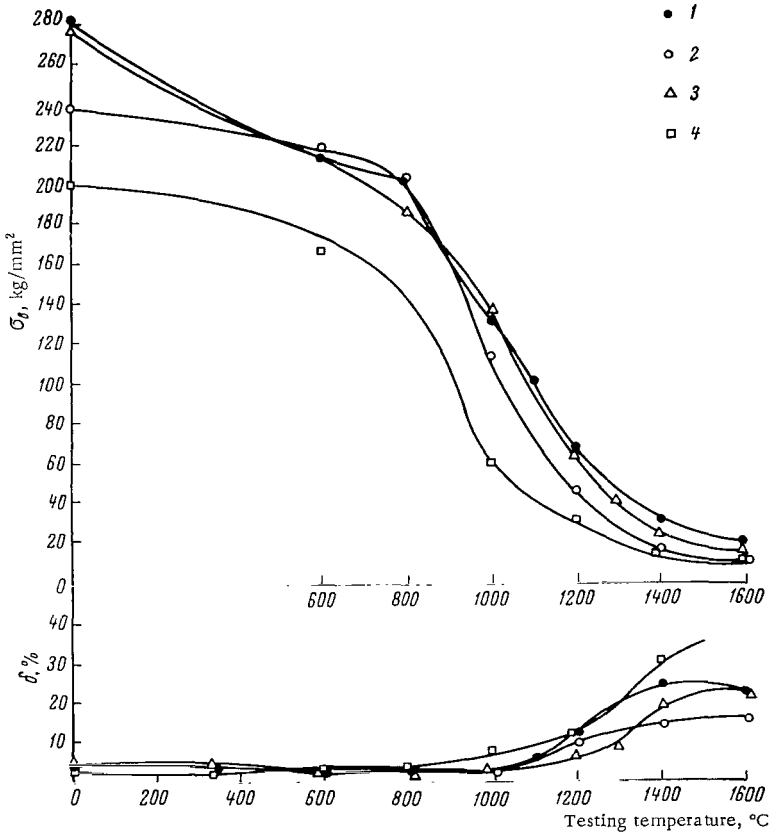

FIGURE 3. Influence of testing temperature on the mechanical properties of wrought alloys of rhenium containing tungsten and molybdenum:

1—VP-27VP; 2—MVR-27VP3; 3—MVR-27VP2; 4—MR-47VP.

The influence of the annealing temperature on the mechanical properties of ternary alloys has been investigated. Figure 2 shows the mechanical properties of one of the ternary alloys MVR-27VP3 which has the highest content of molybdenum (53% molybdenum, 20% tungsten), and the properties

of MR-47VP and VR-27VP binary alloys. It can be seen that annealing at temperatures corresponding to the beginning of recrystallization produces the lowest strength and the highest ductility.

The strength of alloys of the ternary MVR-27VP series is intermediate between that of binary rhenium—molybdenum alloys and rhenium—tungsten alloys, but their ductility is closer to that of the highly ductile MR-47VP alloy.

TABLE 2. Some physical properties of alloys of rhenium with tungsten and molybdenum

Metal	Elasticity modulus, E, kg/mm^2	Shear modulus, G, kg/mm^2	Poisson's ratio, μ	Coefficient of linear expansion, $\alpha_t \cdot 10^6$, 1/degree C	Temperature coefficient of electric resistivity, $\alpha_p \cdot 10^3$, 1/degree C
Tungsten	40,800	16,000	0.28	4.3	5.77
Rhenium	46,900	17,900	0.31	7.7	3.3
Molybdenum	32,200	12,300	0.35	5.6	5.15
VR-27VP	41,600	16,200	0.29	5.4	1.10
MR-47VP	36,400	—	—	6.4	1.7
MVR-27VP1	37,100	—	—	5.4	1.21
MVR-27VP2	37,500	13,600	0.33	5.7	1.88
MVR-27VP3	—	—	—	6.1	1.71

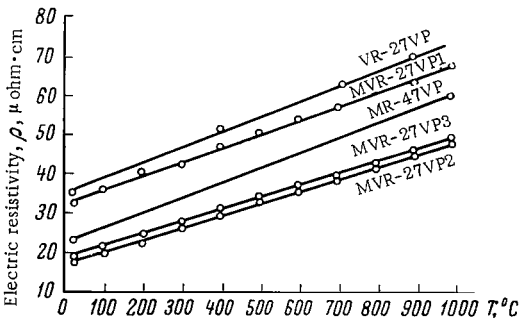

FIGURE 4. Influence of temperature on the electric resistivity of alloys of rhenium containing tungsten and molybdenum.

The mechanical properties of 100 μ diameter strained wire of binary and ternary alloys at elevated (up to 1600°C) temperatures were studied by Amosov and Sokolova, who used an apparatus designed by NIKIMP with a tungsten heater. The vacuum was about 10^{-4} mm Hg and the specimens were loaded gradually to determine ultimate strength, ductility, and elongation (Figure 3).

Figure 3 shows that the strength of the alloys changes little up to 800°C. A considerable drop in strength takes place at 800—1400°C, and then the strength decreases slowly above 1400°C. A considerable increase in ductility begins above 1000°C. Ternary alloys with 27% rhenium have a high strength at all temperatures up to 1600°C ($\sigma_{B_{1600^\circ}} = 10-17$ kg/mm^2).

At these temperatures the elongation is 20—25%, which is relatively low, and equal to the elongation of the annealed alloys at room temperature. The high strength and low elongation make these alloys suitable for service at the above temperature range.

The ultimate strength is somewhat lower and the elongation slightly higher than those of binary and some ternary alloys of rhenium containing tungsten and molybdenum /7, 9/. These discrepancies may be due to differences in shape, treatment, and initial states of the specimens, and also to possible differences in the testing conditions, since the loading of the specimens was carried out by various methods, and in this work was slower.

Other properties of these alloys (shear modulus and elasticity modulus) at room temperatures were determined by Fedotov, who used strained and annealed cast specimens 4 mm in diameter and 60—110 mm in length, and the method of measuring the frequency of longitudinal, transverse, and torsional vibrations (Table 2). The properties of binary and ternary alloys, and also of the pure initial metals, were investigated. The elasticity modulus of binary alloys containing rhenium is higher than that of pure tungsten and molybdenum, but the elasticity modulus of ternary tungsten—molybdenum—rhenium alloys occupies an intermediate position between that of the tungsten—molybdenum and molybdenum—rhenium binary alloys. These alloys can be used for elastic components operating at elevated temperatures.

The average coefficient of linear expansion (Table 2) was found at the temperature range of 100 to 900°C with specimens 4 mm in diameter and 1.5—1.7 mm in length. The measurements were carried out in a vacuum dilatometer. All binary and ternary alloys investigated have a coefficient of thermal expansion close to that of molybdenum, and can be classified as a single group with an average coefficient of linear expansion of $5.7 \pm \pm 0.3 \cdot 10^{-6}$ 1/degree C.

We found that the coefficient of linear expansion of rhenium is equal to $7.7 \cdot 10^{-6}$ 1/degree C, which is somewhat higher than that given in the literature ($6.7 \cdot 10^{-6}$ 1/degree C). Since the literature data are related to cermet materials, and our studies were carried out with cast rhenium, it can be assumed that our results are more reliable.

The electric resistivity of the alloys was measured over a range of temperatures of from 20 to 1000°C, with a potentiometer. The specimens were made of annealed wire 0.3—0.6 mm in diameter (Figure 4, see Table 2). The resistivity of all the alloys studied is higher than that of tungsten and molybdenum, and about the same or higher than that of rhenium. The electric resistivity increases almost linearly with increase in temperature. The average temperature coefficient of the electric resistivity of alloys is $\frac{1}{3}$ to $\frac{1}{2}$ of that of pure metals. For tungsten-rich alloys this coefficient is less ($1.1—1.2 \cdot 10^{-3}$ 1/degree C) than for binary and ternary molybdenum-rich alloys ($1.7—1.9 \cdot 10^{-3}$ 1/degree C. The low temperature coefficient of electric resistivity indicates that the alloys are resistant to combustion when used as heating components.

CONCLUSIONS

We developed a new group of ternary tungsten—molybdenum—rhenium alloys containing 27% rhenium and different tungsten to molybdenum ratios (18—55%). The new alloys of the MVR-27VP series are as readily workable as binary tungsten—rhenium and molybdenum—rhenium alloys. They have the same high strength at room and elevated temperatures characteristic of binary alloys. They also have a high ductility like binary molybdenum—rhenium alloys, a low temperature coefficient of expansion and of electric resistivity, and a high modulus of elasticity. The amount of rhenium in these alloys is 63% of that in binary MR-47VP alloys.

These alloys can be employed in some fields of modern industry at elevated temperatures and with high loads.

Bibliography

1. Savitskii, E.M., M.A.Tylkina, and K.B.Povanova. Splavy reniya (Rhenium Alloys).—Izdatel'stvo Nauka. 1965.
2. Tylkina, M.A., K.B.Povarova, and E.M.Savitskii.—ZhNKh, 5, No. 11. 1960.
3. Hughes, J.and G.Geach. Plansee Proceedings, p. 242. 1955.—London, Pergamon Press, Ltd. 1956.
4. Jaffee, R.I., D.J.Maykuth, and R.D.Douglass. Rhenium and Refractory Platinum Group Metals.—Metallurgy Soc. Conference, USA. 1961.
5. Klopp, W.D., F.G.Holden, and R.I.Jaffee.—T.R.of Battell Memor. Inst., July 12. 1960.
6. Maukuth, D.J., F.G.Holden, and R.I.Jaffee. Rhenium.—Amsterdam—N.Y.Elsevier Publ. Co. 1962.
7. Tylkina, M.A., K.B.Povarova, and E.M.Savitskii.—Izvestiya AN SSSR, OTN, Metallurgiya i Toplivo, 5. 1961.
8. Sims, C.T. and R.I.Jaffee.—Trans. ASM, 52:929. 1960.
9. Savitskii, E.M., M.A.Tylkina, K.B.Povarova, and V.P. Vinokurov.—Proizvodstvenno-tekhnicheskii Byulleten', No. 5:3. 1962.
10. Povarova, K.B., M.A.Tylkina, and E.M.Savitskii. Sbornik—Renii (Collection—Rhenium), p. 155.—Izdatel'stvo Nauka. 1964.
11. Savitskii, E.M., M.A.Tylkina, and K.B.Povarova. Avtorskoe svidetel'stvo, No. 165310 (Russian Patent, No. 165310).—Byulleten' Izobretenii, No. 18. 1964.

V.G.Osipov, V.M.Amosov, E.V.Ushakov, E.K.Drobysheva, N.M.Zelentsova, and A.G.Borisov

THE DUCTILITY OF TUNGSTEN

Until recently the ductility of tungsten was studied mainly in tests on wire for tension and spiral winding. However, unsatisfactory ductility of

the metal during the intermediate stages of production can apparently lead to defects which impair the quality of the final product.

Rotation forging of VA tungsten rods leads to the formation of small transverse cracks on the surface of 10 mm diameter rods. The Moscow electric lamp plant carried out several studies to determine the cause of this cracking. They investigated, firstly, the influence of the composition of the protective atmosphere in the furnace, and found that if hydrogen is substituted by other protective media (carbon-containing atmosphere, nitrogen, argon, gas forming) there is a decrease in the number of cracks, but none of these media completely prevents their formation. Secondly, the influence of temperature was studied, and it was found that a decrease in the temperature of forging of the slabs to 1300°C, and an increase in the reduction per pass at constant temperature, improve the quality of the surface of tungsten rods. A further decrease in the temperature of forging leads to lamination of the material. An increase in temperature, however, increases the amount of surface cracks. To avoid surface cracks by reducing the forging temperature or by increasing the reduction per pass is a rather dangerous method, since it can lead to overworking of the metal.

The purpose of this investigation was to determine the influence of the process of rotation forging on the ductility of tungsten. We used slabs with a cross section of 11 × 11 mm, and rods with a diameter of 10, 5.6, and 3 mm, forged under different conditions.

The slabs were forged to a diameter of 6 mm on rotation forging machines, and were heated in an electric resistance furnace in an atmosphere of hydrogen at 1450°C. The specimens were reduced in diameter to 2.75 mm with heating in gas furnaces at 1400—1300°C. The temperature of forging was gradually reduced as the diameter of the specimens became smaller to avoid recrystallization of the metal.

To homogenize the structure and relieve internal stresses, 10 mm diameter rods were subjected to recrystallization annealing at 2200°C.

Several studies were carried out to determine the ductility of metals at elevated temperatures.

It is well known that the testing conditions should be as close as possible to the process of deformation of the metal in industry /1—3/. However, because of the complex stresses induced during rotation forging it is difficult to choose a method which will exactly simulate the process of forging, and therefore to obtain reliable results we decided to apply several different testing methods and determine the ductility under different stresses.

Since the surface finish greatly influences the ductility of rods during rotation forging, all our specimens had nonmachined surfaces.

For our tests we used the following methods: flattening, bending, stretching, and torsion.

The flattening was carried out on a 100-ton crank press. The average rate of deformation was about 10 sec^{-1}, and the specimens were heated in an electric resistance furnace in an atmosphere of alcohol vapor. The blanks were made of 10 and 6 mm diameter wire and had rounded edges to reduce the stress concentration at the edges. The tests were carried out at temperatures of from 1000 to 1500°C, and the ductility was evaluated from the degree of deformation needed until the appearance of the first crack.

It has been experimentally found that over the range of testing temperatures, the ductility of rods forged at 1300°C to a reduction three times

that produced by accepted techniques is higher than the ductility of rods forged by other processes. The ductility of rods forged by all techniques increases with increase in temperature.

The ductility of the slabs was higher than that of 10 mm diameter rods. This may be because when testing slabs we did not take into account the cracks formed as a result of the concentration of stresses at the edges of the blanks. No such cracks were found on the forged rods.

No cracks were found on flattened rods 3 and 5.6 mm in diameter forged over the temperature range of 800—1500°C, even at a 95% reduction.

The bending tests were also carried out on the crank press with a special device. The average rate of deformation was about 2 sec^{-1}.

The middle part of a specimen 75 mm in length was treated by a mixture of aluminum oxide and kaolin. This material is an additional protection against oxidation if the specimen is heated in a furnace in a protective atmosphere. However, the main task of this material is to protect the specimen against rapid cooling during tests in the air. The specimen was placed on supports which could move along guides and be fastened by screws in the required position.

The deformation was carried out by a cutter with a radius of the champer of 2 mm. The degree of deformation can be varied by changing the length of the connecting rods and the distance between the supports.

As in the above case the ductility was determined from the degree of deformation needed for the formation of the first crack. The degree of deformation was calculated from the external stretched fiber starting from the radius of its maximum curvature. The experimental results shown in Figure 1 indicate that the ductility of 10 mm diameter rods considerably increased from 1300°C for all batches except that treated by the accepted technical process. The ductility of the specimens of this batch was little dependent on temperature.

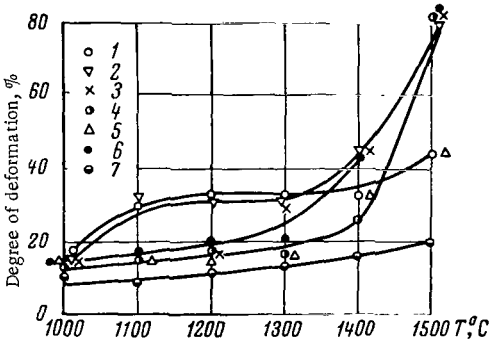

FIGURE 1. Dependence of the ductility of 10 mm diameter rods and of slabs on the temperature of bending tests:

1—forging by an accepted industrial process; 2—temperature of forging 1600°C, reduction by an accepted industrial process; 3—temperature of forging 1300°C; 4—1450°C, increased reduction; 5—1600°C, increased reduction; 6—1600°C, increased reduction; 7—slabs.

The course of the curves over the range of temperatures 1000—1300°C indicates that the rods forged to considerable reductions have a ductility lower than that of rods forged to ordinary reductions accepted in the existing technical process.

If the temperature is increased from 1300 to 1500°C the ductility of rods reduced by the accepted process is equal to that of rods with a reduction three times as great.

It was impossible to determine the dependence of the ductility during bending on temperature for specimens 3 and 5.6 mm in diameter, since even at the greatest bending angles no cracks were noticed at 800—1300°C.

The tensile tests on specimens 3 and 5.6 mm in diameter were carried out at 1000—1300°C on a P-5 machine at a rate of deformation of 0.02 sec^{-1}. Specimens 250 mm in length were heated in an electric resistance furnace in an atmosphere of argon. The calculated length of the specimen was 40 mm. All specimens exhibited a ductile manner of failure and clearly marked necking. The ductility of the metal increased gradually with increase in temperature. From this point of view the most characteristic measure is the constriction. Because of the greatly limited zone of deformation, the elongation does not give a correct picture of ductility. The elongation does not change appreciably over the range of temperatures from 1000 to 1300°C, and according to the data of elongation tests there is no great difference between the properties of rods forged by different industrial processes.

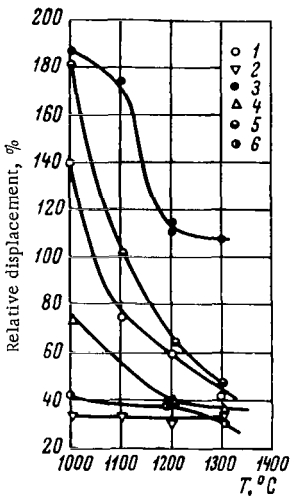

FIGURE 2. Dependence of the ductility of 5.6 mm diameter rods on the temperature during torsion tests:

1—forging by an accepted industrial process; 2—temperature of forging 1450°C, reduction trebled; 3—temperature of forging 1600°C, reduction by an accepted industrial process; 4—1600°C, reduction doubled; 5—1300°C, reduction by an accepted industrial process; 6—1300°C, reduction trebled.

Over the whole range of temperatures rods with a diameter of 3 mm are somewhat stronger than those with a diameter of 5.6 mm. At the upper limit of the temperature range the differences are rather smaller than at the lower limit.

The torsion tests were carried out on an experimental machine of the K-50 type at a rate of deformation of 0.002 sec^{-1}, and in an atmosphere of argon. The calculated length of the specimen was 40 mm. Rods 5.6 mm in diameter forged to a reduction according to the accepted industrial process have a much higher ductility than rods forged to a reduction three times as great. This difference is especially great at 1000—1100°C (see Figure 2). The most ductile rods were those forged at 1600°C, including those with a normal reduction and with a reduction three times as great.

As the testing temperature was increased, the ductility of rods forged according to the accepted industrial process decreased to $\frac{1}{3} - \frac{1}{2}$ of the initial.

An exception was a batch of rods forged at 1450°C to an increased reduction. In this case the ductility was low, and was almost uninfluenced by temperature.

Rods 3 mm in diameter also are very ductile if forged according to the accepted industrial process. When the testing temperature was increased, the ductility also dropped although not so much as that of the rods 5.6 mm in diameter. The ductility remains almost constant over the temperature range of 1100—1300°C.

To study the influence of stresses induced by forging on the ductility, the specimens were forged in dies of different shapes.

According to Osipov /4, 5/ oval external gauges are the most favorable for small deformations. However, after the first blow expansion takes place along the horizontal axis and the spherical blank becomes oval. The radius of the external surface of the oval blank along the horizontal axis will be smaller than the radius of the gauge, and after turning over the deformation will be similar to that induced by forging with flat hammers. Therefore, the oval gauge is not the best.

We should like to point out another change in the stressed state taking place during forging to great reductions. If specimens are forged by flat hammers, they are subjected to the same tensile stresses along the vertical axis. At large deformations, when the contact zone between the hammer and blank is determined by a surface and not by a line along the axis of the blank, a redistribution of stresses takes place in zones close to the contact surface, and the tensile stresses are converted into compressive. The same takes place during forging in angular dies. Here, at large deformations the tensile tangential stresses are appreciably smaller, and are not so dangerous from the point of view of reduced ductility.

This analysis indicates that forging brittle refractory metals and alloys on rotation forging machines with four dies or in angular dies gives the best results from the point of view of the influence of tensile stresses. The drawback of this type of deformation is that elastic zones exist in the center of the blank and that the stretching at the center of the blank under the influence of the peripheral layers leads to the induction of tensile stresses along the axis of the blank. However, these are not very dangerous if the material has a certain ductility.

From the above considerations on the influence of stresses on ductility, square dies instead of oval ones for rotation forging of tungsten will considerably increase the ductility of the metal.

To evaluate the influence of stresses during rotation forging of VA tungsten, the following series of experiments was carried out. Slabs 11.5 × 11.5 mm in cross section were forged on a rotation forging machine in oval dies to obtain approximately octahedral cross sections with an 11.5 mm diameter. The blanks were heated in an electric furnace to 1450°C in an atmosphere of hydrogen. The forging was then continued in dies with a square cross section until a rod with a 10 mm diameter was obtained. In this way six slabs were forged from two batches of the metal. For comparison six other slabs from the same batches were forged to a 10 mm diameter under the conditions of an ordinary process with oval dies.

The ductilities of rods forged by the different processes were compared by bending tests at 1200°C according to the method described above, and the following results were obtained. For specimens of the two batches forged by an ordinary industrial process the degree of deformation of the external fiber which produced the first crack was 29.4 and 38.4%, respectively. The rods of these two batches which had been forged in square dies showed a deformation of 55 and 71.5%, respectively.

Thus, as expected from theoretical considerations, rods forged in square dies were much more ductile than those forged in ordinary oval dies. Only round rods or those similar in shape can be forged in square dies. Consequently, the metal must be forged several times in oval dies before forging in square dies.

CONCLUSIONS

It has been experimentally shown that torsion under conditions when the tangential stresses are equal to or close to normal stresses have the greatest influence on the ductility of tungsten.

Torsion tests on rods 3 and 5.6 mm in diameter showed that the ductility of the metal decreases with the increase in the testing temperature. At low forging temperatures and high reductions the ductility is lower than under conditions of normal temperatures and reductions.

Static tensile tests showed that there are no great differences between the properties of rods forged by different methods.

Flattening tests could be carried out only if the diameter of the rod was not less than 10 mm, since the ductility of thinner rods was so high that no cracks were formed even after the highest degrees of deformation. For the same reasons, rods used for bending tests must not be thinner than 10 mm. Bending tests showed that the ductility increases with the increase in the testing temperature. The ductility of 10 mm diameter rods which had been forged by the usual process was higher than that of specimens with a higher reduction. Increase in the forging temperature to 1600°C under conditions of normal reduction also ensures good ductility. If the forging temperature is reduced to 1300°C the ductility decreases also.

The test results also indicate that there is no direct relationship between the number of surface cracks on the rods and the ductility and strength of the metal.

Comparative studies on the ductility of rods forged by the ordinary process and in square dies showed that the latter have a much higher ductility.

Bibliography

1. Gubkin, S.I. Teoriya obrabotki metallov davleniem (Theory of Press Forming of Metals).—Metallurgizdat. 1947.
2. Pavlov, I.M. Teoriya prokatki (Theory of Rolling).—Metallurgizdat. 1950.
3. Osipov, V.G. Osnovnye metody izucheniya plastichnosti metallov pri obrabotke ikh davleniem (Basic Methods of Studying the Ductility of Metals during Press Forming).—In: Sbornik "Plasticheskaya deformatsiya metallov," Izdatel'stvo Nauka. 1964.
4. Osipov, V.G. Napryazhennoe sostoyanie pri vytyazhke prutkov pod ploskimi boikami (Stresses Induced during Stretching of Rods by Flat Hammers).—Trudy Instituta Metallurgii im. A.A. Baikova, No. 7, Izdatel'stvo AN SSSR. 1960.

5. Osipov, V. G. Napryazhennoe sostoyanie pri szhatii diska (pri rotatsionnoi kovke prutkov) chetyr'mya matritsami (Stresses Induced by Reduction of Disks (during Rotation Forging of Rods) in Four Dies). — Trudy Instituta Metallurgii im. A. A. Baikova, No. 7, Izdatel'stvo AN SSSR. 1960.

V. G. Osipov, E. V. Ushakov, E. K. Drobysheva, V. I. Kashin, and G. Kh. Vasyukov

FORGING TUNGSTEN PRODUCED BY ARC MELTING

Tungsten obtained by vacuum arc melting cannot be shaped by ordinary methods of forging because of its brittleness. Press forming cast tungsten is also difficult.

The ductility of the metal during press forming can be appreciably increased by increasing the hydrostatic compression and the uniformity of deformation /1 — 3/. On this assumption a method of forging has been developed which ensures that the above conditions are fulfilled. It is based on the method of forging highly alloyed steels suggested by Prozorov /4/.

Tungsten ingots produced from slabs of 99.9% purity were forged. The ingots were melted in a vacuum arc furnace (AC) with a 50 mm diameter crystallizer.

Before the ingots were forged they were machined to a diameter of 45 mm, which freed them completely from surface defects.

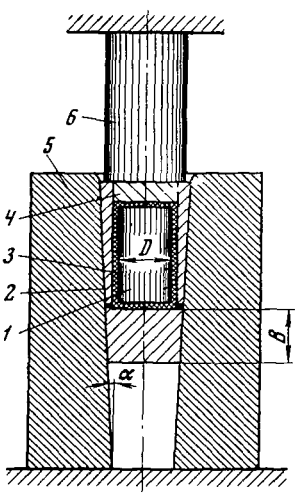

FIGURE 1. Forging tungsten ingots in a die:

1 — ingot; 2 — ring; 3 — thermal insulation; 4 — ring cover; 5 — die; 6 — punch.

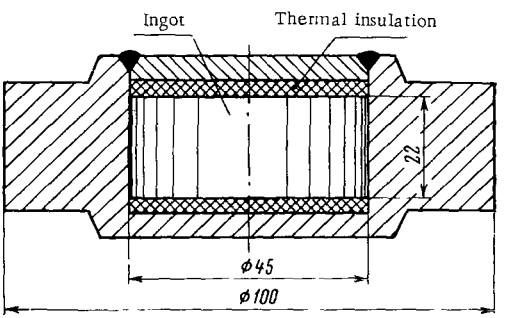

FIGURE 2. Tungsten ingot in a 1Kh18N9T steel ring.

The cast tungsten was forged on the machine shown in Figure 1. The ingot was placed into ring 2 made of 1Kh18N9T stainless steel. To slow down the cooling of the ingot the clearing between the ingot and the ring (2—3 mm) was filled with a mixture of aluminum oxide and kaolin. The thick bottom part of the jacket was used as a support. The thickness of the bottom should be approximately equal to the diameter of the ingot.

The ingot welded in the ring was heated to a temperature of 1300°C, and then placed into a conical die 5. The angle of taper α was 3—5°C. As the angle α was increased the stresses induced by the nonuniform compression at all sides increased, and the ductility of the metal improved. The formation was carried out with a punch 6 and a pneumatic hammer.

A further deformation was carried out after the ingot had been heated in another conical die with a smaller diameter but the same angle of taper. To obtain the necessary degree of deformation 3—4 dies were changed in succession. After the ingot had been elongated by 60—70%, it was further forged in ordinary die without taking it out of the ring into which it had been welded. The ring was removed by etching in a mixture of hydrochloric and nitric acids.

By the above method of forging, deformations of up to 70% can be obtained without any crack formation. The forging took place over the range of 1300—1000°C.

Tungsten sheet was produced by upsetting in 1Kh10N9T steel rings. Kick /1/ was the first to recommend upsetting materials of low ductility in rings. A ring with a welded ingot is shown in Figure 2. Photographs of macrostructures are given in Figure 3. The forging was carried out under pneumatic hammers with flat heads at a temperature of 1200—1300°C. After a deformation of 60—70% the ingots were rolled in rings. Before the material was rolled it was heated in an electric furnace to 1250°C. The rolling in rings was carried out to a thickness of 4 mm. The rings were etched away in a mixture of nitric and hydrochloric acids, and the tungsten was further rolled to 1 mm thick sheet.

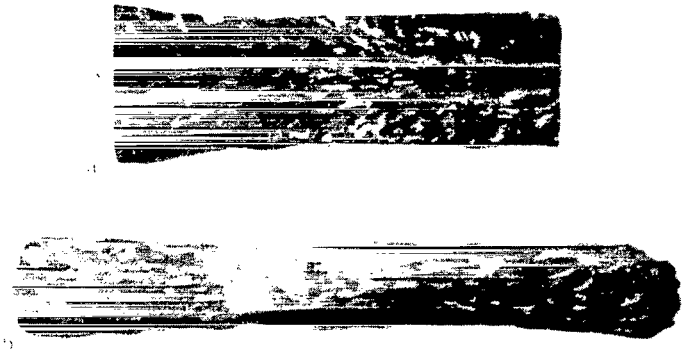

FIGURE 3. Macrostructure of deformed ingots:

1—after forging in dies; b—after upsetting.

Specimens (5 × 1 × 60 mm) for bending tests were cut out of the 1 mm thick sheet for determining the ductile—brittle transition temperature. Before the test the specimens were cleaned and electrolytically polished in a 10% solution of KOH at a current density of 1.5 amp/cm^2. Electropolishing removed a layer of metal 0.05 mm thick from each side.

The specimens were tested in the following three states: a) after rolling; b) after annealing at 900°C for 1 hr (to relieve stresses); and c) after recrystallization annealing at 1350°C for 1 hr.

The bending tests were carried out on a crank press by means of a device described in /5/.

CONCLUSIONS

It has been experimentally found that the critical ductile—brittle transition temperature for recrystallized tungsten is about 500°C. For deformed tungsten this temperature is 150°C and for tungsten annealed at 900°C to relieve stresses, it is also 150°C.

To determine the influence of the surface finish on the ductile—brittle transition temperature, some of the specimens were electrolytically polished. The tests carried out at 200°C showed that electrolytically polished specimens have an appreciably higher ductility. It has been proved that tungsten produced by arc melting can be forged in rings by a hammer at 1200—1300°C. The sheet has a satisfactory ductility. This has been confirmed by a bending test.

Bibliography

1. Kick, F. Die Prinzipien der mechanischen Technologie und die Festigkeitslehre.—Zeitschrift des Vereines deutscher Ingenieure, 36, No. 27. 1892.
2. Gubkin, S.I. Teoriya obrabotki metallov davleniem (Theory of Press Working of Metals).—Metallurgizdat. 1947.
3. Pavlov, I.M. Teoriya prokatki (Theory of Rolling).—Metallurgizdat. 1950.
4. Prozorov, L.V. Kovka vysokolegirovannykh stalei (Forging Highly Alloyed Steels).—Leningradskoe Otdelenie NITOMASh, No. 31.
5. Osipov, V.G., E.K.Drobysheva, E.V.Ushakov, N.M. Zelentsova, and A.G.Borisov. Issledovanie plastichnosti vol'frama marki VA na nachal'nykh stadiyakh obrabotki (Study of the Ductility of VA Tungsten during the Initial Stages of Working).—In: Sbornik "Napryazhennoe sostoyanie i plastichnost' pri deformirovanii metallov," Izdatel'stvo Nauka. 1966.

L. I. Ivanov, E. A. Abramyan, and V. A. Yanushkevich

NATURE OF HIGH-TEMPERATURE CREEP OF REFRACTORY METALS AND ALLOYS

It has been found /1, 2/ that the rate of high-temperature creep of body-centered metals with a high dislocation energy can be written as:

$$\dot{\gamma} = \frac{2\pi\lambda b\sigma D_0\tau^2}{\psi^2\eta^2\mu^2 RT}\exp\left(-\frac{Q}{RT}\right), \qquad (1)$$

where τ is the tangential stress; σ is the normal stress acting in the slip plane of dislocations; ψ is a coefficient representing the real shape of the dislocation loop, ≈ 1; η is the coefficient of screening of the elastic fields of dislocations by the boundaries of the subgrains; μ is the shear modulus; b is Burgers vector; Q is the activation energy of self-diffusion

$$\lambda = \frac{2\pi}{\ln r/R} \approx 0.8—1.3,$$

where R is the average distance between the dislocations in body-centered cubic metals during creep; $r \approx b$.

This equation is based on the assumption that high-temperature creep is completely controlled by the rate of diffusion of vacancies.

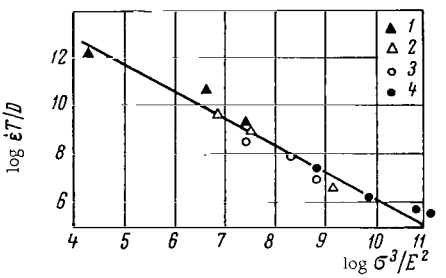

FIGURE 1. Dependence of log $\frac{\dot{\varepsilon}T}{D}$ on $(31\,g\sigma - 21\,gE)$ for tantalum:

1—normal stresses 44, 130, 236 kg/mm^2, temperature 1690°C; 2—normal stresses 11, 22, 44, 70, temperature 2080°C; 3—normal stresses 15, 22, 44, temperature 2390°C; 4—normal stresses 2.4, 2.87, 15, temperature 2630°C.

If the concentration of thresholds on the edge dislocations is insufficient, the shift of blocked dislocations and therefore the process of steady-state creep will be represented by the formula:

$$\gamma = \frac{2\pi\sigma\rho\beta}{RT}\frac{b\tau^2}{\eta^2\psi^2\mu^2}\exp\left(\frac{Q_1}{RT}\right), \qquad (2)$$

where β is a coefficient with the same dimensions as D_0, ρ is the concentration of thermal thresholds; Q_1 approximately corresponds to the activation energy of self-diffusion.

From the above equation of the steady-state high-temperature creep it follows that:

1) the rate of steady-state creep of body-centered metals does not depend on their initial structure at temperatures close to the melting point;

2) the rate of steady-state creep in these metals is strongly influenced by the coefficient of screening η, which is associated with the state of the boundaries of subgrains and of grains in the metal;

3) the relationship between the creep rate and stresses is governed by a formula with an exponent equal to ~ 3;

4) the creep rate depends on the concentration of thermal thresholds.

It has been experimentally shown that the above equations can be used to determine the high-temperature creep of pure body-centered metals /2, 3/.

Figure 1 shows the rates of the steady-state creep of pure tantalum experimentally obtained by Green /4/ for a temperature range of 0.6—0.8 T_s. To calculate these rates Green used formula (1). The theoretical and calculated rates agree well. Similar results were obtained for the creep of iodide β-titanium over a temperature range of 0.5—0.8 T_s /5/. For all these metals the activation energy of the steady-state creep does not depend on the applied stress but corresponds to the activation energy of self-diffusion over the same temperature range. If we calculate the coefficients of screening from these experimental data, we can see that for all the metals investigated these coefficients are equal to ~ 0.3.* The coefficients of screening for various metals and the alloys (α-solid solutions) Fe—Al are given below /6/.

Metal	β-Zr	Ta	Nb	Fe—Al α-solid solution
η	0.24	0.35	0.28	0.2

These coefficients of screening are close to similar coefficients calculated theoretically /7/.

We have already shown /3/ that contaminated metals have appreciably lower rates of high-temperature creep. The exponent, however, increases with the stress applied. This is proof of the influence of the applied stresses on the screening ability of the boundaries of grains and subgrains. The increase in η in contaminated metals, which leads to decrease in γ, is due to the influence of interstitial phases, and the decrease in η with increase in stresses is caused by a partial dissolution of these phases in the matrix.

The dependence of η on the stresses in contaminated metals is one of the reasons for the close exponential dependence of the rate of steady-state creep on stresses. This was confirmed experimentally during an investigation on the creep of commercial metals with a body-centered lattice /8, 9/.

Let us now see how $\mu^2 T$ influences the rate of steady-state creep of body-centered metals. It has been found /1, 10/ that if we take into account the temperature dependence of the shear modulus in the equation for creep, we shall obtain somewhat smaller values for the activation energy of creep.

* The coefficient was calculated assuming that $\psi \approx 1$ and $\lambda \approx 1$

Absolute magnitudes of $\mu^2 T$

Metal	T_{mp}	T/T_{mp}	$\mu^2 T$ at $\nu=0.4$
Nb	2741	0.6	$2.5 \cdot 10^{14}$
		0.89	$1.1 \cdot 10^{13}$—$1.6 \cdot 10^{13}$
Ta	3300	0.6	$5.8 \cdot 10^{14}$
		0.89	$7.3 \cdot 10^{13}$
Mo	2900	0.6	$1.6 \cdot 10^{14}$

However, these changes are usually small. Thus, it has been found that if we consider the temperature dependence of the shear modulus, the activation energy of the steady-state creep of tantalum decreases by ~ 6 kcal/g·atom (5% of the determined activation energy of creep) /4/. The empirical equation of Sherby /11/ was used for these calculations. If we assume that equation (1) is correct, the influence of the temperature dependence of the shear modulus on the activation energy of creep for β-Zr is even smaller /1/. Thus, this product has little influence on the temperature dependence of the rate of steady-state creep. The absolute magnitudes for various metals and alloys (substitutional solid solutions) are very close to one another. This is confirmed by the table, which gives the calculated product $\mu^2 T$ at two homologous temperatures.

For these calculations the data on the shear modulus for Nb and Fe—Al obtained by the authors were used, and literature data for Mo and Ta.

Consequently, for the same stresses, the pre-exponential terms for body-centered metals and for their solutions differ only in the magnitude of D_0. This can be illustrated by the dependence of the creep rate of body-centered cubic metals and of their alloys on their melting point.

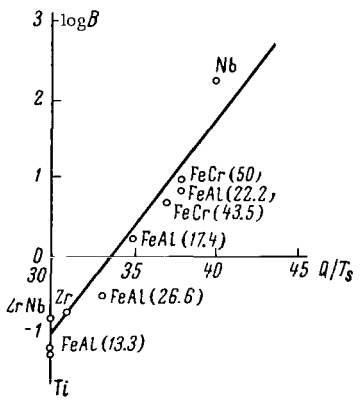

FIGURE 2. Dependence of the pre-exponential term B in the empirical equations of the creep of body-centered cubic metals and alloys on the melting point (the magnitude of $Q_{creep} = Q_{self\text{-}diffusion}$ for Ti and Zr were taken at T_s).

It is well known /12, 13/ that the coefficients of self-diffusion of these metals and alloys at the melting point are almost the same. Therefore, from the above analysis it can be assumed that the rates of steady-state creep will be the same for different metals and alloys at temperatures close to the melting point and under the same stresses.

Figure 2 shows the dependence of the logarithm of the pre-exponential term on Q/T_s, where Q is the activation energy of the steady-state creep; T_s is the melting point.

The experimental points lie on the curve with a slope of ~ 0.28 instead of 0.22 (T/R), i.e., $1/R$.

These differences can be explained by the scattering of the experimental

pre-exponential terms in the equation of creep. From this relationship the following equation for the creep rate can be written:

$$\gamma = 4 \cdot 10^{-8} \exp \frac{Q}{RT_s} \exp - \frac{Q}{RT} \tau^{3-4}, \qquad (3)$$

where γ is given in [1/sec]; Q is [kcal/mole]; and τ is [kg/cm^2].

The correctness of this equation is confirmed by the experimental data on the rate of the steady-state creep of some alloys, Nb—Ti and Nb—W, * at temperatures above 0.5 T_{mp}.

The data on the rate of the steady-state creep agree well with those calculated from equation (3).

An analysis of the theoretical equation of creep of body-centered cubic metals (2) shows that it is possible to calculate theoretically the rate of steady-state creep of metals and alloys from their melting points.

Bibliography

1. Yanushkevich, V.A. and L.I.Ivanov. Svoistva i primenenie zharoprochnykh splavov (Properties and Application of Refractory Alloys), p. 253.—Izdatel'stvo AN SSSR. 1966.
2. Ivanov, L.I. and V.A.Yanushkevich.—FMM, 17(1):112.
3. Abramyan, E.A., L.I.Ivanov, N.S.Kudryavtsev, and V.A. Yanushkevich.—Fiziko-Khimicheskaya Mekhanika, 2(4): 422—425. 1966.
4. Green, W.V. High-Temperature Creep of Tantalum.—Trans. AIME, 233, Oct. 1965.
5. Prokoshkin, L.I., L.I.Ivanov, and V.A.Yanushkevich.— Izvestiya Vuzov, Fizika, No. 5:65. 1961.
6. Ivanov, L.I. and E.A.Surova.—Izvestiya AN SSSR, OTN, Metallurgiya i Toplivo, No. 5. 1961.
7. Armstrong, R.W. and A.Nead.—Acta Met., 15, No. 7. 1965.
8. Bystrov, L.N., L.I.Ivanov, and E.A.Surova. Sbornik— Issledovaniya po zharoprochnym splavam (Collection—Study of Refractory Alloys), 9.—Izdatel'stvo AN SSSR. 1962.
9. Green, W.—Trans. AIME, 215(6):1057. 1959.
10. Barrett, Ardell, and O.Sherby.—Trans. AIME, 230(1):200. 1964.
11. Sherby, O.—Acta Met., 10, No. 2. 1962.
12. Gruzin, P.L. and G.B.Fedorov.—Doklady AN SSSR, 105, No. 2. 1955.
13. Askill, I. and G.Gibbs.—Phys. Status Solid, 11(2):557. 1965.
14. Wolls, B.A. and H.W.Pakton.—Trans. AIME, p. 230, Oct. 1964.

* The investigations were carried out together with N.V.Popov.

A. F. Orlov

CREEP OF NIOBIUM UNDER HIGH STRESSES

The creep of a number of metals and alloys with a face-centered cubic lattice at relatively low temperatures and under high stresses has been studied in /1—3/. It has been found that under high stresses the activation energy of creep decreases at first almost linearly with increase in stress until it reaches a constant value, and it is then no longer influenced by the stress. A quantitative determination of this relationship for Al, Pt, Ni, and Ni—Cu alloys has shown /4/ that in this region the activation energy of creep is determined, after reaching a constant value, by the energy of migration of mobile point defects in the crystal lattice. The purpose of this work is to determine the characteristics of the creep of niobium under high stresses and to find whether the above assumptions are also true for metals with a body-centered lattice.

For our investigations we took sintered niobium, which was remelted in a vacuum arc furnace. The contents of the main impurities (in wt %) were as follows: Ta, 0.21; Ti, 0.09; Si, 0.08; and Fe, 0.09. The rods were melted and then reduced in diameter from 34 to 8 mm by forging. They were then machined into specimens and thus the external oxidized layer of the metal removed. One batch of specimens was tested directly, and the other batch vacuum annealed for 10 hr at 1400°C.

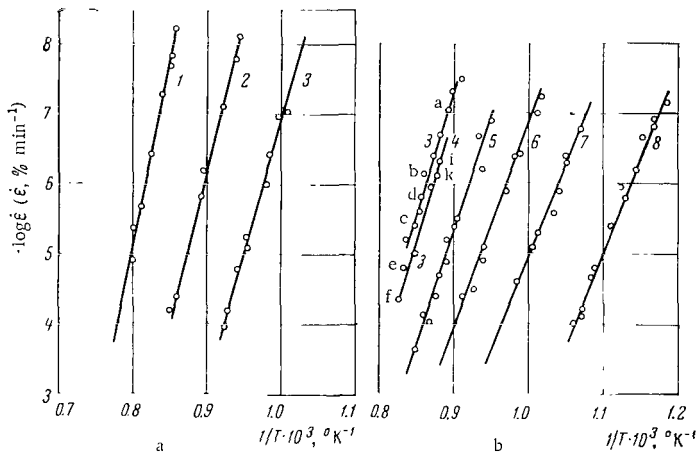

FIGURE 1. Dependence of the creep rate of annealed (a) and deformed (b) niobium on temperature under different stresses:

1—21.0 kg/mm²; 2—29.0; 3—33.6; 4—33.6; 5—42.4; 6—51.4; 7—56.3; 8—64.0. Letters a—k are the serial numbers of tests on the same specimen.

The tests were carried out on a VPM-S2 machine /6/ in a vacuum of $\sim 10^{-4}$ mm Hg under constant stress. The creep of the annealed niobium was studied over a temperature range of 700—1000°C, under stresses of 21.0 to 33.6 kg/mm². If a stress of 33.6 kg/mm² was rapidly applied the specimens failed at a temperature close to room. However, it was found

that slow loading (the stresses were increased at an average rate of 0.25 kg/mm^2 over 1 hr) accompanied by periodic short annealing at about 300°C led to partial strengthening of the specimens, which withstood the maximum load at creep-test temperatures for a prolonged period. Creep tests under higher stresses (up to 64 kg/mm^2) were carried out on deformed specimens over a temperature range of 550—900°C.

The results of the tests are given in Figures 1, a and b as the relationship between the logarithm of creep rate and the reciprocal of temperature for the steady-state creep of annealed and deformed Nb. For annealed niobium the slopes of the straight lines decrease monotonously with increase in stress, which corresponds to a decrease in the activation energy of creep. In the case of deformed niobium this relationship is found up to a stress of 56.3 kg/mm^2, but with further increase in stress the slopes remain constant within the limits of experimental error. The magnitudes of the activation energy of creep and of the pre-exponential term given in the table were found from the formula:

$$\varepsilon = A \exp(-Q/RT), \qquad (1)$$

where ε is the steady-state creep rate in $\%\cdot \text{min}^{-1}$; Q is the activation energy of creep in cal/g·atom; R is the gas constant; T is the temperature, °K.

Magnitudes of the activation energy of creep and of the pre-exponential term

State	σ, kg/mm^2	Q, kcal/g·atom	lnA
Annealed niobium.....	21.0, 29.0, 33.6	102.0, 85.7, 74.8	36.5, 32.8, 30.9
Deformed niobium.....	33.6, 42.4, 51.4	72.3, 63.5, 53.4	24.5,* 22.5, 21.6
	56.3, 64.0	53.7, 53.1	21.0, 23.5

* Not annealed during tests (see below).

It is interesting to note that at a stress of 33.6 kg/mm^2 the activation energy of creep of annealed and deformed niobium are about the same, but the creep rates at different temperatures differ by almost two orders of magnitude. We were unable to determine whether the activation energy of creep for annealed and deformed niobium agree at other stresses also. As we have already mentioned, annealed specimens of niobium fail even at room temperature under higher stresses. On the other hand, under relatively low stresses any noticeable creep rate of deformed specimens takes place at elevated temperatures close to the recrystallization point. The nature of the variation in the creep rate of one deformed niobium specimen during thermal cycling (experimental points for $\sigma = 33.6$ kg/mm^2 on Figure 1, b) apparently indicates that a softening of the deformed specimens takes place during the steady-state creep at these temperatures. In this experiment the total time of creep at temperatures corresponding to points e and f was about 6 hrs.

The dependence of the activation energy of creep on the applied stress is shown in Figure 2. Under stresses of 21—33 kg/mm^2 the activation energy is a decreasing linear function of the applied stress. Over this range the creep rate can be described with a satisfactory degree of accuracy by the equation:

$$\dot{\varepsilon} = A_1 \exp\left(-\frac{Q - \gamma\sigma}{RT}\right), \qquad (2)$$

where $\gamma = 2.3$ cal·mm^2/g·g-atom. A further increase in stress leads to a retardation in the activation energy, and starting at 55 kg/mm^2 the activation energy becomes constant. The section with constant activation energy represents a region in which the exponential law of the dependence of the creep rate on the applied stresses holds

$$\dot{\varepsilon} \sim \sigma^n. \qquad (3)$$

If the exponent in this formula is evaluated from the variation in the logarithm of the pre-exponential term it is found that $n = 18.7$.

A similar variation in the activation energy as a function of the applied stress had already been noted /3—5/, and the constant value of the activation energy for high stresses was believed to be the maximum value which can be reached for a given metal. As we have already mentioned, this value was compared to the value of the energy parameter $\tilde{q}$, calculated on the basis of the hypothesis on localized melting /5/, and to the activation energy of the movement of point defects (vacancies and interstitials in the crystal lattice). For niobium $q = 46.8$ kcal/g-atom /5/, and the activation energy of the motion of interstitial atoms $E_i = 27.7$ kcal/g-atom /7/. The energy of formation of vacancies $E_{f.v}$ in niobium is equal to 47.0 kcal/g-atom /8/, and the activation energy of self-diffusion $E_{s.d}$ in niobium is equal, according to different authors, to 97—106 kcal/g-atom. Hence $E_{s.d} - E_{f.v}$ gives us the activation energy of the motion of vacancies $E_{m.v}$ in niobium, which is equal to 50—59 kcal/g-atom.

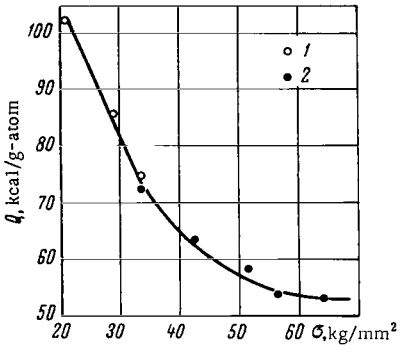

FIGURE 2. Dependence of the activation energy of creep of niobium on the stress:

1—annealed specimens; 2—deformed specimens.

Figure 2 shows that the maximum activation energy of creep of niobium under high stresses is about 53 kcal/g-atom. Such an agreement indicates that the creep of niobium under high stresses, like that of metals with a face-centered cubic lattice, is governed by an energetically activated motion of the point defects in the crystal lattice to the slip dislocations. In this case, such defects are apparently the vacancies. From the results of /9/ it is possible to calculate that in our case (deformation of niobium at the rate of 10^{-2}—10^{-4} % · min^{-1} at 600°C) the concentration of vacancies generated during deformation should exceed their equilibrium concentration at a given temperature by at least 11—13 orders of magnitude. Foudreaux /10/ found by experiment that supersaturation of vacancies in niobium is produced in the process of low-temperature plastic deformation.

It is characteristic that in our experiment the high rate of creep of deformed niobium was reached at temperatures above 500°C only, although according to the data of /11/, the strength characteristics of niobium vary slightly between room temperature and 600°C. At the same time, according to /7/ it can be expected that the single vacancies in niobium become mobile at temperatures of 350—500°C. It is thus indicated that vacancies participate in the creep of niobium over the range of temperatures studied

and under high stresses. At lower temperatures (below 300°K) the deformation point defects in niobium are almost immobile, and the creep rate is governed by the overcoming of the Peierls-Nabarro barriers because of energy fluctuations /12/.

Bibliography

1. Trozera, T.A., O.D.Sherby, and J.E.Dorn.—Trans. ASM, 49:173. 1957.
2. Carreker, R.P.—J.Appl. Phys., 21:1289. 1950.
3. Orlov, A.F. and K.A.Osipov. Sbornik—Svoistva i primenenie zharaprochnykh splavov (Collection—Properties and Use of Refractory Alloys), p. 178.—Izdatel'stvo Nauka. 1966.
4. Orlov, A.F. and K.A.Osipov. Sbornik—Diffuzionnye protsessy v metallakh (Collection—Diffusion Processes in Metals), 2.—Kiev, Izdatel'stvo Naukova Dumka. 1966.
5. Osipov, K.A. Voprosy teorii zharoprochnosti metallov i splavov (Problems of the Theory of Heat Resistance of Metals and Alloys).—Izdatel'stvo AN SSSR. 1960.
6. Sotnichenko, A.L. Peredovoi nauchno-tekhnicheskii i proizvodstvennyi opyt (Progressive Scientific and Technical and Industrial Experience).—Filial VINITI, Tema 32, No. 11—59—68/6. 1959.
7. Stals, L. and J.Nihoul.—Phys. status solidi, 8:785. 1965.
8. Kraftmakher, Ya. A.—Fizika Tverdogo Tela, 5:950. 1963.
9. Wazzan, A.R. and J.E.Dorn.—J. Appl. Phys., 36:222. 1965.
10. Foudreaux, A.M. and A.Wronskii.—Metal Sci. Revue metallurgie, 61: 185. 1964.
11. Prokoshkin, D.A. and E.V.Vasil'eva. Splavy niobiya (Niobium Alloys).—Izdatel'stvo Nauka. 1964.
12. Stone, G.A. and H.Conrad.—Acta metallurgica, 12:1125. 1964.

V. G. Chernyi and I. M. Nedyukha

PHYSICAL FACTORS LEADING TO THE STRENGTHENING OF ALLOYED NIOBIUM

The number of works on the nature of the strengthening of alloys and solid solutions has recently increased. However, most of these were carried out with materials of low melting point. Considerably less attention has been paid to the strengthening of refractory metals which are today being increasingly used in new branches of industry.

The purpose of this work is to investigate the factors which lead to the strengthening of cast niobium alloys and their importance.

We studied solid solutions of niobium with titanium, vanadium, tantalum, molybdenum, and tungsten over wide concentration limits (0—40 wt% of the alloying element).

The alloys were melted in an arc furnace in an argon atmosphere. We used the following metals as starting material: niobium (99.4%, main impurity tantalum), titanium (99.5%), vanadium (99.4%), tantalum (99.9%), molybdenum (99.99%), and tungsten (99.95%). To distribute the components uniformly each alloy was remelted 4—5 times. The alloys were investigated in the cast state.

The elastic properties were determined by the dynamic pulse method using a device similar to that described in /1/. These measurements were carried out with an accuracy of 1—2% (including possible errors). The numerical magnitudes of the elasticity modulus E and of the shear modulus G were found from the known formulas /2, 3/.

The dimensions of the regions of coherent dispersion D (mosaic blocks) and the variation in the crystal lattice parameters $\Delta a/a$ were found from the width of the interference lines (110) and (310) /4/. In our calculations of D and $\Delta a/a$ we introduced corrections for nonmonochromatic light and for the geometric layout of the whole apparatus /4, 5/. The X-ray diagrams were produced by a URS-50I diffractometer with iron irradiation K_α. The density of dislocations was evaluated from the width of the interference lines (110) and from the data on the dimensions of the mosaic blocks and variation in the parameter $\Delta a/a$ /6, 7/.

The microstructure was studied by the MIM-7 optical microscope at a magnification of X 220. The hardness was measured on a TP hardness meter (Vickers) at a load of 20 kg.

In this work we also compared the experimental data with the theory of strengthening of substitutional solid solutions as suggested by Fleischer /8—10/.

According to this theory, the elastic interactions between the dissolved atoms and the dislocations, which are the main cause of the strengthening of alloys by solid solutions, are the result of two effects:

1) the difference in the dimensions of the atoms of the solvent and solute, and 2) their different elasticities.

The first effect which leads to the distortion of the crystal lattice is the dissimilarity in the atomic dimensions, first discovered by Mott and Nabarro. Quantitatively, this effect is determined by the magnitude ε_a, which is equal to $1/a \cdot \frac{da}{dc}$, where a is the lattice parameter and $\frac{da}{dc}$ represents its change as a function of the concentration of alloying elements in the solid solution.

The second effect, which Fleischer calls modulus effect, characterizes the interaction between dislocations and atoms of different rigidities which act as elastic-hard and soft spots (regions) in the matrix. This effect is quantitatively determined by the magnitude $\varepsilon_{G'}$, equal to

$$\frac{1}{G}\frac{dG}{dC}\left(1 + \frac{1}{2G}\left|\frac{dG}{dC}\right|\right)^{-1},$$

where G is the shear modulus, and $\frac{dG}{dC}$ is the variation in the modulus as a function of the concentration of the solid solution.

According to Fleischer, the strengthening of the crystal by different atoms can be monotonous, and increase as a function of $\varepsilon_S = (\varepsilon_{G'} - \alpha\varepsilon_a)$. The magnitude α shows which dislocations, linear or screw, control the slip

process. For linear dislocations, α cannot be less than 16, while for screw dislocations it cannot be greater than 16 /9, 11/.

For an experimental check of Fleischer's theory on strengthening, data are necessary on the dependence of strengthening, lattice parameters, and shear modulus on the concentration of alloying elements in a given matrix. If we have such data, it is possible to plot the dependence of dH_0/dC on ε_a, $\varepsilon_{G'}$, and ε_S, which can clarify the question of what strengthens the metal, and which dislocations govern the slip process.

Figure 1 shows data on E, G, θ and $\sqrt{\overline{u^2}}$ for the alloys studied. These data indicate that alloying niobium with vanadium, tantalum, molybdenum, and tungsten increases their elasticity and shear moduli. Alloying with about 20 at. % of titanium has almost no influence on E or G. Further increase in the titanium content leads to a decrease in E and G.

The characteristic temperature of niobium is appreciably increased by alloying with molybdenum and vanadium, and but is little influenced by alloying with tantalum, tungsten, and titanium. The value of θ is increased if 10 at. % of these elements are added to niobium. Further increase in the content of tantalum and tungsten to 25 at. % and of titanium to 57.5 at. % has almost no influence on the characteristic temperatures of the alloys.

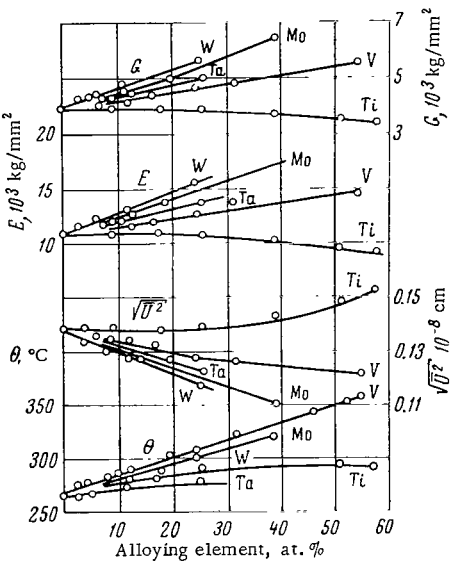

FIGURE 1. Dependence of the normal elasticity E and shear G moduli, the characteristic temperature θ, and the standard deviation $\sqrt{\overline{u^2}}$ of atoms in the crystal lattice of niobium on alloying.

The standard deviation of the atoms in the crystal lattice of niobium decreases in alloys containing vanadium, tantalum, molybdenum and tungsten over the whole range of concentrations studied but in the case of alloys containing titanium $\sqrt{\overline{u^2}}$ is almost uninfluenced up to 25% of Ti, and then it increases.

An analysis of the interference lines showed that the width of line (110) is little influenced by increase in the content of alloying elements in niobium. In the case of niobium—vanadium and niobium—tungsten alloys, the width is somewhat increased, and for niobium alloys containing molybdenum, titanium, and tantalum variations in the width of the line remain within the limits of experimental error. The greatest changes can be seen in the (310) interference lines. The width of line (310) is appreciably increased by adding vanadium and tungsten, and to a lesser degree, molybdenum. The width of line (310) produced by niobium—tantalum and niobium—titanium alloys is increased if the content of tantalum is increased to 15 at. % and the content of titanium to 25 at. %, but then the width of the lines decreases again.

If the elements of fine crystal structure are determined from the width of interference lines (110) and (310), Figure 2 indicates that: the mosaic

blocks of the alloys investigated change little, and in Nb alloys with up to ~ 20% of alloying elements the smallest blocks are found in alloys containing molybdenum and titanium, and in more highly alloyed materials the smallest blocks are in niobium—vanadium and niobium—tungsten alloys.

The greatest variation in the lattice parameters, $\Delta a/a$, over the whole range of concentrations studied can be found in niobium—vanadium alloys, while the smallest variation is characteristic of niobium—titanium alloys.

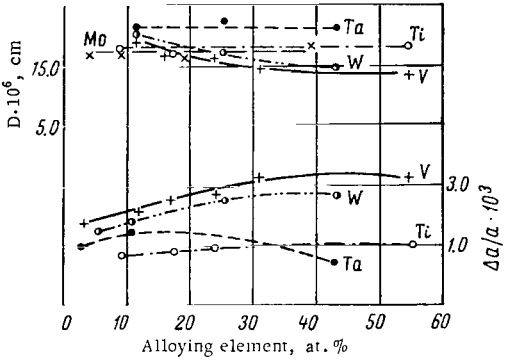

FIGURE 2. Dependence of the dimensions of the mosaic blocks D and of the variation in the lattice parameter $\Delta a/a$ of niobium on the content of alloying elements.

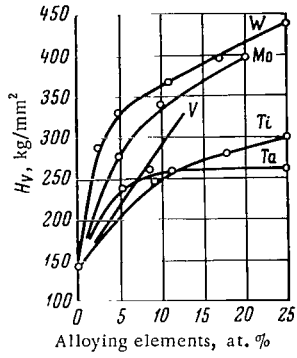

FIGURE 3. Dependence of the hardness of niobium alloys on the content of alloying elements.

The density of dislocations in these alloys was investigated by X-ray analysis, and shows that alloying leads to an increase in the density of dislocations. Thus, alloys with about 5 at. % of alloying elements have a density of dislocations equal to approximately $6-7\cdot10^{10}$ 1/cm^2, alloys with 25—30 at. % of tungsten and vanadium have a density of $2-3\cdot10^{11}$ 1/cm^2, and alloys with the same content of molybdenum, titanium and vanadium have a similar density of dislocations.

The microstructure of niobium alloyed with small amounts of other elements (up to 5 at. %) differs little from the polyhedral structure of cast niobium. If more than 10 at. % of alloying elements are added to niobium its structure changes markedly. If tungsten, vanadium, and titanium are added, the microstructure of niobium is clearly denditric in nature.

Data on the variation in the hardness of the alloys studied are given in Figure 3. According to the decrease in hardness caused by the addition of up to 5 at. % of alloying elements, the alloys can be placed in the following series: niobium—tungsten, niobium—molybdenum, nobium—tantalum, niobium—vanadium and niobium—titanium. After further increase in the content of alloying elements to 25 at. %, the niobium—tungsten and niobium—molybdenum alloys are still the hardest. The softest material with 25 at. % of alloying elements is the niobium—tantalum alloy.

An analysis of the above data indicates that as the content of alloying elements in niobium increases, there is a change in the factors which determine its strengthening. If the concentration of the alloying elements is 0—5 at. %, the chief factor which determines the strength of the alloy

is apparently the strength of the interatomic bonds; the stronger the interatomic bonds become on alloying, the greater is the strengthening produced in the alloy. The greatest strengthening effect is found in niobium—tungsten alloys in which the strength of interatomic bonds is highest, and the smallest strengthening occurs in niobium—titanium alloys in which the strength of the bonds in the lattice is lowest. The data of X-ray and metallographic studies show that the role of structural changes over this range of concentrations is much smaller.

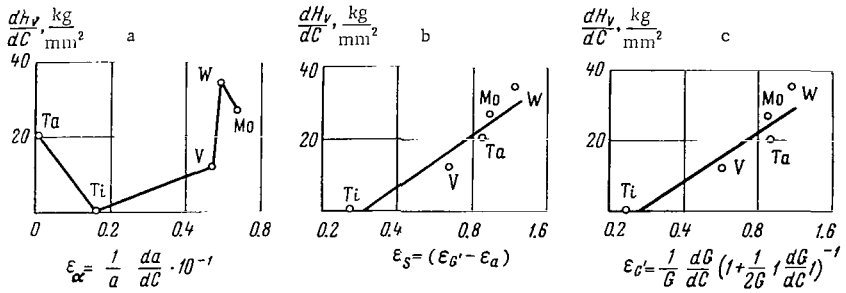

FIGURE 4. Dependence of the strengthening of niobium alloys on the dissimilarity in the atomic dimensions ε_a (a), the dissimilarity in the elastic moduli ε_S (b), and on the total effect of the atomic and elastic dissimilarities $\varepsilon_{G'}$ (c).

As the content of alloying elements is increased, the role of structural changes in the process of strengthening increases.

Figure 4 shows the dependence of the strengthening of niobium on the parameters ε_a, $\varepsilon_{G'}$, and ε_S at a content of alloying elements up to 5 at. % (the data on the lattice constants are taken from /12—16/).

Figure 4, *a* shows that the dependence of dH_V/dC on ε_a is not smooth, and consequently the strengthening cannot be due to the dissimilarity in atomic dimensions only. The dependence of strengthening on the parameter $\varepsilon_{G'}$ is almost smooth, but a certain scattering exists (Figure 4, b). Thus, the strengthening cannot be explained only by the difference between the moduli.

The dependence of dH_V/dC on $\varepsilon_S = (\varepsilon_{G'} - 16\,\varepsilon_a)$ shows a considerable scattering of data, which is increased if the coefficient α is above its lower limit of 16. Considerably less scattering is found if $\alpha = 3$, and even less if $\alpha = 1$ (Figure 4, c), i.e., for coefficients which correspond to screw dislocations.

In this work we checked the accuracy of Fleischer's theory on strengthening for alloys containing more than 5 at. % of alloying elements also, but in this case we could not find any regular dependence of the strengthening of these alloys on the dissimilarity in atomic dimensions, the dissimilarity in elastic moduli, and on the combined effect of these two factors.

This is apparently because the structural changes, which are not considered in Fleischer's theory, are of great importance in the strengthening of alloys.

The data of this part of the work indicate that the strengthening of niobium alloys by tungsten, molybdenum, tantalum, vanadium, and titanium, in amounts of up to 5 at. %, is determined by the stresses necessary for

movement of edge dislocations, and that these stresses are determined by the differences between the atomic dimensions and between the moduli of elasticity of these metals (moduli effect). The moduli effect contributes more to the strengthening than the difference between the atomic dimensions. It should be pointed out that the differences between the moduli of elasticity of niobium and the alloying metals is the cause of from 65 to 90% of the strengthening.

The results of this part of the work agree well with the experimental data of the first part of the work, with the data of Fleischer /9, 10/ who investigated copper-base alloys, and also with the data of McAdam /17/, who studied niobium alloys forged at 600°C.

Bibliography

1. Polotskii, I.G., T.Ya.Benieva, and Z.L.Khodov. Sbornik—Issledovaniya po zharoprochnym stalyam (Collection—Study of Heat-Resistant Steels), 3:310.—Moskva, Izdatel'stvo AN SSSR. 1958.
2. Köster, W.—Z. Metallk., 39:149. 1948.
3. Frantsevich, I.N. Sbornik—Voprosy poroshkovoi metallurgii i prochnosti materialov (Collection—Problems of Powder Metallurgy and Strength of Materials), No. 3.—Kiev, Izdatel'stvo AN USSR. 1956.
4. Lysak, L.I. Sbornik—Voprosy fiziki metallov i metallovedeniya (Collection—Problems of Physics of Metals and Metallurgy), No. 5.—Kiev, Izdatel'stvo AN USSR. 1954.
5. Arbuzov, T.P.—Doklady AN SSSR, 73(1):83. 1950.
6. Williamson, G.K. and R.F.Smallman.—Phil. Mag., 1:34. 1956.
7. Guseva, L.N. and A.A.Babareko.—Izvestiya AN SSSR, OTN, 6:98.
8. Fleischer, R.J.—Acta Met., 9:996. 1961.
9. Fleischer, R.J.—Acta Met., 11:203. 1963.
10. Fleischer, R.J. and W.R.Hibbard. The Relation between the Structure and Mechanical Properties of Metals, 1:261, London. 1963.
11. Stehle, H. and A.Seeger.—Z. Phys., 146:217. 1956.
12. Krimer, B.I.—ZhNKh, 3:895. 1958.
13. Eremenko, V.N.—Ukrainskii Khimicheskii Zhurnal, 20:227. 1954.
14. Wilchelm, H., O.Carlson, and H.Dichinson.—J. Metals, 6:195. 1954.
15. Shakhova, K.I. and P.B.Budberg.—Izdatel'stvo AN SSSR, OTN, 4:56. 1961.
16. Williamson, G.K.—Trans. ASM, 50:1081. 1958.
17. McAdam, G.D.—J. Inst. Metals, 93:559. 1964—1965.

A. P. Semenov and V. V. Pozdnyakov

METHODS AND RESULTS OF A STUDY ON THE FRICTION AND THE ADHESION BETWEEN METALS AT ELEVATED TEMPERATURES IN VACUO AND IN GASES

METHODS OF INVESTIGATION

The main apparatus for studying friction and adhesion of metals at elevated temperatures is a modified high-frequency vacuum furnace of the MVP-3M type with which it is possible to heat specimens up to 200°C in a vacuum of about 10^{-4}—10^{-5} mm Hg. The apparatus /1/ is shown diagrammatically in Figure 1, and specimens which are not in contact with one another can be heated (radiation heating from a tubular graphite or tungsten high-frequency heater), and then brought into contact at the given temperature. The required load is then applied and the contacting surfaces slide against one another. To make accommodation easy, sliding takes place between the butt ends of large tubular specimens.

The lower specimen is mounted at the top of the graphite tube and rotated together with it. The upper specimen is mounted on the graphite rod which passes concentrically through the tube. The lower end of the rod is connected to the loading—measuring mechanism which consists of two systems in the mutually perpendicular planes of the flat exchangeable springs. Each spring reacts individually tc the normal load and to the moment of friction. The load is applied by bending the proper springs. The acting normal loads and the moments of friction are recorded on photographic plates without distortion (there are no places with interfering friction in the loading—measuring mechanism), using high-temperature resistance deformation devices, glued to the springs, a TA-5 amplifier, and a loop oscillograph of the POB-14 type.

With this apparatus it is possible to investigate the following phenomena in vacuo and in gaseous media: a) friction at a constant temperature or during heating or cooling when the specimens slide continuously; b) adhesion; c) chemical reactions between contacting specimens; d) welding under pressure (which is important for the industrial production of articles from these materials and for diffusion welding); and e) mechanical properties.

By this method we investigated the friction of similar and dissimilar pure metals (total load ~5 kg; rate of sliding 0.8 m/min) in vacuo and in gases at elevated temperatures.

The tests in gases were carried out after the tests in vacuo. The total feeding system and the vacuum chamber were flushed with gas at room temperature, and then the gas was evacuated to a final pressure of ~ 10^{-5} mm Hg. The apparatus was heated to the required temperature, and gas was again introduced (to a pressure 50—100 mg Hg below atmospheric pressure), and the tests were carried out with the same volume of gas, and the temperature was increased to the maximum (recording of friction during heating). The gas was then cooled to room temperature (friction during cooling). During both heating and cooling the friction moment and the load were recorded in the same way as during tests in vacuo.

In our studies we used pure argon (content of oxygen less than 0.05%), pure helium (content of oxygen and other impurities about 0.02%) and

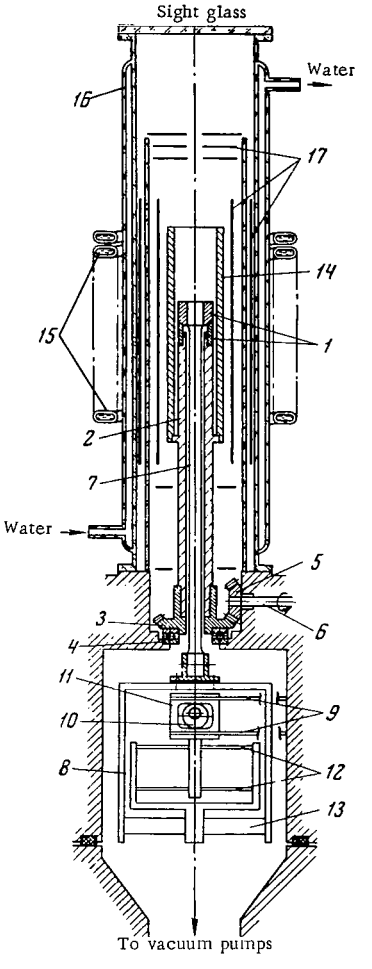

FIGURE 1. Diagram of an apparatus for studying friction and adhesion at elevated temperatures:

1—specimens; 2—graphite tube made to rotate (the lower specimen is fastened to the top end); 3—bevel pinion; 4—ball thrust bearing; 5—driving bevel pinion; 6—drive shaft; 7—graphite rod (the upper specimen is fastened to the top end); 8—loading and measuring mechanism; 9—suspension springs; 10—cam; 11—rigid frame of the loading and measuring mechanism; 12—springs for recording loads along the rod; 13—springs for recording the friction moment; 14—tubular heater; 15—induction coil; 16—water-cooled quartz cylinder; 17—system of molybdenum and quartz screens.

commercial nitrogen (content of oxygen 0.5%). Since the graphite heater and the molybdenum screens become heated to higher temperatures than the specimens themselves, the oxygen in the chamber reacts first with them, producing oxides of molybdenum and carbon monoxide (reduction atmosphere). Thus, the oxygen which enters the chamber together with the inert gas becomes neutralized and has no great influence on the test results at elevated temperatures.

The curves characterizing the dependence of friction on temperature were plotted for the average values of the friction coefficient.

INFLUENCE OF TEMPERATURE ON THE FRICTION AND ADHESION OF SIMILAR AND DISSIMILAR METALS

The metals were tested for friction during heating and cooling under conditions of continuous sliding of the specimens. Before the test the specimens were heated (without contact) in vacuo at 1200°C to free the surface from any traces of impurities. In the adhesion tests different specimens were brought into contact at a given temperature and load, and held under this load for 3 min. The force needed to separate the specimens was recorded. The ability of the metals to adhere was evaluated from the adhesion coefficient, which is the ratio of the breaking force to the compressive force initially applied. The studies in gases were carried out after friction and adhesion tests in vacuo.

We tested pairs of similar metals of group IVB (titanium, zirconium), VB (niobium, tantalum), VIB (molybdenum, tungsten) and VIII (cobalt) of the periodic system of elements and also seven pairs of dissimilar metals. Some characteristics of the metals are given in the table.

The results of adhesion tests on similar metals are given in Figure 2,a in the coordinates: adhesion coefficient versus relative temperature. For the

metals we investigated the temperature at which adhesion starts is 0.3—0.4 T_{mp}. This agrees well with the values already found for temperatures at the beginning of sintering of powders in a reduction atmosphere, and of the adhesion of crossed wires in a vacuum of 10^{-7}—10^{-8} mm Hg /2/. The adhesion under these conditions is apparently due to the beginning of sintering under pressure caused by thermal activation. The surface films, which can be formed in a vacuum of 10^{-4}—10^{-5} mm Hg, either vaporized (oxides of molybdenum and tungsten) or were removed from the zones of contact into the crystal lattices of the contacting specimens (dissolution) as a result of diffusion.

Properties of the metals studied

Metal	Group of periodic system	Crystal lattice	Atomic radius, Å	Melting point, °C	Method of production
Titanium	IVB	Hexagonal, above 882.5°C body-centered cubic	1.47	1668±5	Iodide, forged
Zirconium	IVB	Hexagonal, above 865°C body-centered cubic	1.60	1852	The same
Niobium	VB	Body-centered cubic	1.47	2468±10	Remelted in a vacuum arc furnace furnace
Tantalum	VB	Body-centered cubic	1.47	3000±50	Sintered, forged
Molybdenum	VIB	Body-centered cubic	1.40	2620±10	Remelted in a vacuum arc furnace
Tungsten	VIB	Body-centered cubic	1.41	3380	Sintered (rod)
Cobalt	VIIIB	Hexagonal, above 400°C, face-centered cubic	1.25	1495	Sintered, forged

The adhesion of titanium, which over this range of temperatures has a hexagonal close-packed crystal lattice, starts at the lowest temperature. This metal is followed by the metals of groups VB and VIB /3/, which have a body-centered cubic lattice. The influence of additional mechanical activation on adhesion has been demonstrated on molybdenum and tungsten. A repetition of the adhesion tests on tungsten specimens shortly after the first test led to a less rapid increase in the adhesion coefficient (dashed line in Figure 2, a) which may be due to a relief in the distortion of the crystal lattice (caused by friction) during the first series of adhesion tests. In the case of molybdenum the influence of additional mechanical activation during tests in which the application of a small twisting moment, but without sliding of one specimen over the other, led to additional deformation at the areas of real contact. The application of such a moment under pressure caused a considerable increase in the adhesion coefficient, to a value above 0.2 at relatively low temperatures.

Zirconium, with its hexagonal structure up to 865°C, is less susceptible to adhesion than titanium and the body-centered metals of groups VB and VIB.

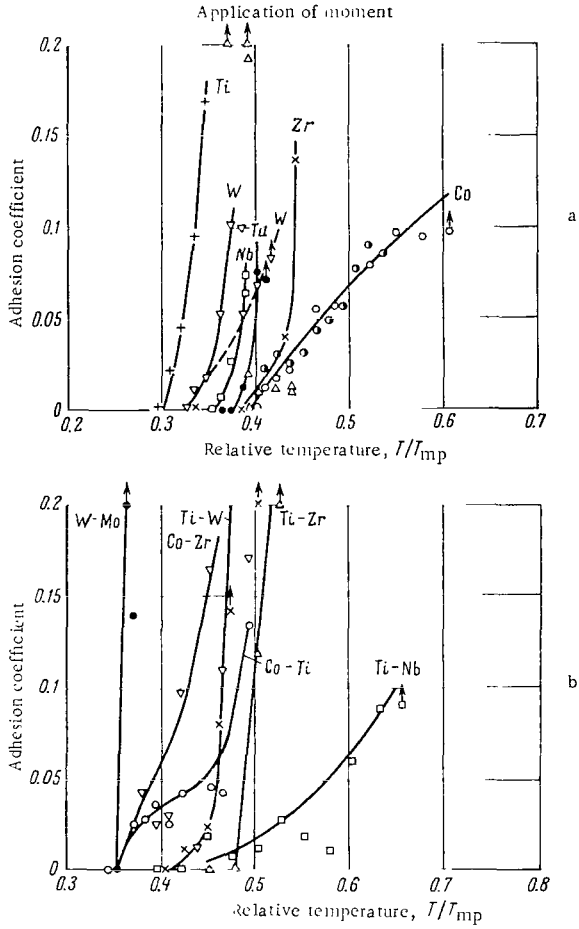

FIGURE 2. Dependence of the adhesion coefficient on the relative temperature:

a—for similar metals (the half-shaded circles for cobalt refer to tests in helium); b—for dissimilar metals (the temperature is calculated for the metal with the lower heat resistance).

Of the metals we investigated, cobalt (group VIIIB) has the lowest susceptibility to adhesion, which only starts at a high temperature. The increase in the adhesion coefficient of cobalt is slow. The adhesion coefficient of cobalt is the same in helium as in vacuo.

The friction tests carried out in vacuo showed that a certain correlation exists between the coefficient of friction and its variation, and the type of crystal lattice and position of the metal in the periodic system. Figure 3, a shows the dependence of the average values of the coefficients of friction (without taking into account fluctuations in the coefficient of friction due to frictional autovibrations) on temperature. The dashed line characterizes the temperatures at which adhesion starts (see Figure 2, a), and the

continuous line the temperature of polymorphic transformations (in the case of cobalt and titanium).

Titanium and zirconium with hexagonal close-packed lattices have low coefficients of friction, which vary little with temperature up to $0.4T_{mp}$. Further increase in temperature leads to a considerable increase in the coefficient of friction (in particular for zirconium). The coefficient of friction of niobium and tantalum (group VB), which are relatively ductile and have a body-centered cubic structure over the whole range of temperatures, decreases appreciably (from a value of above 1) at room temperature to ~0.5, but then increases as rapidly. The minimum coefficient of friction for niobium almost coincides with the temperature at the beginning of adhesion, but for tantalum the minimum coefficient of friction was found to be ~200°C below the temperature at which adhesion starts. The curves for niobium and tantalum representing the dependence of the coefficient of friction on the relative temperatures almost coincide.

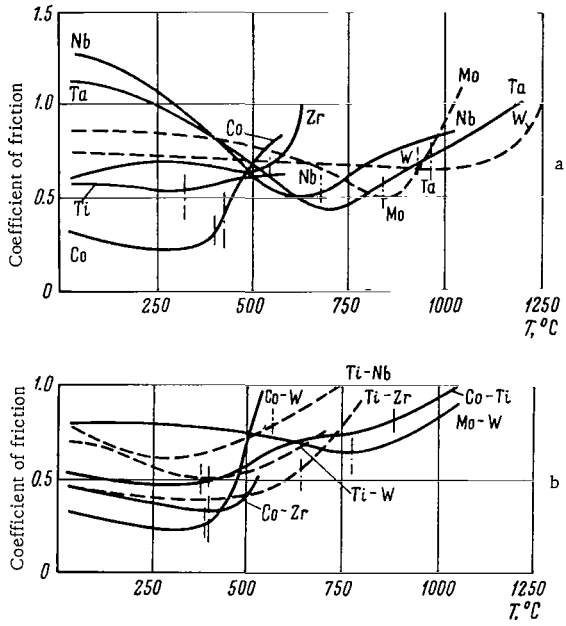

FIGURE 3. Dependence of the average value of the coefficient of friction on temperature:

a—similar metals in vacuo (tested during heating); b—dissimilar metals in vacuo (tested during heating).

Over the range of relatively low temperatures, the coefficient of friction of molybdenum and tungsten (group VIB) is appreciably lower than that of metals of group VB, but it is higher than that of metals of group IVB. The dependence of the coefficient of friction on temperature for molybdenum is similar to that for the more ductile metals of group VB. Tungsten shows a characteristic small decrease in the coefficient of friction from about 1100°C, which is followed by a sharp increase. A comparison of the results

of a study on transition metals of three groups of the periodic systems (IV, V, VI) which have unfilled *d*-shells, indicates that the curves for metals of group VIB lie between the curves for metals of groups IVB and VB.

The results of the study on molybdenum and tungsten are interesting. They show that the oxides of these metals are volatile and the retained oxygen has no influence on the characteristics of friction of these metals as the surfaces are self-abrading /4/. However, we found no fundamental differences between the behavior of all seven metals during the investigation (vacuum $10^{-4}-10^{-5}$ mm Hg).

The results with cobalt are also very interesting. At temperatures up to the start of the polymorphic transformation from the hexagonal close-packed structure to a face-centered cubic structure, at which adhesion starts, the friction of cobalt is very low (coefficient of friction ~ 0.2). Above these temperatures the coefficient of friction increases greatly. If the temperature is increased, the opposite occurs, but with certain hysteresis. This is apparently due to a hysteresis in the reverse polymorphic transformation into a hexagonal close-packed lattice. There are reasons to believe that during friction cobalt can exist in two crystal modifications (hexagonal close-packed and cubic face-centered) over a wide range of temperatures.

The results of investigations of similar metals given in Figure 3, a show that metals with a hexagonal close-packed structure are less susceptible to friction. This conclusion agrees well with the results of other studies carried out in air /5/. The decrease in the coefficient of friction caused by an increase in temperature to about $0.3-0.4\,T_{mp}$ is particularly marked in metals with a body-centered cubic structure. This phenomenon is apparently due to a decrease in the role of work hardening of the volumes of metal which participate directly in friction. At temperatures which are close to that at the beginning of recrystallization (in the case of cobalt also the beginning of polymorphic transformation), the susceptibility of metals to galling and adhesion increases greatly (see Figure 2, a), as already found by the method of combined plastic deformation /6/, and the coefficient of friction starts to increase greatly. These temperatures are very much influenced by the purity of the metal (chemical composition) and by the type of crystal lattice. The latter, in turn, is determined by the position of the metal in the periodic system, and finally by the nature and the alignment of bonds between atoms in the crystal lattice (the role of the exchangeable directional bonds /3/).

A study of the adhesion between seven pairs of different metals has shown (see Figure 2, b) that dissimilar metals adhere to one another, although at higher relative temperatures than similar metals (the relative temperature is calculated for the metal with the lower heat resistance). The lowest temperature at which adhesion starts is found in the molybdenum—tungsten pair, which can be explained by the similar crystal structures and the equality of atomic radii (which differ by only 0.7%), by the complete mutual solubility (formation of a continuous series of solid solutions at all concentrations), and by similar chemical properties, as both metals belong to the same group of the periodic system. A certain influence can also be exerted by the volatility of the oxides of tungsten and molybdenum.

The relatively low starting temperature of adhesion between pairs containing cobalt (cobalt—zirconium, cobalt—titanium, cobalt—tungsten)

is apparently due to the polymorphic transformation of cobalt into a body-centered cubic modification. A reason for this low temperature may also be that in the periodic system cobalt is far from tungsten, titanium, and especially zirconium. The activity of the chemical interaction between these metals should also be influenced. These factors, apparently, lead to considerable adhesion between these metals even though the dimensional factors are unfavorable (considerable difference between atomic radii).

In the titanium—tungsten and titanium—zirconium pairs, the higher susceptibility to adhesion of the first pair may be because the differences between the atomic radii (4%) are smaller than in the second pair (8%). The slow growth in the strength of adhesion between titanium and niobium is unclear (the adhesion starts at a relatively low temperature), especially as the atomic radii of these two metals are the same, though over this range of temperatures, their crystal structures are different.

The friction between different metals depends on the properties of the individual metals and on the relationship between the properties of the metals in the pair, which is determined by the position of these metals in the periodic system.

The curve representing the dependence of the coefficient of friction on temperature for tungsten—molybdenum pairs (Figure 3, b) was plotted from the average data for tungsten and molybdenum. The beginning of the increase in the coefficient of friction coincides with the recorded temperature at which adhesion starts. This point and also the minimum on the curve representing the temperature dependence of the coefficient of friction lie at lower temperatures than that for molybdenum.

The coefficient of friction—temperature relationships for the cobalt—zirconium, and especially for the cobalt—tungsten, pairs are the same as for specimens of cobalt alone. Apparently, during friction between two different metals, the softer and less heat-resistant cobalt is transferred to the surface of the other metal, and as a result cobalt rubs against cobalt with the ease characteristic of this metal at low temperatures.

The dependence of friction on temperature for titanium against cobalt, zirconium, niobium, and tungsten is similar to that of titanium against titanium. The determining factor in all these cases is apparently titanium (except, perhaps, the cobalt—titanium pairs). The metal paired with titanium exerts a certain influence on the friction coefficient. Thus, the friction is highest for the titanium—niobium pair (the atomic radii of these metals are the same), the friction is somewhat lower for the titanium—tungsten pair (the difference between the atomic radii of these metals is 4%), and it is still lower for titanium—zirconium pairs (the difference between the atomic radii of these metals is 8%).

As in the case of two specimens of the same metal, the beginning of adhesion is accompanied by a sharp increase in the coefficient of friction. The polymorphic transformation at elevated temperatures also leads to an increase in the coefficient of friction. This can be seen well on the example of pairs with cobalt. Over this range of temperatures the cobalt—titanium pair undergoes two polymorphic transformations (cobalt at about 400°C and titanium at 882.5°C).

When the metals are cooled in an atmosphere of pure argon and helium, the relationship between the coefficient of friction and temperature is almost the same as that during cooling in vacuo. In commercial nitrogen

the coefficient of friction is somewhat lower than in vacuo, which is due to the relatively high content of oxygen and other impurities in nitrogen, and also to the more active formation of adsorption layers of nitrogen and its possible chemical interaction with the metal (formation of nitrides) during friction at elevated temperatures.

From the studies which we have discussed above we can draw the following conclusions:

1. Adhesion between similar metals starts at a range of temperatures of from $0.3-0.4\ T_{mp}$, but between dissimilar metals at a range of temperatures of from 0.35 to $0.5\ T_{mp}$.

2. Friction experiments, carried out during heating, showed that if the temperature at which adhesion starts (due to thermal activation) is exceeded, friction is greatly increased.

3. The polymorphic transformation influences the magnitude and nature of friction.

4. The friction between similar metals with a hexagonal close-packed crystal lattice is lower than that between metals with a body-centered lattice. The lowest coefficient of friction was found for hexagonal cobalt at temperatures below its transformation into a face-centered modification.

5. The friction and adhesion between similar metals depend on their position in the periodic system, and the friction and adhesion between dissimilar metals depend on their relative position in the system, the relationship between their atomic radii, the type of the crystal structure (which has a considerable influence on the mutual solubility) and on the nature of the bonds between similar and dissimilar atoms.

6. There is a certain hysteresis shown by the coefficient of friction during cooling and the coefficient of friction during heating, which leads to a hysteresis loop on the diagram representing the dependence of the coefficient of friction on temperature.

7. Friction in pure argon and helium differs little from friction in vacuo ($10^{-4}-10^{-5}$ mm Hg).

Bibliography

1. Semenov, A.P. and V.V. Pozdnyakov. Issledovanie antifriktsionnykh svoistv tverdykh tel pri vysokikh temperaturakh v vakuume i nekotorykh gazovykh sredakh (Study of Antifriction Properties of Solids at Elevated Temperatures in Vacuo and in Certain Gases).—Doklady AN SSSR, 160(4):811. 1965.
2. Bowden, F. and D. Tabor. Friction and Lubrication of Solids, Pt. 1. 1954.
3. Grigorovich, V.K. Periodicheskii zakon Mendeleeva i elektronnoe stroenie metallov (Periodic Law of Mendeleev and the Electron Structure of Metals).—Izdatel'stvo Nauka. 1966.
4. Hagstrum, H.D. and C.D'Amico. Production and Demonstration of Atomically Clean Metal Surfaces.—J. Appl. Phys., 31(4):715. Apr. 1960.
5. Sikorski, M.E. The Adhesion of Metal and Factors that Influence it.—Wear, 7: 144—162. 1964.

6. Semenov, A. P. Skhvatyvanie metallov-osnova kholodnoi svarki (Galling of Metals as the Basis of Solid-State Welding).—Avtomaticheskaya Svarka, 134, No. 5. 1964.

A. P. Semenov and V. V. Pozdnyakov

PRELIMINARY RESULTS OF A STUDY ON ADHESION AND FRICTION AT ELEVATED TEMPERATURES BETWEEN OXIDES AND REFRACTORY METALS AND OXIDES IN VACUO AND IN GASES

A study of contact processes between refractory metals and oxides, including external friction and adhesion, is very important for mechanisms working at elevated temperatures, and also for solving problems on the theory, technology, and application of cermets for joining metals to oxides and for machining metals with cermet tools. In this work contact reactions of metals with oxides are studied. To analyze the results of contacts between pairs of dissimilar materials (metal—oxides) correctly, we carried out preliminary investigations with similar materials. The results of studies on similar metals are given above (see p. 110).

Properties of materials studied

Material	Group (metal) of the periodic system	Atomic radius (of metal), Å	Melting point, °C	Crystal structure
Molybdenum	VIB	1.40	2620±10	Body-centered cubic
Iron	VIII	1.27	1534	Body-centered cubic, above 910°C face-centered cubic
Cobalt	VIII	1.25	1495	Hexagonal, above 400°C face-centered cubic
Aluminum oxide (Al_2O_3)	IIIA	1.43	2050±10	Hexagonal (corundum)
Magnesium oxide (MgO)	IIA	1.60	2800±13	Cubic (structure of NaCl)
Cerium oxide (CeO_2)	IVC	1.82	2725±20	Cubic (fluorite CaF_2)

Studies on oxides were carried out with the same apparatus and the same method as that used for studying friction and adhesion of metals. This method has already been described in greater detail /1, 2/. Some general data on the materials we studied are given in the table.

When the adhesion and friction between similar oxides of aluminum, magnesium, and cerium were studied it was shown that these oxides behave fundamentally like refractory metals. The adhesion typical of metals is also characteristic of oxides (Figure 1, a), but starts at higher temperatures, from 0.45 to 0.65 T_{mp} for the oxides we studied. It is interesting to note that adhesion between the oxides of magnesium and cerium, which have a cubic lattice, occurs at lower temperature than that between specimens of aluminum oxide which have a hexagonal lattice.

The friction between similar oxides (Figure 2, a), which is high at relatively low temperatures, falls as the temperature increases, and for oxides of magnesium and cerium the minimum friction occurs at temperatures directly preceding those at which adhesion starts. For aluminum oxide specimens we found no minimum on the curve representing the dependence of the coefficient of friction on temperature, although the coefficient of friction falls continuously with increase in temperature and reaches a fairly low value at 1350—1500°C (about 0.3). Cerium oxide has the lowest coefficient of friction over the range of temperatures from 400 to 1200°C. However, at higher temperatures the coefficient of friction of this oxide increases most rapidly.

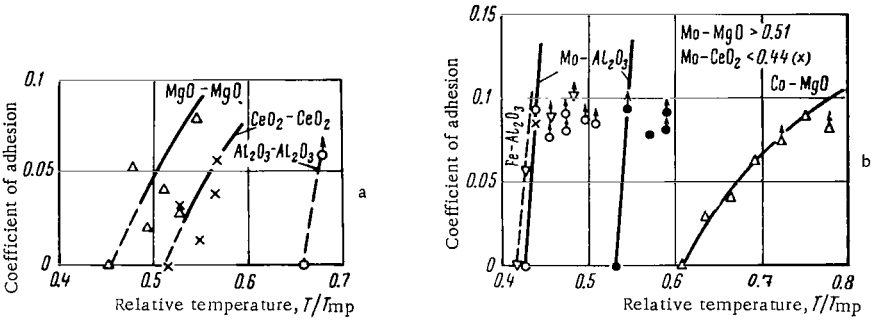

FIGURE 1. Dependence of the coefficient of adhesion on the relative temperature:

a—for similar oxides; b—for a number of metal—oxide pairs (for the Mo—Al_2O_3 pair the data are also related to the melting point of the oxide).

Any further change in the friction of these oxides during further increase in the vacuum cannot be expected, since the decrease in the content of oxygen (which has the greatest influence on the friction between metals) cannot be expected to have any appreciable influence on the friction of oxides.

It has been found that the adhesion between dissimilar materials such as metal—oxide (molybdenum and oxides of aluminum, cerium, and magnesium; iron and aluminum oxide; and cobalt and magnesium oxide, starts at temperatures which are lower than those at which adhesion starts between oxides (Figure 1, b). Thus, if we take as the basis for the calculation of the relative temperature the melting point of the metal (for the molybdenum—aluminum oxide pair plotted, because of the high melting point of molybdenum the results are obtained by two different methods of calculation), the temperature at which adhesion starts lies within the range of 0.4—0.6 T_{mp} (Figure 1, b). Adhesion starts at lowest temperature for iron—aluminum oxide, molybdenum—aluminum oxide, and molybdenum—cerium oxide pairs. In our experiments the adhesion between molybdenum and magnesium oxide did not start up to a temperature of 0.51 T_{mp}. Adhesion starts at the highest temperature for the cobalt—magnesium oxide pair (adhesion between molybdenum and magnesium oxide starts at an even higher temperature). The strength of adhesion increases with temperature rather slowly, and this relationship is similar to that for cobalt specimen pairs.

The results of tests on friction between molybdenum and oxides during heating are given in Figure 2, b. The highest coefficient of friction over the whole range of temperatures was found for the molybdenum—aluminum oxide pair. The coefficient of friction of molybdenum against magnesium oxide is considerably lower (about 0.2 at 1250°C).

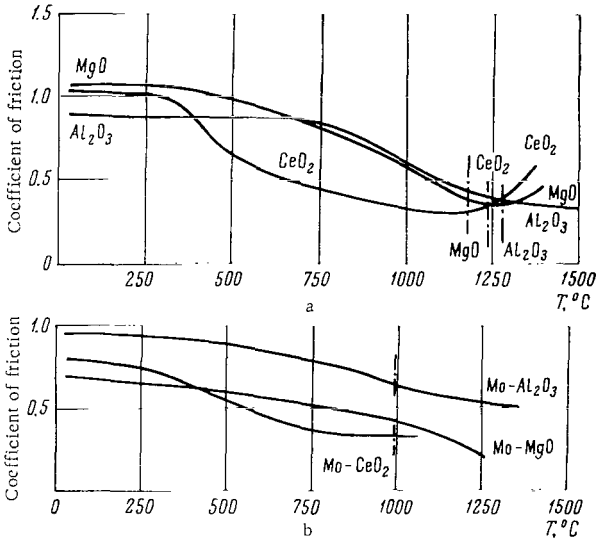

FIGURE 2. Dependence of the mean coefficient of friction on temperature:

a—for similar oxides in vacuo (tests during heating); b—friction of molybdenum against oxides in vacuo (tests during heating).

Up to about 400°C, the curve representing the friction of molybdenum against cerium oxide lies somewhat higher than the corresponding curve for the friction of Mo against magnesium oxide, but then it falls below. Most probably it will rise again above the curve for magnesium oxide on further heating. A comparison of these results with those obtained by friction tests between similar specimens of molybdenum and oxides showed that the oxide has a prevailing influence on the friction between different specimens (although molybdenum also has a certain influence). Heating to the temperature at which adhesion begins does not lead to an increase in friction, as during friction between similar specimens of oxides and metals, and the average value of the coefficient of friction continuously decreases with the increase in temperature. The coefficient of friction for the molybdenum—magnesium oxide pair, for which the temperature of adhesion was not reached, dropped sharply at temperatures above 1000°C, and reached a value of about 0.2 at 1250°C. It should be pointed out that the coefficient of friction of molybdenum against magnesium oxide grows very slowly on cooling, and remains the lowest of the coefficients of friction of the three pairs studied over the whole range of temperatures.

Peculiar curves with a single maximum were obtained for the cobalt—magnesium oxide pair (Figure 3, a). During heating the coefficient of

friction remains low (average value of 0.3) up to the temperature of polymorphic transformation of cobalt from a hexagonal structure to a face-centered cubic modification, then it starts to rise and passes through a maximum at about 700°C (coefficient of friction about 0.7), and finally it drops sharply to about 0.2 at 1100°C. An increase in temperature above the point at which adhesion starts did not lead to the usual increase in the coefficient of friction, but on the contrary to a decrease. During cooling the results were essentially the same although the maximum was shifted toward lower temperatures (by about 200°C). This was repeated several times before adhesion tests were started. The friction between cobalt and magnesium oxide during cooling showed a very different dependence on temperature directly after the adhesion tests (dashed line on Figure 3, a). The difference was even greater in the following tests on the same specimens (also during cooling) in atmospheres of argon and helium. The coefficient of friction increased with decrease in temperature and did not drop to the values characteristic of cobalt. The reason for this change in the characteristics of friction is that after adhesion tests under normal loads the particles of magnesium oxide passed from the oxide specimen and stuck to the surface of the cobalt specimen. A continuation of the friction tests only aggravated the situation, since more worn-out particles of the oxide (the wear increased after the initial damage to the surface) passed onto the metal surface, and the friction between different materials was gradually substituted by friction between similar materials, i.e., between two specimens of magnesium oxide.

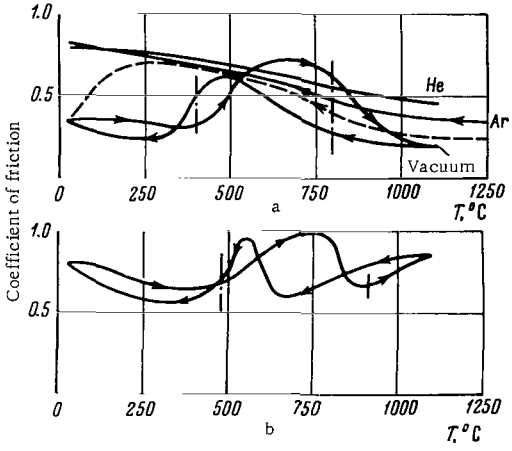

FIGURE 3. Dependence of the average value of the coefficient of friction on temperature:

a—for the cobalt—magnesium oxide pair in vacuo (tests during heating and cooling) and in gaseous media (tests during cooling); b—for the iron—aluminum oxide pair in vacuo (tests during heating and cooling).

Tests on Armco iron—aluminum oxide pairs were started in connection with the machining of steels with cermet tools (on the basis of aluminum oxide). The dependence of the coefficient of friction (Figure 3, b) on

temperature is similar to that for the cobalt—magnesium oxide pair (Figure 3, a) but the curves for heating and cooling lie considerably higher. During heating the coefficient of friction at first fell, but after passing through a minimum it started to rise again. The temperature at which the average coefficient of friction started to increase almost coincided with the temperature at which adhesion began. After passing a maximum at about 750°C the coefficient of friction dropped sharply, but started to rise at the temperature of the polymorphic transformation of iron from a body-centered cubic structure to a face-centered cubic modification. The same happened during cooling, but as in the case of the cobalt—magnesium oxide pair the maximum was shifted toward lower temperatures (by about 200°C). The apparent reason for the analogous behavior of two different pairs (cobalt—magnesium oxide and iron—aluminum oxide) is that both metals belong to the same group of the periodic system. It should be pointed out that the pair with the greater difference between the atomic dimensions of the metals (cobalt—magnesium) has a lower average coefficient of friction over the whole range of temperatures.

According to the existing theory /3/, a strong bond can exist directly between the components and also through oxygen bridges. In addition, it is possible that in this case reduction reactions (although partial) take place in the zone of contact, which lead to the formation of oxygen alloys and of metal—metal—oxygen alloys at the interface. In this connection the ability to adhere is probably influenced by the radii of the metal atoms and by the position of the metals in the periodic system of elements, and also by the nature of the reaction of the metals with oxygen. The influence of the relationship between the atomic radii of the metals of the pair was confirmed by the above experiments on friction and adhesion of cobalt and iron to oxides. The results of tests on molybdenum in contact with oxides are not so clear. However, even here the maximum coefficient of friction and the maximum adhesion are characteristic of the molybdenum—aluminum oxide pairs in which the radii of the metal atoms differ least (2.1%). Results which do not conform to this rule were obtained for the molybdenum—cerium oxide pair only.

The following conclusions can be drawn from the above studies:

1. Pairs of similar oxides, like pairs of similar metals, have a strong mutual adhesion which starts at higher temperatures (0.45—0.65 T_{mp}) than adhesion between metals.

2. Pairs consisting of an oxide and a metal start to adhere to one another at temperatures lower than those for pairs of similar oxides but higher than those for pairs of similar metals (in our studies adhesion started at a range of 0.41—0.6 T_{mp} of the metal).

3. Friction and adhesion of metals and oxides depend on the relationship between the radii of the metal atoms, the polymorphic transformations in the metals, the position of the metals in the periodic system of elements, and their affinity for oxygen.

Bibliography

1. Semenov, A.P. and V.V.Pozdnyakov. Issledovanie antifriktsionnykh svoistv tverdykh tel pri vysokikh temperaturakh v vakuume i nekotorykh gazovykh sredakh (Study of Antifriction Properties of Solids at Elevated Temperatures in Vacuo and in Some Gases).—Doklady AN SSSR, 160(4):811. 1965.
2. Semenov, A.P. and V.V.Pozdnyakov. Metodika issledovaniya treniya i adgezionnogo vzaimodeistviya tugoplavkikh materialov pri temperaturakh do 2000°C (Methods for Studying the Friction and Adhesion of Refractory Materials at Temperatures of up to 2000°C).—In: Sbornik "Teoriya treniya i iznosa," Izdatel'stvo Nauka. 1965.
3. Rykalin, N.N., M.Kh.Shorshorov, and Yu.L.Krasulin.—Fizicheskie i khimicheskie problemy soedineniya raznorodnykh metallov (Physical and Chemical Problems of Joining Different Metals).—Izvestiya AN SSSR, Neorganicheskie Materialy, 1, No. 1. 1965.

S. O. Tsobkallo, M. D. Nikitin, V. A. Chelnokov, V. I. Timofeeva, I. G. Val'ter, and L. A. Privalov

STUDY ON THE VIBRATION ENERGY (INTERNAL FRICTION) AS A RESERVE OF STRENGTH OF REFRACTORY ALLOYS AT ELEVATED TEMPERATURES

PURPOSE OF STUDY

The damping of vibrations of refractory alloys is often of great importance for evaluating their strength under conditions of resonance, for example, when these alloys are used to produce blades of steam and gas turbines. In such cases the amplitude of resonance vibrations, and consequently the maximum stresses in the material, are inversely proportional to the damping of a given system. Since the damping of vibrations is a characteristic greatly influenced by the structure of the metal, it is possible to change it by varying the heat treatment of the material. The strength of the material under conditions of vibration can also be influenced in the same way.

Since there are few data on the ability of modern refractory materials to dissipate energy during vibrations /1—7/, a solution to the problems associated with a study of the damping of vibrations of these materials is very important.

The purpose of this study is to find the chief groups of modern refractory alloys: 1) medium-alloyed ferromagnetic steels on the basis of α-solid solutions of iron (EI415 and 18Kh11MFB); 2) highly alloyed austenitic steels (EI787 and EI696M); 3) nickel-base alloys (EI437B, EI893 and EI765).

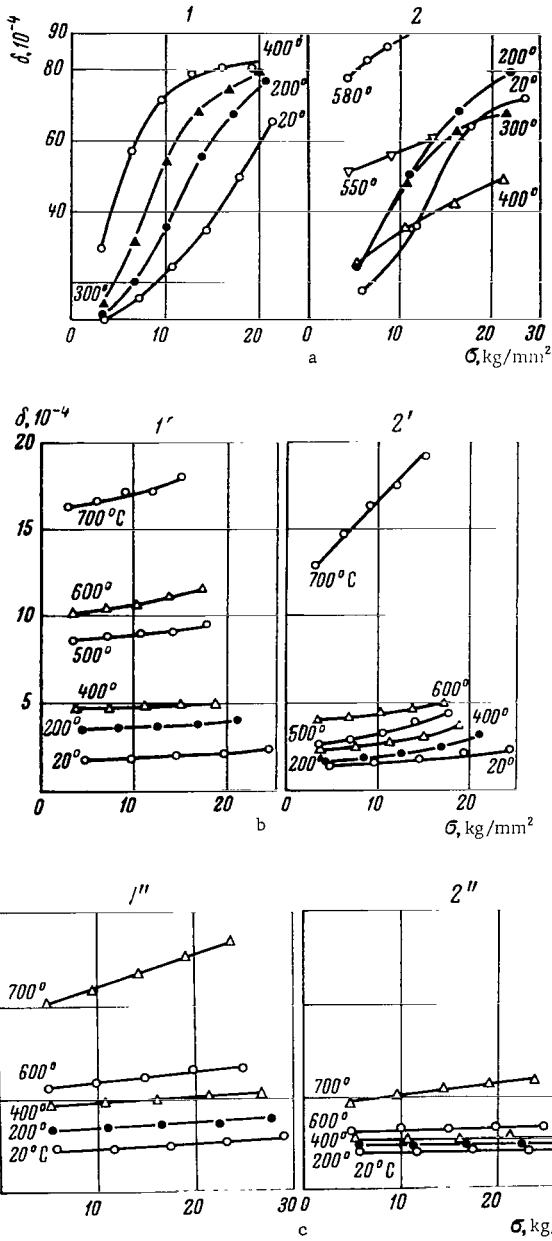

Dependence of the damping of vibrations on the amplitude of stresses at different temperatures:

a—for ferromagnetic steels: 1—perlitic steel EI415; 2—martensitic—ferritic steel 18Kh11MFB; b—precipitation—hardening austenitic steel EI696M: 1'—in the hot-worked initial state; 2'—in the initial cast state; c—nickel-base precipitation—hardening alloy EI893: 1"—in the initial hot-worked state; 2"—in the initial cast state.

Particular attention is paid to a comparison between the properties of hot-worked and cast materials. The properties of cast materials are of particular interest in modern methods of precision casting of refractory alloys, particularly of turbine blades and even of complete turbine wheels. Prior to the investigations, all alloys were given a heat treatment which ensured a maximum heat resistance.

DEPENDENCE OF THE DAMPING OF VIBRATIONS OF REFRACTORY ALLOYS ON THE AMPLITUDE OF VIBRATIONS AT DIFFERENT TEMPERATURES

The problem of dissipation of energy during vibrations has been especially studied in this work. We found the relationship between the damping of vibrations in these alloys and the amplitude of stresses and temperature. These measurements were carried out by the method of impulse counting with special specimens and devices /1, 2/.

The dependence of the damping of vibrations of some of the alloys we studied on the amplitude of stresses at different temperatures are given in the figure. The temperatures were chosen according to the ability of a given alloy to withstand high temperatures under service conditions. For practical use and for a quantitative comparison of the damping abilities of alloys, it is convenient to have numerical data on the damping of vibrations for some static stresses. The static stresses applied were 10, 15, and 20 kg/mm^2. For these magnitudes the table gives the damping for all alloys studied at different temperatures.

DISCUSSION OF RESULTS

1. The specific characteristic of nickel alloys and austenitic steels studied in this work is the existence of solid solutions which are strengthened by the precipitation of intermetallic compounds of borides and carbonitrides /8/. These alloys are nonmagnetic. These properties influence the relationship between the damping of vibrations and the increase in the amplitude and temperature (Figures 1, b and c). As a result of the specific properties of these alloys, the damping of vibrations is little influenced by the amplitude of stresses, and this relationship is only slightly improved by increase in temperature to a maximum value.

These facts can be qualitatively analyzed according to dislocation theories on the dependence of internal friction on amplitude. Of these theories the most important is that of Swartz and Weertman /9/, which is essentially a continuation of the work of Granato and Lücke /10/. These works are based on a model in which the dissipation of energy is determined by the migration of dislocation loops which are fixed not only on the branchings but also on the atoms of impurities.

The differences between the damping of vibrations of wrought and cast alloys are very interesting. It has been found that the damping of vibrations of cast austenitic EI696M steel (Figure 1, b) below 600°C is smaller than that of the same hot-worked steel. The damping of forged nickel-base EI893 alloys (Figure 1, c) and its dependence on the amplitude of stresses

Damping of vibrations of heat-resistant alloys and their fatigue strength characteristics under conditions of resonance

Materal and state	Damping of vibrations at different temperatures (°C) and stresses ($kg/mm^2 \cdot 10^4$)																		Fatigue strength characteristics under conditions of resonance vibrations			
	20			200			400			500			600			700			T, °C	σ_{-1}, kg/mm^2	δ, 10^{-4}	A, $10^{-3} kg/mm^2$
	10	15	20	10	15	20	10	15	20	10	15	20	10	15	20	10	15	20				
EI415 Wrought	22	38	58	35	60	75	72	80	82										400	37	90	33
18Kh11MFB Cast	30	53	69	45	65	76	34	42	48	35	41	47	158						550	19	65	12
EI787 Cast	1.9	2.0	2.2	2.8	3.4	4.0	3.8	4.2	4.5	4.2	4.5	5.1	8.7	9.6	11	17	19	22	650	22	13	2.9
																			700	21	23	4.8
EI696M Wrought	1.9	2.0	2.1	3.7	3.8	4.0	4.8	4.9	5.1	8.9	9.2	9.6	10	11	12	17	18					
Cast	1.6	1.8	2.0	1.9	2.3	2.9	2.6	3.1	4.0	3.2	4.4	5.0	4.4	4.8	5.5	17	19		650	19	13	2.4
EI437B Wrought	1.1	1.1	1.1	1.5	1.5	1.5	2.1	2.1	2.1	2.5	2.5	2.5	3.4	3.4	3.4	18	20	22	20	33	1.1	0.36
																	800°		700	28	24	6.7
																39	52	76	800	23	92	21
Cast*	1.9	1.9	1.9	2.2	2.2	2.2	3.2	3.2	3.2	3.7	3.7	3.7	4.3	4.3	4.3	14	14	14				
Cast**	3.1	3.1	3.1	3.5	3.5	3.5	5.6	5.6	5.6	6.2	6.2	6.2	7.5	7.5	7.5	16	16	16				
EI893 Wrought	2.3	2.4	2.5	3.4	3.6	3.8	4.8	4.9	5.1				5.9	6.1	6.4	11	12	13				
Cast	2.0	2.0	2.0	2.4	2.4	2.4	2.7	2.7	2.7				3.1	3.2	3.3	5.1	5.4	5.7				
EI765 Cast	1.5	1.7	2.0	2.1	2.4	2.7	3.1	3.4	3.7	4.2	4.5	4.8	5.8	6.6	7.3	9.4	11	12	750	28	38	11
																	800°					
																62	68	75				

* Aging at 750°C.
** Aging at 700°C.

are also greater than in cast alloys. The cause of these differences probably lies in the structures of these alloys. In fact, an analysis of the structures has shown that wrought materials have finer dispersed particles than cast alloys. This indicates that in wrought alloys with fine-grained precipitates the dislocations can break more easily through the impurity barrier than in cast alloys with their coarse coagulated particles. Therefore the damping of vibrations of cast alloys (particularly at elevated temperatures) is lower than of wrought alloys.

On the other hand, a decrease in the temperature of aging reduces the amount of intermetallic precipitates and makes them more dispersed. Therefore, in EI437B alloys aged at 700°C the dislocations can break more easily through the barriers than in the same material after aging at 750°C. The damping of vibrations of such alloys is less than of alloys aged at 700°C (see table).

The damping vibrations of ferromagnetic EI415 and 18Kh11MFB steels (see Figure 1, a) is one order of magnitude higher than that of the above alloys. This may be due to the heterogeneous structure and the magnetic properties of these steels. It has been found /6/ that the dissipation of energy in ferromagnetic materials is higher because of the deflection of the fields of spontaneous magnetization under the influence of external stresses.

The irregular variation in the damping of vibrations of 18Kh11MFB steel (see Figure 1, a and the table) with increase in temperature has also been explained by the migration of atoms of carbon along the interstitial sites in the retained austenite /11/.

2. The damping of vibrations of a number of refractory materials studied in this work have a specific scientific and practical interest as characteristics closely related to the structures of the alloys.

However, for practical engineering, the damping of vibrations should be considered together with other characteristics determining the strength of the materials, including one which determines directly the process of failure.

For failure under conditions of vibration, one such characteristic is the fatigue limit of the material at a given temperature. Thus, the fatigue limit should be considered in connection with the damping of vibrations.

Let us now consider the quantitative relationship between these physical characteristics.

It is known /12/ that during resonance the maximum amplitude of vibrations θ_0^m of the system is

$$\theta_0^m = \frac{\pi F_0}{I\omega_r^2\delta}, \qquad (1)$$

where F_0 is the amplitude of periodically acting induced forces; I is an inertion characteristic of the system (mass); ω_r is the frequency of angular resonance of the system; δ is the logarithmic damping of vibrations.

At the same time the permissible amplitude of vibrations of the system θ_0^m is determined by the geometry of the vibrating element (its rigidity), and by the magnitude of permissible stresses. Obviously, under conditions of resonance vibrations the level of permissible stresses is determined by the fatigue limit at a given temperature. At the same time each alloy has an optimum temperature for a given service time. Let us designate the

fatigue limit at this temperature by σ_{-1}. In this case it is possible that

$$0_0^m = B\sigma_{-1}, \tag{2}$$

where B is the rigidity characteristic of the vibrating system. By substituting formula (2) into formula (1), we obtain

$$F_0 = C\sigma_{-1}\delta, \tag{3}$$

where $C = l\omega_r^2 B/\pi$ is a certain constant magnitude characterizing the geometry and elastic properties of the system.

The result given by (3) shows that the maximum value of the induction force F_0 is determined by the product of the fatigue limit and the damping of vibrations of a material under stresses equal to the fatigue limit. Thus, the $\sigma_{-1}\delta$ product is determined by the fatigue strength of the material. Let us designate this product by A, and consider it as a new strength charactersitic of heat-resistant materials under conditions of resonance vibrations.

The above discussion shows that the damping of vibration is a very important reserve of strength in metals used in machine building. If it is possible to increase the damping of vibrations of a metal without reducing its fatigue limit, the strength of the construction is increased also. The damping of vibrations can be increased, for example, by heat-treatment, alloying, surface coating, and other methods.

Since the fatigue limit should always be considered together with the damping of vibrations we have given these characteristics and the values of A at service temperatures for the alloys investigated in the table. It should be pointed out that at 700°C the EI437B alloy has a higher value of A than the EI787 alloy.

CONCLUSIONS

1. From the experimental data on the dependence of the amplitude of vibrations on the amplitude of stresses at different temperatures it is possible to compare the characteristics of 7 refractory alloys in 11 states, since the measurements were carried out by the same method. These data have a direct practical value for designers.

2. The magnitude of the damping of vibrations of refractory alloys depends on their structure, and can be explained on the basis of the dislocation theory of internal friction developed by Swartz and Weertman.

3. Coarse precipitates in the alloys lead to a decrease in the damping of vibrations.

4. For a correct evaluation of the strength of a metal under conditions of vibration, it is necessary to consider both the fatigue limit of the material and its damping of vibrations under stresses equal to the fatigue limit. For a quantitative evaluation of the heat resistance of a material under conditions of resonance vibrations, a magnitude has been introduced equal to the product of the fatigue limit and the damping of vibrations at the service temperature of the alloy.

5. The nonferromagnetic austenitic heat-resistant steels and nickel-base alloys show a damping of vibrations considerably lower than the

ferromagnetic low- and medium-alloyed steels. This is because in addition to the dislocation mechanism of dissipation of energy, these alloys have a magnetomechanical hysteresis which leads to additional great losses of energy in the material.

6. The damping of vibrations in nickel-base alloys increases over the range of service temperatures of which these alloys are heat resistant.

Bibliography

1. Tsobkallo, S.O. and V.A.Chelnokov.—ZhTF, Vol. 24, 499. 1954.
2. Tsobkallo, S.O. and V.A.Chelnokov.—In: Sbornik "Vnutrennee trenie v metallakh i splavakh." Izdatel'stvo Nauka. 1966.
3. Mikhailov-Mikheev, P.B. Spravochnik po metallicheskim materialam trubo- i motorostroeniya (Handbook on Metals in Tube Production and Engine Building).—Mashgiz. 1961.
4. Smithells, C.J., editor. Metals Reference Book.—New York. Second edition. 1955.
5. Panchenko, I.I. Vibratsionnaya prochnost' polatok turbin (Vibration Strength of Turbine Blades).—Mashgiz. 1959.
6. Pisarevskii, M.M. and I.G.Sokolinskaya.—In: Sbornik "Svoistva materialov, primenyaemykh v turbinostroenii, i metody ikh ispytanii." Vol. 2, Mashgiz. 1955.
7. Pisarenko, G.S. Rasseyanie energii pri mekhanicheskikh kolebaniyakh (Dissipation of Energy During Mechanical Vibrations).—Kiev, Izdatel'stvo AN USSR. 1962.
8. Khimushin, F.F. Zharoprochnye stali i splavy (Refractory Steels and Alloys).—Izdatel'stvo Metallurgiya. 1964.
9. Swartz, J.C. and J.Weertman.—J.Appl. Phys., Vol. 32:1860. 1961.
10. Granato, A. and K.Lücke.—J.Appl. Phys., Vol. 27:583. 1956.
11. Krishtal, M.A., Yu.B.Piguzov, and S.A.Golovin. Vnutrennee trenie v metallakh i splavakh (Internal Friction in Metals and Alloys).—Izdatel'stvo Metallurgiya. 1964.
12. Novik, A.S.—In: Sbornik "Uspekhi fiziki metallov," Vol.1. Metallurgizdat. 1956.

II. IRON- AND NICKEL-BASE STEELS AND ALLOYS

I. L. Mirkin, A. A. Yudin, Yu. A. Rybakova, M. B. Guterman, and A. S. Trekalo

SUBSTRUCTURE AND GRAIN BOUNDARY POROSITY UNDER CONDITIONS OF CREEP

Two characteristic processes take place during the creep of metals.

1. A change in the structure, in particular the formation of subgrains whose dimensions and disalignment greatly influence the creep rate.

2. The formation of small centers of fracture along the grain boundaries. The kinetics of the development of these apparently determine the service life of materials under stress.

Substructural changes during creep have been studied in several papers /1—4/. However, the mechanism of formation of substructures is still controversial. Even more doubtful is the mechanism of the nucleation and growth of grain boundary pores. The purpose of this work is to determine the specific conditions under which these processes take place in materials which differ considerably with regard to the formation of a substructure and of grain boundary porosity. We shall first discuss the processes of strengthening in nickel and in nickel-base alloys at different temperatures of deformation, as well as the softening which occurs during subsequent annealing.

We studied the temperature dependence of the strength and the thermal stability of several single-phase nickel alloys containing titanium, molybdenum, and iron.

After a homogenizing anneal the specimens were stretched to a 10% deformation at a constant rate of about $10^{-3} \cdot \text{min}^{-1}$ at different temperatures. The stress-strain curves are well represented by the equation

$$\sigma = \chi \varepsilon^n,$$

where σ is the difference between the acting stresses and the stresses at which flow starts; ε is the elongation.

The parameters χ and n in this equation characterize the strengthening of a given alloy. The first coefficient gives the slope of the stress-strain curve, and should be considered as a characteristic of the ability of the crystal lattice to become strengthened, which is associated with the ease of motion and interaction of dislocations. The coefficient n determines the shape of the curve, and characterizes the development of softening processes. As an example Table 1 gives the values of χ and n for nickel and nickel—titanium alloys.

It can be seen that both parameters decrease with temperature. This is due to a smaller accumulation of defects, and therefore to a smaller

strengthening (χ), and the gradual development of the softening processes (n). It can also be seen that the strengthening ability of pure nickel decreases more rapidly with temperature than that of the nickel-titanium alloy.

The stability of strengthening and the elimination of accumulated microdefects was studied by the calorimeteric method using a special microcalorimeter /5/.

TABLE 1. Magnitude of χ and n

Temperature of deformation	Ni		Ni + 3 at. % Ti		Temperature of deformation	Ni		Ni + 3 at. % Ti	
	χ	n	χ	n		χ	n	χ	n
20	105	0.63	120	0.62	700	—	—	20	0.29
400	45	0.56	108	0.55	800	—	—	14	0.30
500	—	—	50	0.43	900	2.8	0.2	4.5	—
600	16	0.32	46	0.51					

Figure 1 shows the evolution of energy accumulated by deformation at 20, 400, and 900°C during slow heating. An increase in the temperature of deformation from 20 to 400°C greatly increases the stability of microdefects. In addition, the region where energy (A) associated with various unstable point defects is evolved exists during cold deformation only. On the other hand, the region of stable defects during deformation at elevated temperatures is divided into two subregions, apparently because of the formation of two different groups of defects. It is also possible that one of the high-temperature peaks is caused by polygonization, and the other by the existence of complex configurations. A comparison of the properties of nickel and of nickel-base alloys shows that the addition of alloying elements increases the stability of the defects, and consequently of the strengthening, particularly at low temperatures of deformation.

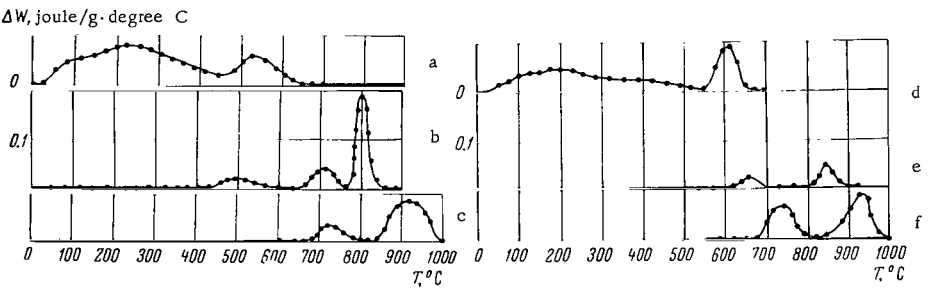

FIGURE 1. Evolution of accumulated energy during annealing of nickel (a—c), and of nickel alloys containing 3 at. % of titanium (d—f), deformed at 20°C (a, d), 400°C (b—e) and 900°C (c, f).

The addition of molybdenum to the alloy shifts the region of stability even more (by almost 200°C) [to higher temperatures], while iron shifts this region toward lower temperatures. It is interesting to note that even after deformation at 900°C certain defects still exist.

The dislocation structure and the substructure were also studied by metallographic methods. Figure 2 shows some of these structures, and

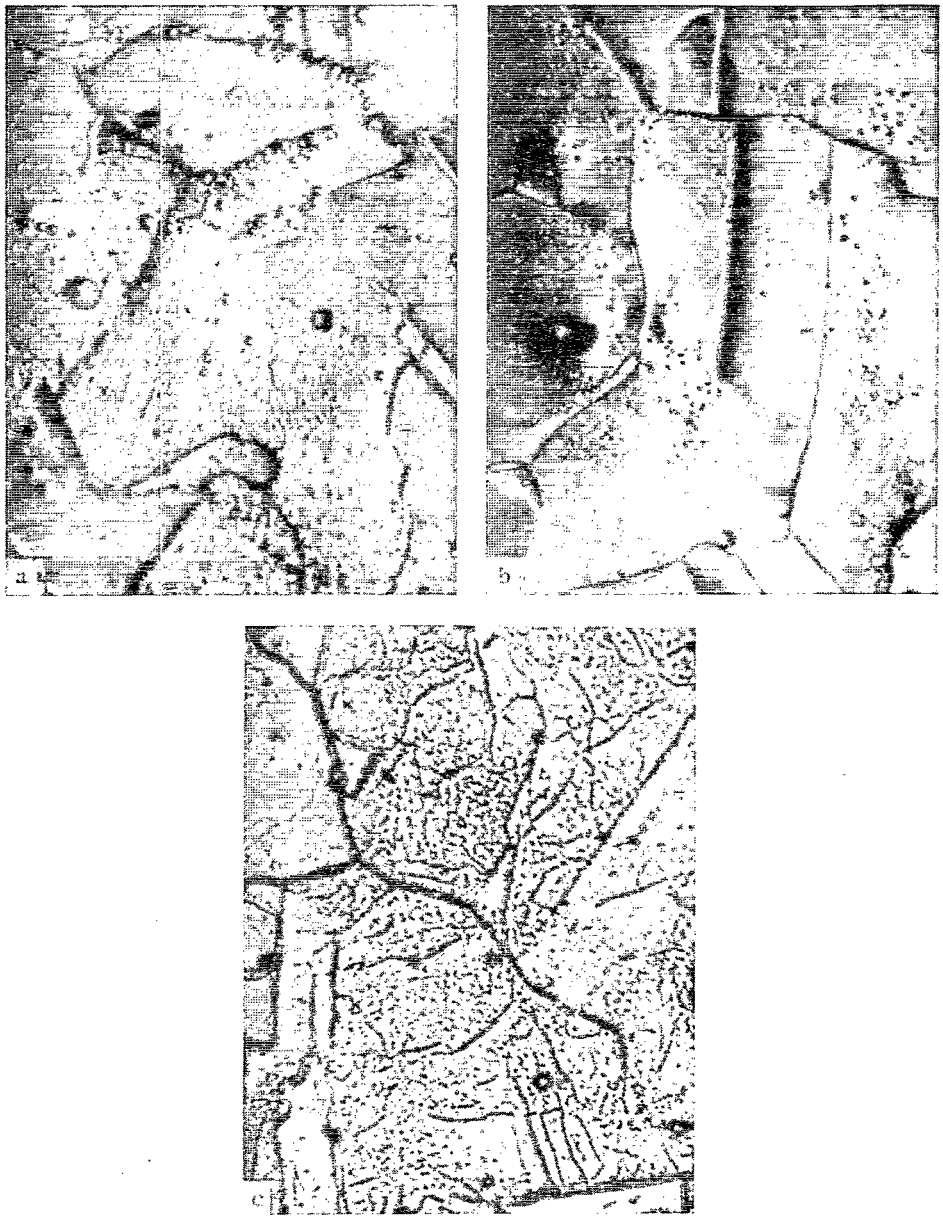

FIGURE 2. Dislocation structure:

a—nickel, T_{def} = 400°C; ×100, b—nickel, T_{def} = 900°C, ×500; c—nickel alloy with 3 at. % of titanium, T_{def} = 900°C, ×1000.

indicates that the density of dislocations in nickel is considerably higher than in nickel—titanium alloys. It can also be clearly seen that a higher temperature of deformation (900°C instead of 400°C) leads to the formation of a substructure during the deformation process proper; the dislocation density in this case is also lower.

Thus, the degree of strengthening and its thermal stability are greatly influenced by the composition of the alloy, the temperature of deformation, and the substructure which is visual even under an optical microscope.

To study the formation of pores and of a substructure during creep, we chose M1 copper (99.9%), NO nickel (99.99%), and three nickel-base alloys: 1) a single-phase solid solution 28.5% Cr—2.6% Al—Ni; 2) a binary nickel-base alloy with a composition similar to that of the first alloy but strengthened by a dispersed γ-phase (Ni_3Al); and 3) the industrial complex refractory EI765 alloy strengthened by carbide and intermetallic precipitates. The nickel was tested at 500—700°C for up to 300 hr. The substructure was revealed metallographically.

The best etchant for nickel is a mixture of three concentrated acids: nitric (40—30 ml), acetic (60—70 ml), and hydrochloric (0.5 ml). The grain boundary porosity in nickel was not revealed, and only the grain boundaries were etched more. The degree of development of the substructure varies between grains, and depends on the orientation of these grains with respect to the axis of tension. The thick, well etched continuous subboundaries are located perpendicular to the direction of shear, and apparently characterize the relatively higher disalignment. These subboundaries can be identified with the bending planes. The thin boundaries can be etched only slightly. They consist of points located along this direction, and have a low carbon content. Therefore, the substructure looks banded. The dimensions l of subgrains have been calculated. The curve representing the distribution of subgrains according to their dimensions is asymmetric to the elongated branch of the coarse grains, and can be given approximately by the logarithmic-normal distribution. The average dimension of subgrains (as found in our experiments) decreases approximately linearly with increase in stress and is equal to 1—2 μ at $t = 500$°C and at $\sigma = 5\ kg/mm^2$ applied for 200 hr. The disalignment of thin boundaries (parallel to the direction of slip) determined from the distance between the etched holes is equal to $\sim 1'$. According to our data, the formation of a substructure is not terminated by the first stage of creep. This fact together with the appearance of the subgrains, as mentioned above, confirms the theory of MacLean, according to which the first stage of creep leads to division of the slip bands, and the formation of bend planes perpendicular to the direction of slip. The next process is the formation of a substructure by polygonization. These processes are probably the cause of the banded substructure, and the orientation of the continuous and point size subgrains discussed before. No substructure could be found in copper (only recently, we found a work in which a substructure with 3.3 μ large blocks was revealed after creep at 465°C by means of a transmission electron microscope). After creep at 350—500°C for up to a few tens of hours large amounts of small pores were found in copper. These pores were located chiefly (about 90% of them) along the grain boundaries perpendicular to the axis of stretching. These pores were oval in shape with an average relationship between the axes of 1:1.2, and were slightly elongated along the grain boundaries. Most

pores were joined in chains in the vicinity of the fracture. Many cracks which preserved the shape of the pore chains were also found.

In specimens with different cross-sectional areas, tested at 450°C for 4 hr, the pore distribution was found in sections corresponding to stresses of 5 and 2.4 kg/mm^2. The curves representing the distribution of pores according to their dimensions at both these stresses have a well-marked maximum at 1.2 μ. The distribution of pores was studied in all cases from 200 measurements. The distribution curves, plotted in semilogarithmic coordinates, are symmetrical. On the distribution versus log d (where d is the dimension of pores) graph, the distribution law is represented by a straight line. This indicates that the distribution of pores according to their dimensions is governed by a logarithmic-normal law of distribution.

The number of pores per unit of microsectional area has been counted for the different diameters of failed specimens. It has been found that the relationship between the number of pores N and the stress σ is almost linear (Figure 3), and therefore $\sigma a = A = \text{const}$, where $a \frac{1}{\sqrt{N}}$ is the average distance between the pores (Table 2).

The dependence of the dimensions of pores on the testing time is shown in Table 3. As the dimension of the pores, we took the diameter of the pore d perpendicular to the boundary (small axis). Every magnitude of d in Table 3 corresponds to an arbitrary magnitude on the curve representing the distribution of pores according to their dimensions, which was plotted from at least 200 measurements. It was found that this dependence is almost a linear function in the $d - \tau^{1/3}$ coordinates.

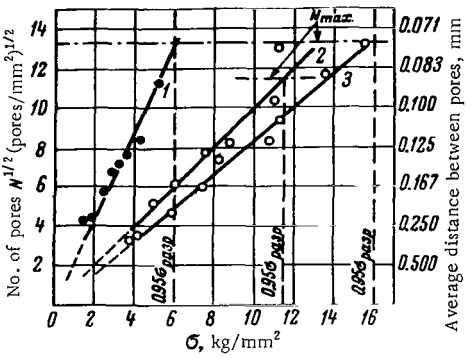

FIGURE 3. Dependence of the number of pores N on the stress σ for nickel alloys:

1—EI765 alloy, T = 850°C; τ = 4202 hr; 2—Ni—Cr—Al alloy, T = 700°C, τ = 993 hr; 3—the same, T = 700°C, τ = 557 hr.

It is interesting to note that such a dependence on time is characteristic of the diffusion processes of sintering and coalescence. Figure 3 and Table 2 show that during intergranular failure the number of pores N_{max} after accelerated spontaneous fracture takes place is almost identical at all temperatures and testing times.

It should be pointed out that the rate at which N_{max} is attained is greatly influenced by the conditions of testing and may vary by one order of magnitude. Thus, in copper at T = 450°C, N_{max} is reached after 43 hr at σ = 3 kg/mm^2 but after 4 hr at σ = 5 kg/mm^2. Pores have also been found along the grain boundaries of nickel alloys creep tested at 700—850°C for from 300 to 10,000 hr. It was found that the laws which govern the mechanism and kinetics of the development of porosity in copper also hold for this whole group of alloys. It is interesting to note that N_{max} for various conditions of testing of different alloys is very similar, but considerably less than N_{max} for copper. The photomicrograph in Figure 4 shows that the

pores in the heterogeneous alloy are formed along the grain boundaries between the precipitates of the strengthening phase. These precipitates, apparently, hinder the joining of the pores into chains and the formation of continuous cracks.

TABLE 2. Dependence of the number of pores in copper on the stresses

T = 500°C, τ = 4 hr			T = 450°C, τ = 4 hr			T = 390°C, τ = 4 hr			T = 450°C, τ = 43 hr		
σ, kg/mm^2	$\sqrt{N}$, pores/mm^2	$\sigma\alpha$	σ, kg/mm^2	$\sqrt{N}$, pores/mm^2	$\sigma\alpha$	σ, kg/mm^2	$\sqrt{N}$, pores/mm^2	$\sigma\alpha$	σ, kg/mm^2	$\sqrt{N}$, pores/mm^2	$\sigma\alpha$
2.85	24.5*	0.114	4.75	24.3	0.195	6.00	25.0	0.240	2.85	21.00	0.135
2.20	17.5	0.125	3.97	17.2	0.200	4.00	17.8	0.224	2.40	20.00	0.120
1.65	13.7	0.120	2.80	14.6	0.185	3.42	14.0	0.224	1.80	13.70	0.132
1.40	11.6	0.122	2.06	10.4	0.204	2.35	11.2	0.210	1.48	11.95	0.125

* N_{max}, corresponds to about 0.95 σ_{break}.

TABLE 3. Dependence of the transverse dimension of pores on the testing time

EI765 alloy, 750°C		Alloy (solution), 700°C	
τ, hr	d, μ	τ, hr	d, μ
288	0.87	200	1.76
974	1.02	557	1.78
10,202	2.34	1000	1.82
		1615	1.92

It can be assumed that the critical number of pores depends on the properties of the basis metal, but if other conditions are equal, the rate at which this critical number of fracture centers is reached, and consequently the life of the material, depend on the degree of strengthening of the grain boundaries by the carbide or intermetallic precipitates.

From these results certain assumptions can be made on the mechanism of deformation and fracture caused by creep. The first stage of creep leads mainly to transient processes of slip and the formation of bend bands and adiathermal fragmentation. Although the initial stage of nucleation of fracture centers has not yet been sufficiently clarified, it can be assumed that the strengthening of the metal gives rise to conditions under which the formation of fracture centers by thermally activated rupture of atomic bonds in small regions becomes possible. The maximum stresses are exerted chiefly at the boundaries perpendicular to the tension axis. A gradual increase in the number of fracture centers up to a certain number N_{max}, which is characteristic of a given material and a given structure, takes place during the whole test, starting at the second state of creep. When the number of pores N_{max} is reached, the total surface of the pores is a small fraction, about 1%, of the surface of the grain boundaries of the microsection.

At the beginning of the process the maximum stresses at the ends of the pores lead to the formation of new pores in the immediate vicinity of those in existence; this results in the formation of pore chains. After N_{max} is reached, the distances between individual pores in the chains becomes so narrow that the maximum stresses at the ends of two neighboring pores overlap, and the stress is sufficient to fracture metal between the pores. As we have already mentioned, the precipitation of a strengthening phase along the grain boundaries is an obstacle to the joining of the pores into a continuous crack. The growth of the pores is due to diffusion processes.

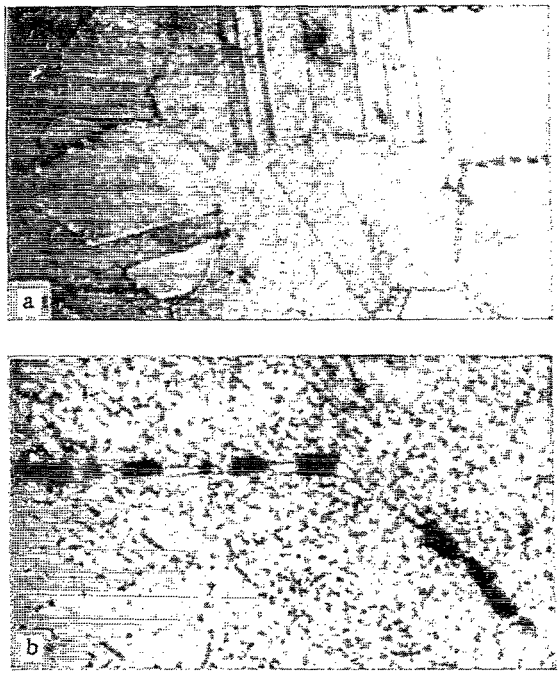

FIGURE 4. Pores in the EI765 alloy after stretching at 850°C for 4000 hr, $\sigma = 6$ kg/mm^2:

a—×300; b—×1000.

We found no direct connection between the formation of a substructure and the susceptibility of a metal to the formation of pores. Although the substructure of nickel and aluminum can easily be revealed, the pores are not discernible. For copper the opposite is true. Pavlov, Mel'nikova and Pecherkina /6/ showed that this behavior of copper may be due to the stacking fault energy.

Bibliography

1. Salli, A. Kh. Sbornik—Uspekhi fiziki metallov (Collection—Progress in the Physics of Metals), 3.—Metallurgizdat. 1960.
2. Rozenberg, V. M. Issledovanie mekhanizma polzuchesti metallov pri povyshennykh temperaturakh (Investigation of the Mechanism of Creep of Metals at Elevated Temperatures). Author's Summary for Doctor Thesis. 1963.
3. Parker, E. R. and J. Washberry. Sbornik—Polzuchest' i vozvrat (Collection—Creep and Recovery).—Metallurgizdat. 1961.
4. Kozyrskii, G. Ya., A. B. Kononenko, and P. N. Okrainets. Sbornik—Voprosy fiziki metallov i metallovedeniya (Collection—Problems of Physics of Metals and Metallurgy), No. 11.—Kiev, Izdatel'stvo AN USSR. 1960.
5. Mirkin, I. L. and M. B. Guterman. Nauchno-tekhnicheskaya informatsiya o rabotakh TsNIITMASh (Scientific-technical Information on the Works of TsNIITMASh), No. 59. 1966.
6. Pavlov, V. A., V. V. Mel'nikova, and N. L. Pecherkina.—Fizika Metallov i Metallovedenie, No. 2. 1966.

K. I. Terekhov

*ALLOYING, STRUCTURE, AND PHASE COMPOSITION OF HEAT-RESISTANT NICKEL-CHROMIUM ALLOYS CONTAINING NIOBIUM**

Most complex alloyed heat-resistant steels and alloys contain several elements which either enter the solid solution (Ni, Cr, Mn, Mo, Co, W) or form the main strengthening intermetallic γ'-phase (Ti, Al), with some carbide phase (Cr, Ti, Nb, C, V).

During the early stages of the development of dispersion-hardened heat-resistant nickel—chromium alloys titanium was the chief strengthening element. Later it was found that aluminum is even more effective in forming the γ'-phase.** Aluminum forms a compound with nickel of the berthollide type Ni_3Al, which has a lattice similar to that of the solid solution, but the γ'-phase has a larger lattice parameter. The above compound can dissolve large amounts of titanium, which leads to the increase in the lattice parameter of the γ'-phase.

The importance of niobium for stabilizing the solid solution and forming the main strengthening phase has long been underestimated, and therefore few niobium-alloyed heat-resistant steels and alloys are produced today in the Soviet Union (EI481, EI607) or abroad (Inko-718, Rene-62, USA, and g-18B and g-32B, England).

* The experimental part of this investigation was carried out with the participation of N. I. Kurkina, A. P. Ozerova, G. G. Georgieva, and E. V. Polyak.

** According to the data given by S. T. Kishkina, N. F. Lashko, et al.

In 1953—1954 the investigations carried out together with N. I. Kurkina on a number of heat-resistant alloys containing up to 2—3% niobium, 2.5—3% molybdenum, and 1.3—1.6% aluminum (the EI437 alloy contains only 0.5—0.90% Al) led to the development of an original heat-resistant alloy with no cobalt or tungsten, which had good mechanical properties (up to 750°C) over the range of the most important working temperatures (550°C—750°C).

The mechanical and high-temperature properties of this Soviet heat-resistant alloy are superior to those of the English Nimonic-90 alloy, which contains 18% cobalt, and are comparable to those of the complex alloyed Rene-41, Waspaloy, and other alloys (USA) with 10—14% cobalt and 4—10% molybdenum. The amounts of alloying elements forming the chief strengthening γ'-phase in nickel-base alloys are about the same, namely, 2.5—3.0% titanium and 1.5% aluminum.

According to literature data the influence of niobium is often similar to that of other alloying elements (Mo, W, Co), as it effectively strengthens the solid solution, inhibits the diffusion processes, and greatly increases the recrystallization temperature. It thus appreciably increases the resistance of alloys to plastic deformation at elevated temperatures.

According to Lashko and Georgieva, more than half the niobium ($\simeq$1%) forms an intermetallic γ'-phase, about one third forms a solid solution, and part (0.2—0.3%) a primary carbide phase of the Nb(CN) type.

The influence of niobium on the structure of heat-resistant steels and alloys is most important. The coarse liquation particles consist of carbonitrides, titanium oxides, and chromium borides. The chief liquation elements in heat-resistant nickel-base alloys are titanium, aluminum, and to some extent boron and carbon. According to the studies of Stepanov et al., the presence of 1.5—2% niobium in the alloys binds the carbon during the early stages of crystallization, and thus changes the physicochemical properties of the mother liquor and creates conditions for reducing the separation of liquation elements.

The presence of heat-resistant initial niobium carbides which are almost insoluble up to 1250—1300°C inhibits the rapid grain growth during the heating of the alloy, and thus prevents the formation of a coarse zonal nonuniform crystal structure during hot pressing and heating for quenching.

INVESTIGATION OF THE PHASE COMPOSITION OF A NICKEL—CHROMIUM ALLOY

The data of a phase analysis given in Table 1 show that quenching this alloy from 1000, 1120°C in water leads to the formation of a solid solution and small amounts of a primary carbide phase NbCN which does not dissolve even if the metal is heated to 1250°C. Slow cooling in the air from the solution heat-treatment temperature leads to the precipitation of considerable amounts of the strengthening γ'-phase, about 10% of the γ'-phase after a single heat treatment and about 14.5% of the γ'-phase after a double.

Aging at 750—775°C for 16 hr leads to an increase in the content of the γ'-phase to 20%, i.e., double the amount produced by a single quenching.

Double aging increases the content of the γ′-phase to 22% and reduces the size of its particles. This leads to an appreciable increase in the strength of the alloy (σ_b, $\sigma_{0.2}$, H_B) and the long-time strength of the EI-698 alloy over the whole range of working temperatures up to 750°C.

TABLE 1. Phase composition of a nickel—chromium alloy after different heat-treatment processes

Heat-treatment process	Content of alloying elements in the γ′-phase, %							Content of elements in the carbide phase, %	
	Ni	Ti	Al	Nb	Cr	Mo	ε, %	Ti	Nb
1120°C, 8hr, air + 1000°C, 12hr, water	0.10	0.04	traces	traces	traces	traces	0.14	0.05	0.22
1120°C, 8hr, air	8.37	0.85	0.4	0.53	0.41	0.10	10.6	0.05	0.11
1120°C, 8hr, air + 1000°C, 4hr, air	11.8	1.05	0.53	0.60	0.37	0.09	14.4	0.06	0.13
1120°C, 8hr, air + 1000°C, 4hr, air + + 750—775°C, 16hr, air	15.7	1.58	1.05	1.1	0.68	0.18	20.20	0.06	0.18
1120°C, 8hr, air + 1000°C, 4hr, air + + 750°C, 16hr, air + 650°C, 16hr	18.0	1.62	1.10	1.18	0.72	0.72	22.8	0.06	0.17

An analysis of the content of alloying elements in the γ′-phase shows that it consists chiefly of Ni, Ti, Al, and Nb. The contents of Al and Nb in the γ′-phase are almost the same. Although chromium and molybdenum also enter the γ′-phase they remain mostly in the solid solution of the alloy. The amount and composition of the strengthening carbide phase (about 0.2%) are almost the same after a single or double solution heat treatment.

An X-ray analysis carried out under the supervision of N. F. Lashko showed that the alloy contains two main phases: the strengthening intermetallic γ′-phase Ni_3 (Al, Nb, Ti, Cr, Mo), the carbide Nb (CN) phase, and very small amounts of TiN and Cr_2B_3.

It should be pointed out that this heat-resistant nickel-base alloy is the only one that does not contain the cubic chromium carbide of the $Cr_{23}C_6$ type, which precipitates mainly along the grain boundaries and appears to be the main reason for the considerable reduction in the impact strength of heat-resistant alloys on heating. This is apparently because the total amount of carbon in this alloy is used up by niobium and titanium, and little is left for the formation of chromium carbide.

A study on the embrittlement of EI-437B alloys during heating showed that heating to 550—650°C for 50—500 hr reduces the impact strength of the metal to 1.5—1.2 kgm/cm². Further heating for 5000 hr does not change this value. After 10,000 hr of heating at 650, 700, and 750°C the impact strength of heat-resistant alloys containing 2% niobium does not drop below 3.5—4 kgm/cm² (Figure 1).

Niobium inhibits the diffusion processes, particularly the process of coagulation of the γ′-phase, which in itself is very slow in the range of 600—750°C.

This is shown by the results of an analysis on the relationship between the composition of the alloys and the temperature during prolonged aging (from 3000 to 10,000 hr) given in Table 2. *

* The specimens were aged and tested for strength after a long time by E. E. Levin and I. G. Taubina.

The data in Table 2 show that even prolonged heating (from 3000 to 10,000 hr) at 650, 700, and 750°C does not influence the relationship between the chief alloying elements in the γ'-phase. The amount of this phase is increased from 14.56 to 19—20% on heating.

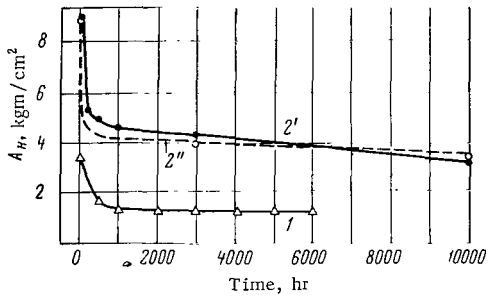

FIGURE 1. Relationship between the impact strength of alloys and the duration of aging:

1 — EI-437B, heated at 600°C; 2 — nickel — chromium alloy, heated at 650°C (2') and 700°C (2").

TABLE 2. Phase composition of nickel-chromium alloys after prolonged heating at elevated temperatures under stress

Temperature, holding time, and stress	Content of elements in the γ'-phase, %							Content of elements in the carbide phase, %				
	Ni	Ti	Cr	Mo	Al	Nb	ε, %	Ti	Cr	Mo	Nb	ε, %
Initial state after heat treatment by the process: 1120°C, 8 hr, 1000°C, 4 hr, +800°C, 16 hr	11.55	1.22	0.30	0.13	0.76	0.60	14.56*	0.08	0.02	0.03	0.24	0.37
The same + 650°C, 3000 hr	14.90	1.55	0.35	0.16	0.9	0.90	19.76	0.08	0.03	0.03	0.28	0.42
" +700°C, 3000 hr	15.29	1.60	0.37	0.18	—0.9	0.98	19.40	0.08	0.037	0.03	0.26	0.40
" +700°C, 10,000 hr	14.96	1.54	0.38	0.17	1.02	0.92	19.2	0.08	0.03	0.04	0.24	0.40
" +750°C, 3000 hr	14.58	1.54	0.37	0.15	1.09	0.95	18.68	0.08	0.03	0.03	0.25	0.39
" +750°C, 10,000 hr	14.44	1.52	0.39	—0.16	1.05	0.96	18.52	0.08	0.04	0.04	0.25	0.41
" 700, σ = 38 kg/mm^2, 4040 hr	15.2	1.50	0.40	0.16	1.12	0.94	19.82	0.09	0.06	0.03	0.26	0.44
" 700, σ = 38 kg/mm^2, 200 hr	15.3	1.54	0.40	0.20	1.10	0.95	19.70	0.09	0.05	0.03	0.26	0.43

* In this heat the content of Al, Ti, and Nb, i.e., of the chief elements in the γ'-phase, was a minimum. The higher temperature of aging (800°C) applied earlier led to a certain coagulation of the strengthening γ'-phase.

The total content of alloying elements in the carbide phase was 0.4—0.43%, compared to 0.20% before aging. This increase was chiefly at the expense of niobium. The data on the phase analysis obtained for alloys heated under stresses at 700°C for 2000 to 4000 hr are very interesting. Specimens stressed by a force of σ = 33 kg/mm^2 at this temperature did

not fail before 4000 hr, but specimens stressed by a force of $\sigma = 38\ kg/mm^2$ failed after about 2000 hr.

Prolonged heating at 650°C leads to additional strengthening of the alloys caused by precipitation of a finely dispersed strengthening phase, which somewhat increases the strength and the hardness of the alloy but considerably reduces ductility and impact strength.

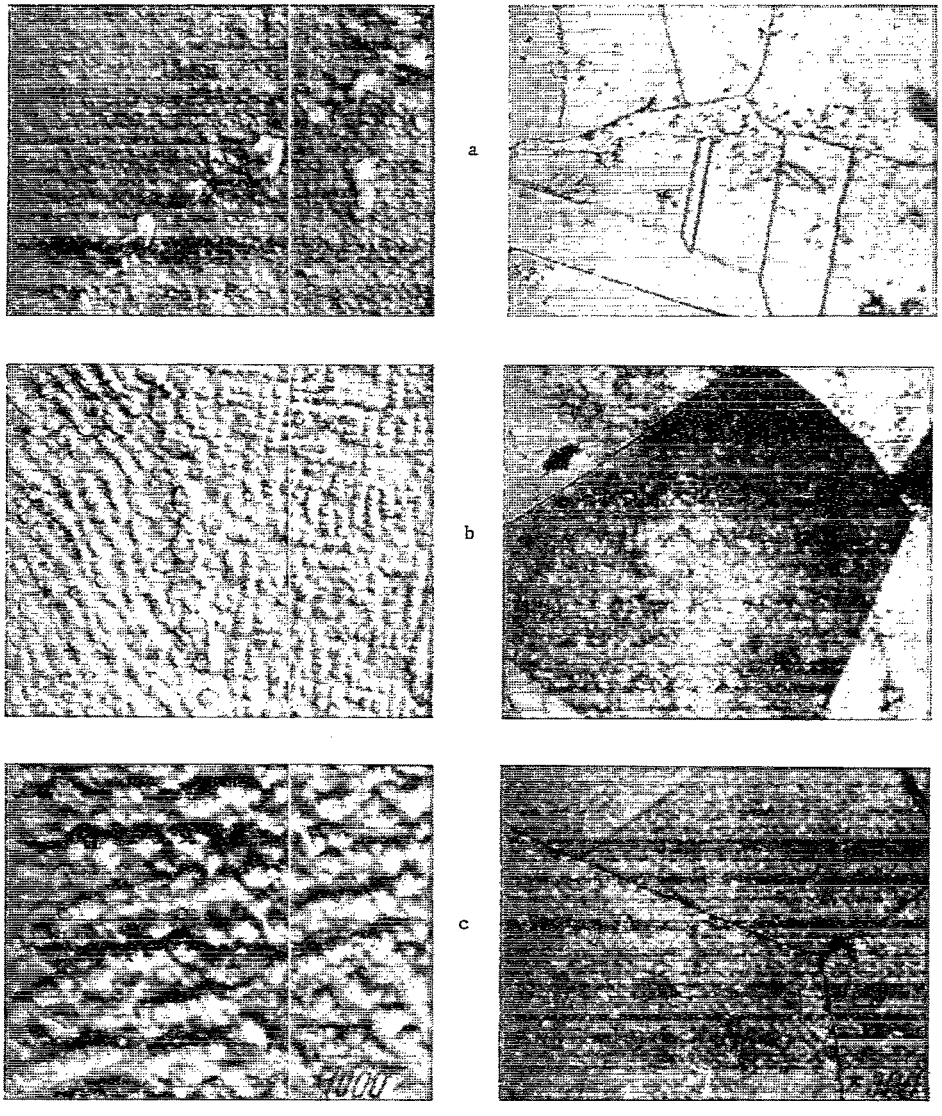

FIGURE 2. Microstructure of heat-resistant nickel—chromium alloys:

a—solution heat-treatment and aging, ×300, ×1000; b—solution heat-treatment +aging at 700°C, for 10,000 hr, ×300 and ×1000; c—solution heat-treatment +aging at 750°C, for 10,000 hr, ×300 and ×1000.

These properties of the alloys, their structural and phase transformations, and also their high thermal stability, indicate that they will be very reliable under conditions of prolonged service, and satisfy the requirements of high-temperature service for engines and stationary gas turbines.

METALLOGRAPHIC ANALYSIS

The microstructure of these alloys was studied by optical and electron microscopes with a magnification of 300 and 10,000,* respectively. The heat-treated alloys consist of a solid solution, γ'-phase, and primary carbides of the Nb(CN) type. The particles of the γ'-phase are very small and cannot be seen at a magnification of 300 (Figure 2, a). These particles, however, become coarser after aging for 3000 and 10,000 hr, and the alloy can be more readily etched. The particles of the γ'-phase in an alloy heated at 700°C for 3000—10,000 hr grow to a size of 0.1—0.15 μ (Figure 2, b). At 750°C the particles of the γ'-phase become coagulated, which leads to a softening of the alloy (Figure 2, c).

* [In Figure 2, ×1000.]

Yu. P. Romashkin

INFLUENCE OF TEMPERATURE AND DEFORMATION ON THE NATURE OF ACTIVATION AND THE BEHAVIOR OF STRESSED METALS AT ELEVATED TEMPERATURES

If we assume that a solid has a certain viscosity, η, then the rate of plastic deformation of this body under a stress $\sigma = \text{const}$ can be written as

$$\dot{\varepsilon} \sim \frac{\sigma}{\eta}. \tag{1}$$

According to the theory of the rate of a reaction /1/,

$$\eta = \eta_n e^{\frac{\Delta F(\sigma)}{RT}}, \tag{2}$$

where ΔF is the free energy of activation of the process, η_n is the viscosity when $\Delta F = 0$.

If we substitute formula (2) into (1), we obtain the well-known formula

$$\dot{\varepsilon} = \frac{a\sigma}{\eta_n} e^{-\frac{\Delta F(\sigma)}{RT}} = \dot{\varepsilon}_n e^{-\frac{\Delta F(\sigma)}{RT}}, \tag{3}$$

where a is a certain arbitrary parameter which can be used as a coefficient of overstress, and

$$\dot{\varepsilon}_n = \frac{a\sigma}{\eta_n}. \tag{4}$$

In general, any molecular-kinetic process, which we shall call $\dot{\xi}_i$ (rate of plastic deformation $\dot{\varepsilon}$, rate of bulk diffusion D_b and grain boundary diffusion D_{gb}, failure, etc.) can be characterized by the formula

$$\dot{\xi}_i = \dot{\xi}_{ni} e^{-\frac{\Delta F(\alpha_i)}{RT}}, \tag{5}$$

where α_i is a certain factor characterizing ΔF or $\dot{\xi}_{ni}$.

In this study an attempt has been made to clarify the nature of the activation of processes such as plastic deformation and diffusion.

1. GENERAL TEMPERATURE DEPENDENCE OF THE RATE OF KINETIC PROCESSES IN SOLIDS

Model of the "hard" activated complex

It can be assumed that activation takes place if the atoms of a certain complex acquire a kinetic energy ΔH_p, which we shall call the activation energy at the "pole," as a result of which the forces of interaction between the atoms of the complex (which we shall call the modulus of normal elasticity E) are overcome. The value of ΔH_p can correspond to a certain temperature of activation at the "pole" T_p so that the activated complex at $T = 0$ will tend to increase by the magnitude.

$$\Delta v_p = \beta_0 T_p V_0.$$

However, since the activated complex is surrounded by a "hard" matrix which has a modulus of bulk elasticity K, the extension of this complex will be counteracted by a certain pressure:

$$P_p = K_0 \frac{\Delta v_p}{V_0}.$$

As a result the extension Δv_p will not take place, and the distances between the atoms will remain almost unchanged. Therefore, we can assume that the relative volume changes of the activated complex $\beta_0 T_p$ is constant, and does not depend on the conditions of the system, such as temperature, and this type of activated complex can be called "hard."

Further on we shall use this model for temperatures above the Debye temperature, and therefore β_0, V_0, E_0, etc., will be magnitudes obtained by extrapolation according to laws governing the relationship between these factors and the temperature (we shall consider $T = 0$).

Activation energy H_p of the activated complex

According to the above model the kinetic energy of the activated complex will be

$$\Delta H_p = E_0 \Delta v_p = \beta_0 T_p E_0 V_0. \tag{6}$$

In the general case we can apparently assume that

$$\Delta v_p = \Delta v_{Ti} + \Delta v_{\delta i}, \tag{7}$$

where Δv_{Ti} is the volume change caused by thermal fluctuation; $\Delta v_{\delta i}$ is the volume change in the lattice caused by any factor other than the thermal (we shall call it the δ-factor). The δ-factor may be a distortion of the lattice caused by deformation, incomplete filling of the lattice by atoms (spheres) even in the case of close-packed structures, vacancies produced by irradiation, etc.

If we connect the free spaces Δv_{Ti} and $\Delta v_{\delta i}$ with certain temperatures (the temperature of fluctuation T_{Ti} and the temperature $T_{\delta i}$ of the δ-factor) then in analogy with (6) we obtain

$$\Delta H_p = \Delta H_{Ti} + \Delta H_{\delta i}. \tag{8}$$

Hence

$$\Delta H_{Ti} = \Delta H_p - \Delta H_{\delta i}, \tag{9}$$

where the magnitude ΔH_{Ti} is the activation energy of some kinetic process, and $\Delta H_{\delta i}$ is a certain configurative energy which can be transformed into the kinetic energy of the motion of atoms at the moment of activation only. For this reason, and since at the moment of activation part of the kinetic energy should correspond to $P_p \Delta v_p$ (the energy consumed to compress the complex), the maximum magnitude of $\Delta H_{\delta i}$ will be

$$\Delta H_{\delta i} \leqslant \Delta H_p - P_p \Delta v_p \tag{10}$$

In general the following equation will apparently be true:

$$\Delta H_{\delta i} = (\Delta H_p - P_p \Delta v_p) f\left(\frac{\delta_i}{\delta_{0i}}\right), \tag{11}$$

where δ_{0i} is a certain characteristic value of δ_i. According to /2/, the function $f(\delta_i/\delta_{0i})$ should be equal to the tangent of the hyperbola, and the activation energy of the process can be written as

$$\Delta H_{Ti} = \Delta H_p - (\Delta H_p - P_p \Delta v_p) \operatorname{th} \frac{\delta_i}{\delta_{0i}}. \tag{12}$$

At $\delta_i > 2\delta_{0i}$ $\operatorname{th} \frac{\delta_i}{\delta_{0i}} \to 1$; therefore from (12) it follows that

$$\lim_{\delta_i > 2\delta_{0i}} \Delta H_{Ti} \to P_p \Delta v_p. \tag{13}$$

This result agrees with the theory of the maximum activation energy of processes developed by Osipov /6/. It should be mentioned that this will be true only if the action of the δ-factor does not upset the isothermal process even in certain microvolumes; otherwise the δ-factor can influence the kinetic term $P_p \Delta v_p$ also, and it will appear that

$$\lim_{\delta_i > 2\delta_{0i}} \Delta H_{Ti} \to 0.$$

It is possible that the dependence of the activation energy of creep on deformation and the resultant unsteadiness of the creep rate /5/ is due to the upsetting of the isothermal conditions in the microvolumes, since according to /5/ the combined action of stresses and deformation may lead to very small activation energies of creep.

Entropy of activation of the process ΔS_{Ti}

Since the temperature of the activated complex is T_p irrespective of the type of process and of the ratio ΔH_p to $\Delta H_{\delta i}$, and the thermal effect of activation is ΔH_{Ti}, the relationship

$$\Delta S_{Ti} = \frac{\Delta H_{Ti}}{T_p} = \frac{\Delta H_p}{T_p} - \frac{\Delta H_{\delta i}}{T_p} = \Delta S_p - \Delta S_{\delta i} \tag{14}$$

can be determined as the entropy of the activation of the process. The terms ΔS_p and $\Delta S_{\delta i}$ are the entropies of activation of the complex and of the δ-factor, respectively.

Free energy of activation of the process and the temperature at the "pole"

From equations (14) and (12), the free energy of activation of the process can be written

$$\Delta F_i = \Delta H_{Ti} - \Delta S_{Ti} T = \Delta H_{Ti}\left(1 - \frac{T}{T_p}\right) =$$
$$= \left[\Delta H_p - (\Delta H_p - P_p \Delta v_p) \operatorname{th} \frac{\delta_i}{\delta_{0i}}\right]\left(1 - \frac{T}{T_p}\right).$$

If we consider that $P_p \Delta v_p = (\beta_0 T_p)^2 K_0 V_0$, and assume that $K_0 \cong E_0$, as is usually the case, then

$$\Delta F_i = \beta_0 T_p \left[1 - (1 - \beta_0 T_p) \operatorname{th} \frac{\delta_i}{\delta_{0i}}\right] EV, \tag{15}$$

where it is assumed that

$$\frac{1}{T_p} \simeq \frac{1}{E_0}\frac{dE}{dT} - \beta, \tag{16}$$

if we disregard second order terms in the expansion of E and V in terms of T.

Formula (15) shows that at $T = T_p$, E should be equal to zero, since $\Delta F_i = 0$. Consequently, the temperature at the "pole" is the temperature at which the binding forces between the atoms in the activated complex are overcome, and a pressure P_p develops.

If we assume that $T = 0$, equation (15) leads to the known laws of Bugakov /3/ and Portevin /4/. On the other hand, if in the laws of Bugakov and

Portevin we disregard the melting point T_{mp} and take into account the temperature dependence of E and V, we obtain an equation of the type (15) in the form

$$\Delta F_i = C_i E V.$$

Since this formula was the real reason for this analysis, and its results are well confirmed by experiments, as shown below, equation (15) should be called the modified Portevin-Bugakov law.

If we substitute ΔF_i from (15) into (5), we obtain the formula

$$\dot{\xi}_i = \dot{\xi}_{ni} e^{-\frac{\Delta H_p - (\Delta H_p - P_p \Delta v_p) \text{th} \frac{\delta_i}{\delta_{0i}}}{RT} \left(1 - \frac{T}{T_p}\right)}, \qquad (17)$$

which is Shestopalov's equation /2/, theoretically derived and experimentally confirmed for plastic deformations.*

Let us take equation (17) as the basis for comparing the proposed theory with experiment. The validity of this theory can be best checked by an analysis of the temperature-rate dependence of the resistance of solids to deformation. In this case we can obtain experimentally the magnitudes of T_p, ΔH_p, $P_p \Delta v_p$, $\dot{\xi}_{ni}$, and $\text{th} \frac{\delta_i}{\delta_{0i}}$. The results can be approximately checked by comparing equation (12) with the data on the activation energy of self-diffusion of pure metals. We shall return to this later.

2. COMPARISON OF THEORY WITH EXPERIMENT

The temperature-rate dependence of the resistance of solids to deformation

According to the results of /2, 5/, it can be assumed that

$$\bar{\dot{\varepsilon}} = \frac{\varepsilon_f}{\tau_f} = \dot{\varepsilon} \frac{\gamma T_{mp}}{T} \simeq \dot{\varepsilon}_p e^{-\frac{\Delta H_p - (\Delta H_p - P_p \Delta v_p) \text{th} \sigma / \sigma_0 + \gamma R T_{mp} \ln e}{RT} \left(1 - \frac{T}{T_p}\right)}, \qquad (19)$$

where $\bar{\dot{\varepsilon}}$ is the average creep rate, τ_f is the time to failure as a result of creep; $\dot{\varepsilon}$ is transient or steady-state creep rate; ε_f is the deformation at the moment of failure, $\gamma \simeq 2-1$.

* Equation (17) is very important for diffusion. Since diffusion in the bulk and along grain boundaries can be described by an equation of type (17), and since

$$D_b = D_p \exp\left[-\frac{\Delta H_d}{RT}\left(1 - \frac{T}{T_p}\right)\right], \quad \text{a} \quad D_{gb} = D_p \exp\left[-\frac{\Delta H_\alpha(\theta)}{RT}\left(1 - \frac{T}{T_p}\right)\right],$$

where θ is the angle of disalignment of neighboring grains, then at $T = T_p$,

$$D_{gb} = D_b = D_p \qquad (18)$$

Together with Fick's formula for diffusion along grain boundaries from the last formula it is possible to determine the absolute magnitudes of D_{gb} and the width of the grain boundary δ_{gb}, if we know the product $D_{gb}\delta_{gb}$.

If ε_f (0.3—3) is sufficiently large, then the γRT_{mp} can be disregarded, and therefore we shall continue to leave it out.

Figure 1 shows the log ε—log σ and log τ_f—log σ relationships at different values of T = const given by different authors for a number of substances /2, 6—10/. These data were also plotted in the log $\dot{\varepsilon}$—$1/T$ and log τ_f—$1/T$ coordinates at different values of σ = const, and the relationships between the activation energy of deformation and stresses, shown in the figure, were also obtained.

According to (19), the point of intersection of the straight lines should correspond to $T = T_p$ and $\dot{\varepsilon} = \dot{\varepsilon}_p$, or $\tau_f = \tau_p$.

The magnitude of ΔH at $\sigma = 0$ should correspond to ΔH_p, and its maximum value corresponds to the product $P_p \Delta v_p$.

All the curves of $\Delta H = f(\sigma)$ are theoretical.

a. Deformation rate at the "pole." According to the graphs given in Figure 1, the following equation is true for all the above substances:

$$\dot{\varepsilon}_p \cong \frac{1}{\tau_p} = 10^{6\pm1}\ \text{sec}^{-1}.$$

Since according to the above model of the activated complex the substance is in the gaseous state at $T = T_p$ and $P = P_p$, so that its density is similar to that of a solid, the viscosity of the activated complex will have an order of magnitude:

$$\eta_p = 10^{-3}\text{poise} \qquad (20)$$

The magnitude of the arbitrary parameter a in equation (4) will be equal to 10^{-5} dimensionless units. If we assume that

$$\eta_{pr} = \frac{\eta_p}{a}, \qquad (21)$$

where η_{pr} is the viscosity of a certain relaxation element, which can be represented as a certain unloaded zone around an activated complex, then the value a indicates that the viscosity of the relaxation element is 10^5 times greater than that of the activated complex. An analysis of the value η_{pr} is difficult. It can be stated only that the solution to this problem requires an exact knowledge of the number of atoms in the activated complex and of the duration of its life.

b. Temperature at the "pole" T_p. Data are given in the following table and in Figure 2 in which a comparison is made between the values of $1/T_p$ calculated according to formula (16) (in certain cases we used the well-known empirical relationship /11/: $(1/E_0)(dE/dT) \cong 8\beta$) and the values of $1/T_p^e$ obtained from Figure 1. T_p^e is the temperature which corresponds to the intersection of the straight lines plotted in the logε — $1/T$ or logτ_f — $1/T$ coordinates. Let us call T_p^e the experimental temperature at the "pole," i.e., the temperature of the activated complex. It can be seen that the calculated data agree satisfactorily with the experimental.

Substance	Cu	Pb	Al	Fe	Sn	Zn	In	Ag	Se	Polymers*
$1/T_p \cdot 10^4$, °K^{-1}	4.5	6.0	6.0	3.6	6.0	6.0	12.0	4.3	30.0	20.0±3
$1/T_p^e \cdot 10^4$, °K^{-1}	4.6	5.0	8.5	2.3	3.0	4.0	9.0	5.0	28.0	16.0—25.0
T_p/T_p^e	1.0	0.8	1.40	6	0.5	0.7	0.8	1.1	0.9	0.8—1.2

* The data for $(1/E_0)(dE/dT)$ were taken from /12, 13/.

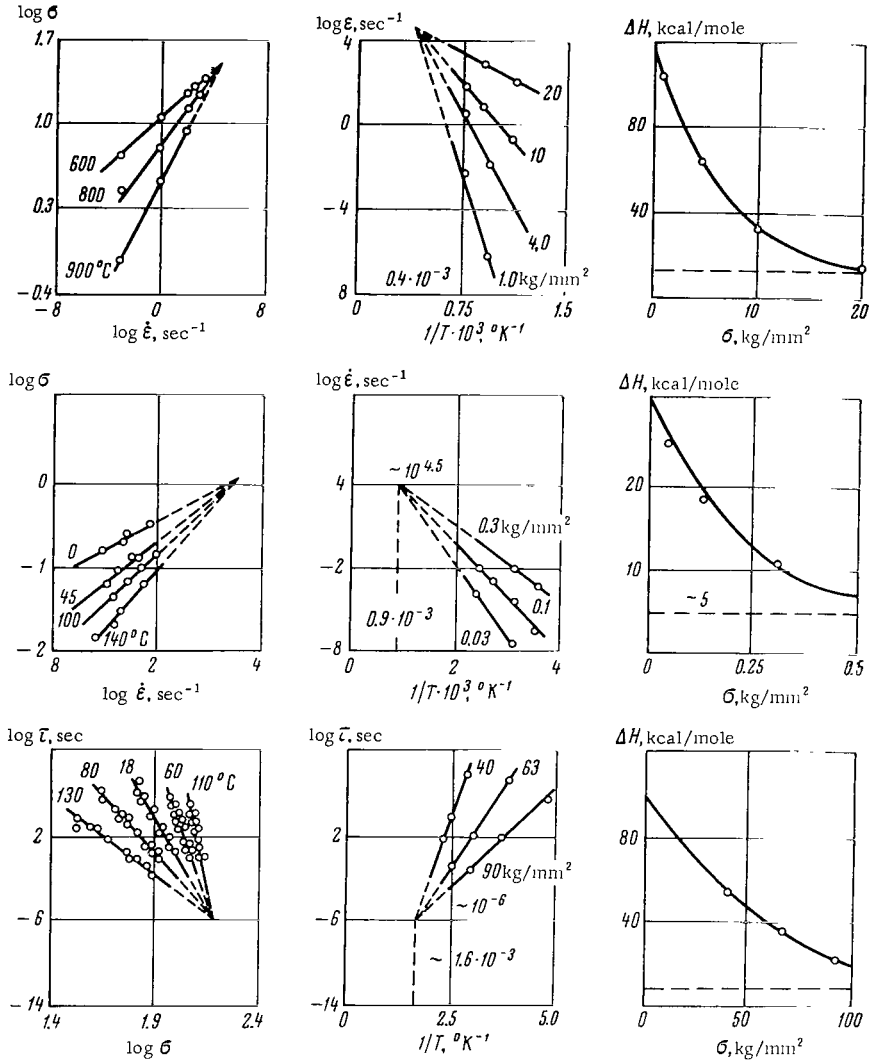

FIGURE 1. Temperature-rate dependence of the resistance to deformation and the dependence of the activation energy of deformation on the applied stress for the following substances (from left to right downward) /27/:

1—copper, ΔH_{mp} = 110—95 th 0.11 σ kcal/mole; 2—silver, ΔH_{mp} = 82—72 th 0.07 σ kcal/mole; 3—indium, ΔH_{mp} = 30—25 th 3.5 σ kcal/mole; 4—amorphic selenium, ΔH_{mp} =110—100 th 0.14 σ kcal/mole; 5—capron fiber, ΔH_{mp} = 96—60 th 0.015 σ kcal/mole; 6—"chlorin" film, ΔH_{mp} = 120—114 th 0.06 σ kcal/mole; 7—polystyrene fiber, ΔH_{mp} = 100—92 th 0.16 σ kcal/mole.

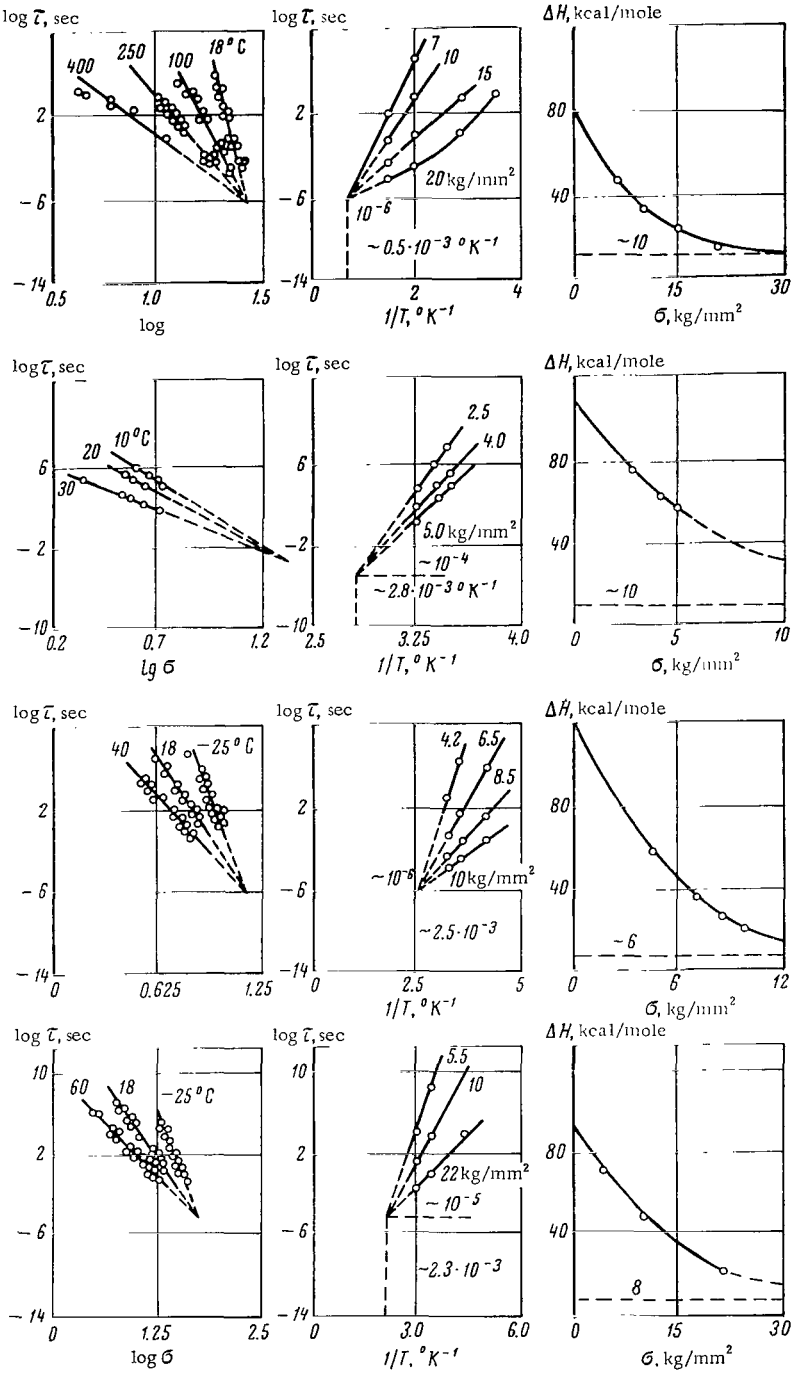
log τ, sec
400
250
100
18° C
2
−6
−14
0.5
1.0
1.5
log
log τ, sec
7
10
15
20 kg/mm²
10⁻⁶
~0.5·10⁻³ °K⁻¹
2
4
1/T, °K⁻¹
ΔH, kcal/mole
80
40
~10
0
15
30
σ, kg/mm²
log τ, sec
20
10° C
30
6
−2
−10
0.2
0.7
1.2
2.5
lg σ
log τ, sec
2.5
4.0
5.0 kg/mm²
~10⁻⁴
~2.8·10⁻³ °K⁻¹
3.25
4.0
1/T, °K⁻¹
ΔH, kcal/mole
80
40
~10
0
5
10
σ, kg/mm²
log τ, sec
40
18
−25° C
2
−6
−14
0
0.625
1.25
log τ, sec
4.2
6.5
8.5
~10⁻⁶
10 kg/mm²
~2.5·10⁻³
2.5
5
1/T, °K⁻¹
ΔH, kcal/mole
80
40
~6
0
6
12
σ, kg/mm²
log τ, sec
10
60
18
−25° C
2
−6
−14
0
1.25
2.5
log σ
log τ, sec
5.5
10
22 kg/mm²
~10⁻⁵
~2.3·10⁻³
3.0
6.0
1/T, °K⁻¹
ΔH, kcal/mole
80
40
8
0
15
30
σ, kg/mm²

It can be seen that if $1/T_p$ is changed by about one order of magnitude, the average agreement between the calculated and experimental results is ± 30%, which is within the accuracy of the estimates.

c. Activation energy at $\sigma = 0 - \Delta H_p$. At $\sigma \to 0$, the activation energy of deformation according to formula (19) can be written as: $\Delta H_p = \beta_0 T_p E_0 V_0$.

Below we compare the calculated activation energies of deformation at $\sigma = 0$ ($\Delta H_p = \beta_0 T_p E_0 V_0$) with the experimental data found for several metals (ΔH_p^e).

Metal	Cu	Pb	Pt	Ag	α-Fe	Al	Mg	In	Zn
ΔH_p, kcal/mole (calculated)	110	38	130	90	80	95	67	37	50
ΔH_p^e, kcal/mole (experimental)	110	35	120	80	80	75	60	30	33
	Fig. 1	[2]*	[	[14,15]	Fig. 1		[2]*	[16]	Fig. 1	[2]*
$\Delta H_p/\Delta H_p^e$	1.0	1.1	1.1	1.1	1.0	1.25	1.1	1.2	1.5

* The data for ΔH_p are given in /2/ and $u = \Delta H_p(1 - T/T_p)$, therefore we have made the necessary recalculation, and T_p has been taken from /2/.

Further data required for ΔH_p of some metals, particularly of refractory metals, were calculated:

Metal	Na	Li	Ni	Ta	Th, Mo, W, Re γ = Fe	Rh	Ir	Ru	Os
T_{mp}, °K	371	459	1728	3270	2000—3500	2239	2723	2773	2973
ΔH_p, kcal/mole	30	12	220	140	160—170	340	570	300	360

These values are compared graphically in Figure 3. It is believed that for metals with a hexagonal close-packed lattice $V_0 = 1.55\, a_{min}^3$ where a_{min} is the minimum distance between atoms. This volume corresponds to the space occupied by an equivalent close-packed body-centered cubic lattice into which the hexagonal lattice is transformed at $T = T_p$ and $P = P_p$, i.e., in the activated state.

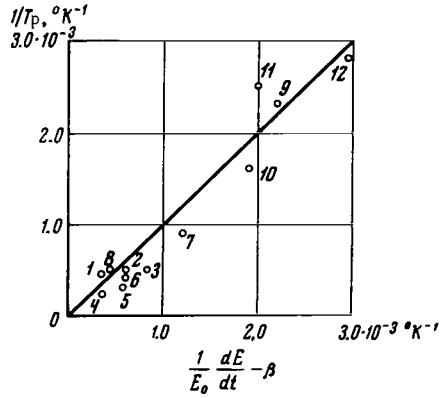

FIGURE 2. Comparison of calculated and experimental data on the inverse temperatures at the "pole" for the following substances:

1—copper; 2—lead; 3—aluminum; 4—iron; 5—tin; 6—zinc; 7—indium; 8—silver; 9—polystyrene; 10—capron fiber; 11—"chlorin" film; 12—amorphous selenium.

The highest value of ΔH_p, and consequently the highest heat resistance, can be expected for iridium, osmium, rhodium and ruthenium, although these metals do not have the highest melting points, but tungsten, molybdenum, tantalum, rhenium, and thorium, can be expected to have a lower heat resistance, although they have higher melting points than, for example, rhodium.

d. Maximum activation energy — $P_p \Delta v_p$. The experimental ($\lim_{\sigma > 2\sigma_0} \Delta H_p$) and calculated ($P_p \Delta v_p$) magnitudes of the maximum activation energy of deformation are given below:

Substance	Cu	Ag	In	Capron	"Chlorin"	Polystyrene
$\lim_{\sigma>2\sigma_0} \Delta H_p$, kcal/mole*	15	10	5	6	6	8
$P_p \Delta v_p$, kcal/mole	12	12	6.5	Tentatively	~7 for all	

* Experimental data taken from Figure 1.

The agreement between these data can be considered satisfactory. Thus, equation (19) conforms well with the experimental data.

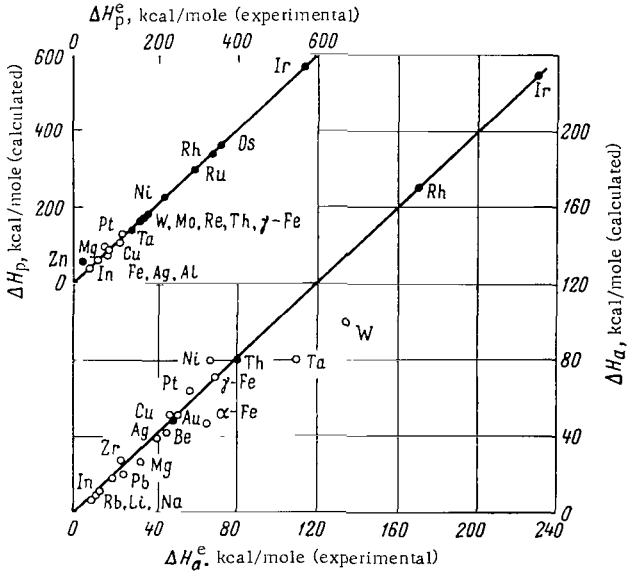

FIGURE 3. Calculated and experimental data on the activation energy of self-diffusion during the process of deformation at $\sigma \to 0$:

Dark circles designate the required calculated values for ΔH_d or ΔH_p.

Activation energy of self-diffusion ΔH_a

In the case of self-diffusion and in the absence of any stresses caused by the δ-factor the crystal lattice can apparently have a free space, i.e.,

$$\frac{\delta_i}{\delta_{oi}} \simeq \frac{\Delta v}{v_{at}} = \frac{(1 - \Pi) V_0}{v_{at}}, \qquad (22)$$

where Π is the packing coefficient, $V_0 = a^3$ (for cubic lattices a is the lattice parameter), $v_{at} = a^3_{min}$, where a_{min} is the minimum distance between atoms, and consequently v_{at} is the minimum volume of a cube in which an atom can be located. In such a case the equation for calculating the activation energy of self-diffusion for cubic structures can be written as:

$$\Delta H_d = \Delta H_p - (\Delta H_p - P_p \Delta v_p) \operatorname{th} \frac{(1 - \Pi) a^3}{a^3_{min}}. \qquad (23)$$

For noncubic structures the problem of determining V_0 and v_{at} should apparently be investigated further. For hexagonal lattices the calculated and the experimental values of ΔH_α agree, if it is assumed that the magnitude of $\Delta v/v_{at}$ is the same as for face-centered lattices, i.e., equal to 0.73.

The values of the activation energy ΔH_α for some metals, calculated from formula (23), and experimental values are given in the table and in Figure 3.

Activation energies (kcal/mole)

Metal	ΔH_p calculated	ΔH_α calculated	ΔH^e_α experimental	$\Delta H_\alpha / \Delta H^e_\alpha$
Copper	110 (12)*	50	48 [17]	1.0
γ-iron	160 (15)	70	70 [17]	1.0
Silver	90 (12)	42	45 [17]	0.9
Gold	130 (10)	50	50 [17]	1.0
Lead	38 (9)	20	24 [17]	0.8
Nickel	185 (25)	80	66 [18]	1.2
Platinum	130 (20)	65	57 [19]	1.1
Magnesium	54 (7)	25	32 [20]	0.8
Indium	36 (7)	18	18 [17]	1.0
Zirconium	85 (10)	40 85**	40	1.0
Zinc	50 (8)	24	23 [17]	1.0
α-Iron	80 (10)	50	60 [17]	0.8
Lithium	15 (2)	9.5 18**	10 [21]	1.0
Sodium	25 (3)	11 15**	10.5 [17]	1.0
Rubidium	12 (1)	7	9 [22]	0.8
Tantalum	140 (15)	80	110 [23]	0.7
Tungsten	175 (25)	100	135 [24]	0.7
Thorium	175 (35)	80	—	—
Rhodium	350 (30)	170 90**	—	—
Iridium	560 (20)	210 110**	—	—
Beryllium	100 (5)	40	—	—

* Values of the product $P_p \Delta v_p$ are given in round brackets.

** Values of ΔH_α which can be expected from Bugakov's law ($20\,RT_{mp}$).

It can be seen that the calculated and experimental data agree, within the limit of the error of evaluation and measurements, with an accuracy of ± 20% (average ± 10%).

It should be pointed out that Bugakov's law does not hold so well. For example, as we can see from the table, the values for lithium and zirconium obtained experimentally are one half of those expected on the basis of this law, while for rhodium and iridium the values of ΔH_α calculated from formula (23) are twice those obtained according to Bugakov's law. An experimental verification of Bugakov's law is of considerable interest.

3. COMPARISON OF THE ACTIVATION ENERGY AT THE "POLE" ΔH_p WITH THE ACTIVATION ENERGY OF SUBLIMATION ΔH_s

Since the activation at the "pole" and the volatilization of atoms from the surface of metals (sublimation) are both associated with the overcoming of binding forces between atoms, it can be assumed that there is a certain relationship between these two magnitudes.

A comparison between these two magnitudes is given in Figure 4. It can be seen that the relationship between them is very remote: usually the deviation of some points from a certain mean line is ± 300%, although if ΔH_p is varied 50-fold, a certain correlation does exist.

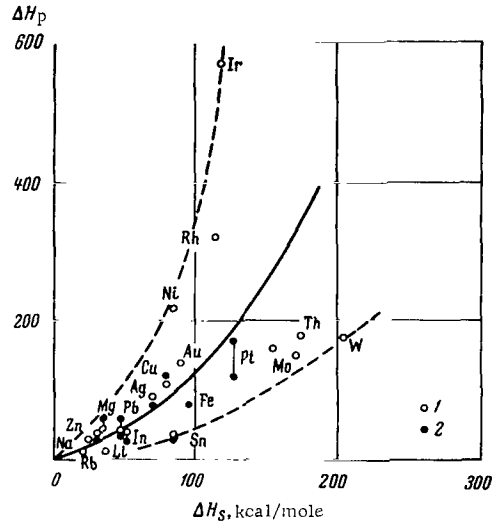

FIGURE 4. Relationship between the activation energies at the "pole" and the activation energy of sublimation (ΔH_s):

The values of ΔH_p were obtained: 1 — by calculation; 2 — from the temperature—rate dependence of the resistance to deformation.

CONCLUSIONS

1. We suggested a model of the activated state.
2. With this model we derived formulas for the free activation energy and for the energy and entropy of activation of deformation and of diffusion. The results of our calculations agree well with the experimental data.

The author wishes to express his gratitude to L. M. Shestopalov for his useful remarks.

Bibliography

1. Glasstone, S., K.I. Laidler, and H. Eyring. The Theory of Rate Processes. [Russian translation. 1948.]
2. Shestopalov, L.M. Deformirovanie metallov i volny plastichnosti vnikh (Wrought Metals and Waves of Plasticity in Them).— Izdatel'stvo AN SSSR. 1958.

2a. Vitman, F.F., N.A. Zlatin, and L.M. Shestopalov.—Sbornik, posvyashchennyi 70-letiyu akademika A.F. Ioffe, Izdatel'stvo AN SSSR. 1951.

3. Bugakov, V.Z. Diffuziya v metallakh i splavakh (Diffusion in Metals and Alloys).—GITL. 1949.
4. Portevin.—Compte Rendus Acad. Sci., 177:634. 1923.
5. Romashkin, Yu.P. Issledovaniya po zharoprochnym splavam (Investigation of Refractory Alloys) (Collection of Articles), 10.— Izdatel'stvo AN SSSR. 1963.
6. Osipov, K.A. Nekotorye aktiviruemye protsessy v tverdykh metallakh i splavakh (Certain Activated Processes in Solid Metals and Alloys).—Izdatel'stvo AN SSSR. 1962.
7. Zhurkov, S.N. and A. Savitskii.—Doklady AN SSSR, 91. 1959.
8. Zhurkov, S.N., V.R. Regel', and T.P. Sanfirova. Vysokomolekulyarnye soedineniya (High-Molecular Compounds), 6:1092. 1964.
9. Weertman, J.—Trans. Met. Soc. AIME, 218:207. 1960.
10. Abasov, S.A., B.B. Kuliev, and Kh.M. Khalilov.—FTT, 8:153. 1965.
11. Lifshits, B.G. Fizicheskie svoistva metallov i splavov (Physical Properties of Metals and Alloys).—Mashgiz. 1956,
12. Wada, Y., H. Hirose, and T. Asano.—J. Phys. Soc. Japan, 14:1064. 1959.
13. Ebnet, Chemistry and Technology of Polymers, No. 1, p. 88.— Izdatel'stvo "Mir," 1965.
14. Zhurkov, S.N. and T.P. Sanfirova.—ZhTF, 28:1719. 1958.
15. Carrecer, R.—J. Appl. Phys., 21:1289. 1950.
16. McTegart, W.J.— Acta Met., 9:615. 1961.
17. Zait, V. Diffusion in Metals. [Russian translation. 1958.]
18. Uptergrouwe, W.R. and M.J. Sinnott.—Trans. ASM, 50:1031. 1958.
19. Breadshow, F.J. and S. Pearson.—Philos. Mag., 1:812. 1956.
20. Shewmon, P.G. and F.N. Rihnes.—Trans. AIME, 200:1021. 1954.
21. Gutowsky, H.S. and B.R. Garwey.—J. Chem. Phys., 20:1472. 1952.
22. Fumi, F.G.—Philos. Mag., 11(46):1007. 1955.
23. Eager, R.L. and D.W. Langmuir.—Phys. Rev., 89:911. 1953.
24. Vasil'ev, V.P. and S.G. Chernomorchenko.—Zavodskaya Laboratoriya, 22:688. 1956.
25. Henderson, J. and L. Vang.—Trans. AIME, 221:72. 1961.

L. A. Ryabtsev, I. I. Kornilov, and L. I. Pryakhina

HEAT RESISTANCE AND PHYSICOCHEMICAL PROPERTIES OF COMPLEX NICKEL-BASE ALLOYS

Modern nickel—chromium heat-resistant alloys usually contain from five to eight or more components.

Of all the phases which can be produced in these alloys (carbides of different composition, nitrides, intermetallic compounds, etc.) the most important for strengthening alloys is the intermetallic phase on the basis of the Ni_3Al compound.

Intermetallic compounds in combination with solid solutions are very important factors in the heat resistance of an alloy. The highly dispersed particles of these phases which precipitate from supersaturated solid solutions lead to additional strengthening of the alloy /1/. However, the intermetallic compound cannot ensure a maximum possible heat resistance of the alloy. Therefore, metals are alloyed with several elements which strengthen both the solid solutions and the intermetallic compound and increase their ability to maintain a high strength for long periods at elevated temperatures. The combined action of alloying elements depends on their individual properties.

A study of the laws governing the physicochemical properties and the heat resistance of complex alloys will help to solve problems of optimum alloying.

The purpose of this work is to investigate the physicochemical properties of nickel-base alloys containing from two to eight elements. The data were compared with those we had obtained earlier /2/. We produced our alloys by introducing successively elements such as chromium, titanium, tungsten, molybdenum, niobium, and cobalt in such amounts that the alloys consisted of a single-phase solid solution.* By adding from 0 to 12 wt % of aluminum we produced alloys with the same strengthening γ'-phase on the basis of the Ni_3Al compound. The table below gives the composition of alloys (in wt %) studied.

Element	Ni	Cr	Ti	W	Mo	Nb	Co	Al
1	Chief		—	—	—	—	—	0—12
2	element	10	—	—	—	—	—	0—11
3	"	10	2	—	—	—	—	0—10
4	"	10	2	6	—	—	—	0—10
5	"	10	2	6	3	—	—	0—10
6	"	10	2	6	3	2	—	0—10
7	"	10	2	6	3	2	5	0—10

The alloys were annealed before the investigation: at 1200°C for 10 hr; at 1150°C for 24 hr; at 1100°C for 24 hr; at 1000°C for 50 hr; and at 900°C for 100 hr. The specimens were then cooled together with the furnace. This heat treatment does not produce the maximum heat resistance, but if facilitates more complete precipitation of the γ'-phase. The purpose of this work was to clarify the influence of the γ'-phase on the physicochemical

* We chose these elements because they are usually used for the production of modern heat-resistant nickel-chromium alloys.

properties and the heat resistance of complex alloys. The dispersion of the precipitated particles was thus not a maximum.

We used the electron microscope to study the nature of the precipitation of the γ'-phase and determine the size of the precipitate particles in alloys of the highest high-heat resistance (Figure 1). We showed that the particles of the γ'-phase are not uniformly distributed in binary and ternary alloys (Ni—Al, 10 wt % Al; Ni—Cr—Al, 9% Al; Ni—Cr—Ti—Al, 8% Al). The size of these particles was up to 10—15 μ. The average size of these particles decreases as we pass from binary to ternary and quarternary alloys. For example, the average size of particles in a binary alloy was 5—7 μ, but it was only 2—3 μ in a ternary alloy. We found very small particles of size 0.1—0.2 μ besides large particles. The precipitate particles in more complex alloys (consisting of six or eight components) are more uniform, their average size in an eight-component alloy is below 1 μ. The deviations from this are very small. The structures of some of these alloys are shown in Figure 2.

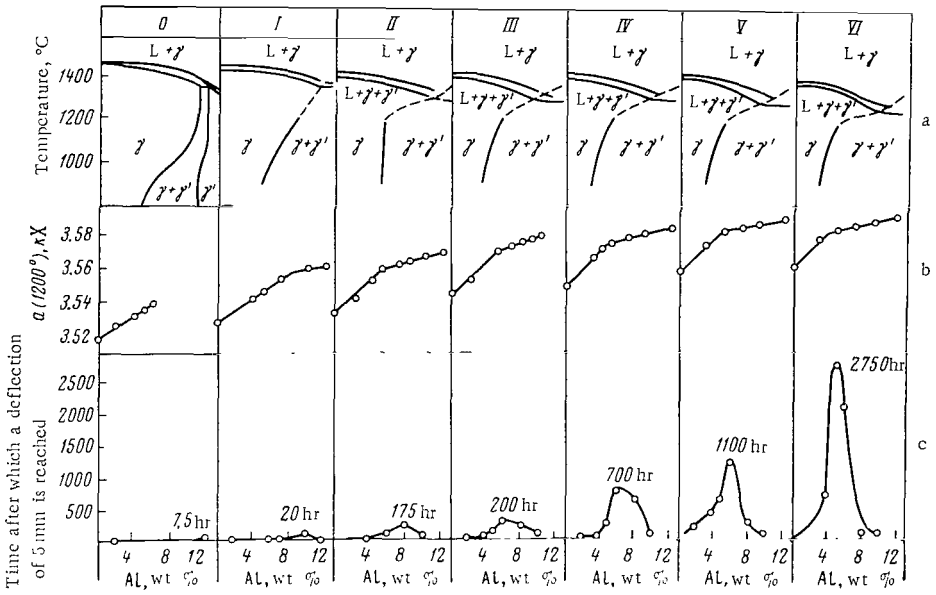

FIGURE 1. Phase diagrams of sections studied (a); crystal lattice parameters of alloys quenched from 1200°C (b); high-temperature strength of alloys at 900°C and $\sigma = 12\ kg/mm^2$ (c):

0— Ni—Al; I—Ni—Cr—Al; II—Ni—Cr—Ti—Al; III—Ni—Cr—Ti—W—Al; IV—Ni—Cr—Ti—W—Mo—Al; V—Ni—Cr—Ti—W—Mo—Nb—Al; VI—Ni—Cr—Ti—W—Mo—Nb—Co—Al.

The photomicrographs show that the dimensions of the particles of the γ'-phase and the nature of their precipitation in alloys with the highest heat resistance are greatly influenced not only by the content of aluminum in the alloy but also by the number of components.

X-ray spectral analysis of the γ-solid solution and of the γ'-phase of five- to eight-component alloys was carried out with a French apparatus

of the "Kameka" type with a 1μ diameter probe. We chose alloys in which the particles were not smaller than 5μ. The data of this analysis agree well with those for intermetallic compounds of similar alloys, and with literature data. Thus, for example, it was found that certain amounts of all components of the alloy are present in both the γ-solid solution and in the γ′-phase. The concentration of chromium, tungsten, and molybdenum in the γ-solid solution is higher than in the γ′-phase (particularly for molybdenum). The concentration of aluminum in the γ′-phase is higher than in the γ-solid solution.

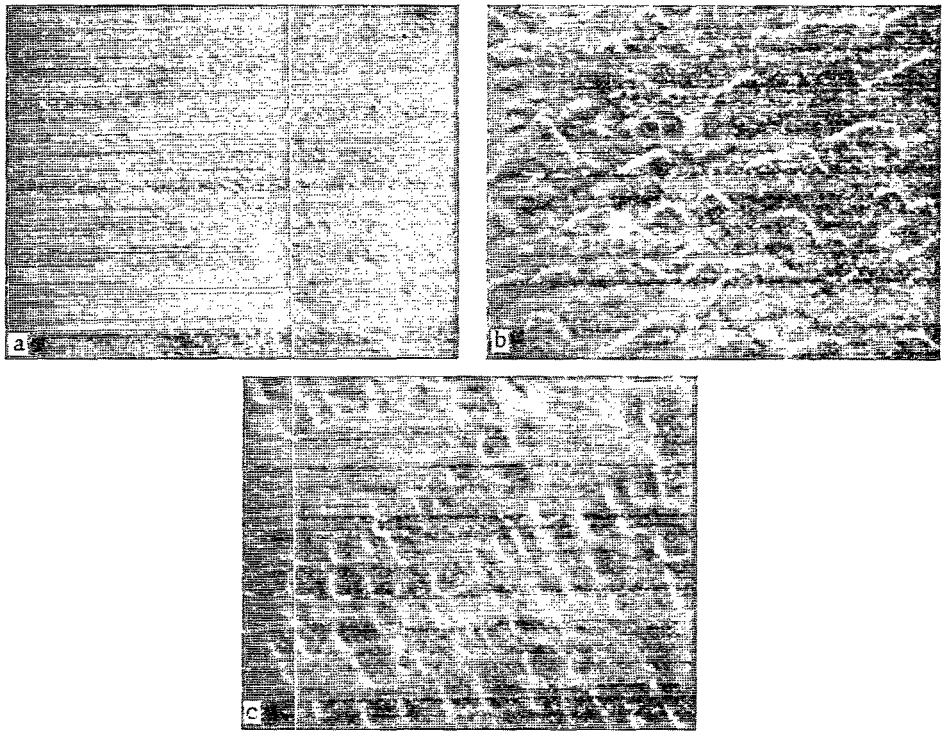

FIGURE 2. Electron photomicrographs of alloys, × 5000:

a—Ni—Al, 10% Al; b—Ni—Cr—Ti—W—Mo—Al, 6% Al; c—Ni—Cr—Ti—W—Mo—Nb—Co—Al, 5% Al.

An earlier X-ray structural analysis showed /3/ (see Figure 1) that with increase in the content of aluminum in the alloy and the number of elements in the alloy, the parameters and the distortion of the crystallattice of the nickel-base solid solution increase.

This has been confirmed by measurements of the electric resistivity of these alloys at elevated temperatures (Figure 3). The electric resistivity increases with increase in the content of aluminum and also with increase in the number of alloying elements in the alloys.

The results of measurements of the coefficients of linear expansion of alloys agree well with literature data for alloys of the Nimonic type /4, 5/.

The dependence of the coefficient of linear expansion of alloys of the Ni—Cr—Ti—W—Mo—Nb—Al systems on temperature and aluminum content is given in the table.

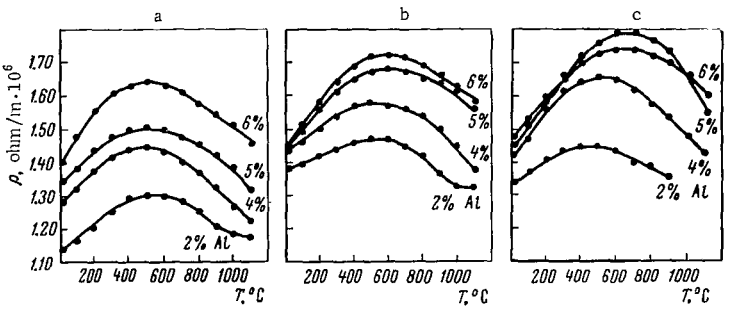

FIGURE 3. Dependence of the electric resistivity of alloys on the temperature and the aluminum content:

a—Ni—Cr—Ti—W—Al; b—Ni—Cr—Ti—W—Mo—Nb—Al; c—Ni—Cr—Ti—W—Mo—Nb—Co—Al.

Coefficient of linear expansion of alloys as a function of temperature and the aluminum content

Content of Al, wt %	Coefficient of linear expansion $\alpha \cdot 10^6$, degree^{-1} over range of temperatures, °C			
	20—1000	20—900	20—800	20—700
2	18.1	17.4	16.6	15.8
4	16.8	15.9	15.1	14.3
5	16.7	15.8	15.0	14.2
6	16.4	15.5	14.6	13.7

The table shows that the coefficient of linear expansion decreases not only with decrease in temperature but also with increase in the content of aluminum. This coefficient decreases also with increase in the number of alloying elements in the alloy.

Thus, for example, in six-component alloys (Ni—Cr—Ti—W—Mo—Al) containing 5 and 6 wt % of aluminum, the coefficient of linear expansion over the temperature range 20—900°C is equal to 16.8 and $16.1 \cdot 10^{-6}$ degree^{-1}, respectively, and for seven-component alloys containing 5 and 6 wt % of aluminum (see table) this coefficient is 15.8 and $15.5 \cdot 10^6$ degree^{-1}, respectively. This variation in the coefficient of linear expansion is a direct proof that if the number of components in the alloy is increased, the binding forces between different atoms increase, and there is a decrease in the root-mean-square displacement of atoms from the equilibrium position.

The microhardness of alloys cooled from 1200°C is shown in Figure 4. We also found the limits of solubility in three-, four-, and five-component systems. It has been shown by experiment that the hardness of the γ-solid solution increases not only with the increase in the aluminum content in the alloy but also as we pass from three- to five-component alloys.

Annealed specimens whose microhardness was measured at a magnification of 1080 behaved similarly. The hardness of the γ-solid solution and of the γ'-phase increased with increase in the content of aluminum and in the number of alloying elements.

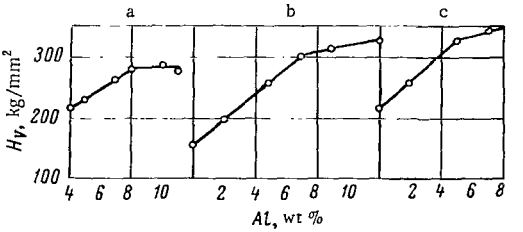

FIGURE 4. Dependence of the microhardness of alloys cooled from 1200°C on their aluminum content:

a—Ni—Cr—Al; b—Ni—Cr—Ti—Al; c—Ni—Cr—Ti—W—Al.

The hardness of the γ'-phase in a five-component alloy with 6 wt% of aluminum was 380—390 kg/mm^2, and in a seven-component alloy with 5 and 8 wt % of aluminum it was 580 kg/mm^2 and 640 kg/mm^2, respectively.

CONCLUSIONS

1. An electron microscopic study showed that an increase in the number of alloying elements in the alloy leads to a decrease in the size of the particles of the γ'-phase, more uniform distribution in the matrix, and greater uniformity of grain size. The increase in the heat resistance as we pass from two- to eight-component alloys can be explained by the influence of the structural factor.

2. The results of an X-ray spectral microanalysis show that the chemical composition of the γ-solid solution and of the γ'-phase becomes more complex if additional elements are introduced into the alloy. All the alloying elements, chromium, titanium, tungsten, molybdenum, niobium, cobalt, and aluminum dissolve in the γ-solid solution and in the γ'-phase. Microhardness measurements confirmed that this leads to a strengthening of the structural components of the alloys.

3. The high-temperature electric resistivity of each of these alloys increased with increase in the content of aluminum and in the number of alloying elements. This phenomenon can be explained by the increase in the distortion of the crystal lattice of solid solutions when additional alloying elements are introduced into the alloy. This assumption agrees with the results of an earlier X-ray structural analysis.

4. The coefficient of linear expansion of alloys decreases as we pass from less complex to more complex alloys. It can thus be concluded that the binding forces between different atoms in the alloys increase when new elements are introduced.

Bibliography

1. Kornilov, I.I. Fiziko-khimicheskie osnovy zharoprochnosti splavov (Physicochemical Principles of Heat Resistance of Alloys).—Izdatel'stvo AN SSSR. 1961.
2. Pryakhina, L.I. and L.A.Ryabtsev.—Doklady AN SSSR, **141**, No. 2. 1961.
3. Pryakhina, L.I., A.Ya.Snetkov, and L.A.Ryabtsev.—Fizika Metallov i Metallovedenie, **11**, No. 5. 1961.
4. Betteridge, U. Heat-Resistant Nimonic Alloys. [Russian translation. 1961.]
5. Mints, R.S. Diagramma sostoyaniya Ni—Cr—NiAl (Phase Diagram of the Ni—Cr—NiAl System). Author's Summary of Candidate Thesis, Moskva. 1954.

M. V. Rastegaev, M. V. Pridantsev, M. Ya. Dzugutov, and Yu. V. Vinogradov

THE NONUNIFORM CRYSTAL STRUCTURE OF THE KhN77TYuR (EI437B) ALLOY

Recrystallization processes can be divided into primary recrystallization (nucleation and formation of new grains), and secondary recrystallization (growth of some grains at the expense of others).

Primary recrystallization is terminated when the grain boundaries of new grains meet. An increase in temperature or prolonged heating after this stage leads to secondary recrystallization, during which some grains grow at the expense of other new grains. Secondary recrystallization is due to the tendency of small grains to decrease their surface energy. As a result, this type of recrystallization leads to the formation of a structure consisting of grains of rather different sizes.

During certain conditions of plastic deformation and subsequent heating, certain grains appear to be in a better position for grain growth than others. As a result, they grow much more rapidly and consume their slower growing neighbors.

It is believed that secondary recrystallization consists of several processes of grain growth. These processes are associated with small (critical) degrees of deformation, with deformation of a texture at a high degree of deformation, or with dissolution of dispersed phases.

The mechanism of the formation of coarse and nonuniform crystal structures has not yet been sufficiently studied.

This problem is difficult because the grain size and the uniformity of the crystals are influenced by many factors, which can be divided into the following three groups:

1) influence of the initial material (chemical composition, impurities, liquation, dispersed phases, and initial structure);

2) influence of the process of deformation (temperature, lack of uniformity, rate and degree of deformation, and also stresses);

3) influence of heat treatment (temperature and duration of heating).

Of these factors the dispersed phases (barrier mechanism) and the "critical" degrees of deformation are particularly important.

The barrier mechanism operates when alloys are heated to temperatures below the point at which dispersed phases start to dissolve. The non-dissolved particles at the grain boundaries hinder diffusion and serve as a barrier which inhibits grain growth /1—4/.

The influence of small ("critical") degrees of deformation on rapid grain growth has been investigated by many authors. The small "critical" degrees of deformation were induced either mechanically /5, 6/, etc., or by a cold-hardening process /7, 8/, etc.

It can be seen that there is no unanimous opinion on the reasons for the formation of nonuniform crystal structures. The different approaches to the problem are due to the fact that in most research the recrystallization was studied under conditions of nonuniform deformation, so that reliable conclusions cannot be formed.

Studies carried out under conditions of a uniform deformation /9/ led to the discovery of a new factor (thermal effect) at the spots where deformation is localized, and a coarse-grained structure is formed during heat treatment of the EI437B alloy.

To find the influence of the thermal factor, experiments were carried out under conditions of very nonuniform deformations induced by stamping specimens with a diameter $D_0 = 45$ mm and a height $H_0 = 62$ mm, as well as specimens with a diameter $d_0 = 26$ mm and $h_0 = 36$ mm high. The specimens were cut from rolled and heat-treated rods of the KhN77TYuR (EI437B) alloy, and were stamped at 1000—1200°C. Large specimens were stamped on a 200-ton hydraulic press, and small specimens on 100-ton eccentric presses.

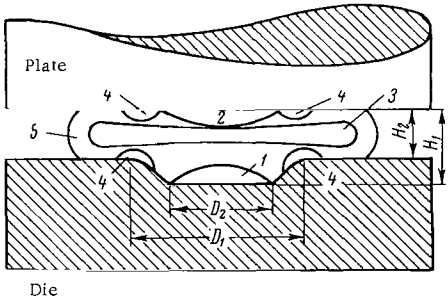

FIGURE 1. Die for deformation of specimens.

The dies were prepared in such a way (Figure 1) that all regions of the specimens were deformed to not less than 20% (Table 1, dies 1 and 2). It has been experimentally found that this minimum degree of deformation was necessary for completion of recrystallization.*

The specimens were divided into two batches. The first batch was subjected to high-temperature deformation at 1200—1000°C, followed by rapid cooling, and the second batch was also given an intermediate recrystallization annealing directly after deformation, and was then rapidly or slowly cooled. For an intermediate recrystallization anneal at the temperature of deformation, we used hot-worked specimens which had not been cooled. The specimens were held at the annealing temperature for 10—30 min.

The purpose of this study was to determine the optimum process of intermediate recrystallization annealing to ensure uniform recrystallization over the whole bulk of the specimen, and to produce a uniform crystal structure.

* The average reduction of specimens deformed in different dies was 70—75%.

TABLE 1. Dimensions of dies and specimens

Degree of deformation at end of specimens, %	No. of die	Dimensions of die, mm				Dimensions of specimens before stamping, mm			
		D_1	D_2	H_1	H_2	D_0	H_0	d_0	h_0
26	1	43	38	15	23	45	62	—	—
20	2	40	30	8	11.4	—	—	26	36

We found by experiment that five characteristic regions can be formed in the stamped disks, depending on the conditions of hot working and heat treatment (see Figures 1 and 2): 1 and 2 are the regions where deformation is difficult (formed as a result of cooling and contact friction); 3 is a region of maximum deformation (formed in the middle of the specimen under the action of regions where deformation is difficult); 4 are circular regions of local deformation which are formed under the influence of contact friction and cooling at the transition points of the center (bosses or wedged-in butt ends); 5 is a lateral region formed as a result of cooling of the lateral face of the specimen.

There are considerable thermal effects in regions 3 and 4 /11/. As a result the temperature in these regions can rise so high that recrystallization may be highly advanced or even completed in a very short time. The temperature then drops sharply as a result of rapid removal of heat by the cold metal of the specimen and instrument, and small grains (0.05—0.08 mm) are formed in regions 3 and 4. The grain boundaries are in this case sufficiently pure. If these specimens are air-cooled from 1080°C, very coarse grains are formed (Figure 2, a—c) where deformation is localized, i.e., in regions 3 and 4. In the other regions (1, 2, and 5) the recrystallization processes start to develop later or may even not take place.

Thus, deformation of the five characteristic regions in hot-worked specimens takes place as a result of cooling or of cooling and contact friction.

It is impossible to eliminate completely the influence of contact friction during stamping. At the ends of the specimens contact friction can be reduced to a level at which deformation in the layers adjacent to the surface will be less than 20%. As we have already mentioned this was achieved by deformation in specially engraved dies.

The resistance of the KhN77TYuR (EI437B) alloys to deformation at 1000°C is about double that at 1200°C. Consequently, it can be expected that the higher thermal effect will take place at lower temperatures of deformation. However, the general temperature in the region and not only the thermal effect should be taken into account. The specimens were therefore stamped over a wider range of temperatures (1200—1000°C). For every experiment we deformed two or three specimens. The results of the experiments are shown in Table 2, and indicate that the thermal effect and the critical degrees of deformation are the main factors which facilitate the formation of nonuniform regional crystal structures. It should be pointed out that the influence of the thermal effect on the formation of a nonuniform crystal structure is closely connected with the temperature of deformation.

Table 2 shows that a coarse-grained structure with a grain size of 3 mm is formed in regions 3 and 4 after deformation at 1200—1170°C (experiments 1 and 2).

FIGURE 2. Microstructure of the KhN77TYuR alloy:

a—after deformation in die 1 at 1000°C, air cooling, and standard heat treatment, ×1; b—the same, macrostructure of region 4, ×20; c—after deformation in die 3 at 1000°C, air cooling, and standard heat treatment, ×1; d—after deformation in die 1 at 1150°C, intermediate recrystallization anneal at 1150°C, slow cooling, and standard heat treatment, ×1.

TABLE 2. Characteristics of structures produced by different deformation and heat-treatment processes

No. of experiment	t, °C and No. of die	t_p, °C/holding time, min	Cooling	Heat treatment	Grain size within the regions, mm					Characteristic of structure and average grain size, mm and degrees (scale of GOST 5639-51)
					1	2	3	4	5	
1	1200, 2	—	Accelerated (in air)	None	0.03—1	0.1	0.1	0.1	0.03—1	ZNG; 0.03—1; 7—(—3)
				Standard	0.8	0.6	3	3	0.8	CGN; 0.8—3; —3 > (—3)
2	1170, 2	—	The same	None	0.03—1	0.1	0.1	0.1	0.03—1	ZNG; 0.03—1; 7—(—3)
				Standard	0.7	1	3	3	0.7	CGN; 0.7—3; —2 > (—3)
3	1140, 2	—	" "	None	0.03—0.1	0.04	0.04	0.03	0.03	NG; 0.03—1; 7—(—3)
			" "	Standard	0.1—1	0.1—1	0.1—1	0.1—1	0.1—1	CG; 0.1—1; 3—(—3)
4	1100, 2	—	" "	None	0.03—0.8	0.03	0.03	0.03	0.03—0.3	ZNG; 0.03—0.8; 7—(—2)
				Standard	0.1—0.7	0.4—0.7	0.4—0.7	0.1—0.7	0.1—0.7	CG; 0.1—0.7; 3—(—2)
5	1000, 1	—	" "	None	0.5—2	0.5—2	0.02	0.005	0.05—1	ZNG; 0.005—2; 12 > (—3)
				Standard	0.3—1	0.3—1	0.25	2	0.3	CGN; 0.25—2; 1 > (—3)
6	1200, 2	1200/10	Retarded (together with furnace)	None	0.25	0.25	0.25	0.25	0.25	RNG; 0.25; 1
				Standard	0.25	0.25	0.25	0.25	0.25	RNG; 0.25; 1
7	1170, 2	1170/30	The same	None	0.7	0.7	0.7	0.7	0.5	RNG; 0.65; —2
				Standard	0.7	0.7	0.7	0.7	0.5	RNG; 0.65; —2
8	1140, 2	1140/30	" "	None	0.7	0.7	0.7	0.7	0.7	RNG; 0.7; —2
				Standard	0.7	0.7	0.7	0.7	0.7	RNG; 0.7; —2
9	1100, 2	1100/30	" "	None	0.5	0.5	0.5	0.5	0.5	RNG; 0.5; —1
				Standard	0.5	0.5	0.5	0.5	0.5	RNG; 0.5; —1
10	1000, 1	1000/30	" "	None	2	2	0.018	0.018—1	0.03—1	ZNG (0.018—2), 8 > (—3)
				Standard	0.3—1.5	0.3—1.5	0.15	0.15	0.15	ZNG; 0.1—1.5; 3 > (—3)
11	1200, 2	1200/10	Accelerated (in air)	None	0.25	0.25	0.25	0.25	0.25	RNG; 0.25; 1
				Standard	0.25	0.25	0.25	0.25	0.25	RNG; 0.25; 1
12	1150, 2	1150/30	The same	None	0.3	0.3	0.3	0.3	0.3	RNG; 0.3; 0
				Standard	0.3	0.3	0.3	0.3	0.3	RNG; 0.3; 0
13	1100, 2	1100/30	" "	None	0.4	0.4	0.4	0.4	0.4	RNG; 0.4; —1
				Standard	0.4	0.4	0.4	0.4	0.4	RNG; 0.4; —1
14	1000, 1	1000/30	" "	None	0.03	0.02	0.02	0.15	0.02	NG; 0.02—0.15; 8—2
				Standard	0.2	0.2	0.2	2.5	0.2	ZNG; 0.2—2.5; 1 > (—3)

Note. Designations: t—deformation temperature; t_p—temperature of intermediate recrystallization annealing; ZNG—regional (zonal) nonuniform grain size; CGN—coarse-grained nonuniform; NG—nonuniform grain size; CG—coarse grained; RNG—relatively nonuniform grain size.

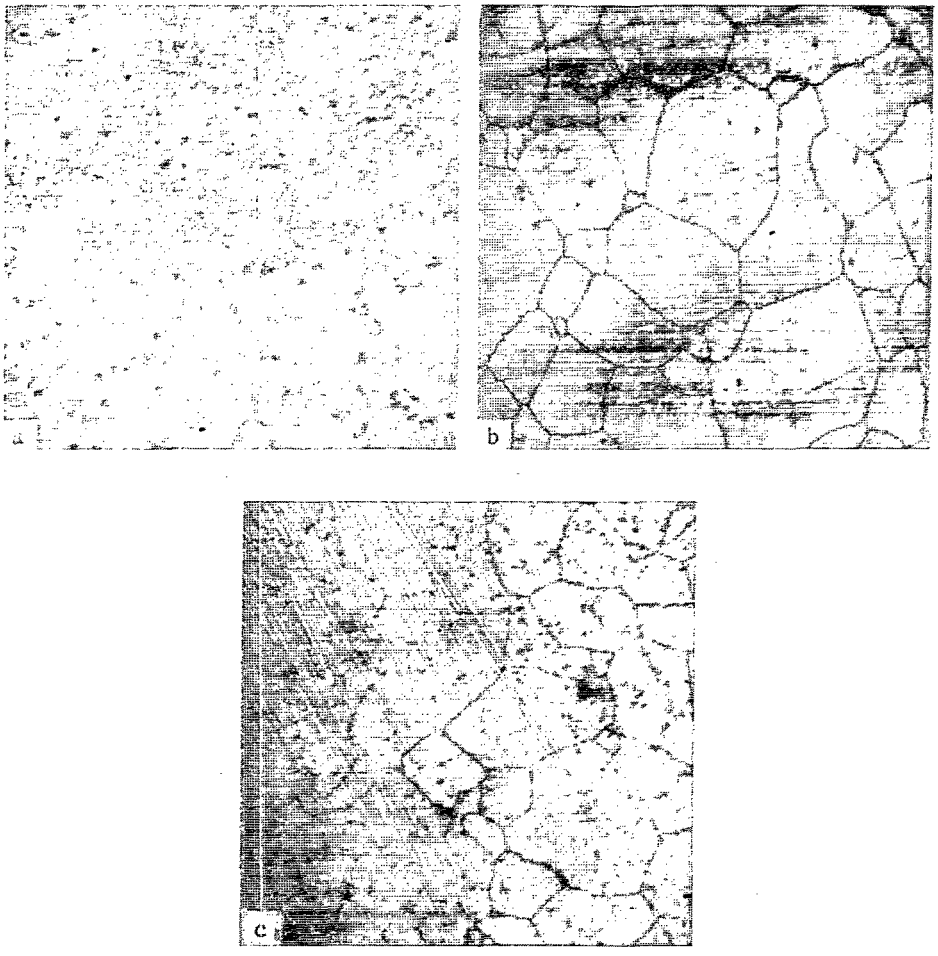

FIGURE 3. Microstructure of the KhN77TYuR alloy:

a—after deformation at 1000°C and rapid cooling, ×100; b—after deformation at 1200°C and accelerated cooling in air, ×100; c—the same, plus standard heat treatment, ×85.

If, however, the recrystallization anneal of the deformed specimen is carried out at the same temperature (without cooling after deformation), no nonuniform structure is formed either directly after the intermediate anneal and cooling or after the regular quenching which does not fundamentally change the grain size. Thus, deformation at 1200—1100°C followed by a recrystallization anneal leads to a structure with a uniform grain size of 0.25 — 0.7 mm in all five regions (depending on the conditions of deformation) (see experiments 6—9, 11—13 and Figure 2, d).*

* The beneficial influence of heat treatment (forging at 1150—1000°C, heating from 1000 to 1150°C for 7—8 min and cooling in the air) on the formation of a uniform fine-grained structure in KhN67MTYuR alloys was found by Chizhov and Bernshtein /10/. The authors believe that metals with such a structure are not susceptible to secondary recrystallization.

Specimens deformed at 1000°C and annealed at 1000°C (experiments 10 and 14) were exceptions, and had a nonuniform grain structure after standard heat treatment (1080°C).

A uniform structure with grain sizes of 0.17 mm can be produced by standard heat treatment if the deformation is uniform and does not cool the specimen. This is achieved by open upsetting, during which the specimens are fully insulated by asbestos against loss of heat.

The formation of a coarse-grained structure, where local heating takes place, can be explained as follows: as we have already mentioned, nonuniform deformation causes thermal effects in certain regions of the deformed metal, and recrystallization occurs. On the other hand, rapid cooling (between cold volumes of metals) leads to the formation in the same regions of small grains (0.02 mm) with very thin intercrystalline layers of second phase precipitates. In certain regions of the metal there are no such layers at the grain boundaries (Figure 3, a).

If the specimens were not cooled by the cold volumes of metal but in the air (from 1200°C), the grain coarsened considerably (to 0.13 mm) as a result of secondary recrystallization (Figure 3, b).

During the standard heat treatment the layers of the grain boundaries start to coagulate and pass into the solid solution so that the barrier obstacles are eliminated (Figure 3, c).

The removal of the barriers in certain regions leads to regular secondary recrystallization.

Therefore, the process of secondary recrystallization (and consequently the formation of a coarse-grained structure) is closely connected with the action of thermal effects at the points of localization of deformation.

CONCLUSIONS

1. It was determined that the thermal effect is one of the chief factors leading to the formation of a coarse-grained structure at points of localization of deformation.
2. Stamping disks of the KhN77TYuR alloy may give rise to five regions in the deformed volume, in which recrystallization does not develop uniformly, and structures of different grain sizes are formed.
3. It was shown that an intermediate recrystallization anneal followed by slow cooling prevents the formation of grain nonuniformity during the standard heat treatment in the various regions of KhN77TYuR alloys, deformed (over the whole bulk) to not less than a 20% reduction at 1200—1100°C.
4. The formation of a coarse-grained structure in a nonuniformly deformed KhN77TYuR alloy can to a certain degree be prevented under the following conditions: 1) the deformation should take place at 1100—1200°C and the reduction should be not less than 20% throughout the whole deformed part; 2) the specimen being deformed should be insulated against loss of heat (the specimens should not become cooled when they are moved from the furnace to the press, during deformation, or for a certain time after this); 3) it is useful to carry out an intermediate recrystallization anneal followed by slow cooling. The temperature and the duration of the anneal depend on the grain size required.

Bibliography

1. Smit, M.K. Osnovy fiziki metallov (Fundamentals of the Physics of Metals).—Moskva, Metallurgizdat. 1959.
2. Dobatkin, V.I., S.K.Bukov, and P.I.Selitskii. Sbornik—Issledovanie deformiruemosti splavov (Collection—Study of the Deformability of Alloys).—Oborongiz. 1959.
3. Mes'kin, V.S. Osnovy legirovaniya stali (Principles of Steel Alloying). 1959.
4. Gorelik, S.S. and E.N. Spektor. Sbornik—Issledovaniya po zharoprochnym splavam (Collection—Investigation of Heat-Resistant Alloys), 8.—Izdatel'stvo AN SSSR. 1962.
5. Maevskii, I.L.—Trudy LKVVNM im. A.F. Mozhaiskogo, No. 257. 1958.
6. Gulyaev, A.P. and R.P.Leshchinskaya.—Metallovedenie i Termicheskaya Obrabotka Metallov, No. 9. 1963.
7. Sidnikhin, A.I. O vliyanii termicheskogo naklepa na strukturu i svoistva zharoprochnykh splavov tipa KhN80T (Influence of Hot Working on the Structure and Properties of Heat-Resistant Alloys of the KhN80T Type).—Trudy Kuibyshevskogo Aviatsionnogo Instituta, No. 7, Kuibyshevskoe Knizhnoe izdatel'stvo. 1958.
8. Makhanek, G.V., S.N.Petrova, and V.D.Sadovskii. K voprosu o raznozernistosti v splave tipa nemonik (EI437B) (Grain Non-uniformity in Nimonic-Type Alloys (EI437B)).—In: Sbornik "Svoistva i primenenie zharoprochnykh splavov," Izdatel'stvo Nauka. 1966.
9. Rastegaev, M.B. Raznozernistost' splava na nikel'khromovoi osnove pri ravnomernoi deformatsii (Grain Nonuniformity of Uniformly Deformed Nickel—Chromium Alloys).—Metallovedenie i Termicheskaya Obrabotka Metallov, No. 1. 1966.
10. Chizhov, V.G. and M.L.Bernshtein. Ustranenie raznozernistosti v pokovkakh zharoprochnykh splavov (Eliminating Grain Nonuniformity im Forgings of Heat-Resistant Alloys).—Kuznechno-shtampovochnoe Proizvodstvo, No. 5. 1965.
11. Rastegaev, M.V. O teplovom effekte pri lokal'noi dinamicheskoi deformatsii (Thermal Effect in Local Dynamic Deformation).—Trudy Instituta Metallurgii AN SSSR, No. 7, Izdatel'stvo AN SSSR. 1960.

M. Ya. Dzugutov and V. P. Stepanov

PREVENTION OF THE FORMATION OF A NON-UNIFORM GRAIN STRUCTURE IN A CRITICALLY DEFORMED KhN77TYuR ALLOY

The mechanical properties at normal temperatures ($\sigma_в$, σ_s, δ, ψ, $a_н$), and the fatigue limit, the long-time strength, and creep resistance of alloys of the KhN77TYuR type over a wide range of temperatures are very dependent on the grain uniformity, as shown by inspecting the final

macrostructure. It has often been found, e.g., in /1/, that the KhN77TYuR alloy, heat treated by the standard process (1080°C, holding for 8 hr; aging at 750°C for 16 hr) has the highest values of $\sigma_к$, σ, ψ, and $a_н$ when the crystal structure is uniform and the grain size is 5—8. If the grain becomes coarsened these properties deteriorate.

The long-time strength increases with increase in grain size from 1 to 3 according to the GOST 5639-51 scale, but decreases if the grain becomes coarser. If the crystal structure is not uniform, the above properties deteriorate more if the nonuniformity is greater.

Alloys of the KhN77TYuR type with optimum composition can have good properties specified by technical conditions or by GOST, and not by a given crystal structure, but only if they have a relatively uniform grain of optimum size.

After hot working these alloys usually have a fine-grained structure but heat treatment leads to nonuniform grain growth and the formation of a nonuniform crystal structure. In some regions the grain growth is inhibited, but in others it is accelerated, and whole regions or aggregates of coarse grains are formed.

As a result of structural studies on this alloy, three main types of structural nonuniformity have been determined:

1. regional grain coarseness, due to a critical deformation imparted to a given region followed by secondary recrystallization during the final heat treatment;

2. the formation of dispersed coarse grains or grain aggregates as a result of the heterogeneity of the phase and chemical composition: absence or low concentration of a second phase, and also secondary recrystallization;

3. the presence of bands of very fine grains, caused by an accumulation of large amounts of precipitates insoluble at the temperature of heat treatment, which inhibit grain growth. This classification agrees well with the data of Gorelik /2/.

The formation of a nonuniform crystal structure of the second type can also be influenced by an increase in the temperature of the final deformation /3, 4/.

A decrease in or annulment of each of these types of nonuniform structures is important, since this improves the properties of the alloy. This improvement can be achieved in different ways for every type of structural nonuniformity. In this work we shall discuss data on the first and second types of nonuniform crystal structures.

Despite the considerable number of investigations /1, 5, 6, and others/, we still have no industrial process of deformation which will prevent critical degrees of deformation in individual regions of forged and stamped specimens. This deformation is at present unavoidable as is the formation of coarse grains in these regions during subsequent standard heat treatment as a result of secondary recrystallization.

In this connection any study carried out to prevent the formation of regions with a coarse-grained structure in KhN77TYuR alloys during standard heat treatment by annealing is of great practical interest. The most important of the papers on this problem from both the practical and theoretical points of views is the one by Gorelik.

The numerous data on the influence of annealing on the recrystallization processes which follow are still contradictory. Thus, Kornfel'd and Pavlov /7/ showed that if the annealing is carried out at 320°C for 20 hr on slightly

deformed fine-grained aluminum, the incubation period increases several times. Other authors /8, 9/ found that such a preliminary annealing during which relaxation and polygonization take place leads to deterioration in the conditions for recrystallization.

The clearest conclusions on the positive influence of preliminary annealing are given by Gorelik /10/. He believes that the relaxation decreases the gradient of elastic stresses between neighboring grains, and thus reduces the tendency of some grains to grow at the expense of others during the recrystallization anneal which follows. The decrease in the grain size is due to the polygonization process.

In this paper data are given on the decrease in the size of recrystallized grains after aluminum with a critical degree of deformation is annealed at temperatures lower than those of the recrystallization anneal.

The purpose of this work is to investigate the influence of annealing KhN77TYuR alloys with a critical degree of deformation on the final structure produced by standard heat treatment (1080°C for 8 hr and cooling in the air).

METHODS AND RESULTS*

For our studies we used specimens with regions with a critical degree of deformation, as well as ones with a smaller or larger degree of deformation, and also regions that were not deformed at all. Our simple method of preparation of specimens produced all these regions in a single specimen. The specimens were prepared from rolled rods 26 and 35 mm in diameter, with a normal fine-grained structure in the rolled state; the standard heat treatment which followed did not upset the structural uniformity.

The specimens which had been cut from rods before heat treatment were heated to 950°C and held at this temperature for 30 min. Then, transverse notches were made on these (with the help of similar cold rods). A study of the macrostructure showed that the notched specimens had a uniform structure. The specimens which had undergone standard heat treatment had coarse-grained regions, produced by a critical degree of deformation followed by secondary recrystallization (Figure 1). In some cases we also found dispersed coarse grains or aggregates of such grains, apparently formed by secondary recrystallization.

The notched specimens were cut longitudinally into two symmetrical equal parts, and one was subjected to a preliminary anneal. The two halves were given a standard heat treatment at 1080°C for 8 hr followed by air cooling.

The influence of the preliminary anneal was found by comparing the macrostructures of the two halves. Our experiments showed that the preliminary anneal of specimens at 600—950°C for 6—40 hr and at 450—750°C for 15—90 min had no favorable influence on the results of the following standard heat treatment. In all cases the specimens had regions of coarse grains coinciding with regions of critical deformation. The same was found in specimens that had not been given a preliminary anneal (Figure 1, b, d, f).

* The experiments were carried out with the participation of V. P. Mironova.

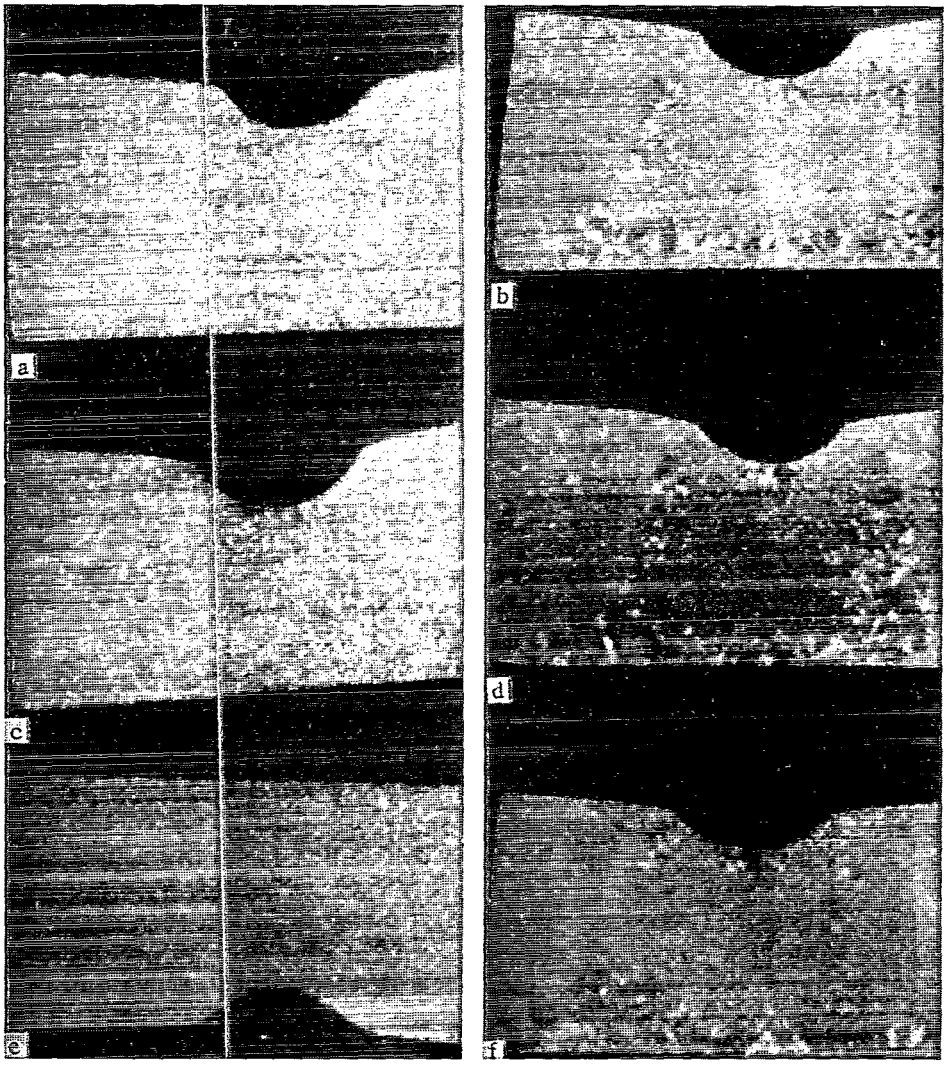

FIGURE 1. Microstructure of KhN77TYuR alloy specimens after heat treatment by the following processes:

a—1130°C, 15 min; cooling in the air, +1080°C, 8 hr; cooling in the air, +750°C, 16 hr; cooling in the air; b, d, f—1080°C, 8 hr; cooling in the air, +750°C, 16 hr; cooling in the air; c—1150°C, 15 min; cooling in the air, +1080°C, 8 hr; cooling in the air, +750°C, 16 hr; cooling in the air; e—1180°C, 15 min; cooling in the air, +1080°C, 8 hr; cooling in the air, +750°C, 16 hr; cooling in the air.

A preliminary anneal at temperatures above that of the standard heat treatment (1080°C) gave a more favorable final structure. All specimens held for 5—35 min at 1100—1160°C and then treated according to the standard process (1080°C for 8 hr plus annealing at 700°C for 16 hr) had a uniform structure with an optimum grain size (Figure 1, a, c, e). At the same time the symmetric halves that had been given standard heat treatment without any preliminary anneal at the above temperatures had a nonuniform structure as a result of secondary recrystallization (Figure 1, b, d, f).

The photomicrographs show that a prolonged preliminary anneal at temperatures above 1100°C prevents secondary recrystallization during subsequent heat treatment and thus also the formation of a nonuniform structure.

This is apparently because during short heating at temperatures above those of the standard heat treatment (1080°C) intense processes of relaxation and polygonization proceed, which finish during the incubation period before recrystallization starts. As a result, secondary recrystallization in regions with a critical degree of deformation are suppressed either completely or to a considerable extent.

To produce a uniform fine-grained structure in KhN77TYuR alloys, the preliminary heat treatment should be carried out over certain ranges of temperatures and time.

Heating above 1190°C and holding at this temperature for 35—40 min first leads to slight grain coarsening, but then the process produces the same structure as ordinary heat treatment. Figure 2 shows the dependence of the structure of the alloy on the temperature and time of the preliminary heat treatment.

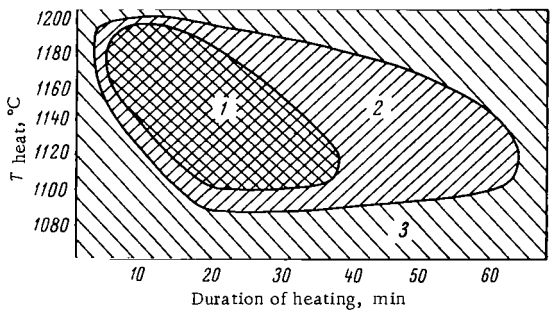

FIGURE 2. Influence of temperature and the duration of heating during preliminary heat treatment on the structure of KhN77TYuR alloys after standard heat treatment:

1—uniform structure; 2—transitional structure; 3—nonuniform structure.

According to the processes represented by area 1, heat treatment of the metal ensures a uniform fine-grained structure after the final treatment. If the metal is treated by a process represented by area 2, the structure is more coarse grained, and processes represented by area 3 give a nonuniform grain size (after the final heat treatment).

Thus, a short preliminary treatment of the KhN77TYuR alloy by heating at 1110—1180°C for from 5 to 35 min ensures a uniform structure of normal grain size, irrespective of the degree of deformation, after the final standard heat treatment.

We studied the influence of the favorable effect of a short preliminary heat treatment on the mechanical properties of the KhN77TYuR alloy.

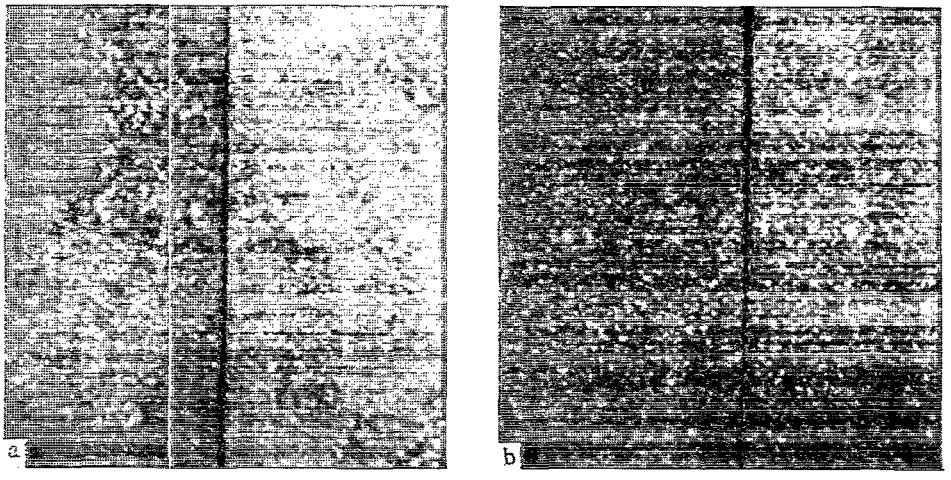

FIGURE 3. Microstructure* of 70 mm diameter specimens made of a KhN77TYuR alloy after the following heat treatment:

a—1080°C, 8 hr; cooling in the air, +750°C, 16 hr; cooling in the air; b—1150°C, 25 min; cooling in the air, +1080°C, 16 hr; cooling in the air, +750°C, 16 hr; cooling in the air.

The mechanical tests were carried out on 70 mm diameter specimens, in which standard heat treatment produced an appreciable nonuniformity of grain size. The specimens were cut longitudinally into two equal halves before the heat treatment. One of these halves was subjected to a preliminary heat treatment at 1150°C for 25 min, and cooled in the air. Then, together with the second half, it was subjected to the standard process: heating at 1080°C for 8 hr, cooling in the air, aging at 750°C for 16 hr, cooling in the air. The macrostructure and the mechanical properties of the specimens were studied after the heat treatment. The macrostructure of the specimens is shown in Figure 3.

Influence of preliminary heat treatment on the mechanical properties of the KhN77TYuR alloy

Heat treatment process	Mechanical properties at 20°C					
	σ_B, kg/mm^2	$\sigma_{0.2}$, kg/mm^2	δ, %	ψ, %	a_K, kgm/cm^2	H_B (d, mm)
1080°C, 8 hr, air + 750°C,	86.0	66.9	12.2	13.6	4.88	3.8
16 hr, air	91.0	66.3	14.4	17.8	5.13	
1150°C, 25 min, air +						
+ 1080°C, 8 hr, air +	104.0	68.6	21.6	21.4	5.13	3.75
+ 750°C, 16 hr, air	101.8	67.8	20.6	21.4	4.8	

* [Macrostructure may be meant.]

Preliminary heat treatment produces a uniform fine-grained structure in specimens which have a nonuniform structure after ordinary heat treatment.

The data confirm that preliminary heat treatment of the KhN77TYuR alloy eliminates the tendency to form a nonuniform grain structure and ensures a uniform structure with a grain size of from −1 to +1 (according to the GOST 5639-51 scale). Thus, the mechanical properties (see table) are better than those of specimens cut out of alloys which have not been given any preliminary heat treatment and have a nonuniform grain structure.

Bibliography

1. Dzugutov, M. Ya. and B. F. Vakhtanov. — Kuznechno-shtampovochnoe proizvodstvo, No. 2. 1960.
2. Gorelik, S. S. and E. N. Spektor. Issledovanie prichin raznozernistosti zharoprochnykh splavov na osnove nikhroma (A Study of the Causes of Nonuniform Crystal Structures of Heat-Resistant Alloys (Nichrome Base)). — In: Sbornik "Issledovanie po zharoprochnym splavam," 8, Izdatel'stvo AN SSSR. 1962.
3. Dzugutov, M. Ya. and B. F. Vakhtanov. — Kuznechno-shtampovochnoe proizvodstvo, No. 3. 1961.
4. Vakhtanov, B. F., E. A. Demidova, and M. Ya. Dzugutov. Sbornik — Novoe v tekhnologii metallurgicheskogo proizvodstva (Collection — News on the Technology of the Metallurgical Industry). — Izd. Moskovskogo Sovnarkhoza. 1962.
5. Il'in, M. M. and T. A. Michin. — Kuznechno-shtampovochnoe proizvodstvo, No. 5. 1959.
6. Zabaluev, I. P., V. I. Travinin, and M. A. Kovaleva. — Stal, No. 10. 1957.
7. Korfel'd, M. and V. Pavlov. — ZhETF, 4:982. 1934.
8. Van Bueren. Imperfections in Crystals. [Russian translation. 1962.]
9. Burke, I. and D. Torball. Uspekhi fiziki metallov (Advances in the Physics of Metals), 1. — Metallurgizdat. 1954.
10. Gorelik, S. S. — Metallovedenie i Termicheskaya Obrabotka Metallov, No. 3. 1961.

B. I. Medovar, L. G. Puzrin, G. A. Boiko and Yu. N. Krokhmal'

ISOTHERMAL CRYSTALLIZATION DURING PRESSURE BRAZING OF HEAT-RESISTANT NICKEL-BASE ALLOYS

The very high susceptibility of chromium-nickel austenitic steels and alloys to cracking has forced welders to look for methods which will not entail local heating to the melting point.

Studies in the field of the so-called pressure brazing have been carried out at the E. O. Paton Institute of Electric Welding (AN USSR). Unlike brazing with hard solders, pressure brazing gives uniform strong joints which can withstand high temperatures.

This new method is based on the interaction between the fused material of the solder and the basis metal.

As a result of the diffusion interaction between the liquid and solid phases an isothermal crystallization of the liquid phase takes place, followed by a diffusion dissolution of the components of the solder in the basis metal.

The joints produced by the pressure brazing method (Figure 1) have no regions with a cast structure with properties and chemical composition differing greatly from those of the basis metal, as in ordinary brazing. The chemical composition of the metal of the joint obtained by pressure brazing differs little from that of the basis metal.

Using this method, the E. O. Paton Institute of Electric Welding (AN USSR) has successfully solved the problem of welding articles made of heat-resistant steels and alloys. Pressure brazing is also used to produce bimetallic tubes, bimetallic sheet, etc.

Today, solid solution and eutectic solders are used in pressure brazing. In both these solders the fused phase can be produced by melting the solder or by contact melting during the reaction of the solder with the basis metal. Contact melting during pressure brazing of heat-resistant nickel-base alloys facilitates a more vigorous dissolution of the strong surface oxide films in the liquid phase. The oxygen is removed from the joint together with excess of the molten metal which is pushed out to the periphery. Contact melting, particularly by a eutectic reaction, of alloys with a strong oxide film is preferable to the independent melting of the solder.

In this report we shall give certain data on the mechanism of the formation of joints during pressure brazing of heat-resistant chromium—nickel alloys.

For pressure brazing chromium—nickel alloys, three elements which with nickel form relatively low-melting eutectics, niobium, vanadium, and titanium, are used mainly today. *

A thin foil of one of these elements is placed between the surfaces to be joined, the articles are fastened together, and heated to the melting point of the eutectic. The joining is usually carried out in vacuo at a pressure not exceeding $1 \cdot 10^{-4}$ mm Hg. However, a vacuum is not essential. The brazing can also be carried out under conditions which prevent access of air to the joint, for example, by a protective gas or a flux.

To compare the mechanism of brazing with the phase diagram, we experimented with pure nickel.

The nickel—niobium system (Figure 2) was usually studied. This system has two eutectics melting at 1270 and 1175°C, respectively.

We found that a liquid phase is formed as soon as 1175°C is reached. This indicates that during contact melting a liquid phase consisting of a eutectic with a melting point of 1175°C (about 50% of niobium) is produced first. Apparently, the composition of the liquid phase remains unchanged until all the niobium is consumed. In our experiments we used niobium foil 20 μ thick.

* S. I. Novak was the first to recommend niobium as a solder for nickel-base alloys.

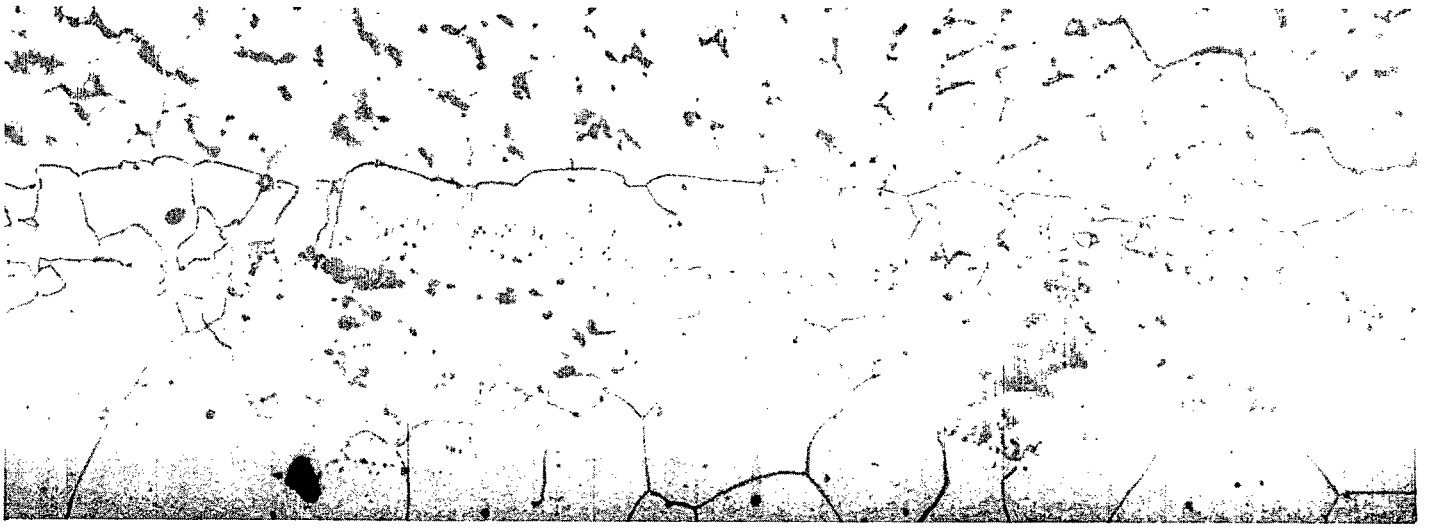

FIGURE 1. Joint between a chromium—nickel alloy and another alloy produced by an intermediate layer of niobium 20μ thick, x100.

The melting is apparently preceded by the formation of a diffusion layer similar in composition and structure to the eutectic.

A photomicrograph of a diffusion region produced when nickel and niobium in the solid state are joined in vacuo at 1150°C and then diffusion annealed in a furnace at the same temperature for 24 hr (diagonal microsection) is shown in Figure 3. The structure of the diffusion region is clearly eutectic.

Further dissolution of nickel in the liquid phase takes place after the whole layer of niobium is molten, and the temperature of the specimen is raised to the temperature of brazing (isothermal heating). On the phase diagram this corresponds to a shift of the point characterizing the composition of the liquid phase to the nickel side.

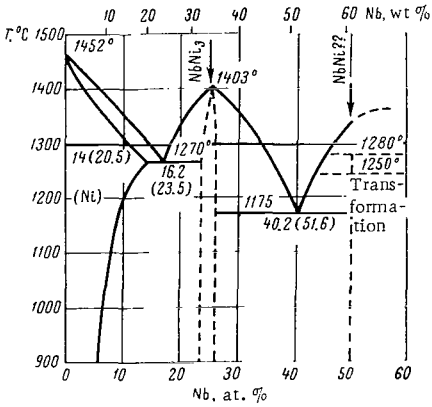

FIGURE 2. Nickel—niobium phase diagram.

In our experiments the temperature of isothermal heating was chosen as 1300°C to accelerate as much as possible the diffusion processes, to produce a solid phase consisting of a solid solution by isothermal crystallization, and to force the remainder of the liquid phase to crystallize in the eutectic field. As a result, the liquid phase in our experiments contained 23.5% of niobium or less.

After the liquid reached a composition corresponding to the point of intersection of the liquids with the 1300°C isotherm, further dissolution of nickel stopped, since this point determines the maximum solubility of nickel in the liquid phase at a given temperature. At such a composition, the liquid is in a state of equilibrium with the solid phase whose composition is determined by the point of intersection of the solidus and the 1300°C isotherm. A solid phase of this composition forms a thin layer on the solid nickel—liquid alloy (nickel—niobium) phase boundary directly after dissolution of nickel in the liquid phase ceases.

The equilibrium during isothermal heating is apparently upset only as a result of a change in the composition of the solid phase (nickel—niobium solid solution on the boundary with the liquid phase) due to concentration diffusion of niobium from the interface toward the interior of nickel. As a result, a solid phase crystallizes from the liquid at the interface. This solid phase has a composition that leads to a continuous renewal of the upset equilibrium. Therefore, the rate of isothermal crystallization is determined by the rate of diffusion of niobium into the solid. The composition of the crystallizing liquid remains constant during the whole process. The rate of crystallization decreases with decrease in the rate of diffusion of niobium, due to a shifting of the interface.

By changing the duration of the isothermal heating we were able to determine the different stages of isothermal crystallization of the liquid layer. A photomicrograph of a joint between nickel and a niobium layer is shown in Figure 4.

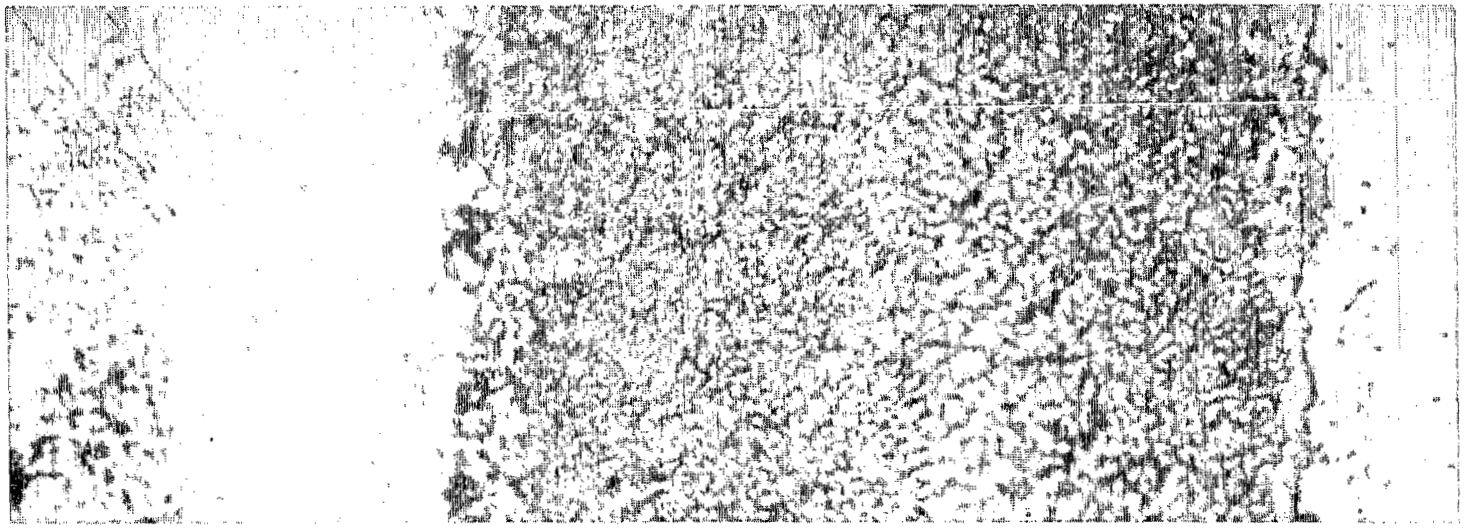

FIGURE 3. Region of mutual diffusion of nickel and niobium at 1150°C (below the melting point of the eutectic). Diagonal microsection, × 500.

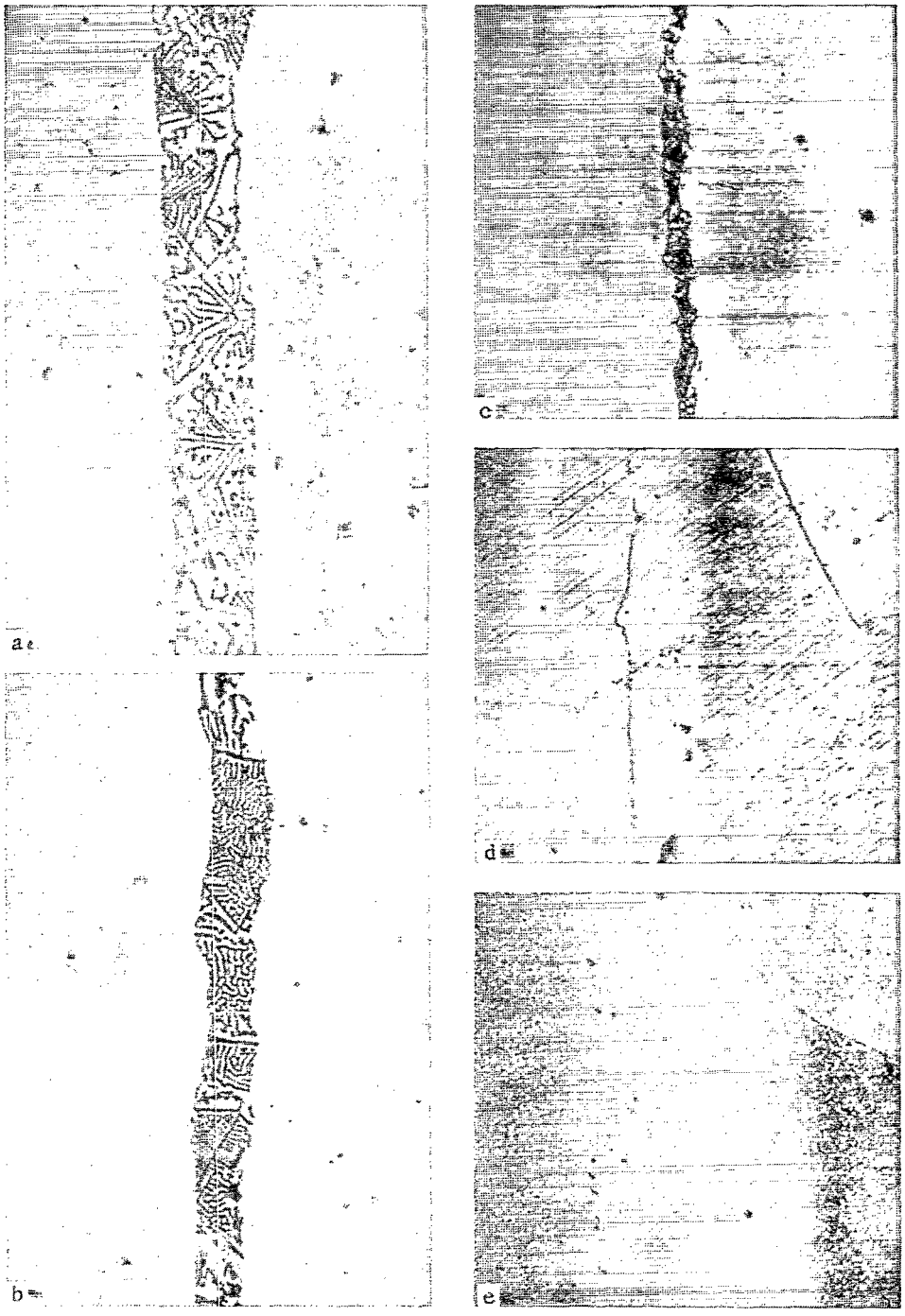

FIGURE 4. Isothermal crystallization of the nickel—niobium eutectic, × 500:
a—1 min; b—2 min; c—4 min; d—8 min; e—16 min.

The variation in the width of the layer with a eutectic structure indicates that an increase in the duration of isothermal heating reduces the amount of liquid phase, and this confirms an earlier assumption on the mechanism of the isothermal crystallization during pressure brazing.

V. G. Volkov, S. A. Yuganova, I. A. Stepanova, and N. S. Kreshchanovskii

INFLUENCE OF METALLURGICAL FACTORS ON THE STRUCTURE OF HEAT-RESISTANT NICKEL ALLOY EI765

The mechanical properties and thermal resistance of metals are greatly influenced by the structure of the material. The structure of alloys depends on a number of factors, including the way these alloys were melted and the conditions of solidification of the castings. The purpose of this work was to determine the structure of EI765 alloys melted in open and vacuum induction furnaces, and cast in chill molds or in ceramic molds heated to 800°C. We paid particular attention to a study on the nature, amount, shape, and distribution of precipitates (carbides in cast and heat-treated alloys and γ'-phases in heat-treated specimens).

METHOD

For our investigations we took alloys of standard composition, and subjected them to standard heat treatment.

We melted the metal according to a process developed by TsNIITMASh for materials of this class. The temperature of the alloys during casting was 1500 ± 10°C.

The structure of this alloy was found by metallographic and electron microscope methods, and also by X-ray and chemical phase analysis.

The microsections were prepared under an optical microscope and etched electrolytically in a 10% aqueous solution of oxalic acid (current density about 0.1 amp/cm^2), or by the Murakami etchant.

The electron microscope studies were carried out by the single-stage method with carbon.

The distribution of carbon in the cast alloy was found by qualitative autoradiography. A C^{14} radioactive isotope was introduced into special heats.

RESULTS AND DISCUSSION

A study of the structure of cast specimens cut from chill mold castings showed that melting in vacuo leads to a certain coarsening of the dendrite

branches, an increase in the total amount and size of primary phase precipitates, and also a change in the nature of their distribution in comparison with metals melted in the air (Figure 1).

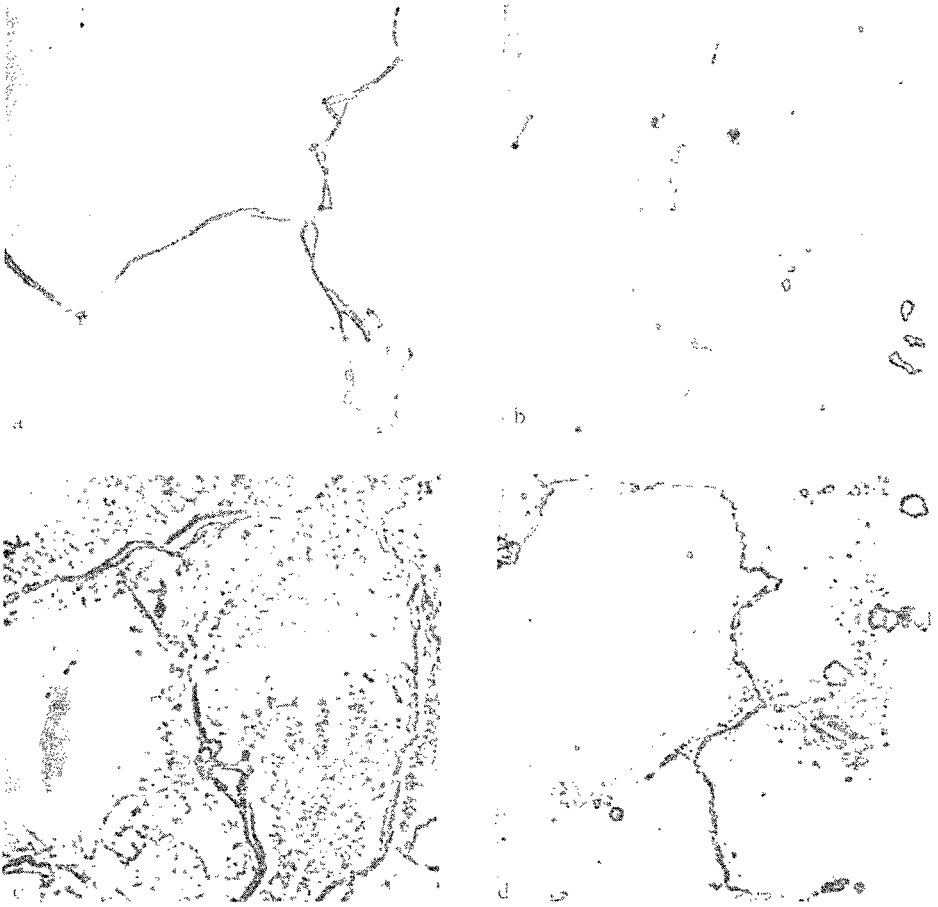

FIGURE 1. Microstructure of EI765 alloy, × 500:

a—melted in vacuo, polished microsection; b—melted in air, polished microsection; c—melted in vacuo, etched in a 10% aqueous solution of oxalic acid; d—melted in air, etched in a 10% aqueous solution of oxalic acid.

The carbide precipitates in specimens obtained by vacuum melting form chains which surround the dendrite branches. The titanium carbide precipitates are elongated, and are similar in shape to the incompletely developed dendrites (Figure 1, a).

If the metal is melted in the air, the carbides are distributed more uniformly and are more regular in shape (Figure 1, b). The metal produced by vacuum melting has a high content of eutectic components, which like columns of titanium carbides accumulate in the interaxial regions of the

dendrites and are clearly visible on polished and etched microsections. If the specimens are etched by the Murakami reagent the eutectic is colored black (Figure 2). This indicates that this eutectic contains carbon. Because of the changes in composition, amount, and distribution of carbides, the grain boundaries of cast vacuum-melted metal are coarser.

A similar, although less pronounced, regularity was found during comparative studies on the microstructures of precision cast metals.

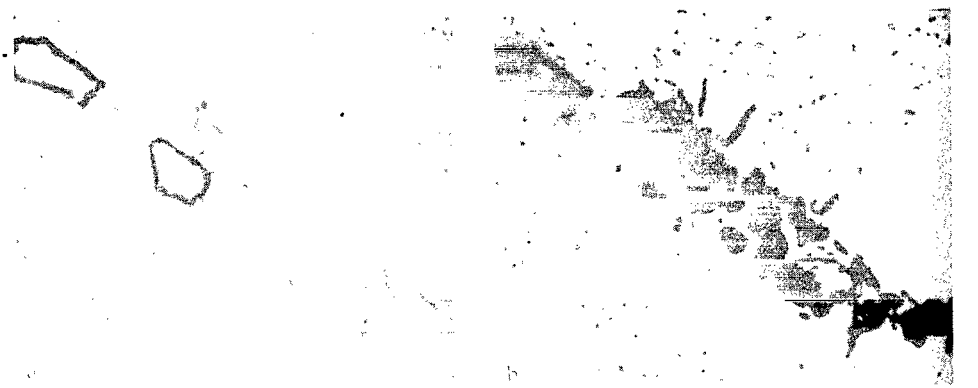

FIGURE 2. Eutectic precipitates in the structure of the EI765 alloy, ×1000:

a—polished microsection; b—microsection etched by the Murakami reagent.

Thermal heat treatment of the alloy leads to an appreciable decrease in the amount and separation of the primary carbides present in the eutectic, and also to an increase in the content of the secondary phase which accumulates in the interaxial regions. The differences between the structures of cast alloys melted in air or in vacuo were generally retained after heat treatment.

A study of the influence of the temperature of the mold on the structure of the cast metal melted in vacuo showed that a decrease in the cooling rate leads to a thickening of the dendrite branches, coarsening of the grains, and a decrease in the total amount of primary phases. At the same time, the titanium carbides become coarser, and the aggregates of the eutectic larger. Because of an increase in the distance between the axes of the second order, the secondary phases form wider bands.

The grain boundaries of alloys cast in ceramic molds were clearer than those of specimens cast in chill molds.

Our metallographic studies showed that the method of melting and the conditions of solidification of the EI765 alloy influence its structure, and in particular the amount and distribution of the different types of carbide phases, and the relationship between them.

Similar results were obtained by studies involving methods of chemical and X-ray phase analysis.

The data in Table 1 show that if the EI765 alloy is melted in vacuo, the total content of the [alloying] elements in the carbide precipitates increases.

This is true also of alloys cast in chill molds, and or in heated ceramic molds.

In both cases the weight of the carbide precipitates in the vacuum-melted alloy was 1.5—2 times that of carbides precipitated in the metal melted in air.

On the other hand, slower cooling during crystallization leads to a decrease in the total amount of carbide precipitates, irrespective of the method of melting.

X-ray studies (see Table 1) showed that the carbide particles precipitated from the cast metal contain titanium carbide and titanium nitride, and also a phase of the M_2C type. This compound has a variable composition, and a hexagonal lattice of the Mo_2C type.

TABLE 1. Results of a phase analysis of the EI765 alloy

Conditions of melting and casting of metal	State of specimen	Phase composition of carbide precipitate	Content of [alloying] elements in precipitate, on the weight of dissolved metal, wt %						
			Cr	Mo	W	Ti	Fe	Ni	total amount of [alloying] elements in precipitate, wt %
Melted in air, cast in chill molds	Cast	TiC; TiN	0.09	0.10	0.07	0.16	0.02	0.004	0.44
	Heat treated	Ti (C; N); $M_{23}C_6$	Not determined						
Melted in vacuo, cast in chill molds	Cast	TiC; TiN; M_2C	0.16	0.17	0.17	0.13	0.02	None	0.65
	Heat treated	$M_{23}C_6$; TiC; TiN	Not determined						
Melted in vacuo, cast in chill molds	Cast	TiC; M_2C; TiN	0.21	0.23	0.24	0.22	0.02	None	0.92
Melted in air, cast in ceramic molds (T = 800°C)	Cast	TiC; TiN; M_2C	0.04	0.04	0.06	0.09	0.01	None	0.25
Melted in vacuo, cast in ceramic molds (T = 800°C)	Cast	TiC; TiN; M_2C	0.15	0.20	0.14	0.16	0.01	None	0.66
	Heat treated	$M_{23}C_6$; TiC; TiN	Not determined						

We found that the M_2C carbide in the vacuum-melted metal cast in chill molds has the following lattice parameters: $a = 2.89$ kX, $c = 4.55$ kX, and $c/a = 1.57$.

According to the data obtained by X-ray spectral microanalysis with the "Comeca" analyzer, this phase contains about 47 wt% Cr, 40% Mo, 8% W, and 1.2%Ti. If we assume that the balance is carbon, the ratio of the total content of carbide-forming elements to carbon (in at. %) is close to 2.

According to the results of X-ray structural analysis, vacuum-melted alloys contain more M_2C-type carbides than metals melted in air. The relative increase in the content of M_2C in the precipitates is also confirmed by data on chemical phase analysis (see Table 1). The concentration of chromium, molybdenum, and tungsten in the precipitate increases. These

elements, as we have already mentioned, enter the complex M_2C carbides.

No M_2C carbides were found by the X-ray method in heat-treated specimens. The precipitates of these specimens were found to contain not only titanium carbides and titanium nitrides, but also $M_{23}C_6$ carbides (Table 1). A comparison of the intensity of the lines of $M_{23}C_6$ and of TiC on the X-ray photographs showed that alloys melted in vacuo have a higher content of $M_{23}C_6$ than metals melted in air. Since vacuum melting leads to an increase in the content of carbides in the alloy, it has been assumed that this is because of an increase in the dendrite liquation of carbon.

The method of qualitative autoradiography with the C^{14} isotope was applied to check this assumption, but it is insufficiently sensitive, and it is not possible to find any difference between the distribution of carbon in the metal melted in air or in vacuo. In both cases the carbon is concentrated in the interaxial regions of the dendrites. As an example, Figure 3 shows one of the autoradiograms recorded from a polished specimen of the EI765 alloy.

FIGURE 3. Autoradiogram of a specimen of the EI765 alloy containing a C^{14} isotope, × 60.

To clarify this problem, quantitative radiographic methods must be used.

We studied not only the carbide phases, but also made an attempt to evaluate the influence of metallurgical factors on the amount, shape, and dimensions of the intermetallic $Ni_3(Al, Ti)$ precipitates.

From a study of the structure of the alloys under an electron microscope it was not possible to determine any specific relationship between the distribution, amount, and dimensions of the particles of the γ'-phase and the method of melting and conditions of crystallization of the metal. In all specimens the γ'-phase was distributed uniformly within the matrix of the alloy, and its amount was determined by the content of aluminum and titanium in the alloy. The particles of the γ'-phase were spherical in shape.

Figure 4 shows photomicrographs of sections typical of all specimens.

No definite relationship was found between the composition of the intermetallic precipitates and the method of production of the alloy. This can be illustrated by the results of phase analysis given in Table 2.

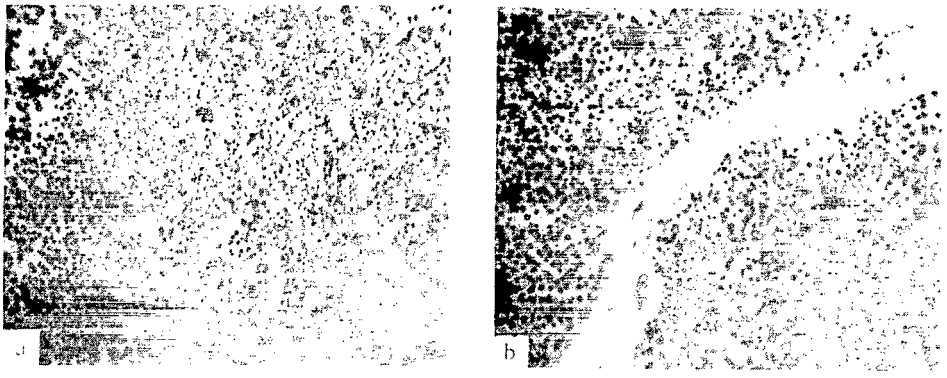

FIGURE 4. Distribution of the γ′-phase in the EI765 alloy, × 10,000:

a—grain; b—grain boundary region.

TABLE 2. Results of a chemical phase analysis of the EI765 alloy

Method of production of metal	Content of elements in alloy		Phase composition of precipitate	Content of elements in precipitates, on the weight of dissolved metal, wt %						
	Al	Ti		Fe	Cr	Mo	W	Ti	Al	Ni
Melting in air, casting in chill molds . . .	2.05	1.21	γ′-phase, Ti (C, N) γ′-phase	0.22	0.75	0.52	0.95	0.73	1.10	9.2
Melting in vacuo, casting in chill molds . . .	1.87	1.03	traces Ti (C, N)	0.24	1.01	0.44	0.82	0.52	0.83	7.10
Melting in vacuo, casting in ceramic mold heated to 800°C	1.82	1.03	γ′-phase	0.24	0.65	0.43	0.80	0.52	0.77	6.65

The higher content of alloying elements in the precipitate produced in the metal obtained by melting in the air is apparently due to the higher concentration of aluminum and titanium in the alloy, and is not connected with the technology of melting.

A comparison of the results of a study on the structure of alloys by metallographic and electron microscope methods and phase analysis shows that the method of melting and the conditions of crystallization of the EI765 alloy greatly influence the formation of carbide phases, but have no influence on the principal characteristics of the γ′-phase.

V. I. Prosvirin, V. D. Mortikov, and S. A. Goryunov

THE SPECIFIC BEHAVIOR OF HEAT-RESISTANT ALLOYS DURING THERMAL CYCLING

The behavior of alloys during thermal cycling has usually been investigated under conditions of stress. The heat resistance of many unstressed alloys and metals has been studied, and this property has been evaluated from a change in the shape of the metal and the formation of cracks. Variation in the state of the alloys during thermal cycling when no external loads are applied has not yet been sufficiently investigated.

A study of repeated heating of nickel—chromium-base heat-resistant alloys containing titanium and aluminum is interesting in order to clarify the interaction between the processes of strengthening and softening. In this article we shall give some data on the influence of thermal cycling on the structure and properties of the EI437B alloy.

The heat-treated specimens (15 mm in diameter and 160 mm in length) were subjected to one of the following three processes of thermal cycling (700—850°C):

700°, 30 min ⇄ 850°, 20 min
700°, 90 min ⇄ 850°, 20 min
700°, 270 min ⇄ 850°, 20 min

Each cyclic process was repeated 50 times. The specimens were heated in one furnace at 700°C and then transferred to another furnace and held at 850°C.

The changes in the properties and structure were evaluated by long-time strength tests on 6 mm diameter specimens at 700°C stressed by a load of 44 and 55 kg/mm^2, microhardness measurements, studies on the microstructure and phase composition, and also from certain data of X-ray analyses.

Long-time strength. The variation in the long-time strength after different heat-treatment processes is shown in Table 1.

TABLE 1. Variation in the long-time strength after different heat-treatment processes

Heat treatment*	Stress, kg/mm^2	δ_{av}, %	ψ_{av}, %	τ_{av}, hr, min
Initial (1080°C, 8 hr, +700, 16 hr) ...	44	3.22	7.65	85.40
Initial + 850°C, 30 min	44	3.3	9.77	69.55
850°C/20 min + 700°C/30 min	44	3.98	12.91	24.00
	55	4.86	16.3	14.05
850°C/20 min + 700°C/90 min	44	3.46	10.5	5.21
	55	4.55	11.74	1.31
850°C/20 min + 700°C/270 min	44	2.57	6.59	72.00
	55	2.38	7.56	4.20

* The tables give the average data obtained from 4—5 specimens.

The data indicate that the duration of heating at the minimum temperature of the cycle greatly influences the strength and ductility of the alloy.

Thermal cycles with 30 min heating periods, and in particular with 90 min periods, decrease the time to failure (τ_{av}) but increase the ductility of the alloy. Cycles with a 270 min heating period do not cause such a sharp drop in the long-time strength.

Microhardness. In Figure 1 are curves showing the dependence of the average (of 200 measurements) microhardness (H_μ) and the dependence of the distribution of microhardness (ΔH) on the duration of heating at the lowest temperature of the thermal cycle.

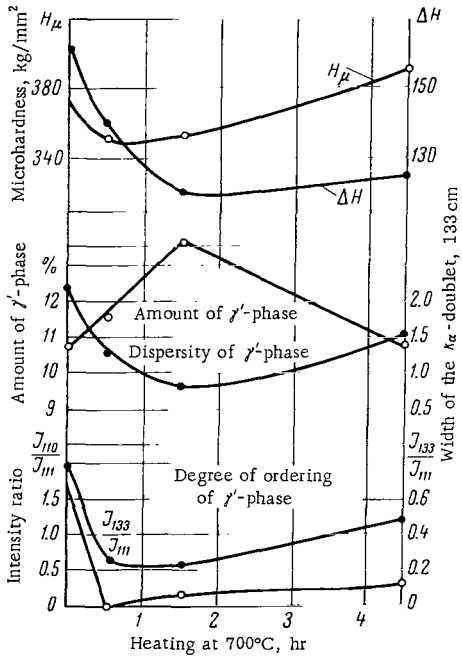

FIGURE 1. Influence of duration of heating on the microhardness and other properties determined by chemical and X-ray structural analyses of the EI437B alloy.

These data indicate that during the first and second heating treatments of the thermal cycle the processes of softening prevail over those of strengthening, and therefore the long-time strength and the mean microhardness decrease greatly. The microhardness of metals subjected to the third process of thermal cycling is even higher than the initial value.

The width of the bands representing the distribution of microhardness levels can to a certain extent indicate structural heterogeneity of the alloy. An increase in the duration of heating at 700°C decreases the difference between the maximum and minimum microhardness (ΔH), which indicates a decrease in heterogeneity.

Phase analyses. The variation in the substructure of the alloys was studied by a complex method of phase analysis (method developed by N. I. Blok and N. F. Lashko). Anodic precipitates were separated from specimens 10 mm in diameter and 40 mm in height in the electrolyte 18.

The specimens were then analyzed chemically and by X-ray methods, using a URS-50 apparatus. The results of the chemical and X-ray analyses are given in Table 2 and Figure 1.

TABLE 2. Content of elements and lattice parameters of the γ'-phase in the EI437B alloy after thermal cycling

Heat treatment	Content of elements, %				Lattice parameters, kX
	Ni	Cr	Al	Ti	
Initial { γ'-phase	77.0	4.58	6.85	11.54	3.5800
Initial { solid solution	76.7	20.35	0.68	2.01	3.5602
850°, 20 min; +700°, 30 min	77.0	4.52	6.82	11.65	3.5800
830°, 20 min; +700°, 90 min	77.22	4.17	7.15	11.43	3.5798
850°, 20 min; +700°, 270 min	77.0	4.86	6.51	11.62	3.5800

The maximum amount of γ'-phase in the alloy was found after cycling by the second process. The increase in the amount of γ'-phase caused the mother solid solution to become depleted of titanium and aluminum. This reduced the heat resistance and increased the ductility of the solid solution.

The average composition and the average crystal lattice parameter of the γ'-phase remain almost unchanged by the different cycling processes (see Table 2). However, X-ray photographs of the γ'-phase in the initial alloy show very diffused lines, particularly for large slip angles (*hkl* -133 and -420) which indicates that individual grains may have very varying compositions. After thermal cycling by the first process, and in particular by the second, the intensity of the lines on the X-ray photographs is increased, they become sharper, and doublets appear, which indicates that the individual grains of the γ'-phase have a highly stable composition.

It can be assumed that the dispersion of individual grains of the γ'-phase is proportional to the width of the interference lines of this phase, since there are almost no stresses of the second type in individual grains of the γ'-phase because of their microscopic dimensions.

The data shown in Figure 2 indicate that the dispersion of the grains of the γ'-phase in alloys after thermal cycling, particularly by the second process, is greatly decreased.

The γ'-phase in heat-treated alloys has an ordered face-centered cubic lattice, and CrK_α-radiation produces superlattice lines on the X-ray photographs. The relationship between the intensity of the superlattice lines and ordinary lines is usually an indication of the ordering of the γ'-phase.

It has been experimentally found that after thermal cycling the superlattice lines of the γ'-phase either disappear completely (after cycling by the first process) or are very weak. This indicates a complete or partial upsetting of the long-range order of atoms in this phase. This may adversely influence the long-time strength of the alloy since in this case the bonds between the chief strengthening phase and the solid solution matrix are disrupted.

The relationship between the integral intensities of the lines of the X-ray photographs are proportional to stresses of the third type, which arise as a result of a change in the state of the crystal lattice of the dislocated regions of the phase. It has been experimentally found that the relationship

between the integral intensities and the nature of thermal cycling of the alloy varies, in the same way as the long-time strength.

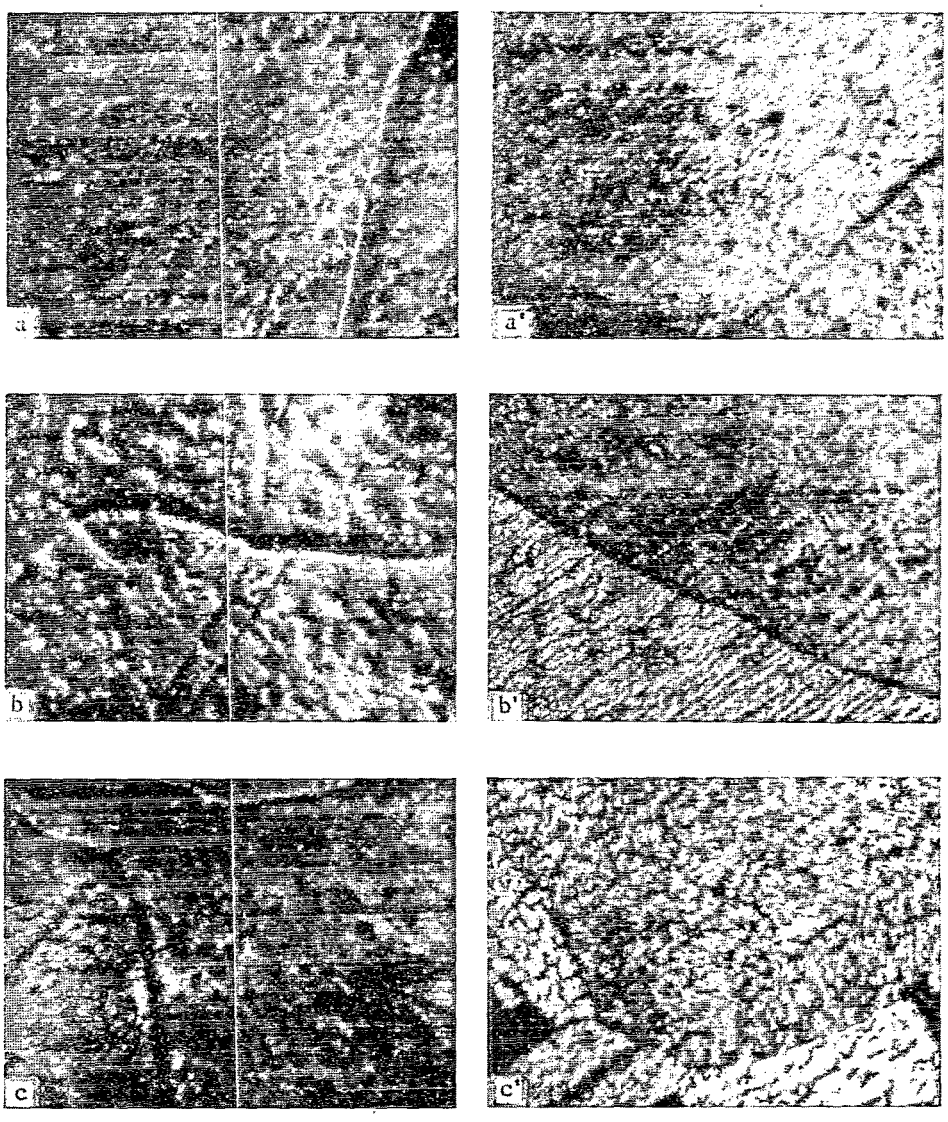

FIGURE 2. Structure of ET437B alloys after many thermal cycles, ×1350:

a—850°, 20 min; +700°, 30 min; b—850°, 20 min; +700°, 1 hr 30 min; c—850°, 20 min; +700°, 4 hr 30 min; a, b, c—electrolytic etching; a', b', c'—chemical etching.

CONCLUSIONS

1. The processes of strengthening and softening in EI437B alloys during thermal cycling (700 ⇄ 850°C) can reduce their long-time strength to a fraction of its initial value. The extent of this decrease depends on the duration of the cycles. One-time overheating of the alloy to 850°C for 30 min decreases the time to failure at 700°C by 18.5% ($\sigma = 44\ kg/mm^2$). After 50 cycles during which the alloy is heated to 850°C after every 30 and 90 min, the time to failure is decreased by 72 and 94%, respectively. If the time interval is increased to 270 min, the decrease in the long-time strength is not so great. The larger decrease in the long-time strength is accompanied by a considerable increase in the ductility of the alloy.

The decrease in the heat resistance of the alloy is caused by:

a) a considerable depletion of the solid solution of those elements consumed for the additional formation of the strengthening γ'-phase;

b) the formation of a highly developed block structure in the micrograins of the alloy, which can facilitate plastic flow and failure of the metal along the boundaries of the blocks during long-time tests;

c) complete or partial upsetting of the superlattice of the chief strengthening γ'-phase, which leads to a change in the bonds between this phase and the solid solution matrix of the alloy.

2. Certain thermal cycling processes of alloys containing molybdenum also lead to softening. Thus, for example, a cycling process at 850°C for 2 hr ⇄ 1050° for 5 min leads to a gradual reduction in the long-time strength if the number of cycles is increased. After 500 such cycles, the long-time strength at 800°C under a stress of $38\ kg/mm^2$ decreases by 88%. Under the same conditions of testing, after 420 cycles at 850°C for 2 hr ⇄ 1050 for 2 min the long-time strength decreases by 58%. An increase in the holding time at the upper temperature of the cycle increases the softening of the alloy. An increase in the holding time at the lower temperature of the cycle first causes softening of the alloy but then this softening is retarded, i.e., the process is similar to that in the EI437B alloy.

A decrease in the heat resistance of the alloy is caused by:

a) depletion of the solid solution of titanium and aluminum because these elements are used to form additional amounts of the γ'-phase;

b) fragmentation of the main grains with the formation of precipitates, which weaken the intergranular bonds at the grain boundaries.

V. K. Tsvetkova, V. N. Zhuchin, V. V. Topilin, A. P. Boyarinova, V. P. Stepanov, L. N. Zimina, and G. F. Kosheleva

*PROPERTIES OF SUPER ALLOYS OF THE EP487 TYPE**

The wrought EP487 super alloy is recommended for welded articles working at 750—900°C and under high stresses.

* M. Ya. Dzugutov, M. M. Klyuev, E. G. Dracheva, G. V. Zaglodina, A. S. Tugai, and E. F. Ignatenko participated with the authors in this work.

The EP487 (KhN60VMT10) alloy has a better weldability and a higher strength over the range of temperatures of 20—950°C than the recently used EP202 (KhN60MVT10) alloy. The ultimate strength and the yield strength of the EP487 alloy are 10—15 kg/mm² higher than those of the EP202 alloy, which is very valuable for increasing the reliability of manufactured articles.

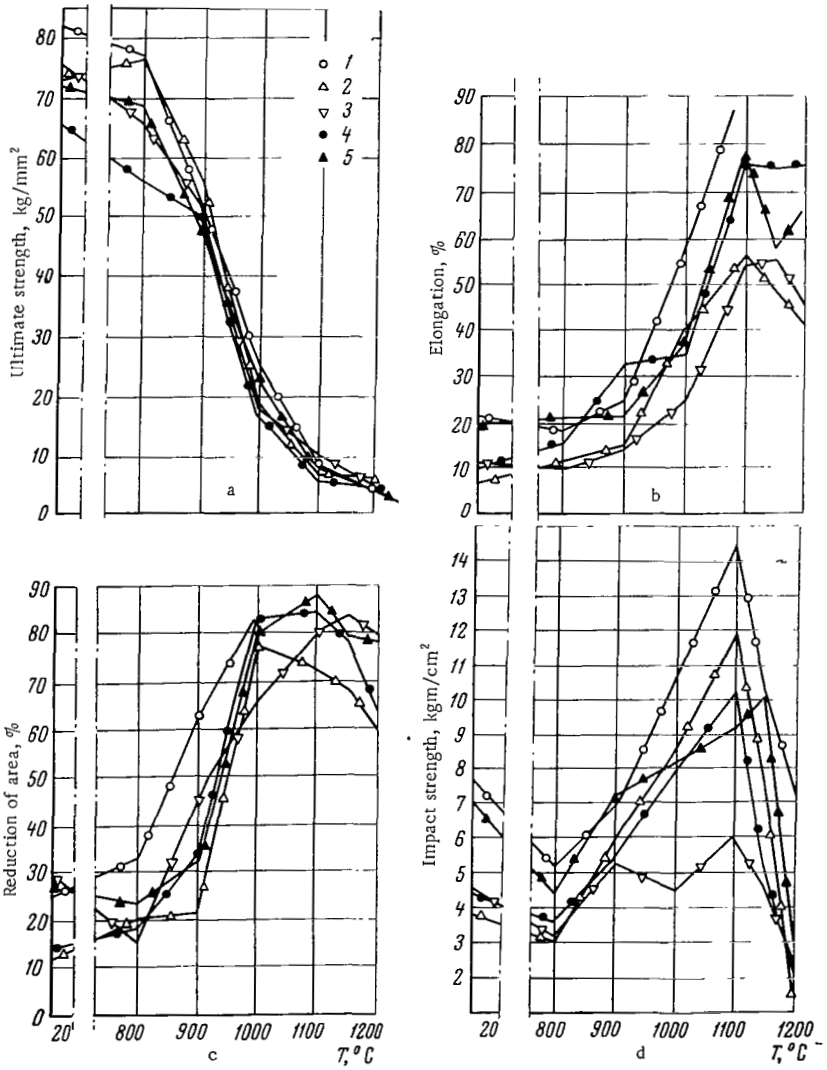

FIGURE 1. Mechanical properties of EP-487 steel at elevated temperatures:

1—along acicular crystals; 2—along ingot, edge; 3—along ingot, middle; 4—across ingot, edge; 5—across ingot, middle.

The molybdenum content of the EP487 alloy is 5% higher than in the EP202 alloy, which increases its resistance to plastic deformation and limits the field of high ductility to a narrower range of temperatures.

We studied the properties of cast and wrought EP487 alloys to choose the correct process of shaping and to determine its deformability at elevated temperatures.

The mechanical properties of cast alloys were studied with specimens cut from 270 kg ingots.

The specimens were cut in the longitudinal and transverse directions of the ingot (edge and middle) and also along acicular crystals.

We investigated the mechanical properties of the metal at 20 and 800—1200°C. The dependence of properties on temperature are shown in Figure 1.

The results show that the ultimate strength is almost independent of the direction and place from which the specimens were cut out, but the ductility of the metal (elongation and reduction of area) is greatly influenced by these factors. Specimens cut out along acicular crystals had the highest impact strength and the highest elongation, while specimens cut longitudinally from the middle of the ingot had the lowest impact strength and elongation over the range of temperatures of hot working.

The ultimate strength of the alloy at 900°C is from 30 to 40 kg/mm^2, but at 1000°C it is only 20 kg/mm^2. This indicates that the alloy has a high resistance to deformation and requires powerful and rapid working equipment. The ductility and impact strength are highest at 1100°C. An increase in the temperature to 1200°C or a decrease to 950°C greatly decreases the ductility. This indicates that the alloy is highly sensitive to overheating and that the strengthening of the alloy due to the precipitation of intermetallic phases starts at relatively high temperatures.

Similar data were obtained during studies on a wrought metal produced in open induction furnaces, and electric furnaces by the slag processes. No great difference between the ultimate strengths of the metals produced by these two methods was found. The metal obtained by the slag process has a higher ductility at elevated temperatures. The impact strength of metal produced by induction melting at 900—1200°C does not exceed 10 kgm/cm^2, while that of the metal produced by the slag process in an electric furnace is as high as 22 kgm/cm^2 (Figure 2).

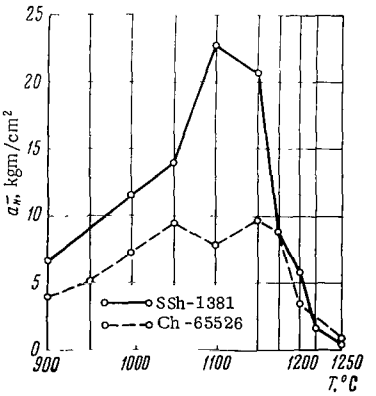

FIGURE 2. Impact strength over the temperature range of 900—1250°C.

It has been experimentally found that in the EP487 alloy a highly effective precipitation hardening takes place rapidly even at high cooling rates. If the metal is cooled in molds the processes of precipitation hardening are apparently almost complete, and therefore this metal is very brittle.

The hardness (H_B) of the ingot after cooling was 277 kg/mm^2, but after quenching in water from 1220°C the hardness was 170 kg/mm^2.

In alloys which undergo no polymorphic transformation tensile stresses can always arise in the interior of the ingot, and can produce internal cracks if the metal has a low ductility. Such cracks usually arise in those regions of the ingot subjected to the highest tensile stresses.

In ingots produced by the ordinary method, the highest tensile stresses usually appear in the lower part of the ingot because the cooling is most rapid there.

Most 500-kg ingots of the EP487 alloy cooled in molds had internal transverse cracks in their lower parts. Attempts to avoid these by different cooling methods available in industry met with little success.

It was found that to avoid the formation of internal transverse cracks the ingots must be forged while hot, without any intermediate cooling after teeming and solidification.

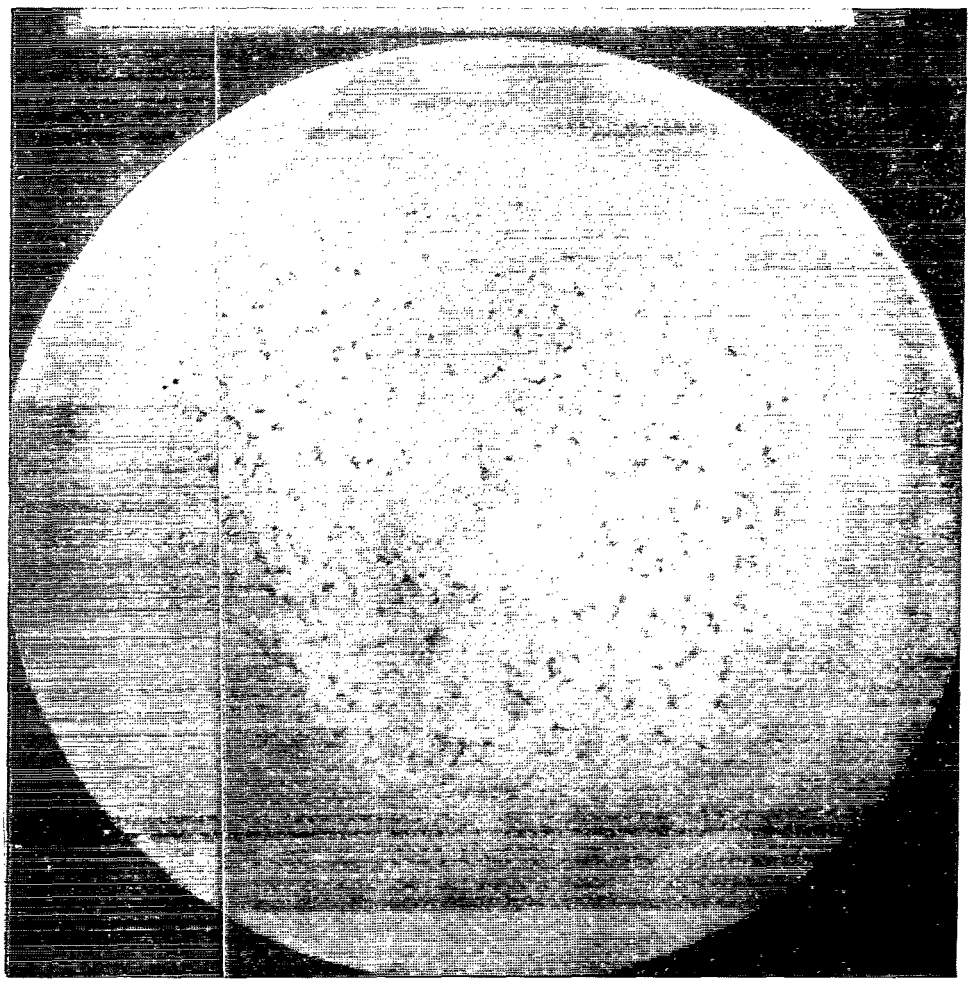

FIGURE 3. Macrostructure of a 350 mm diameter billet cut from a 2100 kg ingot.

The experience obtained with 960 to 2500 kg ingots showed that if these are heated during forging to 550°C (at the surface) or above, no internal cracks are formed and forgings of different dimensions can be produced.

As already mentioned, special industrial processes for deformation must be developed because of the low ductility of the alloy and its high resistance to deformation at low temperatures. With such methods articles with a diameter of from 16 to 350 mm, and also billets of various dimensions can be produced by working 165 kg to 2500 kg ingots of this highly alloyed and deformation-resistant alloy.

The deformation of this alloy must be carried out over a very narrow range of temperatures and at very limited reductions per operation.

A study of the macrostructure of cross sections 200—350 mm in diameter prepared from 960 kg and 2500 kg ingots (produced by induction melting) showed that the alloy is susceptible to extraaxial liquation (see Figure 3). The volume of metal attacked by this liquation is greater in the larger ingots (2100, 2500 kg). Remelting in an electric furnace by the slag process considerably decreases the liquation heterogeneity of the metal.

However, metals prepared in an electric furnace by the slag process have considerable internal cracks in the lower part of the ingots, which appreciably reduces the percentage of usable material and limits the application of this method.

According to technical specifications, rods more than 100 mm in diameter are inspected for mechanical properties during melting by using reforged specimens 80—100 mm in diameter. Rods with a diameter of 100 mm or less are inspected on delivery. Bars 45 mm in diameter are produced from 165 kg ingots so that the conditions of recrystallization exclude any extraaxial liquation. Thicker bars prepared from 960 and 2500 kg ingots produced by induction melting show appreciable extraaxial liquation.

The mechanical properties of specimens prepared from different ingots and from metals produced in electric furnaces by the slag process at 20 and at 800°C are given in Table 1. The specimens were made of round or square billets, cut into four parts, heated to 1100—1120°C for 2.5 hr, cooled in the air and then held for 10 hr at 850°C.

TABLE 1. Mechanical properties

Dimensions of ingot	Testing temperature, °C	$\sigma_в$ kg/mm^2	$\sigma_{0,2}$, kg/mm^2	δ, %	ψ, %	A_k, kgm/cm^2
Ingot 165 kg (40 mm diam)	20	118	80	20	25	2.6
	800	91	73	29	32	3.8
Ingot 960—2500 kg (□90 mm)	20	116	80	15	18	2.4
	800	88	73	23	30	3.5
Slag process in electric furnace, (□90 mm)	20	119	82	20	20	2.7
	800	90	73	27	32	3.8

From the data of Table 1 it can be seen that the ultimate strength and yield strength of 30—40 mm rods prepared in an induction furnace or in an electric furnace by the slag process are almost the same as those of 90 mm square specimens made of large ingots. However, their ductility

is higher, probably because of extraaxial liquation in large ingots.

Characteristically, the metal has a low impact strength at 20 and 800°C. We studied the influence of heat treatment on the mechanical properties of alloys, and found the optimum process (1130°, 2.5 hr + 850°C, 3 hr, air) for an increase in impact strength.

With this new heat treatment the impact strength of 90 mm square specimens can be increased from 2.2 to 5.0 kgm/cm^2 at 20°C (Table 2).

TABLE 2. Mechanical properties of the EP487 alloy after different heat-treatment processes

Heat treatment	Temperature, °C	σ_B, kg/mm^2	$\sigma_{0,2}$, kg/mm^2	δ, %	ψ, %	A_k, kgm/cm^2
1100°, 2 hr 30 min, air, +850°, 10 hr, air	20	120.0	82.7	18.1	18.5	2.2
	800	88.7	73.1	23.9	32.7	4.3
1130°, 2 hr 30 min, air, +850°, 3 hr, air	20	110.4	78.8	29.0	29.4	5.0
	800	92.1	71.7	12.0	25.5	5.61

CONCLUSIONS

1. We developed a technique for the production of large forgings of the EP487 alloy prepared by open electric arc and induction melting.
2. The EP487 alloy has a high resistance to deformation and a narrow temperature range over which hot forming is possible.
3. The EP487 alloy is susceptible to extraaxial liquation heterogeneity, which can be reduced by melting by the slag process in an electric furnace.
4. If the alloy is heat treated at 1130°C for 2.5 hr, air cooled to 850°C, and held at this temperature for 3 hours, it has good mechanical properties.

L. N. Zimina, G. F. Kosheleva, E. A. Kardonov, and V. K. Tsvetkova

STRUCTURE AND PROPERTIES OF THE KhN60MVTYu (EP487) ALLOY*

The new wrought heat-resistant alloy KhN60MVTYu (EP487)** can be used to produce welded articles for service at 750—900°C. The alloy has the following chemical composition (in %):

Element	Ni	Cr	Mo	W	Ti	Al	Fe	C
Content of element, %	Basis	17—20	9—11	4—5	2.2—2.8	1.0—1.5	$\leqslant$ 6	$\leqslant$ 0.08

Over the temperature range of 20—950°C the EP487 alloy has a higher strength than the weldable EP202 alloy used today /1/. The ultimate

* [In last article, KhN60MVT10.]

** The alloy was developed with the cooperation of TsNIIChM and other institutions.

strength and yield strength of the EP487 alloy are 10—15 kg/mm^2 higher than those of the EP202 alloy. If EP487 alloy is used, the performance of manufacturing articles can be improved.

The EP487 alloy is a precipitation-hardening material. At elevated temperatures this alloy consists of a solid solution of the alloying elements in nickel. Quenching in water from a temperature of above 1100°C produces a single-phase solid solution with a relatively low hardness (H_B of 207). If the alloy is air cooled, a small amount of intermetallic compounds and carbides (total about 5.5%) is precipitated, which leads to an increase in the hardness (H_B of 241). Slow cooling causes rapid decomposition of the solid solution with the formation of considerable amounts of precipitates (total 13.7%), and an appreciable increase in hardness (H_B of 302). The strengthening phase starts to precipitate at about 930°C.

Aging leads to additional precipitation of intermetallic compounds and carbides from the solid solution and to a further strengthening of the alloy. Aging at 700°C is slow, and the maximum hardness is not reached even after 25 hr. An alloy aged at 700°C consists of a solid solution with carbide precipitates along the grain boundaries and within the grains (Figure 1, a).

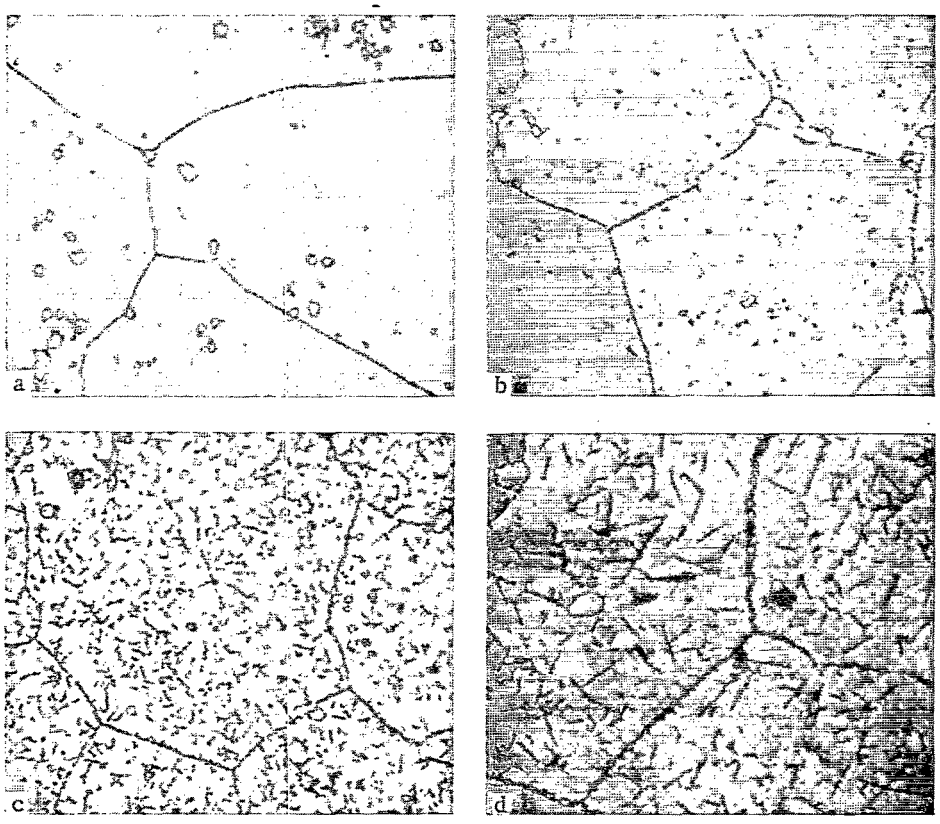

FIGURE 1. Microstructure of the EP487 alloy after aging for 10 hr, × 600:

a—at 700°C; b—at 800°C; c—at 850°C; d—at 900°C.

The strengthening precipitates within the grains are not visible under an optical microscope (× 600) because of the considerable dispersion, although according to a phase analysis the amount of this phase is up to 10% (Table 1).

TABLE 1. Content and composition of intermetallic compounds and of carbide phases in the EP487 alloy*

Heat treatment	Type of precipitation phase	Content of phase, %		Composition of the γ′-phase, at. %						
		Me_6C, TiC, Me_7W_6	$Ni_3(Ti, Al)$	Ni	Fe	Cr	Al	Ti	W	Mo
1100°, 2.5 hr; air	Me_6C, TiC $Ni_3(Ti, Al)$	1.0	4.6	71.7	0.1	3.8	3.7	10.6	1.3	2.8
1100°, 2.5 hr; cooling with the furnace	Me_6C, TiC $Ni_3(Ti, Al)$	1.6	12.1	75.0	0.5	0.1	5.1	16.7	1.4	1.4
1100°, 2.5 hr, air + 700°, 10 hr, air	Me_6C, TiC $Ni_3(Ti, Al)$	0.8	10.0	73.2	0.6	2.3	6.0	14.7	1.4	2.3
1100°, 2.5 hr, air +800°, 10 hr, air	Me_6C, TiC, $Ni_3(Ti, Al)$ Me_7W_6 (traces)	2.0	11.0	74.6	0.1	0.2	5.7	16.7	1.4	1.7
1100°, 2.5 hr, air + 850°, 10 hr, air	Me_6C, TiC $Ni_3(Ti, Al)$, Me_7W_6	3.0	11.6	74.7	0.5	—	4.3	18.9	0.8	1.2
1100°, 2.5 hr, air + 900°, 10 hr, air	Me_6C, TiC, $Ni_3(Ti, Al)$ Me_7W_6	4.6	9.8	74.5	0.2	—	5.9	15.4	1.5	2.5

* The chemical analysis was carried out under the direction of E. F. Yakovleva, and the X-ray analysis by D. N. Zharkova.

Holding the alloy at 750°C leads to a continuous increase in hardness for 25 hours, but no considerable structural changes take place.

The maximum strengthening of the alloy occurs at a temperature of 800—850°C. The hardness increases most rapidly during the first 2—3 hr (R_c is 30). This increase continues, although much more slowly, up to 25 hr, when the alloy has a hardness of R_c is 34. After the alloy is heated for 10 hr at 800°C it consists of a solid solution with γ′-phase precipitates along the grain boundaries and fairly large carbide inclusions. No γ′-phase precipitates were found within the grains, but individual point size particles of Me_7W_6-type precipitates, clearly visible after 25 hr of aging, were found (Figure 1, b). The nature of this phase was determined by an X-ray structural analysis. The amount and dimensions of the particles of the Me_7W_6-type phase increase with increase in temperature and duration of aging. After 5 hr of aging at 850°C the Me_7W_6-type phase is clearly visible under a microscope, and after 25 hr of aging its amount increases rapidly, it coarsens, and is in the form of small lamellas (Figure 1, c). The content of the γ′-phase after 10 hr of aging at this temperature is 11.6%.

Aging at 900°C leads to a certain softening of the material due to a coagulation process at this temperature. Alloys aged at 900°C have γ′-phase precipitates within the grains. Aging at this temperature also leads to coagulation of the γ′-phase along the grain boundaries, and to a coarsening of the Me_7W_6-type particles (Figure 1, d).

According to data obtained by X-ray structural analysis, the Me_7W_6-type phase has a hexagonal lattice with the following parameters: $a \cong 4.75$ kX and $c \cong 25.7$ kX . Chemical analysis of a deposit containing a Me_7W_6-type phase indicates that the formula can be written as $(Ni, Cr)_7 (Mo, W)_6$. This phase can exist over the range of 800—1050°C.

Besides intermetallic compounds, the alloy contains carbides of the Me_6C and TiC types. Rods, forgings, and billets made of large ingots (1—2.5 t) show carbide liquation, which consists chiefly of the Me_6C-type carbide. According to the data of local X-ray spectral analysis, the formula of the carbide can be written as $(Ni, Cr)_3(Mo, W)_3C$ /2/.

Heating to 1100—1200°C has little influence on the shape and distribution of the carbide phase. In the wrought metal the carbide phase is globular or somewhat acicular, and is strung out along the specimen. Heating to above 1200°C leads to a gradual dissolution of carbides in the solid solution. Only nitrides and carbonitrides of titanium remain precipitated, as these dissolve at higher temperatures. At 1250°C, a eutectic precipitates along the grain boundaries. At 1300°C this becomes coarser and appears not only along the boundaries but also in the interior of the grains.

The heat treatment of the alloy was adjusted to satisfy the requirements of welded articles with a short service life. To produce an EP487 steel with good mechanical properties and a high heat resistance, the steel must be solution heat treated and aged. However, even without aging the solution heat-treated alloy has a good strength ($\sigma_b = 100-112$ kg/mm^2), good ductility ($\delta = 50\%$) and high impact strength ($A_k = 14-23$ kgm/cm^2).

Heating to 1100—1130°C produces a fine grain of size 5—8 and has a favorable influence on the mechanical properties of the alloy (Table 2). Heating to higher temperatures (1170°C) leads to a coarsening of the grain (size 3—4), and to a certain decrease in the ductility and strength. If the heating at 1100°C is prolonged from 2.5 to 6 hr, this has almost no influence on the mechanical properties of the alloy.

TABLE 2. Influence of heat treatment on the mechanical properties of EP487 alloys at 20°C

Quenching		Aging		σ_B, kg/mm^2	$\sigma_{0.2}$, kg/mm^2	δ, %	ψ, %	a_k, kgm/cm^2
temperature, °C	time, hr	temperature, °C	time, hr					
1100	3	—	—	112	65	52	52	14
1150	3	—	—	102	60	51	52	23
1100	2.5	850	10	125	81	22	18	4
1130	2.5	850	10	120	80	23	20	4.4
1150	2.5	850	10	118	80	21	17	4.2
1170	2.5	850	10	110	74	17	13	4.2
1100	2.5	850	5	122	81	27	22	3.6
1100	6	850	5	122	82	24	23	4
1100	2.5	750	10	128	89	37	29	6
1100	2.5	800	10	132	94	34	20	5
1100	2.5	850	10	132	89	32	15	3.5
1100	2.5	900	10	124	80	27	10	3
1100	2.5	1050	2	108	66	42	32	5.5
1100	2.5	850	3	120	78	35	32	6
1100	2.5	850	5	120	78	29	26	4
1100	2.5	850	10	120	79	24	20	3.2

We studied the influence of aging at 750—1050°C on the properties of alloys quenched from 1100°C. An increase in the temperature of aging to 850°C improves the strength of the alloy, but decreases the impact strength and ductility. A further increase in the temperature of aging to 1050°C leads to a gradual decrease in strength but to an increase in ductility, which is due to the processes of coagulation taking place in the alloy. If the duration of heating at 800—850°C is increased from 3 to 10 hr, this has little influence on the strength, ductility and impact strength of the alloy.

We found by experiment that articles made of EP487 alloy destined for short service lives should be air hardened from 1100—1130°C and aged at 850°C for 3 hr.

The mechanical properties of the EP487 alloy at 20—900°C after this heat treatment are shown in Figure 2.

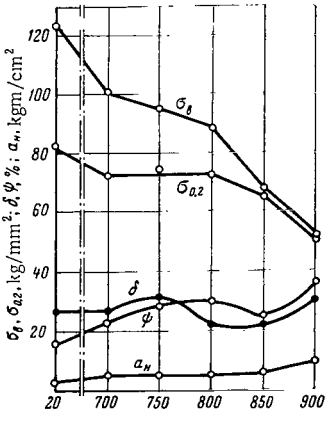

FIGURE 2. Mechanical properties of the EP487 alloy.

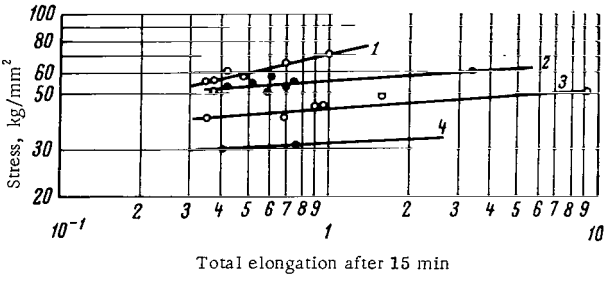

FIGURE 3. Creep strength of the EP487 alloy over a short time: 1—750°C; 2—800°C; 3—850°C; 4—900°C.

The best mechanical properties can be obtained with rolled rods and sheet (Table 3). Mechanical properties of forgings are less stable, since these have a greater carbide heterogeneity.

The creep strength of EP487 alloys over a short time which produces a total elongation of 1% after 15 min of testing is 70 and 55 kg/mm² at 750 and 800°C, respectively (Figure 3).

TABLE 3. Mechanical properties of wrought rods, forgings, and hot-rolled sheet of the EP487 alloy

Semifinished product	Testing temperature, °C	$\sigma_в$, kg/mm²	$\sigma_{0,2}$, kg/mm²	δ, %	ψ, %	a_k, kgm/cm²
Rolled rod, ∅ 43 mm	20	115—124	75—85	25—35	23—37	3.5—4.5
	750	101—114	67—76	23—32	23—36	
Forgings	20	103—128	73—88	10—25	10—25	2—3.5
	800	80—106	66—80	20—28	14—40	3—5
Sheet, 8 mm thick	20	117—132	78—88	20—32	15—20	3.2—4.5
	750	95	74	31	27	5.3
	800	88	74	22	20	5.3

TABLE 4. Physical properties of EP487 alloys

Temperature, °C	E, kg/mm²	λ, cal/cm·sec·g	α·10⁶ mm/mm·°C (from 20°C)	γ, g/cm³	Temperature, °C	E, kg/mm²	λ, cal/cm·sec·g	α 10⁶, mm/mm·°C (from 20°C)	γ, g/cm³
20	22,350	0.030	—	8.56	600	18,400	0.043	13.0	—
100	21,650	0.027	10.8	—	700	17,600	0.048	13.5	—
200	21,250	0.031	11.3	—	800	16,900	0.057	13.9	—
300	20,300	0.034	11.6	—	900	15,650	0.065	14.5	—
400	19,700	0.036	12.1	—	1000	14,100	—	15.3	—
500	19,100	0.039	12.6	—					

The physical properties of the alloy are shown in Table 4.

The EP487 alloy is now being produced on an industrial scale and is available as rods, forgings, and sheet.

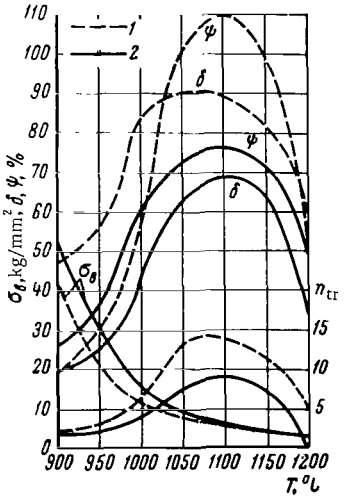

FIGURE 4. Mechanical properties of wrought EP487 alloys (and EP202) at 900—1200°C:

1—EP202 alloys; 2—EP487 alloys.

When planning the processes of hot working of this alloy we must remember that the EP487 alloy contains 5% more of molybdenum than the EP202 alloy and so its resistance to plastic deformation is greater and the temperature limit of such a deformation is narrower (Figure 4). The elongation, reduction of area, and torsion number of EP487 are 20—25% lower than those of the EP202 alloy, and the highest ductility is at a temperature 25—30°C higher than that for the EP202 alloy.

CONCLUSIONS

1. We developed a new wrought, weldable, heat-resistant nickel—chromium alloy KhN60MVTYu (EP487) which has better mechanical properties than the EP202 alloy which is widely used today.

2. The maximum strengthening is achieved by aging at 800—850°C due to precipitation of strengthening $Ni_3(Ti, Al)$ and $(Ni, Cr)_7(Mo, W)_6$ phases from the solid solution. The liquation heterogeneity found in this metal consists chiefly of the $(Ni, Cr)_3(Mo, W)_3C$ carbide phase.

3. The heat-treated EP487 alloy has good mechanical properties. At 800°C these properties are as follows: $\sigma_в = 80—100\,kg/mm^2$, $\sigma_{0.2} = 65—80\,kg/mm^2$, $\delta = 15—30\%$, $A_k = 3—5\,kgm/cm^2$. The creep strength over a short time which produces a total elongation of 1% after 15 min of testing is $52\,kg/mm^2$.

4. From our studies on the mechanical properties of the alloy over the range of temperatures of hot working, we found that EP487 castings should be hot worked at 950—1140°C, while wrought alloys should be hot worked at 1000—1160°C.

Bibliography

1. Pridantsev, M.V., G.V.Estulin, and L.N.Zimina. Vliyanie molibdena i vol'frama na svoistva zharoprochnykh nikelevykh splavov (Influence of Molybdenum and Tungsten on the Properties of Heat-Resistant Nickel Alloys).—Stal', No. 4. 1964.
2. Zimina, L.N., G.F.Kosheleva, and T.V.Egorshina. Dendritnaya i zonal'naya neodnorodnost' v splavakh KhN67VMTYu i KhN60MVTYu (Dendritic and Regional Heterogeneities in KhN67VMTYu and KhN60MVTYu Alloys).—MiTOM, No. 3. 1966.

N. F. Lashko, O. A. Khromova, A. A. Burmistrova, and N. I. Zhuravleva

INFLUENCE OF COBALT ON THE PHASE COMPOSITION OF SOME HEAT-RESISTANT ALLOYS

Cobalt has a great influence on many properties of steels and alloys.

However, it is used much less than it should be, chiefly because of its high price and scarcity. The influence of cobalt on the properties of steels and alloys is very characteristic and very specific. In certain combinations with other alloying elements its influence can be detrimental, and cause softening or even embrittlement of the material. Too high a content of cobalt in certain heat-resistant alloys containing tungsten and molybdenum can lead to the formation of a phase containing Co_7W_6 along the grain boundaries during aging, and this makes the alloy brittle.

Heat-resistant austenitic steels and nickel—chromium alloys alloyed with cobalt have a high ductility during short tests (certain alloys retain

a high ductility even after prolonged heating) and during service, which indicates inhibition of aging. These can be readily hot worked. Heat-resistant steels and nickel-base alloys may contain up to 20% cobalt.

Despite the fact that more and more cobalt is now added to various steels and alloys, the nature of its influence on the properties of metals has not yet been sufficiently investigated. It is characteristic of cobalt that it has a beneficial influence on the properties of steels and alloys when it enters iron- or nickel-base phases, or even if it does not precipitate from the solid solution at all, and not when it forms a phase of its own. We can thus assume that cobalt increases the solubility of alloying elements in the precipitates /1, 2/, or increases the temperature at which these precipitates dissolve /3/.

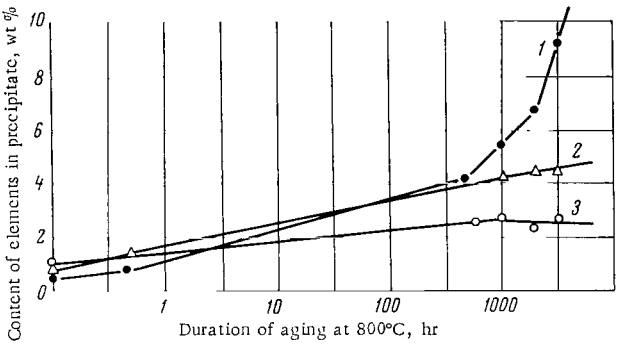

FIGURE 1. Dependence of the total content of alloying elements (Cr + Fe + + Ni + Co + W + Mo) in precipitates separated from austenitic steels by aging at 800°C on the content of cobalt:

1—0% Co; 2—5% Co; 3—20% Co.

We should differentiate between the influence of cobalt on heat-resistant austenitic steels strengthened by carbide precipitates and its influence on nickel-base heat-resistant alloys strengthened by intermetallic compounds on the basis of Ni_3Al or $Ni_3(Al, Ti)$.

The results of a study onthe phase composition of aged wrought steels, particularly of alloys aged at 800°C, are very characteristic. These steels contain an average of 0.20% carbon, 20% nickel, 1% tungsten, 2% molybdenum, with different contents of cobalt (0.5, 9.7, 19.1%). Steels containing no cobalt precipitate an $Me_{23}C_6$ carbide, an $Fe_2(Mo, W)$ intermetallic compound, and a σ-phase on aging. In steels containing 0.5 and 9.7% Co the precipitation of intermetallic compounds is greatly inhibited, but in steels containing 19.1% Co this precipitation does not take place at all. Therefore, alloys with 19.1% of cobalt age very slowly, the alloy is stabilized, and its high ductility and toughness are preserved even after prolonged heating. Figure 1 shows the total content of alloying elements (Cr + Fe + Ni + Co + W + Mo) in precipitates (separated electrolytically) produced by aging at 800°C.

Undoubtedly the increase in the stability of the solid solution of cobalt-alloyed steels and the slowing down of its decomposition during aging are due mainly to an increase in the solubility of carbon and of alloying elements (Cr, W, Mo) which form carbide and intermetallic compound precipitates.

We studied the nickel-base cast alloy which is hardened as a result of the precipitation of intermetallic compound particles $Ni_3(Al, Ti)$. The composition of this alloy was as follows (%): C, 0.1; Cr, 13; Mo, 4.2; W, 5; Al, 4.5; Ti, 2.9; and B, 0.02. The content of cobalt in the different heats was as follows: 0, 4.1, 7.1, 9.8, and 14.1% (the alloys were cast into three-part molds).

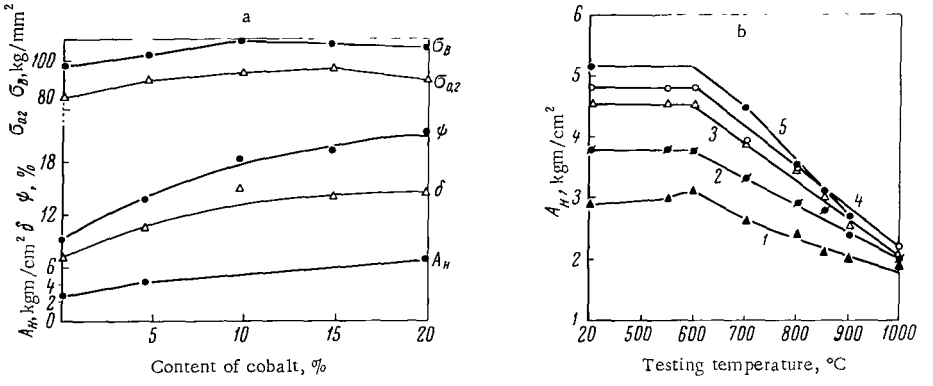

FIGURE 2. Influence of cobalt on the mechanical properties of nickel-base alloys (three-part specimens) (a), and influence of testing temperature on the impact strength of nickel-base alloys with different contents of cobalt (b):

1—0.0% Co; 2—4.1% Co; 3—7.1% Co; 4—9.8% Co; 5—14% Co.

The alloys were hot treated by a homogenizing anneal at 1200—1220°C for 4 hr followed by cooling in the air, which led to rapid decomposition of the solid solution and precipitation of considerable amounts (44—47%) of the strengthening α′-phase on the basis of $Ni_3(Al, Ti)$. Additional aging does not appreciably increase the content of the α′-phase but leads to a change in the shape of the particles and a partial change in their chemical composition.

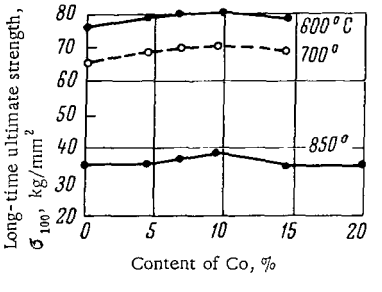

FIGURE 3. Influence of cobalt on the long-time strength of nickel alloys (σ_{100}) at 600—850°C.

The addition of cobalt to the alloy (Co $\geqslant$ 10%) increases the yield strength ($\sigma_{0.2}$) and the ultimate strength by 10 kg/mm^2. The elongation, reduction of area, and impact strength increase proportionally to the increase in the cobalt content (Figure 2, a). The impact strength of nickel-base cast alloys decreases if the temperature is raised above ~600°C. Up to 1000°C cobalt-containing alloys have a higher impact strength than those without cobalt (Figure 2, b).

At 600—850°C the addition of 4—20% of cobalt to such alloys has almost no influence on their long-time ultimate strength (Figure 3).

The change in the mechanical properties of alloys produced by an increase in the cobalt content is due to a change in the phase composition.

This has been determined by electrochemical, X-ray structural, and chemical analyses of primary and secondary precipitates.

The α′-phase particles, like those of carbides and borides, were separated in electrolyte 1 of the following composition: citric acid, 30 g; ammonium sulfate, 10 g; water, 1 liter.

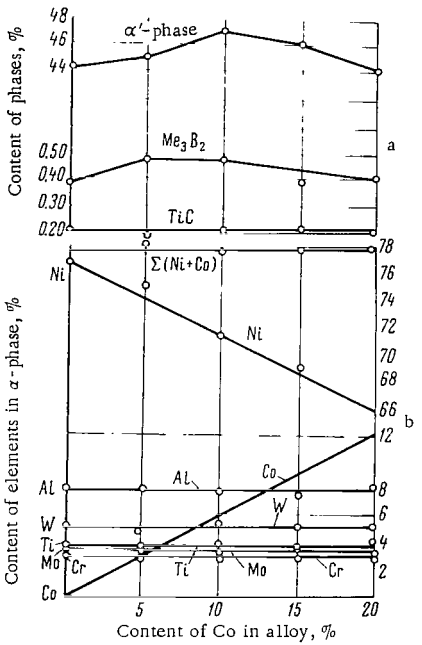

FIGURE 4. Content of α′-phase, TiC and Me_3B_2 in nickel alloys as a function of the cobalt content (a), and the dependence of the chemical composition of the α′-phase of nickel alloys on the content of cobalt (b).

We separated the carbide and boride phases in a nonaqueous electrolyte 2, containing 50 ml HCl (specific gravity 1.19), and 1050 ml of methyl alcohol. Electrolyte 1 dissolves the solid solution, and electrolyte 2 dissolves the solid solution and also the α′-phase.

By comparing the results of the chemical analyses of the anodic deposits precipitated in these two electrolytes, the content of the α′-phase can be found.

According to data of X-ray structural analysis, the anodic deposits precipitated in electrolyte 2 consisted of TiC and Me_3B_2. The content of TiC and Me_3B_2 in the alloy was about 0.65%, irrespective of the content of cobalt. No cobalt was found in the carbides or borides. The results of chemical analysis of the carbide and boride phases are shown in Figure 4, a.

An increase in the cobalt content of the alloy to 20% has little influence on the content of the α′-phase and its chemical composition. If the content of cobalt in the alloy is increased from 4 to 19%, its content in the α′-phase changes from ~1 to 5%, which is about 25% of the average concentration of cobalt in the alloy, and the other 75% of cobalt remain in the solid solution. The content of cobalt in the alloy has almost no influence on the content of tungsten, molybdenum, titanium, and chromium in the α′-phase (Figure 4, b).

Cobalt influences the phase composition of alloys of this type by changing the chemical composition of the solid solution and of the intermetallic compound $(Ni, Co)_3(Al, Ti)$ in which cobalt substitutes part of the nickel. Consequently, cobalt as an alloying element influences heat-resistant austenitic alloys favorably by increasing the solubility of carbon and of certain carbide-forming elements, by stabilizing the solid solution, and by inhibiting its decomposition. In nickel-base alloys cobalt enhances the properties of the solid solution and increases its stability, ductility, and toughness. The stability of the solid solution depends not only on its chemical composition but also on its microstructure, and particularly on the energy of formation of imperfections in the crystal lattice. It is possible that cobalt decreases the energy of formation of imperfections. However, additional investigations are necessary to prove this.

Bibliography

1. Lashko, N.F. and N.I. Eremin. Fazovyi analiz i struktura austenitnykh stalei (Phase Analysis and Structure of Austenitic Steels).—Mashgiz. 1957.
2. Heslop, J.—Cobalt, No. 24, 128. 1964.
3. Cross, H.C.—Metal Progress, Vol. 87, No. 3, 67. 1965.

M. A. Filatova, G. T. Kuz'mina, and L. I. Ostrovskii

*CHANGES IN THE PROPERTIES AND STRUCTURE OF VANES OF GAS TURBINES MADE OF NICKEL-BASE INDUSTRIAL ALLOYS DURING SERVICE IN AN EXPERIMENTAL INSTALLATION**

One of the main problems in the construction of gas turbines is to increase their service reliability. Therefore, experimental data on the material of the vanes (the most stressed parts of the turbine) are of the greatest importance.

The purpose of this work was to investigate the strength and serviceableness of industrial heat-resistant alloys EI765, EI893, EI827, and of the steel EI787.

The vanes were tested in an experimental gas turbine designed by TsNIITMASh (EGTU-1000) at 750 and 800°C for about 3000 hr.

The static stresses in the vanes were induced, taking into account the long-time strength of each alloy. The vanes were tested in the combustion products of diesel fuel which contained 0.3—0.6% of sulfur. The excess air conformed to the norms accepted for combustion chambers of gas turbines using liquid fuel. The content of ash was 0.0016%. The turbine was stopped 60 times during the experiment. The working conditions were reached 40—60 min after the turbine was started.

A study of the constructional strength of the edges of the vanes at the first stages of GTU** in a region removed from resonance showed that the nickel-base EI765, EI893 and EI827 alloys have a high static strength characterized by a coefficient

$$K = \frac{\sigma_{\text{failure}}^{\text{vane}}}{\sigma_{\text{failure}}^{\text{specimen}}} = 0.85 - 0.9.$$

The constructional strength of vanes made of EI787 steel is somewhat inferior, and has a coefficient of 0.6—0.8.

Cyclic vibration stresses of 1—2 kg/mm^2 induced in EGTU† have no influence on the constructional strength of the materials studied.

* The investigation was carried out with the participation of chief technician V.I. Dorofeeva and engineer V.F. Ivanova.

** [Gas turbine.]

† [Gas turbines driving an electric generator.]

The service reliability of vanes of gas turbines depends also on the variation in the properties of the material during service. This is especially true of the surface layers of the vane edges. The shaping of vanes made of heat-resistant alloys induces work hardening and residual stresses. Due to this state of the surface layer of the vane before service, and the fact that these layers are acted on by stresses and the flow of gases more than the core of the vanes, the structural changes in the surface layers of the metal are greater than at its core /1, 2/.

A study of the damage in the surface layers of vanes of stationary gas turbines is very important when evaluating their serviceableness.

Existing data on this problem are mainly on materials used for the production of aircraft engines /3/. The service conditions such as temperature, service life and medium (gas) of metals in aircraft engines differ greatly from those of metals in stationary gas turbines.

As already mentioned, we tested vane edges under conditions close to those of actual service. The experiments were stopped short of failure, and the vanes were removed from the disk after different times of testing.

We found that under the influence of gases the vanes became covered by dark oxide films consisting of spinel $NiO \cdot Cr_2O_3$ and chromium oxide Cr_2O_3. The duration of the test (up to 3000 hr) had no influence on the composition of these oxide films.

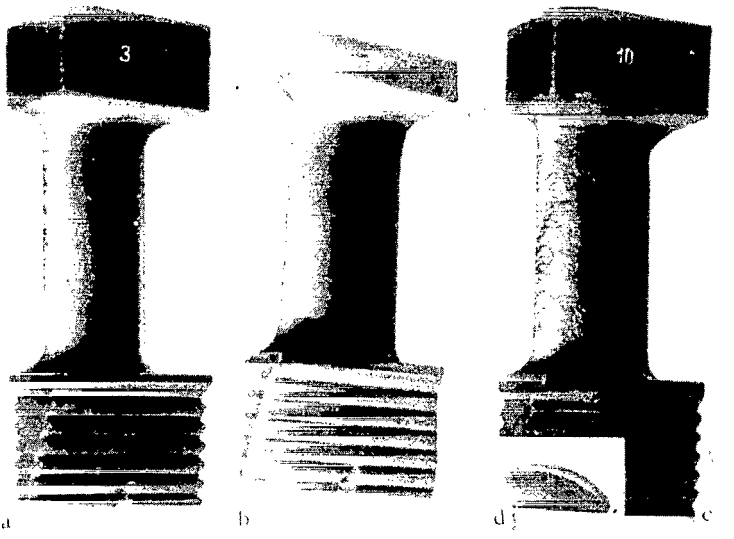

FIGURE 1. Vanes after testing in an EGTU at 750°C:

a—EI893 alloy, $\sigma = 22\,kg/mm^2$; $\theta = 500$ hr; b—EI765 alloy, $\sigma = 20-13\,kg/mm^2$; $\theta = 1834-1366$ hr; c—EI827 alloy, $\sigma = 21\,kg/mm^2$, $\theta = 1220$ hr; d—cross sectional surface area of the edge of the vanes made of EI827 alloy on the inlet edge.

The distribution of oxides on the surface of vanes as a function of the service time is different for vanes of different materials.

On vanes of EI765 and EI893 alloys the oxide film forms a thin but dense and uniform layer, irrespective of the service time.

On vanes of the EI827 alloy, however, the distribution of the oxide changes with time, and its amount is larger at the inlet and in the region of the highest temperature (Figure 1).

A cross section of this part of the vane shown in the figure was cut out from the middle region. We can see a fairly thick oxide layer around the vane at the side of the inlet edge. The penetration of the oxide into the vane varies too. The maximum depth of penetration is about 1mm.

No damage or spalling of the oxides was noticed on the vanes investigated.

An exception was one vane made of the EI827 alloy which was worked for 1220 hr at 750°C under a stress of 21 kg/mm^2. On this specimen a crack was found in the oxide layer at the edge of the vane (see Figure 2).

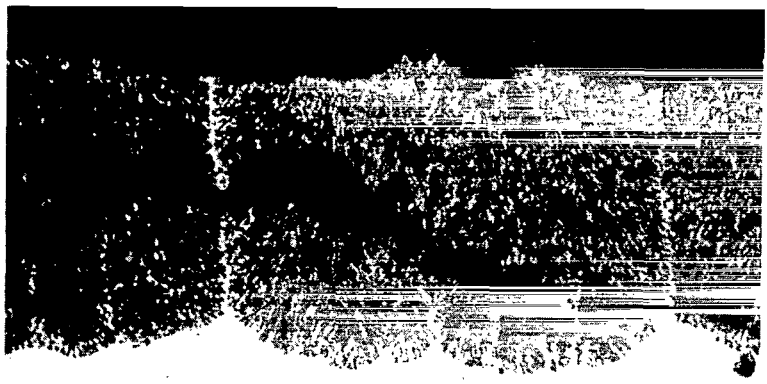

FIGURE 2. Surface layer of vane (from the side of the "back") of EI827 alloy after it has been worked in an EGTU at 750°C, ×100;

σ = 21 kg/mm^2; θ = 1220 hr.

The formation of oxides involves diffusion of alloying elements into the surface layer. As a result the layer of solid solution beneath the oxide film becomes depleted of alloying elements and this greatly influences the properties of the alloys. Thus, for example, the hardness of the oxide layer of vanes of the EI827 alloy is 420 kg/mm^2, but the hardness of the layer beneath the oxide film is only 300 kg/mm^2.

The process of oxidation is not the same in all the alloys we studied. In the EI893 and EI827 alloys the oxidation is frontal and leads to a change in the chemical composition of the metal beneath the oxide film along the grain boundaries and within the grains. The EI765 alloy is oxidized mainly along the grain boundaries (Figure 3).

The depth of the layer depleted of alloying elements in alloys is as follows:

In EI765 at 800°C the depth is 80—120μ after 956 hr
In EI893 at " " " " 60—110μ after 1036 hr
In EI827 at " " " " 500μ after 696 hr

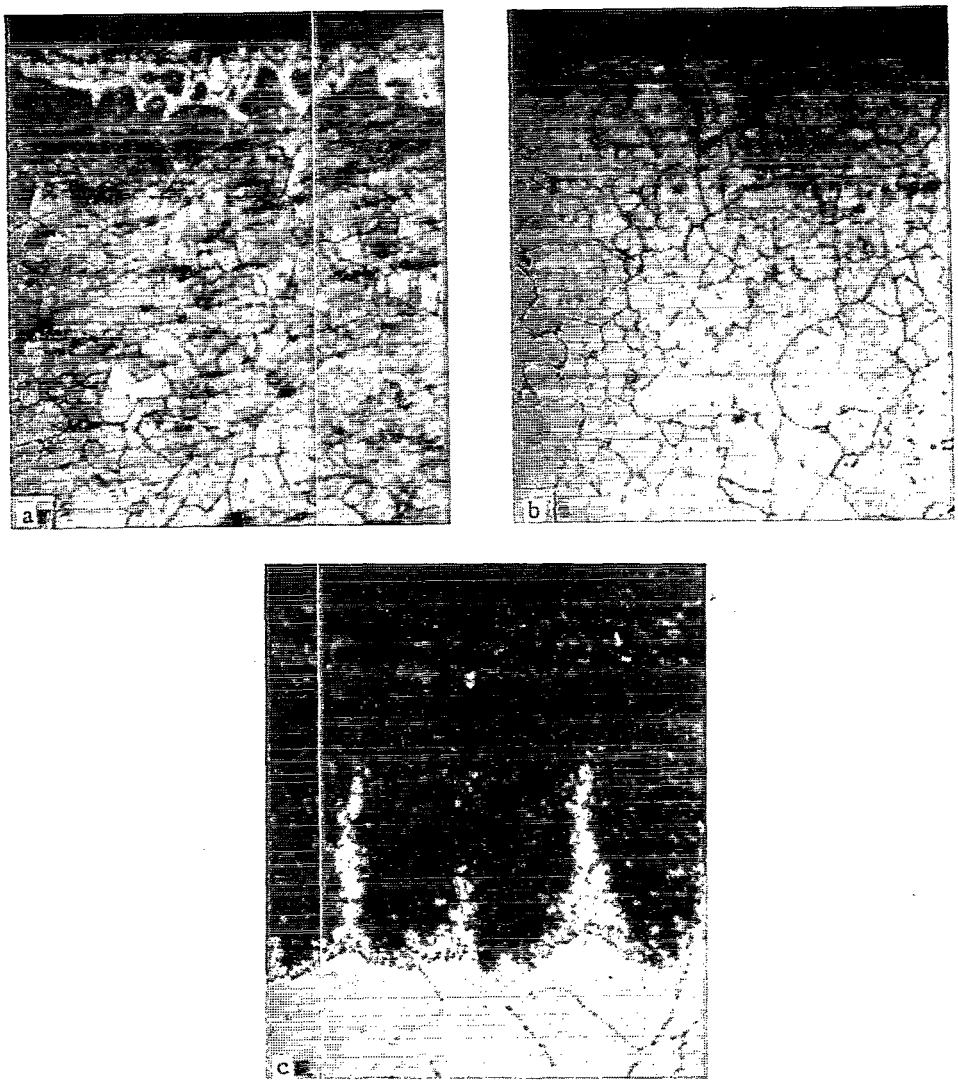

FIGURE 3. Microstructure of the surface layers of vanes (from the side of the "back") after service in an EGTU: a—alloy EI765, $T = 800°C$, $\sigma = 13\ kg/mm^2$, $\theta = 956\ hr$, ×100; b—alloy EI893, $T = 800°C$, $\sigma = 17\ kg/mm^2$, $\theta = 1036\ hr$, ×100; c—alloy EI827, $T = 750°C$, $\sigma = 25\ kg/mm^2$, $\theta = 1840\ hr$, ×200.

By chemical, spectral, and microspectral analysis of the metal of vanes, tested in EGTU, it was found that the basic changes in the chemical composition of the surface layer are caused by chromium, aluminum, and titanium. The content of these metals is lower in the surface layers than in the metal beneath them (Table 1).

The depletion took place mainly when working started. When the vanes worked at 750°C or 800°C this had almost no influence on the chemical composition of the surface layer under the conditions of the investigation.

The depth of the depleted layer increases with increase in the duration of service. But even these changes are greater at the initial stage.

An increase in the static stresses at the edges of the vanes makes the reaction between the medium and the metal of the blades more intense.

TABLE 1. Changes in the chemical composition of surface layers of vanes worked in EGTU

Alloy	Service		Chemical composition of surface layers of vanes,* %		
	T, °C	duration, hr	Al	Ti	Cr
EI765	Not worked		2.07**	1.18**	14.4**
			1.80	1.03	13.9
	750	1660	1.3	0.75	9.13
	750	3200	0.6	0.7	9.8
	800	530	1.2	0.63	Not determined
	800	746	1.15	0.67	The same
	800	1484	1.26	0.77	7.59
EI893	Not worked		1.34**	1.35**	15.9**
	800	1036	0.58	0.92	10.5
EI827	Not worked		4.3**	—	10.0**
	750	380	1.32	—	4.9
	750	1840	1.11	—	5.4

* The analysis was carried out by the spectral method. The depth of penetration of the spark, 0.01 mm.

** Certified data on the chemical composition of the alloys being investigated.

To find the strength of the surface layers and of the cores of vanes we measured the microhardness of the metal of the vanes at different cross sections.

These measurements showed that the core of the blades remains stronger during service than the surface layers.

A study of the mechanical properties of the metal of the vane edges working in a turbine showed that the medium of the GTU has an appreciable influence on the strength of materials working at 750—800°C.

For the mechanical tests we used flat microspecimens 5 mm long and with a 1.5 × 0.5 mm surface area. These were cut from the surface layers of the vane edges. On one side of the specimens we left the layer of worked metal.

It was found that after 2000 hr of service at 750°C the short-time strength of EI765 and EI827 alloys remained relatively high, but the elongation decreased by about 30%.

After working in EGTU at 800°C the short-time mechanical properties of the same metal of the surface layers decreased by about 60% (Figure 4).

A comparison of the experimental results obtained with microspecimens and with standard specimens (diameter 6 mm) shows the influence of the dimensional factor on the short-time ductility. The ductility of microspecimens is only $\frac{1}{3}-\frac{1}{2}$ of that of standard specimens. Nevertheless, the absolute short-time ductility is high.

A study of the short-time mechanical properties of vanes aged for 5000 hr in the air without a load showed that there is no difference in the short-time

strength ($\sigma_в$) and in ductility (δ) of microspecimens of different surfaces (Table 2).

All alloys have a high ultimate strength of more than 100 kg/mm^2. The elongation is not less than 6%.

When the same alloys are tested in an atmosphere containing the products of combustion of diesel fuel (0.3—0.6% of sulfur), it is found that the strength and the ductility decrease after a shorter time than that given above, particularly at a temperature of 800°C.

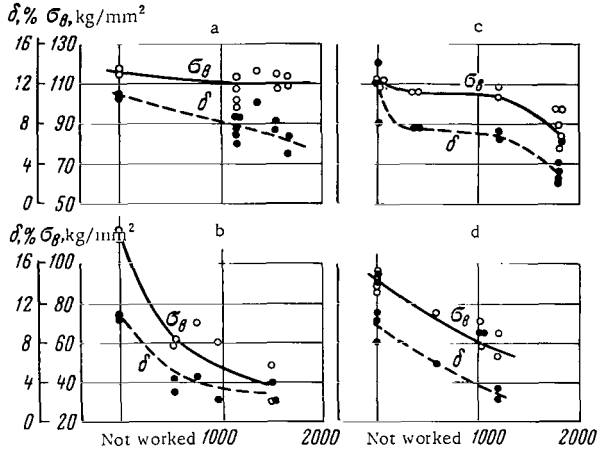

FIGURE 4. Variation in the short-time mechanical properties of the metal of the surface layers of vanes working in an EGTU:

a—EI765 alloy; T_{work} = 750°C; b—the same, T_{work} = 800°C; c—EI827 alloy, T_{work} = 750°C; d—EI893 alloy, T_{work} = 800°C.

TABLE 2. Short-time mechanical properties of heat-resistant alloys after prolonged aging in the air at elevated temperatures

Alloy	Process of aging		State of the surface of the specimens	Mechanical characteristics	
	T, °C	duration, hr		$\sigma_в$, kg/mm^2	δ, %
EI765	750	5000	Covered by oxide film	117.8	7.8
	750	5000	The same	110.9	6.3
	750	5000	With no film	116.4	8.3
	750	5000	The same	115.5	9.1
EI893	750	5000	Covered by oxide film	107.4	9.1
	750	5000	The same	106.9	7.4
	750	5000	With no film	101.6	5.4
	750	5000	The same	92.2	6.3
EI827	800	5000	Covered by oxide film	104.1	6.2
	800	5000	The same	106.2	6.6
	800	5000	With no film	106.3	6.7
	800	5000	The same	113.9	8.5

TABLE 3. Comparative data on the serviceableness of blades under conditions of EGTU TsNIITMASh

Alloy	Service conditions of vanes			Depth of the layer in which changes have taken place, measured by the metallographic method, μ	Microhardness, kg/mm²				Mechanical properties of surface layer		Variation in chemical composition of surface layer, %		
					surface		core				initial	after service	
	T, °C	σ_B, kg/mm²	θ, hr		initial	after service	initial	after service	σ_B, kg/mm²	δ, %	Al	Ti	Cr
EI765	800	13	956	60—120	500	350	500	425	61.0	2.0	—	—	—
	800	14	1484	60—110	500	350	500	400	49.3	3.7	1.80/1.26	1.03/0.77	13.9/7.6
EI893	800	17	1036	30—110	425	300	425	350	58.1	9.1	1.34/0.52	1.35/0.92	15.9/10.5
									71.5	9.1			
	800	19	1211	40—60	425	370	425	425	65.7	3.4			
									53.4	2.2	—	—	—
EI827	800	23	696	500	480	350	480	500	—	—	—	—	—
	750	23	1840	not determined					77.8	2.1	4.3/1.11	—	10.0/5.4
									83.9	6.4			

Comparative data on the properties which characterize the serviceableness of the three materials studied under conditions of service in an EGTU are given in Table 3.

These data show that the strength of the metal can be appreciably reduced mainly due to oxidation of the surface layers of the vanes, but also because the alloy becomes depleted of aluminum and titanium, the chief components of the γ'-phase that strengthen alloys of this type.

The EI827 is the most heat resistant of the three alloys we studied, but is the least resistant under conditions of service in EGTU in the combustion products of diesel fuel.

Service in this medium leads to a considerable change in the chemical composition of the metal (depletion of aluminum). The depth to which these changes reach can vary appreciably (by a factor of approximately 4—5).

An oxide layer which penetrates deep into the metal of the vane (up to 1 mm at a maximum thickness of the vane of 6 mm) indicates that the metal can fail prematurely, particularly if the generator is stopped often as in transport turbines and at the peaks of GTU.

The data we give show that the problem of heat resistance of turbine vanes and of the long-time strength of alloys for prolonged stationary service in GTU is of great significance and very important for increasing the reliability of vanes.

Bibliography

1. Parfenov, V.A.—Teploenergetika, No. 5. 1956.
2. Kolomytsev, P.T., A.A.Samgin, and A.Ya.Snetkov.—Metallovedenie i Termicheskaya Obrabotka, No. 9. 1960.
3. Sporyagina, N.M., A.A.Zhukova, and Z.D.Kharitonova.—Aviatsionnaya promyshlennost', No. 4. 1963.
4. Parfenov, V.A.—Teploenergetika, No. 9. 1957.

E.E.Levin, E.M.Pivnik, M.G.Taubina, D.B.Livshits, and E.F.Trusova

SOME PROBLEMS OF ALLOYING NICKEL-BASE ALLOYS

At service temperatures above 750°C the diffusion processes within the solid solutions, between the precipitates, and also on the surface of the article at the metal—gas interface are so great that it becomes exceedingly difficult to maintain the proper strength, ductility, and toughness of the alloys. The problem of choosing the proper heat-resistant alloy is thus rather difficult.

For our investigations, we chose three alloys: the EI617, EI826, and EI827 alloys.

From a comparative study of these three alloys, we chose a stepwise heat-treatment process. The metal is heated at 1180°C for 6 hr, cooled in

the air to 1000°C, held at this temperature for 4 hr, further cooled together with the furnace to 900°C, held at this temperature for 8 hr, cooled together with the furnace to 850°C, held at this temperature for 15 hr, and then finally cooled in the air. This heat treatment increases the deformability of the alloys during long-time strength tests /2/.

The chief strengthening phase in the three alloys is the γ′-phase. The composition of the γ′-phase is determined by the content of aluminum and titanium in the alloy, and therefore the γ′-phase in the EI827 alloy consists of Ni_3Al, and in the EI826 and EI617 alloys it is $Ni_3(Ti, Al)$. Aluminum influences the content of the γ′-phase more than titanium (Table 1).

TABLE 1. Content of the γ′-phase in EI617, EI826, and EI827 alloys (1180°C, 6 hr; +1000°C, 4 hr; +900°C, 8 hr; +850°C, 15 hr)

Aging		Alloy EI617	Alloy EI826	Alloy EI827
°C	time, hr			
—	—	16.3	24.2	29.8
750	1000	23.0	27.0	42.0
800	1000	22.3	25.0	41.2
850	1000	18.4	27.0	—

A comparison of the EI826 and EI827 alloys shows that if part of the aluminum is substituted by titanium, the content of γ′-phase in the EI826 alloy decreases. The EI827, EI826, and EI617 alloys contain several elements, and therefore heat treatment and aging produces various carbides in them besides the γ′-phase, the chief one being the chromium-base $Me_{23}C_6$ carbide. Alloying with molybdenum and tungsten leads to the formation of other binary carbides $Me^1_nMe^2_mC$, where Me^1_n is Ni or Cr, and Me^2_m is Mo or W. The chromium base $Me_{23}C_6$ carbide and the binary carbide are of the same type, and have a cubic lattice with similar parameters.

The field of the $Me_{23}C_6$ carbide is very much influenced by the content of chromium in the alloy. In the EI827 alloy the $Me_{23}C_6$ carbide exists during the early stage of aging at 800°C only (up to 500 hr), and then it is completely transformed into a binary carbide. An increase in the content of chromium in the EI826 alloy to 14—15% and the presence of titanium widen the field in which $Me_{23}C_6$ exists. This carbide is stable even at a temperature of aging of 850—900°C for more than 5000 hr (Figure 1).

At all aging temperatures we found that the EI827 and EI826 alloys contain a boride phase *T*; in the literature the formula is given as Me_4B_3 /3/. This phase is produced during quenching and remains unchanged during the process of aging at 600—900°C.

Directly after heat treatment the average size of the γ′-particles is about 0.20—0.25 μ, but after 5000 hr of aging at 800°C these particles grow to 0.34 μ in EI826 alloys and to 0.57 μ in EI827 alloys.

Aging at 600—650°C leads to coagulation of the precipitate particles, chiefly along the grain boundaries. Etching showed that these particles are carbide and are acicular in shape. This is particularly true of the EI617 alloy. The unfavorable shape of these carbides decreases the impact strength and the ductility of the metal during long-time strength tests.

If the temperature of aging is increased from 700 to 850°C the γ′-phase particles become coagulated.

It is very important to note that at these temperatures of aging the individual large carbide particles along the grain boundaries of EI826 and EI827 alloys are separated by coagulated particles of the γ′-phase.

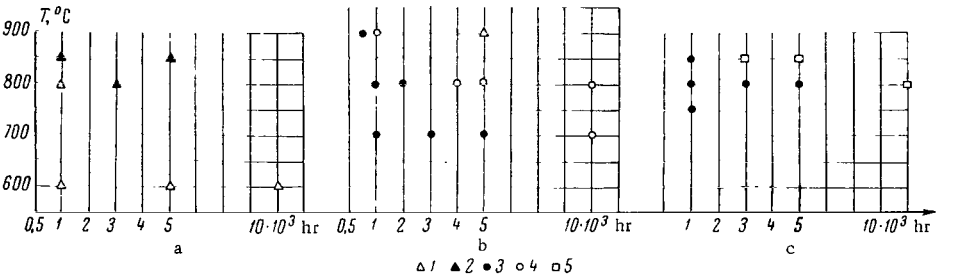

FIGURE 1. Field of existence of complex carbides $Me_{23}C_6$ and $Me_n^1Me_m^2C$ in EI617(a), EI826 (b), and EI827 (c) alloys.

It has been experimentally found that the strength of all three alloys at room and elevated temperatures is almost identical. The EI826 alloy has a higher ductility at 650—850°C.

The ductility of alloys decreases at room temperature as a result of aging. The EI617 alloy has its lowest ductility at 650—700°C. The ductility of EI826 and EI827 alloys is greatly decreased by aging at 700—750°C and the elongation and reduction of area are decreased to 6—8%.

Thus, the coagulation of the γ′-phase at these temperatures and the accompanying softening of the solid solution leads to an increase in the ductility at room temperature only. At elevated temperatures at which the importance of the solid solution in the vicinity of the grain boundaries and of the grain boundaries themselves increases, the ductility of the alloys is low.

The impact strength of all three alloys is decreased to 1—1.5 kgm/cm² by aging at 600—650°C. The impact strength at elevated temperatures is about twice that at room temperature.

We evaluated the deformability and the manner of failure of the alloys by determining their ductility by means of tensile tests at a constant rate of deformation of 0.8%/hr.

To determine the influence of aging on the nucleation and development of cracks, we investigated the process of failure of specimens that had been aged at 850°C for 1000 hr in order to coarsen the particles of the carbide and intermetallic phases, particularly along the grain boundaries. When the EI617 alloy was aged at 850°C for 1000 hr, its ductility was reduced to 3% at a testing temperature of 750—800°C. Figure 2, a shows a photomicrograph of a specimen of this alloy produced by the method of color transformation /4/. The intergranular crack passes along the boundary between the carbide, γ′- and γ-phases, and also between the fractions of carbide particles broken during deformation of the specimen. The crack is continuous without branches leading into the interior of the grain, and no visible traces of deformation or of any upsetting of continuity could be

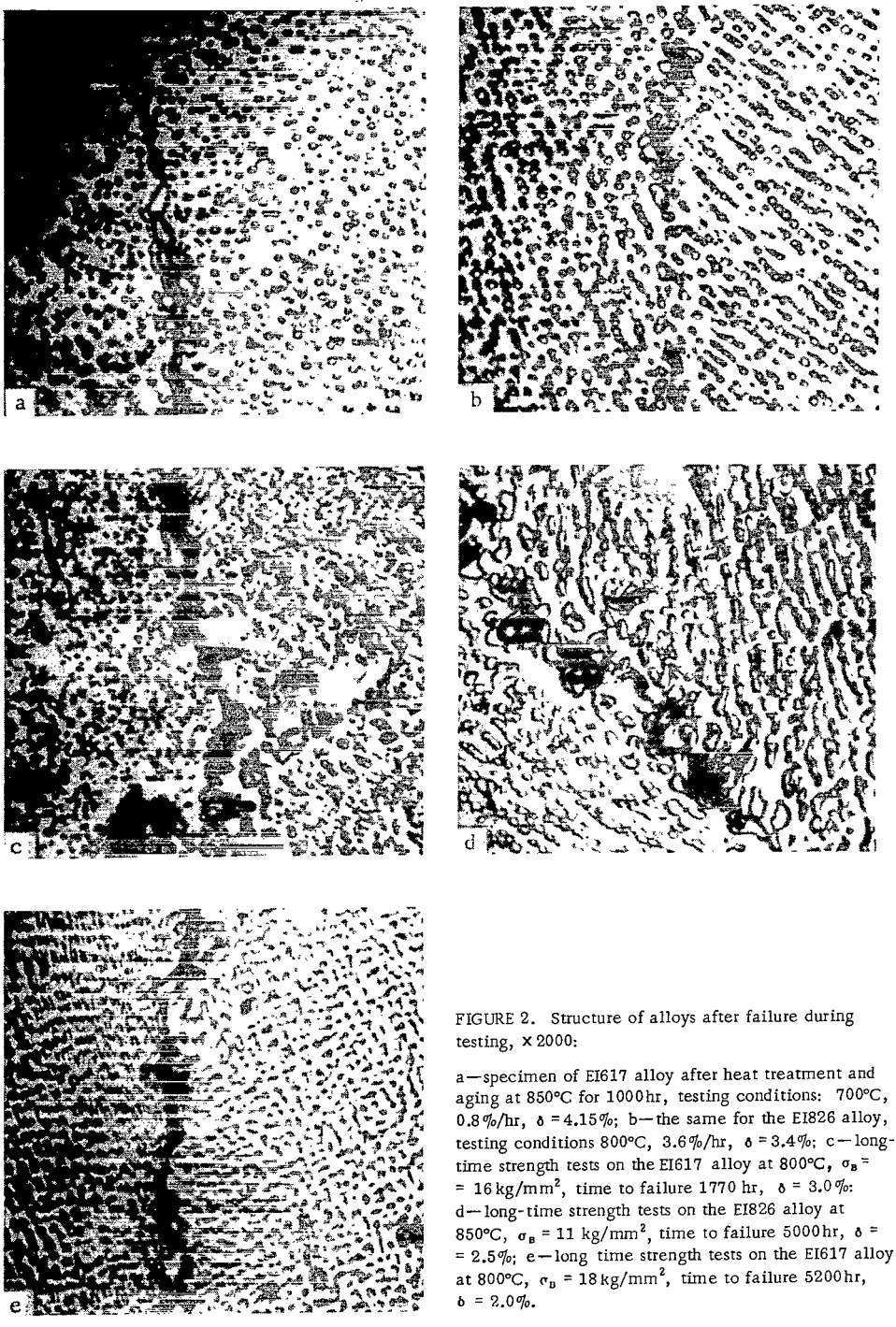

FIGURE 2. Structure of alloys after failure during testing, × 2000:

a—specimen of EI617 alloy after heat treatment and aging at 850°C for 1000 hr, testing conditions: 700°C, 0.8%/hr, δ = 4.15%; b—the same for the EI826 alloy, testing conditions 800°C, 3.6%/hr, δ = 3.4%; c—long-time strength tests on the EI617 alloy at 800°C, σ_B = = 16 kg/mm^2, time to failure 1770 hr, δ = 3.0%: d—long-time strength tests on the EI826 alloy at 850°C, σ_B = 11 kg/mm^2, time to failure 5000 hr, δ = = 2.5%; e—long time strength tests on the EI617 alloy at 800°C, σ_B = 18 kg/mm^2, time to failure 5200 hr, δ = 2.0%.

found within the grains. Such cracks lead to failure at a relatively low level of accumulated deformations.

Under similar conditions, the ductility of the EI826 alloy is considerably higher, $\delta = 7\%$.

The crack nucleating in the zone of carbide particles is stopped by barriers consisting of grain boundaries, mainly of the γ'-phase, which has a crystal lattice and parameters similar to those of the solid solution (Figure 2, b). As a result, a considerably high deformation is accumulated before failure takes place.

The long-time strength of these alloys was studied at 650°C, 700°C, 800°C, and 850°C and some tests lasted up to 10,000 hr (Table 2).

TABLE 2. Ultimate long-time strength of alloys studied

Alloy	Ultimate long-time strength, kg/mm²							
	700°		800°		850°		900°	
	5000 hr	10000 hr	5000 hr	10000 hr	5000 hr	10000 hr	5000 hr	10000 hr
EI617	24	19	13	12.5	—	—	—	—
EI826	39	36	19	17	11	—	—	—
EI827	40	37	17	15	10	—	—	—

The results showed that the EI826 alloy has certain advantages over the EI617 and EI827 alloys at testing temperatures of 800—850°C.

The elongation, determined by long-time strength tests, which is directly connected with the reliability of the material, indicates that the EI826 alloy is much superior to the other two at both 800 and 850°C (Figure 3). A microscopic study of the specimens, tested for long-time strength, clearly illustrates this. Figure 2, c shows the structure of the EI617 alloy close to the spot where the specimen failed at 800°C ($\sigma = 16$ kg/mm² after 1777 hr of testing). The cracks which nucleated at the grain boundaries where carbides accumulate develop chiefly within the grains of the solid solution close to the grain boundaries. In the same way as metal aged at 800°C for about 2000 hr, these specimens are somewhat softened and quite ductile, and the cracks develop at a rate which ensures an accumulation of deformation of $\delta = 3\%$.

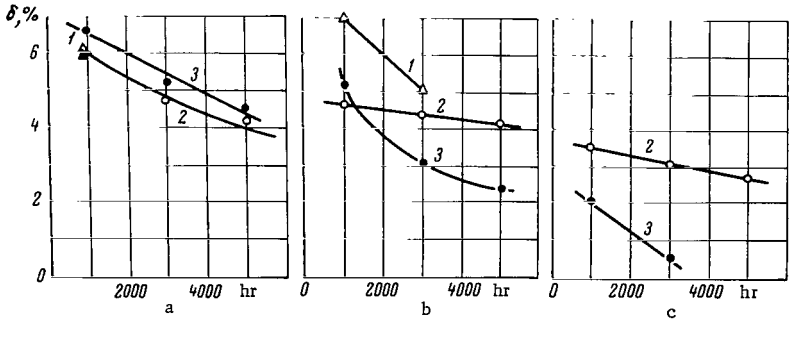

FIGURE 3. Elongation caused by failure of alloys during long-time strength tests:

a—at 750°C; b—800°C; c—850°C; 1—EI617; 2—EI826; 3—EI827.

Figure 2, d is interesting, as it shows the structure of an EI826 specimen tested at 850°C for more than 5000 hr at $\sigma = 11\ kg/mm^2$. The advanced aging under these conditions produced a relatively favorable combination of the strength of the basis solid solution and of the intergranular layers. The latter consist of thin chains of carbides separated by large regions of the dispersed γ'-phase with particles of similar shape and commensurable with the intragranular precipitates of the γ'-phase, or with the irregular large particles of this phase. Under these conditions the beginning of failure leads to the formation of separate pores near the coarse particles of the carbides or γ'-phase. The development of these pores and their combination into cracks is sufficiently slow to accumulate a deformation of 2—3%.

The failure of EI827 alloys is somewhat different (Figure 2, e). The cracks are straight and pass exactly along the intergranular layers consisting of the binary carbide Me_6C and the boride phase.

A decrease in the content of chromium in this alloy leads to the formation of chains of binary carbide particles along the grain boundaries, and since there are no coarse particles of a γ'-phase the conditions are favorable for an accelerated development of nucleated cracks. Therefore, the specimen fails in a brittle manner. At 850°C, $\sigma = 10\ kg/mm^2$, but this value can decrease by 0.56%. At this stage of investigations, a microscope study of failed specimens confirms our theory on the influence of the phase composition and structure on the ductility of alloys during long-time tensile tests.

CONCLUSIONS

Nickel-chromium base alloys which after heat treatment contain 25—30% of the chief strengthening γ'-phase can be used for service at about 800°C.

An important condition for the proper combination of heat resistance and ductility is uniform distribution of the strengthening γ'-phase in the bulk of the grains of the solid solution, and similarity in the size of particles of the γ'-phase and carbides which form intergranular layers. The carbide particles should be separated by particles of the γ'-phase. These conditions are largely satisfied in alloys containing both aluminum and titanium.

For service at 850—900°C, heat-resistant alloys containing cobalt are used today. In these alloys the high heat resistance is ensured by the formation of about 40% of the γ'-phase, preferably of the $Ni_3(Ti, Al)$ type. The content of alloying elements should prevent or inhibit the formation of the $(Ni, Co)_7(W, Mo)_6$ phase, which decreases the ductility and long-time strength under conditions of service.

Bibliography

1. Khimushin, F.F. Zharoprochnye stali i splavy (Heat-Resistant Steels and Alloys).—Moskva, Metallurgiya. 1964.
2. Levin, E.E. and E.M. Pivnik. Issledovaniya po zharoprochnym splavam (Investigations of Heat-Resistant Alloys), 8.—Izdatel'stvo AN SSSR. 1962.

3. Blok, I.I., M.N. Kozlova, N.F. Lashko, and K.P. Sorokina.— Zavodskaya Laboratoriya, No. 9. 1959.
4. Levin, E.E. Mikroskopicheskoe issledovanie metallov (Microscope Studies of Metals).—Mashgiz. 1955.

O.A. Bannykh, I.F. Zudin, R.M. Volkova, Yu.K. Kovneristyi, M.V. Pridantsev, E.D. Surovtseva, and G.A. Sgibneva

STUDY OF THE STRUCTURE AND PROPERTIES OF EP357 STEEL

The 45Kh10G14Yu2 (EP357) steel is an austenitic material containing no nickel, and its heat resistance is not inferior to that of a number of chromium-nickel austenitic steels.

EP357 steel has been suggested for constructing steam superheaters for service at 610—630°C, instead of the nickel-alloyed 1Kh18N10T and 1Kh18N12T steels.

This work brings some results of a study on 45Kh10G14Yu2 tubes (32 × 6 mm) produced by the Southern Pipe Plant (Nikopol').

The EP357 tubes we investigated were quenched in water from 1070°C.

The microstructure studied on two tubes consisted of austenite (grain size 6—7 on the standard scale) with a certain amount of carbides. Apparently, heating the tubes for austenitizing was insufficient to dissolve the carbides completely.

We carried out numerous mechanical tests and technological studies to find whether these tubes can be used for the production of steam superheaters.

The tubes were bent to an angle of 180° at a radius of 75 mm on a bending machine. No defects were found on the external or internal surfaces of the bends. The bending increased the hardness of the stock by 80—90 Brinell units to 255—259 kg/mm^2.

To determine the influence of cold working on the mechanical properties of the tubes, straight tubular specimens were drawn to a 20% elongation. This is equal to the maximum deformation of the extended sections of the bends.

A number of cold-worked specimens were given to the following heat-treatment processes:

a) austenitizing at 1050°C for 30 min, and quenching in water;

b) heating to 950°C, holding for 1 hr, and cooling in the air.

Table 1 shows the results of tensile tests on cold-worked and heat-treated specimens.

Cold working considerably increases the ultimate strength and particularly the yield strength of the steel, but the ductility and the toughness remain quite high.

Heating to 1050°C leads to a partial dissolution of carbides and recrystallization of the austenitic matrix. In this case, the carbides form individual coarse particles or groups of particles, which are not associated with the

boundaries of the austenitic grains. After the steel is heated to 950°C, most of the carbon is bound into carbides which are usually strung out along the grain boundaries and the slip bands of the austenite.

The presence of carbides in the heat-treated steel caused the impact strength to be rather lower than that of the delivered or of the cold-worked steel. The decrease in impact strength was greatest on heating to 950°C.

EP357 steel was resistance welded by processes accepted for austenitic steels, and deburred with a mandrel. No welding defects were found in the cross-sectional specimens of the welded articles.

TABLE 1. Results of tensile tests on cold-worked and heat-treated specimens

State of material	σ_B, kg/mm^2	$\sigma_{0.2}$, kg/mm^2	δ, %	a_k, kgm/cm^2	H_B, kg/mm^2
As delivered	80.0	43.5	58.0	23.0	180
Drawn to a 20% elongation	100.5	80.5	31.0	17.0	229
Drawn to a 20% elongation + austenitized at 1050°C	72.0	35.0	54.5	14.1	156
Drawn to a 20% elongation + heated to 950°C	72.5	44.5	52.0	10.0	170

Of four welded tensile specimens three failed along the zone of melting, and their strength was 66.5—68.0 kg/mm^2 and the fourth specimen failed along the basis metal (σ_B = 71.0 kg/mm^2).

When rings 25 mm high, cut out of the welded tubes, were upset until the internal diameter was half the external diameter, no cracks or other external defects were formed.

The microstructure of a welded joint is shown in Figure 1. The zone of melting (Figure 1, a) consists of small grains of austenite separated by a thick discontinuous network. This network also contains austenite, but this was formed during cooling after welding as a result of the decomposition of the σ-ferrite in steel above 1350°C.

Austenite grains with wavy boundaries (Figure 1, b) can be seen on sections of the tubes which had been plastically deformed during contact welding. Some austenite grains consist of fragments, surrounded by small carbide particles.

The metal in the zone of thermal influence consists of austenite grains with carbide particles at its boundaries (Figure 1, c). The metal of this zone was heated to a temperature sufficiently high for precipitation of carbide particles.

An X-ray analysis of the zone of melting and of the adjacent regions revealed the presence of stresses of the second type equal to 10—12.5 kg/mm^2.

Thus, it has been found that tubes of EP357 (45Kh10G14Yu2) steel can be used to produce steam superheaters.

Since EP357 steel has a higher carbon content than ordinary boiler steel, it can be expected that it will also have rather different mechanical properties after prolonged heating at elevated temperatures (550—700°C). Therefore, when determining the usefulness of EP357 steel, it is most important to find under what conditions its properties change.

We studied the variation in the structure and impact strength of this steel after it had been heated at 610, 650 and 700°C for up to 3000 hr.

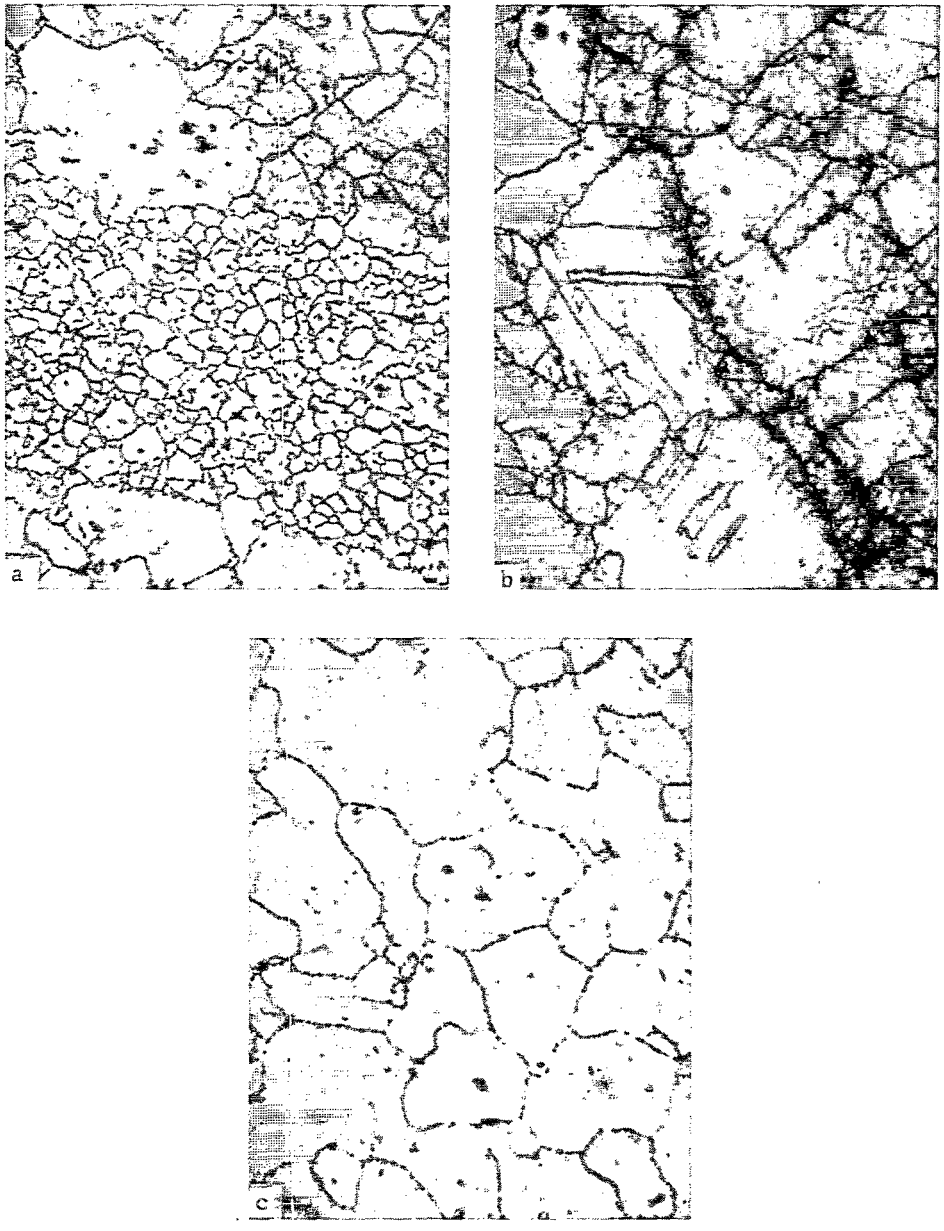

FIGURE 1. Microstructure of joints made by resistance welding, X 400:

a—in the zone of melting; b—in the zone of plastic deformation; c—in the zone of the thermal influence of welding.

The impact strength of tubular specimens dropped considerably during the first 500 hr of heating at these temperatures. Further heating up to 2500 hr did not decrease the impact strength which remained stable (2.3—4.0 kgm/cm^2 (Figure 2)).

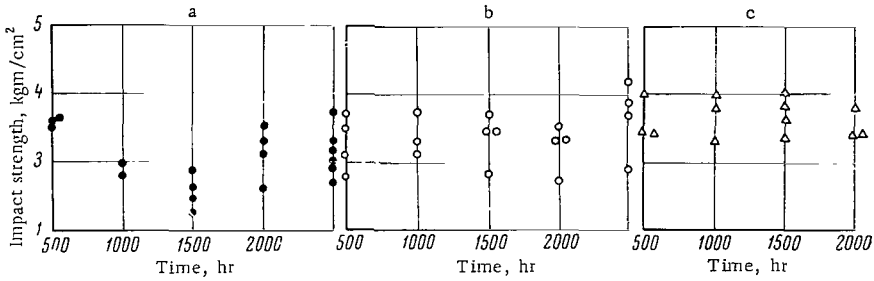

FIGURE 2. Influence of time of heating at various temperatures on the impact strength of EP357 steel: a—610°C; b—650°C; c—700°C.

After 3000 hr of heating the impact strength at 20°C was equal to 2.6—3.5 kgm/cm^2, and at 630°C to 4.0—5.5 kgm/cm^2. More detailed data are given below:

Aging temperature, °C	610		650		700		
Impact strength at 20°C, kgm/cm^2	2.6	3.4	3.5	3.7	3.2	2.6	3.5
The same at 630°C, kgm/cm^2	4.7		5.5	4.9	4.0	4.6	

A study of the microstructure (Figure 3) showed that the reason for the decrease in the impact strength of this steel is the precipitation of carbides from the γ-solid solution.

Heating at 650°C for 50 hr led to the formation of layers of carbide particles between the austenite grains. Figure 3, a shows a network of carbides along the boundaries of the austenite grains and also carbide particles aligned along the slip planes within the austenite grains. A certain amount of ferrite can be found in the carbon-depleted regions adjacent to the carbide network.

After 500 hr heating at 650°C (Figure 3, b) carbide particles can be clearly seen along the boundaries of austenite grains and in the adjacent zones. Carbides are also formed within the austenite grains.

After 1500 hr of heating at 650°C the carbide particles were nearly uniformly distributed within the austenite grains (Figure 3, c), and the content of carbide particles at the boundaries of the austenite grains decreased. A certain coarsening of the carbide particles and alignment can be seen in Figure 3, d.

An X-ray phase analysis showed that 1000—3000 hr of aging had almost no influence on the content of ferrite in the steel (5—8%).

X-ray analysis of precipitates separated electrolytically from aged EP357 steel showed that the chief structural component of these precipitates is the cubic $Me_{23}C_6$ carbide. Local X-ray spectral analysis with the "Kameka" apparatus gave the content of chromium in these carbides as 30—35% and in ferrite 6—7%.

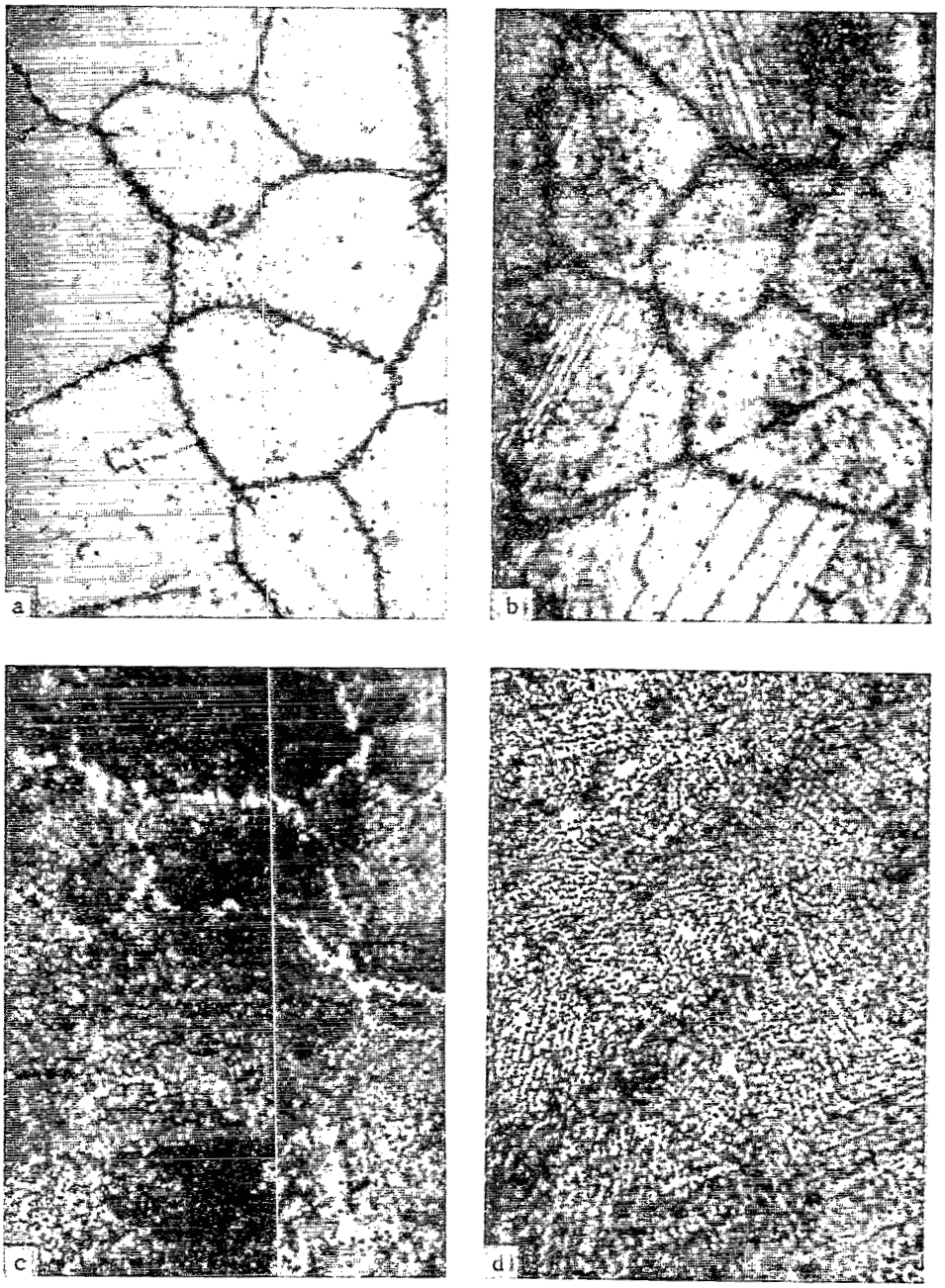

FIGURE 3. Variation in the microstructure of EP357 steel during heating at 650°C, × 600:
a—50 hr; b—500 hr; c—1500 hr; d—3000 hr.

If chromium is distributed thus between the carbide and the ferrite, a σ-phase is rather improbable in EP357 steel after long aging processes.

X-ray phase analysis revealed a certain increase in the content of the α-phase in the zone of failure of impact specimens aged for 500—3000 hr (up to 15—20% just on the surface of the fracture). Obviously, cold working can lead to a martensitic transformation in the austenite of EP357 steel which has been depleted of carbon. Apparently, the formation of martensite during failure of the specimens is one of the reasons why the impact strength of aged specimens is lower at 20°C than at 630°C, i.e., above the point at which martensitic transformation during deformation can take place (see above).

The specimens cut out from tubes were tested for long-time strength at 610, 630, 650 and 700°C.

We tested 20 specimens, and the tests lasted for from 100 to 2000 hr.

The results were processed by the Larson-Miller method. The existence of an unequivocal dependence of the parameter $T(20+\log\tau)$ on stresses (from 50 to 12 kg/mm²) (T is the absolute temperature, °K; τ is the time to failure, hr), and the absence of scattering of the results irrespective of the temperature, indicate that the ultimate long-time strength can be quite accurately calculated from the data obtained. The calculated ultimate long-time strength over a range of temperatures of from 550 to 700°C are given in Table 2.

TABLE 2. Calculated values of long-time strength

Temperature, °C	σ_{LT}, kg/mm²			
	100 hr	1000 hr	10,000 hr	100,000 hr
550	44.0	38.0	31.00	24.0
600	35.0	28.0	19.0	14.0
650	26.0	19.0	11.0	4.5
700	17.0	9.5	3.0	—

All specimens tested for long-time strength had an elongation of not less than 6%.

Our experiments showed that testing experimental coils made of EP357 (45Kh10G14Yu2) tubes would be useful.

The influence of phosphorus on the properties of EP357 steel is of great practical interest. During the first experimental melting of this steel manganese was added to the charge. If electric furnace ferromanganese is used instead of manganese metal, a certain increase in the content of phosphorus in the steel is observed, but the cost is lower.

If the content of phosphorus in the steel is increased from 0.008 to 0.043%, the strength is increased and the ductility and toughness decrease slightly (Figure 4). The strengthening influence of phosphorus is retained even at 630—700°C.

The presence of up to 0.04% of phosphorus in EP357 steel considerably increases the high-temperature strength (increase in time to failure and decrease in creep rate).

The increase in the creep resistance is accompanied by a decrease in ductility (elongation).

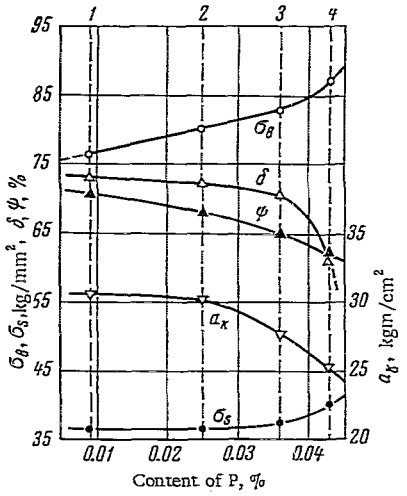

FIGURE 4. Influence of phosphorus on the strength and ductility of EP357 steel.

Small additions of boron to heat-resistant steels have a beneficial influence on the ductility of specimens tested for long-time strength.

The influence of phosphorus and boron on the high-temperature strength of EP357 steel ($\sigma = 18$ kg/mm^2, $t = 630$°C) is shown in Table 3.

At a concentration of 0.0005—0.004%, boron, which decreases the grain size of austenite, somewhat increases the creep rate of steel. The addition of 0.007% B leads to an appreciable increase in both the time to failure and the creep resistance, despite the fact that the grain size of austenite is almost the same as that of steel with 0.004% B.

The addition of boron changes the manner of failure of specimens during long-time strength tests. Specimens with a high content of phosphorus, tested at $\sigma = 18$ kg/mm^2 and $T = 630$°C failed along the grain boundaries, steel specimens containing 0.008% P failed chiefly along the grain boundaries but also in an intragranular manner (Figure 5, a). Steel containing boron failed in an intragranular manner (Figure 5, b).

FIGURE 5. Fracture surface of EP357 steel tested for long-time strength at 630°C and $\sigma = 18$ kg/mm^2: a—without boron; b—with 0.004% boron.

It is interesting to note that the coefficient of strengthening by drawing steels containing 0.008 — 0.025 and 0.036% P is almost the same, but it increases appreciably if the content of phosphorus is increased to 0.043%. From this increase in the coefficient of strengthening it can be assumed that steel with 0.043% P contains phosphides, which hamper the movement of dislocations to the surface or their elimination during plastic deformation, and thus facilitate the accumulation of dislocations in the metal.

Due to the small number of phosphide particles and their small size it is difficult to detect them in a steel with 0.043% P. However, phosphides have been found in steel containing 0.13 — 0.20% P by means of metallographic and local X-ray spectral analysis.

Steel without boron and steel containing 0.0005% B have the same coefficients of strengthening but steel with 0.004% boron has a considerably higher coefficient. An increase in the content of boron to 0.007% leads to an increase in the coefficient of strengthening. This increase cannot be due to the distortion of the crystal lattice of austenite by the atoms of boron. Earlier studies /1/ showed that a variation in the content of carbon in the γ-solid solution of 0.1 — 0.2% has almost no influence on the coefficient of strengthening. The most probable reason for the strengthening influence of boron and phosphorus is the formation of a boride phase.

TABLE 3. Influence of phosphorus and boron on the high-temperature strength of EP357 steel

Addition of phosphorus and boron, %	Time to failure, hr	δ, %	ψ, %	Steady-state creep rate, (% hr)·10^3
Initial (0.008P)	1530	5.72	9.76	2.46
0.025P	2260	4.75	7.95	1.00
0.036P	4248	4.73	12.82	0.50
0.043P	4613	3.42	3.00	0.31
0.0005B	1291	6.80	11.21	3.29
0.004B	2362	8.42	17.66	2.99
0.007B	3599	10.20	19.51	1.37

A certain decrease in the high-temperature strength of EP357 caused by the addition of 0.0005% of boron is possibly due to the refining influence of boron and the fact that this element depletes the γ-solid solution of some alloying atoms such as nitrogen, etc.

Thus, a certain decrease in the ductility of EP357 steel caused by an increase in the content of phosphorus can be compensated by adding small amounts of boron to the steel.

It would be interesting to investigate whether electric furnace ferromanganese with a medium carbon content could be added to EP357 steel instead of metallic manganese, and what the technological properties of such a steel would be.

Bibliography

Bannykh, O.A., Yu.K.Kovneristyi, and I.F.Zudin. Khromomargantsovistye teploustoichivye stali s alyuminiem (Chromium-Manganese Heat-Resistant Steels Containing Aluminum), p. 33.— Izdatel'stvo "Nauka." 1965.

I. L. Mirkin, Z. N. Petropavlovskaya, and I. A. Shchenkova

INFLUENCE OF ALLOYING ELEMENTS ON THE STRENGTH OF INTERATOMIC BONDS OF FERRITE, THE COMPOSITION AND TYPE OF STRENGTHENING PHASES, AND THE RESISTANCE OF STEEL TO STRESS RELAXATION

Detailed studies recently carried out to develop new heat-resistant materials showed that alloying, particularly by several elements, has a great influence on the heat resistance of steel. However, a high total content of alloying elements is not necessarily related to the heat resistance of steel. Sometimes an increase in the content of alloying elements does not increase the heat resistance of steel, but on the contrary decreases it. For proper alloying a study of the interatomic forces in the lattice of α-Fe is very important. It has been found /1, 2, 3/ that the location and shape of the line representing the start and finish of the polymorphic transformation on the iron—alloying element phase diagram influence the creep and relaxation of such alloys. Despite the fact that the strength of interatomic bonds is one of the chief factors determining the heat-resistance of steels and alloys, the dependence of the resistance to stress relaxation on the interatomic forces in the lattice of ferrite has so far been insufficiently studied.

Since most heat-resistant steels are precipitation hardening alloys, their properties are greatly influence by the composition of the solid solution and the state of the strengthening phases /4, 5/.

The role of strengthening phases during the relaxation of stresses at elevated temperatures has not yet been thoroughly studied. In this work we shall discuss the results of a study of the process of stress relaxation in binary and more complex iron-base alloys containing different types of strengthening phases.

To study the dependence of the properties of ferrite on the content of alloying elements we prepared heats containing not more than 0.06% of carbon. The chemical composition of the alloys are shown in Table 1. In binary alloys the content of chromium varied from 1 to 18%. In addition, each of these binary alloys had been additionally alloyed with either molybdenum, vanadium, or niobium or with all three elements. The specimens were annealed at 950°C before the test.

In all cases these alloys consisted of almost pure ferrite. The content of carbides was relatively low (less than 1%, see Table 1). Most of the alloying elements remained in the α-Fe solid solution, and the variation in their content in ferrite determined the strength of the alloys. It was found

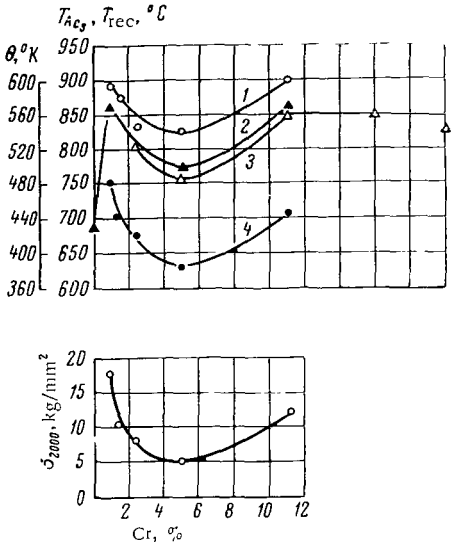

FIGURE 1. Influence of content of chromium in the solid solution containing Mo, 0.5%, and V, 0.15%, on T_{rec}, θ, T_{Ac_3}, and on the resistance to relaxation at 550°C during 2000 hr of testing:

1— T_{Ac_3} (°C) Fe—Cr—Mo—V—ferrite; 2— θ (°K) Fe—Cr—Mo—V—ferrite; 3— θ (°K) Fe—Cr—ferrite; 4— T_{rec} (°C) Fe—Cr—Mo—V—ferrite.

by experiment that the relaxation stability of the α-Fe solid solution, found by the method of I. A. Odding, is a straight-line function of the strength of the crystal lattice.

Figure 1 shows the influence of the content of chromium in binary and in more complex ferrite which contains molybdenum and vanadium also on characteristics of the interatomic forces such as the X-ray characteristic temperature at 20°C (θ), and the temperature of recrystallization (T_{rec}). It can be seen that the addition of 1% of chromium to the ferrite raises the characteristic temperature θ from 430 to 570°K, which indicates a strengthening of the binding forces in the lattice of α-Fe. Further increase in the content of chromium leads to a decrease in θ from 570 to 500°K. The weakest binding forces in the crystal lattice of the solid solution of chromium in iron were found in alloys containing 4—6% of chromium. An increase in the content of chromium to 12% leads to an increase in the characteristic temperature from 500 to 570°K, which shows that the strength of the lattice of ferrite containing 12% of chromium increases again. Further increase in the content of chromium in ferrite to 20% has almost no influence on the characteristic temperature, which remains stable (at about 560°K). This indicates that the strength of the ferrite lattice is little influenced by a content of chromium in excess of 12%.

A similar relationship between the characteristic temperature and the content of chromium was found in ferrite containing 0.5% of molybdenum and 0.1% of vanadium also (Figure 1, curve 2).

Figure 1 also shows the dependence of the recrystallization temperature T_{rec} (Figure 4) and of the temperature of the polymorphic transformation at the point A_{c_3} (curve 1) for Cr—Mo—V-ferrite on the content of chromium. The variation in residual stresses during 2000 hr of relaxation tests under $\sigma_0 = 25\ kg/mm^2$ is shown in the same figure. It is apparent that these characteristics are governed by the same law, and that the curves representing these have the same concave shape as the curve of the characteristic temperature.

It is important to mention that all the above characteristics had a minimum at 4—6% of chromium, which indicates that there is a direct relationship between the resistance to stress relaxation and the α—γ-phase transformations in chromium-alloyed steels. The curve of these characteristics has a typical concave shape. The minimum temperature of the

TABLE 1. Composition of ferrite steels

Composition of alloy, wt %					Composition of ferrite, wt %				Lattice parameter of solid solution, kX	Weight of carbide phase, wt %	Composition of carbides
C	Cr	Mo	V	Nb	Cr	Mo	V	Nb			
0.02	1.3	—	—	—	1.25	—	—	—	2.8610	0.11	Me_3C_6; Me_7C_3
0.06	2.0	—	—	—	1.81	—	—	—	—	0.52	Me_3C; Me_7C_3
0.03	5.6	—	—	—	5.3	—	—	—	—	0.47	Me_7C_3; $Me_{23}C_6$
0.05	11.5	—	—	—	11.2	—	—	—	2.8632	0.37	$Me_{23}C_6$
0.06	18.0	—	—	—	16.0	—	—	—	2.8647	0.49	$Me_{23}C_6$
0.01	1.1	0.7	—	—	1.0	0.7	—	—	2.8617	0.10	Me_7C_3
0.05	5.6	1.0	—	—	5.56	1.0	—	—	2.8643	0.128	$Me_{23}C_6$; Me_7C_3
0.01	11.5	1.15	—	—	11.35	1.1	—	—	2.8654	0.292	$Me_{23}C_6$
0.01	1.3	0.5	0.10	—	1.08	0.45	0.10	—	2.8606	0.35	VC; Me'Me"C
0.06	2.05	0.66	0.15	—	1.85	0.58	0.09	—	—	0.60	Me_7C_3; $Me_{23}C_6$; VC
0.04	1.6	1.3	—	0.75	1.5	1.28	—	0.15	—	0.86	NbC; Me_7C_3
0.04	4.9	0.7	0.17	—	4.5	0.60	0.12	—	—	0.85	Me_7C_3; $Me_{23}C_6$
0.01	11.0	0.65	0.25	—	10.89	0.59	0.23	—	2.8704	0.68	$Me_{23}C_6$

TABLE 2. Composition and phase analysis of steels strengthened by different precipitates

Content of elements in steel, wt %							Content of elements in ferrite, wt %						Lattice parameter of α-Fe	Weight of carbide phase, %	Composition of phases
C	Cr	Mo	V	Nb	Co	W	Cr	Mo	V	Nb	Co	W			
0.06	11.8	0.69	0.33	0.36		—	11.5	0.67	0.31	tr	—	—	2.8654	0.773	NbC, $M_{23}C_6$
0.32	12.9	0.89	0.31	0.72	—	—	11.5	0.77	0.302	tr	—	—	2.8634	2.912	$M_{23}C_6$, NbC
0.05	11.2	0.5	0.4	0.35	4.0	—	11.0	1.0	0.35	0.27	4.0	—	2.8652	0.524	NbC
0.26	12.4	0.9	0.3	0.38	4.34	—	12.25	0.88	0.33	0.12	4.34	—	—	1.92	NbC
0.05	11.5	0.95	0.31	0.56	4.14	1.14	9.56	0.66	0.38	0.18	4.14	0.9	—	2.27	NbC, $M_{23}C_6$, $M_A(M_B)_2$
0.23	12.1	0.95	0.37	0.40	4.16	1.15	10.5	0.75	0.36	0.02	4.16	0.01	—	2.97	$M_{23}C_6$, NbC
0.03	18.0	—	—	—	—	2.25	17.29	—	—	—	—	1.35	2.8851	2.09	$M_{23}C_6$
0.05	18.0	—	—	—	—	7.06	17.0	—	—	—	—	2.36	2.8880	7.6	σ-phase
0.053	18.0	1.0	—	—	—	5.25	17.14	0.87	—	—	—	3.25	2.8820	3.7	$M_{23}C_6$, $M_A(M_B)_2$
0.05	18.0	1.0	—	—	—	7.3	16.0	0.88	—	—	—	2.59	2.8846	12.97	σ-phase

polymorphic transformations in binary Fe—Cr alloys also corresponds to a 5—7% content of chromium, which agrees well with the above data.

Since there is no $\alpha - \gamma$ transformation in Fe—Cr alloys containing more than 12% of chromium, the strength of the binding forces in the α-Fe lattice will depend mainly on the differences between the melting points (T_{mp}).

However, the differences between the melting points of ferrite containing 12 and 20% of chromium are small, and have little influence on the strength of the binding forces in the lattice of ferrite at temperatures of from 20 to 600°C, and therefore the characteristic temperatures for ferrites containing 12 and 20% of chromium are almost identical.

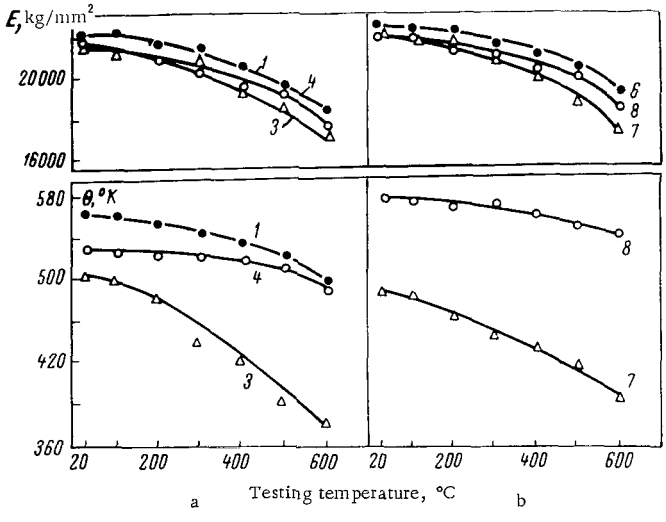

FIGURE 2. Dependence of the modulus of elasticity E and the characteristic temperature θ in Fe—Cr and in Fe—Cr—Mo alloys on the temperature:

a—Fe—Cr—ferrite; b—Fe—Cr—Mo-ferrite; 1, 3, 4, 6, 7, 8—No. of heat according to Table 1.

In chromium alloyed ferrite containing molybdenum (up to 1%), vanadium (up to 0.2%) and niobium (up to 0.15%), the above relationship is retained, and alloys with 4—6% of chromium have the weakest lattices. The resistance of these alloys to stress relaxation is also very low. Thus, to increase heat resistance, the alloy should consist of ferrite alloyed with 1, 12, or 18% of chromium, and also with alloying elements that increase the strength of interatomic forces.

The curves representing the variation in the modulus of elasticity and the characteristic temperature from 20 to 600°C (Figure 2) show that chromium, molybdenum, and niobium increase the strength of the crystal lattice at elevated temperatures also. It should be pointed out that the slope of the curve representing the temperature dependence of θ for alloys with 5% chromium toward the abscissa is greater than that for alloys containing 1 and 12% of chromium.

High-quality ferrite steels containing 12 and 18% of chromium were produced with different strengthening phases, such as carbides of the $Me_{23}C_6$, Me_7C_3, NbC, type, etc., a σ-phase or a Laves phase.

The chemical composition of steels is given in Table 2.

The chief strengthening phases in steels containing 12% of chromium are the carbides of the $Me_{23}C_6$, NbC, and VC types, and in steels with a content of 18% of chromium, not more than 0.05% of carbon, 1% of molybdenum, and from 2 to 7% of tungsten, these phases are either the $Me_{23}C_6$ carbides, a σ-phase, or a Laves phase.

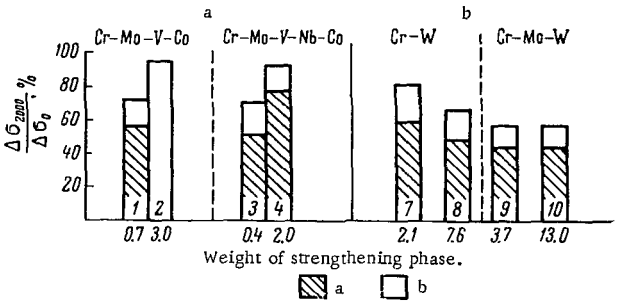

FIGURE 3. Influence of amount and type of strengthening phases on the relaxation stability of steels at 525°C (a) and 580°C (b):

a—steels strengthened by carbides; b—steels strengthened by intermetallic compounds: 1, 2, 3, 4, 7, 8, 9, 10—No. of heat according to Table 2.

Figure 3 shows the relative decrease in stresses caused by relaxation during 2000 hr of testing as a function of the types and amount of strengthening phases in steels in which the ferrite is similar in composition but the strengthening phases have different compositions.

The above data show that the ratio of ferrite to strengthening phase has an appreciable influence on the process of stress relaxation in steel.

In all steels strengthened by carbides, the highest relaxation stability at 525 and 580°C was found when the content of the strengthening particles was low. An increase in the content of carbides from 0.4—0.7 to 2—3 wt% raised the relative decrease in stress caused by heating for 2000 hr at 580° from 70 to 90%.

In steels strengthened by intermetallic compounds, an increase in the content of precipitates has a favorable influence on the resistance to relaxation. Thus, if the content of the strengthening phase in Cr—W steel is increased from 2 to 7% and in Cr—Mo—W from 4 to 13% the stress decrease after 2000 hr of heating is 40—60% at 525°C and 60—80% at 580°C.

It can be clearly seen from Figure 4 that steel strengthened by intermetallic precipitates has a higher relaxation stability than that strengthened by carbides. The figure shows the dependence of residual stresses after 10,000 hr of testing from 550 to 580°C on temperature. Steels strengthened by carbides (curve 1) lose much of their relaxation stability when tested over the temperature range of 550—580°C. This test leads to a decrease in $\sigma_{10,000}$ from 11.5 to 6.5 kg/mm^2.

Steels strengthened by both carbides and intermetallic precipitates (curve 2) have a higher relaxation stability at 580°C, when the residual stress is about 30% higher.

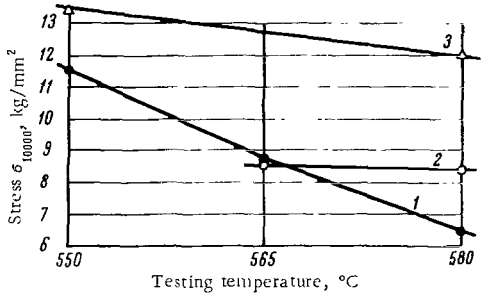

FIGURE 4. Dependence of relaxation stability of steels on the testing temperature at $\sigma = 25$ kg/mm^2:

1—0.17% Cr; 10.5% Cr; 0.45% Mo; 0.4% W; 0.24% V; 0.43% Nb (strengthened by carbides); 2—0.05% C; 11.5% Cr; 1.00% Mo; 0.3% V; 0.56% Nb; 4.14% Co; 1.14% W (strengthened by carbides and intermetallic compounds); 3—0.05% C; 18% Cu; 1.0% Mo; 5.0% W (strengthened by intermetallic compounds).

Steel containing 18% of chromium, 5% of tungsten, and 1% of molybdenum, has a higher relaxation stability at temperatures of from 550 to 580°C. The stress retained after 10,000 hr of testing at 580°C is higher than that retained at 550°C in steel strengthened by carbides.

CONCLUSIONS

1. It has been found by experiment that stress relaxation in alloys with an α-Fe matrix is closely connected with the strength of interatomic bonds in the lattice of ferrite, with the temperature of phase transformations, and with the thermal stability of the strengthening secondary phases.

2. Alloys containing ferrites with one or more alloying elements and with 1.5 or 12% of chromium have a solid solution whose crystal lattice is most elastic over a temperature range of 20—600°C, and the lowest rate of relaxation processes. Ferrite containing about 4—6% of chromium corresponds to the minimum on the $\alpha - \gamma$ transformation curve, and has a crystal lattice with the lowest strength and the lowest resistance to stress relaxation at temperatures of up to 550°C. Therefore it is not advisable to produce relaxation resistant steels containing 5% of chromium.

3. It has been found that to obtain good resistance to stress relaxation at elevated temperatures up to 600°C, the steels should be alloyed with elements that will strengthen the ferrite lattices and lead to the formation of strengthening phases in the steel with a high thermal stability under service conditions.

4. Chromium-alloyed steels strengthened by intermetallic compounds have a higher stability to relaxation than steels strengthened by carbides, and they are not very sensitive to an increase in the testing temperature. An increase in the content of the carbide phase in the steel does not increase the relaxation stability, but on the contrary decreases it.

Bibliography

1. Grigorovich, V.K. and Yu.S. Safonov. Polimorfizm zheleza i polzuchest' splavov na osnove zheleza (Polymorphizm of Iron and Creep of Iron-Base Alloys).—Sbornik "Trudy IV konferentsii po fiziko-khimicheskim osnovam proizvodstva stali." Izdatel'stvo AN SSSR. 1964.
2. Shteinberg, M.M. Struktura i svoistva legirivannogo ferrita (Structure and Properties of Alloyed Ferrite).—Doctorate's Thesis. Sverdovsk. 1959.
3. Mirkin, I.L. and Z.N. Petropavlovskaya. Zavisimost' protsessa relaksatsii napryazhenii v stali ot stepeni legirovaniya ferrita (Dependence of the Process of Relaxation of Stresses in Steel on the Degree of Alloying of Ferrite).—Sbornik TsNIITMASh, No. 105. Mashgiz. 1962.
4. Mirkin, I.L. and Z.N. Petropavlovskaya. Vliyanie sostava ferrita na relaksatsionnuyu stoikost' khromistoi stali (Influence of the Composition of Ferrite on the Relaxation Stability of Chromium-Alloyed Steel).—Metallovedenie i Termoobrabotka, No. 8. 1964.
5. Mirkin, I.L. and Z.N. Petropavlovskaya. Vliyanie sostava faz i struktury metalla na kharakter plasticheskoi deformatsii (Influence of Phase Composition and Structure of Metals on the Character of Plastic Deformation).—Sbornik TsNIITMASh, No. 45. Moskva, ONTI. 1964.

K.V. Gorev, L.I. Shvedov, Z.D. Pavlenko, and S.L. Lifshits

STUDY OF STRUCTURAL CHANGES IN CHROMIUM-NICKEL STEEL ALLOYED WITH ALUMINUM

The heat-resistant steels and alloys produced today contain large amounts of nickel, which is expensive and rare.

Earlier papers /1, 2/ showed that it is possible to produce high-quality austenitic heat-resistant steels containing little nickel by alloying these steels with aluminum. However, aluminum greatly facilitates the formation of an α-phase, and thus introduces a ferrite component into the austenitic steel. The content of aluminum in alloys for service at elevated temperatures must therefore be strictly limited.

The purpose of this work was to study the influence of aluminum on the nature of the structural changes taking place at elevated temperatures in chromium-nickel Kh17N13 steel containing 0.2 and 0.4% of carbon. The boundaries of phase equilibria were usually determined by metallographic and X-ray methods. We also used the methods of measuring hardness, electric resitivity, and magnetism. All the alloys contained 17% Cr, 13% Ni and different amounts of aluminum (alloys with 0.2% C contained up to 7.15% Al, and those with 0.4% C up to 8.5% Al). The alloys were melted in an induction furnace, generally in crucibles. As the starting material we used Armco iron, N1 nickel, type 1 chromium, and AV000 aluminum.

The required amount of carbon was introduced by adding Armco iron that had been carburized by charcoal. The weight of the heats was 1 kg. The metal was cast into metal molds. The ingots were forged at 1100—900°C into square slabs to an average deformation of 50%. After the slabs had been forged they were annealed at 1150°C for 10 hr and then cut into microsections for hardness measurements. The specimens were heat treated in evacuated quartz ampules. All the specimens were homogenized at 1150°C for 15 hr, and some were quenched in water. The temperature of the remaining specimens was reduced by steps, and they were cooled from 1050, 950, 850, and 750°C, after holding at these temperatures for 15, 25, 45, and 75 hr, respectively. The heat-treated specimens were cut into two. One part, 1—2 mm thick, was analyzed by an X-ray structural method, and the second was used for a microstructural analysis and hardness measurements. To detect the structural components we used the Marble, Murakami, Villel, and Rozenhein agents, and also a 5% solution of HNO_3 in alcohol /3, 4/.

The lattice parameters of the alloys were determined by an X-ray structural analysis. The variation in the phase equilibrium was determined from the relationship between the lattice parameters found by the X-ray method and the content of aluminum in the alloy. The X-ray diffraction photographs were recorded in a KROS-1 chamber using an iron target (master method). The parameter was calculated from the (222) lines of austenite and from the (222) lines of nickel foil used as a master.

A microstructural analysis showed that steel containing 0.2% of carbon and cooled from 1150°C has a single-phase austenite structure when the content of aluminum is from 0 to 3.4% (Figure 1, a). If the content of aluminum is 4.25% the steel contains considerable amounts of ferrite besides the austenite (Figure 1, b), and if the content of aluminum is increased to 5.6% the steel contains carbides also. These carbides can be seen in Figure 1, c as white inclusions with diffuse boundaries. Such steels consist mainly of ferrite. If the content of aluminum is increased further to 6.15%, the steel consists of ferrite and of carbides located mainly along the grain boundaries.

Alloys containing 0 to 3.4% Al cooled from 1050°C consist of austenite and comparatively large amounts of chromium carbide (Figure 1, d). The Murakami reagent colors the chromium carbide brown. If the content of aluminum is increased, the concentration of carbides increases and the particles become coarse. The concentration of carbides increases with increase in the content of aluminum because aluminum, which is soluble in austenite, decreases the solubility of carbon and facilitates the precipitation of carbides.

Alloys containing 4.25—5.6% aluminum consist of austenite, carbides, ferrite, and a new β-phase which precipitates as small particles within the crystals of austenite and ferrite (Figure 1, e). Consequently, this new phase is the result of a transformation in the austenite and ferrite. An X-ray study of a powder of this phase, separated electrolytically, showed that it has a body-centered cubic lattice with a parameter corresponding to that of NiAl (2.878 kX). This result agrees with the data of /4, 5/.

Alloys containing 6.2—7.15% Al consist of ferrite, the β-phase, and carbides. A similar structure, formed at a lower temperature, is shown in Figure 1, f. Here the small dark precipitates belong to the β-phase and the coarser black precipitates are chromium carbides.

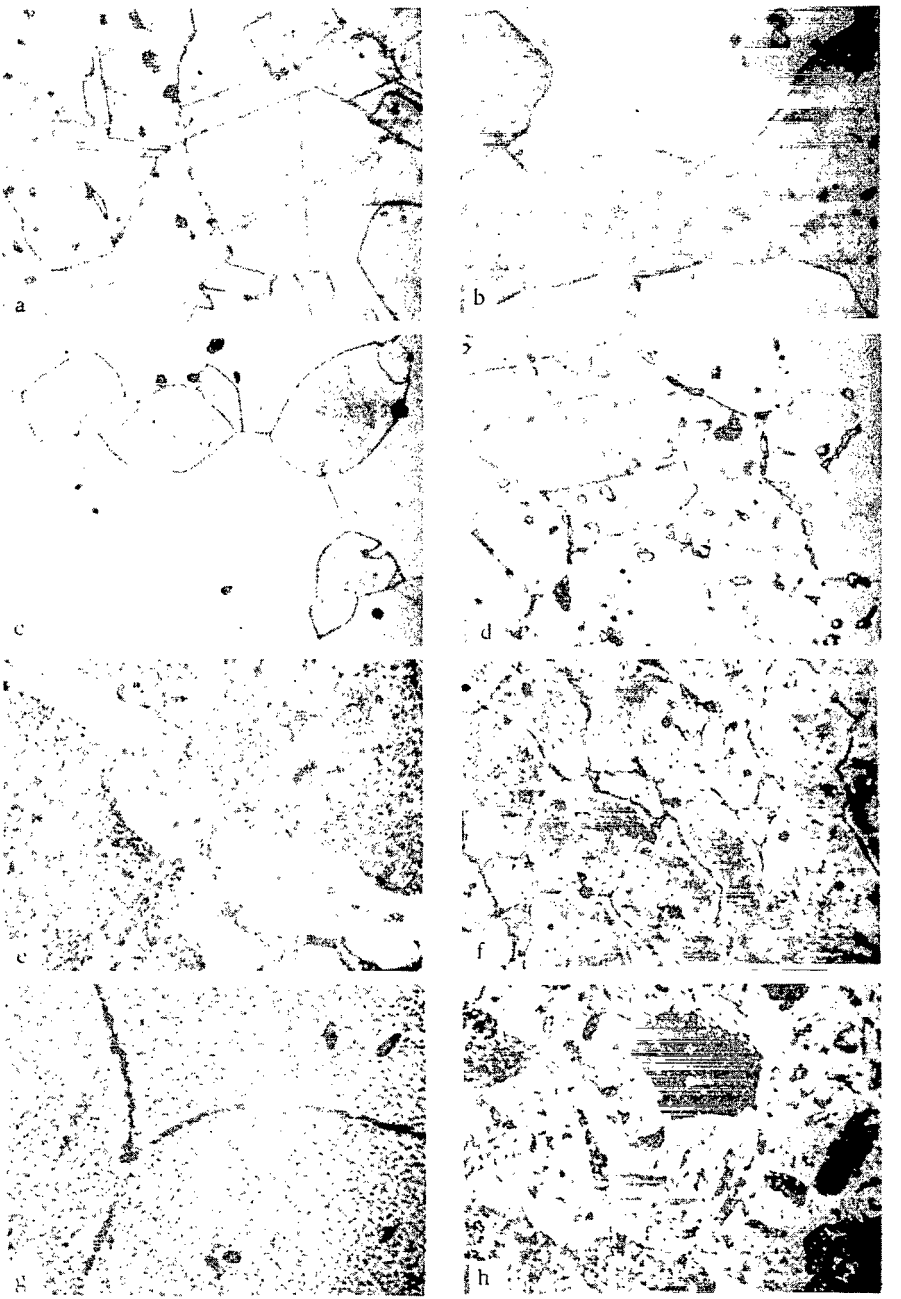

FIGURE 1. Microstructure of steel, containing 0.2% C, 17% Cr, 13% Ni, and different contents of aluminum, after cooling from different temperatures, × 340:

a—cooled from 1150°C, 0.0% Al; b—the same, 4.25% Al; c—the same, 5.6% Al; d—cooled from 1050°C, 3.4% Al; e—the same, 5.0% Al; f—cooled from 850°C, 3.1% Al; g—the same, 7.15% Al h—cooled from 750°C, 4.25% Al.

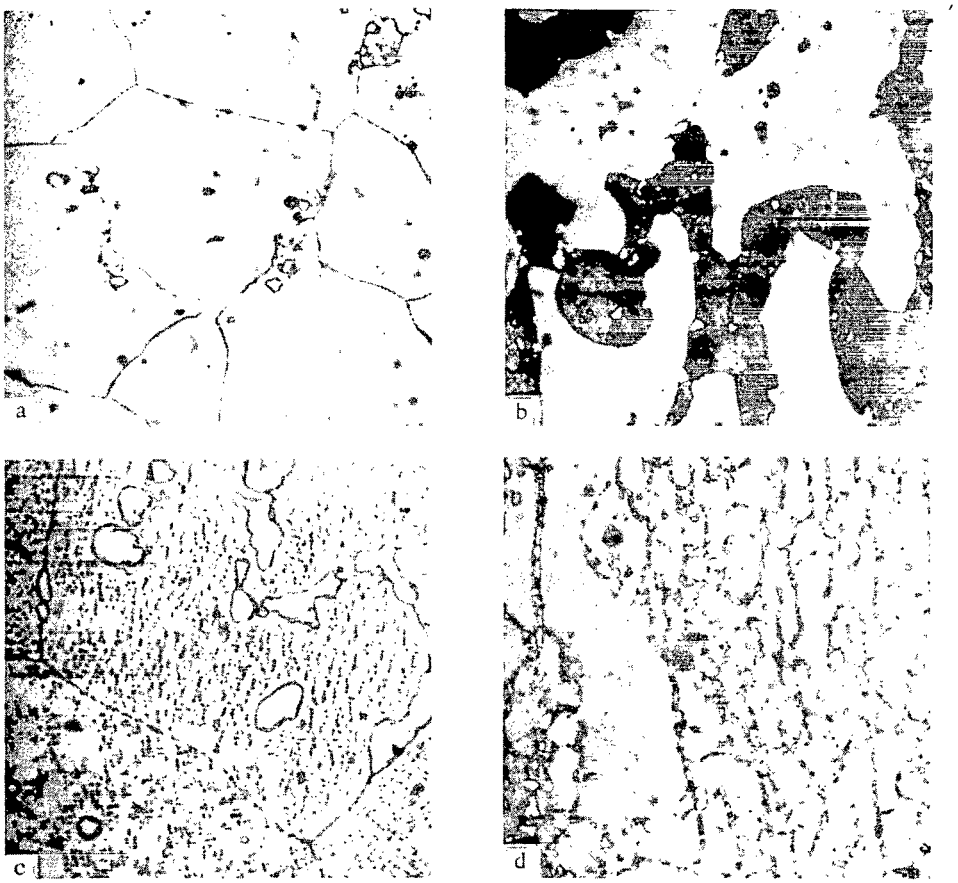

FIGURE 2. Microstructure of steel containing 0.4% C, 17% Cr, 13% Ni, and different contents of aluminum, × 340:

a—cooled from 1150°C, 0.0% Al; b—the same, 6.2% Al; c—cooled from 1050°C, 8.5% Al; d—cooled from 950°C, 4.5% Al.

At 950°C, alloys containing up to 2.9% Al have an austenitic structure with carbide inclusions. If the content of aluminum in the alloy is increased, the carbide particles become coarser. In steel containing 3.1—3.4% Al the austenite decomposes to give a finely dispersed β-phase.

Alloys containing 4.25—5.6% Al have an austenitic—ferritic matrix with large amounts of β-phase and carbide inclusions. Little austenite is formed in alloys containing 6.15—7.15% Al.

At 850°C, alloys with up to 2.15% Al have an austenitic structure with chromium carbide inclusions. In alloys with 2.3% Al fine-grained inclusions of the β-phase are formed along the grain boundaries.

In alloys with 2.9% Al, besides the β-phase small amounts of ferrite are formed along the grain boundaries (Figure 1, g). A four-component structure (austenite, ferrite, chromium carbide, and β-phase) is characteristic of alloys containing up to 6.15% Al. Alloys containing 7.15% Al

have no austenite, and consist of ferrite, a β-phase, and carbides precipitates mainly along the grain boundaries.

At 750°C, alloys with less than 2.15% Al have an austenitic matrix with carbide inclusions. In alloys with 2.15% Al the austenite decomposes at this temperature to give a finely dispersed β-phase.

Alloys with 2.9% Al have small ferrite particles precipitated along some grain boundaries, besides the β-phase and carbides. As the concentration of aluminum in the alloy is increased, the content of ferrite increases and that of austenite decreases. The four-phase structure of the alloys is preserved up to an aluminum content of 6.2%. The structure of alloys in this field of concentrations is shown in Figure 1, h.

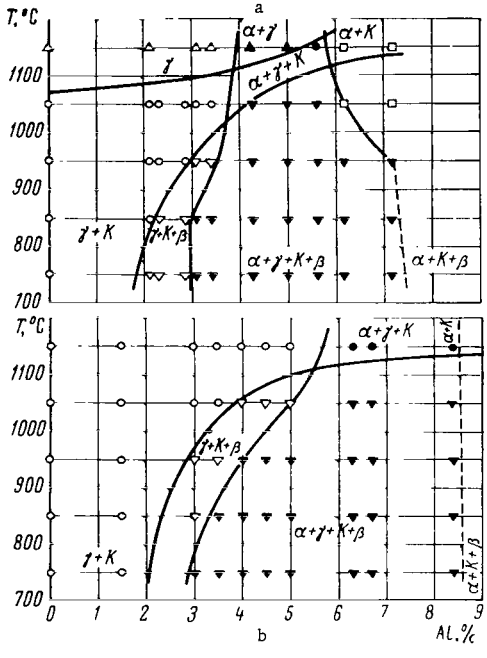

FIGURE 3. Polythermal section of Fe—Cr—Ni—Al alloys containing 17% Cr, 13% Ni, and different contents of aluminum, with 0.2% C (a) and 0.4% C (b).

Alloys containing 7.15% Al produce almost no austenite. The alloy consists of ferrite, a β-phase, and carbides.

Alloys with a carbon content of 0.4%, unlike those with 0.2%, have carbide inclusions at all the temperatures studied, irrespective of the content of aluminum.

At 1150°C, alloys containing up to 5% Al consist of austenite and carbide inclusions only (Figure 2, a). Those with 6.2% Al have appreciable amounts of ferrite (Figure 2, b). An increase in the concentration of aluminum raises the content of ferrite and decreases the content of austenite until at 8.5% Al there is very little austenite.

Chemical composition of chromium-nickel steel

Chemical composition, %				Temperature from which specimens were cooled, °C	Crystal lattice parameter of austenite a, kX	Microstructure
C	Ni	Cr	Al			
0.19	13	17	—	1150	—	A*
				1050	3.5757	A + Cbd
				950	3.5757	A + Cbd
				850	3.5757	A + Cbd
				750	3.5757	A + Cbd
0.1	13	16.75	2.1	1150	—	A
				1050	3.5844	A + Cbd
				950	—	A + Cbd
				850	—	A + Cbd
				750	3.5829	A + β + Cbd
0.24	13	17	2.3	1150	—	—
				1050	3.5844	A + Cbd
				950	3.5852	A + Cbd
				850	3.5852	A + β + Cbd
				750	3.5833	A + β + Cbd
0.21	12.8	17	3.1	1150	—	—
				1050	3.5894	A + Cbd
				950	3.5894	A + Cbd
				850	3.5875	A + F + β + Cbd
				750	3.5852	A + F + β + Cbd
0.21	13	17	3.4	1150	—	A
				1050	3.5948	A + Cbd
				950	3.5894	A + β + Cbd
				850	3.5894	A + F + β + Cbd
				750	3.5864	A + F + β + Cbd
0.19	13	17	4.25	1150	—	A + F
				1050	3.5956	A + F + β + Cbd
				950	3.5914	The same
				850	3.5914	» »
				750	3.5894	» »
0.22	13	17	5.0	1150	—	A + F
				1050	3.5956	A + F + β + Cbd
				950	—	The same
				850	—	» »
				750	—	» »
0.1	13	17	5.5	1150	—	A + F + Cbd
				1050	3.5875	A + F + β + Cbd
				950	—	The same
				850	—	» »
				750	—	» »
0.27	13	19.17	6.25	1150	—	F + Cbd
				1050	—	F + β + Cbd
				950	—	F + A + β + Cbd
				850	—	The same
				750	—	» »
0.18	13	17.68	7.15	1150	—	F + Cbd
				1050	—	F + β + Cbd
				950	—	F + A + β + Cbd
				850	—	The same
				750	—	» »
0.36	13	17	—	1150	—	A + Cbd
				1050	3.5768	The same
				950	3.5768	» »
				850	3.5768	» »
				750	3.5768	» »
0.36	13	17	1.5	1150	—	A + Cbd
				1050	3.5852	The same
				950	—	» »
				850	3.5852	» »
				750	3.5837	» »

* [A, F, Cbd respectively stand for austenite, ferrite, carbide.]

(continued)

Chemical composition, %				Temperature from which specimens were cooled, °C	Crystal lattice parameter of austenite a, kX	Microstructure
C	Ni	Cr	Al			
0.31	13	17	3	1150	—	A + Cbd
				1050	3.5032	The same
				950	3.5883	A + β + Cbd
				850	3.5852	The same
				750	3.5848	A + F + β + Cbd
0.32	13	17.62	3.5	1150	—	A + Cbd
				1050	—	The same
				950	3.5883	A + β + Cbd
				850	3.5865	A + F + β + Cbd
				750	—	The same
0.37	13	17	4	1150	—	A + Cbd
				1050	3.5970	A + β + Cbd
				950	3.5910	A + F + β + Cbd
				850	3.5898	The same
				750	3.5871	» »
0.42	13	17	4.5	1150	—	A + Cbd
				1050	—	A + β + Cbd
				950	—	A + F + β + Cbd
				850	—	The same
				750	—	» »
0.33	13	17	5.1	1150	—	A + Cbd
				1050	3.5990	A + β + Cbd
				950	3.5948	A + F + β + Cbd
				850	3.5948	The same
				750	3.5848	» »
0.34	13	17	6.2	1150	—	F + A + Cbd
				1050	3.6014	F + A + β + Cbd
				950	—	The same
				850	3.5852	» »
				750	—	» »
0.4	13	17	6.8	1150	—	F + A + Cbd
				1050	—	F + A + β + Cbd
				950	—	The same
				850	—	» »
				750	—	» »
0.34	13	15.3	8.5	1150	—	F + Cbd
				1050	—	F + β + Cbd
				950	—	The same
				850	—	» »
				750	—	» »

If there is less than 4% Al in the alloy, at 1050°C the alloy consists of austenite and carbides. Alloys containing 4% Al consist of austenite, carbides, and a β-phase produced as a result of the decomposition of austenite, and alloys with more than 6% Al contain ferrite also. This four-component structure (ferrite, austenite, carbide, and β-phase) is retained up to a content of 8.5% Al (Figure 2, c).

Alloys cooled from 950°C have a β-phase besides austenite and carbide inclusions if the content of Al is 3%, but if the content of aluminum is raised to 4%, ferrite is precipitated (Figure 2, d). At this temperature the four-phase structure is retained to a concentration of aluminum of 8.5%.

The dependence of the structure of alloys cooled from 850 and 750°C on their aluminum content is similar to that of alloys cooled from 950°C, except that at 850°C ferrite is produced if the content of aluminum is 3.5%, and at 750°C it already appears at an aluminum content of 3%. The results of

a microstructural analysis are given in Figures 3, a and b in the form of polythermal sections of phase diagrams.

These figures show that alloys with 0.2% C have eight structural fields over the ranges of concentration of aluminum and of temperatures studied: at elevated temperatures, γ, $\gamma + \alpha$, $\gamma + \alpha +$ Cbd and α + Cbd, and at low temperatures γ +Cbd, γ + Cbd + β, $\alpha + \gamma +$ Cbd + β, and α + Cbd + β. Over the temperature ranges studied in alloys containing 0.4% C only the γ and ($\gamma + \alpha$) fields are missing. Otherwise, the dependence of the structure of these alloys on temperature and on the concentration of aluminum is the same as that of alloys containing 0.2% C. The two-phase field (γ +Cbd) broadens as the temperature is increased. A change in the content of carbon from 0.2 to 0.4% has almost no influence on the line of saturation of austenite by the β-phase. The β-phase is formed as a result of the decomposition of both austenite and ferrite. At elevated temperatures the upper limit of aluminum corresponding to the beginning of ferrite formation is higher in alloys containing 0.4% C than in alloys containing 0.2% C. This indicates that at 850°C and above aluminum facilitates the formation of ferrite less effectively as the content of carbon in the alloy is increased.

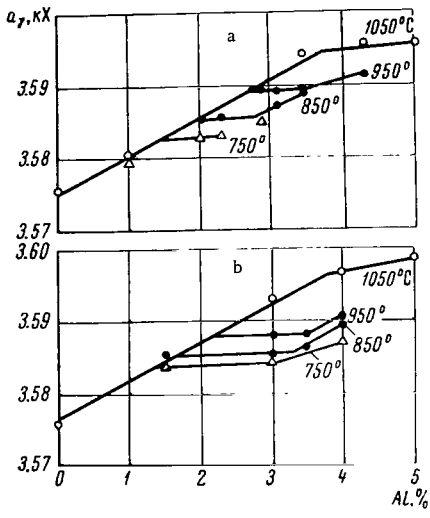

FIGURE 4. Dependence of the lattice parameters of austenite in steel containing 0.2% (a) and 0.4% C (b) on the content of aluminum.

The lattice parameters of austenite in the alloys studied are shown in Figure 4 as curves giving the dependence of the lattice parameters of austenite on the content of aluminum at different temperatures. The first inflection on these curves corresponds to the beginning of the precipitation of the β-phase from austenite, and the second to the beginning of the formation of ferrite. Figure 4 also shows that the data of X-ray structural analysis agree well with the results of microstructural analysis.

This agreement is even better at higher temperatures. The data obtained by X-ray analysis at lower temperatures indicate that the β-phase and the ferrite start to form at somewhat lower concentrations of aluminum than is indicated by the metallographic method. The results of magnetic measurements, hardness measurements, and measurements of electric resistivity, also agree well with those of the microstructural analysis.

CONCLUSIONS

1. We studied the structural changes in chromium-nickel steels (Kh17N13) which are due to changes in the concentration of aluminum and in temperature.

2. It was found that a variation in the carbon content from 0.2 to 0.4% does not influence the position of the line of saturation of austenite by the β-phase.

3. The efficiency of aluminum as an agent for facilitating the formation of ferrite in the alloys at elevated temperatures decreases with increase in the content of carbon.

Bibliography

1. Gorev, K.V. and L.I. Shvedov. Vliyanie alyuminiya na svoistva splavov zheleza s khromom, nikelem i margantsem (Influence of Aluminum on the Properties of Iron Alloys Containing Chromium, Nickel and Manganese). — Inzhenerno-fizicheskii Zhurnal, No. 6. 1958.
2. Shvedov, L.I. Vliyanie alyuminiya i vanadiya na uprochnenie Fe—Cr—Ni—Mn austenita pri vysokikh temperaturakh (Influence of Aluminum and Vanadium on the Strengthening of Fe—Cr—Ni—Mn Austenite at Elevated Temperatures). — In: "Issledovanie stalei i splavov." Izdatel'stvo "Nauka." 1964.
3. Kuo, K. Isothermal Transformation of Delta-Ferrite in a Low-Carbon 27—5—1.5 Cr—Ni—Mo Corrosion-Resistant Steel. — J. Iron and Steel Institute. 181:2. 1955.
4. Bradley, A.J. Microscopical Studies on the Iron—Nickel—Aluminum System. — J. Iron and Steel Institute. 168:3. 1951.
5. Hughes, H. Precipitation in Alloy Steels Containing Chromium, Nickel, Aluminim and Titanium. — J. Iron and Steel Institute. 203. p. 10. October 1965.

O.A. Bannykh, M. Ya. Dzugutov, V.M. Doronin, I.F. Zudin, M.V. Pridantsev, V.V. Topilin, A.M. Uglova, E.G. Fedorinova, and E.V. Shal'nev

*STUDY OF THE HEAT RESISTANCE OF CHROMIUM-MANGANESE-ALUMINUM AUSTENITIC STEELS**

Chromium-manganese steels containing aluminum are resistant to scale formation up to 850—900°C. We studied the heat resistance in the air of steel containing 15% Cr, 14% Mn, 0.45% C, and up to 2.0% Al. One batch of steel contained about 0.3% Si (EP499), and the second batch about 1.5% Si (EP577). We compared the resistance of these steels to scaling with that of 45Kh10G14Yu2 (1) and 1Kh18N10T steels.

We studied specimens from 500 kg heats produced in electric induction furnaces. The 500 kg ingots were scalped and then forged into square billets (135 and 35 mm), which were further rolled into 18 mm diameter rods. The specimens for heat-resistance tests were machined from these rods into cylinders 8—12 mm in diameter and 15—25 mm high.

* The experimental part of this work was carried out with the participation of A.M. Evteeva and M.M. Teplinskii.

The investigations were carried out in two directions:

a) We studied the relationship between the weight gain and the testing time over the temperature range of 800—1100°C. From these data we plotted curves showing the dependence of the weight gain and the oxidation rate on time at a given temperature.

b) We studied the crystal structure of the scale formed on the specimens by an X-ray method.

The first group of tests was carried out by means of a device for studying the kinetics of oxidation.

The specimens were placed into a platinum crucible suspended from a platinum wire attached to the pan of an analytic balance. The crucible was then transferred to a vertical tubular furnace. The changes in weight were recorded after every hour of testing.

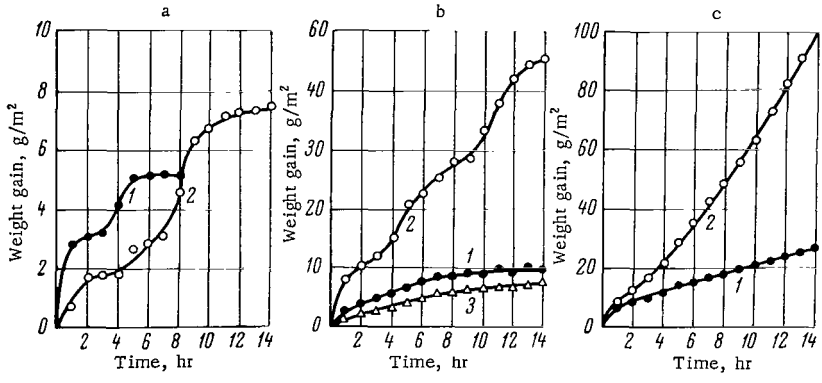

FIGURE 1. Dependence of the weight gain on the duration of oxidation:

a—800°C; b—900°C; c—1000°C; 1—EP577 (45Kh15G14YuS) steel; 2—EP499 (45Kh15G14Yu); 3—1Kh18N10T.

Figure 1, a shows the dependence of the weight gain (g/m^2) of EP499 and EP577 steel at 800°C on the testing time. During the first 7 hr of testing the steel containing 0.3% Si (EP499) oxidized rather more slowly than that containing 1.5% Si (EP577). At 900°C (Figure 1, b) the absolute weight gain of both steels was higher than at 800°C. However, the steel containing 1.5% Si increased in weight when the temperature rose from 800 to 900°C relatively little, but the increase of the steel with 0.3% Si was 6—7 times as great. The rate of oxidation during 10 hr of testing is 3.8 $g/m^2 \cdot hr$ for the EP499 steel, and only 0.9 $g/m^2 \cdot hr$ for the EP577 steel.

As a comparison, Figure 1, b shows the dependence of the weight gain of 1Kh18N10T steel on time. The resistance to scaling of 1Kh18N10T steel at 900°C is very similar to that of EP577 steel. The oxidation rate of 1Kh18N10T steel during 10 hr of testing is equal to 0.7 $g/m^2 \cdot hr$.

At 1000°C the EP577 steel is more resistant to scaling than the EP499 steel (Figure 1, c). During 14 hr of testing the oxidation rate of the EP577 steel decreased continuously, and at the end of the test was equal to 2.1 $g/m^2 \cdot hr$, but the oxidation rate of EP499 steel decreased during the first 3 hr only, and increased during the next 10 hr (from 5.5 to 6.9 $g/m^2 \cdot hr$).

It should be pointed out that after tests at 800°C the scale formed on EP577, and on EP499 steel adhered well to the surface, did not spall, and did peel off on cooling.

The scale formed at 900°C on EP577 and 1Kh18N10T specimens was dense; however, on EP499 (0.3% Si) specimens the scale lamellas spalled off during cooling to room temperature.

The 500 hr test for resistance to scaling was carried out by the following method: the specimens were placed into corundum crucibles heated to a constant weight. Then, the specimens together with the crucibles were held in the furnace for 50 hr. The specimens were cooled in a desiccator to 20°C, and were weighed together with the crucibles. They were then reheated in the furnace to the necessary temperature, etc.

We carried out two series of tests. In the first series we compared the resistance to scaling of EP577 and EP499 steels with that of the 45Kh10G14Yu2 steel. At 900°C, the 45Kh10G14Yu2 steel had the lowest resistance to scale, and an oxidation rate during a 500 hr test of 3.6 $g/m^2 \cdot hr$. The oxidation rate of EP499 during the same time was 2.0 $g/m^2 \cdot hr$, and that of the EP577 steel was 0.3 $g/m^2 \cdot hr$.

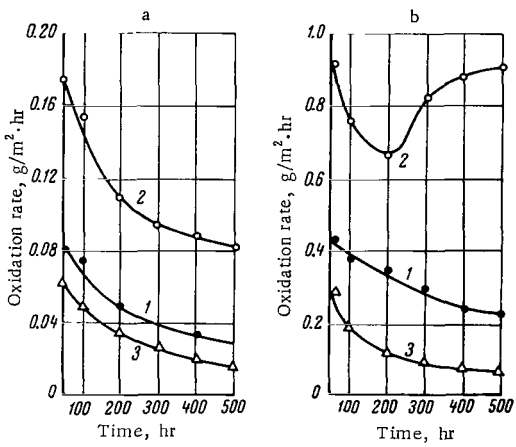

FIGURE 2. Influence of the duration of heating at 800°C (a) and at 900°C (b) on the oxidation rate of steel:

1—EP577 steel (45Kh15G14YuS); 2—EP499 (45Kh15G14Yu); 3—1Kh18N10T.

The scale did not spall off the EP577 steel specimens.

In the second series of tests we compared the resistance to scaling of EP499, EP577, and 1Kh18N9T steels. The experiments were carried out at 800 and 900°C. At 800°C the oxidation rate of all three steels was low (Figure 2, a) and the most scale-resistant steel was the 1Kh18N10T (oxidation rate during 400 hr test was 0.021 $g/m^2 \cdot hr$). The oxidation rate of the EP577 steel was similar to that of 1Kh18N10T steel (0.032 $g/m^2 \cdot hr$). Under the same conditions the oxidation rate of EP499 steel was equal to 0.087 $g/m^2 \cdot hr$. The oxidation rates of all three steels decreased with time.

At 900°C (Figure 2, b) the 1Kh18N10T steel was still the most resistant to scaling. The oxidation rate of EP577 steel during a 500 hr test was $\frac{2}{5}$ of that of the first steel (0.08 instead of 0.21 $g/m^2 \cdot hr$). The oxidation rates of these steels tend to decrease with time. The scale on these specimens is dense and does not spall off during cyclic heating and cooling.

At 900°C the oxidation rate of EP499 steel was somewhat lower than in the first series of tests (after 500 hr the oxidation rate was 0.9 $g/m^2 \cdot hr$).

When the heating lasted more than 200 hr the scale started to crumble and spall off the EP499 steel specimens, which led to an increase in the oxidation rate (Figure 2, b).

X-ray diagrams were recorded by a URS-50I apparatus with an iron target, at a range of angles from 18 to 25°. At these angles it was possible to record the most intense lines of oxides of iron and other elements present in the steel.

We oxidized the prepared microsection in furnaces in an atmosphere of air at the given temperature. The X-ray photographs were recorded directly from the oxidized microsections.

We studied the crystal structure of scale formed at 800°C on EP577 and 1Kh18N10T steels.

We studied the change taking place in the structure of scale formed on EP499 steel very thoroughly to find the causes of spalling of scale at 900°C and above. We therefore oxidized specimens at 800°C, 900°C, 1000°C, and 1100°C for from 15 min to 5 hr.

Figure 3 shows X-ray photographs of scale formed on 1Kh18N10T and EP577 steel at 800°C.

The scale on 1Kh18N10T steel consists of two phases: Me_2O_3 and Me_3O_4. The intensity of the lines of these phases is little influenced by the duration of oxidation at 800°C, and consequently it can be assumed that as the duration of heating at 800°C is increased the layer of scale grows without any noticeable changes in its phase composition.

It is interesting to point out that instead of two close interference maxima, which correspond to reflections from the (101) plane of Me_2O_3 and the (311) plane of Me_3O_4, the X-ray photographs of scale formed on 1Kh18N10T steel have a single maximum corresponding to an interplanar distance of 2.52 kX.

The line corresponding to the interplanar distance of 2.52 kX was the most intense obtained when specimens heated at 800°C were studied at all the holding times.

The main structural component of the scale formed on EP577 steel is the Me_2O_3 compound. The most intense line corresponds to an interplanar distance of 2.71 kX, which coincides with the interplanar distance of the (112) planes of Fe_2O_3. As the heating at 800°C is prolonged, the layers of scale become thicker and the integral intensity of the (112) line of Me_2O_3 increases. The X-ray photographs show relatively weak lines of reflections from the (311) and (220) planes of Me_3O_4 besides the (112) line. This indicates the presence of a certain amount of this oxide in the scale.

The X-ray photograph recorded from EP499 specimens oxidized at 800°C was similar to that recorded from EP577 specimens. The chief structural component is also Me_2O_3. At 900°C the scale consists of two phases, Me_2O_3 and Me_3O_4, and the (112) line of Me_2O_3 is the most intense of those recorded.

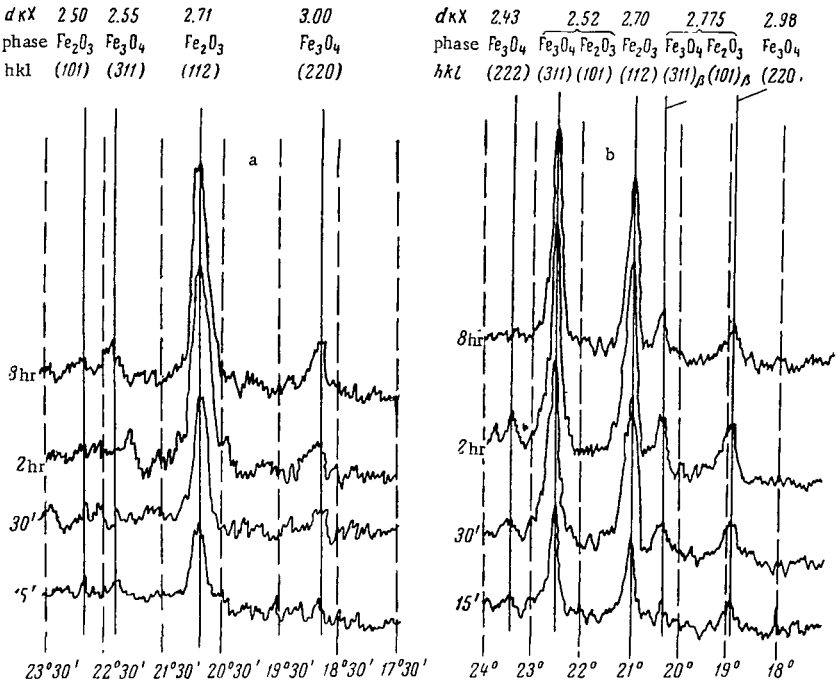

FIGURE 3. X-ray photograph recorded at 800°C for the following steel specimens: a—EP577 (45Kh15G14YuS); b—1Kh18N10T.

An increase in the temprature of oxidation from 1000 to 1100°C leads to an increase in the relative amount of the Me_3O_4 phase in the scale (Figure 4, a and b). The intensity of the (311) and (200) lines of Me_3O_4 is considerably increased, but after oxidation at 1000°C the most intense line is still the (112) line of Me_2O_3 up to a heating time of 1 hr 45 min. If the heating time is increased, this scale spalls off the specimen, and no X-ray photograph can be recorded from the microsections.

After the specimens had been heated at 1100°C for 1 hr 45 min, the X-ray photographs of the scale had (311) and (220) lines of Me_3O_4, which were more intense than the (112) line of Me_2O_3. Thus, it can be said that as the temperature of oxidation is increased the amount of Me_3O_4 (spinel of complex chemical composition) in the scale is increased. As we have already shown /2/, the surface layer of scale formed on chromium steel consists of Me_2O_3. The spalling of scale from 45Kh10G14Yu2 steel /1/ took place when an Me_3O_4 layer developed under the Me_2O_3 layer. We found such a relationship also between the structural changes in the oxide film and its spalling from EP499 steel. This steel differs from that studied in /1/ as it has a higher content of chromium.

It is interesting to point out that the intense development of Me_3O_4 under Me_2O_3, and the spalling of the oxide films when the specimens are cooled,

take place in EP499 (45Kh15G14Yu) steel at temperatures 50—100°C higher than in 45Kh10G14Yu2 steel.

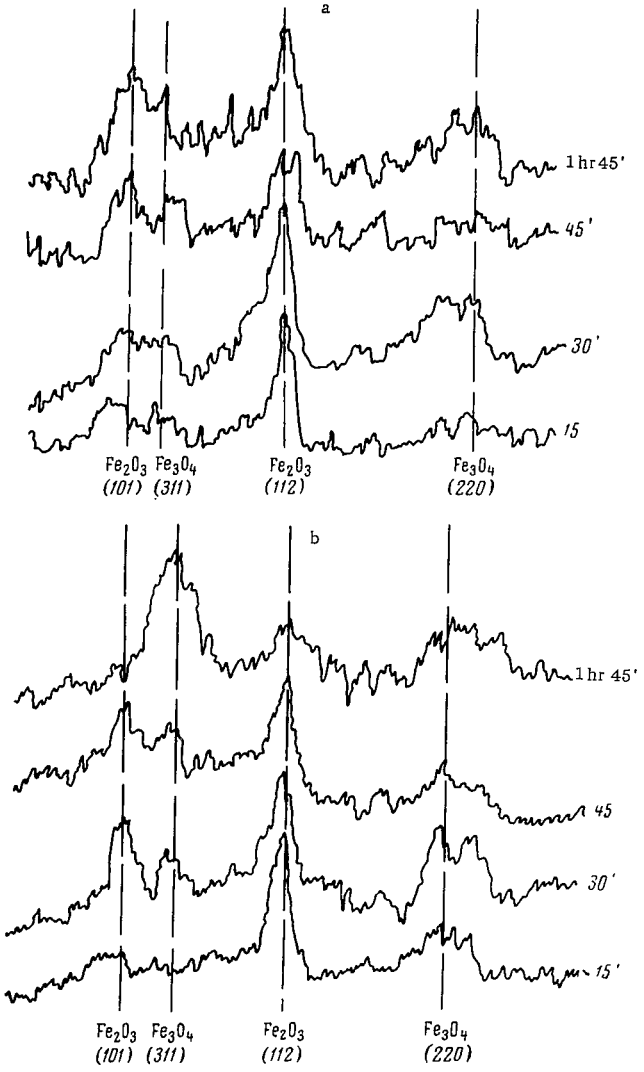

FIGURE 4. X-ray photograph of scale produced on EP499 (45Kh15G14Yu) steel at 1000°C (a) and 1100°C (b).

CONCLUSIONS

1. We studied the scaling of EP499, EP577 steels, and for comparison EP357 (45Kh10G14Yu2) and 1Kh18N10T steels, by means of weight gain and

weight loss in the air at 800—1000°C. We showed that at 800°C and 900°C the resistance of EP577 steel to scaling is close to that of 1Kh18N10T steel. The resistance to scaling of EP499 and EP577 steels considerably exceeds that of the EP357 (45Kh10G14Yu2) steel.

2. By the method of X-ray analysis we found the phase composition of scale formed on the surface of EP577 (45Kh15G14YuS) and 1Kh18N10T steel up to 800°C and on EP499 (45Kh15G14Yu) steel at 800—1100°C. We showed that the increase in the oxidation rate of the EP499 steel at temperatures above 900°C is due to the development of a spinel (Me_3O_4) layer under the protective Me_2O_3 layer and to the spalling of the scale.

Bibliography

1. Bannykh, O.A., Yu.K.Kovneristyi, and I.F.Zudin. Khromomargantsovistye teploustoichivye stali s aluminiem (Chromium—Manganese Heat-Resistant Steel Alloyed with Aluminum).—Izdatel'stvo "Nauka." 1965.
2. Sbornik: "Skorost' okalinoobrazovaniya na metallakh i splavakh" (Collection: Rate of Scale Formation on Metals and on Alloys).—Uchenye Zapiski LGU, No.175, Issue 14. 1954.

Yu.P.Belolipetskii, M.A.Endzelin, M.A.Filatova, S.P.Barabanov, L.R.Alishoev, and D.I.Berezhkovskii

STUDY OF THE INFLUENCE OF THE GRAIN SIZE AND OF GRAIN SIZE NONUNIFORMITY ON THE HEAT RESISTANCE AND STRENGTH OF VANE MATERIALS

This study was undertaken because when turbine vanes made of heat-resistant nickel alloys were produced by foring or drop forging, the heat treatment that followed sometimes led to a nonuniform grain structure.

Thus, drop forged vanes of stationary gas turbines made of EI765 alloy often consist of more or less uniform grains (1—3 mm), or of a combination of small grains (0.1—0.2 mm) and regions of large grains up to 5—10 mm in size.

The difficulty of producing a completely uniform structure when drop forging vanes from nickel alloys is apparently due to the high resistance to deformation, the relatively narrow range of forging temperatures, the complex shape of the vanes, and their large size, particularly those for high-power turbines.

Therefore, it is necessary to evaluate correctly the serviceability of vanes of different grain size or of nonuniform grain structure.

Although the literature data indicate that a coarse-grained structure is detrimental, the data are incomplete and sometimes contradictory, apparently because of the different methods of producing and studying the materials, and also because of the nonmonotonous dependence of some properties of the materials on the grain size /1—4/.

In this work we investigated nickel-chromium EI765 and EI893 alloys. The material was obtained by hot and cold working combined with high-temperature heating. To make the conditions of preparation of metals (drop forging in two passes) of a given structure similar to those under which vanes are produced we used a two-stage deformation.

To produce a metal with a uniform structure but with a nonuniform grain size along the specimens, the deformation was produced by drawing, and in specimens with a nonuniform grain size across them by torsion.

Metals of different grain size were produced by different degrees of deformation of the stock, including critical degrees of deformations.

Our deformation processes were similar to those used in industry for drop forging vanes from EI765 and EI893 steel.

Before the specimens were prepared, the material was heat treated by the usual method for these alloys. The macrostructure of each billet was then checked. The material in each batch was fairly uniform.

The EI765 alloy we produced had a structure like that prepared industrially: grain size up to 0.1—0.2 mm; up to 1, up to 3, up to 5, and up to 0.1—0.3—3—5 (grain size nonuniformity in the transverse or longitudinal direction of the specimen).

We studied the properties which determine the serviceability of the metals at room and at service temperatures (750°C). We also studied the short-time mechanical properties and the long-time strength (at constant temperature and under conditions of thermal cycling), creep, fatigue, constructional strength (asymmetric cycle), thermal fatigue (cycle 20°C—650°C—20°C) and the logarithmic decrement of damping. We also tested real vanes. The results are as follows:

The short-time strength of the EI765 alloy at room and service temperatures (750°C) (Figure 1) in the hot- and cold-worked state is decreased most (by 30—40%) if the grain size is increased from 0.1—0.2 to 2—3 mm. Further coarsening of the grain to 5—10 mm has much less influence.

Such grain coarsening influences the ductility of the metal more than its strength, and if the grain size is increased to 3 mm the ductility is decreased by a factor of 2—2.5.

If the grain becomes coarser, the ductility deteriorates even more.

The long-time strength is also decreased by a coarsening of the grains.

If the grain size is increased from 0.1 to 1 mm, the long-time strength is decreased by about 3 kg/mm^2, i.e., by 10%. The long-time strength is decreased most if the grain size is increased to 3 mm (~20—25%).

Further coarsening of the grain to 5 mm or more causes little change in the long-time strength.

It has been found that the slope of the curve representing the long-time strength of hot-worked materials with a grain size of 1.5 to 3—4 mm is greater than that of the curve representing the long-time tensile strength of fine-grained steel (Figure 2).

If the grain size is increased the ductility during long-term tensile tests decreases to about $\frac{1}{3}$, and the scattering increases. Sometimes the ductility of the coarse-grained material at the time of failure (about 1000 hr) is very low (0.5—1.5%).

The results of long-time strength tests under conditions of thermal cycling (750 ± 25°C) confirm the data obtained under conditions of constant

temperature, which indicated that the long-time strength characteristics of coarse-grained materials are low.

The results of creep tests at 750°C under a load of 17 kg/mm^2 showed that there is no real relationship between the creep rate and the coarsening of the grains of the metal. However, a certain tendency toward a creep rate increase was found in materials with a grain size of 2.5 mm.

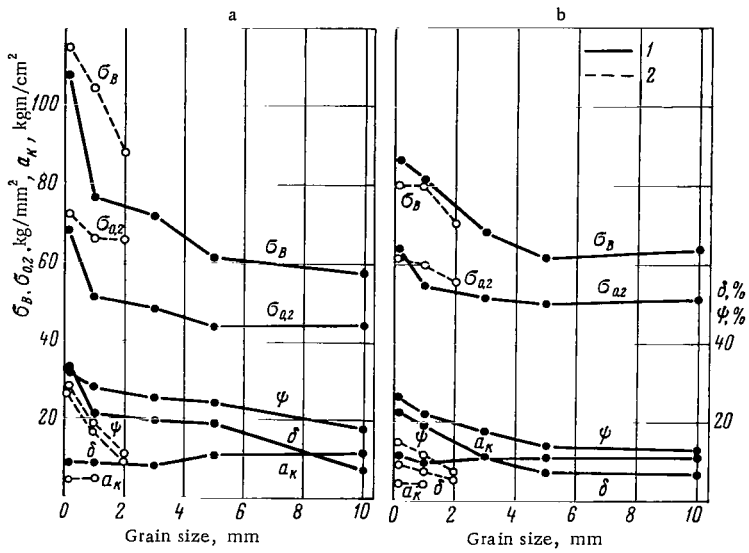

FIGURE 1. Dependence of the mechanical properties of EI765 alloy on the grain size:

a—20°C; b—750°C; 1—properties of cold-worked metal with uniform grain size; 2—properties of hot-worked metal with uniform grain size.

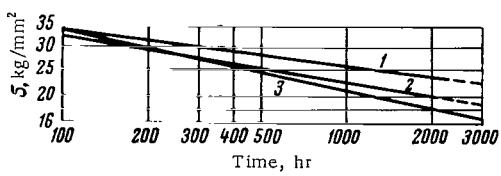

FIGURE 2. Influence of grain size and of grain-size nonuniformity on the long-time strength of EI765 alloy at T = 750°C:

1—fine grained; 2—nonuniform grain size; 3—coarse grained.

The fatigue strength of the EI765 alloy at 750°C (Figure 3) under conditions of symmetric and asymmetric cycling is greatly influenced by the grain size.

If the grain size is increased from 0.25 mm the decrease in the fatigue strength (on the basis of 10^8 cycles) is as follows:

For a grain size up to 1 mm about 20%
For a grain size up to 3 mm about 25%.

The fatigue strength under asymmetric cycles (static tension $\sigma = 15\ kg/mm^2$ plus cycling) decreases even more, and in materials with a grain size of 3—5 mm the decrease is about 40%.

Service tests on vanes showed that the variation in the fatigue strength of the vane edges with a uniform structure and various grain sizes is similar to the variation in the fatigue strength of experimental specimens.

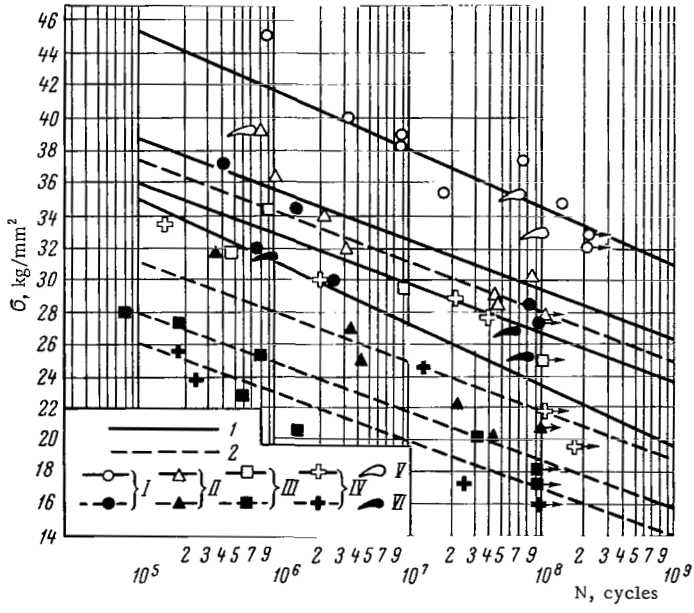

FIGURE 3. Dependence of the fatigue strength (symmetric and asymmetric cycles) of the EI765 alloy at 750°C on the grain size:

1—symmetric cycle; 2—asymmetric cycle; I—grain size up to 0.1 mm; II—up to 1 mm; III—up to 3 mm; IV—0.1—3—5 mm; V—specimens of drop forged vanes, symmetric cycle; VI—the same, asymmetric cycle.

The resistance of the alloy to thermal fatigue is not a monotonous function of the grain size but has a minimum at a grain size of about 3 mm when the number of cycles to failure decreases by a factor of 6—10.

If the grain size is increased to 5 mm or more, the resistance to thermal fatigue increases to that of fine grained material.

Data on the influence of the grain size on the damping capacity of metal indicates that coarsening decreases this value.

At room temperature, at an amplitude of stresses equal to 0.5 $\sigma_{0.2}$, the logarithmic decrement of damping of coarse-grained material of tuning

forks is about $\frac{2}{3}$ of that of materials with a grain size of about 0.1 mm.

The strength of materials which have a nonuniform grain size structure over the cross section of the specimens is determined during short-term and long-term testing by the grain size and the relationship between the cross-sectional areas of the specimen occupied by the coarse and fine grains. The mechanical and thermal fatigue strength, and also the fatigue strength under asymmetric cycles, are determined by the properties of the grain at the peripheral part of the specimen.

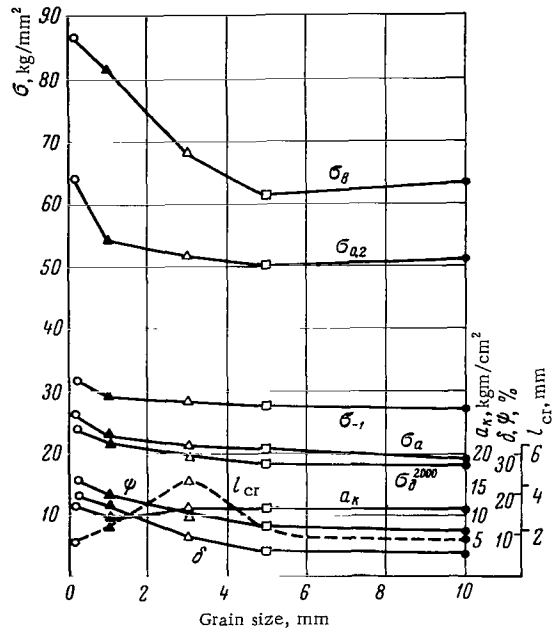

FIGURE 4. Dependence of the properties of EI765 alloy on grain size:

σ_{-1} —fatigue strength under symmetric cycles (10^8 cycles); σ_a = constructional strength (fatigue strength under asymmetric cycles); l_{cr} —depth of crack.

During all the tests, the strength of specimens with a nonuniform grain size in the longitudinal direction was determined by the strength of the more coarse-grained part of the specimen.

Thus, we found that the structure of the metal (grain size and grain size nonuniformity) considerably influence the properties which determine the serviceability of vanes (Figure 4).

EI765 alloy specimens with a uniform fine-grained structure (grain size about 0.25 mm) have an optimum combination of strength and ductility. If the grain size is increased to 1 mm there is a decrease in the properties of about 10—15%.

The properties are worst in a structure with grains 3 mm in size.

The results of a study on the EI893 alloy with different grain sizes agree well with those of an EI765 alloy. Therefore, it can be assumed that the above structure-properties relationships can be extended to other nickel alloys to determine the properties of turbine vanes and other stressed articles (for example, disks).

The above data indicate that vanes made of EI765 and EI893 alloys should have a uniform structure with a grain size of 0.25—0.1 mm, and that grain size differences must remain within these limits.

The TsNIITMASh institute developed heat treatment and mechanical processes for drop forging vanes made of EI765 steel and recommended these to industry. These produce a high-quality material with a relatively uniform structure and a grain size of up to 0.5 mm.

A study of the vanes produced according to these recommendations by various plants showed that the articles have properties close to the optimum obtainable for this alloy.

Bibliography

1. Khimushin, F.F. Zharoprochnye stali i splavy (Heat-Resistant Steels and Alloys).—Metallurgizdat. 1964.
2. Dzugutov, M.Ya. and B.V. Vakhtangov. Kuznechno-shtampovoe proizvodstvo, No. 2. 1960.
3. Getsov, L.B., D.F. Zhirnov, K.I. Terekhov, and M.G. Taubina.—Metallovedenie i termicheskaya obrabotka metallov, No. 9. 1960.
4. Morozova, G.G. and M.A. Endezilin.—In: "Issledovaniya po zharoprochnym splavam." Izdatel'stvo AN SSSR. 1963.

L. Ya. Liberman

RELAXATION AND CREEP STRENGTH OF HARDENING STAINLESS CHROMIUM STEELS

Stainless steel containing 12% of chromium and carbide-forming elements (W, Mo, V, Nb) are widely used in the electric machine-building industry for the production of articles by hot working (disks, vanes, forgings) and by casting (cylinders, etc.). The advantages of hardening heat-resistant martensitic-ferritic stainless steels are their high long-time strength, resistance to scaling, forgeability, and ease of rolling. Because of these properties these steels can be used at temperatures of up to 600°C. The disadvantage of martensitic-ferritic stainless steel is their low creep resistance which leads to a considerable deformation at the beginning of the period of transient creep and during the long initial period. According to the data of ordinary long-time strength tests (2000—3000 hr), the creep limit corresponding to a creep rate of $1 \cdot 10^{-5}$%/hr at 550°C is equal to 10—12 kg/mm^2, which is about one half of the long-time ultimate strength for 100,000 hr.

It has been found that under conditions of a prolonged stationary load and isothermal conditions the creep rate of 1Kh12VNMF (EI802) steel systematically decreases to a very low level /1, 2/. Thus, at 550°C and under a stress of 10 kg/mm^2 the creep rate decreases continuously from $1.0 \cdot 10^{-5}$%/hr for 2000—3000 hr of testing to $0.2 \cdot 10^{-5}$%/hr for 500,000 hr of testing. This factor is of considerable importance for articles made of this steel.

Articles made of hardening stainless steels must be joined by bolts and pins made of steel of the same type to avoid any weakening of the joint because of possible difference between the coefficients of linear expansion.

The use of stainless steels for high-temperature service for bolts and pins has caused difficulties because of the low relaxation stability of the steel at 550—565°C as a result of the low creep during the initial stage of loading.

It is well known that thermomechanical treatment to a 10% reduction increases the resistance to creep and the heat resistance for certain periods of time. It hs been found that this is true also for the 1Kh18N9T austenitic steel and for some other alloys /3, 4, 5/.

The increase in creep strength is achieved even by a small reduction of 0.2—3.0% which can be produced by creep tests and heating at the testing temperature.

Creep tests on 1Kh18N9T steel were carried out under stresses which either exceeded the yield strength of the steel or were equal or close to it.

Hardening stainless steels can work under stresses within the limits of elasticity but considerably lower than the yield point at service temperature.

The relaxation processes were studied with two types of standard steels widely used in power-machine building, 1Kh12VNMF (EI802) and 2Kh12VMFBR (EI993), and also several martensite-ferrite steels. The chemical composition and mechanical properties of these are shown in Table 1.

TABLE 1. Chemical composition (in %) and mechanical properties of steels

Type of steel	C	Mn	Si	Cr	Ni	W	Mo	V	Other elements	T, °C	$\sigma_{0.2}$, kg/mm^2	σ_B, kg/mm^2	δ_5, %	ψ, %	a_H, kgm/mm^2
1Kh12VNMF (EI802)	0.19	0.47	0.14	11.43	0.7	0.90	0.58	0.16	—	20	77.0	90	17	53	8.7
										550	51	54	21	78	13
2Kh12VMBFR (EI993)	0.18	0.35	0.27	12.1	0.17	0.70	0.53	0.29	0.38Nb	20	74	87	18	55	5.9
									0.03B	550	48	51	15	65	14
EP280	0.21	0.73	0.17	11.2	0.7	1.16	1.28	0.26	0.37Co	20	77	94	18	55	11.5
									0.01B	565	49	54	21	76	13.7

The EI802 and EI280 steels were quenched from 1050°C in oil and tempered at 700°C. The EI993 steel was normalized at 1050°C, cooled in the air, and tempered at 700°C.

All steels had identical mechanical properties, and our investigations were based on this.

Two methods were used: relaxation by bending ring specimens, designed by I. A. Oding, and relaxation by stretching cylindrical specimens 10—12 mm in diameter with a calculated length of 150 mm on a UIM5 machine.

The relaxation curves of EI802 and EI993 steel specimens at 565°C under an initial load of 30 kg/mm^2 obtained by both the above methods (Figure 1, a) indicate that in these steels the stresses drop considerably, and after 2000 hr the residual stresses in the ring specimens were 10.5—11.0 kg/mm^2, which is about 30% of the initial stress. In cylindrical specimens the same stress decrease was achieved under conditions of stretching after 1000 hr. The level of residual stresses does not satisfy the requirements.

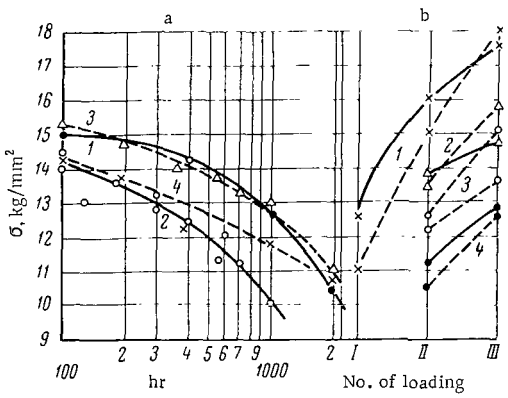

FIGURE 1. Relaxation stability at 565°C, σ_0 = kg/cm^2:

a—initial state; 1, 2—EI802 steel shaped into rings and cylindrical specimens, respectively; 3, 4—EI993 steel shaped into rings and cylindrical specimens, respectively; b—at three consecutive loadings up to 30 kg/mm^2 (ring specimens: first loading 2000 hr, 2nd and 3rd loadings 10,000 hr each); 1, 2, 3, 4—1000, 3000, 5000 and 10,000 hr, respectively. Continuous line—EI802 steel, dashed line—EI993 steel.

The above data indicate that relaxation by stretching reduces the stress by 8—14% more than in ring specimens. Similar discrepancies were found during a study of pearlite and austenite steels.

Our investigations by both methods showed that in the initial state the stainless steels have a low relaxation stability.

Experiments with repeated loadings to the initial level of stresses showed that the relaxation stability of both types of steel increases appreciably under these conditions (Figure 1, b). While the first loading produced a residual stress of 10.5—11.0 kg/mm^2 after 2000 hr, the second loading with up to 30 kg/mm^2 produced the same residual stress after 10,000 hr, and a third loading produced a residual stress of 12.5 kg/mm^2. Ring specimens of both steels EI802 and EI993) show identical behavior under conditions of relaxation, and have almost identical residual stresses.

According to these data, and to clarify whether an increase in the creep strength of stainless steel by small deformations is possible, we tested EI802 and EP280 steels, so that the accumulation of plastic deformation

under conditions of creep took place at 580°C and at 600°C, and the creep strength was evaluated from data of tests at 565°C (Table 2).

The results of these tests show that the plastic deformation accumulated under conditions of creep in amounts of up to 0.2% at temperatures above or below the testing temperature decreases the steady-state creep rate and the duration of the first stage of creep by a factor of 2—3, and also decreases the total deformation after 3000 hr of testing by 35—40%.

Under conditions of relaxation small plastic deformations are accumulated (0.10—0.15% after 10,000 hr of testing).

TABLE 2. Creep strength under a stress of 10 kg/mm^2

Type of steel	Accumulation of plastic deformation		Creep under a stress of 10 kg/mm^2			
	temperature, °C	ε_{pl}, %	T, °C	duration of test, hr	total deformation, %	steady-state creep rate, 10^{-5}%/hr
EI802	—	0.0	565	3100	0.174	1.6
EI802	580, 600	0.160	565	3100	0.100	0.5
EP280	—	0.0	580	2400	0.224	3.0
EP280	565, 600	0.20	580	2700	0.147	2.0
EI802	565, 580	0.14	600	2000	0.165	3.0

To clarify the possibility of increasing the relaxation stability by small plastic deformations, we carried out a series of tests with cyclic loads (repeated every 50—100 hr), which were followed by a 20,000 hr long-time test. Figure 2, a gives data obtained with ring and cylindrical specimens of EI802 and EP280 steels. In both cases the residual stresses increase, and reach a maximum after 5—7 cycles; they then become stabilized. The discrepancies between the results of the two different methods are within the above limits. The residual stresses in EI802 and in EI993 steels obtained under conditions of relaxation by stretching after a plastic deformation of 0.23 and 0.11% (curves 5 and 6) are identical, and higher than the initial stresses (curve 3).

Figure 2, b shows the dependence of the residual stresses (average data) in EI802 steel after different periods of testing by both methods on the accumulation of stresses induced by plastic deformation before the relaxation process started. According to the data obtained by both methods the relaxation stability increases with increase in the plastic deformation. The curves of relaxation for ring specimens show that the plastic deformation greatly influences relaxation up to 3000—4000 hr of testing. Tensile tests on cylindrical specimens showed that for 500—1000 hr of testing the optimum increase in the relaxation stability corresponds to a plastic deformation of 1.0%. If the deformation exceeds 1.0% there is a tendency to lose the effect of strengthening after 100—500 hr of testing. This tendency is particularly well marked for EI802 and EP280 steels after 1000 hr of testing (curves 4 and 5). These data indicate that preliminary deformation increases the relaxation stability by 35—40%.

To find the influence of the conditions of accumulation of plastic deformation on the relaxation stability, we carried out a series of experiments

with cyclic loading under stresses of from 20 to 50 kg/mm^2 and at different temperatures. Table 3 shows that after 5—7 short cycles of 20—25 hr, the residual stresses increase by about 50%. Long-term tests (15,000 hr) carried out after cyclic prestressing (Table 4) showed that the relaxation stability is almost uninfluenced by the prestress loads. The differences between the residual stresses are 14—20%. A comparison of these results with those shown in Figure 1, a shows that in this case the residual stresses after 15,000 hr of testing are 10.2—12.7 kg/mm^2, compared to 10.5 kg/mm^2 after 2000 hr of testing in the initial state.

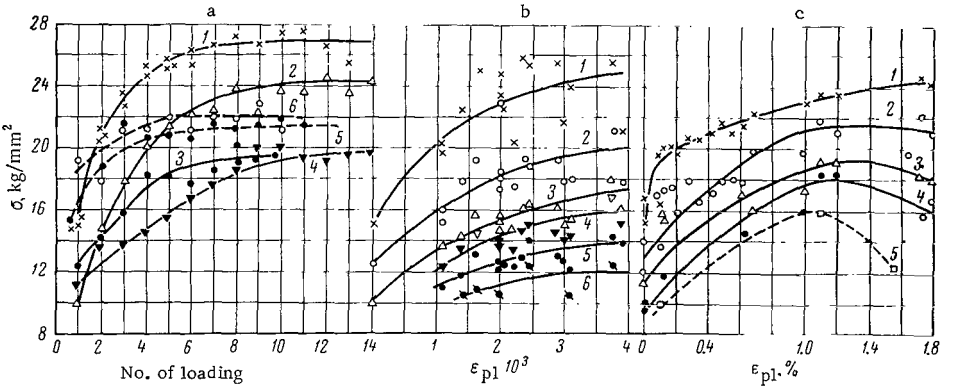

FIGURE 2. Dependence of residual stresses under cyclic loads and dependence of relaxation stability of steel on plastic deformation:

a—cyclic loading repeated every 50 hr (up to 30 kg/mm^2); steel EI802; 1, 3—ring and cylindrical specimens, respectively, initial state; 5—cylindrical specimen, 0.23% reduction; EP280 steel; 2, 4—ring and cylindrical specimens, respectively, initial state; steel EI993; 6—cylindrical specimen, 0.11% reduction; b—EI802 steel 565°C; ring specimens, σ_0 = 30 kg/mm^2. 1—100 hr; 2—1000 hr; 3—3000 hr; 4—5000 hr; 5—10,000 hr; 6—16,000 hr; c—EI802 steel, 565°C; cylindrical specimens, σ_0 = 30 kg/mm^2, 1—5 hr, 2—100 hr; 3—500 hr; 4—1000 hr; 5—EP280 steel, 1000 hr.

TABLE 3. Influence of initial stresses on the relaxation stability of EI802 steel

σ_0, kg/mm^2	σ_τ after prestressing, kg/mm^2							Plastic deformation, mm × 10^{-4}
	1	2	3	4	5	6	7	
20 + 30	12.6	17.2	16.8	18.0	18.0			16.3
	—	—	—	—	—	23.8	24.6	
25	15.0	21.0	20.0	22.0	22.5	—	—	14.1
30.0	17	24.0	22.7	25.4	26.0	26.7	26.2	23.7
35.0	19.3	26.0	24.8	27.4	28.0	—	—	24.4
50.0	21.4	28.0	—	—	—	—	—	29.2

TABLE 4. Relaxation stability at 565°C, σ_0 = 30 kg/mm^2 after cyclic prestressing to different levels

σ_0 after prestressing, kg/mm^2	σ_τ (kg/mm^2) after (hr)					
	100	1000	3000	10,000		16,000
20, 25, 30, 35 and 50	22.4—25.4	17.9—19.2	14.3—16.2	13.7—15.1	11.9—14.0	10.2—12.7

TABLE 5. Relaxation stability at 565°C and at an initial stress of 30 kg/mm^2 after accumulation of plastic deformation at different temperatures

Type of steel	Method of testing	Conditions of accumulation of plastic deformation		Residual stresses (kg/mm^2) after, (hr)					
		T, °C	ε_{pl}	100	500	1000	3000	5000	10,000
1Kh12VNMF (EI802)	Ring	500	$33.4 \cdot 10^{-4}$	—	—	20.8	18.2	16.6	14.9
1Kh12VNMF (EI802)	Stretching	500	0.44%	19.2	17.0	—	—	—	—
	"	580	1.40%	19.0	17.0	16.0	—	—	—
2Kh12VMBFR (EI993)	Ring	450	$5.0 \cdot 10^{-4}$	21.1	19.2 (400 hr)	17.5	14.2	13.2	10.0

The results of tests on both types of specimens at 565°C and at an initial stress of 30 kg/mm^2 (Table 5) also show that the relaxation stability increases irrespective of the temperature at which the plastic deformation is carried out, and that the residual stresses agree with the above data for similar deformations.

Figure 3 shows the optimum curves of the relaxation stability of EI802 and EP280 steels, which characterize long-term tests on ring and cylindrical specimens at 565°C and an initial stress of 30 kg/mm^2. The results of tests on ring specimens show that each consecutive loading increases the relaxation stability of the EI802 steel (curves 1, 2, 3). The second and third loadings at an initial plastic deformation of $11.3 \cdot 10^{-4}$ and $22.3 \cdot 10^{-4}$ ensure a high relaxation stability during 10,000 hr of testing, which leaves a residual stress of 11 — 12.5 kg/cm^2. Preliminary prestressing of EI802 and EP280 steels repeated 12 times at intervals of 50 hr produces even higher residual stresses, which after 10,000 hr of testing are 14 kg/mm^2 for both steels. The residual stresses in EI802 steel after 20,000 hr of testing are equal to 12 kg/mm^2 (curves 4, 5). Similar residual stresses were produced in cylindrical specimens which had first been subjected to a creep test for 15 hr at 35 kg/mm^2, leading to a 1.1% reduction (curve 6). Similar data were obtained with ring specimens of the EI993 steel (Table 6). The residual stresses after the second and third loadings increased considerably as a result of the plastic deformation which took place during the test.

TABLE 6. Optimum relaxation stability of EI993 steel at 565°C, $\sigma_0 = 30$ kg/mm^2 (ring specimens)

No. of loading	Plastic deformation, mm·10^{-4}	σ_τ (kg/mm^2) after (hr)				
		100	1000	3000	5000	10,000
1	0.0	13.2	11.4	10.3 (2000 hr)		
2	11.5	19.9	16.6	14.7	13.9	12.2
3	21.0	—	18.2	16.4	15.6	13.3

It has been experimentally found that hardening stainless steels which have a low relaxation stability in the initial state at elevated temperatures become strengthened during creep and relaxation due to the small plastic deformations. The latter can be produced at various temperatures and loads by several short-time (20—50 hr) prestressings under conditions of relaxation, or by long-time creep under a constant load at service or other temperatures. An optimum relaxation stability is produced by an initial plastic deformation of 1.0%.

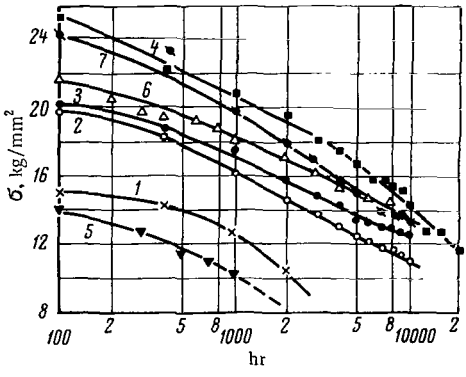

FIGURE 3. Optimum relaxation stability at 565°C, $\sigma_0 = 30$ kg/mm²:

Steel EI802, ring specimen; 1, 2, 3—first, second and third loadings at an initial plastic deformation of $0.113 \cdot 10^{-4}$ and $22.3 \cdot 10^{-4}$, respectively; 4—at $\varepsilon_{pl} = 37.5 \cdot 10^{-4}$ after 12 prestressings at intervals of 50 hr; stretching; 5—first loading; 6—after creep to $\varepsilon_{pl} = 1.1\%$; 7—EP280 steel, ring specimens after 12 loadings.

During service the tightening of bolts which is always necessary under static conditions of service or during the assembly or repair of apparatus is sufficient to ensure the necessary relaxation stability of stainless steel.

The ability of stainless steel to improve its creep strength and relaxation stability under the influence of small plastic deformations is determined by the influence of the latter on the structure of the metal. The structural changes, in turn, are due to a number of factors connected with the dislocation mechanism of deformation. These factors are the increase in the dislocation density, the distribution of dislocations in the deformed metal, the development of a substructure during creep, and the development of a polygonization process. Special studies can determine which of these factors predominate.

CONCLUSIONS

1. Heat-treated hardening stainless steels containing 12% of chromium have a low creep strength at elevated temperatures and a low relaxation

stability. This has been confirmed by the data of a study on 1Kh12VNMF (EI802), 2Kh12VMBFR (EI993) and EI280 steels.

2. The creep strength of EI802 and EP280 steels is considerably increased by a 0.1—0.2% plastic deformation. Such a deformation of 1Kh12VNMF (EI802) steel decreases the creep rate at 565°C by a factor of 2, shortens the period of transient creep by a factor of 2—3, and decreases the total deformation (during 3000 hr of testing) by 50%.

3. The relaxation stability of these steels is increased appreciably by preliminary plastic deformation produced by cyclic loading, by repeated prestressing during service, or by a short-time creep. The maximum relaxation stability of 1Kh12VMF (EI802) steel at 565°C is produced by a plastic deformation of about 1.0%

4. Under these conditions the residual stresses after 20,000 hr of tests on 1Kh12VNMF (EI802) at 464°C and at an initial stress of 30 kg/mm^2 are equal to 12 kg/mm^2, compared to a residual stress of 11.5 kg/mm^2 after 2000 hr of tests on steel which has not undergone plastic deformation. These data show that this steel can be used as a bolting material for power constructions.

Bibliography

1. Liberman, L. Ya. Dlitel'naya polzuchest' zharoprochnykh stalei. Issledovaniya po zharoprochnym stalyam-splavam (Long-Time Creep of Heat Resistant Steels. Studies of Heat-Resistant Steels and Alloys), Vol. 10.—Izdatel'stvo AN SSSR. 1963.
2. Liberman, L. Ya. Dlitel'noe soprotivlenie polzuchesti zharoprochnykh stalei (Long-Time Resistance to Creep of Heat-Resistant Steels).—Metallovedenie i Termicheskaya Obrabotka Metallov, No. 1. 1964.
3. Oding, I. A. and Z. G. Fridman. Povyshenie zharoprochnosti metallicheskikh splavov metodom mekhaniko-termicheskoi obrabotki (Increasing the Heat Resistance of Metal Alloys by Thermomechanical Treatment).—Izv. AN SSSR, OTN. Metallurgiya i Toplivo, No. 5. 1961.
4. Ivanova, V. S. and L. K. Gordienko. Novye puti povysheniya prochnosti metallov (New Methods of Increasing the Strength of Metals).—Izdatel'stvo "Nauka." 1964.
5. Ivanov, V. S. et al. Rol' dislokatsii v uprochnenii i razrushenii metallov (Role of Dislocations in Strengthening and Failure of Metals).—Izdatel'stvo "Nauka." 1965.

A. S. Tereshkovich, S. P. Nestertsev, and A. E. Runov

AUSTENITIC HEAT-RESISTANT STEEL FOR CASTINGS

For the construction of power plants, some high-temperature castings (turbine body and mountings) are required.

To produce cast parts for steam turbines working at 600—650°C, austenite-ferrite steels have been developed with good weldability (1Kh20N12T-L, 1Kh16N9V4B (TsZh-15) and EI402M steels). However, these steels cannot be used at 700°C or above because of their relatively low high-temperature strength.

New austenitic casting steels for service at 700—750°C have been developed during the last years /1—3/.

The choice of the type of strengthening for steel has been influenced by the following considerations:

1. Good long-time heat resistance of the steel can be achieved by precipitating several strengthening phases in the steel during different stages of aging.

2. For casting it is undesirable to have aluminum in the steel, as this leads to the formation of oxide layers in the castings. Consequently, the Ni_3Al strengthening phase, which is often present in heat-resistant wrought materials, must be substituted by another phase.

3. For good weldability, it is advisable to make the austenitic structure heterogeneous by the precipitation of primary phases during crystallization.

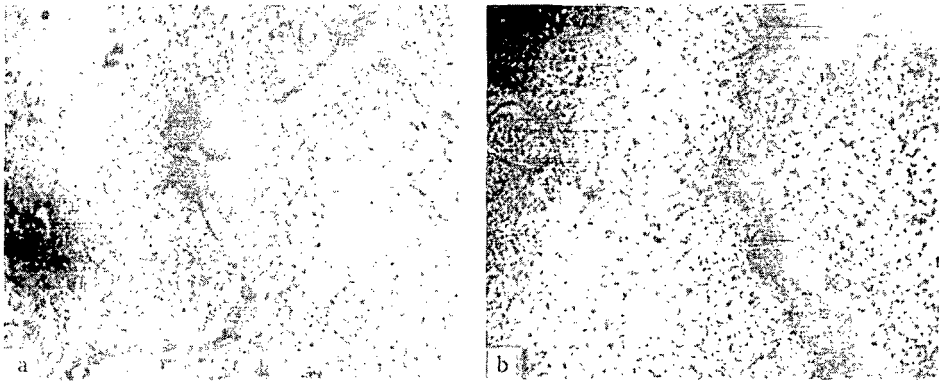

FIGURE 1. Microstructure of steel, ×500:

1—after austenitizing and tempering; b—after aging at 750°C for 5000 hr.

Therefore, after investigating a number of alloys we chose a steel with the following composition, which has the optimum properties for service and weldability: C, 0.25%—0.3%; Cr, 15%—17%; Ni, 21%—23%; W, 5.5%—6.5%, and Nb, 0.8%—1.2%.

In the steel the role of the primary phase which facilitates weldability is fulfilled by the NbC carbide. The strengthening phase during the initial stages of aging is the secondary chromium carbide ($Me_{23}C_6$), and the strengthening phase during the later stages is the Fe_2W intermetallic compound, which precipitates as highly dispersed particles after isothermal heating at 750°C for 1000—3000 hr (Figures 1, a and b).

During our studies we also chose the proper heat-treatment process. From the kinetic curves hardness vs temperature and hardness vs duration of heating, and also by determining the short-time properties, we found that

the best heat treatment is austenitizing the steel at 1200°C for 2 hr, quenching in water, and giving a stabilizing anneal at 800°C for 10 hr followed by cooling in the air.

Under these conditions a steel was produced that satisfies the chief requirements of austenitic steel casting for service at 700 and 750°C:

$$\sigma_{1ts^*}^{10^5} \geqslant 8 \text{ kg/mm}^2;\ \sigma_n^{10^{-5}} \geqslant 5 \text{ kg/mm}^2;\ \sigma_{0.2} \geqslant 13 \text{ kg/mm}^2.$$

During adaptation of this steel to industrial conditions it has been found that in thick-walled castings, i.e., at a low rate of cooling during crystallization, the ductility of the steel decreases greatly. The elongation of a large casting is only about one-fourth of that of wobbler-like test specimens (5 and 20%, respectively).

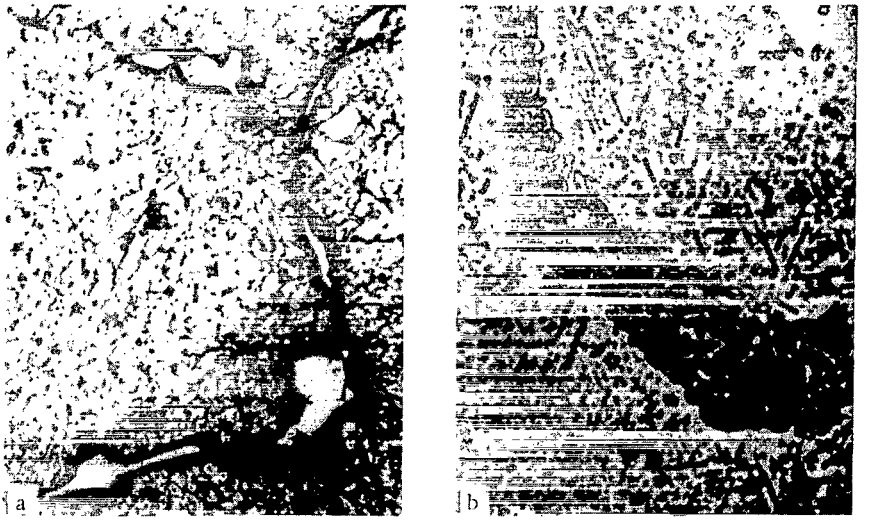

FIGURE 2. Microstructure of a thick-walled sand casting, × 500.

The macrostructure of thin-walled parts (wall thickness about 25 mm) consists of a continuous zone of acicular crystals. In castings with a wall thickness of 200 mm there is a small surface zone of acicular crystals and a well-developed zone of coarse equiaxial crystals with the lowest ductility.

It has been experimentally found that the rather low ductility of thick casting is due to the considerable coarsening of the niobium carbide particles (Figure 2, a), and also to the formation of coarse eutectic inclusions, which apparently consist of a carbide eutectic according to the data of microanalysis (2, b).

The content of chromium in this phase** is 43%, of tungsten, 13%, and of niobium, 1.2%.

* [Long-time strength.]

** According to the data of TsNIIChermet.

The low ductility of thick-walled castings of this metal, which is particularly undesirable for weldability (formation of cracks near hard welded joints) forced us to develop a special technique of large castings which cool rapidly during crystallization and consequently ensure high ductility.

In this method external metal coolers are used, which ensure good elasticity of the metal molds and a relatively uniform cooling of the different sections of the casting.

This new process of casting was tested and improved under industrial conditions by this method. We produced complex-shaped ring parts 2.4 m in diameter, 260 mm in height. With metallic chills parts were produced with a fine-grained acicular structure along the whole section of the casting, and a maximum thickness of 220 mm. A small zone of equiaxial crystals was found in the upper part of the casting only, which also had a low ductility.

TABLE 1. Chemical composition of the steel

Number of heat	Content of element, %								
	Cr	Si	Mn	Cr	Ni	W	Nb	S	P
D3-17	0.26	0.26	0.75	14.99	21.06	6.30	0.96	0.017	0.028
D3-236	0.30	0.27	0.95	16.25	22.00	6.41	0.90	0.020	0.020
D4-285	0.30	0.29	1.06	14.65	20.10	6.40	0.80	0.008	0.018
D5-54	0.25	0.20	1.0	14.18	21.65	6.08	0.89	0.011	0.018
12655 (NZL)	0.26	0.49	1.03	16.40	22.02	5.95	1.00	0.007	0.017

The results of a study on the properties of metal castings of different diameters cast into sand or metal molds after austenitizing at 1200°C and stabilizing at 800°C for 10 hr are given below.

The chemical composition of the heat studied is given in Table 1.

The short-time tensile and impact tests were carried out at room and service temperatures. The results at 20°C are given in Table 2.

TABLE 2. Mechanical properties of the steel at 20°C

Number of heat	Shape of casting	Mold	$\sigma_{0.2}$, kg/mm^2	σ_B, kg/mm^2	δ_5, %	ψ, %	a_k, kgm/cm^2
D3-17	Wobblers	Sand	34	63	20	26	2.7
D3-236	1/6 rings	"	36	45	4.0	8.5	1.6
D4-285	1/6 rings	Metal	33—36	52—61	5—15	7—16	1.7—2.0
12655	1/6 rings	"	28—36	50—61	8—21	10—30	2.0—4.0

These data show that castings can be obtained with good properties.

However, the ductility, elongation, and reduction of area of thick-walled sand castings are reduced by several percent. Correspondingly, the ultimate strength decreases from 63 to 45 kg/mm^2 as a result of premature brittle failure.

Castings produced in metal molds have better mechanical properties. The elongation varies from 5—8 to 15—20% in different zones of the casting. The worst properties were found in the zone of coarse equiaxial crystals, particularly near the shrinkage head.

The mechanical properties at 700°C of thin-walled and thick-walled castings produced in metal molds are as follows: $\sigma_{0.2} = 20-25$ kg/mm^2; $\sigma_в = 30-40$ kg/mm^2; $\delta_5 = 17-20\%$; $\psi = 25-40\%$; $a_k = 2.5-6.0$ kgm/cm^2.

The strength of the metal is little changed by prolonged (3000—5000 hr) isothermal heating at 750°C. Under these conditions the ductility (δ_5 and ψ) decrease to 6—7 and 10—12%, respectively.

However, the ductility decreases during the first 1000 hr of heating, and further heating retards this detrimental decrease.

The same is true of the impact strength, which decreases from 3.0 to 1.5—2.0 kgm/cm^2 during the first 1000 hr of heating at 750°C, but it remains at the same level on further heating for 3000—5000 hr.

Thin-walled and thick-walled castings were tested for long-time strength at 700 and 750°C. Figure 3 shows the dependence of the time to failure on the stresses of wobbler specimens. It can be seen that an arbitrary extrapolation of these data to 100,000 hr fixes the ultimate strength at 700°C as 10 kg/mm^2, and at 750°C as 8 kg/mm^2, which satisfy technical requirements.

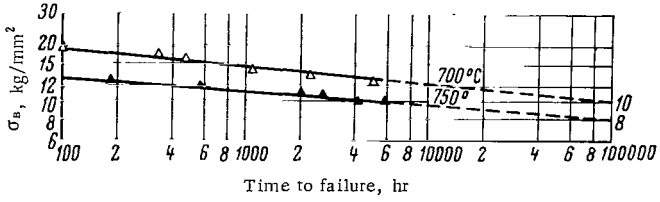

FIGURE 3. Long-time strength of steel (thin-walled castings, D3-17 heat).

The long-time strength of thick-walled specimens cast into metal molds is about the same, i.e., at 750°C σ_{10^5} is equal to 8 kg/mm^2 (Figure 4). The elongation on failure after 2000 hr of testing is 10—12%.

The creep strength of this steel was determined at 750°C by 4000—5000 hr-long tests. Under a stress of $\sigma = 5$ kg/mm^2 the steady-state creep rate did not exceed $0.5-1.0 \times 10^{-5}$%/hr. Thus, the creep limit at 750°C at a rate of 1×10^{-5}%/hr was not less than 5 kg/mm^2, and so satisfies technical requirements.

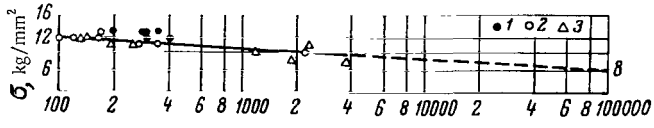

FIGURE 4. Long-time strength of TsZh13 steel at 750°C (thick-walled castings made in metal molds):

1—melt D4-285; 2—melt D5-54; 3—melt 12655.

Resistance to scaling is also one of the characteristics of heat-resistant materials.

The resistance to scaling was tested by heating in the air at 750°C for up to 10,000 hr. The corrosion rate was determined from the weight loss and was 0.03 mm/year. This metal can therefore be classified as resistant to scaling.

The conditions of crystallization of TsZh13 steel considerably influence its weldability as regards the formation of cracks near the joint.

Cracks which propagate from the joint into the basis metal are easily formed in brittle welds of a large casting. Similar cracks can sometimes appear when welding castings which were produced in metal molds but were not given high-temperature austenitizing treatment.

The formation of cracks near the weld can be avoided if the chill casting is heated to 1200—1250°C before welding and rapidly cooled (preferably water quenched).

When choosing welding electrodes their influence on the final product must be considered, particularly low sensitivity to the formation of crystallization cracks. In addition, the metal of the weld should be sufficiently heat resistant and have other satisfactory properties.

We studied and recommended two electrode metals* of the 1Kh14N65M15V4 type (electrodes TsT-28 and welding wire EP367) and the 3Kh15N35V3B2 metal (KTI-7 electrodes made of the EP198 welding wire).

The KTI-7 electrodes are rather less suitable, since crystallization notches are sometimes formed in the first layers of the weld diluted by the basis steel and with a lower niobium content (sufficient resistance to cracking of 3Kh15N35V3B2-type metal in the joint is ensured by the presence of a high content of niobium carbide). Such undesirable influence of dilution can be removed by filling the first layers of the weld by means of special KTI-7 electrodes with a niobium-rich coating which produce a joint with a high content of niobium.

At 750°C the metal of the welds produced by TsT-28 electrodes has a long-time strength during 100,000 hr of 6 kg/mm^2; welds made by KTI-7 electrodes have a long-time strength of 8 kg/mm^2 which is almost the same as that of the basis metal.

This welding technique successfully passed industrial test on welding pilot-plant parts.

CONCLUSIONS

We developed an austenitic steel for casting articles for service at 700—750°C. We also developed a new casting process by accelerated crystallization, which ensures the necessary mechanical properties of the metal, and a welding technique (filling in defects) for castings which ensures reliable service of welded assemblies.

* These compositions were developed by TsNIITMash and TsKTI im. Polzunov.

Bibliography

1. Mirkin, I. L. and M. I. Fantaeva. Svoistva litykh austenitnykh splavov s intermetallidnym uprochneniem (Properties of Precipitation-Hardening Austenitic Alloy Castings Containing Intermetallic Compounds). — In: "Issledovanie novykh zharoprochnykh splavov dlya energetiki," No. 101. Mashgiz. 1961.
2. Mirkin, I. L. and A. S. Tereshkovich. Svoistva litykh austenitnykh splavov s karbidnym i smeshannym uprochneniem (Properties of Precipitation-Hardening Austenitic Alloy Castings Containing Carbides or Carbides and Intermetallic Compounds). — In: "Issledovanie novykh zharoprochnykh splavov dlya energetiki," No. 101. Mashgiz. 1961.
3. Mirkin, I. L., R. P. Zaletaeva, and A. S. Tereshkovich. Fazovyi sostav i svoistva slozhnolegirovannykh austenitnykh stalei (Phase Composition and Properties of Complex Austenitic Steels). — In: "Issledovaniya po zharoprochnym splavam," Vol. 10. Izdatel'stvo AN SSSR. 1963.

III. STRENGTHENING OF STEELS AND ALLOYS

V. D. Sadovskii, B. D. Titorov, E. N. Sokolkov, V. K. Farafonov, V. D. Negodyaev, and M. M. Nichkova

HIGH-TEMPERATURE AUSFORMING OF LARGE STEEL FORGINGS

The purpose of this work is to determine the applicability of high-temperature ausforming to strengthening large forgings of EI612K steel.

Forgings 450 mm in diameter and 250 mm thick were subjected to high-temperature ausforming by upsetting at the rate of 0.5—1%/sec. A 25% deformation was obtained by upsetting under a 3 ton press in two passes after heating to 1100°C. Three minutes after upsetting the forging was quenched in water.

A microstructural study showed that under these conditions high-temperature ausforming produces a nonrecrystallized structure with characteristically twisted grain boundaries. This structure is also characteristic of fragmentation of grains. By X-ray structural analysis it was found that the maximum dimensions of the fragments which form individual grains is 50—100μ, and that they are disaligned by 3—5 min. These data were obtained by analyzing the X-ray photographs of an inverse recording method using 0.4 mm diameter diaphragms when the distance between the specimen and the film was 25—30 mm. Under such conditions of recording the reflections from the grains can be divided into those corresponding to the individual fragments. By recording from two distances the dimensions of the fragments formed can be evaluated. The distances between the most intense reflections indicate the disalignment between the fragments.* From the forgings which had undergone high-temperature ausforming we cut out specimens for studying the kinetics of aging and for evaluating the mechanical properties. All master specimens were cut out from forgings after high-temperature ausforming and a second quenching in water from 1100°C.

A study of the kinetics of aging according to hardness (at 650°C, 700°C, 750°C, and 800°C) indicates that in material that has undergone high-temperature ausforming the decomposition of the solid solution is very intense. Therefore, these specimens have a much higher hardness after almost any aging process than specimens hardened in the ordinary way (Figure 1).

High-temperature ausforming has the same influence on the metal from any spot in the forging. From these results we chose a temperature of aging (700°C) at which we treated specimens for mechanical testing at room and elevated temperatures. An evaluation of the mechanical properties by tensile tests at room temperature indicates that high-temperature ausforming and aging at 700°C considerably increase the strength of the steel, which

*Data on the disalignment between the fragments were prepared statistically.

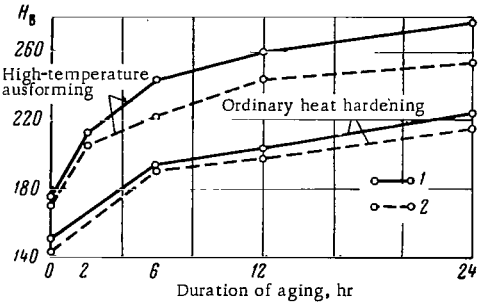

FIGURE 1. Influence of aging on the hardness of material after high-temperature ausforming (T = 700°C):

1 — upper; 2 — middle.

at the same time remains sufficiently ductile (Figure 2). Here it should be pointed out that differences between the strength of the metal from different sections of the forgings are small (Figure 3). The high-temperature strength of the metal (specimens with a 6 mm diameter working part) was tested at 600 and 650°C under stresses of 44 and 38 kg/mm^2, respectively, after aging at 700°C for 24 hr. It was found that the time to failure at 600°C and under a stress of 44 kg/mm^2 was 3000—5000 hr for specimens that had been given a high-temperature ausforming, compared to 500—700 hr for specimens hardened ordinarily (the strength increased 6 times on an average).* This increase is apparently due mainly to decrease in the creep rate of the ausformed steel (elongation at failure of specimens hardened ordinarily and of those hardened by high-temperature ausforming was 3—4 and 0.7—1%, respectively).

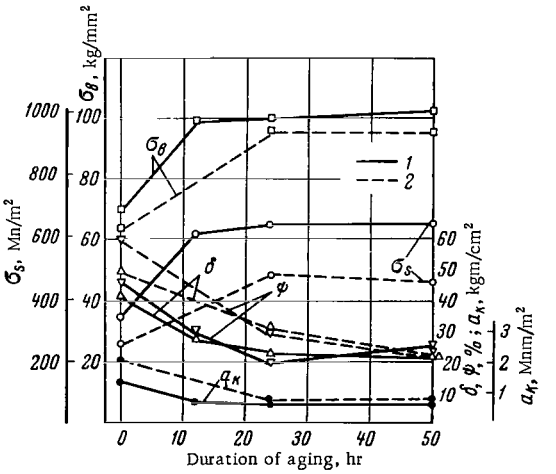

FIGURE 2. Mechanical properties of EI612K steel after high-temperature ausforming and aging at 700°C:

1 — high-temperature ausforming; 2 — ordinary hardening.

* The specimens were cut from the peripheral part of the forging.

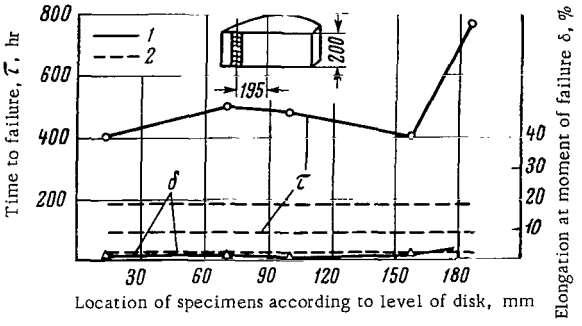

FIGURE 3. Influence of high-temperature ausforming on the long-time strength at 650°C:

1 — high-temperature ausforming; 2 — ordinary hardening.

Tests carried out at 650°C and under a load of 38 kg/mm^2 show that the strengthening produced by high-temperature ausforming is retained although not completely, and the time to failure is approximately doubled. These tests, unlike those carried out at 600°C, show that specimens which have undergone high-temperature ausforming have a higher ductility at the moment of failure (5—7% compared to 0.7—0.9% for specimens which have been quenched a second time). It is quite possible that the increase in the time to failure of a specimen that has undergone high-temperature ausforming is due to increase in the ductility of the material. A final conclusion on this problem can be obtained by analyzing the creep curve.

A comparison of the heat resistance produced by high-temperature ausforming and by ordinary heat treatment is somewhat complicated. This is because ordinary hardening was performed on small billets (cut from forgings) which had a grain size different from that of the metal subjected to high-temperature ausforming.

Comparisons, however, can be made by means of statistical values of the time to failure for a given steel under specific testing conditions. Such a comparison shows that high-temperature ausforming doubles or trebles the time to failure (this almost coincides with the conclusions based on this work). Finally, we should like to point out that high-temperature ausforming of EI612K steel produces a yield strength that cannot be attained by any other heat treatment (see Figure 2). This together with the increase in the heat resistance of the steel are apparently of great importance.

The favorable influence of high-temperature ausforming on the properties of EI612K steel is due to at least three factors:

1. Intensification of aging, which leads to an increase in the content of the strengthening phase and to its more uniform distribution within the grains; this apparently increases the strength of the metal.
2. Fragmentation of the structure and the formation of boundaries between subgrains which form obstacles to migration of dislocations.
3. Twisting of the grain boundaries, which slows down intergranular failure during high-temperature tests.

CONCLUSIONS

1. High-temperature ausforming at a rate of deformation equal to 0.5—1%/sec can be carried out on large forgings.
2. High-temperature ausforming of EI612K steel produces a nonrecrystallized structure in forgings 500 mm in diameter and up to 200 mm in thickness.
3. High-temperature ausforming of forgings of this size increases their strength and their heat resistance quite uniformly throughout the diameter of the forging.
4. The favorable influence of high-temperature ausforming is due to intensification of aging, fragmentation of the structure, and twisting of the grain boundaries.

V. S. Ivanova and N. A. Vorob'ev

KINETICS OF FAILURE OF HEAT-RESISTANT ALLOYS DURING HIGH-TEMPERATURE DEFORMATION

Due to the increasing demands of industry, materials which have a high strength at elevated temperatures must be used.

As the service conditions endured by materials (higher service parameters, allowance for local plastic deformations during service, and in certain cases even local failure) become more rigid, parts and constructions must be produced with a higher safety coefficient. Therefore, the properties of the metal in the region of plasticity, and the mechanisms of failure under various service conditions, must be tested besides the ordinary strength characteristics of a metal.

Failure is a process caused by plastic deformation which develops with time. It is therefore necessary to investigate the kinetics of the accumulation of damage during plastic deformation.

By studying the damaging process, it is possible to find the amount of plastic deformation just before failure of the material during strengthening processes.

In this work we studied the kinetics of the process of damaging heat-resistant chromium—nickel stainless steel 1Kh18N9T and the nickel-base EI437A alloy to determine the point at which damage becomes irreversible under conditions of static tensile deformation at room and elevated temperatures.

The chemical composition and the heat-treatment processes of these alloys are shown in Table 1.

The damage was studied by direct and indirect methods. In the first methods cracks are observed directly by electron or light microscopes, and in methods of the second type the regularity of the variation in a number of physical properties as well as mechanical and other characteristics (the so-called structurally sensitive properties) is studied during the deformation of metals.

TABLE 1. Chemical compositions and heat treatment processes of the materials studied

Material	Content of elements, wt %										Heat treatment
	C	Si	Mn	S	P	Cr	Ni	Fe	Ti	Other elements	
1Kh18N9T	0.038	0.70	0.80	0.01	0.04	17.0	10.0	traces	0.27	—	Heating to 1100°C, quenching in water
EI437A	0.04	0.29	0.30	0.007	0.008	20.3	traces	0.35	2.63	0.88	Heating to 1150°C, quenching in water, aging at 700°C for 1600 hr

To find the damage to materials in the process of deformation caused by tensile stresses at room and elevated temperatures, we carried out the following:

1) electron microscopic analysis of specimens stretched to various elongations;

2) determination of the variation in the electric conductivity, measured at room temperature, as a function of the degree of deformation of the metal at a given temperature;

3) determination of the variation in the specific energy of maximum deformation, measured at room temperature, as a function of the degree of preliminary deformation of the metal at elevated temperatures;

4) determination of the dependence of the cross-sectional area of specimens on elongation;

5) determination of the dependence of the Irwin criterion K_{IC}, which characterizes the resistance to crack propagation, on the degree of deformation.

We deformed cylindrical specimens with a measured length of 25 mm and a diameter of 5 mm, by the IM-4R tensile test machine.

The electron microscope studies were carried out by a TESLA BS-242 microscope using carbon replicas applied to the unetched surface of deformed specimens at an angle close to 90° without any special shadowing.

The electric conductivity was measured by a potentiometer device. The readings were taken from the most deformed region of the specimen and the error was ± 0.5% on a basis of about 1.4 mm /1/.

The specific energy of the maximum deformation was determined by the method of Shwinning /2/ by measuring the $\sigma = f(\delta)$ experimental curve with a planimeter, where $\sigma = P/F$ (P is the actual load, F is the initial cross-sectional area of the specimen) and $\delta = (d_0/d_i)^2 - 1$ (d_0 is the initial diameter of the specimen and d_i is the actual diameter of the specimen during tensile tests). To determine d_i, the specimen was periodically unloaded. In this case the specific energy of the maximum deformation characterizes the specific energy consumed for plastic deformation and for destruction of the specimen in the dangerous section.

To plot the dependence of the cross-sectional area on the elongation, we measured the diameter d_i in the dangerous section during the periodical unloadings of the specimen until it failed, according to the method developed by Oding and Liberov /3, 4/.

The criterion of resistance to the propagation of cracks was found for individual specimens deformed to a given elongation. In this case we used the method of determining K_{1C}, suggested by Irwin /5/ for cylindrical specimens with round and very sharp notches (radius of notch 0.025 mm). If the notch decreased the cross-sectional area to half its initial magnitude, K_{1C} was calculated from the formula $K_{1C} \simeq 0.414\sigma_N D^{1/2}$, where D is the diameter of the specimen outside the notch; σ_N is the nominal breaking force ($\sigma_N = P_{max}/F_{notch}$), and the energy necessary for unstable propagation of the crack (per unit length) was found from the formula

$$G_{1C} = \frac{K_{1C}^2}{E}(1 - \nu^2),$$

where E is Young's modulus and ν is Poisson's ratio.

Figure 1 shows diagrammatically a stress-strain curve and curves representing the variation in the structurally sensitive properties of materials during deformation. These include the variation in the cross-sectional surface area S (curve d_i^2), the resistance to propagation of cracks (criterion K_{1C}), the specific energy of maximum deformation A_p, and the electric conductivity $1/\rho$ during elongation.

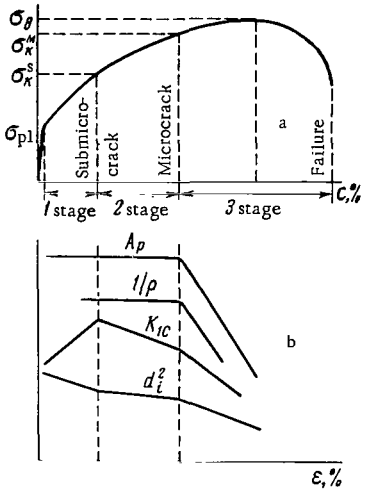

FIGURE 1. Stress-strain curve (a) and variation in the specific energy of maximum deformation A_p, electric conductivity $1/\rho$, resistance to the propagation of cracks K_{1C}, and the cross-sectional surface area d_i^2 during deformation (diagrammatic representation) (b).

From these studies the stress-strain curve can be divided into certain sections corresponding to the characteristic changes in these properties.

Section 1 is characterized by a linear decrease in the cross-sectional surface area with increase in the deformation to the moment where this decrease starts to lag behind elongation (deformation ε_k^s), and by an increase in K_{1C} to a maximum; A_p and $1/\rho$ do not yet change significantly; in section 2, S lags behind ε and K_{1C} decreases. The values of A_p and $1/\rho$ change little; in section 3 $\varepsilon \geqslant \varepsilon_k^M$, and $S(d_i^2)$, K_{1C}, A_p and $1/\rho$ decrease more rapidly.

Examples of the variation in structurally sensitive properties of the materials we studied are given in Figures 2 and 3.

Electron microscope studies (Figure 4) showed that plastic deformation exceeding ε_k^s leads to the formation of cracks in the metal. The latter are 0.4—7 μ in length, and their maximum width is a few tenths of a micron. These cracks usually lie in the slip bands. Their nucleation can apparently be explained by the dislocation theory suggested by Gilman /6/ and Rozhanskii /7/.

Sometimes the cracks nucleate in the vicinity of nonmetallic inclusions or of second-phase particles (Figure 4, b). As the degree of deformation increases the number of cracks in the slip bands and their length increase, and at deformations exceeding ε_k^M, microcracks are formed.

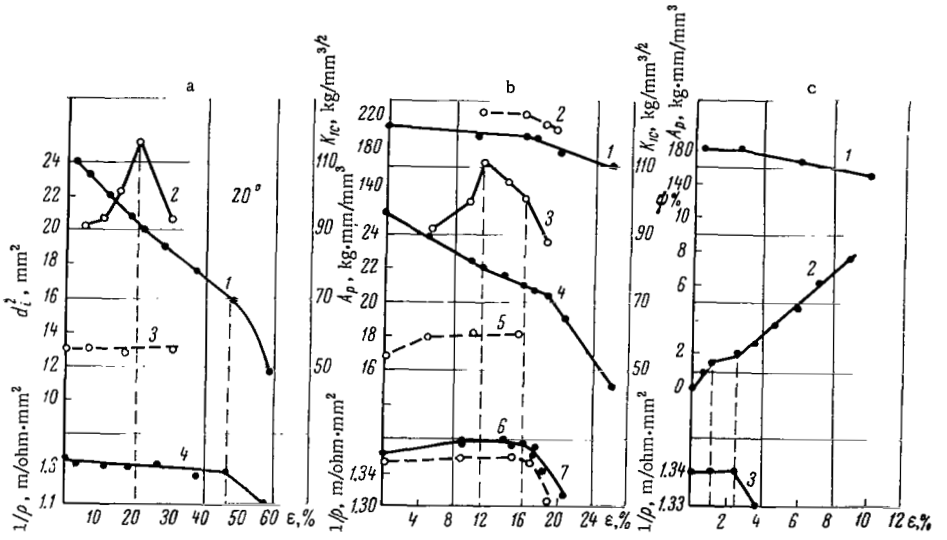

FIGURE 2. Dependence of the structurally sensitive properties of 1Kh18N9T steel on elongation:

a) $T = 20°C$: $1 - d_i^2 = f(\varepsilon)$, $2, 3 - K_{1C} = f(\varepsilon)$, $4 - 1/\rho = f(\varepsilon)$; b) $T = 600°C$: $1, 2 - A_p = f(\varepsilon)$, $3, 5 - K_{1C} = f(\varepsilon)$, $4 - d_i^2 = f(\varepsilon)$, $6, 7 - 1/\rho = f(\varepsilon)$; c) $T = 700°C$: $1 - A_p = f(\varepsilon)$, $2 - \psi = f(\varepsilon)$, $3 - 1/\rho = f(\varepsilon)$.

Thus, there is a certain connection between the changes in the structurally sensitive properties and in the microstructure of the metal during stretching.

The decrease in K_{1C} and the lagging of S behind ε (see Figure 2) confirm the formation of submicrocracks at $\varepsilon \geqslant \varepsilon_k^s$.

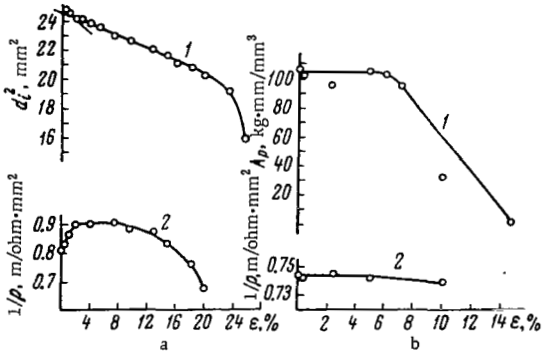

FIGURE 3. Dependence of the structurally sensitive properties of the EI437A alloy on elongation:

a) $T = 20°C$: $1 - d_i^2 = f(\varepsilon)$, $2 - 1/\rho = f(\varepsilon)$; b) $T = 700°C$: $1 - A_p = f(\varepsilon)$, $2 - 1/\rho = f(\varepsilon)$.

From the above it follows that the process of plastic deformation from the start until the spontaneous growth of the crack can be divided into the following three stages:

I—accumulation of defects in the crystal lattice (dislocations and vacancies) until submicroscopic cracks start to form in the local volumes which have a critical density of defects;

II—growth of submicroscopic cracks to the dimensions of microscopic cracks;

III—growth of microcracks to macroscopic dimensions and final failure of the metal.

This sequence of processes of failure is similar to the failure of metals under conditions of fatigue /8/. It can, apparently, be assumed that this sequence of processes is quite general for different methods of loading.

From these results it is possible to construct a stress-strain diagram which shows not only the usual criteria of strength (ultimate strength, limit of proportionality, etc.) but also certain values of stresses or deformations which represent the start of the formation of submicroscopic (σ_k^s, ε_k^s) and microscopic cracks (σ_k^M, ε_k^M).

A change in the structurally sensitive properties caused by deformation and austenitizing at 1100°C for 30 min shows that the damage caused by submicrocracks is reversible (see Figure 2, dashed lines), while the microcracks cannot be annealed by such heat treatment.

It should be pointed out that our experimental data for σ_k^s of a material consisting of a uniform solid solution agree well with the calculated.

Since no other stress relaxation is possible, the applied stress which leads to the formation of a crack is determined, according to the dislocation theory, by the Stro formula /10/

$$\sigma = 4\{6\gamma G/\pi(1-\nu)d\}^{1/2}, \qquad (1)$$

where γ is the surface energy, G is the shear modulus, ν is Poisson's ratio, and d is the diameter of the grain.

According to Cottrell /11/ the length of the crack produced in the region of accumulated dislocations can be calculated from the formula

$$l = 2\gamma G/\pi(1-\nu)\sigma^2, \qquad (2)$$

where γ, G, σ and ν are the same as in equation (1).

From these formulas we calculated the length l of submicrocracks arising during the deformation of 1Kh18N9T steel and of the EI437A alloy, and the stresses σ_k^s which induce these cracks. The calculated and experimental data for l and for σ_k^s are given in Table 2. The calculated and experimental data for the 1Kh18N9T steel agree well if the metal consists of a homogeneous solid solution. The experimental data for σ of aged EI437A alloys are higher than the calculated. This is possibly because in this case the slip bands are less than half the diameter of the grain due to the presence of second-phase obstacles. The magnitudes of σ_k^s and ε_k^s can be used for calculating the stresses necessary for the various strengthening deformations and also for determining the optimum conditions for thermomechanical treatment.

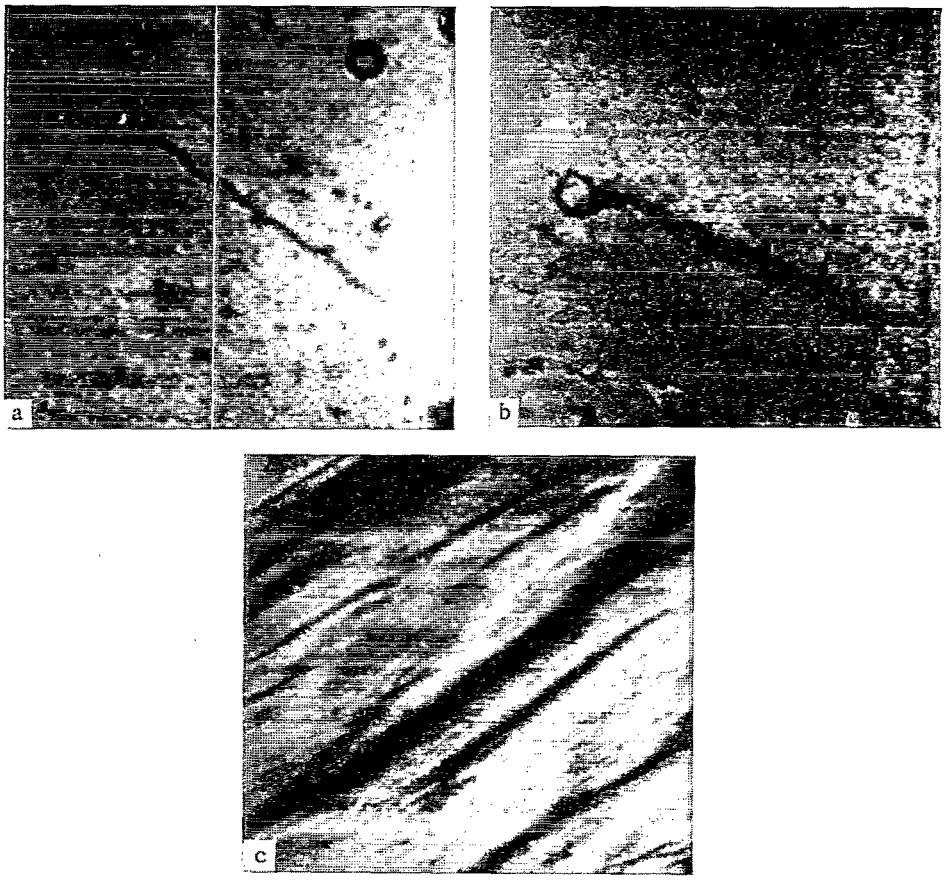

FIGURE 4. Variation in the microstructure of 1Kh18N9T steel during stretching at 20°C:
a and b — $\varepsilon = 23\%$, ×30,000; c — 55, ×15,000.

TABLE 2. Comparison of calculated and found lengths l of submicrocracks and stresses σ_k^s which lead to the production of such cracks, under conditions of static tension of 1Kh18N9T steel and of EI437A alloy

Material	Testing temperature, °C	Shear modulus, $G \cdot 10^{-5}$ kg/cm^2	Minimum crystal lattice parameter, 10^{-8} cm	Surface energy* $\gamma \cdot 10^{-3}$ kg/cm^2	Poisson's ratio, ν	Diameter of grain d, cm	Stress σ_k^s, kg/mm^2		Length of crack $l \times 10^2$, mm	
							calculated	found	calculated	found
1Kh18N9T	20	7.87	2.49	1.96	0.285	0.0015	66.5	70	0.03	0.04—0.7
1Kh189T	600	5.77	2.49	1.44	0.326	"	50	41	—	—
EI437A	20	7.87	2.49	1.96	0.285	0.02	18.2	90.5	—	—

* The values of the coefficient of elasticity are taken from /12/. It has been assumed that $\gamma = 0.1\ Gb$.

Oding, Gordienko, and Fridman /9/ found that the optimum and at the same time maximum degree of plastic deformation for thermomechanical treatment of 1Kh18N9 steel at 600°C is a 10% reduction.

The optimum degree of deformation $\varepsilon_k^s = 11\%$ is close to the deformation which according to our data leads to the formation of submicrocracks in 1Kh18N9 steel. The variation in the structurally sensitive properties of 1Kh18N9 steel is similar to that of 1Kh18N9T steel (see Figure 3). This shows that in this case the maximum degree of deformation in thermomechanical treatment leads only to the formation of submicrocracks during the process of high-temperature deformation.

The experimental data shown in Figure 2, b, c, indicate that the optimum degree of deformation depends on temperature, and for 1Kh18N9T steel it is equal to 10% at 600°C and 1% at 700°C.

CONCLUSIONS

By studying the variation in the structurally sensitive properties (electric conductivity, specific energy of maximum deformation, resistance to the propagation of cracks, etc.) during plastic deformation, and by electron microscope analysis, we found:

1. The laws that govern failure of heat-resistant 1Kh18N9T steel and of the EI437A alloy under conditions of static stresses at 20°C, 600°C, and 700°C.
2. That the process of deformation and of failure during static strain proceeds in three stages: I — accumulation of crystal lattice defects until submicroscopic cracks are formed; II — growth of submicroscopic cracks to the dimensions of microscopic cracks; III — growth of microscopic cracks to macroscopic dimensions and final failure of the metal.
3. The experimental values for the true stresses which lead to the formation of submicrocracks agree well with the theoretical, calculated from dislocation models for single-phase alloys. In the case of alloys containing considerable amounts of a finely dispersed second phase, there are considerable discrepancies between the theoretical and experimental data.
4. We found criteria of forces with which it is possible to determine the maximum permissible plastic deformation leading to reversible or irreversible damage. These criteria can be used to choose the optimum degree of deformation during thermomechanical treatment.

Bibliography

1. Gordienko, L.K.— Filial VINITI AN SSSR, PNTO, No. P-59-36/2, tema 32. 1959.
2. Gillemot, L. and G. Sinay.— Acta Techn. Acad. Sci. Hungaricael, Vol. 22, 1—2. 1958.
3. Oding, I.A. and Yu. P. Liberov.—Izv. AN SSSR, OTN. Metallurgiya i Toplivo, No. 6. 1962.

4. Oding, I.A. and Yu.P.Liberov.—Izv. AN SSSR, OTN. Metallurgiya i Gornoe Delo, No.1. 1964.
5. Irwin, G.R.—Appl. Materials Research, Vol.3, No.2. 1964.
6. Gilman, J.J.—Trans. ASME, Vol.212, No.6. 1958.
7. Rozhanskii, V.N.—Doklady AN SSSR, 123. 1958; Fizika Tverdogo Tela, Vol.2. 1960.
8. Ivanova, V.S. *Ustalostnoe razrushenie metallov* (Failure of Metals by Fatigue), p.149.— Moskva, Metallurgizdat. 1963.
9. Oding, I.A., L.K.Gordienko, and Z.G.Fridman. — In: "Issledovanie splavov tsvetnykh metallov." Izdatel'stvo AN SSSR. 1963.
10. Cottrell, A.H. — In: "Atomnyi mekhanizm razrusheniya," p.30 Moskva. 1963.
11. Cottrell, A.H.—Trans. ASME, Vol.212, 192. 1958.
12. Clark, C.L. High Temperature Alloys. Pitman's Metallurgical Series. 1953.

L.K.Gordienko, Z.G.Fridman, and V.N.Stepanov

INFLUENCE OF TEMPERATURE ON THE STABILITY OF HEAT-RESISTANT ALLOYS STRENGTHENED BY THERMOMECHANICAL TREATMENT (TMT) AND MULTISTAGE THERMOMECHANICAL TREATMENT (MSTMT)

A new method of increasing the heat resistance of steel by TMT, suggested by Oding et al. /1, 2/ and now being developed at the Institute of Metallurgy AN SSSR /3—5/ and some other institutions, has been tested in several plants producing power units and constructional materials. Research has recently been started on the adaptation of this method to industry. Special studies have been carried out on the behavior of materials strengthened by TMT under various conditions of temperature and stresses during service.

To produce a highly heat-resistant alloy it is very important not only to obtain high strength by the known methods of thermomechanical treatment, but also to retain this strength under the prolonged action of stresses and temperature. To determine the effectiveness of the strengthening treatment, it is necessary to find the thermal stability of the structure produced by TMT and to determine the maximum temperature at which the effect of strengthening is retained under a static load. The purpose of this study is to determine the increase in the heat resistance (long-time strength, creep resistance, and short-time strength) produced by TMT below the recrystallization temperature and by multistage thermomechanical treatment (MSTMT) /6/ over a wide range of stresses and temperatures in a number of materials used in the machine-building industry. We studied the following materials: heat-resistant pearlitic 12Kh1MF steel, heat-resistant nickel-chromium EI617 alloy, and three types of austenitic steels hardened by carbide and intermetallic precipitates (1Kh18N9, EI481, EI696M). The thermal stability and the upper temperature limit of service of these steels

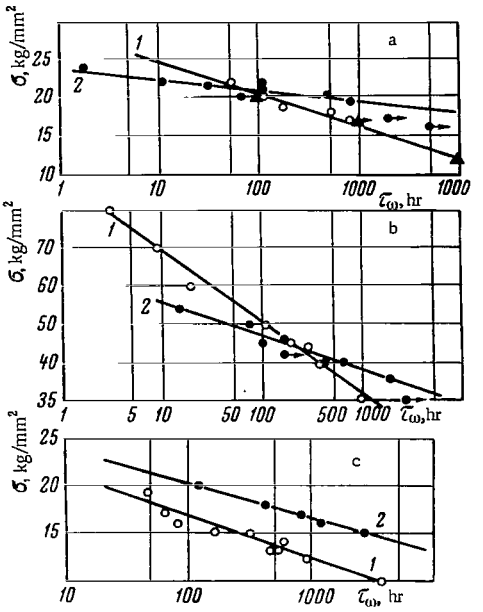

FIGURE 1. Long-time strength curves of:

a — 12Kh1MF steel at 585°C; b — EI617 alloy at 700°C; c — 1Kh18N9 steel at 650°C; 1 — not strengthened; 2 — after TMT (in the case of 12Kh1MF steel after MSTMT).

were also determined. We attempted to make a general evaluation of the behavior of hardening materials using a general diagram of the criteria of creep (complex).

LONG-TIME STRENGTH OF 12Kh1MF STEEL AFTER MSTMT

The experiments were carried out on specimens which had been cut out of tubes of steam boiler superheaters according to the method described in /7/. The long-time strength tests were carried out on the following batches of specimens:

a) after ordinary heat treatment (normalizing at 965°C for 2 hr, cooling in the air, and tempering at 740°C for 5 hr);

b) after MSTMT of normalized specimens (the MSTMT was carried out by successive deformation of the specimens by drawing to a 1.2, 1.0, and 0.8% reduction with intermediate heatings. After this process the articles were aged at 150°C for 6 hr).

The long-time strength curves constructed for these two batches of specimens are shown on Figure 1,a. It was found /7/ that after such a MSTMT process the long-time strength of 12Kh1MF steel at 510°C is considerably increased over the whole range of stresses. An increase in

the service temperature to 585°C annuls the effect of strengthening under relatively high stresses (above 20 kg/mm^2). However, the rate of softening is rather low (curve 2), and if the service life is more than 100 hr the strengthening produced by MSTMT increases continuously. The long-time strength ($\sigma_{10,000}$) of specimens is increased by MSTMT from 12 to 18 kg/mm^2, and the service time under a stress of 15 kg/mm^2 increases (according to data obtained by extrapolation) from 2000 to 100,000 hr.

These data were confirmed by the results of service tests on sections of steam superheater tubes strengthened by MSTMT (in the industrial boiler BKZ-210-140 PT at the "Kievenergo" ERU system) at 585°C. We did not overlook the possibility that the temperature can rise periodically to 610–630°C. The tubes which underwent this treatment had a high creep resistance under stresses that were 1.5–2.0 times those calculated during 10,000 hr of continuous service. This experiment shows that the method of MSTMT can be very useful for increasing the heat resistance and reliability of pearlitic boiler steel.

INFLUENCE OF TMT ON THE HEAT RESISTANCE OF THE EI617 ALLOY AT 700°C

Specimens of the nickel-chromium EI617 alloy after solution heat treatment and an optimum process of TMT /4/ (deformation by stretching to a 1% reduction at 600°C followed by a polygonization anneal for 100 hr at the same temperature) were tested for creep on IP-5 machines at 700°C, which is 100°C higher than that of the previous tests on the strengthened alloy /4–5/. An example of the creep curves is shown in Figure 2.

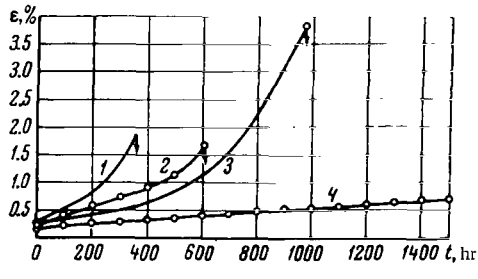

FIGURE 2. Creep curves of the EI617 alloy recorded at 700°C:

1 – untreated; 2 – after TMT; 3 – untreated; 4 – after TMT:
1, 2 – σ = 40 kg/mm^2; 3, 4 – σ = 35 kg/mm^2.

Under a stress of 40 kg/mm^2 the time to failure of the alloy after TMT was almost twice that of the untreated specimens (curves 1 and 2), but the ductility remained almost the same (1.7–1.9%). As the stress is decreased, the creep strength of the alloy increases after TMT. Under a stress of 35 kg/mm^2 (curves 3 and 4) the creep rate of the alloy after TMT is one

third of that of the initial alloy ($3.3 \cdot 10^{-4}$% per hr). After 1500 hr of testing the creep of the hardened alloy proceeds at a minimum constant rate (under these conditions the untreated specimen failed after 972 hr). The total duration of the test of specimens subjected to TMT was 3000 hr, and even after this period the creep rate did not increase.

Thus, the thermomechanical treatment of the EI617 alloy greatly increases its heat resistance not only at 600°C but also at 700°C. However, as in the case of pearlitic steel, strengthening is attained under stresses of long duration only.

This is particularly apparent from the curves representing the long-time strength of the alloy (Figure 1,b). At 700°C the effect of TMT is marked under stresses of less than 45 kg/mm^2 (i.e., after 200 hr of service) as a result of the slower softening of the treated alloy (curve 2). Under stresses of 35 kg/mm^2 the service life of specimens increases about 10 times after TMT and this effect is augmented as the stress which causes creep is reduced and approaches the real service stresses for a given alloy.

Thus, the optimum process of TMT at 600°C is an effective means of increasing the heat resistance of the EI617 alloy at 700°C under stresses of less than 45 kg/mm^2.

Gordienko /8/ studied internal friction in the EI617 alloy, and showed that the lack of any strengthening effect of TMT under very high loads is due to loss of thermal stability of the polygonized structure as a result of combined thermal and mechanical activation under conditions of high temperature creep. However, from the temperature dependence of the internal friction found in this work it can be assumed that under appropriate stresses of creep the positive effect of TMT will be noticeable at temperatures up to 800°C. It is only at higher temperatures that the internal friction of the strengthened alloy recovers completely, which indicates an irreversible annulling of the strengthening effect of the polygonized structure.

INFLUENCE OF TMT ON THE HEAT RESISTANCE OF AUSTENITIC STEEL 1Kh18N9. COMPLEX EVALUATION OF THE EFFECT OF TMT BY MEANS OF GENERALIZED DIAGRAMS OF CRITERIA OF CREEP

Earlier studies /4—5/ showed that TMT of 1Kh18N9 steel (drawing at 600°C to a 10% reduction followed by a 100-hr-long annealing at 600°C) is an effective means of increasing the creep resistance of this steel at 600°C. The effect of this TMT process has also been tested at a temperature of 650°C. The service temperature of steel could be increased on the basis of the dependence of the effect of TMT on the temperature of the polygonization anneal. The curve representing this relationship has a broad peak at temperatures from 550°C to 650°C (Figure 3). This dependence shows that annealing at 650°C leads to the formation of a stable polygonized structure, and therefore it can be expected that a steel subjected to creep tests at 650°C will have a high heat resistance.

Creep tests on specimens that had not been hardened and aged, and on specimens after TMT (650°C), showed that TMT decreases the creep rate (from $1.8 \cdot 10^{-1}$ to $4.0 \cdot 10^{-4}$% per hour at $\sigma = 16$ kg/mm^2, and from $1.35 \cdot 10^{-1}$

to $2.0 \cdot 10^{-4}$% per hour at $\sigma = 15$ kg/mm^2) and increases the service life of the metal. TMT increases the heat resistance of the steel over the whole range of stresses (from 10 to 20 kg/mm^2).

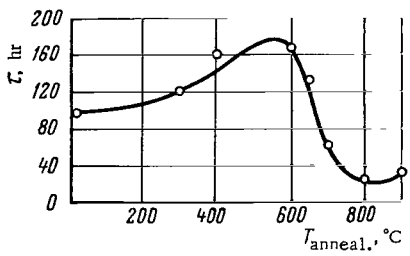

FIGURE 3. Influence of the temperature of the polygonization anneal after TMT on the time to failure of 1Kh18N9 steel creep-tested at 600°C under a load of $\sigma = 27$ kg/mm^2.

The long-time strength curves constructed from creep tests (carried out until failure (Figure 1,c) show that after TMT the 1Kh18N9 steel softens at 650°C much less than after the ordinary process of heat treatment. As a result of the optimum TMT process, under conditions of creep at 650°C and a stress of 15 kg/mm^2, the service life increases from 250 to 2600 hr, i.e., more than ten times, and the long-time ultimate strength σ_{1000} increases from 12 to 16.5 kg/mm^2. The different slopes of the curves of long-time strength (different rates of softening) show that the effect of strengthening of the steel increases with decrease in the creep stress.

The data given above show that TMT and MSTMT of heat-resistant steels lead to a considerable change in two basic criteria of heat resistance — the ability of the metal to resist deformation under conditions of creep, and its ability to resist failure. For constructional materials these two criteria are fundamental. A change in these criteria means the production of an entirely new material, which in fact is achieved as the result of TMT that produces a stable dislocation structure /9/.

In this connection the constructional features of hardening materials must be considered again. The evaluation of the maximum ductility of alloys under conditions of high-temperature creep is of particular importance in the field of the construction of electric machines. Oding et al. /1/ suggested a criterion which he calls ductility resource. This criterion should be used to evaluate the maximum ductility of the metal over long service periods when this cannot be determined experimentally because of the length of time that such an experiment would require. The permissible stresses and the strength of metals required for the production of machine parts working under conditions of creep can also be found by means of this criterion.

To analyze the criteria of creep and of long-time strength, and also the ductility resource, general diagrams of creep criteria of 1Kh18N9 steels before and after TMT were constructed for 600 and for 650°C (Figures 4,a and b) /1/.

The long-time strength curve and the curves representing the dependence of the creep rate on stresses (left and right quadrants of the diagrams, respectively) were plotted by means of serial creep tests on steel. The ductility resource was calculated from the formula

$$\varepsilon_r = v\tau,$$

where v is the rate of established creep under a stress σ; τ is the time to failure under the same stress.

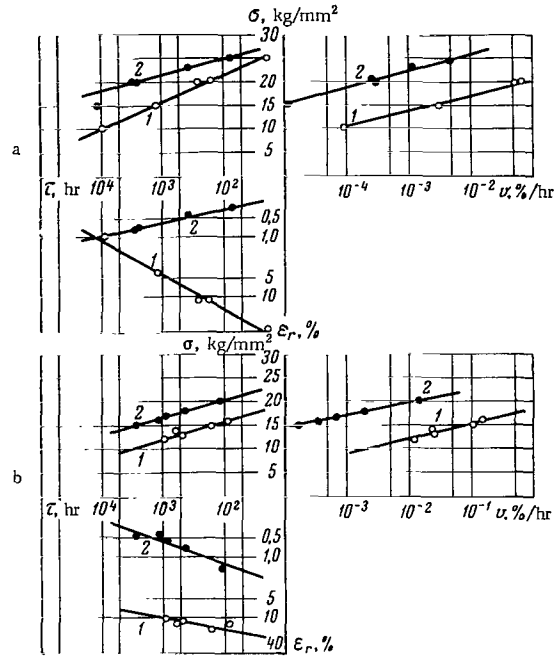

FIGURE 4. General diagrams of creep criteria of 1Kh18N9 steel at 600°C (a) and at 650°C (b):

1 — initial state (before TMT); 2 — after TMT.

The results of these calculations are shown as straight lines in the left lower quadrant of the diagram together with the experimental points representing the results of the direct determination of deformation accumulated during creep from the creep curves at various stresses.

The generalized diagrams of the criteria of creep show that at 650°C 1Kh18N9 steel has a high resource of ductility before TMT and a considerably lower resource after TMT (Figure 4,b). This is the direct result of a sharp decrease in the rate of steady-state creep before TMT. Both before and after TMT the resource of ductility of the steel decreases with increase in the duration of service at 650°C.

At 600°C the dependence of ε_r on the time to failure is entirely different (Figure 4,a). As before, the resource of ductility of steel before TMT rapidly decreases with the time. But after TMT the opposite is true: the resource of ductility of hardening steel increases continuously, and after 10,000 hr is equal to the ε_r of steel before TMT, and then becomes even greater. This variation in the resource of ductility can be explained by the sharp increase in the long-time strength of steel produced by an optimum structure of the polygonized metal for the given conditions of creep, particularly during long periods of service. This shows that for the above process of TMT the most favorable service conditions of the 1Kh8N9 steel is a temperature of 600°C and stresses corresponding to long-time service periods (10,000 hr or more).

The above examples on the behavior of alloys with a thermally stable dislocation structure show that it is necessary to carry out a complex evaluation of the heat resistance of materials hardened by TMT. This should be based on the long-time ultimate strength, creep rate, maximum service temperatures, and the resource of ductility, using the generalized diagrams of the criteria of creep.

INFLUENCE OF MSTMT ON THE STATIC STRENGTH OF AUSTENITIC STEELS PRECIPITATION HARDENED BY INTERMETALLIC COMPOUNDS AND CARBIDE PHASES

In some branches of industry austenitic heat-resistant steels are used for parts that have to withstand very high stresses (close to the yield point) for short times. As an example of these parts we give the power rods of electrically heated hoists used for industrial construction with mobile formwork. The efficiency, capacity, and reliability of such hoists depend on the strength of the power rods made of austenitic steel which are periodically heated by an electric current to 550—600°C and subjected to maximum tensile stresses at elevated temperatures.

Below we shall give the results of a study to find the most effective process of TMT for increasing the constructional strength of EI696M steel (hardened by intermetallic compound precipitates), and of EI481 steel (hardened by carbide precipitates) under tensile stresses at 500—600°C. We used cylindrical specimens with a diameter of the working part of 6 mm for the EI696M steel, and 5 mm for the EI481 steel. These specimens were prepared from hot-rolled rods with a 16—20 mm diameter.

The purpose of the heat treatment was to increase the short-time strength of the steel, and we chose an MSTMT process which not only increased the strength of the steel under prolonged static loads but also greatly improved the properties of the steel under conditions of dynamic loading /4, 6/. Preliminary studies by micromechanical tests showed that the MSTMT process should be preceded by solution heat treatment and aging for 5—6 hr, at temperatures 100—130°C lower than the temperature of rapid precipitation of intermetallic or cabide particles. In this case the following initial stage of strain aging during MSTMT is very favorable for effective blocking of dislocation concentrations. Micromechanical tests were also very useful for determining the optimum processes of MSTMT during which the metal was drawn at room temperature (degree of deformation per cycle, temperature of strain aging, total preliminary deformation, and number of treatment cycles).

Specimens of EI696M steel were subjected to TMT after they had been cooled in the air from 1050°C and aged for 5 hr at 650°C. The deformation produced by MSTMT was induced by drawing the specimens on an IM-4R machine at the rate of 2.5 mm/min, and the number of cycles of MSTMT varied from 3 to 5. The total reduction of the specimens did not exceed 30% (this reduction was chosen to compare the results with those obtained by a

single stage TMT). After each deformation cycle the specimens were held at 650°C for 2 hr (heating and cooling together with the furnace).

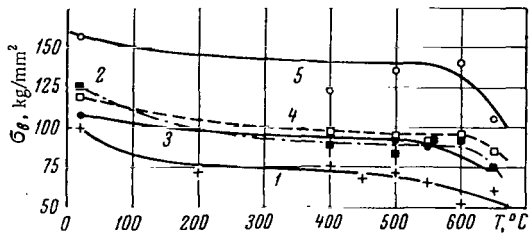

FIGURE 5. Influence of testing temperature on the ultimate strength of EI696M steel:

1 — without TMT (solution heat treatment + aging); 2 — after 3 cycles of MSTMT (ε_{cycle} = 2—4%); 3 — after 5 cycles of MSTMT (ε_{cycle} = 4—6%); 4 — after single stage TMT (ε = = 30%); 5 — after 6 cycles of MSTMT (ε_{cycle} = 2—4%).

The temperature dependence of the ultimate strength of EI696M steel after various processes is shown in Figure 5. Three cycles of MSTMT with an average reduction of ε_{cycle} = 3% per cycle increased σ_B by 25% at room temperature and by 40—45% at 600°C. Almost the same effect was obtained by a single stage TMT, which produced a 30% reduction (curve 4) and by 5 cycles of MSTMT with an ε_{cycle} = 5.5%. In the last case the σ_B at 600°C was increased from 60 to 95 kg/mm^2, i.e., by almost 60%, but because of the greater total deformation the high temperature ductility δ fell from 44 to 8—10%, while after 3 cycles of MSTMT it decreased to 18—20% only.

The highest strengthening was obtained after 6 cycles of MSTMT with an $\varepsilon_{cycle} \approx 3\%$ (Figure 5, curve 5). In this case too the strength of the steel at room temperature was increased from 99 to 155 kg/mm^2 (56%). The limit of proportionality σ_p increased from 52 to 145 kg/mm^2 (180%), but the elongation remained at 15%.

This process caused an increase in the ultimate strength (σ_B) at 600°C of 115% (from 60 to 130 kg/mm^2), and the limit of proportionality, which is close to the yield point, was increased by 300% (from 34 to 135 kg/mm^2).

The curves showing the temperature dependence of the strength of EI696M steel after MSTMT indicate that specimens are softened less by an increase in the testing temperature from room to 550°C or even to 600°C than by conventional heat treatment and tempering. This indicates that MSTMT produces a stable strength, particularly after 5—6 cycles. However, further increase in the number of cycles of MSTMT is not useful, since it leads to a decrease in the high-temperature ductility of the metal.

In Figure 5 the properties produced by MSTMT and aging are compared. The full effect of precipitation hardening as a result of the low temperature and of the short heating time is not given.

Figure 6 shows curves representing the temperature dependence of the ultimate strength of EI696M steel after conventional heat treatment (according to ChMTU/TsNIICHM 856-63 /10/) and of EI696MU steel after the most

effective processes of MSTMT. The same figure also gives the temperature dependence of the ultimate strengh $\sigma_в$ of EI696M steel which has not been subjected to any special heat treatment. These curves show that there is a considerable increase in the short-time strength of the EI696M steel after MSTMT over the whole range of temperatures studied.

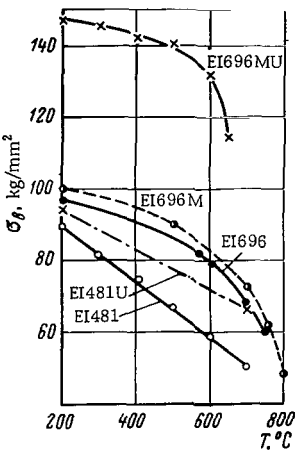

FIGURE 6. Temperature dependence of the strength of EI696M, EI696, and EI481 steels after conventional heat treatment and after MSTMT (index U).

MSTMT is particularly effective for service temperatures of 500—600°C. The increase in the static strength over this range of temperatures is 55—60%. An extrapolation of the temperature dependence of $\sigma_в$ to higher service temperatures shows that the softening of the structure of EI696M steel produced by MSTMT starts near 700°C.

The EI481 steel hardened by carbide precipitates was subjected to the TMT processes which had been most effective for the EI696M steel. The specimens were heated at 1070°C for 3 hr, air cooled, and aged at 680°C for 6 hr (cooling together with the furnace). They were then given four cycles of MSTMT producing a reduction of $\varepsilon_{cycle} = 4—6\%$ per pass (total reduction 23—24%). Between each two reductions the specimens were aged at 680°C for 2 hr. Some of the specimens were subjected to a single-stage TMT with an average reduction of 24%. For steel hardened by carbide precipitates the most effective was single-stage TMT (with the same total reduction which increased the ultimate strength of the metal at room temperature by 43%, and its ultimate strength at 600°C by 14.5%. A comparison of the temperature dependence of the ultimate strength ($\sigma_в$) of hardened EI481 steel with the literature data showed that the strength increase at service temperatures of 500—600°C as a result of TMT can be 17—25%. As in the case of EI696M steel, TMT increased the limit of proportionality σ_p, which is close to the yield strength $\sigma_{0.2}$, even more. The limit of proportionality (σ_p) of the EI481 steel at 600°C was increased by TMT from 17.5 to 58.6 kg/mm², i.e., three times (MSTMT increased the limit of proportionality 2.3 times). Thus the application of this steel as a constructional material is appreciably increased. However, the general strength of EI481 steel even after the most effective strengthening is still less than the strength of EI696M steel after conventional heat treatment (Figure 6).

From the data obtained in this work it can be concluded that the complex evaluation of the effect of strengthening produced by TMT and MSTMT from the temperature dependence of the short-time and long-time strengths and from a generalized diagram of criteria of creep is necessary for the correct choice of permissible stresses and of the ductility resources of materials working under conditions of dynamic and static loads at elevated temperatures. From this evaluation together with an analysis of the thermal stability of hardened steels it is possible to determine the temperatures and stresses that can be withstood by metals with a stabilized dislocation structure. This will considerably widen the applicability of thermomechanical treatment in industry.

Bibliography

1. Oding, I.A., V.S.Ivanova, V.V.Burduksii, and V.N.Geminov. Teoriya polzuchesti i dlitel'noi prochnosti metallov (Theory of Creep and Long-Time Strength of Metals). — Metallurgizdat. 1959.
2. Ivanova, V.S. — In: "Prochnost' metallov," p.20. Izdatel'stvo AN SSSR. 1956.
3. Ivanova, V.S. and L.K.Gordienko. Novye puti povysheniya prochnosti metallov (New Methods of Increasing the Strength of Metals). — Izdatel'stvo Nauka. 1964.
4. Ivanova, V.S. et al. Rol'dislokatsii v uprochnenii i razrushenii metallov (The Role of Dislocations in the Strengthening and Failure of Metals). — Izdatel'stvo Nauka. 1965.
5. Ivanova, V.S., L.K.Gordienko, Z.G.Fridman, and P.V.Zubarev.— Fiziko-khimicheskaya mekhanika materialov, Vol.2, No.1. 1966.
6. Oding, I.A., V.S.Ivanova, and L.K. Gordienko.—Doklady AN SSSR, Vol.160, No.2. 1965.
7. Gordienko, L.K., Zh.Ts.Golyanskii, Z.G.Fridman, and E.Ya.Veksler. Metall v sovremennykh energoustanovkakh (Metals in Modern Power Plants). — Izdatel'stvo Energiya. 1966.
8. Gordienko, L.K. Otsenka strukturnykh izmenenii i termicheskoi stabil'nosti uprochneniya pri MTO po parametram temperaturnoi zavisimosti vnutrennego treniya (Evaluation of Structural Changes and Thermal Stability of Metals Strengthened by Thermomechanical Treatment Processes from the Temperature Dependence of Internal Friction). — In: "Relaksatsionnye yavleniya v tverdykh telakh." Metallurgizdat. 1966.
9. Gordienko, L.K.—Izv. AN SSSR, Metally, No.5. 1965.
10. Khimushin, F.F. Zharoprochnye stali i splavy (Heat-Resistant Steels and Alloys). — Izdatel'stvo Metallurgiya. 1964.

M.I. Zakharova, Yu.S. Egorov, and A.B. Ivanova

THE STRUCTURE OF ALUMINUM AND ALUMINUM ALLOYS CONTAINING 3% OF COPPER AFTER THERMOMECHANICAL TREATMENT

Studies during the last years /1, 2, 3/ have shown that high-temperature thermomechanical treatment (HTTMT) leads to a considerable increase in the heat resistance of alloys. Microstructural studies have shown /4/ that HTTMT produces a substructure in the alloys. The size of this is greatly influenced by the temperature, rate, and also the degree of plastic deformation.

To increase the strength of metals as much as possible by HTTMT, the fine structure after HTTMT and after heating the deformed materials must be thoroughly studied.

In this work we investigated the structure of single crystals and polycristals of Al and of Al+3% Cu alloys after deformation by drawing to a 10—100% reduction at various temperatures.

Single crystals of 99.99% aluminum were produced by recrystallizing plates 1 mm thick, 5 mm wide, and 100 mm long. The deformation by drawing was carried out at the rate of 0.07 and 1.6 mm/min by a machine with automatic recording of the stress-strain curve /5/.

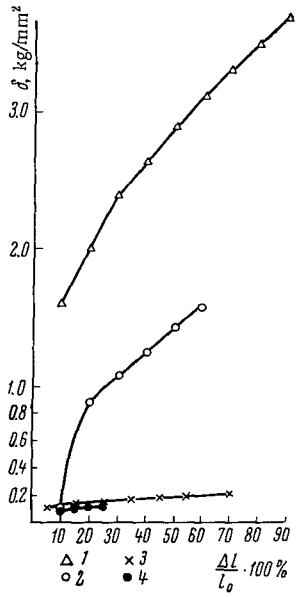

FIGURE 1. Curves representing the true stresses during deformation of single crystals of aluminum by drawing at the rate of 1.6 mm/min.

The orientation of crystals towards the axis of tension is as follows: 1 — at 150°C [312] it is +3°; 2 — at 250°C [100] it is +7°; 3 — at 630°C [312] it is +3°; 4 — at 655°C [115] it is +7°.

The structure of aluminum after deformation at 150°C was determined by the Laue and Guinier-Tennevin methods, and from the stress-strain curve.

The sharp rise in true stresses with increase in deformation at 150°C (Figure 1) shows that the metal is deformed under conditions of cold deformation.

The Laue spectrograms of aluminum single crystals deformed at 150°C have broad maxima with continuous dark fields. This proves that the distortion of the crystal lattice is characteristic of cold deformation.

From studies by the Guinier-Tennevin method the disalignment of blocks produced by thermomechanical treatment was found. The disalignment of blocks increases mainly up to a 10% deformation. Further increase in the degree of deformation to 100% does not greatly affect the total disalignment of blocks. The disalignment of crystals with reference to the axis of drawing was up to 7—10° (irradiated surface area was 80 mm²).

An analysis of the diffraction peaks of {111} planes on the Guinier spectrograms, after aluminum single crystals had been drawn to a 10—100% reduction at 150°C, shows that the diffraction peaks of individual blocks are diffuse and join to form continuous blackenings over a range of several degrees (Figure 2). An increase in the rate of deformation from 0.07 to 1.6 mm/min does not essentially change the diffraction photograph.

This nature of the Guinier diffraction photograph shows that aluminum deformed at 150°C is in a cold-worked state, which agrees with the data obtained from Laue photographs and from the true strain-stress curves.

After a 30—75% deformation at 630°C the distribution of the peaks on the Laue photographs is the same, but each peak consists of several smaller ones. This indicates that deformation at 630°C does not lead to recrystallization but to disalignment of large and small sections of the crystals due to the processes taking place during deformation.

The lack of any strong distortions of the crystal lattice during deformation at 630°C is confirmed by the almost horizontal position of the true strain-stress curves (Figure 1).

X-ray photographs produced by the Guinier-Tennevin method, like Laue photographs, show that no recrystallization takes place as a result of deformation at 630°C or even at 655°C.

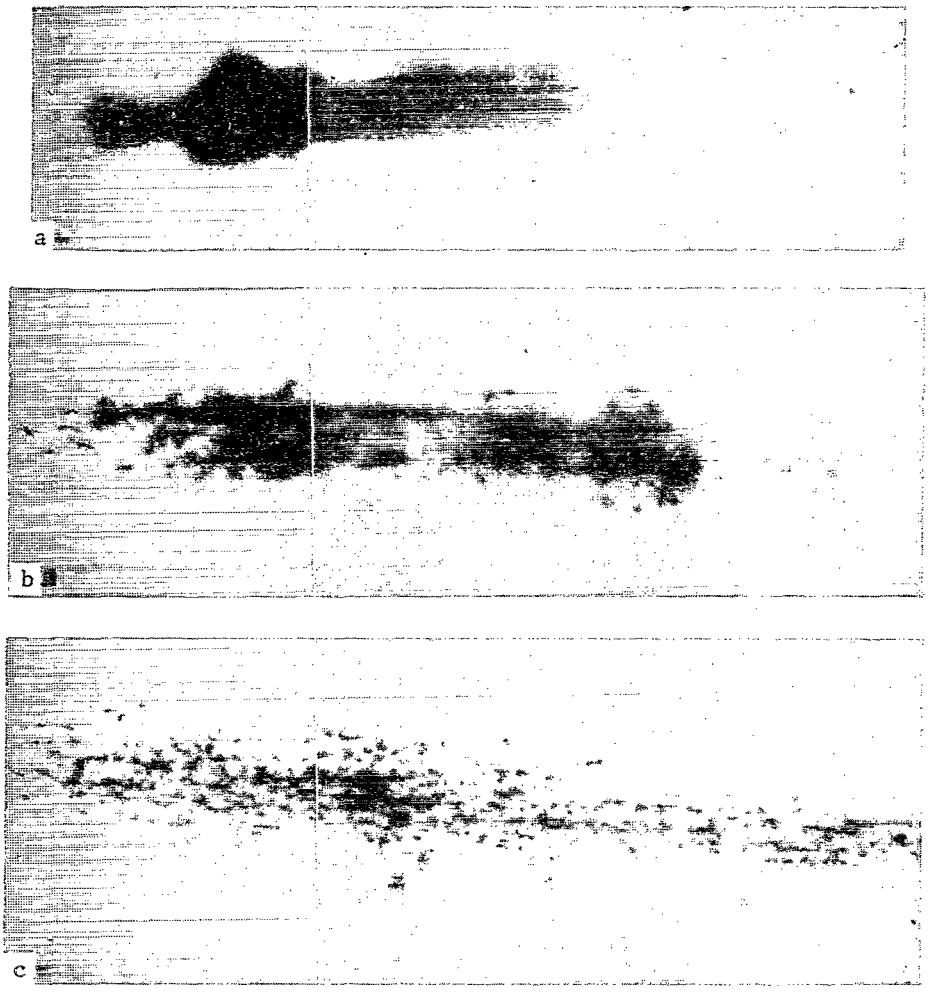

FIGURE 2. Diffraction peaks of [111] planes on Guinier photographs:

a — after deformation by drawing to a 75% reduction at 150°C; b — after drawing to a 36% reduction at 630°C; c — after drawing to a 36% reduction at 630°C and heating for 3 hr at 600°C.

If recrystallization had taken place, this would be evident from a gradual reduction of the diffraction peaks of (111) until they disappeared completely as the nuclei of the new crystals grew, and from formation of new diffraction peaks.

The diffraction peaks of (111) planes on the Guinier photographs show that the total disalignment of blocks in a single crystal with a surface area of 80 mm^2 increases to 6—10° as in deformation at 150°C. However, the

diffraction photograph is quite different: it consists of clear maxima which are the result of reflections from individual blocks, and the disalignment between neighboring blocks is up to several minutes. In addition to these blocks, there are many others which have a disalignment smaller than can be discerned by the Guinier method (40' at a distance between the crystal and the film of 50 cm). The reflections from such blocks cannot be seen separately (Figure 2a).

The sharpness of the individual small reflections indicates that after deformation at 630°C the single crystal consists of disaligned macro- and microvolumes with an undistorted lattice. The reflections are sharp after both slight and considerable deformation.

During the deformation of single crystals of aluminum at 250°C an increase in the degree of deformation led to an increase in the true stresses (see Figure 1), which indicates that stress increase leads to increased distortion of the lattice.

The total disalignment of the blocks after deformation of single crystals at 250°C is also several degrees.

The diffraction peaks on the Guinier photographs consist of several small reflections on a continuous background formed by diffuse reflections.

The structure of the deformed crystals has also been studied by watching the etching pits which correspond to the distribution of dislocations. After deformation at 150°C and at 250°C the etching pits do not form closed circuits, but in aluminum single crystals that have been deformed at 655°C these pits form closed circuits, and thus indicate that the dislocation walls are located along the boundaries of the polygons (Figure 3).

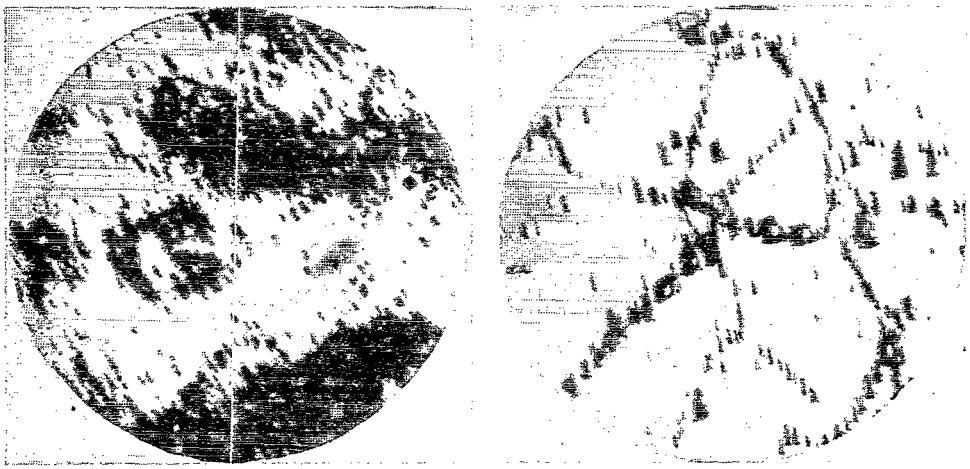

FIGURE 3. Distribution of etching pits over the surface of the crystal after drawing: a — at 150°C to a 14% reduction; b — at 655°C to a 27% reduction.

After deformation at 630°C the etching pits form circuits but not completely closed ones. A study of crystals (Figure 2) deformed at 630°C and at 655°C, and then heated at 630°C for 30 hr, showed that no recrystal-

lization takes place. Hence, we can conclude that a polygonized state is established during the deformation process at 655°C and 630°C.

When specimens which had been deformed at 150°C and at 250°C were annealed, further heating led to recrystallization if the degree of deformation was above the critical.

The structure of single crystals and of coarse-grained specimens of Al+3% Cu alloys was studied after deformation by drawing at 560°C. At this temperature the alloy consists of a single-phase and α-solid solution.

Single crystals were produced by recrystallization. After deformation by drawing to a 3% reduction the specimens were heated to 350°C for 20 min, and the temperature was increased during 20 hr from 350 to 550°C. The specimens were then held at this temperature for 25 hr. The single crystals of the Al+3% Cu alloy were lamellas 1 mm thick, 5 mm wide, and 6 cm long.

The disalignment of the blocks of initial single crystals was equal to several minutes. After drawing at 560°C from a 12% to a 30% reduction, the disalignment of the blocks in the same volume of crystals (80 mm^3) varied from 3 to 8°, depending on the degree of deformation and on the alignment of the initial crystals.

The Laue photographs of single crystals of Al+3% Cu alloys drawn to a 20% reduction show that this process does not lead to recrystallization of the alloy, and does not produce any strong distortions of the lattice characteristic of cold working.

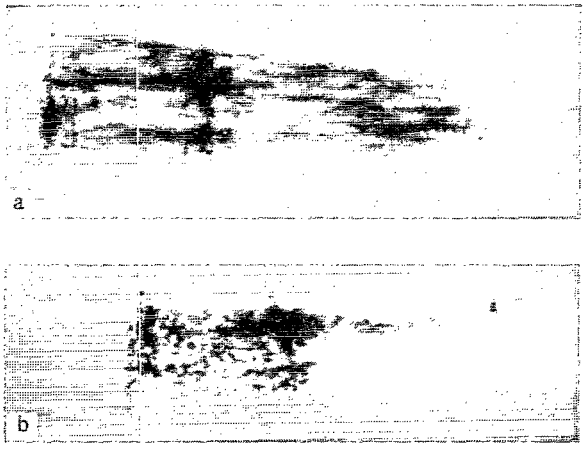

FIGURE 4. Diffraction peaks on the Guinier photographs of single crystals of Al+3% Cu alloys after drawing at 560°C to a 20% reduction (a); after drawing at 560°C to a 20% reduction and heating at 560°C for 27 hr (b).

The peaks of the (111) planes on the Guinier photographs are made up of individual small reflections and of a combination of reflections from neighboring blocks. Consequently, the structural changes in single crystals of Al+3% Cu alloys during deformation at 560°C lead to disalignment of small volumes of crystals of from several seconds to several minutes, without any considerable distortions of the lattice (Figure 4,a).

The Laue X-ray photographs of specimens that have been heated after deformation at 560°C for 27 hr show no recrystallization. The peaks of the (111) planes on the Guinier photographs indicate that no continuous background exists, and there is a certain enlargement of individual reflections (Figure 4,b).

If the alloy is heated for 27 hr at 40°C below the melting point, no recrystallization occurs. This shows that deformation of Al+3% Cu alloys at 560°C leads to polygonization which is very stable at elevated temperatures.

The structure of coarse-grained aluminum specimens after deformation at 150°C and 630°C, and of the Al+3% Cu alloy after deformation at 560°C, is similar to the structure of single crystals deformed under the same conditions.

Bibliography

1. Ivanova, V.S. et al. Rol' dislokatsii v uprochnenii i razrushenii metallov (Role of Dislocations in the Strengthening and Failure of Metals). — Izdatel'stvo Nauka. 1965.
2. Issledovaniya po zharoprochnym splavam (Investigation of Heat-Resistant Alloys), Vol. 7. — Izdatel'stvo AN SSSR. 1961.
3. Issledovaniya po zharoprochnym splavam (Investigation of Heat-Resistant Alloys), Vol. 8. — Izdatel'stvo AN SSSR. 1962.
4. Sokolov, E.N., Yu.P. Surkov, and D.I. Gurfel'. — Fizika Metallov i Metallovedenie, Vol. 20, No. 4. 1965.
5. Kuznetsov, G.F. — Zavodskaya Laboratoriya, No. 3. 1964.

I. A. Epshtein

INFLUENCE OF LOW-TEMPERATURE THERMO-MECHANICAL TREATMENT (LTTMT) ON THE PROPERTIES OF MANGANESE AUSTENITIC STEELS

As austenitic steels in which nickel is partially or completely replaced by manganese are being introduced into industry, it would be interesting to find out whether the heat resistance of these steels can be increased by thermo-mechanical treatment.

We chose chromium-manganese steel of the Kh14G14N3T (EI711) type, which contains 0.01% of boron (nominal). Kh14G14N3T (EI711) steel is used instead of Kh18N9T steel in the construction of electric furnaces for parts used at temperatures up to 700°C.

By modifying Kh14G14N3T (EI711) steel by the addition of boron, the creep limit was increased 1.5—1.7 times.

We chose the following process of LTTMT: quenching from 1100°C, cooling in the air, and cold working (drawing) to a 10, 25, 50, and 60% reduction.

Cold working during thermomechanical treatment leads to the formation of martensite in amounts which increase with the degree of deformation (Figure 1).

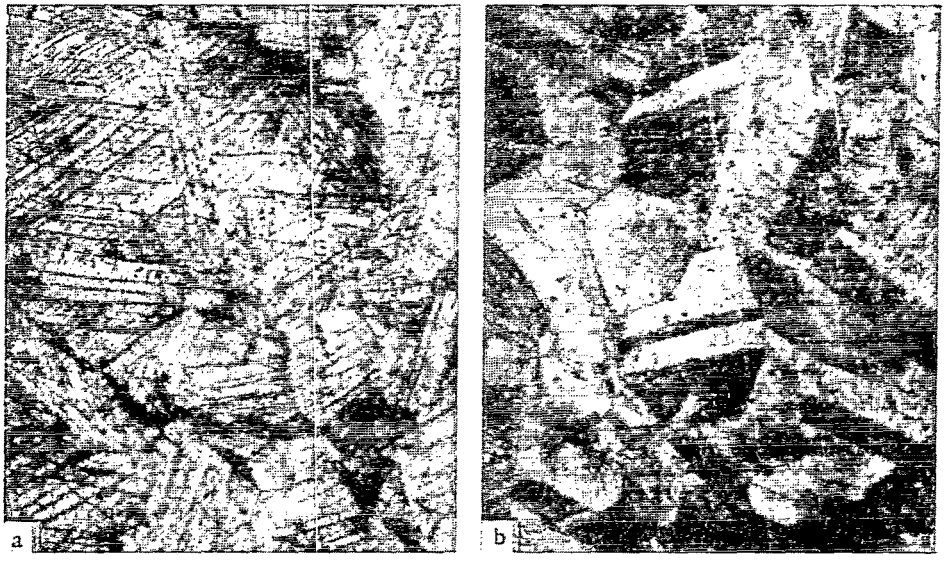

FIGURE 1. Structure of steel after low-temperature thermomechanical treatment produced by drawing to a 10% reduction (a); and to a 25% reduction (b), ×300.

The magnetic saturation of steel after a 60% deformation is about 4500 gauss, which corresponds to about 25—30% of the magnetic component of steel.

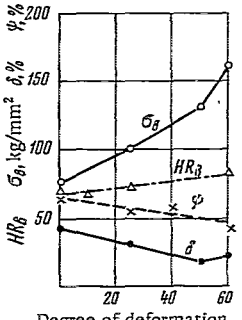

FIGURE 2. Influence of low-temperature thermomechanical treatment on the mechanical properties of steel.

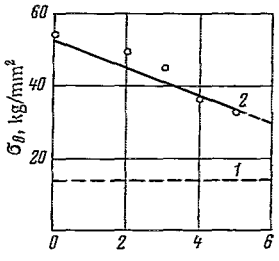

FIGURE 3. Influence of prolonged heating at 700°C on the strength of steel:

1 — λ = 0%; 2 — λ = 25%.

Low-temperature thermomechanical treatment leads to a considerable increase in the strength of steel during short-time tests (Figure 2). This increase is retained over the whole range of testing temperatures from 20 to 700°C.

The increase in the ultimate strength produced by this treatment is not retained at elevated temperatures, and heating to 700°C decreases the effect of thermomechanical treatment (Figure 3).

Thus, heating for 2 hr at 700°C decreases the ultimate strength from 54 to 48 kg/mm^2, and heating for 5 hr to 32 kg/mm^2.

The ultimate strength of nondeformed steel at 700°C is about 20 kg/mm^2.

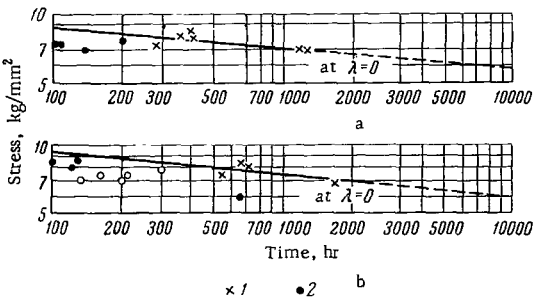

FIGURE 4. Dependence of the creep limit on the deformation produced by high-temperature thermomechanical treatment, = 700°C:

a — δ = 0.5%; b — δ = 1%; 1 — λ = 10%; 2 — λ = 25%.

Figure 4 shows the ultimate strength of steel at 700°C at an elongation of 0.5 and 1.0%. It can be seen from this figure that low-temperature thermomechanical treatment with a reduction of 10% has almost no influence on the ultimate strength of the Kh14G14N3TR steel. As the degree of deformation is increased, there is a tendency toward a decrease in the creep resistance.

Under all the stresses studied, specimens with a 25% reduction have a lower creep limit than steels that have not been subjected to cold working.

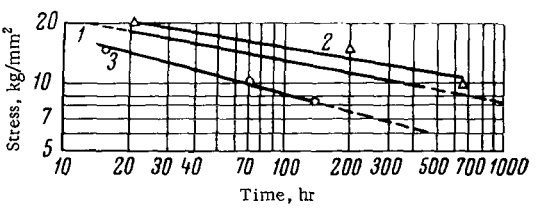

FIGURE 5. Dependence of the long-time ultimate strength on the degree of deformation produced by low-temperature thermomechanical treatment:

1 — λ = 0%; 2 — λ = 25%; 3 — λ = 60%.

The specimens for long-time strength tests were cut from rods that had been drawn to a 25 and 60% reduction (Figure 5). It was found that deformation to a 60% reduction leads to a sharp drop in the long-time ultimate strength (by a factor of approximately 1.5 during 1000 hr). In addition to the decrease in the absolute long-time ultimate strength there is a change in the slope of the curve plotted in the log σ vs. log τ coordinates, and the rate of steel softening increases.

Thus, low-temperature thermomechanical treatment greatly increases the ultimate strength of steel during short tests because of the formation of a metastable state. At elevated temperatures this strength increase diminishes as the time of testing is increased.

M. G. Lozinskii, A. S. Nikishov, N. Z. Pertsovskii, and Yu. I. Kaplin

INFLUENCE OF HIGH-TEMPERATURE THERMOMECHANICAL TREATMENT ON THE HEAT RESISTANCE OF KhN70VMTYu ALLOY

Great attention has been paid during the last years to exploring new sources of strength of constructional metals in order to improve their performance under stress at elevated temperatures. One of the promising methods of increasing the strength of metals at elevated temperatures is high-temperature thermomechanical treatment (HTTMT), which combines plastic deformation at elevated temperatures with hardening.

Later we shall discuss some results of studies on different processes of high-temperature thermomechanical treatment, by hot forging billets of the nickel-base heat-resistant EI617 (KhN70VMTYu) alloy.

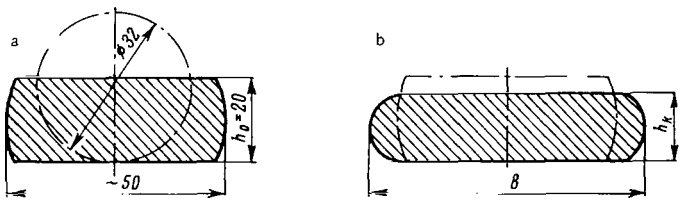

FIGURE 1. Schematic representation of the initial upsetting (a), and of high-temperature thermomechanical treatment (b), of EI617 billets.

For the high-temperature thermomechanical treatment we used 2500 ton crank presses. To fix the effect of hot working the billets were quenched in ice water that was continuously agitated by compressed air. The time that elapsed between the end of forging and the start of quenching was about 0.5 sec. The influence of the rate of cooling on the effectivity of high temperature thermomechanical treatment was found by cooling some billets in air during all the experiments.

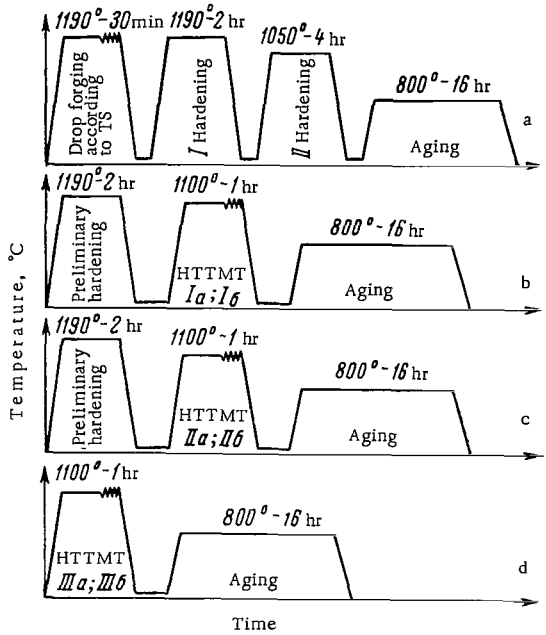

FIGURE 2. Heat treatment according to technical specifications (a), and experimental high-temperature thermomechanical treatment processes (b — d) of EI617 alloys.

High-temperature thermomechanical treatment was carried out on flat billets with a shape and size similar, within certain limits, to those of billets used to drop forge turbine vanes. The formation of the cross section of a billet is shown in Figure 1. The first operation was upsetting 32 mm diam. rods (the initial length of the billet was 90—95 mm) at 1190°C to flat billets 20 mm high (Figure 1,a), and cooling in air. These billets were subjected to different high-temperature thermomechanical treatments (see below) during which they were further upset to a height of h_k (Figure 1,b). The degree of deformation produced by high-temperature thermomechanical treatment was calculated from the change in height of the billet:

$$\frac{h_0 - h_k}{h_0} 100\%.$$

A schematic representation of heat treatment according to technical specifications (TS) and of several experimental processes of high-temperature thermomechanical treatment of EI617 alloy is shown in Figure 2. We shall discuss the following chief processes: 1) treatment according to technical specifications (Figure 2,a); 2) process I: high-temperature thermomechanical treatment at 1100°C after a preliminary hardening of the billets (Figure 2,b); 3) process II: the same at 1050°C (Figure 2,c); 4) process III: high-temperature thermomechanical treatment at 1100°C without preliminary hardening (Figure 2,d). After all these processes the metal was aged according to technical specifications. During each process of high-

temperature thermomechanical treatment the billets were upset to a 9—12% reduction (processes Ia, IIa and IIIa) and to a 20—25% reduction (processes Ib, IIb and IIIb). The specimens were then cooled in water and in the air. Thus, we studied 12 different high-temperature thermomechanical treatment processes. A preliminary investigation showed that these processes of high-temperature thermomechanical treatment very effectively increase the heat resistance of the alloys studied at service temperatures.

Results of short-time tensile tests on specimens of the EI617 alloy at 700—800°C*

Process	Reduction, %	Testing temperature, °C	$\sigma_{0.2}$, kg/mm²	σ_B, kg/mm²	δ_4, %	ψ_k, %
TS	(21.5)	700	63.5	96.5	10.2	15.2
Ia	10.9		73.4	104.5	16.2	19.0
Ib	24.0		80.0	105.2	14.4	17.5
IIa	8.9		75.2	99.6	13.4	15.2
IIb	21.5		85.0	103.0	12.0	14.6
IIIa	12.9		80.8	101.3	15.1	18.7
IIIb	23.5		85.2	105.8	10.8	15.6
TS	(21.5)	750	61.5	89.0	8.0	9.6
Ia	10.9		70.3	91.4	11.8	15.9
Ib	24.0		79.6	98.8	12.7	16.8
IIa	8.9		73.2	96.5	15.5	18.0
IIb	21.5		83.2	91.5	9.9	14.8
IIIa	12.9		79.4	98.2	13.5	18.7
IIIb	23.5		83.5	98.0	10.3	22.4
TS	(21.5)	800	59.8	77.5	6.5	9.3
Ia	10.9		—	77.6	12.0	12.0
Ib	24.0		76.7	83.0	10.6	12.0
IIa	8.9		72.3	88.5	11.7	17.2
IIb	21.5		80.5	88.5	8.6	16.2
IIIa	12.9		—	85.4	11.8	21.4
IIIb	23.5		75.2	85.0	10.3	20.9

* The average data were calculated from two—three specimens. The high-temperature thermomechanical treatment was always carried out by quenching the billets in water.

The long-time strength tests were carried out on a YaB-1M machine under the following conditions: 1) $T=700$°C, $\sigma=50$ kg/mm²; 2) $T=750$°C, $\sigma=40$ kg/mm²; 3) $T=800$°C, $\sigma=30$ kg/mm². For the short-time tensile tests at 700, 750, and 800°C an IM-4R machine was used. The billets were studied metallographically before and after aging, and their hardness was measured. We also studied the microstructure of some specimens after the long-time strength tests.

The hardness of the EI617 alloy at 20°C after high-temperature thermomechanical treatment and aging is 15—20% higher than that of the same alloy after treatment according to technical specifications ($H_V=330$—380 kg/mm² and 290—315 kg/mm², respectively).

The table gives the results of short-time tensile tests. After high-temperature thermomechanical treatment with a 9—12% reduction, the yield strength ($\sigma_{0.2}$) at 700—800°C is 15—25% higher than that of the alloy after treatment according to technical specifications, but σ_B is only 5—10% higher.

In specimens deformed to a 20—25% reduction, the yield strength and ultimate strength increase by 25—35 and 5—15%, respectively.

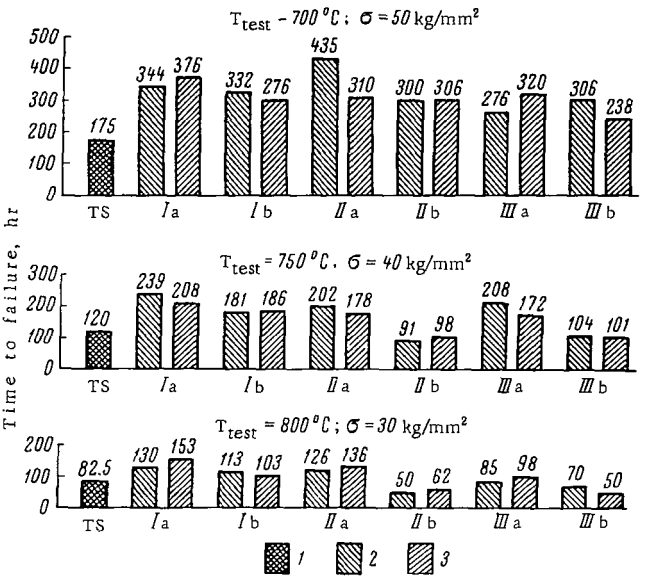

FIGURE 3. Average time to failure (in hours) of EI617 speciments at 700, 750, and 800°C under tensile stresses of 50, 40, and 30 kg/mm², respectively:

1 — heat treatment according to technical specifications; 2 — high-temperature thermomechanical treatment followed by cooling in air; 3 — high-temperature thermomechanical treatment followed by quenching in water.

The variation in the ductility is more complex. We found that an increase in the reduction produced by high-temperature thermomechanical treatment decreases ductility, but that ductility increases if the temperature is raised from 700 to 750—800°C. For example, at 700°C the reduction of area of specimens after high-temperature thermomechanical treatment is in the first case 1.2—1.3 times, and in the second case 1.5—2 times the reduction of area of specimens after heat treatment according to technical specifications.

Because of the large number of high-temperature thermomechanical treatment processes we carried out on EI617, the long-time strength tests were limited to the determination of the time to failure at 700, 750, and 800°C under the above tensile stresses. Under these conditions the master specimens had a life of 100—200 hr. The results of these tests are shown in Figure 3. The numbers above the columns designate the mean time to failure in hours (average of two—three tests) of specimens of EI617 alloys. The numbers below the columns (on the abscissa) designate the treatment.

The time to failure of specimens treated according to technical specifications is 175 hr at σ=50 kg/mm² and 700°C. After high-temperature thermomechanical treatment the time to failure is 1.5—2.5 times as much. The

heat resistance of the alloy increased most after high-temperature thermomechanical treatment according to processes Ia and IIa (forging at 1050°C and 1100°C to a 9—12% reduction and a preliminary hardening according to technical specifications); these specimens failed after 350—450 hr.

However, under the given conditions of testing processes Ib and IIb (similar to processes Ia and IIa except that the reduction produced by high-temperature thermomechanical treatment was 20—25%), and also processes IIIa and IIIb (high-temperature thermomechanical treatment at 1100°C without any preliminary hardening) proved to be sufficiently effective and the time to failure of the specimens was 250—350 hr.

At 750°C and $\sigma=40\,kg/mm^2$ the mean time to failure of the master specimens was 120 hr. Under these conditions of testing high-temperature thermomechanical treatment increased the life of specimens 1.5—2 times. The high-temperature thermomechanical processes that produce a 9—12% reduction (processes Ia and IIa, and also IIIa) which increase the time to failure to 180—240 hr are the most effective. An increase in the reduction by forging to 20—25% (process Ib) is less effective, and after processes IIb and IIIb the specimens have a shorter life than those obtained by heat treatment according to technical specifications.

At 800°C and $\sigma=30\,kg/mm^2$ the time to failure of the master specimens was 82.5 hr. In this case processes Ia and IIa were again the most effective, and increased the time to failure to 120—150 hr, i.e., 1.5—1.8 times. An increase in the degree of deformation to 20—25% during high-temperature thermomechanical treatment at 1100°C (process Ib) gives worse results. High-temperature thermomechanical treatment by process IIIa does not increase the time to failure above that of the master specimens, and processes IIb and IIIb lead to a time to failure shorter than that obtained by heat treatment according to technical specifications.

Despite the fact that high-temperature thermomechanical treatment of EI617 alloys by processes I and II increases their strength, their long-time ductility over the whole range of temperatures that we studied does not decrease, and sometimes even increases. For example, after heat treatment according to technical specifications the reduction of area at 800°C and at $\sigma=30\,kg/mm^2$ was 6.9%, and after high-temperature thermomechanical treatment according to process Ia it was 8—9% after quenching in water, and 10—12% after cooling in air. Processes IIIa and IIIb, which under the given conditions do not increase the heat resistance of the alloy (process IIIa at 800°C, and process IIIb at 750 and 800°C), considerably increase the ductility ($\Psi_k=18—25\%$) at 750—800°C.

According to /1/, the maximum heat resistance of the EI617 alloy at service temperatures (700—800°C) is obtained after double hardening and aging (see Figure 2). Preliminary hardening according to technical specifications (heating to 1190°C, holding at this temperature for 2 hr, and cooling in the air), ensures the necessary grain growth and the maximum alloying of the solid solution, and repeated heating to 1050 and 1100°C in the high-temperature thermomechanical treatment proper acts as a second hardening.

High-temperature thermomechanical treatment with a reduction of 9—12% carried out according to processes I and II produced almost no recrystallization in the microstructure of the billets. High-temperature thermomechanical treatment with a 20—25% reduction according to the same processes (I and II) leads to a limited recrystallization along the boundaries of the initial grains — the new grains occupy not more than 10—20% of the

total surface of the microsection. It has been experimentally found that in EI617 alloys these processes do not lead to a recrystallization during subsequent hardening or long-time strength tests.

The beneficial influence of these two processes of high-temperature thermomechanical treatment on the heat resistance of the EI617 alloys is possibly due to polygonization and to an increase in the content of strengthening phases (particularly of the intermetallic γ'-phase) which precipitate during aging. A similar increase in the content of the strengthening phase was found in EI481 austenitic steel /2/ and in the EI437B alloy /3/. It should, however, be noted that an increase in the degree of deformation during high-temperature thermomechanical treatment from 9—12% to 20—25% apparently leads to more intense diffusion processes on further heating, which somewhat accelerates the over-aging of the alloy. This is apparently why processes Ib and IIb are less effective than processes Ia and IIa.

This was confirmed earlier during a study on the influence of the degree of deformation during high-temperature thermomechanical treatment on the heat resistance of the EI617 alloy. In these experiments an increase in reduction during drop forging from 9—12% to 20—25% had little influence on the heat resistance of the material, but a 30—35% reduction always greatly impaired it. The more intense recrystallization which took place in the more deformed specimens can clearly not fully account for the decrease in the long-time strength. It has been found /4/ that partial recrystallization does not annul the favorable effect of high-temperature thermomechanical treatment on the heat resistance of a number of alloys.

As already mentioned, a short single-stage heating to 1100°C during high-temperature thermomechanical treatment (process III, Figure 2) considerably increases the heat resistance of the EI617 alloy at 700—750°C only. This fact agrees fairly well with the data of /5/, in which a similar treatment had no favorable influence on the long-time strength (100 hr) of the EI598 (KhN70MVTYuB) alloy above 650°C, although the composition of this alloy differed very little from that of the EI617 alloy. In /5/ it is reported that the efficiency of high-temperature thermomechanical treatment of EI598 alloys above 650°C is considerably decreased. This is apparently because the solid solution is not sufficiently alloyed, and process III does not involve double hardening.

Thus, the heat resistance of the EI617 alloy is most effectively improved by processes Ia and IIa because of the optimum combination of the operations of heat treatment and work hardening.

A study on the influence of the rate of cooling during high-temperature thermomechanical treatment on the long-time strength of the EI617 alloy at 700—800°C did not show that quenching in water is preferable to cooling in air (see Figure 3). Metallographic analyses indicated that processes Ia and IIa (9—12% reduction) produce almost the same structure, and processes Ib and IIb (20—25% reduction) lead to a somewhat greater recrystallization as the result of air cooling. It should also be remembered that processes I and II, during which the metal is cooled in the air, considerably improve the ductility of the alloy.

Hence, from all these data we consider that the optimum process of high-temperature thermomechanical treatment of the EI617 alloy is drop forging at 1100—1050°C to a 9—12% reduction and air cooling of preliminarily hardened billets.

Our results indicate that high-temperature thermomechanical treatment is very useful for drop forging turbine vanes from EI617 alloys.

CONCLUSIONS

1. High-temperature thermomechanical treatment of EI617 alloys increases their short-time strength and their ductility at 700—800°C.
2. We found the optimum process of high-temperature thermomechanical treatment which ensures the greatest increase in the long-time strength of the EI617 alloy at 700—800°C.

Bibliography

1. Khimushin, F.F. Zharoprochnye stali i splavy (Heat-Resistant Steels and Alloys). — Izdatel'stvo Metallurgiya. 1964.
2. Lozinskii, M.G., E.N.Sokolkov, K.V.Varli, and Yu.A.Skakov.— Fizika Metallov i Metallovedenie, Vol.13, No.1. 1962.
3. Kishkin, S.T., M.G.Lozinskii, S.Z.Bokshtein, and E.N.Sokolkov.— Metallovedenie i termicheskaya obrabotka metallov, No.1, p.38. 1962.
4. Kagan, D.Ya.— Metallovedenie i termicheskaya obrabotka metallov, No.1, p.27. 1964.
5. Kagan, D.Ya. and M.L.Bernshtein.—Metallovedenie i termicheskaya obrabotka metallov, No.1, pp.2—5. 1966.

E.N.Sokolkov, M.A.Smirnov, M.G.Gaidukov, and M.M.Shteinberg

INFLUENCE OF THE TEMPERATURE OF PRELIMINARY PLASTIC DEFORMATION ON THE LONG-TIME STRENGTH OF AUSTENITIC STEELS

The strengthening of age-hardening steels after thermomechanical treatment, consisting of a combination of plastic deformation, hardening, and aging, is greatly influenced by the preliminary work hardening and by the degree of decomposition of the solid solution during aging. An increase in the temperature of preliminary deformation from 20 to 1100°C in order to decrease the work hardening should generally lead to a decrease in the strength of the metal /1, 2/. However, the strengthening is greatly influenced by the processes of aging of the deformed material. These features differ for the various types of precipitates. Thus, preliminary deformation not only intensifies the precipitation of a carbide phase but also greatly accelerates its coagulation. Preliminary deformation has a smaller influence on the coagulation of the Ni_3[Ti, Al] intermetallic compound. The preliminary decomposition during cooling from the homogenizing temperature

to the temperature of deformation can also have different effects on the processes of the precipitation of carbide and intermetallic phases during subsequent aging /1, 2/.

Thus, the temperature of the preliminary deformation can affect the strengthening of steels hardened by carbide and intermetallic precipitates differently /2/. These differences are apparently also observed in the high-temperature mechanical properties.

In this work we studied the influence of plastic deformation at temperatures from 20 to 1100°C on the high-temperature strength of two age-hardened steels with carbide and intermetallic precipitates.

METHODS

We used the steel EI481, age-hardened by carbides of chromium and vanadium, and the EI612K steel, hardened chiefly by the γ'-phase ($Ni_3[Ti, Al]$). The chemical compositions of these steels are given in Table 1.

TABLE 1. Chemical composition of the steels studied

Type of steel	Content, %										
	C	Cr	Ni	Mn	Co	V	Mo	W	Al	Ti	Nb
EI481	0.36	12.4	7.5	8.9	—	1.25	1.23	—	—	—	0.25
EI612K	0.08	14.9	36.1	—	3.8	—	—	3.25	0.65	1.26	—

For the plastic deformation at 1100°C—20°C grooved rolling mills were used, and the billets were rolled at a rate of 15 m/min to a reduction of 25—30%. The 13×13×70 mm billets were first heated to 1180°C and held at this temperature for 1 hr 45 min (EI481 steel), or for 2 hr (EI612K steel). The specimens were then cooled to different temperatures within the range of 1100—400°C, and held for 3 min. The billets were then deformed and immediately (after not more than 0.2 sec) quenched in water. This prevented any recrystallization because of the high temperatures of deformation. One batch of billets was quenched in water without any preliminary cooling, and some were deformed after quenching at room temperature.

The degree of decomposition of these steels was evaluated from the variation in the lattice parameters of austenite by means of a URS-501 apparatus, using an iron target (line 311)α, with an accuracy of ± 0.0003 kX. The fine structure of the steels was determined from the shape and construction of the (220)α and (311)β reflections on the X-ray photographs obtained in a Kros-1 chamber with a chromium target and a fixed adapter and specimens. The initial X-ray was limited by two diaphragms with a 0.4 mm diameter. The distance between the specimen and the adapter was 28 mm.

The electron microscope studies on the structure were carried out with a BS-242 microscope and carbon replicas.

TsKTI-2 machines were used for the long-time strength tests. The diameter of the specimens was 5 mm, and the calculated length 30 mm. We

found the time to failure and the steady-state creep rate at 650°C, which is the service temperature for both types of steels. For the short-time high-temperature tensile tests a P5-type machine was employed. The specimens of EI481 steel were drawn at the rate of 0.16 mm/min, and the specimens of EI612K steel at the rate of 0.4 mm/min, so that the durations of the tests were almost the same (15 min) for specimens of different ductilities.

RESULTS AND DISCUSSION

Figure 1 shows the dependence of the mechanical properties of EI481 steel subjected to two-stage aging (660° for 16 hr + 760°C for 16 hr) on the temperature of preliminary deformation. It can be seen that preliminary cold working does not increase the short-time strength characteristics at 650°C after ordinary aging, despite the existence of preliminary work hardening and the considerable increase in the content of carbides due to a more intense decomposition.* This can be explained by the greatly accelerated coagulation of the carbide phase (Figure 2,b) and possibly by intense relief of preliminary work hardening of the matrix /1/. The yield strength and the ultimate strength are increased if the deformation is carried out at 400°C—800°C only, i.e., when the rate of coagulation of the carbides (Figure 2,c) and the intensity of relief of preliminary work hardening during aging are lower than in the previous case.

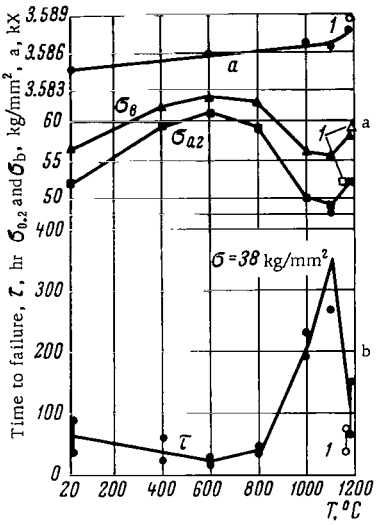

FIGURE 1. Dependence of the mechanical properties of EI481 steel (a) and of the time to failure (b) on the temperature of preliminary deformation:

Aging at 660° for 16 hr + 760° for 16 hr; 1 — without deformation; T_{test} = 650°C.

After high-temperature deformation at 1000—1100°C, the EI481 steel also has a somewhat lower strength than nondeformed steel. This is due to the detrimental influence of premature decomposition during cooling and deformation on the dispersion of carbides precipitated during aging (Figure 2,d) /1/. Specimens deformed at 1180°C have a higher strength than those deformed at 1000—1100°C. This is because there is no premature decomposition of the solid solution.

Comparative creep tests at 650°C under a stress of 38 kg/mm² (see Figure 1) show that specimens subjected to preliminary deformation at 20—800°C do not have a lower creep rate or longer time to failure than nondeformed specimens, despite the work hardening and higher content of

* If we assume that the degree of decomposition of the hardened (without deformation) and aged specimen is 100%, then the decomposition of a specimen subjected to cold deformation and aging will be 125%. The data of X-ray structural analysis agree with those of a study on the precipitated carbides.

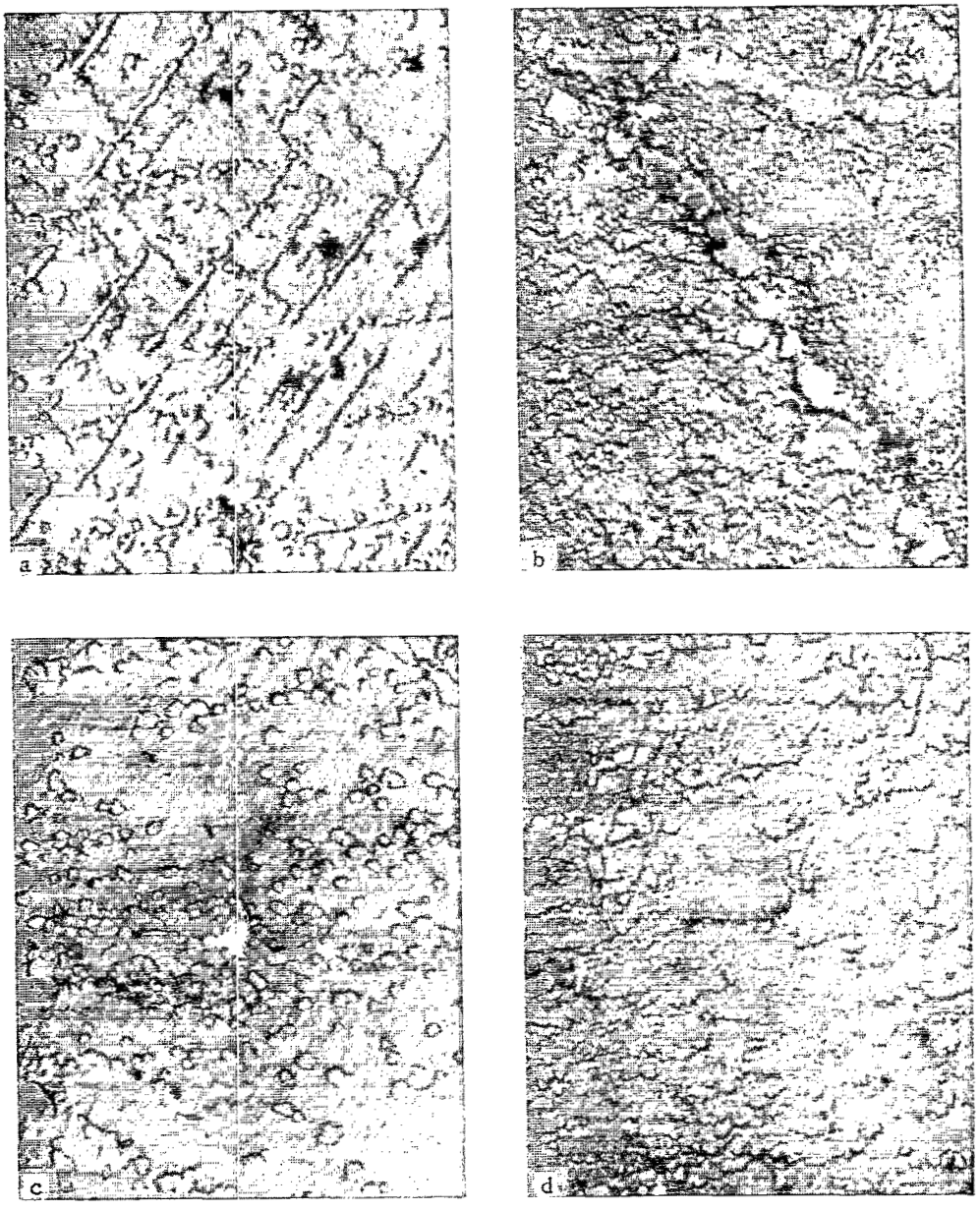

FIGURE 2. Structure of E1481 steel after quenching (a), after deformation at 20°C (b), at 600°C (c), and 1100°C (d), followed by aging at 660°C for 16 hr + 760°C for 16 hr, × 7500.

carbide phase. This is apparently due to the small dispersion of the strengthening phases. In this case the preliminary work hardening of the matrix produced by deformation at 20—800°C (followed by relaxation during aging) cannot compensate for the negative influence of the low dispersion of the strengthening phase on the properties of this steel. It is also possible that the fine structure produced by the above processes of deformation and aging is not effective in increasing the creep strength of steel under the given conditions of testing.

High-temperature deformation at 1000°C—1100°C (see Figure 1) increases the time to failure of EI481 steel 5—7 times, and decreases the creep rate from $8.0 \cdot 10^{-3}$ to $2.5 - 4.0 \cdot 10^{-3}$%/hr. It is important to note that this effect is produced despite the low dispersion of the carbide phase in the specimens after high-temperature thermomechanical treatment. Apparently, this increase in the creep strength of steel is due to the fine structure produced by high-temperature deformation /3/. A study of inverse X-ray photographs showed that high-temperature deformation at 1000—1180°C leads to the formation of a fragmented structure. This is confirmed by the separation of the reflections $(220)\alpha$ and $(311)\beta$ which correspond to individual grains into a large number of sub-spots. According to the data obtained from X-ray photographs the fragments are $10—100\mu$ in size, and the angle of disalignment between them varies from a few minutes to ten times this value (Table 2).*

TABLE 2. Dependence of the angle of disalignment δ between the fragments on the deformation temperature

Deformation temperature, °C	EI481 steel		EI612K steel	
	range of δ, min	δ_{av}, min	range of δ, min	δ_{av}, min
1000	3—18	9	4—16	9
1100	3—21	12	6—23	14
1180	6—27	17	10—32	21

We should expect this fragmented structure with boundaries reinforced by impurity atoms and carbide particles to effectively inhibit creep and increase the time to failure. It is also possible that the wavy grain boundaries, the result of high-temperature deformation, also increase the time to failure. It has been found /4/ that wavy grain boundaries can inhibit the development of intergranular failure during creep tests.

An increase in the deformation temperature to 1180°C leads to a considerderable decrease in the time to failure (Figure 1) due to the presence of recrystallized grains formed during high-temperature deformation.

It has already been mentioned that plastic deformation, which leads to an increase in the precipitation of intermetallic phases, accelerates the coagulation of these phases less than that of carbides. Therefore, all processes of deformation of EI612K steel (20°C—1100°C) lead to a considerable increase in the amount of the γ'-phase during subsequent aging at 700°C for

• The dimensions of the fragments could not be determined more accurately because of the great diffuseness of the sub-spots.

25 hr, but accelerate its coagulation very little. This greatly increases the short-time strength of the above metal at 650°C (Figure 3). This increase is also favored because the presence of a finely dispersed phase in deformed specimens inhibits the relief of work hardening during aging.

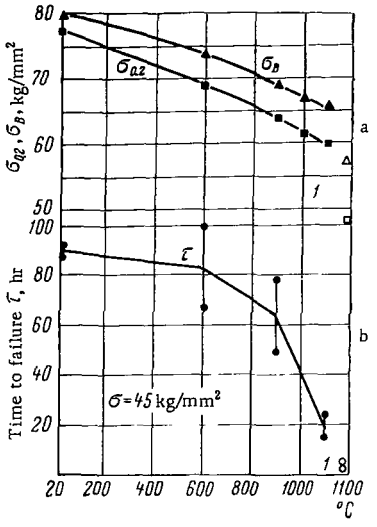

FIGURE 3. Dependence of the mechanical properties of EI612K steel (a) and of the time to failure (b) on the temperature of preliminary deformation:

Aging at 700°C for 25 hr; 1 — without deformation; T_{test} = 650°C.

Cold working greatly increases the strength characteristics (yield strength and ultimate strength are increased by 60 and 40%, respectively), since this treatment gives a higher work hardening of the matrix and a more complete precipitation of the strengthening phase during aging than other treatments /2/. If the temperature of preliminary deformation is increased, the increase in strength decreases monotonously because of the decrease in the amount of preliminary work hardening and in the intensifying influence of plastic deformation on aging. Plastic deformation is favorable for strengthening steel if it is carried out at elevated temperatures (1000—1100°C), since in contrast to the case of EI481 steel there is no detrimental influence of premature decomposition during cooling and of deformation on aging /2/. Thus, high-temperature thermomechanical treatment at 1100°C can increase the yield strength by 25% and the ultimate strength by 15%.

Preliminary deformation at 20—1100°C followed by aging leads to a considerable increase in the time to failure and to a decrease in the creep rate of EI612K steel at 650°C (see Figure 3). The maximum increase in the creep strength can be achieved by deformation at 20°C and at 600°C, i.e., under conditions which produce the highest work hardening of the matrix and lead to the precipitation of the maximum amount of intermetallic phases during aging. Thus, these processes of preliminary deformation decrease the creep rate of steel under a load of 45 kg/mm² from $17—18 \cdot 10^{-2}$ to $5—6 \cdot 10^{-3}$%/hr. At the same time, the time to failure increases 15—20 times. Preliminary deformation at 20°C and at 600°C can lead to an increase in the long-time strength (100 hr) at 650°C of 35—40%.

If the temperature of deformation is increased to 1100°C, the increase in the time to failure is less and the creep rate decreases. Thus, high-temperature thermomechanical treatment at 1100°C increases the time to failure to 3—6 times that of the nondeformed metal, and reduces the creep rate to $18—20 \cdot 10^{-3}$%/hr. The increase in the long-time strength (100 hr) is only 10—15%. The increase in the long-time strength of EI612K steel produced by high-temperature thermomechanical treatment is due to an increase in the content of the strengthening phase and to fragmentation of the structure.

It should be pointed out that despite their wavy grain boundaries, specimens that have undergone high-temperature thermomechanical treatment at 1000—1100°C have a small elongation during the third stage of creep (in contrast to specimens that have undergone other processes of deformation). This is possibly due to the increase in the density of the particles of the strengthening phase formed near the grain boundaries during aging /2/.

Thus, we found the different dependence of the time to failure on the temperature of preliminary deformation for the steels studied under almost similar conditions of testing (temperature and testing procedure). The long-time strength of EI612K steels is considerably increased by preliminary deformation processes which lead to the formation of a large amount of a finely dispersed strengthening phase during aging. In the EI481 steel, in which a combination of plastic deformation and aging does not lead to optimum dispersion of the strengthening phase because of considerable coagulation, an increase in the long-time strength can be obtained only by processes of thermomechanical treatment which ensure fragmentation of the structure.

It should, however, be pointed out that the long-time tests on steel were relatively short, and were carried out at moderate temperatures. If the testing temperature is increased and the test prolonged, the role of the stability of work hardening produced by plastic deformation may increase. This in turn may change the dependence of the long-time strength on the temperature of preliminary deformation. The above assumption is confirmed by the data in Figure 4, which indicate that if the acting stresses are reduced to 38 kg/mm^2 (i.e., if the duration of the test is increased), the time to failure of cold-worked EI612K specimens is shorter than that of specimens deformed at 600°C. Apparently, this is because the changes in the fine structure produced by deformation at elevated temperatures are more stable than the changes introduced by cold working.

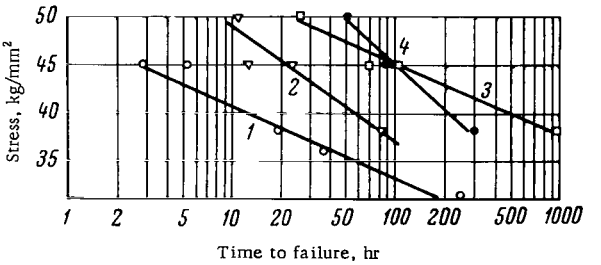

FIGURE 4. Dependence of the long-time strength of EI612K steel at 650°C on the temperature of preliminary deformation.

Aging at 700°C for 25 hr; 1 — without deformation; 2 — deformation at 1100°C; 3 — the same at 600°C; 4 — at 20°C; T_{test} = 650°C.

CONCLUSIONS

The peculiar influence of plastic deformation on the processes of precipitation and coagulation of carbide and intermetallic phases leads to different dependences of the high-temperature mechanical properties of EI481 and EI612K steels on the temperature of deformation during thermomechanical treatment. In the EI481 steel, which contains carbide precipitates, the short-time strength at 650°C increases only if the deformation is carried out at 400—800°C, and an increase in the long-time strength is ensured if the deformation is carried out at 1000—1100°C.

All the processes of deformation (20°C—1100°C) studied lead to an increase in the short-time and long-time strengths (at 650°C) of EI612K steel containing intermetallic precipitates. These properties are increased most after deformation at 20°C and at 600°C.

Bibliography

1. Sokolkov, E.N., M.A.Smirnov, M.M.Shteinberg, and M.M.Nichkova. Vliyanie temperatury plasticheskoi deformatsii na kinetiku stareniya zharoprochnoi austenitnoi stali s karbidnym uprochneniem (Influence of Temperature of Plastic Deformation on Kinetics of Aging of Heat-Resistant Austenitic Steel Containing Carbide Strengthening Precipitates). — Fizika Metallov i Metallovedenie, Vol. 20, No. 1. 1965.
2. Smirnov, M.A., E.N.Sokolkov, and M.M.Shteinberg. Vliyanie temperatury plasticheskoi deformatsii na kinetiku stareniya zharoprochnykh austenitnykh stalei (Influence of Temperature of Plastic Deformation on Kinetics of Aging of Heat-Resistant Austenitic Steels). — Izv. AN SSSR, OTN. Metally, No. 5. 1965.
3. Sadovskii, V.D. et al. Vliyanie vysokotemperaturnoi termomekhanicheskoi obrabotki na svoistva zharoprochnosti splava XN77TYuR (Influence of High-Temperature Thermomechanical Treatment on the High-Temperature Properties of the KhN77TYuR Alloy). — Fizika Metallov i Metallovedenie, Vol. 17, No. 6. 1964.
4. Sadovskii, V.D. et al. Vliyanie termomekhanicheskoi obrabotki na svoistva zharoprochnosti austenitnoi stali (Influence of Thermomechanical Treatment on the Properties of Heat-Resistant Austenitic Steels). — In: "Issledovaniya po zharoprochnym splavam," Vol. 7. Izdatel'stvo AN SSSR. 1961.

N. S. Alferova and T. M. Bogdanova

INCREASE IN WORKABILITY DURING PRESSING OF HEAT-RESISTANT STEELS OF THE MARTENSITIC AND MARTENSITIC-AUSTENITIC TYPES

The experience gained in pipe plants shows that a number of high-strength chromium steels with a low content of nickel and additions of tungsten, molybdenum, vanadium, niobium, aluminum, etc., are very difficult to press in the cold state. Even after being softened by heat treatment these steels have a high strength and a low ductility as a result of alloying, leading to appreciable distortions of the lattice of the solvent metal and of age hardenings, martensitic deformations, and other processes which are detrimental to workability.

We therefore began to study ways of increasing the workability of high-strength steels during pressing. We started by investigating possible methods of increasing the workability of martensitic and martensitic-austenitic steels by better softening heat-treatment processes, by hot rolling, and by rolling supercooled austenite.

We used the high-strength heat-resistant EP56 and EP451 steels.

The first steel is martensitic and has a high resistance to tempering as the result of precipitation of niobium carbides. The second steel is an age-hardening martensitic-austenitic steel, which hardens when heated to 350—600°C.

The characteristic feature of both these steels is the low-temperature of the $\alpha \rightarrow \gamma$-transformation, and the existence of a considerable hysteresis of the polymorphic transformation on heating and cooling. The critical temperatures of the polymorphic transformation, determined dilatometrically for EP56 steel, are at 625°C and 785°C on heating, and at −250°C (M_f) on cooling. For the EP451 steel the range of the $\alpha \rightarrow \gamma$ transformation on heating is 630°C—760°C, and on cooling it is −125°C (M_f). For both these steels the temperature of the end of the martensitic transformation is below 0°C. The supercooled austenite of both steels has a high stability even if cooled together with the furnace (1.5—2°C/min), and the decomposition of austenite leads to the formation of martensite (Figure 1).

The softening of these steels before plastic deformation is particularly difficult because of the high resistance of the EP56 steel to softening, or the age hardening of EP451 steel, the low temperature of the $\alpha \rightarrow \gamma$ transformation, and the high stability of austenite during continuous cooling.

A study of the mechanical properties of forged billets and hot-rolled tubes in the as-delivered state (without heat treatment) showed that the EP56 and EP451 steels have a high strength, and what is even more important their yield strength and ultimate strength are very close. These steels have a low ductility also (for EP56: σ_b = 125.0—145.0 kg/mm^2; σ_τ = 118.0—130.0 kg/mm^2; δ_5 = 6.0—9.0%; and for EP451: σ_b = 107.0 kg/mm^2; σ_τ = 101 kg/mm^2; δ_5 = 7.0%). This combination of properties makes cold-rolling very difficult.

To develop a softening heat treatment for EP56 steel we started from the theory that a decrease in the effective content of carbon and niobium (in the γ-solid solution) leads to softening of the martensite and a decrease in the resistance of steel to softening. The content of effective carbon and

of alloying elements depends on the temperature of heat treatment. It was experimentally found that the minimum strength of EP56 steel after hardening is produced by cooling from temperatures near the A_{c_3} point (780°C—820°C). Subsequent tempering below the A_{c_1} point (tempering temperature 590—610°C, while A_{c_1} = 625°C) considerably decreases the strength and increases the ductility of the steel.

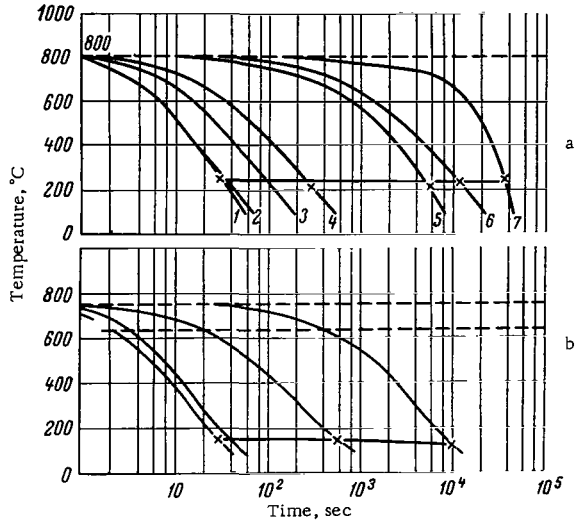

FIGURE 1. Thermokinetic diagrams of the decomposition of austenite during continuous cooling:

a — EP56 steel; b — EP451 steel.

Thus, a maximum softening of the EP56 steel is possible by heat treatment consisting in normalizing at 780—820°C, and tempering at 590°C—610°C for 2 hr. The mechanical properties of the steel after this heat treatment are as follows: σ_b = 96.2 kg/mm^2; σ_T = 81.5 kg/mm^2; δ_5 = 14.7%; ψ = 65.0%; α_k = 13.7 kg/cm^2. The hardness H_B = 306.

From the experience gained in producing tubes from EP56 steel it was found that the properties obtained by heat treatment made it possible to draw tubes, but only to a limited degree of deformation. It should be pointed out that the above heat treatment is too complicated for industrial conditions because of the very narrow permissible range of tempering temperatures, and the closeness of this range to A_{c_1}. Heating above A_{c_1} leads to a sharp increase in the strength and to a drop in the ductility of the steel, while tempering below 550°C leads to embrittlement of the steel. As a result, the necessary properties are difficult to attain and the drawing of tubes becomes complicated.

It was experimentally shown that the EP451 steel, like other austenitic-martensitic steels, cannot be transformed into martensite by air hardening. The steel consists of martensite, austenite, and σ-ferrite, irrespective of the austenitizing temperature (we studied the range of 800—1350°C), and therefore it was experimentally found that the hardened tubes cannot be drawn on the KhPT mill.

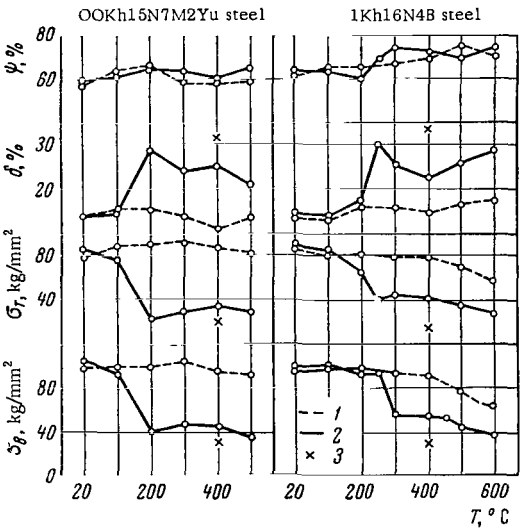

FIGURE 2. Dependence of the mechanical properties of steel containing supercooled austenite during ordinary heating on the testing temperature:

1—ordinary heating; 2—supercooled austenite; 3—properties of supercooled austenite at elevated austenitizing temperatures.

By heat treating this steel we failed to obtain properties that would enable a normal process of plastic deformation on cold rolling mills. All attempts to produce cold-drawn tubes of EP451 steel have so far been unsuccessful.

It was experimentally found that hot drawing tubes from EP56 and EP451 steels is not more advantageous than cold drawing. In addition, deformation at elevated temperatures is accompanied by further development of dispersion hardening processes, which lead to inhibition of the softening of EP56 steel and to a certain increase in the yield strength; this resists the initial stages of plastic deformation of EP451 steel (Figure 2).

Low-temperature thermomechanical treatment, which consists in deforming supercooled austenite followed by quenching to martensite, is normally used to increase the strength of low- and medium-alloyed constructional and tool steels. The above steels have a sufficiently high workability during both hot and cold pressing.

We attempted to use low-temperature thermomechanical treatment (in the field of supercooled austenite) to improve the workability of steels with a high hardness because of alloying and therefore difficult to cold work.

It is well known that it is much easier to cold work metals with a face-centered cubic lattice than metals with a body-centered cubic lattice. In the steels we studied the γ-phase (supercooled austenite) should have certain advantages over the α-phase for plastic deformations. The high stability of supercooled austenite in EP56 and EP451 steels at 200—600°C indicates that these metals can be deformed in the austenitic state at temperatures suitable for the operation of cold working mills (up to 600°C).

We studied the mechanical properties of EP56 and EP451 steels consisting of supercooled austenite at 200—600°C and after ordinary heating to the same temperatures, and plotted the stress-strain curves. We showed that the strength and ductility of these steels are higher and also the range and nature of work hardening are more favorable for rolling supercooled austenite than for rolling heated metals (see Figure 2). Thus, in the case of ordinary heating the yield strength of the EP451 steel even increases (from 78.5 kg/mm^2 at room temperature to 92.0 kg/mm^2 at 200—300°C). The yield strength of the EP56 steel at 200—300°C is only 2—3 kg/mm^2 lower than at room temperature. At the same time supercooling austenite at the same temperatures leads to a sharp decrease in the yield strength (24.0—30.0 kg/mm^2 for EP451 steel and 38.0 kg/mm^2 for EP56 steel). The ductility of both these steels consisting of supercooled austenite increases 1.5 and 1.7 times, but the ductility remains unchanged if the steels are only heated to the same temperatures.

An increase in the austenitizing temperature leads to further reduction in strength and to an increase in the ductility of the supercooled austenite (see Figure 2).

The influence of the conditions of testing on the properties of steel differs because in these steels plastic deformation at 200—600°C (hot rolling) is different from deformation of supercooled austenite. This is because the structures of the steels differ. At 200—600°C the structure of the steels is heterogeneous. EP56 steel then consists of an α-solid solution, a certain amount of γ-solid solution, and a disperse carbide phase, but EP451 steel consists of an α-solid solution, a γ-solid solution, and dispersed Ni_3Al intermetallic particles. If, however, supercooled austenite is deformed, the steel consists only of austenite (with small contents of σ-ferrite in both steels). It is clear that deformation will be more difficult in the first case than in the second.

The first experiments on drawing 50×2, 5×300 mm tubes of EP56 steel, which consists of supercooled austenite, were carried out on a continuous drawing mill, and confirmed the data of laboratory studies.

Thus, our investigations indicated a way of improving the workability of alloyed high-strength martensitic and martensitic-austenitic steels by working them at the temperature of supercooled austenite (low-temperature thermomechanical treatment).

Besides the above advantages, if supercooled austenite is deformed no special anneals are necessary between operations.

A. A. Chizhik

A NEW METHOD FOR INVESTIGATING CREEP AND RELAXATION IN METALS AND ALLOYS

We developed a new method for testing creep and relaxation in metals that requires no complicated apparatus and can be used for large-scale relaxation tests. Soft specimens are used with a working part shaped like a cylindrical spring and a square (rectangular) cross section (Figure 1).

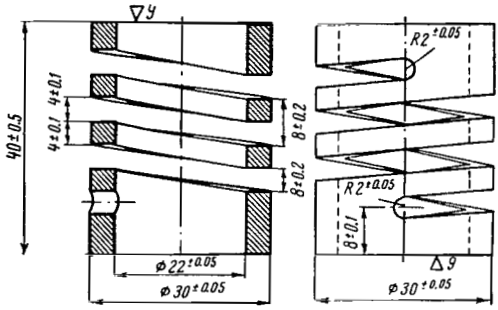

FIGURE 1. Specimens for testing creep and relaxation.

With these specimens expensive and complicated devices are unnecessary, and the accuracy of the measurements of creep deformation is appreciably increased. For the first time a large-scale evaluation of the creep strength of boiler tubes of any shape, including tubes of superheaters, screen tubes, and tubes of heat exchangers, has been possible.

Specimens for large-scale tests on creep and relaxation can be prepared from billets of any dimensions. To obtain the same results it is only necessary that the ratio of the average diameter of the specimen D_{av} to the width 2α be constant. Therefore, this method can be used for large-scale relaxation tests on metals and alloys, particularly when I. A. Oding's method with ring specimens is difficult because of the preparation of the specimen.

In this work we shall discuss three variants of tests carried out according to this method: 1) creep tests; 2) relaxation tests; 3) evaluation of creep strength according to data of relaxation tests. Each of these variants will be discussed separately.

CREEP TESTS

Creep tests were carried out under conditions of direct load. Compression (tension) of spring specimens leads to a twisting of the working coils, and to an irreversible distortion of the cross section of coils under conditions of creep. This distortion leads to certain mathematical difficulties during the calculation of stresses in specimens of this shape.

We calculated the steady-state creep by torsion in a sector of a ring (springs with small pitches) of rectangular cross section. This calculation was based on the existence of an exponential law connecting the creep rate (H) and the stress (T), $H=BT^m$, where B is a coefficient; m is the coefficient of creep. By introducing the function of stress u, the system of equations on the equilibrium and common rates of creep is reduced to a complex nonlinear differential equation of the second order, with partial derivatives

$$P_u \equiv \frac{\partial}{\partial \xi}\left(\frac{T^{m-1}}{(k-\xi)^3}\frac{\partial u}{\partial \xi}\right)+\frac{\partial}{\partial \eta}\left(\frac{T^{m-1}}{(k-\xi)^3}\frac{\partial u}{\partial \eta}\right)+\frac{2}{(k-\xi)^3}=0, \qquad (1)$$

where

$$T_* = \frac{1}{(k-\xi)^2}\sqrt{\left(\frac{\partial u}{\partial \xi}\right)^2 + \left(\frac{\partial u}{\partial \eta}\right)^2}\ ;\ k = \frac{R+a}{a} = i+1.$$

R is the average radius of the spring; a is half the base of the spring coil; $i=R/a$ is the coil index. The magnitude of P (at $m>1$) is a quasilinear differential operator of the elliptic type, with degeneration along the corners and at one of the internal points of the field, which influences numerous functions that meet the extreme conditions at contour G: $u_g = 0$.

Integration of the nonlinear differential equation (1) during the formulation of the above extreme conditions was carried out on a digital computer "Ural-2" by the Kantorovich—Newton method of consecutive approximations. At each approximation step formula (1) is substituted by a formula which is linear with respect to the function of stresses to the n-th approximation

$$P'(u_{n-1})u_n = P'(u_{n-1})u_{n-1} - P(u_{n-1}),$$

where $P'(u_{n-1})u_n$ is the Gato derivative of the nonlinear operator. The conversion of the $P'(u_{n-1})$ operator was carried out by the Ritz method. For function u we assumed the existence of a double sine expansion which automatically meets the limiting conditions for the field contour. As an initial approximation we took the solution of the formulas of torsion of the sector of the circumferential ring of the rectangular section in the elastic field. Our calculations showed that: a) the steady-state creep of spring specimens leads to redistribution of the initial elastic stresses leading to a decrease in the maximum stress; b) the nature of the redistribution of the tangential stresses depends on the magnitude of m, and it is also a function of the geometry of the specimen (of the coil index i); c) the stresses become more symmetrical as a result of their redistribution; d) if the coil index i is increased the distribution of stresses becomes similar to that of the torsion of a straight rectangular rod.

Our calculations show that the maximum stress in spring specimens can be calculated from the formula

$$\tau_{max} = \frac{\gamma_{max} M}{ab^2}, \qquad (2)$$

where $M=P\cdot R$ is the torsion moment; P is the axial force; R is the average radius of the spring; a is half the base section of the spring; b is half the height of the coil pitch. The coefficients γ_{max} for different m and $\mu = b/a$ values are given in Table 1.

To calculate the equivalent stresses during direct creep tests we assumed that $\sigma_{eq} = \sqrt{3}\tau_{max}$.

To determine the connection between the rate of compression of springs during creep, ξ_c, and the creep rate during monoaxial stretching, ξ_s, a fictitious or equivalent beam is introduced. In such a case the spring is substituted by a beam with a straight axis. During axial deformation the rigidity of the beam corresponds to the rigidity C of a spring specimen determined experimentally before the test.*

* The rigidity C is the force (in kg) necessary for a 1 mm elastic compression of a spring specimen.

TABLE 1. Coefficients γ_{max} for different values of m

$i = R/a$	$m=1$	$m=2$	$m=3$	$m=4$	$m=5$	$m=10$
			$\mu = b/a = 0.5$			
2	1.037	0.637	0.512	0.450	0.425	0.375
3	0.637	0.475	0.425	0.387	0.375	0.325
4	0.525	0.437	0.400	0.375	0.350	0.325
6.5	0.437	0.387	0.362	0.350	0.337	0.312
10	0.400	0.362	0.350	0.337	0.325	0.312
			$\mu = b/a = 1.0$			
2	1.400	0.850	0.700	0.630	0.590	0.520
3	0.950	0.680	0.600	0.560	0.540	0.500
4	0.800	0.620	0.570	0.540	0.520	0.500
6.5	0.705	0.590	0.550	0.525	0.505	0.490
10	0.630	0.540	0.510	0.500	0.480	0.460
			$\mu = b/a = 2.0$			
2	2.250	1.425	1.175	1.050	0.975	0.875
3	1.575	1.125	1.000	0.925	0.875	0.800
4	1.375	1.050	0.937	0.887	0.850	0.800
6.5	1.200	0.962	0.875	0.837	0.825	0.787
10	1.087	0.912	0.850	0.812	0.775	0.762

in a spring are uniform, and if the cylindrical specimen is subjected to a monoaxial stretching, the above relationship can be written as

$$\xi_s = \frac{\sqrt{3}\,CR}{EW}\,\xi_c \qquad (3)$$

where E is the modulus of normal elasticity at 20°C; W is the resistance moment during torsion of a straight rectangular rod with parameters corresponding to the dimensions of the actual coils of the specimen.

The above relationships were experimentally verified for EP182 steel specimens at 580°C, and for 1Kh18N9T steel specimens at 600°C. Our theoretical calculations of stresses were based on three assumptions: 1) there is no redistribution of stresses; the stresses were calculated from the formulas which hold for the torsion of a straight rod in the elastic field; 2) the redistribution of stresses can be represented by formula (2); and 3) a complete redistribution of stresses takes place, which corresponds to ideal plastic torsion of a straight beam.

To find out to what extent the results of creep tests on spring specimens agree with the results of creep tests on cylindrical specimens, and which method of calculation of stresses in springs is preferable, we plotted the results in logarithmic coordinates as graphs representing the dependence of the creep rate on stress (Figure 2). It can easily be seen that the results of creep tests on spring specimens are more scattered. Nevertheless Figure 2 shows that the best results are obtained by testing specimens of both steels according to the second assumption on the relationships which exist under conditions of steady-state creep of spring specimens. In fact, the average discrepancies between the theoretical and experimental data over the range of creep rates of $(10-600)\cdot 10^{-6}$ %/hr are 8% for EP182 steel and 6.5% for 1Kh18N9T steel. Calculations on the above relationships, without taking into account the redistribution of stresses, is not permissible since the average differences are 48—54%. Calculations based on an ideal plastic torsion involve considerable errors also (13—15%).

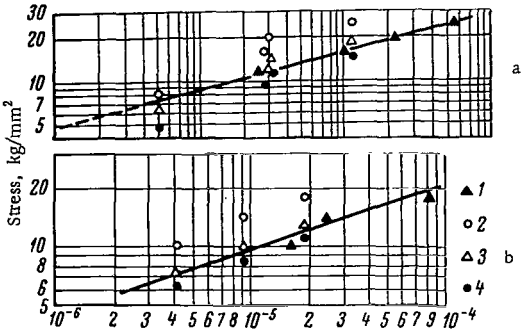

FIGURE 2. Comparison of experimental data on the creep strength of spring specimens with the data of direct tensile tests:

a — EP182 steel (580°C); b — 1Kh18N9T steel (600°C); 1 — standard creep tests; 2 — process 1; 3 — process 2; 4 — process 3.

A characteristic feature of this method of testing creep is the high accuracy of the measurement of small deformations. According to assumption (3) the specimens used for serial tests (see Figure 1) are equivalent to cylindrical tensile test specimens with a working length of about 1250 mm from the point of view of the accuracy of deformation measurements. This method can thus be used to study creep at low rates of deformation.

RELAXATION TESTS

Relaxation tests are carried out by a method similar to that for testing ring specimens with the same bending strength. Indentations were made on the tip of the tubes by a diamond pyramid, using a Vickers tester. These indentations are used to measure the deformation of creep. The specimens were tested in batches of 20—30 pieces and were loaded by compressing with nuts to a given initial position. We used cylindrical bushings of moderate length as a wedge that maintained a constant total deformation. This is the basic condition for pure stress relaxation.

To use this testing method to evaluate the relaxation stability of heat-resistant materials, a method for converting the data obtained by testing spring specimens into data representing relaxation by stretching or bending (Oding's method) had to be developed. This involved solving the problem of relaxation of rectangular springs with small pitches. The solution of this problem was based on the principle of minimum additional forces during deformation, and the data obtained were as follows: a) the intensity of relaxation of spring specimens is determined by the geometry of the coil and by the creep factor; b) if the maximum initial stress is the same, the relaxation of spring specimens becomes more rapid as the curvature of the coil increases (smaller coil index); c) if the coil index is above 6, at the

same initial stresses the relaxation of spring specimens is almost the same as during torsion of a straight rectangular beam.

These calculations lead to the following formula representing the dependence of the maximum tangential stress on the normal stress during monoaxial stretching or bending by Oding's method

$$\tau_{max} = p\frac{\sigma}{\sqrt{3}}.$$

The coefficients p for spring specimens with square coil sections are given on Table 2. From a review of these data it can be concluded that: a) the coefficient p is little influenced by the creep factor and can be considered to be constant irrespective of the curvature of the coil; b) if we consider that the permissible error during the calculation of stresses in ring specimens is 5%, and take into account the scattering of the test results, it is obvious that the use of the criterion $\sigma_{eq} = \sqrt{3}\tau_{max}$ to calculate the initial equivalent stresses for springs at $i > 3$ can give identical relaxation curves for both methods over a wide range of temperatures. In other words, if we choose the initial equivalent stresses correctly, the ring method of I.A.Oding and the method of testing spring specimens will give the same results under conditions of relaxation; c) the agreement between the relaxation curves under conditions of monoaxial stretching during testing of spring specimens (using the criterion $\sigma_{eq} = \sqrt{3}\tau_{max}$) is reflected by the same agreement between the relaxation curves for monoaxial stretching and for ring specimens if $\sigma_{str} = \sigma_{bend}$.

TABLE 2. Magnitudes of coefficient p for rectangular spring specimens

$i = R/a$	p, monoaxial stretching					p, bending by Oding's method				
	$m=2$	$m=3$	$m=4$	$m=5$	$m=10$	$m=2$	$m=3$	$m=4$	$m=5$	$m=10$
3	0.98	0.93	0.88	0.85	0.86	0.88	0.86	0.83	0.87	0.78
4	1.07	1.03	0.98	0.95	0.87	0.98	0.95	0.93	0.99	0.80
6.5	1.08	1.17	1.11	1.11	—	1.10	1.08	1.08	1.15	0.85
10	1.27	1.20	1.13	1.13	0.95	1.12	1.11	1.12	1.16	1.00

With the above criterion it is possible to obtain a dependence between the upsetting of the spring during relaxation and the equivalent stresses (stresses induced by monoaxial stretching)

$$\Delta = \frac{K_2}{\sqrt{3}}\frac{E_{20^\circ}}{E_t}\frac{(2a)^2(2b)}{C \cdot R}\sigma,$$

where Δ is the upsetting of spring specimen; K_2 is a coefficient; $2a$ and $2b$ are the sides of the cross section of the coils; R is the average radius of the specimen; C is the rigidity; E_{20} and E_t are the moduli of normal elasticity at 20°C and at the testing temperature, respectively (equivalent stresses). These relationships should be used to determine the initial upsetting of spring specimens corresponding to the initial stress σ_0.

The coefficients K_2 are given below:

b/a	1.0	1.5	2.0	3.0	5.0	10.0
K_2	0.208	0.231	0.246	0.267	0.294	0.312

To check these relationships experimentally we carried out comparative relaxation tests on spring specimens and rings with the same bending strengths, made of EP182 steel at 580°C and 1Kh18N9T steel at 600°C. The initial relaxation curves of these steels are given in Figure 3, and show that there is good agreement between the theoretical and experimental results. The greatest differences between the stresses do not exceed 5% during 2000 hr of testing. Since the tests were carried out in different laboratories with different equipment, this difference does not exceed the possible experimental error.

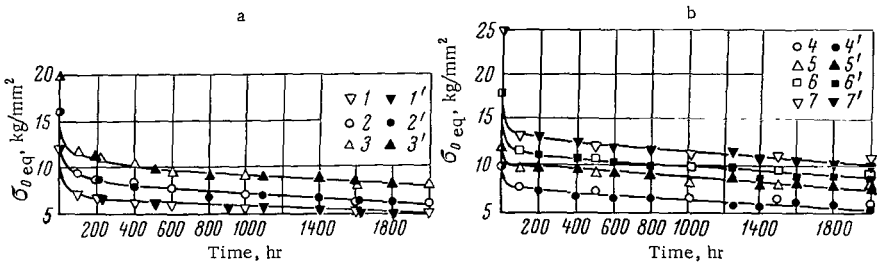

FIGURE 3. Comparison of relaxation curves of spring and ring specimens with the same resistance to bending:

a — EP182 steel (580°C); b — 1Kh18N9T steel (600°C). 1 — $\sigma_b = 12$ kg/mm²; 2 — 16 kg/mm²; 3 — 20 kg/mm² for ring specimens; 1', 2', 3' — the same for spring specimens; 4 — $\sigma_b = 10$ kg/mm²; 5 — 14 kg/mm²; 6 — 18 kg/mm²; 7 — 25 kg/mm² for ring specimens; 4', 5', 6', 7' — the same for spring specimens.

The above theoretical calculations and experimental data show that the method of relaxation tests on spring specimens is quantitatively equivalent to I. A. Oding's method, and can be used as an independent method for evaluating the relaxation stability of metals and alloys.

EVALUATION OF THE CHARACTERISTICS OF CREEP STRENGTH BY DIRECT EXPERIMENTS (RELAXATION TESTS)

Relaxation tests on soft specimens are the easiest way of evaluating the creep strength of heat-resistant materials. This method can be used on a very large scale. One of the advantages is that a low creep rate can be determined with a high degree of accuracy, and it is possible to study the process of creep under variable loads by a few tests only. The method for determining the characteristics of creep strength (deformation and steady-state creep rate) from relaxation tests is indirect, and is based on the assumption that the mechanisms of relaxation and creep are the same.

The phenomenological problems on the connection between relaxation and creep are discussed in the work of A. A. Chizhik.* Methods for calculating

* Chizhik, A. A. The Relationship between the Phenomena of Relaxation and Creep in Metals and Alloys. Collection of articles "Properties and Uses of Heat-Resistant Alloys." — Izdatel'stvo "Nauka." 1966.

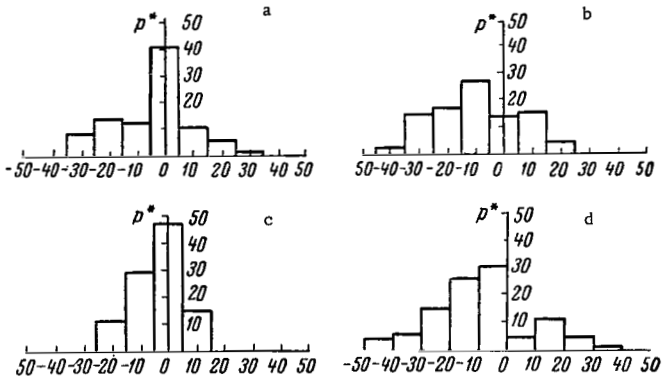

FIGURE 4. Histograms of the distribution of the deviations of the theoretical data from the experimental on creep strength for different theories on creep:

a — theory of flow; b — theory of aging; c — theory of hereditary phenomena; d — combined theory.

the characteristics of creep strength from data on relaxation have been developed from theories on flow, aging, hereditary phenomena, and combined theories. In this work we shall discuss the results of the experimental verifications of the relationships obtained for spring specimens made of 6 different metals (EP182, EI802, 1Kh18N9T, EI695R, EI572, and EI612) over a wide range of temperatures. The results of theoretical calculations on relaxation during creep were compared with the results of direct experiments for two characteristics of creep strength: deformation and rate of deformation during steady-state creep.

The results of these comparisons on deformation during creep showed that the average deviations for the steels studied are as follows according to the theories of: flow, 10.5%; aging, 16%; hereditary phenomena, 7%; and combined theory, 9.5%. This shows that the results of calculations according to these theories do not differ much (the deviation of the average values was only 5—9%).

To compare the theoretical and experimental data on creep rate during steady-state creep, we used elements of statistical analysis. The number of experiments carried out according to the three theories (theory of flow, theory of aging, and combined theory) was 155, and the theory of hereditary phenomena was checked by 28 experiments. The results obtained by comparing the creep limits are given in Figure 4. The statistical agreement between the theoretical and experimental data on the creep limit are plotted on the ordinate (for a given range of deviations) and the deviations from the creep limit obtained by tensile tests on the abscissa. The best agreement between the theoretical and experimental data, as in the case of ring specimens with the same bending strength /1/, is given by the theories of flow and hereditary phenomena. For these theories the differences between the calculated and experimental data are not greater than ±10%. The greatest discrepancies were obtained for the theory of aging, where the calculated values on the creep limit are on an average 10% less than those obtained by tensile tests. The combined theory gives intermediate results.

These results show that relaxation tests on spring specimens can be used for large-scale determinations of the characteristics of creep strength of heat-resistant metals. This method is simple, does not require any expensive equipment, and can be carried out in any industrial laboratory.

N. V. Ageev, S. G. Glazunov, L. A. Petrova, G. N. Tarasenko, and L. P. Grankova

SHORT-TIME AND LONG-TIME STRENGTH OF THE β-ALLOY OF THE Ti—Mo—Cr—Fe—Al SYSTEM AT ELEVATED TEMPERATURES

The β-titanium alloy (Ti—7% Mo—5.5% Cr—3% Fe—3% Al) heated for one hour at 800°C, quenched in water, and aged at 550°C and 525°C for 15 hr (processes 1 and 2), at 500°C for 20 hr (process 3), or at 450°C for 50 hr (process 4), and then cooled in the air, has the following mechanical properties at room temperature: σ_b=140—170 kg/mm^2; δ=10—5%; ψ=22—11%. The mechanical properties of the alloy treated according to processes 1 and 2 changed little when the alloy was held at the required service temperature of 350°C for 100, 500, and 1000 hr (Table 1). This shows that at 350°C this alloy is thermally stable.

TABLE 1. Mechanical properties of alloy

Heat-treatment process	Mechanical properties			Heat-treatment process	Mechanical properties		
	σ_b, kg/mm^2	δ, %	ψ, %		σ_b, kg/mm^2	δ, %	ψ, %
Process 1	143.6	5.59	21.56	Process 2	155.7	5.20	17.26
The same + 350°—100 hr	131.2	9.05	20.8	The same + 350°—100 hr	145.0	5.8	15.5
" " + 350°—500 hr	130.2	8.4	21.4	" " + 350°—500 hr	143.0	5.5	12.6
" " + 350°—1000 hr	130.2	6.6	15.1				

COMPARISON OF THE HEAT RESISTANCE OF THE ALLOY SUBJECTED TO DIFFERENT HEAT-TREATMENT PROCESSES

To find whether this alloy can be used at elevated temperatures, and to compare the above processes of aging, it was interesting to study the heat resistance of alloys by the centrifugal method of bending /1/. This method is based on the deformation of specimens during heating under the continuous action of a centrifugal force, and both creep and long-time strength can be studied simultaneously. The bending force which acts on the specimen is determined by the length of the specimen, its mass, and the rate of rotation. To increase the stress, that is the bending force, additional loads can be added to the free end of the specimens. Since the alloy we studied is relatively light (specific gravity 4.83 g/cm^3) and has a

high strength, we added a tungsten load of 70 g (10 mm in diameter and 46 mm long) to the end of the specimen. The experiments were carried out at 350°C in the air, with specimens 4 mm in diameter and 60 mm long. These specimens were heat treated according to processes 1—4. After these heat-treatment processes, some specimens were additionally heated at 350°C for 100 hr. Other specimens were subjected to processes 1 and 4, and then heated at 350°C for 500 hr. The creep rate was determined by the deflection (in mm) after a given time.

The tests for heat resistance were in three stages: during the first stage the specimens were tested under a load of 100 kg/mm^2 for 75 hr, during the second stage under a load of 110 kg/mm^2 for 125 hr, and during the third stage under a load of 115 kg/mm^2 for 50 hr. Thus, the total testing time was 250 hr. For some specimens the testing time was shorter as the tungsten loads failed before the end of the test because of their brittleness.

An analysis of the dependence of the deflection on the duration of deformation during 3 processes of testing showed that the alloy is little softened at these testing temperatures, and can withstand the above testing conditions. The best results (deflection of 1.5 mm after 250 hr) were obtained on specimens subjected to process 1 and then held at 350°C for 500 hr. The microstructure of these specimens after 250 hr of stressing differs little from the initial structure after aging, except that subgrains appear within the initial β-grains. The fragmentation of the coarse β-grains and the production of a subgrain structure are apparently due to the action of the load during the test.

Specimens treated according to process 1 and held at 350°C for 100 hr showed good properties without any additional heating: the deflection was $\varepsilon = 2$ mm after 250 and 200 hr.

An analysis of the creep curves of the alloy at 350°C showed that the smallest deflection is found in the alloy aged at 550°C for 15 hr. Tests on the mechanical properties at room temperature of aged alloys that had been additionally heated at 350°C for 100 and 500 hr, and the determination of the heat resistance by the centrifugal method, indicated that the alloy is thermally stable at 350°C for 100 and 500 hr, and also that after heating at 350°C for 500 hr the alloy has a higher heat resistance than after heating for 100 hr.

MECHANICAL PROPERTIES OF THE ALLOY AT TEMPERATURES FROM 20°C TO 700°C

The mechanical properties (σ_b, δ and ψ) of the alloy were tested over the temperature range from room to 700°C on KRD-3 specimens with a 10× × 1.5 mm thread, a diameter of the working part of 5 mm, and with a working and total length of 28 and 60 mm, respectively. The tests were carried out in a vertical electric tube furnace filled with air. The testing machine was of the IM-4R type, and the rate of deformation was 1.25 mm/min. The heat treatment of the alloy consisted in quenching in water from 800°C and holding for 1 hr, aging at 550°C (process 1) or at 525°C (process 2) for 15 hr, and cooling in the air. The billets thus treated were 60 mm in length and 12 mm in diameter, and were heated in an air-filled furnace.

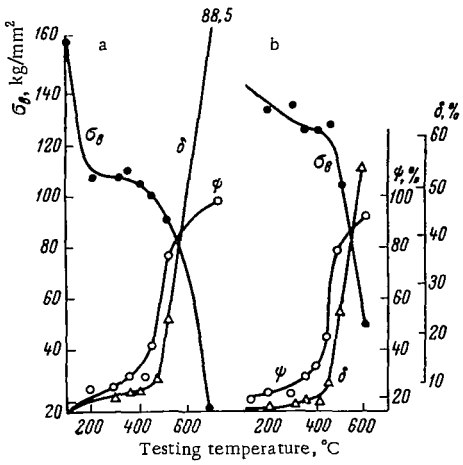

FIGURE 1. Dependence of mechanical properties of the ß-alloy (Ti — 7Mo — 5.5Cr — 3Fe — 3Al) quenched from 800°C for 1 hr in water, and aged at two different temperatures, on the testing temperature (200—700°C):

a — at 525°C for 15 hr; b — at 550°C for 15 hr.

After the heat treatment, specimens were cut from these billets. The specimens were heated in the furnace to the necessary temperature, held for 15 min, and then loaded for 20 to 30 min. The results of these tests are given in Figure 1. They show that the alloy aged at 550°C for 15 hr has the best mechanical properties, and that after aging by processes 1 and 2 the mechanical properties, particularly the strength, change little over the range of temperatures from 200—450°C. At 500°C the strength of the alloy decreases, but it still remains sufficiently high (92 and 105.5 kg/mm^2 for specimens aged at 525°C and 550°C, respectively). At 600°C the alloy that had been aged at 550°C for 15 hr had an ultimate strength of 51 kg/mm^2.

The curves representing the ultimate strength of alloys, aged according to different processes, show that in alloys aged at 525°C, over the temperature range from room to 200°C the ultimate strength decreases more rapidly than in alloys aged at 550°C. The ultimate strength of the alloy decreases sharply because the grains of the α-phase separated as the result of decomposition (Figure 2,a) during aging at 525°C for 15 hr are larger than those in the initial state at room temperature or those formed at 200°C in specimens aged at 550°C for 15 hr (Figure 2,b). Also, in specimens aged at 525°C for 15 hr, after testing at 200°C, more nondecomposed regions are found in the vicinity of the boundaries of β-grains (light edges) than in specimens aged at 550°C for 15 hr, where we find dark edges around the β-grain boundaries.

The light regions near the boundaries of the β-grains are apparently rich in β-alloying elements. The dark regions around the boundaries of the β-grains have less of these elements than the light regions, but are still richer than the bulk of the β-grains. When designating the dark and light regions as those containing more or less alloying elements, we must remember that the difference in the concentration of these elements in the

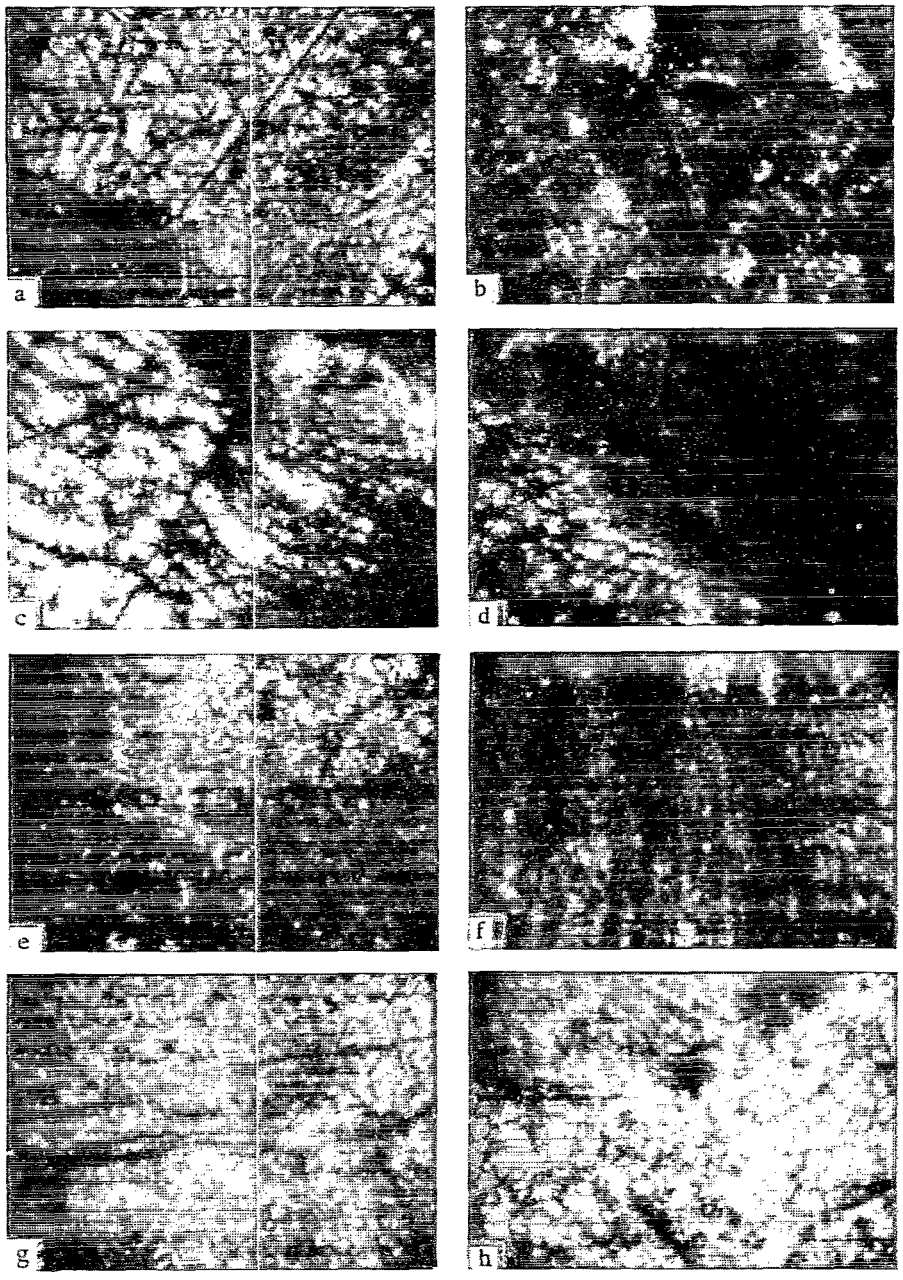

FIGURE 2. Microstructure of β-alloy (×1350), quenched from 800°C (1 hr) in water and aged:

a — at 525°C for 15 hr; b, h — at 550°C for 15 hr; a, b — testing at 200°C; c — at 400°C; d — specimen failed after testing at 500°C for 56.5 hr, at σ_b=60 kg/mm^2; e — after testing at 20°C, the specimen was turned out on a lathe after a test carried out at 350°C under a load of 90 kg/mm^2 for 942 hr, σ_b=242 kg/mm^2, δ=2.8%; f, g — σ_b=243 kg/mm^2, δ=1.4%; h — σ_b=234 kg/mm^2, δ=0.6%.

light and dark regions is less than 1% since point X-ray analysis,* with an accuracy within 1%, showed no differences between the concentrations of Mo, Cr, Fe, and Al in the dark and light regions of the β-grains.

When the alloy is heated to the tempering temperature decomposition starts in the region depleted of alloying elements. If the heating is prolonged, new α-grains are formed in these regions and grains formed earlier coagulate. The mobility of atoms in the alloys is increased, and the regions with a higher content of β-alloying elements start to decompose until the β-alloying elements are unstable, and a fine-grained α-phase is precipitated. Since the α-phase is very fine grained it occupies a larger surface, and therefore after etching these regions are darker than the bulk of the α-grains previously precipitated in the β-grains. If the specimens have light edges (non-decomposed regions with a high content of β-alloying elements), the alloy fails more rapidly than those with dark edges (regions which decompose later), since the fine-grained α-phase blocks plastic deformation more. However, both light and dark edges around the β-grains are stress raisers, and are therefore undesirable.

A study of the microstructure of alloys aged at different temperatures showed that the α-phase formed by aging at 525°C for 15 hr is coarser than the α-phase formed by aging at 550°C for 15 hr, irrespective of the testing temperature. The α-phase formed during decomposition of the β-solid solution as a result of aging at 550°C for 15 hr is more fine-grained than that formed at 525°C, since the larger number of crystallization centers of the α-phase formed at 550°C make the grain growth more difficult than at 525°C. Prolonged aging makes it possible for the α-phase to grow and to precipitate from the β-solid solution.

If the testing temperature is increased, the β-solid solution probably continues to decompose, the grain size of the α-phase increases, and at relatively high temperatures of 600°C and 700°C partial dissolution of the α-phase is possible. If we can judge from the properties of the alloy, decomposition of the β-solid solution takes place even at 350°C, but the strength decrease indicates that at 400°C coagulation of the earlier formed α-grains takes place more rapidly than the formation of new α-grains. Even if the decomposition continues, its influence on the strength of the alloy is suppressed by the coarsening of the α-grains formed earlier, and the growth of these predominates over the number of new α-grains formed. As a result the strength of the alloy during tests at 400°C is somewhat lower, but it remains almost constant up to 450°C. At 500°C and at 600°C the alloy aged at 550°C for 15 hr has a finer α-phase grain than the alloy aged at 525°C for 15 hr. A fine-grained structure of the α-phase means a higher strength.

The microstructure of alloys shown in Figure 2,c indicates that after testing some β-grains have wavy slip lines. The presence of these indicates that under stress shear deformation takes place along two systems of crystallographic planes.

Thus, alloys aged at 550°C for 15 hr have better mechanical properties than those aged at 525°C for the same time. Alloys aged at 550°C for 15 hr can be used as a heat-resistant material up to 450°C, since at these temperatures it retains a uniform strength within the limits of 130—127 kg/mm^2, and a ductility (elongation) of 6—8%.

* We should like to express our gratitude to I. B. Borovskii and V. A. Batyrev for carrying out X-ray spectral point analysis.

LONG-TIME STRENGTH OF ALLOYS AT 350, 400, AND 500°C

To find the resistance of alloys aged at 550°C for 15 hr to failure at 350, 400, and 500°C we found their long-time strength under various stresses. The tests were carried out on standard threaded specimens with a KRD-3 machine. Billets were subjected to heat treatment (solution heat treatment and aging) and test specimens were then prepared from these. The results are shown in Figure 3. The duration of stress was plotted on the abscissa and its magnitude on the ordinate. The data in Figure 3 indicate that at 350°C the alloy does not fail under a stress of 110 kg/mm^2 for 1240 hr, at 400°C it does not fail under the same stress for 11 hr, and under a stress of 100 kg/mm^2 it does not fail for 32.5 hr. At 500°C the breaking stress drops sharply, but the alloy withstands a load of 60 kg/mm^2 for 56.5 hr.

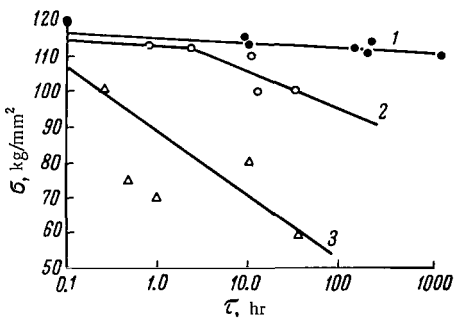

FIGURE 3. Dependence of the long-time strength of a β-alloy quenched from 800°C in water (1 hr) and aged at 550°C for 15 hr, on the time of loading:

1 — 350°C; 2 — 400°C; 3 — 500°C.

A study of the microstructure of alloys after tensile tests showed that the higher the testing temperature the coarser the α-phase. A coarse α-phase apparently inhibits plastic deformation less than a fine, and facilitates softening of the alloy. Since some slip lines were found in the β-grains (Figure 2,d), it can be assumed that the applied stresses cause not only a creep along the grain boundaries but also shear deformation.

The results of a study on the long-time strength show that at 350°C the alloy can withstand a stress of 110 kg/mm^2 for 1240 hr, at 400°C it can withstand the same stress for 11 hr, and at 500°C it can withstand a stress of 100 kg/mm^2 for 32.5 hr.

Specimens which were removed from the testing machine after 942 hr under a stress of 90 kg/mm^2 at 350°C had an elongation of 1.78%. From these specimens we prepared three microspecimens: from the end, from the working part, and a longitudinal microsection running along both the end and the working part. These were subjected to a tensile test on a micro-machine at room temperature. The total length and the working length of these specimens were 15.5 and 7.5 mm, respectively. The diameters of the end and the working part were 3 and 1.5 mm, respectively.

The specimens turned out from the end and from the working part had a very high strength of 242 and 243 kg/mm^2, and an elongation of 2.8 and 1.4%, respectively. The longitudinal specimen turned out from the end and from the working part showed brittle failure at σ_b= 232 kg/mm^2 and an elongation of 0.6%.

A study of the microstructure of specimens with an ultimate strength of 243—234 kg/mm^2 showed that all specimens had a polygonal structure with fine-grained precipitate particles which, according to the data of an X-ray analysis, were an α-phase. The specimen from the end (σ_b= 242 kg/mm^2 and δ = 2.8%) had a sharp polygonal structure with the smallest α-phase grains (see Figure 2,e). The specimen with δ = 1.4% had a less distinct polygonal structure and in some β-grains the slip lines terminated in microcracks (see Figure 2,f and g). The specimen that showed brittle failure differed from the above two specimens as it had β-grains of a nonuniform size (see Figure 2,h).

The lattice parameters of the β-solid solution of all three specimens were similar (3.176—3.183 kX), which indicates the same concentration of the β-solid solution. Powder specimens made from annealed alloys had a similar lattice parameter (3.187 kX). The data obtained on the lattice parameters of the β-solid solution of alloys subjected to different heat-treatment processes show that because the concentration of β-solid solution is the same, this solution decomposes to a certain extent even before intermetallic compounds are precipitated, when the concentration of the β-solid solution changes little. As the concentration of the β-solid is the same, it can be assumed that if this concentration is constant the strength of the alloy is determined by the size and the shape of the grains of the α-phase.

Thus, it can be seen that the heat resistance of the alloy can be improved /2/ by choosing the proper processes of thermomechanical treatment to produce a polygonal structure of the β-grains which leads to a more uniform distribution of the precipitated α-phase (along the walls of dislocation).

Bibliography

1. Kornilov, I.I.— Zadovskaya Laboratoriya, No.1, p.76. 1949.
2. Ivanova, V.S. and L.K.Gordienko. Novye puti povysheniya prochnosti metallov (New Methods of Increasing the Strength of Metals).—Izdatel'stvo "Nauka," p.38. 1965.

A.M.Korol'kov, L.M.Gurova, and E.V.Bezus

HEAT-RESISTANT COPPER ALLOYS

Low-alloyed copper alloys are widely used in electrical technology, in the radio and electronic industries, and in many other fields of industry which require materials with a good electric conductivity.

Due to the rapid development of industrial vacuum apparatus for electronics, these alloys must have not only a high electric conductivity but also a certain heat resistance.

The electric conductivity of these alloys must not be lower than 80—60% of the electric conductivity of copper, and the long-time strength at 400—600°C should be at least 2—3 times that of copper. Such alloys appreciably increase the reliability and the life of the apparatus, which is particularly important if the devices cannot be repaired.

Many such alloys of copper with chromium, zirconium, cadmium, and magnesium /1—3/ and with chromium, zirconium, hafnium, and arsenic /4/ have been studied both in the Soviet Union and outside. The content of alloying elements in these alloys does not exceed 0.6—1.0% so that the electric conductivity of the material is not decreased too much.

In the above works the heat resistance of the alloys was found mainly by measuring their hardness, and no curves of long-time strength or of creep, which represent more completely and more quantitatively the heat resistance of alloys, have been constructed.

A number of copper alloys have been studied in connection with theories on heat resistance. The chief types of composition—heat-resistance diagrams /5—6/, which make the study of the heat-resistance of alloys easier, have also been investigated. One of these composition—heat-resistance diagrams is particularly suitable for a study on the alloys that interest us. The phase diagrams of these alloys show a very limited region of solid solutions and the formation of intermetallic compounds, which have a very high heat resistance. Some properties of alloys can be changed in the desired direction by the addition of alloying elements. Of these properties we should like to mention the following: the temperature dependence of the solubility, a high recrystallization temperature of the solid solution, and a high solidus temperature. The nature, the amount, and the shape of second phases which hinder plastic deformation, etc., can also be changed by alloying /6—11/.

The alloys with the best properties belong to the following systems: Cu—Cr and Cu—V (high solidus, and a field of a copper-base solid solution) and Cu—Cr and Cu—Zr (existence of a solid solution, the solubility changes little with variation in temperature, existence of intermetallic precipitates). Of considerable interest are ternary alloys on the basis of the above binary systems. One of these alloys (Cu—Zr—Cr) has already been studied and satisfactory results have been obtained /1, 3/.

HEAT RESISTANCE OF COPPER AND OF COPPER ALLOYS

To study the influence of alloying components on the heat resistance of copper a certain criterion of heat resistance must be chosen. According to I. A. Oding and V. N. Geminov /11/, the long-time strength can be chosen, as it can give a relative evaluation of heat resistance, and the optimum composition of the alloys can thus be chosen.

We evaluated the heat resistance of copper and copper alloys from their ultimate long-time strength for 100 hr (σ_{100}), which was found from the

long-time strength curves. The heat resistance of some alloys was determined from their individual ultimate long-time strength. Before carrying out long-time tensile tests, we first evaluated the heat resistance of alloys by measuring their hot hardness. With this method the influence of alloying components can be qualitatively compared and the influence of the composition of alloys on their heat resistance evaluated. The heat resistance of alloys was evaluated from the absolute value of long-time hardness and from their softening, i.e., from the relationship between the hardness measured during 30 and during 3600 sec. The tests were carried out on specimens forged and annealed at 750—800°C.

The heat resistance of binary and ternary copper alloys containing cerium, vanadium, zirconium, and other alloying elements, was studied with specimens that had been melted in graphite crucibles placed in induction furnaces in a current of argon. Before the test the specimens were forged and annealed at 750—800°C for 3 hr. In this state almost all alloys consisted of two or three phases.

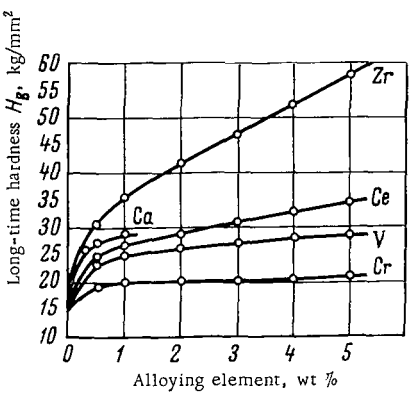

FIGURE 1. Long-time hardness of copper alloys at 400°C.

The structure of the binary alloys agreed with the existing phase diagrams.

The results of comparative measurements of the long-time strength of various binary alloys at 400°C are given in Figure 1.

It can be seen that zirconium has the greatest influence on the long-time hardness of copper. If the content of zirconium increases from 0.5 to 5%, the long-time hardness of copper increases smoothly. The general level of hardness of alloys containing zirconium is appreciably higher than that of other alloys.

Vanadium, and in particular chromium, exert the least influence on the long-time hardness of copper. Chromium up to a concentration of 1% increases the long-time hardness of copper.

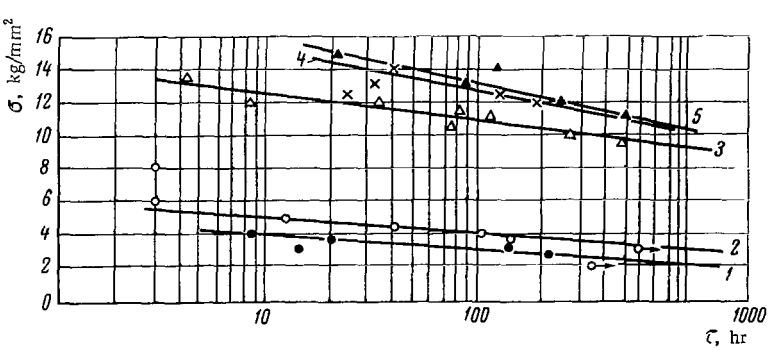

FIGURE 2. Long-time strength of copper and of copper alloys at 400°C:

1 — vacuum-melted copper; 2 — oxygen free copper; 3 — Cu—Ce—Zr vacuum-melted alloy; 4 — Cu—Ce—Zr alloy; 5 — Cu—Zr alloy after melting in the air.

TABLE 1. Long-time strength of copper and of copper alloys at 400°C

Number of melt	Composition of alloy, %*	Electric conductivity, % of electric conductivity of copper	Stresses, kg/mm²	Time to failure, hr
	Oxygen-free copper	99	See curve 2 on Figure 2	
	Vacuum-melted copper	101	See curve 1 on Figure 2	
194	1.48% Cr	87	6.0	43
			7.0	22
294	3.5% V**	80	7.0	130
			9.0	13
301	2.22% Ce	79	7.0	215
333			9.0	52
333	0.73% Zr	83	10.0	355 (did not fail)
			11.0	31
			12.0	28
			14.0	23
334	2.65% Zr	79	See curve 5 on Figure 2	
332	0.7% Zr + 0.7% Ce	81	See curve 4 on Figure 2	
363	0.86% Zr 0.81% Ce	78	10.0	277
			11.0	624
			13.0	146
487	0.75% Zr 0.3% Cr 0.3% V		11.0	631
			13.0	205 (did not fail)
			14.0	5
572	0.69% Ce + 0.91% Zr	85	See curve 3 on Figure 2	

*Balance copper.
**Composition of the alloy according to charge.

The heat resistance of alloys was evaluated chiefly by tensile tests. The results of tests on pure copper and on a number of alloys with an electric conductivity of 75—85% of the electric conductivity of copper are given in Table 1 and Figure 2. The stresses are plotted on the vertical axis and the time to failure in a semilogarithmic scale on the horizontal axis.

With this method the relationship between the strength and testing time is obtained as a straight line function /11/, which is very convenient, particularly when comparing the heat resistance of a number of alloys.

The study on the heat resistance of alloys was started by determining the heat resistance of copper by the method of long-time strength.

Numerous data on the mechanical properties of copper measured at various temperatures up to 1000°C can be found in the literature /7/, but they do not characterize the heat resistance of copper and can be used only to choose conditions for the production of copper parts by hot working.

Existing literature data on the long-time strength of commercial copper of the M1 grade show that this material has a long-time strength σ_{100}^{400} of 2.5 kg/mm² /12/.

We constructed long-time strength curves for two types of copper, oxygen-free copper, and vacuum-melted copper, which are used to produce electronic devices.

The results are given in Table 1 and Figure 2, and show that at 400°C the long-time strength of oxygen-free copper, in 100-hr long tests, does not exceed 4 kg/mm^2, and the long-time strength of vacuum-melted copper is only about 3 kg/mm^2. The long-time strength of oxygen-free copper at 600°C in an atmosphere of argon does not exceed 1.5 kg/mm^2 (Figure 3).

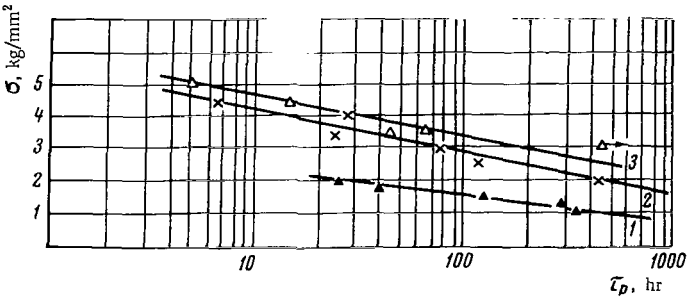

FIGURE 3. Long-time strength of copper and copper alloys at 600°C:

1 — oxygen-free copper; 2 — Cu—Ce—Zr alloy; 3 — Cu—Zr alloy.

The data on the long-time strength of copper alloys at 400°C are given in Table 1 and Figure 2.

These data indicate that zirconium is the best alloying element to add to copper. At 400°C the long-time strength of Cu—Zr alloys in 100-hr long tests (10—13 kg/mm^2) is higher than that of other binary alloys (Cu—Cr, Cu—Ce, Cu—V) (7—8 kg/mm^2). Thus, the heat resistance of alloys at 400°C is 2—4 times that of pure copper. At 400°C, the best heat-resistant alloy of ternary and more complex alloys are the Cu—Zr—Ce and the Cu—Zr—Cr—V alloys ($\sigma_{100}^{400} \approx$ 12—14 kg/mm^2).

For Cu—Zr and Cu—Zr—Ce alloys which have a high long-time strength at 400°C, we constructed long-time strength curves at 600°C (see Figure 3).

The tests at 600°C were carried out in an atmosphere of argon.

From long-time strength curves we found the long-time strength for 100-hr tests, for Cu + 2.01% Zr alloys (3.3 kg/mm^2) and for Cu + 0.69% Ce + + 0.91% Zr alloys (2.8 kg/mm^2). Under these conditions the long-time strength of oxygen-free copper is equal to 1.5 kg/mm^2.

When analyzing the reasons for the various degrees of heat resistance of binary and more complex alloys, it should be remembered that Cu—Cr and Cu—V alloys are heat resistant because their solidus temperature is higher than that of Cu—Zr and Cu—Ce alloys (1075—1100°C against 965—875°C). However, the strengthening phases of Cu—Zr and Cu—Ce alloys are chemical compounds, which are more disperse than elementary inclusions of chromium and vanadium, and therefore hamper deformation. Also, solubility in Cu—Zr, Cu—Ce, and apparently in Cu—Zr—Ce alloys, is much less influenced by temperature than solubility in Cu—Cr and Cu—V alloys

/13—15/. Consequently, the diffusion exchange in these last alloys is much greater, which leads to a greater softening of stressed parts at elevated temperatures /8—10/.

CONCLUSIONS

1. By means of hot hardness and of long-time strength, we studied the influence of a number of alloying elements (Cr, V, Ce, Zr, and others) on the heat resistance of copper at 400°C.
2. It was found that zirconium has the greatest influence on the heat resistance of copper, and the influence of cerium and of vanadium and chromium is more moderate.
3. The strength of copper is increased most by alloying it with two or three components (alloys Cu — Zr — Ce, Cu — Cr — V).
4. We found ductile copper alloys which combine a good heat resistance with a high electric conductivity (not less than 75% of the electric conductivity of copper). The long-time strength of these alloys at 400°C found by 100-hr long tests is equal to 12—13 kg/mm^2, which is 3—4 times that of copper, and at 600°C the long-time strength is equal to 2.8—3.3 kg/mm^2. These alloys contain 2—3% of Zr, or 1.5—2.0% of (Zr+Ce).

Bibliography

1. Zakharov, M.V. et al. Provodnikovye mednye splavy povyshennoi prochnosti (Conducting Copper Alloys (High Strength)). — In: "Issledovanie splavov tsvetnykh metallov," No. 4. Izdatel'stvo AN SSSR. 1963.
2. Zakharov, M.V. K voprosu o printsipakh legirovaniya zharoprochnykh tsvetnykh splavov (Principles of Alloying Heat-Resistant Nonferrous Alloys). — In: "Fasonnoe lit'e mednykh splavov." Mashgiz. 1957.
3. Zakharov, M.V. et al. Novye provodnikovye mednye splavy, printsipy ikh legirovaniya, svoistva i naznachenie (New Conducting Copper Alloys, the Principles of Their Alloying Properties and Application). — Izv. Vysshikh Uchebnykh Zavedenii, Tsvetnaya Metallurgiya, No. 6. 1965.
4. Saarivirta, M.—Metal Industry, No. 20, p. 103. 1963.
5. Zakharov, M.V. K voprosu ob osnovnykh tipakh diagramm sostav—zharoprochnost' metallicheskikh sistem (Basic Types of Composition—Heat-Resistance Diagrams). — In: "Issledovanie splavov tsvetnykh metallov," No. 1. Izdatel'stvo AN SSSR. 1955.
6. Kornilov, I.I. Fiziko-khimicheskaya teoriya zharoprochnosti (Physicochemical Theory of Heat Resistance). — Izdatel'stvo AN SSSR. 1961.
7. Smiryagin, A.P. Promyshlennye tsvetnye metally i splavy (Industrial Nonferrous Metals and Alloys). — Metallurgizdat. 1956.
8. Bochvar, A.A. Metallovedenie (Metallurgy). 1956.

9. Bochvar, A.A. O raznykh mekhanizmakh plastichnosti v metallicheskikh splavakh (Different Mechanisms of Ductility in Metal Alloys). — OTN, No. 5. 1948.
10. Kurdyumov, G.V. et al. O roli diffuzionnykh peremeshchenii splavov v zharoprochnosti (The Role of Diffusion Migration in Heat-Resistant Alloys). — In: "Issledovaniya po zharoprochnym splavam," Vol. 2. Izdatel'stvo AN SSSR. 1957.
11. Oding, I.A. and V.N. Geminov. Mekhanizm razuprochneniya metallov pri polzuchesti v usloviyakh povyshennykh temperatur (Mechanism of Softening Metals during Creep at Elevated Temperatures). — In "Issledovaniya po zharoprochnym splavam," Vol. 6. 1960.
12. Maksimov, S.K. Dlitel'naya prochnost' i polzuchest' krasnoi medi M1 (Long-Time Strength and Creep of Red Copper M1). — Metallovedenie i Termicheskaya Obrabotka Metallov, No. 6. 1955.
13. Zwiker, V. Metall, No. 5, p. 16. 1962.
14. Duisemaliev, U.K. and A.A. Presnyakov. Rastvorimost' tseriya v medi i fiziko-khimicheskie svoistva mednotserievykh splavov (Solubility of Cerium in Copper and the Physicochemical Properties of Copper-Cerium Alloys). — ZhNKh AN SSSR, Vol. 9, No. 9. 1964.
15. Savitskii, E.M. and U.K. Duisemaliev. Mednyi ugol diagrammy sostoyaniya sistemy med'—vanadii (Copper Corner of the Copper —Vanadium Phase Diagram). — Vestnik AN KazSSR, No. 5, p. 55. 1962.

IV. KINETICS AND MECHANISM OF OXIDATION, AND PROTECTIVE COATINGS

N. N. Kozlova and A. R. Krylova

PRINCIPLES OF LONG-TIME OXIDATION OF HEAT-RESISTANT STEELS AND ALLOYS

To increase the power of engines, the heat resistance of materials that have to withstand prolonged service must be carefully studied.

The oxidation rate of metals and alloys at elevated temperatures depends mainly on the protective properties of the scale /1/. The scale should satisfy the following conditions:

1) it must be continuous and have no through-cracks or pores;

2) it should adhere well to the surface of the metal;

3) the diffusion of metal ions and of oxygen through the scale should be hampered.

These conditions are sufficient for stationary service if there are no rapid variations in temperature or stress. In practice, the scale of heat-resistant materials must satisfy other requirements also. Thus, the scale must not be too brittle so that it will not fail under external loads, particularly during vibration; its coefficient of linear expansion should be as close as possible to that of the metal to avoid cracking during change in temperature.

Although the problem of heat resistance of steels and alloys has been widely studied, the tests carried out above 1000°C did not usually last longer than 100–1000 hr.

In 1944 Kornilov /2/ found that in chromium–aluminum steel specimens aluminum is preferentially oxidized from the surface layers. Thus the content of aluminum at the surface decreases, and this metal diffuses from the interior of the specimens.

The selective oxidation of some elements in alloys and the decrease in their content in the surface layers after prolonged heating is particularly important since as time passes the composition of the alloy being oxidized differs from that of the initial material. This considerably influences the oxidation process.

The purpose of this work was to investigate the long-time heat resistance (up to 10,000 hr) of heat-resistant industrial steels and alloys at 1050, 1150, and 1200°C, during continuous and cyclic tests. Other research workers /1/ studied short heating cycles, not longer than a few minutes each, but we investigated the influence of 200, 500, and 1000 hr long cycles on the heat resistance of steels.

We used industrial heats of ordinary heat-resistant steels and alloys (GOST 5632-61),* which are widely used in industry. The specimens were 10 mm in diameter and 20 mm thick, and their surface finish was ∇8.

The principle for following the kinetics of oxidation during prolonged heating (from 5000 to 10,000 hr) is the determination of weight gain. The

*Kh25N16G7AR, Kh23N18, 4Kh18N25S2, Kh25N20S2, KhN78T, KhN60Yu, KhN70Yu.

specimens were placed in wide crucibles, and oxidized in the air in electric furnaces. Three specimens were tested for each point on the graph.

The relationship between the average weight gain and time showed that the oxidation of the materials studied is governed by a parabolic law. However, as has already been shown /3/, this regularity holds up to a certain time only, and then the oxidation rate coefficient changes rapidly. This change is shown on the oxidation curve by an inflection. After this the oxidation rate is also represented by a parabolic curve, but the oxidation rate constant at this stage is appreciably greater than at the first stage. If the specimens are heated for a sufficiently long time, several such inflections can be recorded. This relationship can then be written as

$$\Delta q^2 = k_1\tau_1 + k_2\tau_2 + \ \dots\ + k_n\tau_n,$$

where Δq is the weight gain during time $\tau=\tau_1+\tau_2+\dots+\tau_n$; $k_1, k_2, \dots, k_n$ are the oxidation rate constants for the corresponding stages; $\tau_1, \tau_2, \dots, \tau_n$ are the duration times of the oxidation stages at a constant value of k.

Figure 1 shows the curves representing the dependence of the square of the weight gain on the oxidation time at 1050°C for 1000-hr and 200-hr long cycles. The tests were carried out on four materials (Figures 1,a and b). The KhN78T alloy was tested at 1150 and 1200°C for 200 hr-cycles and continuous tests (Figure 1,c). The calculation of the oxidation rate constants for the straight line sections is shown in Tables 1 and 2.

The influence of the frequency at which the specimens were cooled between the heatings on the heat resistance at a constant temperature is clear. Firstly, if the cooling takes place more frequently, the total oxidation rate is higher, i.e., the weight gain of scale increases. Secondly, with increase in the frequency of cooling the duration of the first stage, during which the oxidation rate is slowest, decreases and the value of k at this stage increases. Thirdly, it has been found that if the heating cycles for Kh23N18 steel are shortened from 1000 to 200 hr, the oxidation changes from a parabolic to a linear function. It can be assumed that if the frequency of cooling is increased, the oxidation will become a linear function for other materials also.

The oxidation rate during cyclic tests on KhN78T steel is most influenced by an increase in temperature over the range 1050—1200°C. It is interesting to point out that the weight gain after 10,000 hr of testing at 1050°C and a 1000 hr-cycle is higher than the weight gain after 10,000 hr of continuous testing at 1150°C. It is also characteristic that the oxidation curve representing cyclic tests has two inflections, and the curve representing continuous heating has only one inflection. The oxidation rate constant for 10,000 hr of testing with cyclic tests is twice that with continuous tests ($37.5 \cdot 10^{-8}$ and $20.3 \cdot 10^{-8}$ respectively).

Above 1050°C we tested not only KhN78T alloy but also the following steels: Kh25N20S2 (1150°C), and the alloys KhN70Yu and KhN60Yu (1150°C and 1200°C).

The results of the tests are shown in Table 3. The tests on steel were stopped at 1150°C because of the low heat resistance: the continuous tests were stopped after 4000 hr (weight gain 583.5 g/m^2 and weight loss 1568 g/m^2), and the cyclic tests were stopped after 2000 hr (weight gain 1588 g/m^2 and weight loss 3878 g/m^2).

TABLE 1. Oxidation rate constants k of Kh25N16G7AR, Kh23N18 and 4Kh18N25S2 steels at 1050°C, and of Kh25N20S2 steel at 1150°C

Duration of heating cycle, hr	Section of oxidation curve	Kh25N16G7AR — 1050°C			Kh23N18 — 1050°C			4Kh18N25S2 — 1050°C			Kh25N20S2 — 1150°C		
		total oxidation time, hr	duration of single stage, hr	$k \times 10^7$, $g^2/cm^4 \cdot hr$	total oxidation time, hr	duration of single stage, hr	$k \times 10^7$, $g^2/cm^4 \cdot hr$	total oxidation time, hr	duration of single stage, hr	$k \times 10^7$, $g^2/cm^4 \cdot hr$	total oxidation time, hr	duration of single stage, hr	$k \times 10^7$, $g^2/cm^4 \cdot hr$
200	I	700	700	2.5	—	—	—	1100	1100	0.9	800	800	8.2
200	II	1200	500	11.4	—	—	—	1500	400	4.9	1580	780	134
200	III	2300	1100	18.4	—	—	—	2500	1000	24.0	1900	320	422
200	IV	3000	700	30.0	—	—	—	3800	1300	63.6	—	—	—
200	V	3700	700	53.6	—	—	—	4300	500	95.4	—	—	—
500	I	1000	1000	2.3	500	500	0.5	—	—	—	—	—	—
500	II	2000	1000	7.3	1600	1100	4.1	—	—	—	—	—	—
500	III	3500	1500	16.2	3500	1900	31.0	—	—	—	—	—	—
500	IV	5000	1500	22.6	5000	1500	52.6	—	—	—	—	—	—
500	V	7000	2000	29.0	6000	1000	157.6	—	—	—	—	—	—
500	VI	8500	1500	53.1	—	—	—	—	—	—	—	—	—
1000	I	1500	1500	1.5	2000	2000	1.2	2000	2000	4.3	1000	1000	5.6
1000	II	3700	2200	4.7	4000	2000	16.2	3600	1600	26.7	3800	2800	14.8
1000	III	7000	3300	12.4	—	—	—	5000	1400	54.5	—	—	—

TABLE 2. Oxidation rate constants k of the Kh78T alloy at 1050, 1150, and 1200°C, for individual stages of the process

Duration of single cycle, hr	Section of oxidation curve	1050°C			1150°C			1200°C		
		total oxidation time, hr	duration of single stage, hr	$k \times 10^8$ $g^2/cm^4 \cdot hr$	total oxidation time, hr	duration of single stage, hr	$k \times 10^8$ $g^2/cm^4 \cdot hr$	total oxidation time, hr	duration of single stage, hr	$k \times 10^8$ $g^2/cm^4 \cdot hr$
200	I	900	900	2.4	800	800	22.0	1000	1000	37.0
200	II	2100	1200	7.3	2500	1700	132.2	1650	650	205.0
200	III	2850	750	13.3	6000	3500	558	2000	350	1540
200	IV	4100	1250	35.6	—	—	—	—	—	—
500	I	1200	1200	2.1	—	—	—	—	—	—
500	II	3300	2100	7.0	—	—	—	—	—	—
500	III	7000	3700	17.8	—	—	—	—	—	—
1000	I	1700	1700	1.2	—	—	—	—	—	—
1000	II	5000	3300	7.6	—	—	—	—	—	—
1000	III	7600	2600	14.5	—	—	—	—	—	—
1000	IV	10000	2400	37.5	—	—	—	—	—	—
Continuous oxidation	I	—	—	—	3800	3800	3.8	2000	2000	5.5
	II	—	—	—	10000	6200	20.3	—	—	—

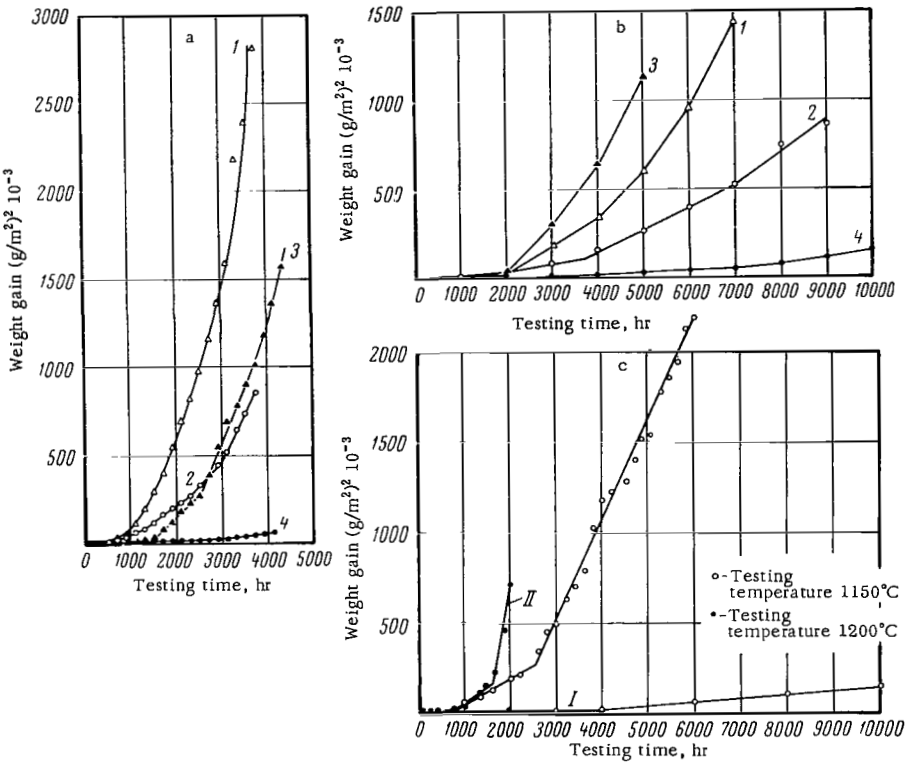

FIGURE 1. Curves of $\Delta q^2 = f(\tau)$:

a — testing temperature 1050°C, duration of cycle 1000 hr; b — the same, 200 hr; c — 1150 and 1200°C, KhN78T alloy; 1 — K23N18 (EI417); 2 — Kh25N16G7AR (EI835); 3 — 4Kh18N25S2 (EYa3S); 4 — KhN78T (EI435): I — continuous heating; II — periodic cooling of specimens after 200 hr of heating.

The KhN70Yu and KhN60Yu alloys have a very high heat resistance at 1150°C for 10,000 hr and at 1200°C for 3000 hr. The weight gain of these alloys for the maximum testing time does not exceed 70 g/m^2. Intermediate coolings to room temperature after every 200 hr of heating had almost no influence on the oxidation rate of these alloys.

X-ray and chemical analyses on the spalled scale showed that prolonged heating leads to a change in phase composition and in chemical composition of the scale. As the duration of heating increases, the content of chromium in the scale decreases and that of nickel increases, and therefore the protective properties of the scale decrease with time.

A study of the microstructure of specimens after heating showed that the metal directly under the scale changes appreciably during prolonged oxidation processes. To study the processes in the surface layers of metals during prolonged oxidation, we analyzed successive layers of metal specimens by X-ray spectral methods with a microprobe of the "Kameka" type.*

* The analysis was carried out in TsNIIChM.

TABLE 3. Heat resistance determined by the weight gain method (continuous heating)

Testing time, hr	Kh70Yu		KhN60Yu		Kh25N20S2	
	g/m^2	$g/m^2 \cdot hr$	g/m^2	$g/m^2 \cdot hr$	g/m^2	$g/m^2 \cdot hr$
	Testing temperature, 1150°C					
100	4.1	0.040	8.7	0.090	50.5	0.50
1000	28.3	0.028	37.5	0.038	236.0	0.24
2000	30.8	0.015	36.4	0.020	575.8	0.29
4000	38.3	0.010	44.3	0.011	583.5	0.15
6000	48.2	0.008	68.2	0.011		
8000	64.1	0.008	60.3	0.008		
10000	66.1	0.007	68.4	0.007		
	Testing temperature, 1200°C					
100	20.1	0.210	25.1	0.260		
780	31.0	0.040	23.5	0.033		
2000	56.8	0.028	48.9	0.024		
3000	60.3	0.020	62.7	0.021		

At 1050°C the chromium and iron contents of the layers directly beneath the scale decrease regularly in all materials. The Kh25N16G7AR steel loses manganese also from these layers. It should be pointed out that in this steel the oxidation of chromium is appreciably slower than in the Kh23N18 steel and in the KhN78T alloy.

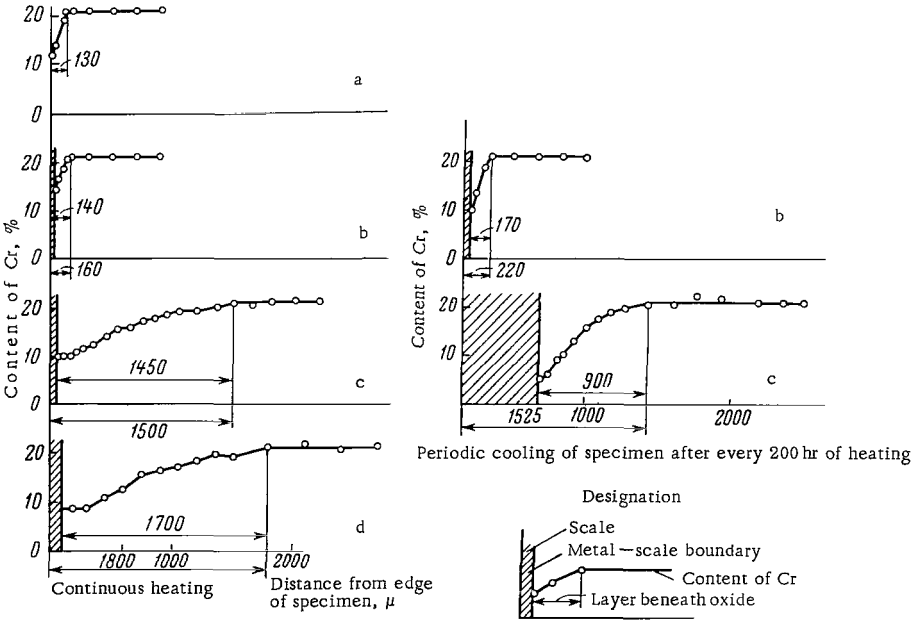

FIGURE 2. Chemical composition of the layers of the KhN78T alloy beneath the scale, testing temperature = 1150°C:

a — testing time, 100 hr; b — 1000 hr; c — 6000 hr; d — 8000 hr.

The thickness of the layers that undergo such changes is considerably smaller in steel than in the alloys. One of the reasons for this is that the heat resistance of steels is lower since the external layers are more oxidized. If, however, we compare the contents of oxidized elements in the depleted layer together with the oxidized layer, the values in Kh25N16G7AR steel are lower than those in the alloy, which means that under identical service conditions parts made of Kh25N16G7AR steel will be less deeply attacked than those made of the KhN78T alloy, despite the fact that the latter has a higher heat resistance.

At 1150°C oxidation of Kh25N20S2 steel leads to a considerable decrease in the contents of chromium and silicon in the layers beneath the scale. Silicon becomes oxidized more than chromium; this result agrees well with the data of /4/.

The results of studying the layers of KhN78T alloys beneath the scale are given in Figure 2.

The content of chromium in the layers of KhN78T alloys beneath the scale decreases. As we have already mentioned, periodic cooling leads to a considerable increase in the thickness of the scale. Figure 2 shows that the total depth of the oxidized metal is not greatly influenced by intermediate coolings.

A study of the chemical composition of the layers of KhN70Yu and KhN60Yu alloys beneath the scale gave no definite results. It is clear that changes in the content of readily oxidizable elements and the depth of the attacked metal are small, and therefore they could not be determined by X-ray spectral microanalysis. In these alloys, changes in the microstructure and in the microhardness of the layers beneath the scale are apparently caused by the oxidation of carbon and by the decomposition of chromium carbides, and also by the formation of vacancies and of micropores due to vacancy diffusion.

CONCLUSIONS

The selective oxidation of elements as a result of prolonged heating leads to a change in the composition of the surface layers of alloys which determines the change in the composition and in the protective properties of the scale formed. Prolonged oxidation of chromium—nickel steels and of the KhN78T alloy leads to a decrease in the content of chromium, chromium and manganese, or chromium and silicon, in the layers beneath the scale. The resulting decrease in the heat resistance is shown by an inflection on the $\Delta q^2 = f(\tau)$ curve. Cyclic tests intensify the oxidation process, but the total amount of metal attacked changes very little.

For long-time service at 1050°C we recommend the Kh25N16G7AR steel and the KhN78T alloy, and at 1150°C and 1200°C the KhN70Yu and KhN60Yu alloys. If these materials are used under the above conditions, the formation of scale and of underscale layers must be taken into account.

Bibliography

1. Kubashevskii, O. and B. Gopkins. Okislenie metallov i splavov (Oxidation of Metals and Alloys). Moskva. 1965.
2. Kornilov, I.I. Doklady AN SSSR, Vol. 42, No. 4. 1944.
3. Krylova, A.R., N.N. Kozlova, and D.N. Zharkova. Spetsial'nye stali i splavy (Special Steels and Alloys). — Sbornik trudov.
4. Kornilov, I.I. and A.I. Shpikel'man. Doklady AN SSSR, Vol. 54, No. 6. 1946.

P. T. Kolomytsev, R. I. Andreeva, L. A. Kostina, and S. A. Strekopytov

BEHAVIOR OF DIFFUSION COATINGS ON NICKEL ALLOYS AT ELEVATED TEMPERATURES

Heat-resistant nickel-base alloys are commonly protected against corrosion in gases by diffusion coatings, especially by calorizing. Therefore data on the protective ability of aluminum coatings are of great interest.

The authors of /1/ studied the behavior of calorized coatings on nickel and nickel—chromium alloys, and showed that the structure of the surface layers changes appreciably at elevated temperatures.

The NiAl compound appears to be unstable on nickel parts and dissociates fairly rapidly. The NiAl compound is replaced by Ni_3Al, which has a lower resistance to corrosion in gases than NiAl.

Therefore, it was very interesting to determine the transformations in the surface diffusion layers containing not only aluminum but also elements which might increase the protective properties of the surface layers by alloying.

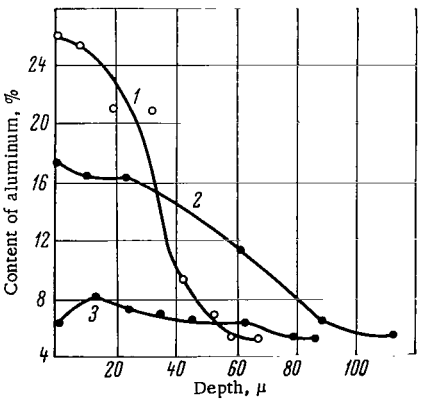

FIGURE 1. Concentration of aluminum in the surface layers of calorized ZhS alloy specimens after tests for heat resistance at 1100°C:

1 — initial; 2 — 5 hr; 3 — 100 hr.

Chromium can apparently be very useful in this respect since it increases the stability of Ni_3Al.

Arbuzov and Zelenkov /2/ studied the influence of third elements on the structure and on the recrystallization of Ni_3Al, and found that the addition of 10% Cr increases the recrystallization temperature of Ni_3Al from 878°C for Ni_3Al to 1113°C for Ni_3(Al, 10% Cr).

For our studies we used calorized and chromized-calorized specimens of the ZhS alloy, which is one of the most widely used modern heat-resistant materials.

The calorizing was carried out at 950°C for 4 hr in a mixture containing 98% of ferroaluminum and 2% of ammonium chloride. The chromizing-calorizing process was carried out in vacuo.

The thickness of the diffusion layer on calorized specimens and on chromized-calorized specimens measured by a metallographic microscope was 35—40μ. The concentrations of chromium and aluminum in the surface layers were determined by spectral analysis of successive layers, and the structure was studied by metallographic methods and X-ray analysis.

After ZhS-type alloys (and other nickel—chromium heat-resistant alloys) have been calorized, the surface layer consists of two zones: an external zone and an internal one. The basic structural component of both zones is the NiAl nickel aluminide. However, in the internal zone, which is about 15 to 25% of the whole layer, we found a considerable amount of a component consisting of a solution on the basis of metals with a body-centered cubic lattice.

The exchange reactions during the calorizing of heat-resistant alloys are apparently of little importance. The surface layer is formed as a result of the diffusion of aluminum, leading mainly to the formation of the internal zone of the layer, and of the diffusion of nickel, which with aluminum forms the NiAl intermetallic compound, in the opposite direction.

The maximum concentration of aluminum in the surface layer is fairly high (about 30% in the calorized specimens studied).

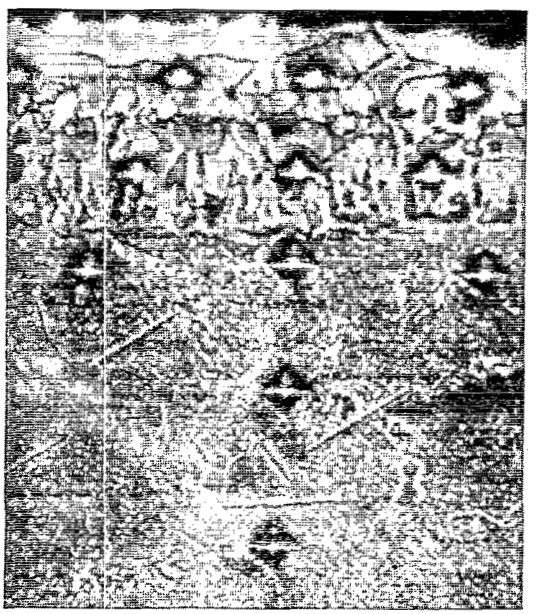

FIGURE 2. Microstructure of the surface layer of a chromized-calorized ZhS alloy specimen after tests for heat resistance at 1100°C for 100 hr.

If calorized specimens are heated at elevated temperatures, the concentration of aluminum in the surface layer decreases, as can be seen in Figure 1, and after 100 hr of heating at 1100°C the maximum concentration of aluminum is 8%.

After 5 hr of heating at 1100°C the content of aluminum in the surface layer is insufficient for the existence of an NiAl phase, and the layer consists chiefly of Ni_3Al.

These structural transformations in the surface layer are accompanied by an increase in its thickness (it is sometimes more than doubled) and by a certain change in its volume.

The surface layer of chromized-calorized specimens contains an NiAl phase also. However, the internal zone of the surface layer of chromized-calorized specimens includes up to 30—40% of the thickness of the whole layer. The internal zone of the surface layer of chromized-calorized specimens contains a large amount of a component consisting of a chromium-base solid solution.

At 1100°C the concentration of aluminum in the surface layer decreases most during the first hours of heating (for example it falls from 21 to 13% of aluminum during the first 5 hr). However, during the following 95 hr the decrease in the content of aluminum in the surface layer is retarded, apparently because of the stabilizing influence of chromium dissolved in the Ni_3Al intermetallic compound.

After prolonged heating, the surface layer of chromized-calorized chromium-containing specimens consists of a phase on the basis of Ni_3Al and of coarse particles of a chromium-base solid solution which dissociates rather slowly at 1100°C.

The photomicrographs of a surface layer of a chromized-calorized specimen (Figure 2) clearly shows the presence of inclusions of the chromium-base solid solution in the internal zone, and this imparts a high microhardness to the specimen.

The results of the determination of the chromium content in the surface layer (Figure 3) agree with this type of structure. Figure 3 also shows that heating at 1100°C for 100 hr decreases the maximum concentration of chromium in the surface layer by not much more than 2%. Consequently, the rate of decrease in the chromium content in the surface layer at 1100°C is appreciably lower than the rate of change in the aluminum content. The same relationship between the rate of decrease in the content of chromium and aluminum at elevated temperatures has also been found in other nickel—chromium heat-resistant alloys coated by diffusion layers.

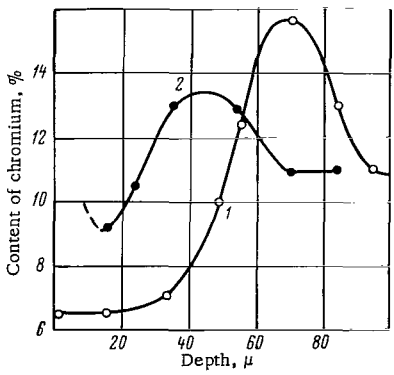

FIGURE 3. Concentration of chromium in the surface layers of chromized-calorized ZhS specimens after testing for heat resistance at 1100°C:

1 — initial alloys; 2 — after 100 hr of testing.

It is very interesting to determine the possible mechanism by which the content of aluminum in the surface layer is decreased.

It is only natural to assume that the decrease in the content of aluminum in the surface layer is due to oxidation and the formation of scale only. However, the volume of scale formed is relatively small, and studies on the heat resistance of calorized specimens and chromized-calorized specimens show that although the former loses much more metal from the surface

layer, the weight increase of the latter is 2—3 times that of calorized specimens, particularly during the initial period of testing.

These experimental data indicate that we must apparently assume that appreciable evaporation of some components of the alloys or of their oxides is possible at elevated temperatures.

If oxides evaporate the loss of chromium from the surface layer will be greater, since evaporation of Cr_2O_3 or $NiCrO_4$ is much more rapid than evaporation of Al_2O_3 or $NiAlO_4$ /3/.

Since no such loss has been observed, we can assume that it is aluminum that evaporates chiefly from the surface layer. This assumption appears to be natural if we consider the evaporation rates of the corresponding components. It has been found /3/ that the evaporation of Cr_2O_3 during 100 hr of heating at 1100°C is 2 mg/cm^2, which means that its evaporation rate is $2 \cdot 10^{-5}$ g/cm$^2 \cdot$ hr.

If we express the evaporation rate of chromium and of aluminum in the same units, using the data of V. E. Ivanov we find that the evaporation rate of chromium at 1100°C is $1.9 \cdot 10^{-3}$ g/cm$^2 \cdot$ hr, and of aluminum $6.48 \cdot 10^{-2}$ g/cm$^2 \cdot$ hr.

Although the evaporation rates of these elements from alloys differ from their evaporation rates from pure metals, nevertheless the above data show that the evaporation rate of aluminum is more than 30 times that of chromium, and this can to a certain extent explain the rapid decrease in the content of aluminum in the surface layers of calorized specimens and chromized-calorized specimens.

The evaporation of aluminum is possible since the oxide film formed on the surface of the metal is porous, and fails if the volume of the surface layer is changed.

CONCLUSIONS

1. Heating at 1100°C leads to an appreciable reduction in the content of aluminum, and to a much smaller reduction in the content of chromium, in the surface layer of calorized and chromized-calorized specimens.

2. It has been assumed that the high loss of aluminum is due to its evaporation.

Bibliography

1. Bruchle, H. and J. Moisan. Recherches sur la diffusion de l'aluminium et beryllium. — "Recherche Aéronautique," No. 64, pp. 27—33. 1958.
2. Arbuzov, M. P. and I. A. Zelenkov. Vliyanie tret'ego elementa na strukturu i protsessy rekristallizatsii (Influence of a Third Element on the Structure and on the Processes of Recrystallization). — In: "Issledovanie po zharoprochnym splavam." Izdatel'stvo AN SSSR. 1963.
3. Hauffe, K. and K. Pschera.—Z. anorg. Chem., Vol. 262, Nos. 1—5. 1950.

O. S. Ivanov, I. I. Raevskii, and M. S. Skryabina

COMPARATIVE STUDY ON THE OXIDIZABILITY AND HEAT RESISTANCE OF NIOBIUM-BASE ALLOYS

Niobium is a metal with very remarkable physical and mechanical properties: its high melting point (2415°C) makes it a suitable base for heat-resistant alloys, its relatively low density (8.4 g/cm^3) makes it very valuable in the aircraft industry and other fields, and due to its high ductility niobium is more readily shaped than tantalum, molybdenum, or tungsten. These features of niobium have promoted the development of niobium alloys during the last ten years /1—6/.

A number of studies to determine the structure and the properties of niobium alloys have been carried out in the A. A. Baikov Institute of Metallurgy, AN SSSR. Among the subjects studied were the influence of 2—10 at.% of Ti, V, Cr, and Mo on the kinetics of oxidation and on the absorption of gases by the surface layers of niobium alloys containing 10 and 30 at.% of zirconium at 500 and 1000°C in the air /6/. Investigations were also carried out on the microstructure, forgeability at 1100°C, hardness at 1000°C, recrystallization temperature, cold working, and the heat resistance of alloys of the niobium corner of the Nb—W—V system containing up to 40 wt% of tungsten and vanadium, and obtained by arc and electron-arc melting. The oxidizability in the air and the penetration of gases in niobium alloys containing 0.4—3 wt% of Cr + Ti have also been studied. Tests were carried out to find the microstructure of these alloys, forgeability at 1100°C, recrystallization, cold working, hardness at 400—1000°C, and the corrosion resistance in water and in carbon dioxide at elevated temperatures and under high pressures of binary alloys Nb—Ta (up to 35 wt% Ta), Nb—Mo (up to 20 wt% Mo), and of ternary niobium-base alloys Nb—Ta—W (up to 35 wt% of Ta + W) and Nb—Mo—W (up to 20 wt% Mo + W) melted under argon in an arc furnace. We also studied the microstructure of alloys of the niobium corner of the ternary Nb—Ti—Zr (up to 30 wt% Ti + Zr) system melted under argon in an arc furnace, their forgeability at 1000°C, workability during cold rolling, recrystallization, tensile strength at 800°C, and their oxidizability in the air at 800°C and corrosion in water at elevated temperatures and at high pressures. In the same way, alloys were studied and isothermal sections of the niobium corner of the ternary Nb—Zr—Cr (up to 30 wt% Zr + Cr) system were constructed. Ternary Nb—V—Zr alloys, including alloys containing Mo, Ti, Cr, and W, and also Nb—Cr—Mo alloys containing Be, Ce, V, and Ti, were tested for oxidizability in the air at 500—1000°C, in water, and in carbon dioxide at elevated temperatures and under high pressures.

As a result of these studies we found the optimum properties of alloys.

Due to the large number of alloys that have been proposed for industrial use, it was necessary to carry out comparative tests to find their workability, heat resistance, and high-temperature strength. The results of the first stage of these comparative tests are given below.

The compositions of the alloys studied are given in Table 1. Alloys Nos. 1—12 were taken from the above papers. Some alloys are known from foreign literature or are variants of alloys which we developed.*

* Some variants of alloys (Nos. 15—18, 21, 22, 28) were suggested by L. I. Gomozov. Alloy No. 31 was developed in VIAM.

TABLE 1. Compositions of alloys studied

No. of alloy	Composition, wt %	Source
1	Nb + 4Ti + 1Zr	Experimental specimens
2	Nb + 8Ti + 2Zr	
3	Nb + 16Ti + 4Zr	
4	Nb + 3.3Mo + 1.7W	
5	Nb + 1.7Mo + 3.3W	
6	Nb + 7.5W + 2.5Ta	
7	Nb + 5Mo	
8	Nb + 5V	
9	Nb + 3.3Mo + 3.1Al	
10	Nb + 3.1Mo + 4.9Zr	
11	Nb + 3.2Mo + 1.5Al	
12	Nb + 10Ti + 3V + 3.75Mo + 1.25Cr	
13	Nb + 7Ti + 20W + 3Mo + 1Zr	(8)
14	Nb + 7Ti + 20W + 3Mo + 1Zr + 1Mn	
15	Nb + 40Ti + 5Mo + 8Cr + 5Al + 1Mn	
16	Nb + 40Ti + 10W + 8Cr + 5Al + 1Mn	Experimental specimens
17	Nb + 49Ti + 5Mo + 10Cr + 5Al + 1Mn	
18	Nb + 44Ti + 10W + 10Cr + 5Al + 1Mn	
19	Nb + 20Ti + 10Mo + 1Zr	
20	*FS*-85(9), 26—*F*-50(10), 27—*F*-48(4)	
21	Nb + 45Ti + 14W + 4.3Al + 4Cr + 0.7Mn	
22	Nb + 44.7Ti + 14W + 4.3Al + 4.0Cr + 0.7Mn + 0.3C	Experimental specimens
23	Nb + 40Ti + 5Mo + 8Cr + 1Mn	
24	Nb + 40Ti + 5Mo + 5Al + 1Mn	
25	Nb + 40Ti + 5Mo + 1Mn	
28	Nb + 41Ti + 3Cr + 3V + 5Al + 4W + 1Mn	
29	Nb + 4Mo	
30	*Cb*-74(9), 32—*D*-43(11)	
31	BH-2	

PREPARATION OF ALLOYS AND METHODS OF INVESTIGATION

Preparation of alloys. The alloys were melted in an arc furnace with a nonconsumable tungsten electrode in an atmosphere of argon. The weight of each ingot was 100 g. To mix the components better, all the alloys were initially cast into 25 g ingots. After 4—5 consecutive meltings these ingots were melted together by adding one at a time into the crucible. The alloys containing Cr, Al, V and Mn, were melted in an arc furnace under increased pressure of argon (400—500 mm of Hg); evaporation during melting was thus reduced. The composition of the alloys was determined by selective chemical analysis. Cast alloys with a high content of titanium (45%) and of tungsten (14—20%) showed strong liquation, but after the alloys had been homogenized the liquation disappeared. This was shown by microstructural analysis. The alloys were homogenized for 3—5 hr in a TVV-4 furnace at 1500°C in a vacuum of 10^{-4} mm Hg. The alloys were not subjected to plastic deformation.

Method of evaluating the heat resistance of alloys. For these tests we used cylindrical specimens 5—6 mm in diameter and about 10 mm high. The surface of the specimens was electrolytically etched. The resistance of the alloys to oxidation in the air was found by weighing periodically and

calculating the weight gain per unit surface area. The alloys were oxidized in celite [lined] furnaces in Al_2O_3 crucibles heated to a constant weight. The temperature of the furnace was controlled by a platinum—platinum-rhodium thermocouple, and was constant with an accuracy of ±10°C.

Evaluation of the heat resistance of alloys. The heat resistance of alloys was found by measuring their hardness at 800, 900, 1000, 1100, 1200, 1300, and 1400°C. The hardness was measured by a tester designed by IMET in a vacuum of 10^{-4} mm Hg. The specimens for these measurements were shaped as cylinders about 14 mm in diameter and 4—5 mm high. The surface of the specimen on which measurements were carried out was polished. The indentor was made of a saphire crystal in the form of a four-plane pyramid, with an angle at the apex of 136°. The indentor was loaded with a 2.5 kg weight. The diagonals of the indentations were measured under a microscope after the specimen was cool, and the hardness was calculated from these data. The temperature of the specimen was measured by a W-(Mo + Al) thermocouple connected to a PP-type potentiometer. The hot end of the thermocouple was placed into an opening in the lower end of the specimen.

RESULTS AND DISCUSSION

All data on the oxidation of alloys and on their hardness at elevated temperatures are the average data of 2—3 measurements carried out on different specimens prepared from an ingot of the same melt.

Resistance of alloys to oxidation at 800, 900, 1000, and 1200°C. The resistance of alloys to oxidation at 800°C is shown in Figure 1,a. At this temperature the best alloys (21 and 22) have the following composition: Nb + 45Ti + 14W + 4.3Al + 4Cr + 0.7Mn, Nb + 44.7Ti + 14W + 4.3Al + 4Cr + 0.7Mn + + 0.3C. These alloys have a high titanium content besides W, Al, and Cr, and differ from one another in the carbon content (0.3% C in alloy No. 22). The weight gains of these alloys after 100 hr of testing were 7.5 and 22 mg/cm^2, respectively. The somewhat poorer resistance of alloy No. 22 is due to the presence of carbon. Alloy No. 28 (Nb + 41Ti + 3Cr + 3V + 5Al + 4W + 1Mn) and the binary alloy No. 8 containing 5% V are also very resistant, but the latter has a poor resistance to oxidation at elevated temperatures. Alloys No. 15 and 19 with 40 and 20% of Ti and Mo, Zr, Al, Cr, and Mn also have a good resistance to oxidation, and their weight gains after 100 hr of testing were 84 and 50 mg/cm^2, respectively. Alloy No. 6 containing 7.5W and 2.5Ta has a low resistance to oxidation at 800°C. Its weight gain after 20 hr of testing was 289 mg/cm^2. The well-known industrial high-strength alloys FS-85 (alloy 20), F-50 (alloy 26) and F-48 (alloy 27) have a very low resistance to oxidation. The FS-85 alloy oxidizes more rapidly than unalloyed niobium.

The multicomponent alloys (Nos. 16, 18, 21, 22, and 28) containing 40—45% Ti, 4—14% W, and 3—10% Cr, 4—5% Al, 0.7—1% Mn, and 3% V have the highest resistance to oxidation at 900°C. None of these alloys contains molybdenum. For example, by comparing the oxidizability of alloys 15 and 16 it can be seen that if 10 wt % W is substituted by 5 wt % Mo (about identical contents of tungsten and molybdenum calculated in at.%) there is a decrease in the heat resistance of the alloy. Alloys 16 and 18 contain not only chromium, aluminum and manganese, but also 10% of tungsten, and after 150 hr

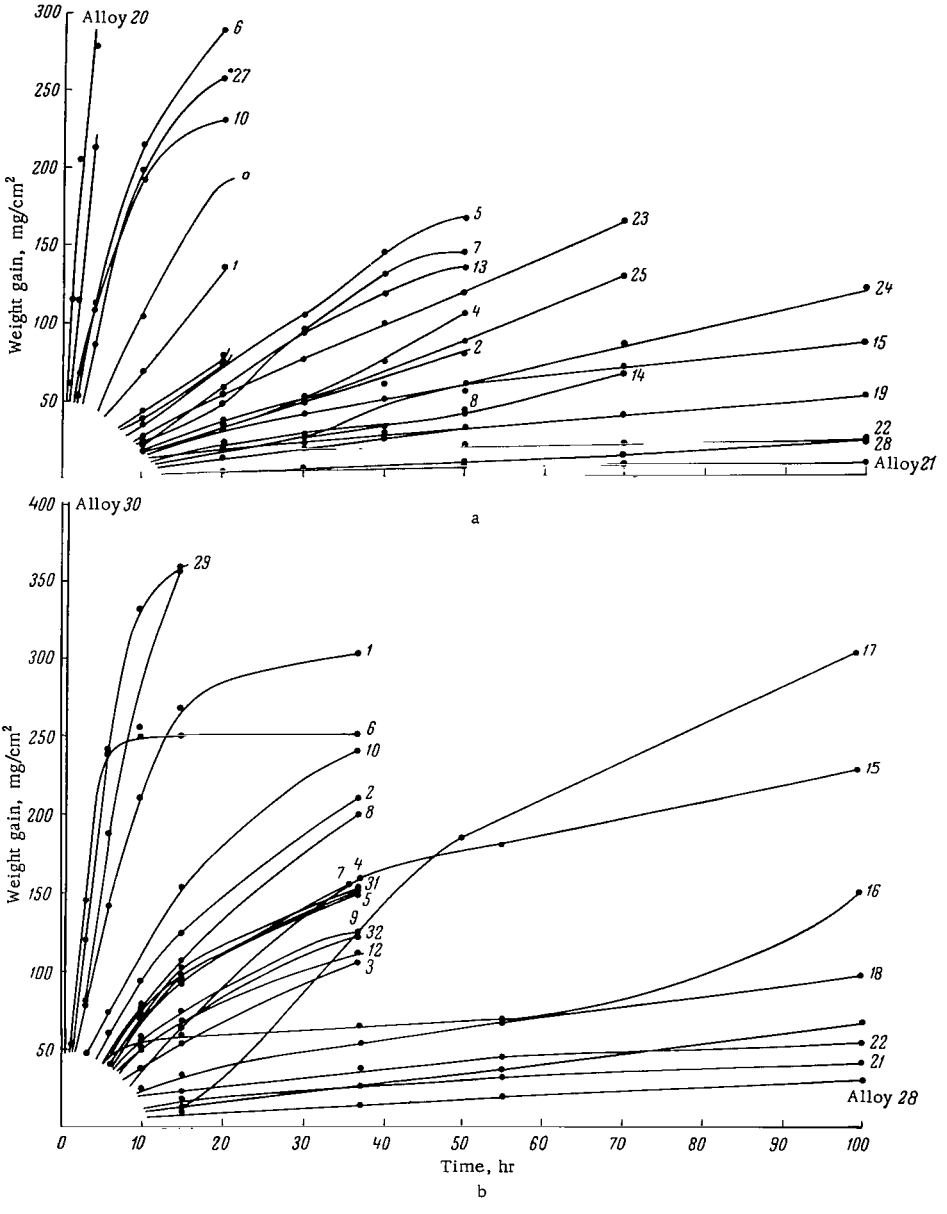

FIGURE 1. Resistance of alloys to oxidation:

a — at 800°C; b — at 1000°C.

of testing their weight gains were 15 and 21 mg/cm^2, respectively. Alloys 21 and 22 have the highest contents of titanium and tungsten; they showed the highest resistance to oxidation at 800°C, and remained the best at 900°C. The most heat-resistant alloy is alloy No. 21 (Nb + 45Ti + 14W + 4.3Al + 4Cr +

+0.7Mn). Its weight gain after 150 hr of heating was 11 mg/cm^2. An alloy of similar composition (No. 17) with molybdenum in place of tungsten has considerably lower heat resistance.

Data on the oxidizability of alloys at 1000°C are given in Figure 1,b. Alloys No. 28 (Nb + 41Ti + 3Cr + 3V + 5Al + 4W + 1Mn) and No. 21 (Nb + 45Ti + 14W + + 4.3Al + 4Cr + 0.7Mn) have the highest resistance at this temperature. The weight gains of these alloys after 100 hr of testing were 26 and 37 mg/cm^2, respectively. It is interesting to point out that the multicomponent alloys containing 40% of Ti or more can be placed in the following series according to descending heat resistance at 1000°C: alloy No. 28 (41Ti—4W), alloy No. 21 (45Ti—14 W), alloy No. 18 (44Ti—10W), alloy No. 16 (40Ti—10W), alloy No. 15 (40Ti—5Mo) and alloy No. 17 (49Ti—5Mo). The substitution of tungsten by molybdenum once again reduces the resistance of the alloys to oxidation. Of the alloys containing more than 70% Nb, the most heat-resistant is alloy No. 3 (Nb + 16Ti + 4Zr). The Cb-47 alloy (alloy No. 30), which at 1000°C has a lower heat resistance than unalloyed niobium and the Nb + 7.5W + 2.5Ta alloy, is the least resistant to oxidation at this temperature.

At 1200°C almost all alloys have a low resistance to oxidation and fail after 10—20 hr of testing. An exception are alloys No. 15 (Nb + 40Ti + 5Mo + + 8Cr + 5Al + 1Mn) and No. 17 (Nb + 49Ti + 5Mo + 10Cr + 5Al + 1Mn). After 150 hr of testing the weight gains were 91 and 149 mg/cm^2, respectively. Alloys Nos. 21 and 22 with 45% Ti and 14% W, with additions of aluminum, chromium, and manganese, were the most heat resistant at 800—1000°C, but failed during the first hours of testing at 1200°C. Of the alloys with more than 70% Nb, the alloy Nb + 10Ti + 3V + 3.75Mo + 1.25Cr has the highest resistance at 1200°C.

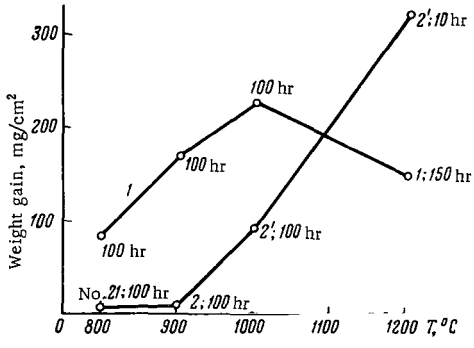

FIGURE 2. Influence of additions of molybdenum (1) and of tungsten (2) on the resistance of alloys to oxidation at 800—1200°C:

1— alloy No. 15 (Nb+ 40Ti+ 8Cr+ 5Al+ 1Mn+ 5Mo);
2— alloy No. 21 (Nb+ 45Ti+ 4Cr+ 4.3Al+ 0.7Mn+14W);
2'— alloy No. 18 (Nb+ 44Ti+ 10Cr+ 5Al+ 1Mn+ 10W).

Alloys with the highest heat resistance in air at 800—1200°C had a weight gain of up to 100 mg/cm^2. These alloys can be divided into two subgroups, one contains tungsten and the other molybdenum. These multicomponent alloys with a high content of titanium and some tungsten are much more

resistant to oxidation at 800—1000°C than alloys of similar composition containing molybdenum. At 1200°C, the opposite is true and alloys containing molybdenum are more resistant.

Our data on resistance to oxidation at 800—1000°C contradict the data of Sims and Klopp /7/, who found that tungsten has a detrimental influence on the resistance of niobium to oxidation at 1000°C. We also found that the oxidizability of alloys containing tungsten is greatly increased (by almost one order of magnitude) if the temperature is increased from 900 to 1000°C (Figure 2). The beneficial influence of molybdenum on the heat resistance of niobium alloys at elevated temperatures was confirmed by Ardzhent and Felps /12/ who believe that this is due to the sintering of the Mo (MoO_3) oxide.

The addition of 8—10% Cr is less effective than the addition of 3—5% Al. This agrees well with the data of Sims and Klopp /7/, who explained that the reason for the low effectiveness of the addition of chromium to niobium in amounts of less than 20% is that chromium has about the same affinity for oxygen as niobium. We found that the heat resistance of niobium alloys is increased most by adding chromium and aluminum in amounts of 10—12%.

If the heat resistance at 800°C of alloy No. 14 (Nb—7Ti—20W—3Mo—1Zr—1Mn) is compared to that of alloy No. 13, which differs from the former in the presence of 1% manganese, it is seen that this addition more than doubles the heat resistance.

Heat resistance and hot hardness of alloys. An analysis of the dependence of the hardness of alloys on temperature over the range 800—1400°C shows that all alloys with a high titanium content have a low hardness at elevated temperatures. The hardness of 50 kg/mm^2 at 800°C drops to 1—2 kg/mm^2 at 1300—1400°C. Alloys with more than 70% of niobium and additions of tungsten, molybdenum, tantalum, and chromium, have a better hot hardness. The hardest alloys are F-48 (Nb—15W—5Mo—1Zr—0.1C), F-50 (Nb—15W—5Mo—5Ti—1Zr—0.1C), and No. 14 (Nb—7Ti—20W—3Mo—1Zr—1Mn). At 1400°C the hot hardness of these alloys is 40—50 kg/mm^2. The addition of 1% Mn to the Nb—7Ti—20W—3Mo—1Zr alloy makes it a little harder at temperatures up to 1200—1300°C. However, the increase is insignificant at 1400°C.

The heat resistance and the hot hardness of most of the alloys that we studied are shown in the diagram in Figure 3. The most favorable combination of heat resistance and hot hardness at 1200—1400°C was found in the alloy Nb—7Ti—20W—3Mo—1Zr—1Mn.

CONCLUSIONS

1. We studied the resistance to oxidation of niobium-base alloys, suggested by different authors, in the air at 800, 900, 1000, and 1200°C. Of the alloys prepared by arc melting the most resistant to oxidation at 800—1000°C are the following: Nb—45Ti—14W—4.3Al—4Cr—0.7Mn (alloy No. 21) and Nb—41Ti—4W—5Al—3Cr—3V—1Mn (alloy No. 28). The weight gain of these alloys over the above temperatures varies from 7 to 36 mg/cm^2 after 100 hr of oxidation. At 1200°C all alloys, except No. 15 (Nb—40Ti—5Mo—8Cr—5Al—1Mn), have a low resistance to oxidation. The weight gain of alloy No. 15 after 150 hr of testing was 91 mg/cm^2. Of the alloys

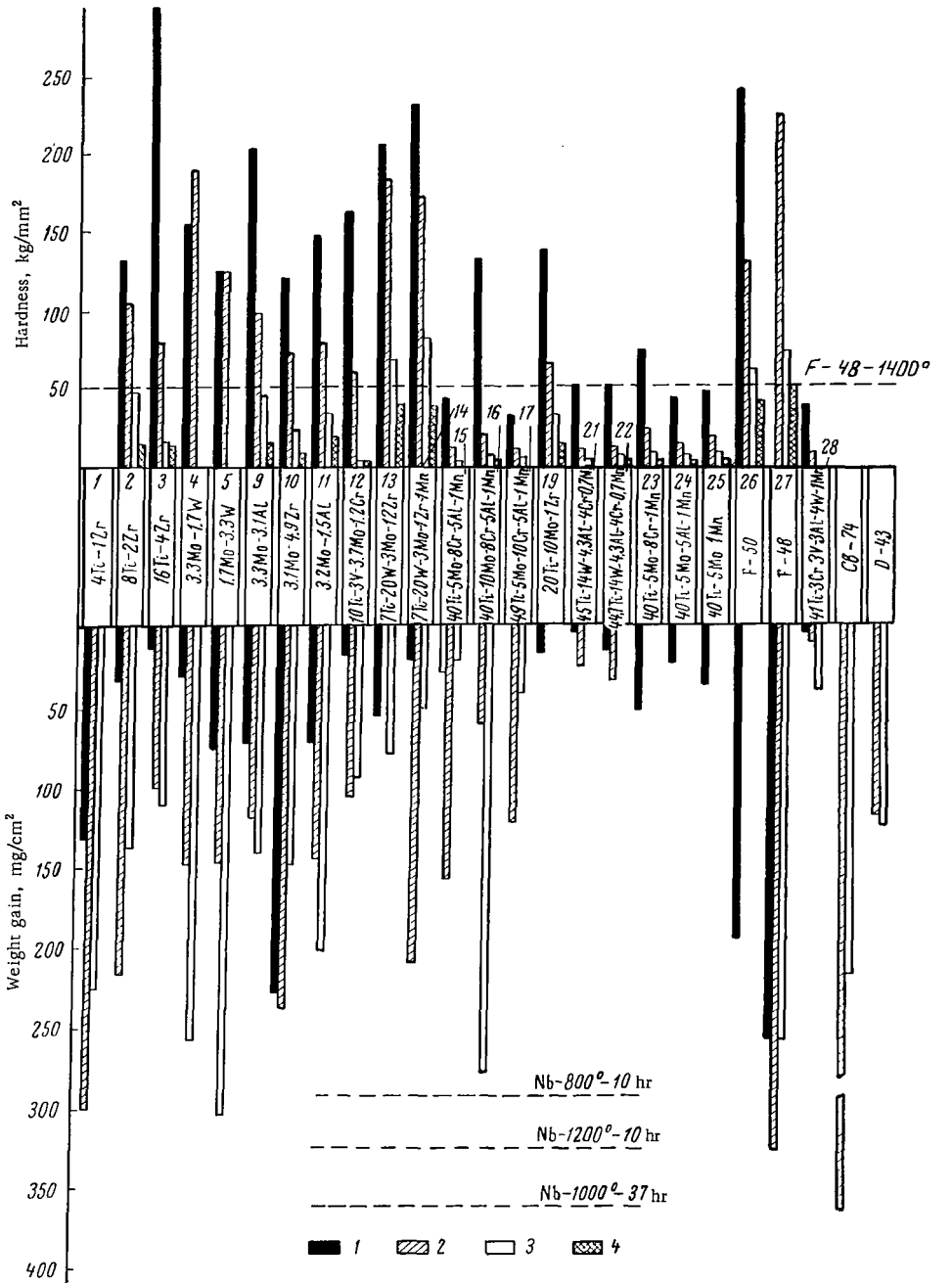

FIGURE 3. Heat resistance and hot hardness of alloys at 800—1400°C:
1 — 800°C; 2 — 1000°C; 3 — 1200°C; 4 — 1400°C.

containing more than 70 wt% of niobium, No. 3, Nb—16Ti—4Zr, and No. 12, Nb—10Ti—3V—3.75Mo—1.25Cr, have the highest resistance to oxidation at 800—1200°C.

We found the influence of a number of elements (tungsten, molybdenum, chromium, aluminum, manganese and carbon) on the resistance of niobium alloys containing 40—45% Ti to oxidation at 800—1000°C. It was found that the addition of tungsten to these alloys is more effective than additions of molybdenum. At 1200°C additions of molybdenum are more favorable than additions of tungsten.

2. We determined the heat resistance of some alloys prepared by arc melting, by measuring their hot hardness at 800—1400°C. It was found that alloys F-50 and F-48, and No. 14 (Nb—7Ti—20W—3Mo—1Zr—1Mn) are the most heat resistant at these temperatures. Their hardness at 1400°C lies between 40 and 50 kg/mm^2.

3. It should be pointed out that the niobium-base alloy No. 14 (Nb—7Ti—20W—3Mo—1Zr—1Mn) has the optimum combination of oxidation resistance and heat resistance, and high-strength alloys such as F-48 and F-50 have a resistance to oxidation differing little from that of unalloyed Nb.

Bibliography

1. Prokoshkin, D.A. and E.V.Vasil'eva. Splavy niobiya (Niobium Alloys). — Izdatel'stvo "Nauka." 1964.
2. Creep of Columbium Alloys, June. 1963.
3. McCedam, G.D.— J. Inst. Metals, 93. 1965.
4. Columbium. Metallurgy. 1961.
5. Arkharov, V.I., A.F.Gerasimov, and T.V.Ushakov.— Fizika Metallov i Metallovedeniya, Vol. 12, No. 5. 1961.
6. Grigorovich, V.K. and A.I.Dedyurin.— Trudy Instituta metallurgii im. A.A.Baikova, No. 12. 1962.
7. Sims, C.T., W.D.Klopp, and R.J.Jaffee.— Trans. ASM, Vol. 51, p. 256. 1959.
8. Industry Pwr, Vol. 27, No. 11. 1960.
9. Materials in Design Engineering. Vol. 34, No. 7, pp. 107—116. 1961.
10. J. Less-Common Metals, Vol. 2, Nos. 2—4. 1960.
11. Properties of Columbium Alloy. Symposium. 1963.
12. Proceedings of the International Conference on Heat-Resistant Metals and Alloys 1960. — Moskva, IL, p. 70. 1962.

G. V. Zemskov, R. L. Kogan, and A. V. Kostenko

STUDY OF BINARY HEAT-RESISTANT SILICON-BASE DIFFUSION COATINGS FOR NICKEL ALLOYS

As metals and alloys are used at elevated temperatures and in highly corrosive media, the problem of their protection against corrosion in gases is very important. Studies carried out to increase the resistance of nickel-

base alloys to corrosion in gases are of the greatest theoretical and practical significance.

The heat resistance of nickel-base alloys is particularly low in gas media containing sulfur, as the formation of low-melting sulfides and their eutectics with nickel and nickel oxides is facilitated /1, 2/. Vanadium pentoxide dissolves the oxide film on the alloys and leads to the formation of pits /3/. If the gas contains large amounts of seawater vapor the high content of chloride ions leads to an attack on the surface of nickel alloys /4/. The heat resistance of nickel—chromium alloys can be increased by protective coatings.

This work was carried out to develop and investigate single-component and multicomponent silicon-base diffusion coatings for the ZhS nickel—chromium alloy. Such coatings will protect the alloy against gas corrosion in an atmosphere of combustion products of sulfur-containing fuel, or in one with seawater vapors. These coatings also increase the heat resistance of the ZhS alloy in the air.

We studied diffusion coatings containing silicon and aluminum, silicon and titanium, and silicon and chromium. The coatings were produced by simultaneous or separate diffusion of these elements.

In our choice of elements for producing the two-component coatings for the ZhS alloy, we were guided by the following considerations.

Silicon, aluminum, and chromium, increase the general heat resistance of the alloy, and form a passivating film of oxides on its surface. On the other hand, aluminum and titanium increase the heat resistance of nickel—chromium alloys, since heating at elevated temperatures leads to a decrease in the content of these elements which determine the high-temperature strength of the alloy in the surface layer. The increase in the content of titanium and aluminum in the diffusion layer will avoid secondary factors such as the formation of cracks and of open-grain boundaries.

Diffusion coatings of several elements produce complex and not simple oxides on the surface layer of the element. The diffusion rate in complex oxides is lower than in oxides of individual elements. Thus, the formation of spinels is accompanied by an increase in the resistance of alloys to oxidation. If the composition of spinels is more complex, there is a change in their lattice parameters. The smaller the lattice parameter of spinels formed during the oxidation of metals and alloys, the more effective is their protective action /5/.

Diffusion coatings of several elements lead to the formation of complex compounds of diffusion elements with the elements of the alloy in the surface layer, and also of intermetallic compounds between the diffusion elements themselves. A homogeneous zone of silicides on the surface of the metal will greatly increase its resistance at elevated temperatures and in corrosive media. Thus, for example, titanium disilicide, $TiSi_2$, has a high resistance to scaling. When oxidized $TiSi_2$ becomes covered by a dense adherent vitreous film of oxides, apparently consisting of a mixture of titanium silicates of the eutectic type /6/.

Finally, to produce a protective coating, low-melting eutectics between the oxides and other compounds should not be formed. If the corrosive medium contains sulfur, the diffusion elements will probably bind it into high melting sulfides. The most favorable elements are silicon, titanium, and chromium (T_{melt} $Cr_2S_3 > 1550°C$, $Ti_2S - 1200°C$, $SiS_2 > 1090°C$).

To cover ZhS alloys specimens by a diffusion coating, the alloys were immersed into a vessel containing the correct powder and heated to 900—1000°C. The vessels were closed by fusible seals. We studied the influence of the temperature and of the duration of the diffusion process and of the composition of the powders on the properties of the coatings (thickness of diffusion coating, microhardness, phase composition, and behavior during service).

To study complex diffusion coatings a new method was suggested for determining possible complex diffusion coatings, and also the compositions of the powders from which two-component diffusion coatings should be produced. This is very important since because of the different diffusion coefficients of the diffusion elements in the alloy, and also because of the mutual influence of these elements on one another, at a certain composition of the powder the depth of diffusion and the concentration of one or of both elements in the surface layer may become very small. Thus, we studied the influence of the composition of the diffusion mixtures during diffusion coating by two elements on the properties of the final diffusion coatings. When the diffusion was carried out with both elements simultaneously, the content of each element in the mixture varied from 0 to 100% in 10% stages. If the diffusion was carried out first with one element and then with the other, the second element diffused from mixtures in which its content was 15, 25, 50, 75, and 95%.

Coatings produced by the optimum processes were tested for corrosion in gases and for heat resistance.

Corrosion in gases was tested on a special semi-industrial set-up simulating service conditions of vanes of gas turbines in an atmosphere of combustion products containing sulfur and seawater vapors at 900°C (the experiments were carried out by K. I. Lutsenko).

The heat resistance was tested in the atmosphere at 1000°C for 100—300 hr.

The heat resistance of the diffusion coatings was measured from the microstructure, penetration of corrosion, and also the phase composition determined by the X-ray method.

For two-component coatings the results can be represented in graphical form: properties of coating versus composition of the diffusion powder.

Such a diagram for Si + Ti, Si + Cr, and Si + Al compositions is shown in Figure 1. The common and characteristic feature of these three compositions is that the thickness of the diffusion layer decreases smoothly with increase in the content of titanium, chromium, and aluminum, in the powder. Let us consider the curves representing silicon + titanium compositions. If the content of titanium in the powder is up to 20%, siliconizing is the predominant process. The microhardness of the coating is the same as that of siliconized layers (1085—1123 kg/mm^2). If the content of titanium in the powder is from 20 to 95% both elements diffuse into the alloy. However, the coating is thinner than during siliconizing. The formation of a complex coating is confirmed by its microhardness, which decreases smoothly with increase in the content of titanium in the powder. A predominantly titanizing process takes place only from mixtures containing from 95 to 100% of titanium. In this case the microhardness of the surface corresponds to that of the external zone of a titanized coating (800 kg/mm^2).

The dependence of the depth of the diffusion coating on the content of elements in the powder was similar at other temperatures of the diffusion

coating also. If the temperature of the process is increased, the depth of the complex titanium-silicon coating increases. However, the optimum conditions for complex impregnation by silicon and titanium is a temperature of 900°C for 10 hr. At more elevated temperatures the quality of the resulting surface is inferior.

The shape of the curve representing the dependence of the linear dimensions on the content of elements in the powder is similar to that of the curve showing the depth of impregnation.

The formation of a complex diffusion coating is accompanied by the formation of a qualitatively new structure. Siliconized coatings consist of a uniform finely dispersed mixture of nickel silicide Ni_2Si and chromium silicides $CrSi_2$ and CrSi, but the coatings produced by a mixture containing from 20 to 35% of titanium consist of three characteristic zones. The upper nonetchable zone has a high microhardness (1035 kg/mm^2), and consists mainly of titanium disilicide but phases of the NiSi type are also found.

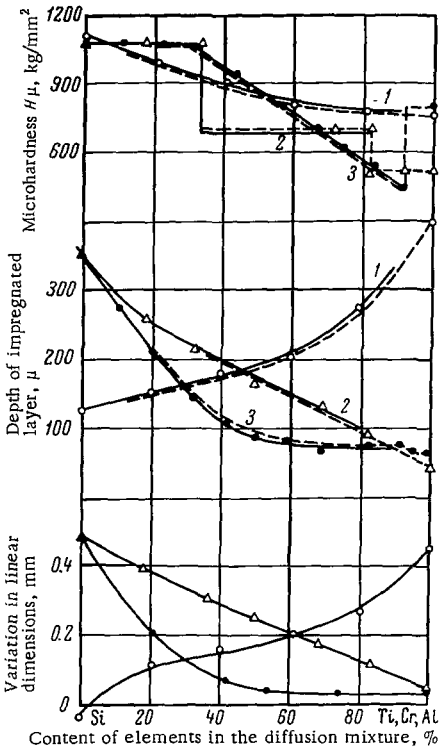

FIGURE 1. Dependence of the basic characteristics of diffusion coatings on the composition of the diffusion powders:

1 — Si+ Al; 2 — Si+ Cr; 3 — Si+Ti.

The structure of the second zone of the diffusion coating is different. It resembles the structure of a titanized coating, but after etching it can clearly be seen that the upper zone consists of two layers. According to the data of an X-ray analysis, the upper part of the coating consists of phases similar to those obtained by titanizing (Ni_3Ti and NiTi). Obviously the influence of silicon is apparent in the deeper part of the coating.

Thus, these results show that this method of studying the complex diffusion process is very valuable since regions of impregnation by both elements can be investigated.

A study of ZhS alloys impregnated by chromium and silicon also showed that a region of impregnation by both elements also exists. If the content of chromium in the powder is from 35 to 85%, the diffusion coating contains phases with a lattice of the Cr_3Si, $CrSi_2$, and Cr_5Si_3 type only. The microhardness of the surface of the complex coating is lower than that of siliconized surfaces, but higher than that of chromized surfaces (750 kg/mm^2). This relationship also holds if the process is carried out at other temperatures, or if powders with an inert material are used.

The Al—Si compositions are of particular interest when preparing complex diffusion coatings, since each of these elements appreciably

increases the resistance of the surface to corrosion in gases. To avoid the formation of brittle coatings, 45% of aluminum oxide is added to the mixture. Figure 1 shows that the depth of the diffusion coating increases with increase in the content of aluminum.

In these coatings it is impossible to determine the individual regions of the complex coating by metallographic analysis, since the coatings of silicon and aluminum are of the same type, and consist of a finely dispersed mixture of a solid solution with nickel and chromium silicides produced by siliconizing, and of nickel—aluminium compounds produced by calorizing. The microhardness changes smoothly from siliconizing to calorizing. In all the calorized—siliconized specimens that we studied, the predominant phase is of the Ni_2Al_3 type. Silicon is present in the diffusion coating as chromium silicides CrSi or $CrSi_2$. In addition, silicon apparently dissolves in the lattice of Ni_2Al_3.

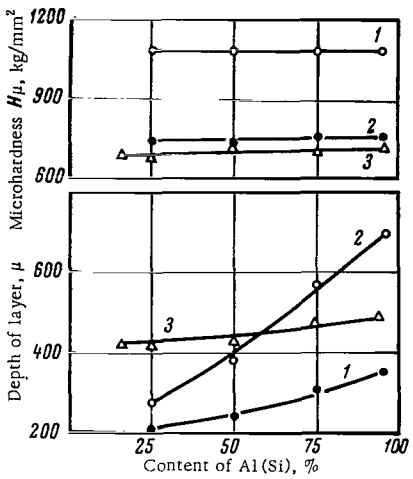

FIGURE 2. Dependence of the chief characteristics of aluminum—silicon coatings on the content of aluminum in the powder. The diffusion coating was produced by separate diffusion of the individual elements:

1 — Si—Al, 800°C; 2 — Si—Al, 900°C; 3 — Al—Si, 900°C.

The production of a complex coating by the diffusion of one element after the other was of great interest. It has been experimentally shown that impregnation by silicon and then by titanium, chromium, or aluminum, or vice versa, produces good diffusion layers on ZhS alloys with a clean surface. The diffusion of silicon into the alloy through a titanium or aluminum undercoat is difficult, and therefore this leads to adsorption of silicon on the surface, not to its diffusion.

In all our experiments siliconizing was carried out at 900°C for 10 hr.

Titanizing siliconized specimens leads to the production of a diffusion coating with a microstructure rather similar to that of siliconized materials. However, these specimens have a new zone which cannot be etched and a microhardness of 1035 kg/mm^2. This zone consists mainly of titanium disilicide. The depth of this zone is little influenced by the content of titanium in the powder, but is greatly increased by an increase in temperature.

The impregnation of siliconized specimens by aluminum from mixtures containing from 25 to 95% of aluminum leads to a thickening of the diffusion coating (Figure 2), and to a change in the dispersion of the microstructure. The microhardness of such coatings produced in a mixture containing 50, 75, and 95% of aluminum is close to that of calorized layers. The upper regions of such coatings consist mainly of the Ni_2Al_3 compound. These coatings also contain another phase, but its composition has not yet been determined. The content of this phase is not influenced by the concentration of aluminum in the powder.

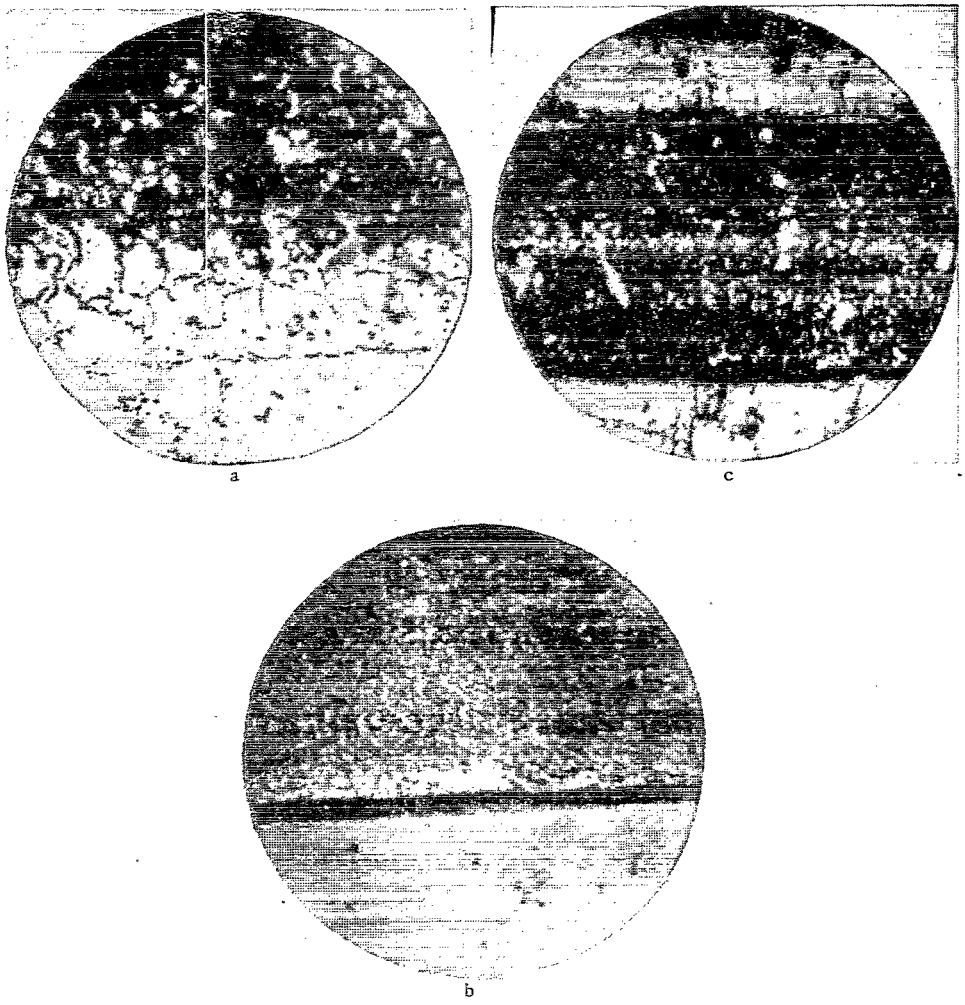

FIGURE 3. Microstructure of diffusion coatings after tests for corrosion in gases: a — without coating; b — Al+ Si, ×200; c — Si — Ti, ×340.

The thickness of the diffusion coating does not increase if calorized specimens are impregnated by silicon (see Figure 2) which indicates that silicon does not diffuse through calorized layers. The microhardness of such layers decreases toward the interior due to coagulation of the aluminum—nickel compounds and because these compounds are very little resorbed by the calorized layer.

The coatings produced by chromizing siliconized specimens have a microstructure similar to that of siliconized specimens. However, the upper part of such coatings has an additional zone consisting of chromium silicides. The depth of the coating is little influenced by an increase in the content of chromium in the powder.

A study of the resistance of the above coatings to corrosion in combustion gases containing sulfur and seawater vapors, and of their heat resistance

in air showed that on uncoated specimens considerable damage can be seen even with the naked eye, but diffusion-coated specimens have a completely smooth surface on which no damage is visible.

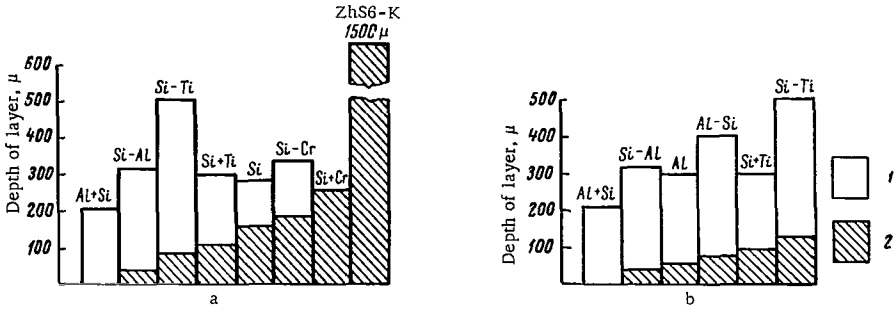

FIGURE 4. Diagrammatic representation of the results of tests on diffusion coatings:

a — corrosion in gases; b — heat resistance, 1 — total thickness of coating; 2 — damaged part of coating.

From the microstructure of coated and uncoated specimens (see Figure 3), it was seen that in uncoated alloys the corrosion penetrates deeply, and is intergranular in nature. In coated specimens the damage, if it exists at all, is local. A diagrammatic representation of the results showing the total thickness of the coating and the thickness of the damaged layers is given in Figure 4.

The diagram shows that complex silicon—aluminum coatings produced by the simultaneous diffusion of both elements are the most resistant to corrosion in gases, and that the microstructure of the specimen is not changed by this corrosion.

Coatings produced by the method of consecutive diffusion were damaged to a depth of 35μ, but in unprotected alloys to a depth of 1000—1500μ.

Of the titanium—silicon diffusion coatings, the most resistant are those produced by the method of successive alloying. The damage occurs at separate points. The resistance of titanium—silicon diffusion coatings (to corrosion) is rather inferior to that of aluminum—silicon coatings. An X-ray analysis of the surface of complex diffusion coatings showed that they consist mainly of spinel-type phases, and to a lesser extent of oxides of the elements in the coating. No nickel oxide was found in the scale.

Chromium—silicon diffusion coatings have a low corrosion resistance in gases. Oxidized chromium silicides do not form a dense film impermeable to gases. A thin protective silicate film may be absent because Cr_2O_3 does not dissolve in SiO_2.

The results of tests on heat resistance show that aluminum—silicon diffusion coatings produced by the simultaneous diffusion of both elements have the best properties. The surface of aluminum—silicon diffusion coatings does not change its external appearance as a result of the test, and no change in microstructure has been found.

Aluminum—silicon diffusion coatings produced by the method of successive alloying are damaged to a depth of 35—70μ. The Si—Al coatings are more resistant than the Al—Si coatings.

Titanium—silicon coatings are rather less resistant than aluminum—silicon ones. Chromium—silicon coatings have the lowest resistance, and the zone of chromium silicides is completely damaged.

CONCLUSIONS

1. We studied the process and developed a technique for coating ZhS alloys with two-component diffusion coatings of silicon and aluminum, silicon and titanium, or silicon and chromium.

We found that the most important factor which determines the quality of two-component diffusion coatings is the composition of the powder, and we found the dependence of the basic characteristics of the diffusion coating (depth, microhardness and phase composition) on this factor.

2. We found that the coatings studied greatly increase the resistance of the metal against corrosion in gases and in combustion atmospheres containing sulfur and seawater vapors, and also their heat resistance in air. Two-component coatings are more resistant to corrosion than single-component ones.

Bibliography

1. Hessenbruch, W. Metalle und Legierungen für höhe Temperaturen. — Verlag Springer. Berlin. 1940.
2. Ipat'ev, V.V. and D.V.Zheltukhin.— Zhurnal Prikladnoi Khimii, Vol.30, No.9. 1957.
3. Lipshtein, R.A., S.E.Khaikina, and E.S.Ginsburg.— Teploenergetika, No.8. 1960.
4. Tomashev, N.D. Teoriya korrozii i zashchita metallov (Theory of Corrosion and Protection of Metals). Moskva. 1959.
5. Arkharov, V.I.—Izv. AN SSSR, No.1, p.127. 1946.
6. Samsonov, G.V. Silitsidy i ikh ispol'zovanie v tekhnike (Silicides and Their Application in Industry).— Kiev, Izdatel'stvo AN UkrSSR. 1959.

D. V. Ignatov, R. S. Ivanova, and N. B. Abramova

ELECTRON DIFFRACTION AND KINETIC STUDIES ON THE REACTION BETWEEN HEAT-RESISTANT METALS AND OXIDES, AND RESIDUAL GASES AND VAPORS IN VACUO (10^{-3}—10^{-6} torr) AT ELEVATED TEMPERATURES

A study of the reaction between heat-resistant metals and oxides and their reaction with residual gases and vapors (O_2, N_2, H_2O, CO_2, CH_4, etc.) in vacuo at elevated temperatures is of great theoretical and practical importance.

In this article we shall report the generalized results of electron diffraction studies on the reaction between thin films of tungsten and oxides (Al_2O_3, ZrO_2 and HfO_2), and their reaction with gases and vapors at a pressure of 10^{-5}—10^{-6} torr.

We shall also discuss the results of the kinetic and electron diffraction studies on the reaction of molybdenum with gases and vapors at a pressure from $9 \cdot 10^{-3}$ to 10^{-6} torr over the temperature range of 600—1000°C.

As the starting specimens we used firstly thin films of tungsten and of oxides. The films of tungsten and of other metals (300—400 Å) were produced by evaporation and condensation on other materials (mica, sodium chloride). From these substances the films were separated by immersion in water, and were then taken from the water and placed on frames made of iridium (strips 20 mm long, 0.1 mm thick, and 3 mm wide, with openings 0.5—0.8 mm in diameter). The thin films of heat-resistant oxides were produced by oxidizing Al, Zr, and Hf foils.

To obtain electron diffraction photographs with sharp lines, the tungsten and molybdenum specimens were placed into piles of tantalum and annealed in vacuo (10^{-4} torr) at 800°C for one hour. Preliminary studies showed that annealing in tantalum piles completely prevents the Mo and W specimens from carburizing. Under these conditions thin foils of Al, Zr, and Hf were completely oxidized during annealing. Therefore, the two-layer specimens consisting of $W + Al_2O_3$, $W + ZrO_2$, and $W + HfO_2$, were first prepared in the form of two-layer foils of metals (W + Al, W + Zr, W + Hf) by the above method of evaporation and condensation, and then the thin foils were annealed in tantalum piles.

The initial thin foils of tungsten, oxides, and the two-layer foils of tungsten and the corresponding oxide, were annealed in a vacuum of 10^{-5}—10^{-6} torr over the temperature range of 800—1800°C. The device in which this annealing was carried out is described in /1/. The oil vapors of prevacuum and high-vacuum pumps, and also the lubricants of the ground stoppers and valves, were frozen by liquid nitrogen.

The molybdenum specimens were made of thin foils (obtained in the same way as the tungsten foils), or of 15×10×4 mm plates.

The kinetics of the reaction between the plate specimens was studied by the weight method, using torsional vacuum microbalances with a sensitivity of 10^{-6}—10^{-7} g per division of the microscale of the microscope. This balance is described in detail in /2/. The molybdenum specimens were heated in an electric furnace of special design which produced no magnetic field. The temperature was measured with an accuracy of ± 10°C by a platinum—platinum-rhodium thermocouple introduced into the working space of the balance. The different pressures of residual gases and vapors (from $9 \cdot 10^{-3}$—10^{-6} torr) in the balance was produced by evacuating the atmosphere by prevacuum and diffusion pumps. The vapors of the pump oils and the lubricants of valves and ground stoppers were, if necessary, frozen by liquid nitrogen.

The surface of the plate specimens was ground by emery paper and rinsed with acetone and alcohol. The specimens were then annealed in a vacuum of $5 \cdot 10^{-6}$ torr at 800°C in tantalum piles for 1 hr. The impurities in the starting molybdenum consisted of 0.02 wt% of carbon.

Composition of thin foils heated for 1 hr in a vacuum of 10^{-5}—10^{-6} torr

Heating temperature, °C	Composition of foil						
	W	Al_2O_3	ZrO_2	HfO_2	$W + Al_2O_3$	$W + ZrO_2$	$W + HfO_2$
Initial state	W	γ-Al_2O_3	ZrO_2(cub + mncl)	HfO_2mncl	W + γ-Al_2O_3	W + ZrO_2(cub + mncl)	W + HfO_2mncl
1000	W + WO_2 + tr WC	γ-Al_2O_3	ZrO_2(cub + mncl)	HfO_2mncl	W + γ-Al_2O_3	W + ZrO_2(cub + mncl)	W + HfO_2mncl
1200	W + WC + tr WO_2	(γ + tr α)-Al_2O_3	ZrO_2(cub + mncl)	HfO_2mncl	W + (γ + tr α)-Al_2O_3	W + ZrO_2(cub + mncl) + ZrC	W + HfO_2mncl + HfC
1400	W + WC + W_2C	(α + γ)-Al_2O_3	ZrO_2(cub + mncl)	HfO_2mncl	(α + γ)-Al_2O_3 + W	W + ZrO_2(cub + mncl) + ZrC	W + HfO_2mncl + HfC + WC
1600	W + WC + W_2C	(α + γ)-Al_2O_3	ZrO_2(cub + mncl) + ZrC	HfO_2mncl	(α + γ)-Al_2O_3 + WC	ZrC + ZrO_2(cub + mncl) + WC	HfO_2mncl + HfC + W + tr WC
1700—1800	W + tr WC 1700°, 1 hr	(α + tr γ)-Al_2O_3 1800°, 1 min	—	HfO_2mncl 1800°, 30 min	—	ZrC + WC + ZrO_2(cub + mncl) 1700°, 20 min	—

Key to abbreviations: cub = cubic; mncl = monoclinic; tr = traces.

RESULTS AND THEIR DISCUSSION

The results of electron diffraction studies on the reaction between thin foils of tungsten and of refractory oxides with residual gases and vapors of hydrocarbons at a pressure of 10^{-5}—10^{-6} torr are given on the table. Typical electron diffraction photographs of both the initial specimens and of carbides formed when these specimens were heated in vacuo are shown on Figure 1.

These data can be summed up as follows: thin foils of tungsten (300—400 Å) interact most intensely at 1400—1600°C with hydrocarbon vapors to form WC and W_2C according to the reactions $W + CH_4 = WC + 2H_2$, $2W + CH_4 = W_2C + 2H_2$. It is also possible that oxidation occurs since the residual gases contain small amounts of O_2, CO_2, and H_2O. However, the chief tungsten oxide WO_3 starts to evaporate at 800°C, and therefore it cannot be found in the film. Small amounts of WO_2 are found at 1000—1200°C. Unfortunately, we were unable to analyze the composition of the gases and vapors while the specimens were being annealed.

It can be seen from the table that Al_2O_3 and HfO_2 are thermodynamically stable in a vacuum of 10^{-5}—10^{-6} torr. From 1200°C γ-Al_2O_3 is gradually transformed into the more stable α-Al_2O_3. According to the data in /3/, thin films of γ-Al_2O_3 can be completely transformed into α-Al_2O_3 by heating for 5 hr at 1300°C in an electric furnace in an ordinary atmosphere. In our case γ-Al_2O_3 was slowly transformed into α-Al_2O_3 apparently because the specimens were heated by the electric current passing through the frame. Since the thermal conductivity of Al_2O_3 is low, the edges of the film in contact with the frame were heated intensely, but particularly during short annealings the middle part of the film was not heated to the necessary

temperature. In this way we can explain the presence of traces of γ-Al_2O_3 in a foil heated to 1800°C.

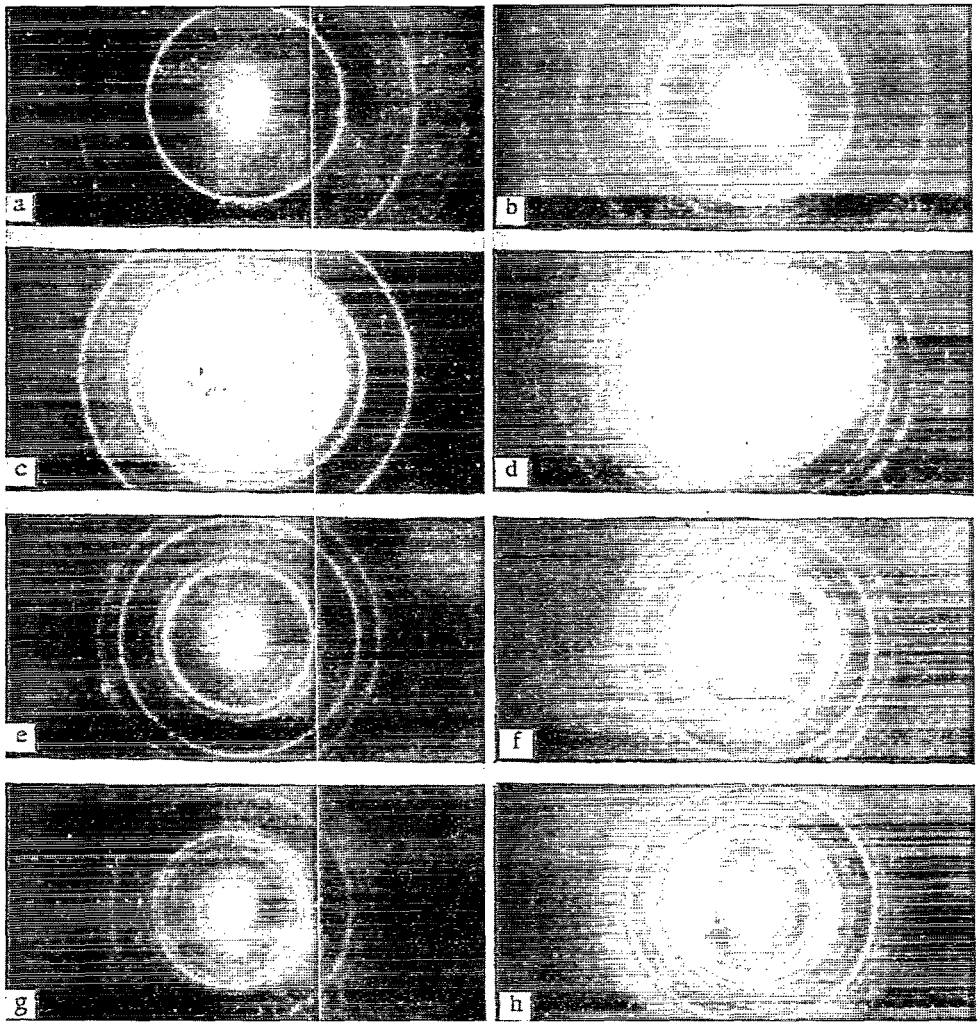

FIGURE 1. Electron diffraction photographs of thin foils of tungsten and of Al_2O_3, ZrO_2, and HfO_2 oxides heated in a vacuum of 10^{-5}—10^{-6} torr:

a — W, initial foil; b — W, 1500°C, 1 hr (W + WC + W_2C); c — Al_2O_3, initial foil (γ-phase); d — Al_2O_3, 1800°C, 1 min (α + traces of γ-phase); e — ZrO_2, initial film (cubic + monoclinic); f — ZrO_2, 1600°C, 1 hr [ZrO_2, (cubic + monoclinic) + ZrC]; g — HfO_2, initial film (monoclinic); h — HfO_2, 1800°C, 30 min (monoclinic).

The ZrO_2 oxide with a cubic and monoclinic structure is stable up to 1600°C. At 1600°C zirconium carbide ZrC was found in addition to the oxide.

The reactions between two-layer specimens and gases under the same conditions are quite different. In all three systems W + Al_2O_3, W + ZrO_2 and

$W + HfO_2$, the content of tungsten in the foils decreases with increase in the temperature of annealing. This was qualitatively confirmed from the decrease in the intensity of the diffraction rings on the electron photographs. Thus, for example, no free tungsten was found in foils consisting of tungsten and oxides of aluminum and of zirconium at 1600°C. In Table 1 the phases in the foils with the greatest intensity of reflections are placed first.

Another peculiarity of the interaction of these systems with gases is that ZrC and HfC are formed in the double-layer foils at lower temperatures than in pure oxide foils. For example, in ZrO_2 zirconium carbide is formed in small amounts at 1600°C, but in the double-layer foils it is formed in about the same amounts at 1200°C. Hafnium carbide does not form at all in HfO_2 foils at 1000—1800°C, but in double-layer foils starts to form at 1200°C.

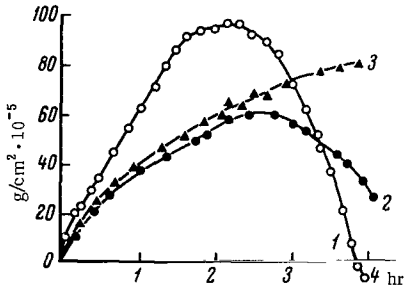

FIGURE 2. Kinetic curves of the reaction between molybdenum and gases and vapors at 1000°C:

1 — pressure $5 \cdot 10^{-3}$ torr after freezing out the oil vapors; 2 — pressure $9 \cdot 10^{-3}$ torr without freezing out the oil vapors; 3 — pressure $3 \cdot 10^{-5}$ torr after freezing out the oil vapors (prevacuum pump).

Thus, the reaction between tungsten or double-layer foils of tungsten + oxide (Al_2O_3, ZrO_2, or HfO_2) with residual gases at a pressure of 10^{-5}—10^{-6} torr in vacuum devices fitted with liquid nitrogen traps, leads to the formation of carbides of tungsten, zirconium, and hafnium. In other words, the reaction of tungsten and ZrO_2 and HfO_2 oxides with vapors of hydrocarbons (of the CH_4 type) is more intense than their oxidation by CO_2, O_2, and water vapor under the same conditions. The intense carburizing of tungsten /1/ under a pressure of 10^{-4} torr and at a temperature of 900—1000°C when the oil vapors were not frozen out (the films were completely transformed into W_2C and WC), and the less intense carburizing under a pressure of 10^{-5}—10^{-6} torr at 1400—1600°C after these vapors had been frozen out can be explained by the fact that the carbides of tungsten are more thermodynamically stable than the oxides over this range of temperatures.

In addition, the reaction of tungsten with a mixture of CO_2, O_2, H_2O, and CH_4 (and similar groups) will lead to the decomposition of CH_4 into carbon and four atoms of hydrogen which can bind the free oxygen atoms according to the reaction $4H + O_2 = 2H_2O$. Water vapor and CO_2 are frozen out more than oil vapors which continuously enter the system from the diffusion pump. Thus, the concentration of CH_4, formed as a result of the decomposition of vapors of vaseline oil on the surface of heated specimens, will always be

higher in the device than the concentration of CO_2, O_2, and H_2O. The CH_4 decomposes on the surface of the hot specimens, and the carbon enters directly into a reaction with tungsten, while hydrogen forms a local protective atmosphere around the specimen.

As already mentioned, the process of formation of zirconium and hafnium carbides in double-layer foils is intense and starts at 1200°C. As the temperature increases the content of carbides in these foils increases, but the content of tungsten decreases. These phenomena can apparently be explained by the influence of the reaction between tungsten and oxides on the usual reaction between tungsten oxides and CH_4. The reason for this influence is that the dissociation of ZrO_2, HfO_2, and Al_2O_3 at the tungsten—oxide interface is accelerated, and the oxygen evolved reacts with tungsten to form the volatile WO_3. Similar reactions of tungsten with Al_2O_3 and with BeO, and also of tantalum with ZrO_2, were for the first time proved by a mass spectrometric method /4, 5/. These phenomena were later observed during a study of the properties of heated cathodes made of tungsten wire and alundum ceramics /6/.

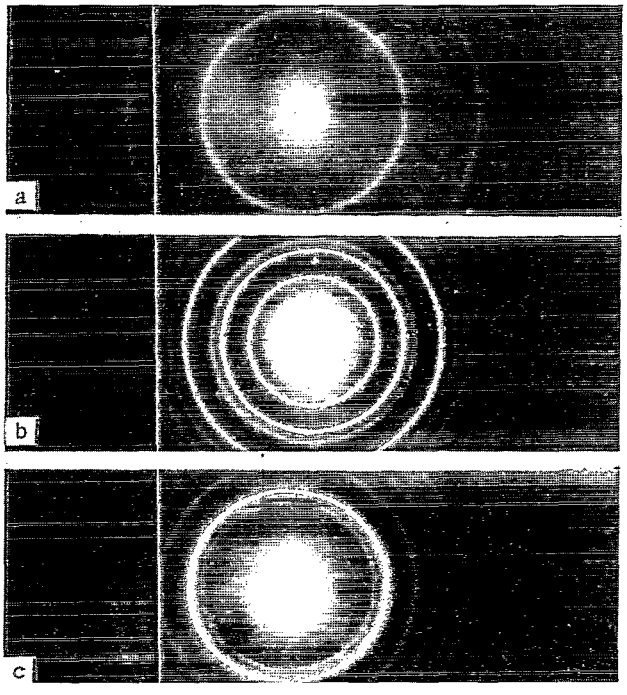

FIGURE 3. Electron diffraction photographs of thin foils of Mo heated in vacuo at 600—1000°C:

a — Mo, initial foil; b — MoO_2, formed under a pressure of $9 \cdot 10^{-3}$—$5 \cdot 10^{-3}$ torr; c — Mo_2C, formed under a pressure of $5 \cdot 10^{-5}$—$3 \cdot 10^{-5}$ torr.

An analysis of the data given in Table 1 also shows that no crystallochemical reactions (formation of new phases) occur between tungsten and

Al_2O_3, ZrO_2, and HfO_2, at 1000—1800°C. The results of a study on the kinetics of the interaction of molybdenum with residual gases and vapors are shown as curves in Figure 2 for the most characteristic case, i.e., at 1000°C and a pressure of $9 \cdot 10^{-3}$ and $3 \cdot 10^{-5}$ torr without freezing out the vapors, and at $5 \cdot 10^{-3}$ torr with freezing out the vapors. Under these conditions, the reaction of molybdenum with gases and vapors is the most intense. The electron diffraction photographs of films of oxides and carbides of molybdenum, formed on the metal as a result of reactions under various conditions, are shown in Figure 3.

The data of electron diffraction analysis of the phase composition of surface films on plate specimens and thin foil specimens of molybdenum show that at 600, 800, and 1000°C, and at a pressure of gases in the device of $(5-9) \cdot 10^{-3}$ torr molybdenum is oxidized to MoO_2 and MoO_3, whether or not the vapors are frozen out. At 800 and 1000°C and at a pressure of $1.5-3 \cdot 10^{-5}$ torr molybdenum becomes carburized to Mo_2C whether or not the vapors are frozen out.

Under these conditions, the mechanism of the formation of molybdenum carbide is the same as that of tungsten carbide described earlier, i.e., according to the reaction: $2Mo + CH_4 = Mo_2C + 2H_2$.

Figure 2 (curve 3) shows that carburizing of molybdenum is governed by a parabolic law, and that the rate constant of this law is $k = 2.9 \cdot 10^{-11}$ g^2/cm^2. The parabolic nature of the kinetic curve indicates that carburizing is due to the diffusion of carbon into the molybdenum. At a pressure of $1.5 \cdot 10^{-5}$ torr and at 1000°C (the oil vapors of both pumps were frozen out) the kinetics of carburizing could not be determined by means of the available balance, but a weight gain of $3 \cdot 10^{-6}$ g/cm^2 after 4 hr was found.

Figure 2 (curves 1 and 2) shows that if the oil vapors of the prevacuum pump are frozen out the average rate of oxidation at 1000°C, under a pressure of $5 \cdot 10^{-3}$ torr, is 1.5 times the oxidation rate of molybdenum under a pressure of $9 \cdot 10^{-3}$ torr, i.e., when the vapors are not frozen out. This is apparently because in the last case the oil vapors and the products of their decomposition (hydrocarbons) decrease the oxidation rate. We were unable to determine in greater detail the mechanism of oxidation of molybdenum under these conditions because we could not analyze the gases in the system during the reaction between the specimens and the mixture of hydrocarbons and oxygen-containing gases. The weight loss of specimens starts about 2 hr after the beginning of the process, and indicates that the rate of evaporation of MoO_3 at 1000°C is greater than the rate of formation of MoO_2 and MoO_3.

Bibliography

1. Ivanova, R.S., D.V.Ignatov, and A.A.Zaitsev. Svoistva i primenenie zharoprochnykh splavov (Properties and Application of Heat-Resistant Alloys). — Izdatel'stvo AN SSSR. 1966.
2. Ignatov, D.V. Trudy Instituta metallurgii im. A.A.Baikova, No.5. 1960.
3. Ignatov, D.V. Kristallografiya, Vol.2, No.4. 1957.
4. Toropov, N.A. and V.P.Barzakovskii. Vysokotemperaturnaya khimiya silikatnykh i drugikh okisnykh sistem (High-Temperature

Chemistry of Silicates and other Oxide Systems). — Izdatel'stvo AN SSSR. 1963.
5. Dushman, S. Scientific Foundations of Vacuum Techniques.—J. Wiley.
6. Semenov, Yu. A. Proizvodstvo podogrevatelei kadotov elektrovakuumnykh priborov (Production of Heating Cathodes of Electric Vacuum Apparatus). — Moskva—Leningrad, Gosenergoizdat. 1962.

N. F. Shur

INVESTIGATION OF THE SERVICEABILITY OF HEAT-RESISTANT STEELS IN CARBON-CONTAINING ATMOSPHERES

The purpose of this research was to study the behavior of heat-resistant materials in carbon-containing atmospheres and to choose steels for furnace equipment working in such atmospheres.

Carbon-containing atmospheres of various compositions which react to different extents with heat-treated steels and heat-resistant materials of furnace equipment are used in industrial electric furnaces.

To choose heat-resistant steels correctly for furnace equipment we took the "carbon potential" as a criterion. This characterizes the activity of the medium of the atmosphere, and all carbon-containing atmospheres can be classified irrespective of their exact chemical composition on the principle of the same carbon potential. Heat-resistant materials which can be used for all or for some groups of carbon-containing atmospheres can be chosen.

The carbon-containing atmospheres most widely used in heat-treatment equipment to protect different steels against oxidation, cementation, etc., can be divided into three groups containing 0.3—0.4, 0.8—0.9, and 1.3—1.5% of carbon.

We took the carbon potential of air as zero for reference.

For our studies we chose the heat-resistant chromium nickel steels Kh18N35, Kh23N18, and Kh25N20S2, and also the chromium steel Kh25. These steels are widely used for the production of electric equipment.

According to literature data, the oxidation of metals in the air, i.e., in a highly corrosive medium, is governed by the Arrhenius equation, and accelerates as the temperature is increased.

The reactions in controlled atmospheres are governed by other laws. Shchmakov /1/ showed (Figure 1) that in controlled atmospheres the thermodynamic probability of oxidation at the equilibrium temperature is equal to 0, since the difference between the thermodynamic potentials of oxidation and of reduction of oxides is also equal to zero. As a result, the difference between the oxidation rate and the rate of reduction of oxides is equal to zero. In the field of oxidation, the rates of oxidation and of reduction of oxides increase with increase in temperature. Hence, it follows that at a certain temperature, lower than the equilibrium, the difference between the oxidation rate and the rate at which oxides are reduced has a maximum, which is a peculiarity of the process of oxidation in protective atmospheres.

We confirmed this theory by experiments on specimens of heat-resistant steels at 700—1000°C for 100 hr in a carbon-containing atmosphere.

Our results showed that at a carbon potential of 0.3—0.4% C (Figure 2,a) the maximum oxidation rate is 800—900°C, and the equilibrium temperature is above 1100°C. At a carbon potential of 1.3—1.5% C (Figure 2,b) the temperature of the maximum oxidation rate shifts to 1050°C.

When the heat resistance of these steels was studied at 1050°C in the air and in carbon-containing atmospheres with different carbon potentials (Figure 3,a), it was shown that in the air and at a carbon potential of 0.3—0.4 and 0.8—0.9% C, the most heat-resistant steel is Kh25N20S2, followed by the Kh23N18, Kh25, and Kh18N35 steels. At a carbon potential of 1.3—1.5% C, the Kh23N18 steel is inferior to the Kh25 steel. This is because the Kh23N18 steel is highly carburized under these conditions (Figure 4). The KhN35 steel is more carburized than any other steel (up to 2.5% of carbides of all three types). When the steels are heated in the air a σ-phase is formed in all those studied, but when they are heated in a carbon-containing atmosphere almost the total content of chromium combines with carbon, and so carbides are formed and not a σ-phase.

The structures of heat-resistant steels Kh18N35, Kh23N18, Kh25N20S2, and Kh25 were determined by an X-ray analysis after heating at 1050°C for 500 hr, and are shown below.

Atmosphere	Structure
Air	γ-solid solution+σ-phase+[$(Fe, Cr)_{23}C_6$]
Carbon-containing atmosphere with a carbon potential:	
0.3—0.4	γ-solid solution+σ-phase+$(Fe, Cr)_{23}C_6$
0.8—0.9	γ-solid solution+$(Fe, Cr)_{23}C_6$+$(Fe, Cr)_7C_3$
1.3—1.5	γ-solid solution+$(Fe, Cr)_{23}C_4$+$(Fe, Cr)_7C_3$+$(Fe, Cr)_3C_2$

From Figure 4 it can be seen that an increase in the carbon potential of the atmosphere up to 0.8—0.9% C reduces the rate of oxidation of the steels. However, further increase in the potential to 1.3—1.5% C reduces the heat resistance of steel, although it still remains higher than the heat resistance of steels in the air. This is because chromium, which is the chief alloying element and increases the heat resistance of the alloy, becomes bound into carbides as a result of this strong carburizing. This leads to a decrease in the chromium content of the solid solution and to a decrease in the heat resistance of the steel.

An X-ray structural analysis of oxide films showed that oxidation in the air leads to the formation of double oxides of the spinel type ($NiFe_2O_4$) with a lattice parameter of 8.34 kX and of chromium oxide α-Cr_2O_3. Under these conditions the Kh25 steel becomes covered by a ($FeCr_2O_4$) spinel with a lattice parameter of 8.34 kX.

In carbon-containing atmospheres chromium oxides and small amounts of iron oxides are the main products.

This is because in highly corrosive air all elements of the alloy are oxidized, but in carbon-containing atmospheres only chromium, which has the highest affinity for oxygen, is oxidized.

Consequently, carbon-containing atmospheres protect materials being heat treated but do not protect furnace parts made of heat-resistant steels containing chromium.

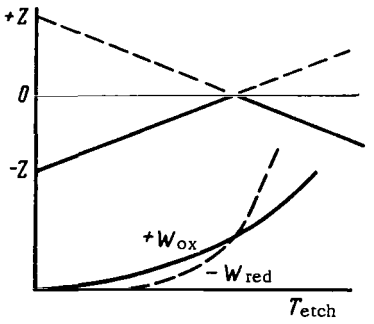

FIGURE 1. Schematic representation of oxidation in protective atmospheres.

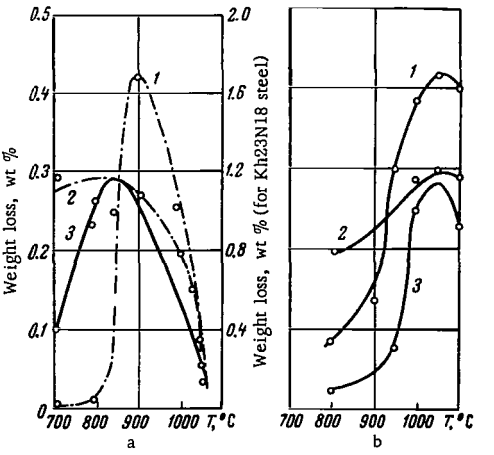

FIGURE 2. Dependence of the weight loss of heat-resistant steels on the temperature of heating (100 hr) in a carbon-containing atmosphere with different carbon potentials:

a — 0.3—0.4%; b — 1.3—1.5%; 1 — Kh23N18; 2 — Kh18N35; 3 — Kh25N20S2.

A check of electric furnaces working under carbon-containing atmospheres was carried out by several plants and showed that the main cause of premature failure of heat-resistant parts is cracking as a result of carburizing. The carburizing is especially high in poorly welded joints and in casting faults.

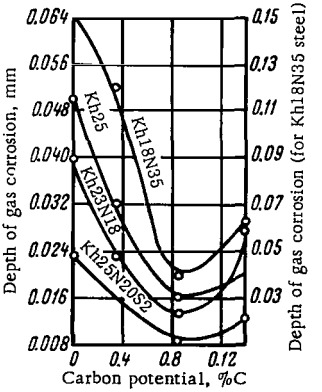

FIGURE 3. Dependence of the depth of gas corrosion in heat-resistant steels on the carbon potential of the atmosphere. The specimens were heated at 1050°C for 1000 hr.

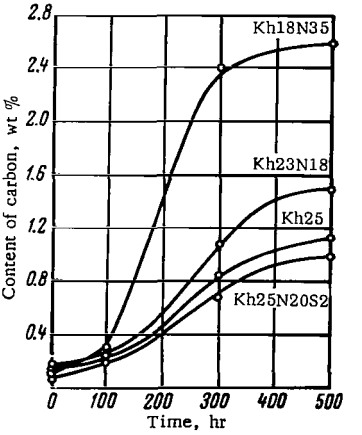

FIGURE 4. Dependence of carburization of heat-resistant steels on the holding time in a carbon-containing atmosphere with a carbon potential of 1.3—1.5% C.

It is thus necessary to develop more heat-resistant steels which will not become carburized at high carbon potentials, and will be sufficiently heat resistant and have a good high-temperature strength at 1000–1100°C in carbon-containing atmospheres.

Of the available steels, Kh25N20S2 and Kh25 steels have the optimum properties, and are recommended for use in carbon-containing atmospheres up to 1050°C. The Kh25 steel can be used for low-stressed parts (screens, guides, etc.).

Bibliography

1. Shmakov, A.A. Teoreticheskie osnovy bezokislitel'nogo nagreva stali (Theoretical Principles of Oxygen-Free Heating of Steels). — Dissertation for Degree of Doctor, Moskva. 1956

V. S. Postnikov, I. M. Sharshakov, V. V. Usanov, A. M. Belikov, and I. V. Zolotukhin

THE MECHANISM OF THE HARDENING OF SOME Fe–Cr–Ni ALLOYS

The hardening of alloys of the martensitic–austenitic type, Kh16N6 and Kh17N5M3, is mainly due to the transformation of austenite into martensite. Aging at 350–550°C leads to additional hardening of these steels. However, aging processes have not yet been sufficiently clarified and we have no unequivocal data on the question as to which phases and structural changes lead to hardening of these steels /1–13/. The aim of this work is to study this problem.

MATERIALS AND METHODS.

For our experiments we used 1 mm diam wire and 25 mm diam rods made of Kh16N6, Kh17N5M3, and Kh15N9Yu steels.

We measured the mechanical properties (ultimate strength, elongation, microhardness, and internal friction) of specimens after various stages of aging.

The internal friction of wire specimens was measured by the ordinary torsional pendulum at a frequency of 0.6 to 18 cps.

The microhardness was measured on a PMT-3 tester fitted with a special device for readings at elevated temperatures.

The ultimate strength and the elongation were measured on 1.0 mm diam specimens by means of an MR-0.5 tensile test machine.

We also carried out X-ray and electron diffraction studies with a URS-50IM diffraction meter and an EG-100A electronograph. These studies

were limited to a high-temperature analysis of the content of martensite and austenite in the specimens, and a phase analysis of the electrodeposited precipitates.

RESULTS AND DISCUSSION

The chief heat-treatment process for all the alloys before aging was normalizing at 750—950°C. This process produced a high content of martensite and a high ultimate strength.

The influence of the aging temperature of the internal friction (Q^{-1}), microhardness ($H\mu$), and ultimate strength (σ_b), of Kh17N5M3 specimens cooled to 20°C is shown in Figure 1. The heating time at this temperature was 1 hr. Before it was aged the steel was normalized at 930°C and deep cooled (at −78°C) for two hours.

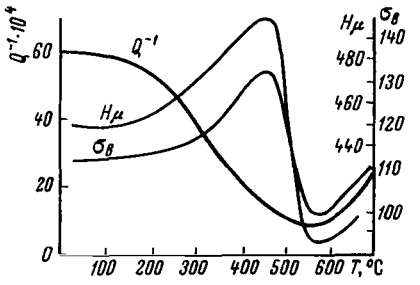

FIGURE 1. Influence of aging temperature on the internal friction, microhardness, and ultimate strength of Kh17N5M3 steel.

Aging at temperatures of up to 200°C has little effect on the above characteristics. Further increase in the aging temperature to 450°C leads to a considerable increase in σ_b and $H\mu$ and a decrease in Q^{-1}. Aging at 450—550°C decreases σ_b and $H\mu$, but a further increase in the aging temperature above 550°C again increases σ_b, $H\mu$, and Q^{-1}. A similar dependence was found for the two other alloys. The influence of the duration of aging at various temperatures on the microhardness measured at room temperature is shown on Figure 2. Aging has the greatest effect on the Kh15N9Yu alloy and the smallest on the Kh16N6 alloy. The hardness is appreciably increased by aging at 430—550°C. The temperature dependence of microhardness is determined by the structure of the alloys.

In alloys with an initial austenitic structure the microhardness decreases smoothly with increase in temperature (Figure 3,a). However, the decrease in the microhardness of austenitic—martensitic steels (Figure 3,b) at 300—450°C (Kh17N5M3 alloy) is much slower, and the microhardness of the Kh15N9Yu alloy even increases if the steel is heated at 350—470°C..

According to literature data, the hardening may be due to the following:

1) precipitation of carbides from the martensite /1—5/;

2) formation of dispersed phases during decomposition of martensite /6—13/;

3) additional formation of martensite as a result of cooling after aging /10/.

We verified these assumptions by X-ray and electronographic studies.

The specimens were analyzed by an X-ray method using a URS-50IM diffractometer fitted with a specially designed high-temperature vacuum device. It was found that heating to 450—500°C and cooling does not appreciably change the content of martensite in the above alloys.

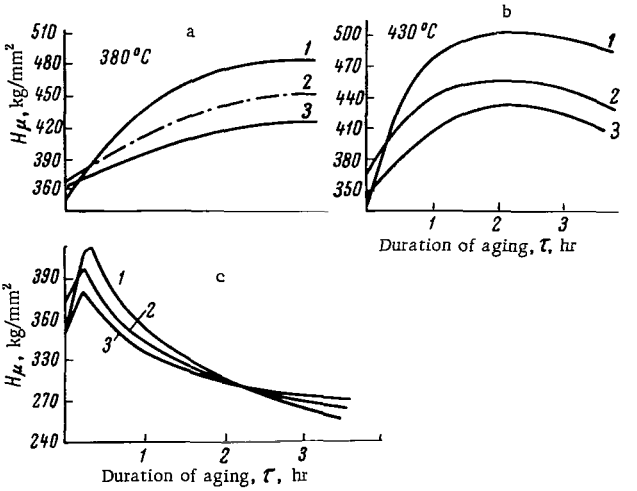

FIGURE 2. Influence of the duration of aging at various temperatures on the microhardness of alloys:

a — 380°C; b — 430°C; c — 550°C; 1 — Kh15N9Yu alloy; 2 — Kh17N5M3 alloy; 3 — Kh16N6 alloy.

If the metals are heated above 500°C the content of austenite increases and that of martensite decreases.

In specimens heated to 700—800° C the content of martensite produced after cooling to room temperature increases with increase in the duration of isothermal heating. This is the result of a decrease in the content of alloying elements and of carbon in the γ-solid solution with a consequent decrease in the stability of the austenite. These results agree well with the data on internal friction which show that isothermal heating at 700—800°C increases the $H\mu$ point. To find which phases are precipitated by aging, we carried out a qualitative phase analysis of the anodic precipitates of specimens aged at 350—500°C after normalizing at 800°C. The electron diffraction photographs recorded for "reflection" and "transition" after etching in "carbide" and "intermetallic" electrolytes /14, 9/ indicated the presence of a $Me_{23}C_6$ carbide and of a phase with a structure of ordered ferrite of the CsCl type, with a lattice parameter of 2.91 Å (Figure 4), in all the alloys studied /11—13, 15/.

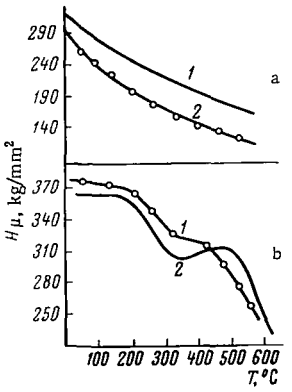

FIGURE 3. Temperature dependence of microhardness of the Kh17N5M3 alloy (1) and the Kh15N9Yu alloy (2):

a — normalizing at 1000°C; b — at 800°C.

No diffraction photographs can be recorded from specimens normalized at 1000°C.

Debye photographs of anodic precipitates of Kh15N9Yu alloys in an intermetallic electrolyte indicated the existence of a Ni_3Al phase besides the above.

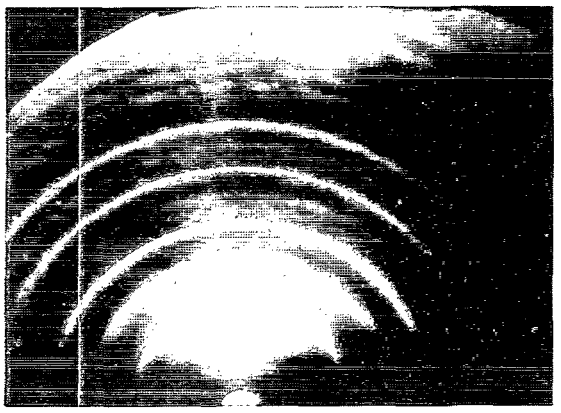

FIGURE 4. Electron diffraction photograph of a Kh17N5M3 alloy (carbide electrolyte), after normalizing and aging for 1 hr at 450°C.

CONCLUSIONS

We can assume that the hardening of the above alloys by aging is due mainly to the formation of an ordered ferrite with a lattice parameter of 2.91 Å (the so-called α'-phase). In fact, it has been experimentally shown that the content of martensite does not change appreciably when the alloy is cooled from an aging temperature up to 500°C. The content of precipitated carbides $Me_{23}C_6$ is not great, even if the specimens are aged at 700—800°C, as can be seen from the intensity of the carbide lines on the electron diffraction photographs. Consequently, the strengthening cannot be due to the presence of carbides only. If the aging temperature is increased above 500°C, the formation of the α'-phase is accompanied by a martensite→austenite transformation. The decrease in the hardness as a result of prolonged heating at elevated temperatures is apparently due to coagulation of the precipitated phases and the start of the martensite→austenite transformation.

The Kh15N9Yu alloy contains not only the α'-phase but also large amounts of the Ni_3Al intermetallic compound, which gives additional strengthening.

Bibliography

1. Potucek, V. and K. Löbe. Hanus Tuma Material. — Collection by SVUMT, Praha, 21. 1963.
2. Cihal, V. and F. Jezek.— J. Iron Steel Inst. Vol. 202, No. 2. 1964.
3. Chekis, Kh. I. and S. I. Vol'fson.—*Metallovedenie i Obrabotka* Metallov, No. 4, p. 16. 1958.
4. Yuonoshin, J. and M. Tsuyoshi.— Sci. Repts. Res. Inst. Tohoku Univ., A13, No. 1, p. 1. 1962.
5. Perry, D. S., H. Tangzyn, and W. C. Clarke.—*Metal Progress*, 6. 1963.

6. Murphy, I.I.—Aeron. Soc., 61. 1957.
7. Underwood, E.E., A.E.Austin, and G.K.Manning.—J. Iron Steel Inst., Vol.200, No.8. 1960.
8. Fel'dgandler, E.G. and M.V.Pridantsev.—Metallovedenie i Termicheskaya Obrabotka Metallov, No.11. 1961.
9. Lashko, N.F. and K.P.Sorokina.—FMM, Vol.14, No.1. 1962.
10. Krauss, G. and B.L.Auerbach.—Trans. ASM, Vol.52. 1960.
11. Antony, K.C.—J. Metals, Vol.15, No.13. 1963.
12. Burnett, H.C., R.Duff, and H.C.Vacher.—J. Res. Nat. Bur. Standards, No.2, p.66. 1962.
13. Varli, K.V., Yu. A.Skakov, N.G.Sokolova, and A.L.Shpitsberg.—Metallovedenie i Termicheskaya Obrabotka Metallov, No.4. 1964.
14. Gorelek, S.S., A.N.Rastorguev, and Yu.A.Skakov. Rentgenograficheskii i elektronograficheskii analiz metallov (X-Ray Diffraction and Electron Diffraction Analysis of Metals).—Metallurgizdat. 1963.
15. Brodley, A.J.—J. Iron Steel Inst., Vol.171, p.41. 1952.

M. Ya. Dzugutov, Yu. V. Vinogradov, S. A. Golovanenko, and A. N. Chernov

STUDY OF THE MACROSTRUCTURE AND PROPERTIES OF EXTRUDED RODS OF HIGH-STRENGTH ALLOYS

The macrostructure of the initial billets was studied by cutting transverse macrosections before the heat treatment.

The macrostructure of the extruded rods was studied by cutting transverse and longitudinal macrosections before and after heat treatment. The specimens were cut from the middle part of the rods and from the parts remaining after extrusion. The specimens for mechanical testing were taken from the middle part of the rods.

The rods were heat treated by processes according to the technical specifications for rods. Rods 70—40 mm in diameter were heat treated after they had been cut along the axis into four parts, and rods 30 mm in diameter or less were heated without cutting.

The macrostructure of all heat-treated rods of KhN70VMTYu, A and B, alloys (except 30 mm diam rods of alloy B, melt No. 967) extruded from a 1000 t press after heat treatment according to technical specifications (see table) was uniform and fine-grained. The 30 mm diam rods of alloy B had a coarse and nonuniform grain. Radial cracks 3—5 mm long were found in the 30 mm diam rods of alloys B and A. These cracks were apparently caused by excessive (for these alloys) degree of deformation produced by extrusion, and the unduly high temperature of the billets before extrusion.

The 60, 38, 29, and 24 mm diam rods of alloys KhN77TYuR, KhN70VMTYu and A extruded on a 1500-ton press from wrought and cast billets did not show much nonuniformity in grain size.

If the diameter of the rod is reduced the grain becomes smaller. In general, the macrostructure does not differ from the structure of rods

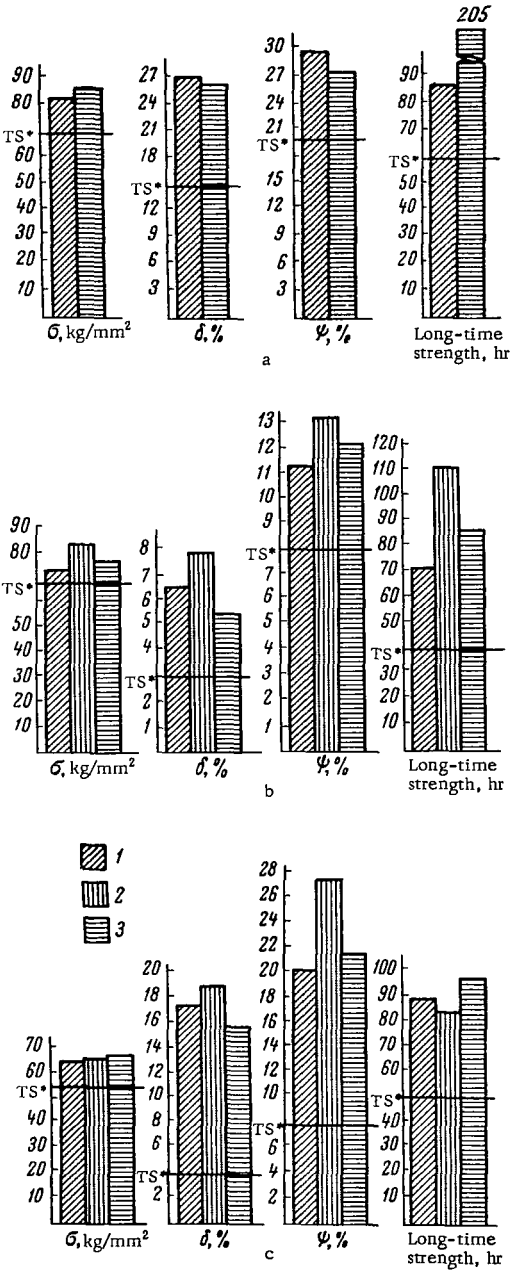

FIGURE 1. Properties of extruded rods of KhN77TYuR (a), KhN70VMTYu (b) and A (c) alloys:

1 — extruded rods; 2 — rolled rods (metal produced in an electric furnace by the slag method); 3 — rolled rods (open-hearth melts).

*[Technical specifications.]

Heat treatment and testing of extruded rods

Designation of alloy	Heat-treatment process		Temperature of short-time tests, °C	Conditions of long-time tests, °C kg/mm²
	hardening	aging		
KhN77TYuR	1080°—8 hr, air	700°—16 hr, air	700	700°—44
	1190°—2 hr, air	800°—16 hr, air		
KhN70VMTYu	1050°—4 hr, air		800	850°—20
A	1200°—4 hr, air	850°—8 hr, air	900	900°—22
B	1220°—4 hr, air	850°—8 hr, air	900	900°—27

produced by ordinary rolling. If other conditions are equal, rods produced from wrought billets have a coarser grain than rods produced from cast billets.

The specimens for determining the properties of initial cast and wrought billets and also of extruded rods of all sizes, except those of 24 and 29 mm diam, were taken from the middle of the material, while specimens from the 24 and 29 mm diam rods were taken from the center.

The shape and dimensions of the specimens for short-time hot tests satisfied the specifications for SMI 204-56, and those for long-time tests were suitable for SMI 205-56.

The short-time tests were carried out at 700, 800, and 900°C, and the long-time tests at 700, 800, and 900°C, under loads of 44, 20, 22, and 27 kg/mm². Specimens of alloys KhN77TYuR, KhN70VMTYu, and A, had stable properties comparable to those of high-quality rolled rods of the corresponding metal.

The average data of tests on KhN77TYuR, KhN70VMTYu, and A alloys are given in Figure 1. For comparison we give a diagrammatic representation of the average annual characteristics of strength, ductility, and long-time strength, of high-quality rolled metal. We give also the average data on rolled rods of KhN70VMTYu and A alloys produced by the slag method.

These data show that all the properties of extruded rods of KhN77TYuR, KhN70VMTYu, and A alloys (except the long-time strength of the KhN77TYuR alloy) are comparable to the properties of rolled rods, and considerably exceed those required by technical specifications (TS). The long-time strength of rolled rods of the KhN77TYuR alloy is appreciably higher than that of extruded rods produced under the given conditions.

Not all specimens of the alloy B have properties that meet the technical specifications, and their properties are inferior to those of rolled rods. The main reason is apparently the grain size nonuniformity, which is greater in extruded rods.

CONCLUSIONS

1. It was found that extrusion of ingots of the above alloys leads to complete breaking up of the cast structure at reductions of 70% upward. The alloys thus acquire a uniform structure with a grain size No. 2—4 according to GOST 5639-65.

2. The data show that extrusion increases the strength and stabilizes the ductility of the alloys. All properties are superior to those required by the technical specifications (TS) and are approximately equal to those of rods (rolled) produced by ordinary techniques, except long-time strength of alloys B and KhN77TYuR.

3. It was found that extrusion can substitute forging and rolling for the production of billets and finished parts. If forging is eliminated, the efficiency is increased. However, the extrusion technique should be further studied under industrial conditions.

National Aeronautics and Space Administration

WASHINGTON, D. C. 20546

OFFICIAL BUSINESS

POSTAGE AND FEES PAID
NATIONAL AERONAUTICS AND
SPACE ADMINISTRATION

5439

Printed in Jerusalem, Israel

NASA TT F-557
TT 69-55020